

DIFFUSION WITH REVERSIBLE CHEMICAL REACTION
IN HETEROGENEOUS MEDIA

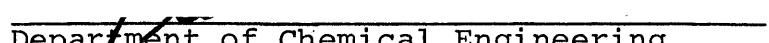
by

PIETER STROEVE


B.S. University of California, Berkeley (1967)
M.S. Massachusetts Institute of Technology (1969)

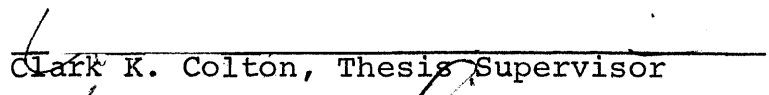
Submitted in Partial Fulfillment
of the Requirements for the
Degree of
DOCTOR OF SCIENCE
at the
Massachusetts Institute of Technology
August 1973

Signature of Author



Department of Chemical Engineering

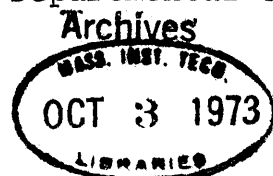
Certified by


Kenneth A. Smith, Thesis Supervisor


Clark K. Colton, Thesis Supervisor

Accepted by


Glenn C. Williams, Chairman
Departmental Committee on Graduate Theses




Department of Chemical Engineering
Massachusetts Institute of Technology
Cambridge, Massachusetts
August 3, 1973

Professor David B. Ralston
Secretary of the Faculty
Massachusetts Institute of Technology
Cambridge, Massachusetts

Dear Professor Ralston:

In accordance with the regulations of the faculty, I herewith submit a thesis, entitled "Diffusion with Reversible Chemical Reaction in Heterogeneous Media", in partial fulfillment of the requirements for the degree of Doctor of Science in Chemical Engineering at the Massachusetts Institute of Technology.

Respectfully submitted,


Pieter Stroeve

ABSTRACT

DIFFUSION WITH REVERSIBLE CHEMICAL REACTION

IN HETEROGENEOUS MEDIA

by

PIETER STROEVE

Submitted to the Department of Chemical Engineering on August 3, 1973, in partial fulfillment of the requirements for the degree of DOCTOR OF SCIENCE at the Massachusetts Institute of Technology.

.....

A theoretical and experimental program was undertaken to study diffusion with reversible chemical reaction in heterogeneous media. The heterogeneous systems considered are media where one phase is dispersed in a second continuous phase, and where reversible chemical reactions may occur in either phase.

Theoretical equations describing steady-state diffusion with reversible chemical reaction in heterogeneous media were solved using approximate analytical methods. Equations were developed for several reaction kinetic schemes including the four-step model of Adair. Expressions derived for the effective permeabilities showed that the effect of the reversible chemical reaction is to facilitate the transport of the diffusing species. The equations take into account deviations from chemical equilibrium. The effective permeability is a maximum when the reaction is at equilibrium. In the case that the reaction departs sufficiently from equilibrium facilitated transport becomes negligible, and the theoretical equations reduce to Maxwell's equation for inert heterogeneous media.

An experimental program was undertaken to measure transport rates in both inert and reactive suspensions. Effective oxygen permeabilities were measured in thin liquid slabs of inert dispersions, inert and reactive emulsions, and reactive red blood cell suspensions. The measured permeabilities showed good agreement with the theoretical predictions. Hemoglobin facilitated oxygen transport is significant in red blood cell suspensions at low oxygen partial pressures. Comparison of the experimental results on the diffusion of oxygen in red blood cell suspension with theoretical predictions suggests that the oxygen-hemoglobin reaction inside the red blood cell is near but not at equilibrium.

The theoretical framework presented here can be used to model and predict mass transport phenomena in a variety of other reactive heterogeneous systems. Important biological and chemical engineering problems of a similar nature can be studied with the presented theoretical framework.

Thesis Supervisors: Kenneth A. Smith
Professor of Chemical Engineering

Clark K. Colton
Associate Professor of Chemical Engineering

ACKNOWLEDGEMENTS

After many years, this thesis represents the climax of a long period of intellectual, emotional, and physical up and downs. Like so many other theses, the course of this work has affected the lives of not only the author but also those of his family and friends. There is much that can be said, but that would be inappropriate here; a book would be a better forum. However, it is in all sincerity that I express my appreciation and gratitude to those people who have made personal contributions of some kind. In particular I wish to thank:

Professors R. C. Reid, L. B. Evans, H. P. Meissner and others for teaching intellectually stimulating chemical engineering courses;

Scott Stricoff, Steve Emmer, Abdalla I. El-Twaty, Joseph Zahka, and Bob Tuntunjian who collaborated with me in various aspects of this thesis;

Drs. B. Bunow, P. A. Drinker, M. B. Laver, and N. N. Li who either offered their facilities or gave professional advice to me;

My brother Wilbert Stroeve, who, while vacationing in Cambridge, performed many calculations;

My colleagues and laboratory partners Jerry Meldon, Joseph Zahka, and Larry Lewandowsky who provided stimulating and challenging discussions during the course of this thesis;

Stan Mitchell and Paul Bletzer, who were of invaluable help with the construction of the apparatus;

My typists, Mrs. Francine (Gedziun) Page and Mrs. Elenore Kehoe for a job well-done;

My advisor, Dr. Clark K. Colton, who suggested to me to investigate the problem of the diffusion of oxygen in blood, and who continually helped focus on problems of importance;

My advisor, Dr. Kenneth A. Smith, who was instrumental in the development of the theoretical framework presented in the thesis, and who provided leadership during the course of this work.

Both advisors constantly provided stimulating ideas and discussions. Their contributions pervade all aspects of this thesis.

Financial support in the form of a National Science Foundation Traineeship, a National Institutes of Health Fellowship (#4-F01-GM-49, 254-03), an E. I. du Pont de Nemours Fellowship, and funding made available to the Chemical Engineering Department by E. I. du Pont de Nemours and Shell Oil Companies are deeply appreciated.

Finally I wish to thank my wife, Barbara, and my daughters, Dale and Maryke, who in their own ways have made great sacrifices in order that I could complete this thesis. Without their continual love and support this work would not have been possible.

*To my parents
and
Barbara, Dale, and Maryke*

TABLE OF CONTENTS

<u>Chapter Number</u>		<u>Page Number</u>
	ABSTRACT	3
	ACKNOWLEDGEMENT	5
	DEDICATION	7
1	SUMMARY	23
	1.1 Introduction	23
	1.2 Theoretical Developments	25
	1.2.1 Systems Studied in This Thesis	25
	1.2.2 Details of the Derivations	31
	1.2.3 Average Effective Permeability	36
	1.3 Analysis of Theory	38
	1.4 Experimental Materials and Apparatus	39
	1.5 Experimental Results and Discussions	42
	1.6 Conclusions and Recommendations	46
2	INTRODUCTION	49
	2.1 General Introduction	49
	2.2 Introduction to the Problem	50
	2.3 Heterogeneous Systems Studied in This Thesis	53
3	LITERATURE SURVEY	58
	3.1 Diffusion in Inert Heterogeneous Media	58
	3.1.1 Analysis of Theoretical Equations	68
	3.1.2 Comparison of Experimental Data	74
	3.2 Diffusion with Reversible Chemical Reaction in Homogeneous Media	78
	3.2.1 Historical Background	78
	3.2.2 Theoretical Developments	81
	3.3 The Oxygen-Hemoglobin System	90
	3.3.1 Homogeneous Systems	91
	3.3.2 Heterogeneous Systems	94
	3.3.2.1 Inert Suspensions	94
	3.3.2.2 Reactive Suspensions	95

<u>Chapter Number</u>		<u>Page Number</u>
	3.3.2.2.1 Experimental Work	95
	3.3.2.2.2 Theoretical Developments . . .	98
	3.3.3 Physico-Chemical Parameters	99
	3.3.3.1 Oxygen and Hemoglobin Diffusivities	99
	3.3.3.2 Kinetic Rate Parameters . . .	102
	3.3.3.3 Solubility Coefficient of Oxygen	103
	3.4 Discussion	106
4	DEVELOPMENT OF THEORETICAL MODELS	109
	4.1 General Mathematical Formulation of the Problem	110
	4.1.1 Outside the Sphere	119
	4.1.2 Inside the Sphere	122
	4.2 Impermeable Carrier Model	125
	4.2.1 Solution for the Concentrations for the Species Inside and Outside the Sphere	125
	4.2.2 Application of the Model to Other Cases	129
	4.2.3 Effective Permeability for a Suspension of Spheres	134
	4.2.4 Effective Permeability for Other Heterogeneous Media	137
	4.3 Permeable Carrier Model	138
	4.3.1 Solution for the Concentrations for the Species Inside and Outside the Sphere	139
	4.3.2 Application of the Model to Other Cases	145
	4.3.3 Effective Permeability for a Suspension of Spheres	147
	4.3.4 Effective Permeability for Other Heterogeneous Systems	148
	4.4 Adair Reaction Scheme Inside the Dispersed Phase - No Reaction in the Continuous Phase	149

<u>Chapter Number</u>		<u>Page Number</u>
5	ANALYSIS AND APPLICATION OF THEORY	157
	5.1 Reaction in the Dispersed Phase Only	157
	5.1.1 One-Step Model	157
	5.1.1.1 Single Sphere in a Continuum	157
	5.1.1.2 Permeability of a Suspension of Spheres: Application to the Oxygen-Hemoglobin System	170
	5.1.1.3 A Note on Kinetic Parameters	184
	5.1.2 Four-Step Model	185
	5.1.3 Comparison of One-Step and Four-Step Model	199
	5.2 Reaction in the Dispersed and Continuous Phase. The Impermeable and Permeable Model	213
	5.2.1 Single Sphere in a Continuum	213
	5.2.2 Effective Permeability of a Suspen- sion of Spheres	223
	5.2.3 A Note on the Impermeable Model	237
6	EXPERIMENTAL PROGRAM, METHODS, AND APPARATUS	240
	6.1 Introduction	241
	6.2 Inert Systems	242
	6.2.1 Dispersions	242
	6.2.2 Emulsions	250
	6.3 Reactive Systems	258
	6.3.1 Immobilized Hemoglobin Films	248
	6.3.2 Hemoglobin Solutions	263
	6.3.2.1 Preparation of Hemoglobin Solutions	264
	6.3.3 Red Blood Cell Suspensions	265
	6.3.3.1 Preparation and Analysis of Red Blood Cell Suspensions	265
	6.3.3.2 Equilibrium Saturation Curve Considerations	267
	6.3.3.3 Equilibrium Saturation Curve Measurements	269

<u>Chapter Number</u>		<u>Page Number</u>
	6.3.4 Model Systems	272
	6.3.4.1 Motivation for Working with a Model System	272
	6.3.4.2 Methods of Encapsulation	275
	6.4 Gas Permeation Experiments	282
	6.4.1 Experimental Apparatus	282
	6.4.2 Experimental Procedure	289
	6.4.3 Game Plan and Analysis of Experimental Results	292
7	EXPERIMENTAL RESULTS AND DISCUSSION	297
	7.1 Characterization of the Permeation Apparatus	297
	7.1.1 Permeability of Support Membranes	297
	7.1.2 Oxygen-Water Runs	298
	7.1.2.1 Effect of Support Material	305
	7.1.2.2 Assemblage of Sample Holder	306
	7.1.2.3 Permeability of Other Gases in Water	307
	7.1.2.4 Oxygen Permeability at Different Temperatures	308
	7.2 Inert Systems	308
	7.2.1 Dispersions	308
	7.2.2 Inert Emulsions	320
	7.3 "Reactive" Systems	329
	7.3.1 Immobilized (Reactive) Hemoglobin Films	329
	7.3.2 Inert Hemoglobin Solutions	333
	7.3.3 Red Blood Cell Suspensions	341
	7.3.3.1 Inert Red Blood Cell Suspension	341
	7.3.3.2 Reactive Red Blood Cell Suspension	342
	7.3.3.2.1 Details on the Oxygen Permeation Experiments on Reactive Red Blood Cell Suspensions	372
	7.3.4 Model System	379

<u>Chapter Number</u>		<u>Page Number</u>
8	CONCLUSIONS AND RECOMMENDATIONS	384
9	APPENDICES	386
	APPENDIX A: MAXWELL PROBLEM	387
	A.1 Single Sphere in a Continuum	387
	A.2 Effective Permeability for an Ensemble of Spheres	390
	APPENDIX B: THE NATURE OF BLOOD AND HEMOGLOBIN .	393
	B.1 Constituents of Blood	393
	B.2 The Hemoglobin Molecule	396
	B.3 Reaction of Hemoglobin with Oxygen .	403
	APPENDIX C: DETAILS OF THE ADAIR DIFFUSION- REACTION SCHEME. THE FOUR-STEP MODEL	409
	C.1 Equilibrium Solution	411
	C.2 Nonequilibrium Solution	416
	C.3 Single Point Linearization Technique for Slab Geometry	428
	APPENDIX D: COMPILATION OF EXPERIMENTAL RESULTS	437
	APPENDIX E: LISTING OF THE COMPUTER PROGRAMS . .	459
	APPENDIX F: SAMPLE CALCULATION FOR DATA REDUCTION	491
	APPENDIX G: NOMENCLATURE	493
	APPENDIX H: LITERATURE CITATIONS	500
	BIOGRAPHICAL NOTE	515
	PUBLICATIONS	516

LIST OF FIGURES

<u>Figure Number</u>	<u>Title</u>	<u>Page Number</u>
2.1	GRAPHICAL REPRESENTATION OF THE DIFFUSION OF SOLUTES IN BLOOD	52
2.2	BASIC COMPONENTS OF SYSTEMS TO BE STUDIED . . .	55
3.1	COMPARISON OF VARIOUS EQUATIONS FOR NON- CONDUCTING SPHERICAL PARTICLES	69
3.2	COMPARISON OF VARIOUS RELATIONSHIPS FOR THE CASE $K_d = 5$	70
3.3	COMPARISON OF RELATIONSHIP FOR THE CASE OF $K_d = 100$	71
3.4	K_m AS A FUNCTION OF K_d at $\Phi = 0.3$ FOR VARIOUS RELATIONSHIPS	72
3.5	DIFFUSION WITH REVERSIBLE CHEMICAL REACTION IN A ONE DIMENSIONAL FILM	82
3.6	THE FUNCTION $f(L/\lambda)$ VERSUS L/λ	89
3.7	PLOT OF AVAILABLE DATA FOR O_2 DIFFUSION IN Hb SOLUTIONS AT $25^\circ C$	100
3.8	PLOT OF AVAILABLE DATA FOR Hb DIFFUSION COEFFICIENT IN Hb SOLUTIONS AGAINST Hb CONCENTRATION AT $20-25^\circ C$	101
4.1	REACTING SPHERE IN AN INFINITE REACTING MEDIUM	111
4.2	SINGLE REACTING SPHERE IN A REACTING CONTINUOUS MEDIUM	113
4.3	SPHERICAL CLUSTER OF REACTIVE SPHERES IN A REACTIVE CONTINUUM	135
5.1	COMPARISON OF THE FACILITATION FACTOR FOR SPHERE AND SLAB	160
5.2	CONCENTRATION PROFILES INSIDE THE SPHERE FOR THE SPECIES A AND B FOR DIFFERENT a/λ'	161
5.3	POTENTIAL FIELD (LOCI OF CONSTANT PARTIAL PRESSURE OF A) AROUND INERT SPHERES	164
5.4	LOCI OF CONSTANT OF CONSTANT PARTIAL PRESSURE OF SPECIES A INSIDE AND OUTSIDE SPHERE	165

<u>Figure Number</u>		<u>Page Number</u>
5.5	COMPLETE FLUX AND POTENTIAL PLOTS	168
5.5a	LOCI OF CONSTANT PARTIAL PRESSURE OF SPECIES A INSIDE AND OUTSIDE THE SPHERE	169
5.6	COMPARISON OF SIGMOIDAL SATURATION CURVE WITH HYPERBOLIC CURVES	173
5.7	CHARACTERISTIC LENGTH FOR RED BLOOD CELL CONDITIONS	176
5.8	THE FACILITATION FACTOR AS A FUNCTION OF OXYGEN PARTIAL PRESSURE AND EQUIVALENT SPHERE RADIUS . . .	177
5.9	LOCAL EFFECTIVE PERMEABILITY FOR WHOLE BLOOD AT 25°C	179
5.10	AVERAGE EFFECTIVE PERMEABILITY RATIO	181
5.11	FLUX VERSUS DRIVING FORCE PLOT WITH $p_{O_2}^{x=L} = 0$ mm Hg	183
5.12	ADAIR SATURATION CURVES FOR STRIPPED AND UNSTRIPPED HEMOGLOBIN	186
5.13	THEORETICAL EIGENVALUES FOR THE ADAIR FOUR-STEP MODEL	188
5.14	ADAIR FACILITATION FACTOR FOR SPHERE AND SLAB . . .	190
5.15	ADAIR FACILITATION FACTOR FOR STRIPPED HEMOGLOBIN	191
5.16	ADAIR FACILITATION FACTOR FOR UNSTRIPPED HEMOGLOBIN	192
5.17	EFFECTIVE LOCAL PERMEABILITY FOR STRIPPED WHOLE BLOOD	194
5.18	EFFECTIVE LOCAL PERMEABILITY FOR UNSTRIPPED WHOLE BLOOD	195
5.19	AVERAGE EFFECTIVE PERMEABILITY RATIO FOR STRIPPED AND UNSTRIPPED RED BLOOD CELL SUSPENSIONS; ZERO BACKPRESSURE	197
5.20	AVERAGE EFFECTIVE PERMEABILITY RATIO FOR STRIPPED AND UNSTRIPPED RED BLOOD CELL SUSPENSIONS; 2 mm Hg BACKPRESSURE	198

<u>Figure Number</u>		<u>Page Number</u>
5.21a	AVERAGE EFFECTIVE PERMEABILITY RATIO FOR THE FOUR-STEP MODEL FOR THE CONDITIONS SHOWN	15 202
5.21b	AVERAGE EFFECTIVE PERMEABILITY RATIO FOR THE FOUR-STEP MODEL FOR THE CONDITIONS SHOWN	203
5.22	AVERAGE EFFECTIVE PERMEABILITY RATIO FOR A DRIVING FORCE OF $p_{O_2}^{x=0} = 15 \text{ mm Hg}$ and $p_{O_2}^{x=L} = 5 \text{ mm Hg}$	205
5.23	AVERAGE EFFECTIVE PERMEABILITY RATIO FOR A DRIVING FORCE OF $p_{O_2}^{x=L} = 0 \text{ mm Hg}$ AND $p_{O_2}^{x=0} = 5 \text{ mm Hg}$	206
5.24	ATTEMPTED FIT OF FOUR-STEP MODEL WITH ONE-STEP MODEL FOR WHICH $K = 1.675 \times 10^4 \text{ l/mole}$	207
5.25	COMPARISON OF THE FOUR-STEP AND ONE-STEP NORMALIZED FACILITATION FACTORS AS A FUNCTION OF SPHERE RADIUS AND PARTIAL PRESSURE	209
5.26	COMPARISON OF THE ONE-STEP MODEL IN TERMS OF THE EQUILIBRIUM SATURATION CURVES	211
5.27	FLUX PLOT FOR THE FOUR-STEP MODEL	212
5.28	ISO-PARTIAL PRESSURE LINES FOR A REACTING SPHERE IN A REACTING CONTINUUM. IMPERMEABLE CASE	216
5.29	ISO-PARTIAL PRESSURE LINES FOR A REACTING SPHERE IN A REACTING CONTINUUM. PERMEABLE CASE	217
5.30	LOCI OF CONSTANT TOTAL FLUX DIFFERENCE FOR THREE VALUES OF THE CHARACTERISTIC LENGTHS. IMPERMEABLE MODEL	220
5.31	LOCI OF CONSTANT TOTAL FLUX DIFFERENCE FOR THREE VALUES OF THE CHARACTERISTIC LENGTHS. PERMEABLE MODEL	222
5.32a	THE FUNCTION $f_2(r)/f_1(r)$ AS A FUNCTION OF r/a AND SPHERE RADIUS. IMPERMEABLE MODEL	230
5.32b	THE FUNCTION $f_2(r)/f_1(r)$ AS A FUNCTION OF r/a AND SPHERE RADIUS. PERMEABLE MODEL	231
5.33	AVERAGE EFFECTIVE PERMEABILITY RATIO FOR THE IMPERMEABLE MODEL (FOR CONDITIONS SHOWN)	233

<u>Figure Number</u>		<u>Page Number</u>
5.34	AVERAGE EFFECTIVE PERMEABILITY RATIO FOR THE PERMEABLE MODEL (FOR CONDITIONS SHOWN)	235
5.35	FLUX VERSUS DRIVING FORCE PLOT FOR THE IMPERMEABLE MODEL	238
6.1	CHARACTERISTIC LENGTH AS A FUNCTION OF HEMOGLOBIN CONCENTRATION	274
6.2	MULTIPLE EMULSION OBTAINED IN METHODS 2 AND 3 (SEE TEXT)	279
6.3	SCHEMATIC DIAGRAM OF EXPERIMENTAL APPARATUS . . .	283
6.4	DETAIL OF THE SAMPLE HOLDER AND THE RUBBER GASKET	284
7.1	UNSTEADY STATE AND STEADY STATE RESPONSE OF OXYGEN DIFFUSION IN WATER	300
7.2	DIFFUSION OF OXYGEN IN WATER	304
7.3	DIFFUSIVITIES OF OXYGEN IN WATER PLOTTED VERSUS THE PARAMETER T/μ	310
7.4	PERMEATION OF OXYGEN IN POLYSTYRENE DISPERSIONS .	312
7.5	ELECTRON MICROGRAPH OF POLYSTYRENE DISPERSION . .	313
7.6	PERMEATION OF CARBON DIOXIDE IN FEP 120 DISPERSIONS	315
7.7	ELECTRON MICROGRAPH OF FEP 120 DISPERSIONS . . .	316
7.8	PERMEATION OF CARBON DIOXIDE IN TFE 30 DISPERSIONS	318
7.8a	ELECTRON MICROGRAPH OF TFE 30 DISPERSIONS . . .	319
7.9	PERMEABILITY OF OXYGEN IN CASTOR OIL EMULSIONS (O/W)	322
7.10	PERMEABILITY OF OXYGEN IN CASTOR OIL (10% SPAN 80) EMULSIONS (O/W)	323
7.11	PERMEABILITY OF OXYGEN IN WESSON VEGETABLE OIL EMULSIONS (O/W)	324
7.12	OXYGEN PERMEABILITY IN FLUOROCARBON EMULSIONS . .	328
7.13	NORMALIZED STEADY-STATE OXYGEN PERMEATION RATE AS A FUNCTION OF IMPOSED PARTIAL PRESSURE DRIVING FORCE	332

<u>Figure Number</u>		<u>Page Number</u>
7.14	OXYGEN PERMEABILITY IN INERT HEMOGLOBIN SOLUTIONS	334
7.15	COMPARISON OF THE CALCULATED OXYGEN DIFFUSIVITIES WITH KREUZER'S PLOT FOR ALL PREVIOUS DATA	337
7.16	COMPARISON OF CALCULATED OXYGEN DIFFUSIVITIES WITH EQUATION (7.6)	340
7.17	OXYGEN PERMEATION THROUGH INERT RED BLOOD CELL SUSPENSIONS AT 25°C	344
7.18	COMPARISON OF HERSHEY AND KARHAN'S DATA (RBC IN PLASMA) WITH MAXWELL'S EQUATION	346
7.19a	AVERAGE EFFECTIVE OXYGEN PERMEABILITY IN REACTIVE RED BLOOD CELL SUSPENSIONS FOR CONDITIONS AS SHOWN. COMPARISON WITH ONE-STEP MODEL ($D_{Hb} = 7.0 \times 10^{-8} \text{ cm}^2/\text{sec}$)	350
7.19b	AVERAGE EFFECTIVE OXYGEN PERMEABILITY IN REACTIVE RED BLOOD CELL SUSPENSIONS FOR CONDITIONS AS SHOWN. COMPARISON WITH ONE-STEP MODEL ($D_{Hb} = 6.0 \times 10^{-8} \text{ cm}^2/\text{sec}$)	351
7.20a	AVERAGE EFFECTIVE OXYGEN PERMEABILITY IN REACTIVE RED BLOOD CELL SUSPENSIONS FOR CONDITIONS AS SHOWN. COMPARISON WITH ONE-STEP MODEL ($D_{Hb} = 7.0 \times 10^{-8} \text{ cm}^2/\text{sec}$)	352
7.20b	AVERAGE EFFECTIVE OXYGEN PERMEABILITY IN REACTIVE RED BLOOD CELL SUSPENSIONS FOR CONDITIONS AS SHOWN. COMPARISON WITH ONE-STEP MODEL ($D_{Hb} = 6.0 \times 10^{-8} \text{ cm}^2/\text{sec}$)	353
7.21a	AVERAGE EFFECTIVE OXYGEN PERMEABILITY IN REACTIVE RED BLOOD CELL SUSPENSIONS FOR CONDITIONS AS SHOWN. COMPARISON WITH ONE-STEP MODEL ($D_{Hb} = 7.0 \times 10^{-8} \text{ cm}^2/\text{sec}$)	354
7.21b	AVERAGE EFFECTIVE OXYGEN PERMEABILITY IN REACTIVE RED BLOOD CELL SUSPENSIONS FOR CONDITIONS AS SHOWN. COMPARISON WITH ONE-STEP MODEL ($D_{Hb} = 6.0 \times 10^{-8} \text{ cm}^2/\text{sec}$)	355
7.22	COMPARISON OF EXPERIMENTAL DATA AND ONE-STEP MODEL WITH $D_{Hb} = 1.5 \times 10^{-7} \text{ cm}^2/\text{sec}$	358
7.23	COMPARISON OF EXPERIMENTAL DATA AND ONE-STEP MODEL WITH $D_{Hb} = 3.0 \times 10^{-8} \text{ cm}^2/\text{sec}$	359

<u>Figure Number</u>		<u>Page Number</u>
7.24	SATURATION CURVE FOR RED BLOOD CELL SUSPENSIONS .	361
7.25	COMPARISON OF EXPERIMENTAL DATA AND FOUR-STEP MODEL $D_{Hb} = 6.0 \times 10^{-8} \text{ cm}^2/\text{sec}$	363
7.26	COMPARISON OF EXPERIMENTAL DATA AND FOUR-STEP MODEL WITH $D_{Hb} = 6.0 \times 10^{-8} \text{ cm}^2/\text{sec}$	364
7.27	COMPARISON OF EXPERIMENTAL DATA AND FOUR-STEP MODEL WITH $D_{Hb} = 6.0 \times 10^{-8} \text{ cm}^2/\text{sec}$	365
7.28	HEMOGLOBIN SATURATION CURVE FOR RED BLOOD CELL SUSPENSIONS AT CONDITIONS SHOWN	367
7.29	AVERAGE EFFECTIVE PERMEABILITY RATIO FOR PHYSIOLOGICAL DRIVING FORCE CONDITIONS	370
7.30	EFFECT OF HEMOLYSIS ON THE AVERAGE EFFECTIVE PERMEABILITY RATIO	374
7.31	EFFECT OF HEMOLYSIS ON THE AVERAGE EFFECTIVE PERMEABILITY RATIO	375
7.32	DEOXYGENATION OF RED BLOOD CELL SUSPENSION IN SEALED SYRINGES	377
7.33	COMPARISON OF EXPERIMENTAL RESULTS WITH THEORETICAL PREDICTIONS FOR THE ONE-STEP MODEL FOR THE REACTIVE EMULSIONS	381
A.1	SINGLE SPHERE IN AN INFINITE MEDIUM	387
A.2	SPHERICAL SUSPENSION OF SPHERES	391
B.1	A REPRESENTATION OF THE β CHAIN OF HUMAN HEMO- GLOBIN SHOWING THE LOCATION OF THE AMINO ACIDS .	399
B.2	THREE DIMENSIONAL MODEL OF THE HORSE HEMOGLOBIN MOLECULE. TOP FIGURE SHOWS SEGMENTS INVOLVED IN THE CONTACT $\alpha_1 \beta_1$. LOWER FIGURE SHOWS SEGMENTS INVOLVED IN THE CONTACT $\alpha_1 \beta_2$	401
B.3	OXYGEN-HEMOGLOBIN SATURATION CURVE AT PHYSIOLOGICAL CONDITIONS	405

LIST OF TABLES

<u>Table Number</u>	<u>Title</u>	<u>Page Number</u>
1.1	EFFECTIVE PERMEABILITY RATIO FOR THE IMPERMEABLE MODEL	34
1.2	EFFECTIVE PERMEABILITY RATIO FOR THE PERMEABLE MODEL	35
3.1	L_3 FOR SPHEROIDS ($b = c$)	64
3.2	MAXIMUM RATIO (K_m author/ K_m Maxwell) AND VOLUME FRACTION AT WHICH IT OCCURS	73
3.3	BUNSEN SOLUBILITY COEFFICIENT OF OXYGEN IN VARIOUS FLUIDS CC(STP)/CC/ATM	105
5.1	PARAMETERS EMPLOYED IN CALCULATIONS	175
5.2	PARAMETERS USED FOR THE COMPARISON OF THE IMPERMEABLE AND PERMEABLE MODEL	214
5.3	MAXIMUM ALLOWABLE VOLUME FRACTION FOR IMPERMEABLE MODEL AS A FUNCTION OF SPHERE RADIUS	234
5.4	MAXIMUM ALLOWABLE VOLUME FRACTION FOR PERMEABLE MODEL AS A FUNCTION OF SPHERE RADIUS	236
5.5	PHYSICO-CHEMICAL PARAMETERS USED IN SECTION 5.2.3 FOR THE IMPERMEABLE MODEL	239
6.1	PHYSICAL PROPERTIES OF 120 FEP DISPERSIONS (BLEND 283)	245
6.2	PHYSICAL PROPERTIES OF 30 TFE DISPERSIONS (BLEND 2400)	246
6.3	RECIPE FOR MONODISPERSE POLYSTYRENE LATEX (S-6)	248
6.4	PROPERTIES OF POLYSTYRENE LATEX SAMPLE S-6	249
6.5	CLASSIFICATION OF EMULSIFIERS ACCORDING TO H.L.B. VALUES	252
6.6	H.L.B. VALUES FOR SOME SURFACE ACTIVE AGENTS	253
6.7	EMULSION SYSTEMS STUDIED	255
6.8	PHYSICAL PROPERTIES AND DESCRIPTION OF ORGANICS AT 25°C	256

<u>Table Number</u>		<u>Page Number</u>
7.1	TABULATION OF OXYGEN PERMEATION IN DISTILLED WATER RUNS	303
7.2	PERMEABILITY OF NITROGEN AND CARBON DIOXIDE IN DISTILLED WATER	307
7.3	EXPERIMENTAL OXYGEN PERMEABILITIES AT A VARIETY OF TEMPERATURES	309
7.4	OXYGEN PERMEABILITIES AND CALCULATED OXYGEN DIFFUSIVITIES IN INERT HEMOGLOBIN SOLUTIONS (T = 25°C)	336
7.5	OXYGEN PERMEABILITY IN INERT HEMOGLOBIN SOLUTION (15.4 gr/100 ml) AS A FUNCTION OF TEMPERATURE	339
7.6	OXYGEN PERMEABILITIES IN INERT RED BLOOD CELL SUSPENSIONS AT 25°C AND pH = 7.0	343
7.7	AVERAGE EFFECTIVE PERMEABILITIES OF OXYGEN IN REACTIVE RED BLOOD CELL SUSPENSION FOR THREE DIFFERENT DRIVING FORCE CONDITIONS	348
7.8	PARAMETERS USED IN THEORETICAL CALCULATIONS	356
7.9	PARAMETERS EMPLOYED IN CALCULATIONS FOR THE MODEL SYSTEM	383
B.1	DIMENSIONS OF THE HUMAN RED CELL	395
D.1	OXYGEN PERMEABILITY IN MEM-213 MEMBRANES	437
D.2	OXYGEN PERMEATION THROUGH THIN LIQUID SLABS OF WATER	438
D.3	MISCELLANEOUS GAS (O ₂ , N ₂ , CO ₂) PERMEATION RUNS THROUGH THIN LIQUID SLABS OF WATER (T = 25°C)	440
D.4	PERMEATION OF OXYGEN THROUGH THIN LIQUID SLABS OF POLYSTYRENE DISPERSIONS	442
D.5	PERMEATION OF CARBON DIOXIDE THROUGH THIN LIQUID SLABS OF 120 FEP DISPERSIONS	443
D.6	PERMEATION OF CARBON DIOXIDE THROUGH THIN LIQUID SLABS OF 30 TFE DISPERSIONS	444
D.7	PERMEATION OF OXYGEN IN THIN LIQUID SLABS OF SURFACTANT SOLUTIONS USED FOR EMULSIONS	445

<u>Table Number</u>		<u>Page Number</u>
D.8	PERMEATION OF OXYGEN THROUGH THIN LIQUID SLABS OF CASTOR OIL EMULSIONS (O/W)	446
D.9	TYPICAL SIZE DISTRIBUTION DATA FOR EMULSIONS	447
D.10	PERMEATION OF OXYGEN THROUGH THIN LIQUID SLABS OF CASTOR OIL (10% SPAN 80) EMULSIONS (O/W)	448
D.11	PERMEATION OF OXYGEN THROUGH THIN LIQUID SLABS OF WESSON VEGETABLE OIL EMULSIONS (O/W)	449
D.12	PERMEATION OF OXYGEN THROUGH THIN LIQUID SLABS OF FLUOROCARBON	450
D.13	PERMEATION OF OXYGEN THROUGH THIN LIQUID SLABS OF PLD EMULSIONS (O/W)	451
D.14	PERMEATION OF OXYGEN THROUGH THIN LIQUID SLABS OF INERT HEMOGLOBIN SOLUTION (pH = 7.0) ISOTONIC RESULTS	452
D.15	OXYGEN PERMEABILITY IN THIN LIQUID FILMS OF RED BLOOD CELL SUSPENSIONS UNDER INERT CONDITIONS AT T = 25°C	453
D.16	OXYGEN PERMEATION EXPERIMENTS IN "REACTIVE" RED BLOOD CELL SUSPENSIONS	454
D.17	OXYGEN PERMEATION EXPERIMENTS IN "REACTIVE" RED BLOOD CELL SUSPENSIONS	455
D.18	OXYGEN PERMEATION EXPERIMENTS IN "REACTIVE" RED BLOOD CELL SUSPENSIONS	456
D.19	OXYGEN PERMEATION EXPERIMENTS THROUGH RED BLOOD CELL SUSPENSIONS AT 37°C	457
D.20	OXYGEN PERMEATION EXPERIMENTS ON THE MODEL SYSTEM	458

1. SUMMARY

- 1.1 Introduction
- 1.2 Theoretical Developments
 - 1.2.1 Systems Studies in This Thesis
 - 1.2.2 Details of the Derivations
 - 1.2.3 Average Effective Permeability
- 1.3 Analysis of Theory
- 1.4 Experimental Materials and Apparatus
- 1.5 Experimental Results and Discussion
- 1.6 Conclusions and Recommendations

1. SUMMARY

1.1 Introduction

The understanding of transport processes in heterogeneous media is an important problem in science and engineering. In the chemical industry, heterogeneous media such as emulsions, slurries, foams, dispersions, and solid mixtures are frequently encountered as process streams or materials of construction. Processes such as the drying of textiles, air or moisture permeation through paint films, and the migration of plasticizers into and out of polymers need to be understood in order to rationally design or choose equipment to perform a specified task.

In the field of biology one deals almost exclusively with heterogeneous systems, because organisms are constructed from a unit building block, the cell. Engineers and scientists are increasingly interested in how biological systems have solved complicated transport requirements. Such knowledge may lead to applications in industrial or chemical processes, as well as to the design of devices that can take over biological functions. For example, with the development of highly permeable membranes, it is now recognized that the blood phase is often the limiting resistance to mass transfer in membrane oxygenators and artificial kidneys. Hence, a fundamental quantitative understanding of solute transport

in blood is a prerequisite for the design of more efficient devices that carry out the mass transfer operations normally performed by the human body.

This thesis is concerned with steady state diffusion with reversible chemical reaction in heterogeneous media. Although the relevant literature is large, this phenomena is not fully understood and experimental results are often contradictory or insufficient. For the most part, previous work has dealt with diffusion without chemical reaction in heterogeneous media and with chemical reaction in homogeneous media, but the combined problem has not been considered with any rigor. A theoretical and experimental program was undertaken in this thesis. Systems were studied where mass transport is influenced only by diffusive and chemical reaction effects. The heterogeneous media considered are those for which one phase is dispersed in a second continuous phase, and for which the characteristic size of the dispersed particles is much smaller than the characteristic dimension of the overall system. Theoretical expressions were derived for the effective permeability for a variety of cases. The specific systems studied experimentally include primarily oxygen permeation through inert suspensions, model reactive suspensions, and whole blood. The latter system was used because the data can be of utility in the design of artificial oxygenators, and, in addition, many physicochemical parameters are available for this particular system.

Some experimental work on the diffusion in stagnant blood is available in the literature. Stein et al (1971) and Hershey and Karhan (1968) measured the oxygen diffusivity in red blood cell suspensions under conditions for which the oxygen-hemoglobin reaction inside the red blood cells was completely saturated (inert suspension). Kutchai and Staub (1969) measured significantly larger diffusivities in packed red blood cells under conditions for which the reaction was unsaturated than for conditions for which the reaction was saturated. However, no theoretical framework that can account for these results has previously been done.

1.2 Theoretical Developments

1.2.1 Systems Studied in this Thesis

A conceptual framework for the problem area considered in this thesis is shown in Figure 2.2.

Case 1 is steady state Fickian diffusion of species A in a one-dimensional film. Simple modifications are shown by cases 2 and 3. Case 2 is diffusion in a heterogeneous medium in which one phase is dispersed in a continuous phase, for example an emulsion or dispersion. Such an inert suspension is a reasonable model for diffusion of solutes in blood where no significant solute interactions occur with the plasma proteins or hemoglobin molecules. Transport in inert heterogeneous media is fairly well understood. The steady state mass transport rate (in the case of a gas) is given by

$$N_A = \bar{P} \frac{(p_A^{x=0} - p_A^{x=L})}{L} \quad (1.1)$$

where \bar{P} is the effective permeability. (Permeability as used here is the product of the diffusivity times the solubility). The classical mathematical approach to the problem has been to solve Laplace's equation

$$\nabla^2 \phi = 0 \quad (1.2)$$

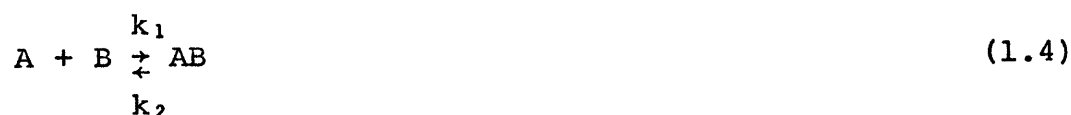
where ϕ is the potential. For example Maxwell (1881), considered a single sphere in an infinite continuum where the field is unidirectional and linear at large distances from the sphere. By solving Laplace's equation for the potential in spherical coordinates both inside and outside the sphere, one obtains the potential variation due to the presence of the sphere in the continuum.

For the analysis of a dilute suspension of spheres, Maxwell considered the suspension to be confined to a spherical region and located in an infinite continuous medium. By assuming the perturbation associated with each of the smaller spheres inside this spherical suspension to be independent of each other, Maxwell obtained an effective permeability for the suspension by equating the perturbation caused by the spherical suspension region with that caused by each of the small individual spheres. The resulting expression for the effective relative permeability is given by

$$\frac{\bar{P}}{P_c} = \frac{P_d + 2P_c - 2\phi[P_c - P_d]}{P_d + 2P_c + \phi[P_c - P_d]} \quad (1.3)$$

where ϕ is the volume fraction of the dispersed phase, P_c is the permeability of the continuous phase, and P_d is the permeability of the dispersed phase. Other relationships include those derived by Fricke (1924) for a suspension of randomly oriented ellipsoidal particles, and Bruggeman (1935), who took into account the interaction of neighboring particles.

Case 3 corresponds to diffusion with reversible chemical reaction in a homogeneous system. Reactant B is constrained to remain within the film and combines with the permeating species A to form product AB



If both species B and AB have significant molecular diffusivities, they can increase the mass transfer of A beyond that which is possible from purely physical diffusion of A alone. This phenomena has been termed carrier-facilitated transport, and the steady state mass transport is given by

$$N_A^T = P(1+F) \left(\frac{P_A^{x=0} - P_A^{x=L}}{L} \right) \quad (1.5)$$

where F is termed the facilitation factor and accounts for the contribution of the carrier molecules to the total mass flux. In order to determine the facilitation factor, the differential

mass conservation equation for A, B, and AB in the film must be solved subject to the associated boundary conditions. If the reaction is at equilibrium everywhere in the film, the facilitation factor is a maximum and is given by (Olander 1960)

$$F_{eq} = \frac{D_B k_1 k_2 C_T}{D_A (1 + k_1 C_A^{x=0}) (1 + k_1 C_A^{x=L})} \quad (1.6)$$

When the reaction deviates from equilibrium within the film, the problem is more difficult since the equations are non-linear. An approximate solution can be obtained if the equations are linearized, and solutions available in the literature differ from each other depending upon the method of linearization employed. Friedlander and Keller (1965) presented a single point linearization solution valid for small driving forces only. For large driving forces the method of matched asymptotic expansions has proven useful in giving accurate predictions of flux for near equilibrium conditions (Goddard et al 1970, Kreuzer and Hoofd, 1970, 1972). Recently Smith et al (1973) have presented approximate analytical solutions corresponding to a perturbation from purely physical diffusion on one hand (thin films), and from reaction equilibrium at each point within the film on the other (thick films). In all solutions, the facilitation factor is found to be a function of F_{eq} and the ratio of the film thickness L to the characteristic length λ . The latter is the ratio of diffusional to chemical reaction effects and is given by

$$\lambda = \left| \frac{k_1 \bar{C}_A + k_2}{D_B} + \frac{k_1 k_2 C_T}{D_A (k_1 \bar{C}_A + k_2)} \right|^{-1/2} \quad (1.7)$$

for the reaction $A+B \rightleftharpoons AB$. The characteristic length also gives a measure of the thickness of the region near the boundaries of the film where the departure from chemical equilibrium is significant. The dimensionless parameter is similar to the Thiele modulus as has been pointed out by Perelson and Katchalsky (1972), and in a general context by Weisz (1973). As L/λ increases, nonequilibrium effects become negligible, and the facilitation factor F reaches the asymptotic value given by Olander (1960).

Combinations of cases 2 and 3 are shown in cases 4 and 5 which are examples of diffusion with reversible chemical reaction in heterogeneous media. In Case 4, the carrier species is present only in the dispersed phase. An example is the diffusion of oxygen in whole blood where hemoglobin is present only inside the red blood cells. In Case 5 the carrier species is present only in the continuous phase. Such a situation may arise in gas absorption with chemical reaction in a slurry or in the diffusion in blood of metabolites, drugs, or amino acids that interact with plasma proteins but not with hemoglobin.

Case 6 and 7 are more complicated reactive heterogeneous systems where the carrier species is present in both

the continuous and dispersed phase. In Case 6, two different carriers are constrained to remain within their respective phases and cannot permeate across the boundary between dispersed and continuous phases. In Case 7, one carrier species is present in both phases, and it can diffuse from one phase into the other.

The same approach utilized by Maxwell was employed here to obtain effective permeabilities for the heterogeneous media shown in Figure 2.2. First a solution was obtained for the concentration and potential field of the diffusing species inside and outside a single sphere in an infinite continuum. With this in hand the average effective permeability of a suspension of spheres was obtained as described above.

The general solutions for Cases 6 and 7 of Figure 2.2 will be referred to as the impermeable and permeable models respectively. These two general solutions can be reduced to give solutions for Cases 2, 4, and 5. The general utility of the mathematical approach was demonstrated by employing for Case 4 the four-step reversible reaction scheme proposed by Adair (1925) to model the reaction of oxygen with hemoglobin:



The Adair reaction scheme is an approximation to an extremely complicated reaction mechanism, but it is a better approximation than a one-step reaction scheme as given by (1.4).

1.2.2 Details of the Derivations

Consider a single sphere, of radius a and permeability P_d , immersed in an infinite medium of permeability P_c , with a constant uniform mass flux of the diffusing species A imposed at large distances from the center of the sphere. A single step reversible reaction with carrier B and B' occurs in the continuous and discontinuous phases, respectively:



Reactions (1.9) and (1.10) were chosen as an example only, and the theoretical development can be extended to other reaction schemes. The steady state diffusion equations in spherical coordinates for species A , B , AB outside the sphere and A' , B' , AB' inside the sphere are given in Figure 4.2, along with the associated boundary conditions for both the impermeable and permeable model. The boundary condition at $r=0$ fixes the partial pressure of A at the center of the sphere, and the boundary condition at $r=\infty$ fixes the total flux of A and, in addition, imposes equilibrium between

all reacting species. These boundary conditions apply to both the impermeable and permeable model, but the boundary conditions at the sphere boundary are of course different. Boundary conditions at $r=a$ insure continuity of species flux and potential, and do or do not constrain the carrier species to remain in its respective phase. For small driving forces across the sphere, an approximate solution can be obtained by utilizing single point linearization about the partial pressure at the center of the sphere. For the sake of simplicity it was assumed that the diffusivities of all the carrier species in both phases are equal and that Henry's Law is applicable. It can be shown that as a consequence of the single point linearization technique the concentrations at the center of the sphere are at equilibrium. Once the concentration and potential variation has been determined the effective permeability of a suspension of spheres can be obtained. Tables 1.1 and 1.2 summarize the relationships obtained for the impermeable and permeable model. The parameters λ and λ' are the continuous and dispersed phase characteristic lengths and are defined analogously to equation (1.7). They give a measure of the thickness of shells outside and inside the sphere where deviations from chemical equilibrium are significant. The factor F_d is the dispersed phase facilitation factor, and the terms F_{eq} and F_{eq}' are the equilibrium continuous- and dispersed-phase facilitation factors and are

defined as

$$F_{eq} = \frac{D_B k_1 k_2 C_T \alpha_A}{P_C (k_1 + k_2 \alpha_A p_A^o)^2} \quad (1.11)$$

$$F'_{eq} = \frac{D_B' k_1' k_2' C_T' \alpha_A'}{P_d (k_1' + k_2' \alpha_A' p_A^o)^2} \quad (1.12)$$

It should be noted here that the general equations in Table 1.1 and 1.2 are for a suspension of reactive spheres in a reactive continuum that is at equilibrium throughout the continuum except locally near the boundary of the spheres. This is a consequence of the boundary conditions at $r \rightarrow \infty$ which fixes the species to be at equilibrium. The general equations can give solutions for the other heterogeneous media if the parameters are allowed to attain certain values. To make the spheres inert a/λ' must approach zero so that F_d approaches zero. To make the continuum inert F'_{eq} must be set to zero since reduction of a/λ will increase nonequilibrium effects around the spheres but will not make the continuum inert. Inspection of the equations show that the equations are similar in form to Maxwell's equation and in fact reduce to Maxwell's equation as shown for Case 2. The continuous phase permeability, P_C , is increased by the factor $(1+F_{eq})$, and the dispersed phase permeability is increased by the factor $(1+F_d)$.

The Adair reaction scheme for oxygen combination with hemoglobin has been given by equation (1.8). For the case of

TABLE 1.1
EFFECTIVE PERMEABILITY RATIO FOR THE IMPERMEABLE MODEL

Type of Media	Relationship	Comments
Reaction inside Reaction outside Case VI	$\frac{\bar{P}}{P_c(1+F_{eq})} = \frac{2P_c(1+F_{eq})+P_d(1+F_d)(1-2F_{eq}f_c)-2\phi[P_c(1+F_{eq})-P_d(1+F_d)(1+F_{eq}f_c)]}{2P_c(1+F_{eq})+P_d(1+F_d)(1-2F_{eq}f_c)+\phi[P_c(1+F_{eq})-P_d(1+F_d)(1+F_{eq}f_c)]}$	General relationship for no shell.
Inert inside Reaction outside Case V (impermeable carrier)	$\frac{\bar{P}}{P_c(1+F_{eq})} = \frac{2P_c(1+F_{eq})+P_d(1-2F_{eq}f_c)-2\phi[P_c(1+F_{eq})-P_d(1+F_{eq}f_c)]}{2P_c(1+F_{eq})+P_d(1-2F_{eq}f_c)+\phi[P_c(1+F_{eq})-P_d(1+F_{eq}f_c)]}$	$\frac{a}{\lambda'} \rightarrow 0$
Reactive inside Inert outside Case IV	$\frac{\bar{P}}{P_c} = \frac{2P_c+P_d(1+F_d)-2\phi[P_c-P_d(1+F_d)]}{2P_c+P_d(1+F_d)+\phi[P_c-P_d(1+F_d)]}$	$F_{eq} = 0$
Inert inside Inert outside Case II	$\frac{\bar{P}}{P_c} = \frac{2P_c+P_d-2\phi[P_c-P_d]}{2P_c+P_d+\phi[P_c-P_d]}$	$\frac{a}{\lambda'} \rightarrow 0$ $F_{eq} = 0$

where:

$$f_c = - \frac{1 + \frac{\lambda}{a}}{2 + 2 \frac{\lambda}{a} + \frac{a}{\lambda}}$$

$$F_d = \frac{F'_{eq} \left[\frac{(3 \frac{\lambda'^2}{a^2} + 1) \tanh \frac{a}{\lambda'} - 3 \frac{\lambda'}{a}}{(2 \frac{\lambda'^2}{a^2} + 1) \tanh \frac{a}{\lambda'} - 2 \frac{\lambda'}{a}} \right]}{1+F'_{eq} \left[1 - \frac{(3 \frac{\lambda'^2}{a^2} + 1) \tanh \frac{a}{\lambda'} - 2 \frac{\lambda'}{a}}{(2 \frac{\lambda'^2}{a^2} + 1) \tanh \frac{a}{\lambda'} - 2 \frac{\lambda'}{a}} \right]}$$

TABLE 1.2

EFFECTIVE PERMEABILITY RATIO FOR THE PERMEABLE MODEL

Type of Media	Relationship	Comments
Reaction inside Reaction outside Case VI	$\frac{\bar{P}}{P_c(1+F_{eq})} = \frac{2P_c(1+F_{eq})+P_d(1+F'_{eq})\left[\frac{1}{1-Q}\right]-2\phi\{P_c(1+F_{eq})-P_d(1+F'_{eq})\left[\frac{1}{1-Q}\right]\}}{2P_c(1+F_{eq})+P_d(1+F'_{eq})\left[\frac{1}{1-Q}\right]+\phi\{P_c(1+F_{eq})-P_d(1+F'_{eq})\left[\frac{1}{1-Q}\right]\}}$	General relationship.
Inert inside Reaction outside Case V (permeable carrier)	Same as Case V, Table 1.1 only if $F'_{eq} = 0$	$\frac{a}{\lambda'} \rightarrow 0$
Reactive inside Inert outside Case IV	Same as Case IV, Table 1.1	$F_{eq} = 0$
Inert inside Inert outside Case II	Same as Case II, Table 1.1, Maxwell	$\frac{a}{\lambda'} \rightarrow 0$ $F_{eq} = 0$

where:

$$Q = \frac{\frac{f_c}{F'_{eq}} \left[\frac{F'_{eq} - F_{eq}}{1 + F_{eq}} \right]^2}{\frac{P_c(1+F'_{eq})F_{eq}}{P_d(1+F_{eq})F'_{eq}} + f_c \left[\frac{2 - \tanh \frac{a}{\lambda'} \left(2 \frac{\lambda'}{a} + \frac{a}{\lambda'} \right)}{1 - \frac{\lambda'}{a} \tanh \frac{a}{\lambda'}} \right]}$$

an Adair reaction scheme inside the dispersed phase with no reaction in the continuous phase the mass conservation equation for species A', B', AB', A₂B', A₃B', and A₄B' inside the dispersed phase and species A in the continuous phase must be coupled with the boundary conditions in order to be solved. Again, single point linearization about the center point concentrations was the technique utilized to linearize the equations; this led to an eigenvalue problem. An effective permeability was obtained which is of the form

$$\frac{\bar{P}}{P_c} = \frac{P_d(1+F^{\text{Adair}}) + 2P_c - 2\phi[P_c - P_d(1+F^{\text{Adair}})]}{P_d(1+F^{\text{Adair}}) + 2P_c - \phi[P_c - P_d(1+F^{\text{Adair}})]} \quad (1.13)$$

The parameter F^{Adair} is the facilitation factor in the dispersed phase for the case of four-step Adair kinetics. When equilibrium conditions are attained throughout the sphere, the Adair facilitation factor approaches its equilibrium value

$$F_{\text{eq}}^{\text{Adair}} = \frac{4D_B 'C_T' \left(\frac{dy}{dp_A} \right) \circ}{P_d} \quad (1.14)$$

where dy/dp_A is the slope of the oxygen-hemoglobin saturation curve

1.2.3 Average Effective Permeability

The equations so far derived were for local permeabilities and facilitation factors in terms of the partial pressure of species A at the center of the sphere. Thus the

effective permeability is uniquely defined only at a local point within the suspension. If one considers a liquid slab composed of a suspension of spheres and across which a large partial pressure gradient of A is imposed, then the average effective permeability of the slab may be calculated by integrating the local expression across the thickness of the film

$$\bar{P}_{ave} = \frac{\int_{p_A^{x=0}}^{p_A^{x=L}} \bar{P} dp_A}{(p_A^{x=0} - p_A^{x=L})} \quad (1.15)$$

1.3 Analysis of Theory

The behaviour of the equations for the various heterogeneous media shown in Figure 2.2 were analysed. Heavy emphasis was placed in the analysis on Case 4 (oxygen diffusion through blood) and on a comparison of the one-step and four-step reaction schemes, represented by equations (1.10) and (1.8) respectively. Physicochemical parameters used for the calculations were taken from Kreuzer (1970), Gibson (1959, 1970) and Altman and Dittmer (1971), and are given in Table 5.1. Figure 5.8 shows the local dispersed-phase facilitation factor as a function of sphere radius a and oxygen partial pressure p_{O_2} for the one-step model. As the size of the spheres increases, the facilitation factor reaches the equilibrium facilitation factor. As the partial pressure increases the reaction saturates and facilitation effects become negligible. Figure 5.9 shows the local effective permeability as a function

of sphere radius and partial pressure, as calculated for whole blood. Curves are shown for radii corresponding to one-half the minimum and maximum red cell dimension, and for a radius based on equivalent red blood cell surface area. The local effective permeability is a maximum at zero partial pressure because the one-step reaction scheme predicts a hyperbolic oxyhemoglobin saturation curve with a maximum slope at that point. Figure 5.10 shows the integrated average effective permeability for red cell suspensions in plasma for two driving force conditions. The equations show that the chemical reaction inside the dispersed phase increases the effective permeability over that of the inert case, consistent with Maxwell's equation.

Analysis was also carried out with the four-step reaction scheme for two cases for which kinetic parameters were available (Gibson 1970): red cells containing (1) normal amounts and (2) "stripped" of 2,3 diphosphoglycerate (2,3 DPG). The Adair facilitation factor for unstripped (normal) blood is shown in Figure 5.16. The facilitation factors maximize near the partial pressure for which the sigmoidal four-step saturation curve has a maximum slope. Local permeabilities for whole blood are shown as a function of oxygen partial pressure and sphere radius in Figure 5.18. The effective permeabilities maximize near the point where the oxygen-hemoglobin saturation curve is steepest. Blood depleted of 2,3DPG exhibits higher facilitation factors because of the higher oxygen affinity of

the "stripped" hemoglobin and consequent steeper saturation curves. The effective permeabilities are therefore large in the low oxygen partial pressure range, but decrease rapidly as the reaction saturates. The average effective permeability for unstripped red blood cell suspensions is shown in Figure 5.21 for the same conditions as those shown in Figure 5.10. It can be seen that the one-step model and the four-step model give reasonably good agreement. This was anticipated in view of: (1) the large driving force (with consequently large hemoglobin saturation differences); and (2) the use of kinetic rate constants for each model which are of the same order of magnitude. A number of driving force conditions were investigated, and the one-step and four-step reaction schemes compared. It was concluded that the one-step reaction scheme fails to agree with the four-step scheme only when both boundary conditions fall within the steep portion of the sigmoidal hemoglobin saturation curve.

In addition to the model for oxygen diffusion in blood, the behaviour of the equations for the other cases discussed above were also analysed.

1.4 Experimental Materials and Apparatus

Gas permeabilities (mainly oxygen) were measured for thin liquid slabs of heterogeneous media. Since diffusion in inert heterogeneous media (for which there is little data in the literature) is relevant to the general problem of reactive

heterogeneous media, experiments were performed with unreactive media prior to utilizing reactive red blood cell and model suspensions. It was expected that if the experimental results showed good agreement with Maxwell's equation, then further experimental results could be obtained with confidence on reactive media. The following media (inert and reactive, homogeneous or heterogeneous) were investigated in the order given:

- 1) inert dispersion
- 2) inert emulsions
- 3) inert and reactive hemoglobin solutions
- 4) red blood cell suspensions
- 5) reactive emulsions

The inert dispersions investigated were as follows:

- i) Teflon 120 FEP-fluorocarbon dispersions
- ii) Teflon 30 TFE-fluorocarbon dispersions
- iii) Polystyrene latex dispersions

Carbon dioxide permeabilities were measured in the fluorocarbon dispersions and oxygen permeabilities were measured in all other systems. The inert emulsions investigated were O/W emulsions of the following organics

- i) Castor oil
- ii) Vegetable oil
- iii) PlD Fluorocarbon

These dispersions and emulsions gave a wide variation in the dispersed to continuous phase permeability ratio.

The hemoglobin solution and red blood cell suspensions in saline were prepared by accepted standard methods. Fresh whole human blood (type O, positive) was purchased from the Massachusetts General Hospital Bloodbank and stored at 4°C prior to use. Red blood cells were removed from blood by centrifugation, washed, and resuspended in saline (pH=7.0). Hemoglobin solutions were prepared by freeze-thawing packed red blood cells.

Reactive emulsions (W/O) were made by emulsifying aqueous hemoglobin solution in a continuous organic phase. Oxygen permeation experiments were carried out on emulsions where the dispersed hemoglobin droplets had either a relatively large or small average particle size in order to demonstrate nonequilibrium effects. By appropriate control of the emulsification procedure the particle size distribution of the "large" and "small" emulsion could be controlled.

Thin liquid films of the various types of media were supported on each side by two thin silicone support membranes in a sample holder as shown in Figure 6.4. The mass transfer resistance of the membranes to oxygen was small in comparison to the total mass transfer resistance (3 to 6%) and was taken into account in the data reduction. Liquid film thicknesses

employed were from 0.5 to approximately 2 mm. Film thickness was controlled by placing thin metal spacers in a gasket of the same thickness. The rubber gasket acted as a seal when the sample holder was completely assembled.

The experimental apparatus was designed as a modification of Barrer's classical time-lag apparatus (Barrer and Skirrow 1948) and is shown in Figure 6.3. The apparatus was run at partial vacuum to eliminate gas phase resistance. To insure that the liquid in the film did not evaporate, a saturator containing the same material as that in the sample holder, was utilized to saturate the upstream and downstream volumes. The experiments involved the introduction of O_2 into the upstream volume and recording of the downstream pressure change with time as the gas diffused from the upstream volume, through the membrane-liquid-membrane layer, and emerged into the downstream volume. Oxygen permeabilities were obtained from the quasi-steady state mass transfer rate for known conditions of driving force, thickness of liquid film, and total mass transfer area.

1.5 Results and Discussion

Effective permeabilities for oxygen transport in inert dispersions and emulsions compared well with Maxwell's equation for moderate differences between the continuous and dispersed phase permeabilities. For the dispersions, the dispersed to continuous phase permeability ratio, P_d/P_c , was

near zero. Figure 7.6 shows a comparison between the theory and the experimental results for the permeation of carbon dioxide in FEP 120 dispersions. Figure 7.11 shows the results of oxygen permeation experiments in vegetable oil-in-water emulsions. In this case the dispersed phase to continuous phase permeability ratio is

$$\frac{P_d}{P_c} = 1.67$$

For larger differences in the permeability ratio of the two phases the data deviates from Maxwell's equation at high dispersed phase volume fractions as is shown in Figure 7.12. for the fluorocarbon emulsions.

Oxygen permeabilities were measured in inactivated hemoglobin solutions in order to measure the permeability when no reaction effects are present. Hemoglobin can be "inactivated" by conversion into the inactive methemoglobin form, or operating the mass transfer experiment under conditions such that the hemoglobin is fully saturated and no longer participates in the reaction ("inert"). This then becomes a case of pure Fickian diffusion. The calculated diffusivities, obtained from the permeability data and published oxygen solubilities (Altman and Dittmer 1971) compared well with those published in Kreuzer's review article (1970) as shown in Figure 7.15.

In order to check the mobile-carrier, facilitated transport hypothesis, active hemoglobin was partially

immobilized by adsorption in swollen collodion membranes. The active hemoglobin in the collodion membranes did not facilitate oxygen transport as is shown in the normalized plot of Figure 7.13. Hemoglobin soaked in Millipore membranes, which does not adsorb the hemoglobin, does facilitate oxygen transport since it retains its mobility. The results in Figure 7.13 are consistent with the mobile carrier transport hypothesis. It should be noted that the membranes were clamped inside a specially constructed sample holder without the use of the silicone membranes. Additional details are available elsewhere (Zahka 1971).

Average effective oxygen permeabilities were measured in red blood suspension for conditions where the hemoglobin inside the red blood cells was either partially or fully saturated. In the latter case the chemical reaction effects are negligible and the situation is equivalent to diffusion in inert heterogeneous media as is shown in Figure 7.17. For the reactive suspensions, experiments were carried out with three different oxygen partial pressure driving force conditions (in the unsaturated portion of the oxygen-hemoglobin saturation curve). These results were compared with theoretical predictions obtained from equation (4.99) and are shown in Figures 7.19a, 7.20a and 7.21a. The experimental results fall between the theoretical curves for the "minimum" red blood cell radius, $1 \mu\text{m}$, and the "maximum" red blood cell radius, $4 \mu\text{m}$. Clearly, the hemoglobin inside the red blood cells facilitates the

oxygen transport. As the driving force is increased the relative effect of the hemoglobin facilitated oxygen transport decreases in relation to the total oxygen transport. The comparison of theory and experimental results suggests that the oxygen-hemoglobin reaction is not at equilibrium inside the red blood cell. However, note the relatively small effect to be expected from the departure of the reaction within the red cells from equilibrium at a volume fraction of $\phi=0.45$ which is consistent with that of whole blood. The parameters used for the theoretical comparisons were either measured values or values previously published.

In addition to the reactive red blood cell experiments, oxygen permeation experiments were carried out with a model reactive suspension aqueous hemoglobin solution emulsified in oil. This is a desirable system since the dispersed hemoglobin particles are indeed spherical as assumed in the theory. Further the particle size of the emulsion can be changed so that non-equilibrium effects can be shown experimentally. In addition the hemoglobin diffusivity is not precisely known at red blood cell hemoglobin concentrations, but at lower hemoglobin concentrations experimental agreement between published values is reasonable (Kreuzer 1970). In this work a hemoglobin solution of 16.3 gr/100 ml was used. Emulsion was made with either a volume average particle radius of 1.5 μm ("small" emulsion) or 8.2 μm ("large" emulsion). Hemoglobin activity

after emulsification was measured with the van Slyke technique. Figure 7.33 shows the experimental results. The theoretical equations were corrected for hemoglobin deactivation, 42% of total for the large and 54% for the small emulsions, and for the particle size distributions. Additional details are available elsewhere (Tuntunjian 1973). The results clearly indicate the effect of particle size. It should be noted that the reaction is nearly at equilibrium for the large size emulsion.

Since the theory and the experimental results gave good agreement the theory was utilized to predict the effective relative permeabilities at physiological conditions and driving forces. In artificial oxygenators or the lung, the venous blood is nearly 75% saturated and as a consequence facilitation effects should be relatively small. Figure 7.29 shows the predictions at 37°C for transport from a partial pressure level of 100 mmHg to a level of 35 mmHg. At a volume fraction of $\phi=0.45$ the effect of the chemical reaction increases the effective permeability only about 8 percent.

1.6 Conclusions and Recommendations

A theoretical framework has been developed that models diffusion with reversible chemical reaction in heterogeneous media. The theoretical framework incorporates general aspects of previously published work on mass transport phenomena in

inert heterogeneous media and diffusion with reversible chemical reaction in homogeneous media. As an example, several models have been developed for various types of heterogeneous media and reaction schemes. Effective permeabilities were derived which show that the effect of reversible chemical reactions is to increase the transport rate of the diffusing species in heterogeneous media. The effective permeability is a maximum when the chemical reactions are at equilibrium. In the case that nonequilibrium effects become important, facilitated transport becomes negligible and the theoretical equations reduce to Maxwell's equation for inert heterogeneous media.

Coupled with the theoretical developments, an experimental program was undertaken to investigate mass transport phenomena in both inert and reactive media. Experimentally measured oxygen permeabilities in thin liquid films of inert dispersions, inert emulsions, reactive red blood cell suspensions, and reactive emulsions showed reasonable agreement with the theoretical equations. It was concluded that in the operation of an artificial oxygenator at normal physiological conditions, hemoglobin-facilitated oxygen transport contributes only a fraction of the total mass transport rate. This same conclusion appears to be valid for oxygen uptake in the lung; but in the tissues and muscles, where the partial pressure of oxygen can be low, hemoglobin facilitated oxygen transport may become significant.

2. INTRODUCTION

- 2.1 General Introduction
- 2.2 Introduction to the Problem
- 2.3 Heterogeneous Systems Studied in This Thesis

2. INTRODUCTION

2.1 General Introduction

The understanding of transport processes in heterogeneous media is an important problem in science and engineering. Whereas a transport process may be well understood in a homogeneous system, a similar process in a heterogeneous system can be of such a complexity that no theoretical solutions or experimental data may be available. Since many physical systems are of a heterogeneous rather than homogenous nature, it is not surprising that researchers have increasingly turned their attention to the study of transport processes in heterogeneous media. In the chemical engineering literature alone, hundreds of articles are published each year on transport processes such as heat transfer, mass transfer, and fluid flow in heterogeneous media (Tavlarides et al. 1970). In the chemical industry, heterogeneous media such as emulsions, slurries, foams, dispersions, and solid mixtures are frequently encountered as process streams or materials of construction. For example, processes such as the drying of textiles, air or moisture permeability of paint films, the migration of plasticizers into and out of polymers, and heterogeneous catalysis of feed reactants need to be understood in order to rationally design or choose the equipment to perform the required task.

In the field of biology one deals almost exclusively with heterogeneous systems, because organisms are made of a

unit building block, the cell. The cell itself is a heterogeneous system of intricate complexity. The knowledge of how biological systems can exist depends to a great extent on the understanding of the heterogeneous transport processes within these systems. In addition, engineers and scientists are increasingly interested in how biological systems have solved complicated transport requirements. Such knowledge may lead to applications in industrial or chemical processes, as well as to the design of devices that can take over biological functions.

Transport processes in heterogeneous media occur of course in many other disciplines, but space limits a full discussion of these phenomena. This thesis is mainly concerned with the problem of diffusion with reversible chemical reaction in heterogeneous media, and in particular with the application of the solution to biological transport processes. Fortunately, different transport phenomena are often analogous so that the extension of this work to related phenomena may be relatively straightforward if appropriate modifications are made.

2.2 Introduction to the Problem

In this laboratory, researchers have been interested for some time in the performance and characterization of artificial kidneys and blood oxygenators (Buckles et. al. 1968; Colton et. al. 1971b). Since the development of highly permeable membranes, it is now recognized that the blood phase

is often the limiting resistance to mass transfer. Hence a fundamental quantitative understanding of solute transport in blood is a prerequisite for the design of more efficient devices that carry out mass transfer operations normally carried out by the human body. Mass transport of a solute in blood is a complex phenomenon because blood is a heterogeneous system as shown in Figure 2.1. Solute molecules must diffuse around plasma proteins and around or through the red blood cells. The equilibrium distribution of solute between plasma and the red blood cell may be unequal. The solute may undergo chemical combination with any of the many species present in the plasma or the red blood cell phase, and deviations from chemical equilibrium of the reactions between the solute and these species may be important. Further the red blood cell membrane may offer a significant resistance to mass transfer. Since the main function of blood is to act as a transport fluid, most of the reactions that take place in blood are reversible. The phenomenon of diffusion with reversible chemical reaction in heterogeneous media is of course not limited to the diffusion of solutes in blood, but such phenomena also take place in the transport of nutrients, metabolites, and drugs to tissues, organs, or any ensemble of cells. At present, despite scores of publications, this phenomena is not fully understood, and experimental results are often contradictory or insufficient. In general, systems have been studied for which only a few of the described processes are operative. For example, numerous theoretical solutions have been given for mass transport without chemical

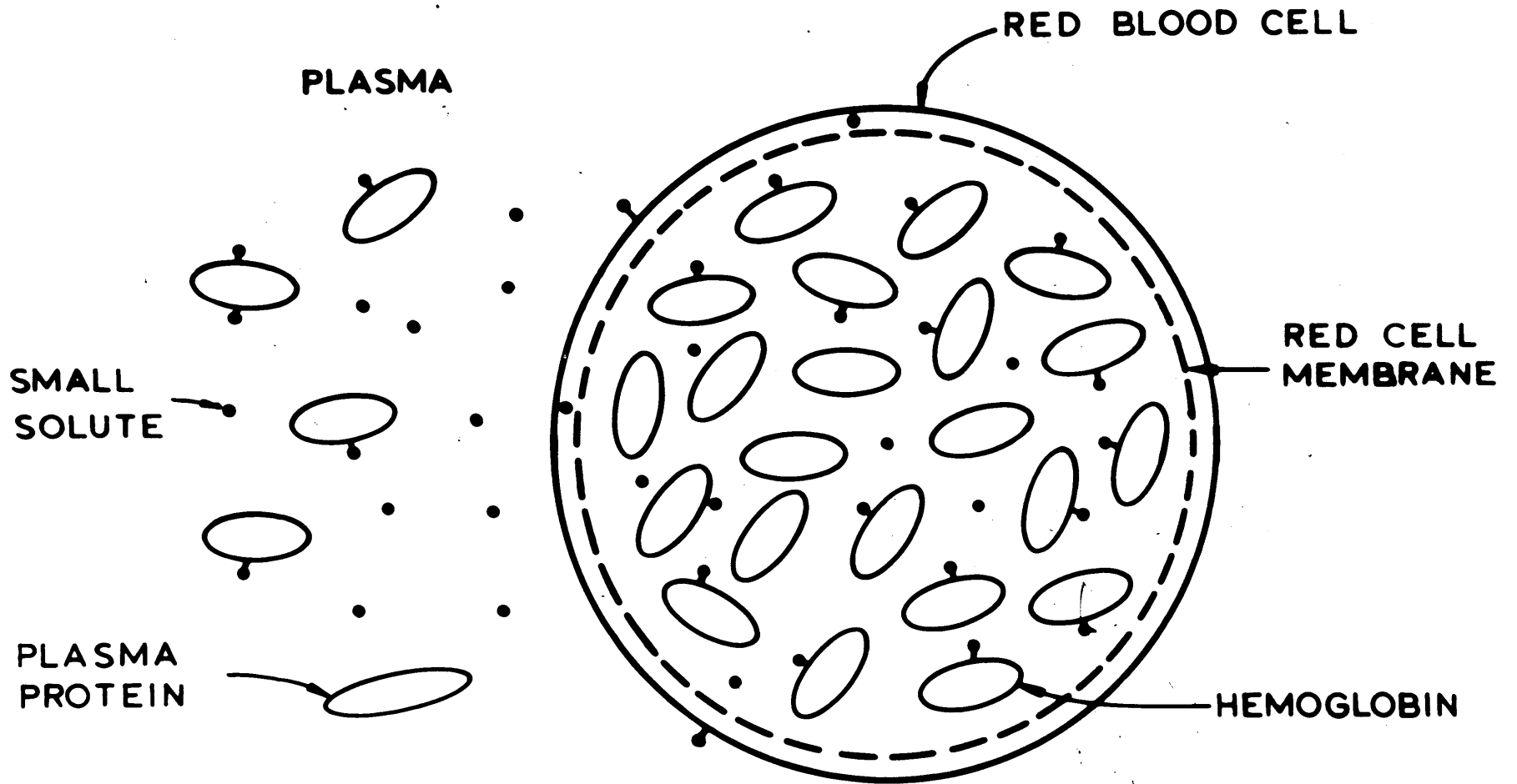


FIGURE 2.1
 GRAPHICAL REPRESENTATION OF THE DIFFUSION OF SOLUTES IN BLOOD.

reaction in heterogeneous media, and diffusion with chemical reaction in homogeneous media. An integrated application of the results of the work on simplified systems toward the more complex situation has not been done previously. Considering the need for a theoretical frame work to model diffusion with reversible chemical reaction in heterogeneous media, a theoretical and experimental program was undertaken in this thesis. The specific experimental systems utilized includes oxygen permeation through blood for the reason that the data can be of utility in the design of artificial oxygenators, and in addition many physical parameters are available for this particular system.

2.3 Heterogeneous Systems Studied in This Thesis

The purpose of this thesis is to gain a quantitative understanding of mass transport with reversible chemical reaction in heterogeneous media. The following restrictions apply. Systems will be considered where mass transport is influenced only by diffusive and chemical reaction effects. The only heterogeneous media considered are those for which one phase is dispersed into a second phase with the characteristic size of the dispersed particles much smaller than the characteristic dimensions of the overall system. A conceptual framework is shown on Figure 2.2. Case 1 is steady state Fickian diffusion in a one dimensional film. Here A is the permeating species (a gas in this thesis). Modifications that may arise in many systems are shown by cases 2 and 3. Case 3 corresponds to diffusion with reversible

chemical reaction in a homogeneous system. Reactant B is constrained to remain within the film, and combines with the permeating species A to form product AB. If both species B and AB have significant molecular diffusivities they can increase the mass transfer of A beyond that which is possible from purely physical diffusion of A alone. This case has been termed carrier-facilitated transport. An example of such a system is the diffusion of oxygen in hemoglobin solutions.

Case 2 is diffusion in a heterogeneous medium where one phase is dispersed in a continuous phase, for example an emulsion or dispersion. Such an inert suspension is a reasonable model for diffusion of solutes in blood where no significant solute interactions occur with the plasma proteins or hemoglobin molecules. The diffusion of urea in whole blood can be an example of such a system.

Combinations of cases 2 and 3 are shown in cases 4 and 5 which are examples of diffusion with reversible chemical reaction in heterogeneous media. Case 4 is the situation where the carrier species is present only in the discontinuous phase. The diffusion of oxygen in whole blood is analogous to case 4 because hemoglobin is present only inside the red blood cells. In case 5 the carrier species is present in the continuous phase but not in the dispersed phase. Such a situation may arise in gas absorption with chemical reaction in a slurry or in the diffusion of metabolites, drugs, or amino acids that interact solely with plasma proteins and not with hemoglobin.

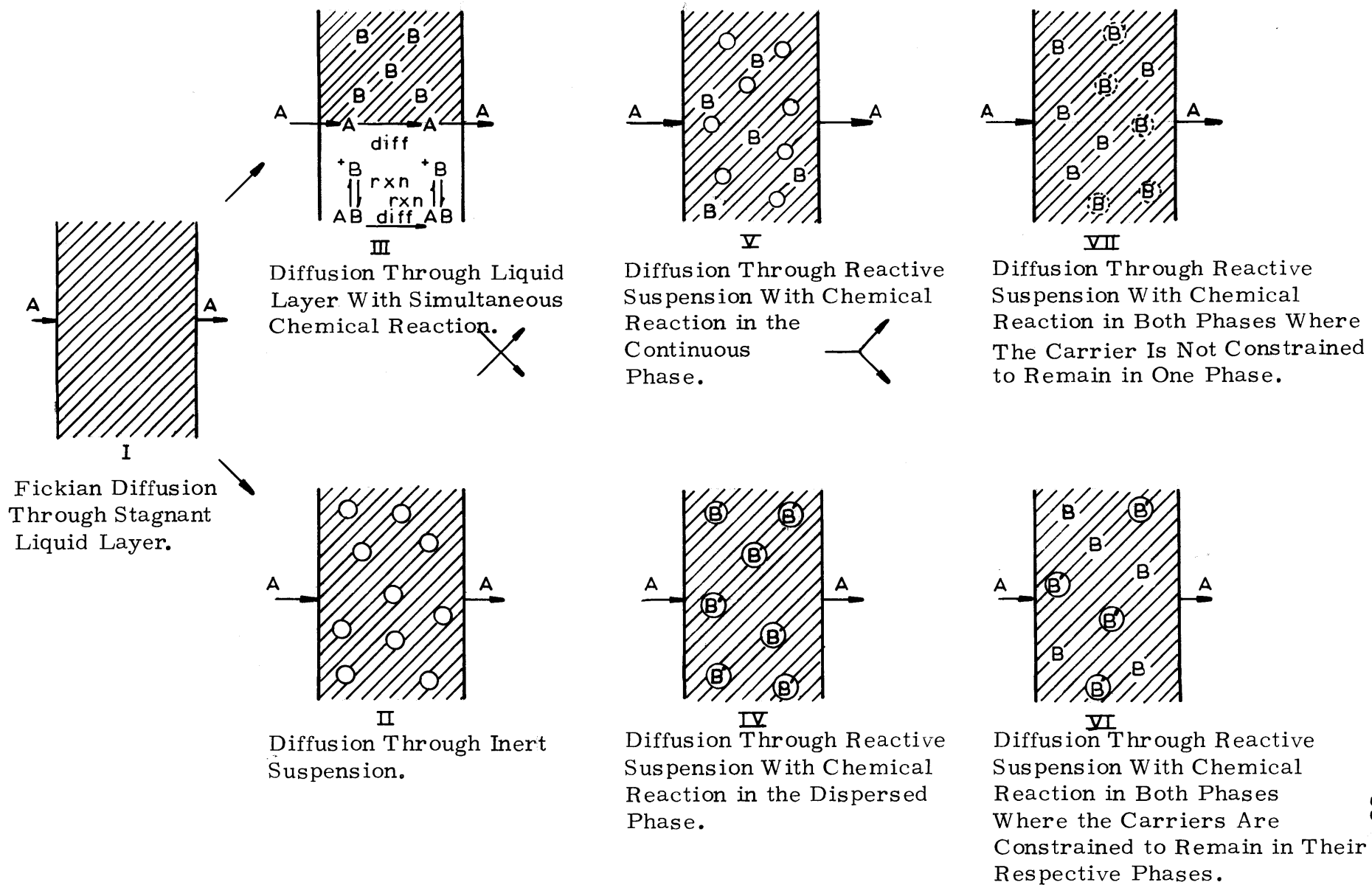


FIGURE 2.2. BASIC COMPONENTS OF SYSTEMS TO BE STUDIED .

Cases 6 and 7 are more complicated reactive heterogeneous systems where the carrier species is present in both the continuous and dispersed phase. In case 6 the two different carriers are constrained to remain within their respective phases and cannot permeate across the boundary between dispersed and continuous phases. In case 7 only one carrier species is present in both phases and this species can diffuse from one phase into the other. Before proceeding into the development of a theoretical model and a discussion of the experimental program, a literature review is necessary to discuss previous work on transport in heterogeneous media, and diffusion with chemical reaction in homogeneous media. It will be shown later that the mathematical model incorporates general aspects of each subsystem, and the approach of the experimental program is to work with systems of increasing complexity.

It should be emphasized here, that the theoretical models developed in this thesis have application not only to biological transport phenomena, but also to similar processes of chemical engineering interest, such as, for example, absorption and reversible reaction of reactants into emulsions, dispersions, or encapsulated enzyme suspension and the transport of ions through ion selective heterogeneous membranes that utilize selective carriers (ion selective electrodes).

3. LITERATURE SURVEY

- 3.1 Diffusion in Inert Heterogeneous Media
 - 3.1.1 Analysis of Theoretical Equations
 - 3.1.2 Comparison of Experimental Data

- 3.2 Diffusion with Reversible Chemical Reaction in Homogeneous Media
 - 3.2.1 Historical Background
 - 3.2.2 Theoretical Developments

- 3.3 The Oxygen-Hemoglobin Systems
 - 3.3.1 Homogeneous Systems
 - 3.3.2 Heterogeneous Systems
 - 3.3.2.1 Inert Suspensions
 - 3.3.2.2 Reactive Suspensions
 - 3.3.2.2.1 Experimental Work
 - 3.3.2.2.2 Theoretical Developments
 - 3.3.3 Physico-Chemical Parameters
 - 3.3.3.1 Oxygen and Hemoglobin Diffusivities
 - 3.3.3.2 Kinetic Rate Parameters
 - 3.3.3.3 Solubility Coefficient of Oxygen

- 3.4 Discussion

3. LITERATURE SURVEY

A review of the literature reveals that extensive work has been done on transport without chemical reaction in heterogeneous media (inert heterogeneous media), and on diffusion with reversible chemical reaction in homogeneous media. Work in these areas will be discussed before considering the system of primary interest involving the reaction of oxygen with hemoglobin.

3.1 Diffusion in Inert Heterogeneous Media

The literature contains many models that predict the effective physical properties of heterogeneous media. Parameters of interest include the electrical conductivity, magnetic permeability, mass permeability, thermal conductivity, and dielectric displacement. In view of the many properties of the composite in which one may be interested, it is fortunate that for the above parameters there is similarity of treatment, and the equations derived for each parameter are interchangeable. The articles of Barrer (1968), Reynolds and Hough (1957), and Meredith and Tobias (1962) are excellent reviews of the published equations.

Nearly all of the analysis published to date consider the solution of the steady state problem. At steady state many phenomena associated with heterogeneous media are expected to obey Laplace's equation

$$\nabla^2 \phi = 0 \quad (3.1)$$

where ϕ is the potential. In the case of the diffusion of solutes in heterogeneous media, Laplace's equation is the mass conservation relationship. Examination of the literature yields the following conclusions (emphasis on mass transfer):

- i) Most of the equations are for two component systems.
- ii) At present, due to the complexity of the problem, no rigorous solution is available. Exceptions are the relations derived for purely parallel or series arrangements or infinitely dilute suspensions of spheres or spheroids.
- iii) Most existing solutions differ from one another in the approximations made in their development.
- iv) The solutions indicate that the effective relative (dimensionless) permeability of the medium is dependent only on the volume fraction of the dispersed phase, the shape of the dispersed particles, and the relative permeabilities of the two phases

$$\frac{\bar{P}}{P_c} = f(\phi, \text{shape } d, \frac{P_d}{P_c})$$

where \bar{P} = effective permeability

P_c = permeability of the continuum

P_d = permeability of the dispersed phase

ϕ = volume fraction of dispersed phase

d = dispersed phase

the particle size is not important as long as it

is much smaller than the characteristic dimension of the system, but much greater than the size of a molecule.

v) A few solutions are a function of the particle size distribution.

vi) Experimental verification of existing solutions is meager.

The solutions for parallel or series arrangements of components in a composite are not of interest, since in this work only media where one phase is dispersed into the other phase will be considered (see Figure 2.2, case 2). Because there are dozens of relationships published in the literature, only the better known equations will be discussed. From a physical standpoint, it is desirable that the following criteria be met,

$$\phi = 0 \quad K_m = 1 \quad (3.2)$$

$$\phi = 1 \quad K_m = \frac{P_d}{P_c} \quad (3.3)$$

where the permeability ratio K_m is defined as

$$K_m = \frac{\bar{P}}{P_c} \quad (3.4)$$

Permeability, as used here is the product of diffusivity times solubility $P = D\alpha$. For the heterogeneous medium the solubility is

$$\bar{\alpha} = \alpha_c(1 - \phi) + \alpha_d\phi \quad (3.5)$$

In the case of a nonvolatile solute the permeability ratio is better expressed as

$$K_m = \frac{\bar{D}[\phi R_{d/c} + 1 - \phi]}{D_c}$$

where $R_{d/c}$ is the equilibrium solute distribution coefficient between dispersed phase and continuous phase ($R_{d/c} = (C_A^d/C_A^c)|_{eq}$).

Some equations need not satisfy the criteria given by (3.2) and (3.3) because they only apply for ordered arrangements of particles in a continuum, and in that case there is an upper limit of volume fraction. For instance, for the case of a cubical array of spheres, the maximum volume fraction occurs when the spheres are close-packed ($\phi = \pi/6$). For a random dispersion of spheres, $\phi = 1$ can be approached if there is a large size distribution of the spheres, or if the spheres can be deformed.

The simplest kind of two phase dispersion consists of spherical particles of mass permeability P_d imbedded or dispersed in a medium of permeability P_c . Maxwell (1881) considered a single sphere in an infinite continuum where the field is unidirectional and linear at large distances from the sphere. By solving the Laplace equation for the potential in spherical coordinates inside and outside the sphere, he obtained the potential variation due to the presence of the sphere in a continuum. For a dilute suspension he considered the suspension itself spherical and located in the continuous medium. By assuming the perturbation associated with each of the smaller spheres inside this spherical suspension to be independent of each

other, he obtained an effective permeability for mass transfer for the suspension by equating both the perturbation caused by the spherical suspension, and that caused by all the small spheres. Maxwell obtained for the effective relative permeability

$$K_m = \frac{K_d + 2 - 2\phi (1 - K_d)}{K_d + 2 + \phi (1 - K_d)} \quad (3.6)$$

where $K_d = \frac{P_d}{P_c}$

Lorentz (1880), and Lorenz (1880) independently derived the same relationship. A detailed derivation of Maxwell's equation is given in Appendix A. Equation (3.6) is rigorously valid only for a dilute suspension of randomly-oriented spheres, where the particles are of uniform size. For ϕ approaching zero all other relationships derived for spheres in a continuum must give the same numerical value as Maxwell's equation. It should be noted that if the permeabilities of the suspended phase P_d and the continuous phase P_c are nearly the same, Maxwell's equation can be applied over the full range of the volume fraction.

Fricke (1924) considered a suspension of randomly oriented ellipsoidal particles. Fricke's procedure is similar to that of Maxwell, but instead of solving the potential problem for a single sphere, he considered the more general case of a spheroid and worked in confocal ellipsoidal coordinates. He obtained

$$K_m = \frac{1 + \phi (WK_d - 1)}{1 + \phi (W - 1)} \quad (3.7)$$

where

$$W = \sum_{i=1}^3 \frac{\frac{1}{3}}{[1 - (1 - K_d) L_i]} \quad (3.8)$$

The three values of L_i involve elliptic integrals of the second kind and are purely numerical. These values depend only on the axial ratio of the dispersed particles. Solutions have been obtained for particles which are spheroids (i.e., when two of the principal axes of the particle are of equal length), and in that case only one value of L_i is needed since

$$L_1 + L_2 + L_3 = 0 \quad (3.9)$$

and

$$L_2 = L_3 \quad (3.10)$$

If the principal axes of the spheroids are designated by a , b , and c (where $b = c$), the value of L_3 may be obtained from Table 3.1 which was given by Meredith and Tobias (1962). For the case of spheres, $a = b = c$, all L_i 's are equal to $1/3$ and Fricke's equation reduces to Maxwell's. Fricke's equation is rigorously valid only for dilute dispersions of spheroids, and the volume fraction range in which the equation is accurate should be the same as for Maxwell's equation.

Bruggeman (1935) derived a relationship for suspensions of spheres in which he attempted to take into account the interaction of neighboring particles:

TABLE 3.1
 L_3 FOR SPHEROIDS ($b = c$)*

Shape	b/a	L_3
Rods	0	0.5000
Prolate Spheroids	1/6	0.4784
	1/5	0.4720
	1/4	0.4624
	1/3	0.4465
	1/2	0.4134
	Spheres	1
Oblate Spheroids	2	0.2383
	3	0.1823
	4	0.1477
	5	0.1245
	6	0.1077
Disks	∞	0

* Values from Meredith and Tobias (1962).

$$\frac{(K_m - K_d)}{K_m^{1/3} (1 - K_d)} = 1 - \Phi \quad (3.11)$$

The above expression was derived for dispersions of random particles in the concentrated range of volume fractions by approximations based on Maxwell's relation. Bruggeman used an integral procedure of adding infinitesimal fractions of the dispersed phase to the mixture and considering the surrounding medium (mixture) for the added particles to be the continuum. Maxwell's equation is used to derive the differential change of the effective permeability with a differential change in the volume fraction, and subsequent integration yields equation (3.11). Meredith and Tobias have pointed out that a limitation (on physical arguments) of the Bruggeman approximation arises because the surrounding medium may be treated as a continuum only if the successively added infinitesimal volume fractions of the dispersed phase consists of particles which are much larger than the ones added previously. They suggested that Bruggeman's equation should be a good approximation when a large range of particle sizes is present in the dispersion. In addition, however, the particle size distribution should be poly-model.

Meredith and Tobias (1962) derived a relationship utilizing not an integral but a stepwise Bruggeman technique (as described above) and Fricke's equation. The result they obtained is:

$$K_m = \left[\frac{2 + \Phi(WK_d - 1)}{2 + \Phi(W - 1)} \right] \left[\frac{2(1 - \Phi) + WK_d\Phi}{2(1 - \Phi) + W\Phi} \right] \quad (3.12)$$

where W is defined by equation (3.8). Meredith and Tobias' equation does not follow the criterion given by equation (3.3) and therefore fails for concentrated volume fractions.

Bottcher (1945) also considered the interaction of particles with their neighbors. Bottcher also assumed that the permeability around a particle is that of the mixture and not that of the continuous phase. Using this assumption, Bottcher obtained the following relationship for the average permeability

$$\frac{K_m - 1}{3K_m} = \left[\frac{K_d - 1}{K_d + 2K_m} \right] \phi \quad (3.13)$$

Niesel (1953) derived equations for randomly oriented lamellae and cylinders in a continuous medium

$$K_m = K_d \left[\frac{3 + 2\phi(K_d - 1)}{3K_d - \phi(K_d - 1)} \right] \text{ lamellae} \quad (3.14)$$

and

$$1 - \phi = \left[\frac{K_d - K_m}{K_d - 1} \right] \left[\frac{K_d + 5}{K_d + 5K_m} \right] \text{ cylinders} \quad (3.15)$$

Niesel's equation for lamellae is the same as Fricke's for the case of infinite flat discs.

In order to determine the effect of interacting particles, the problem is simplified when the position of the particles is fixed and symmetric. Rayleigh (1892) considered the case of parallel cylinders in a square array, and spheres of uniform size in cubical lattices. For a cubical array of

spheres where the field is perpendicular to a side of the cube he obtained

$$K_m = 1 - \frac{2\phi}{(2+K_d)/(1-K_d) + \phi - 0.525(1-K_d)\phi^{10/3}/(\frac{4}{3}+K_d)} \dots \quad (3.16)$$

For small volume fractions equation (3.16) reduces to that of Maxwell. Meredith and Tobias (1960) have evaluated one more term in the denominator for the Rayleigh's expression for spheres and Runge (1925) improved Rayleigh's expression for cylinders. In addition Barrer and Petropoulos (1961) derived an equation for lattices of parallelepipeds in a continuum.

Many empirical relations have been derived by various authors. Some of these do not approach Maxwell's and Fricke's relationship for small volume fractions. Empirical relationships have been proposed by Slawinsky (1926), Pearce (1955), Topper (1955), Higuchi (1958) and others. Meredith and Tobias (1962) have reviewed these relationships and have discussed their limitations.

The equations reviewed here are just a drop in the bucket compared to all the equations that have been published. However many derivations have been duplicated and are known by different names in different disciplines. At present this field is still quite active, and new relationships with varying degrees of sophistication appear continually in the literature.

3.1.1 Analysis of Theoretical Equations

The primary emphasis in this thesis is on randomly dispersed spherical particles in a continuum, and the equations of Maxwell, Bruggeman, Fricke, and Bottcher are of special interest. The solutions of various relationships is shown graphically in Figures 3.1, 3.2, and 3.3 for the following three cases: $K_d = 0$; $K_d = 5$, $K_d = 100$. For the case of an impermeable suspended phase in a continuum ($K_d = 0$) the largest differences between Maxwell's relationship and those of others occurs at concentrated volume fractions. Bottcher's equation appears to fail at volume fractions greater than approximately 0.35.

When the mass permeability of the dispersed phase is of the same order of magnitude as the mass permeability of the continuous phase, differences in the equations are small as shown by Figure 3.2. For a large dispersed phase permeability relative to the continuous phase permeability the equations again show large deviations when compared to Maxwell's equation in the concentrated volume fraction range (see Figure 3.3). The dashed straight lines on Figures 3.1, 3.2 and 3.3 are given as a basis of comparison, and represent an effective permeability linearly weighted with volume fraction. For small volume fractions the equations of Bruggeman, and Bottcher must agree with that of Maxwell, but as ϕ increases the difference between these relationships increases to a maximum at some value of ϕ less than one. In

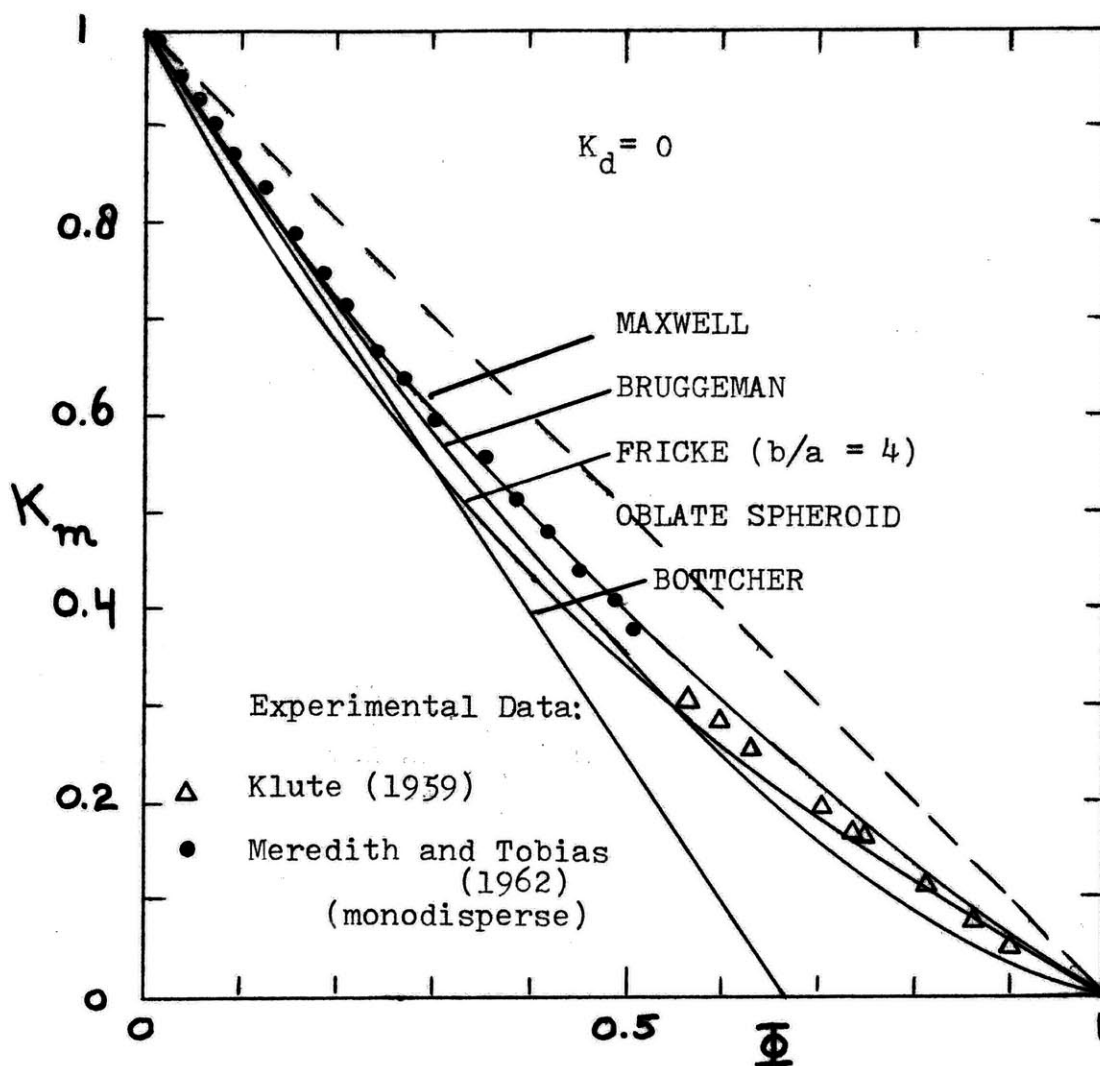


FIGURE 3.1

COMPARISON OF VARIOUS EQUATIONS FOR NON-CONDUCTING SPHERICAL PARTICLES

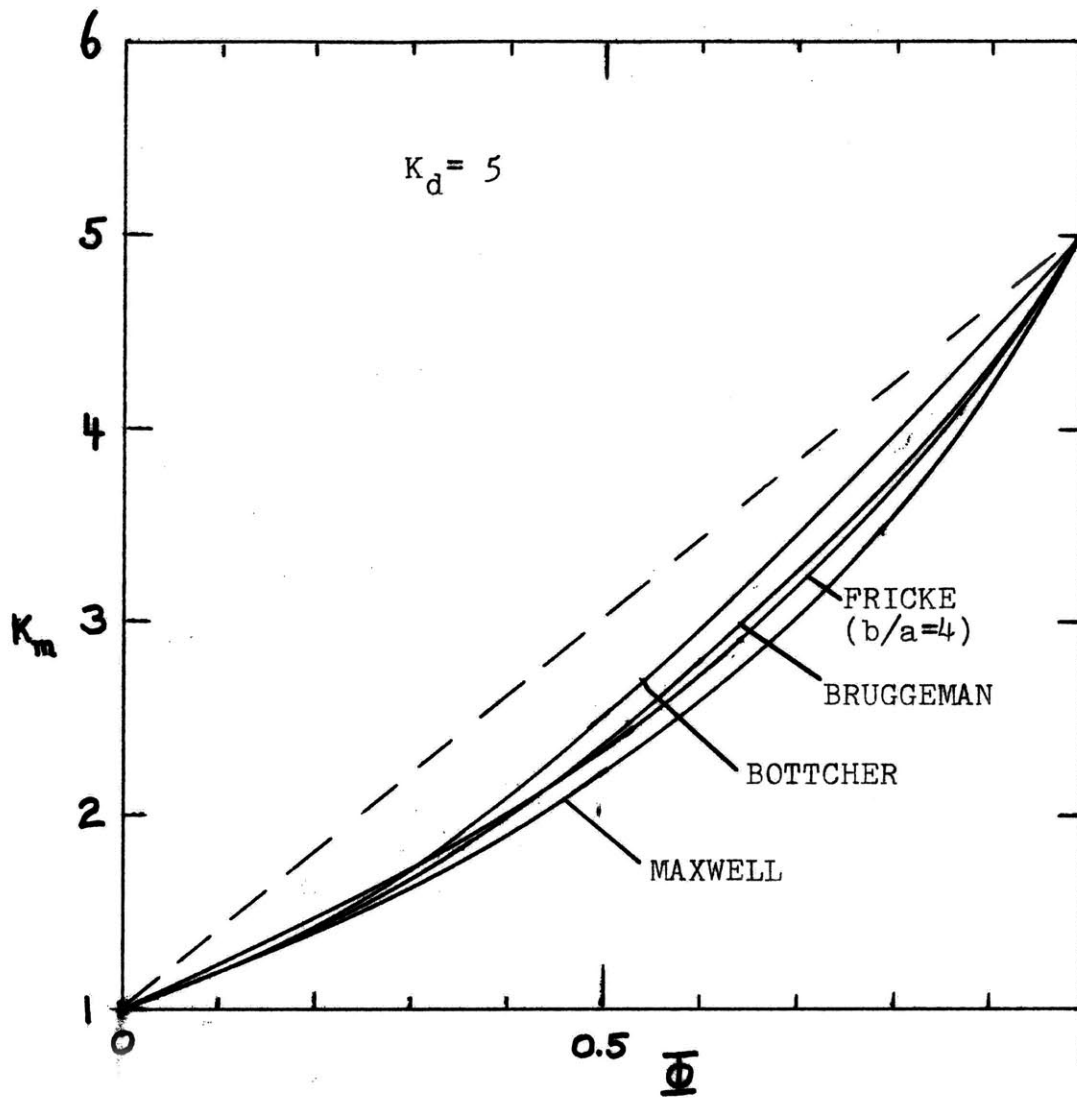


FIGURE 3.2

COMPARISON OF VARIOUS RELATIONSHIPS FOR THE CASE
 $K_d = 5$

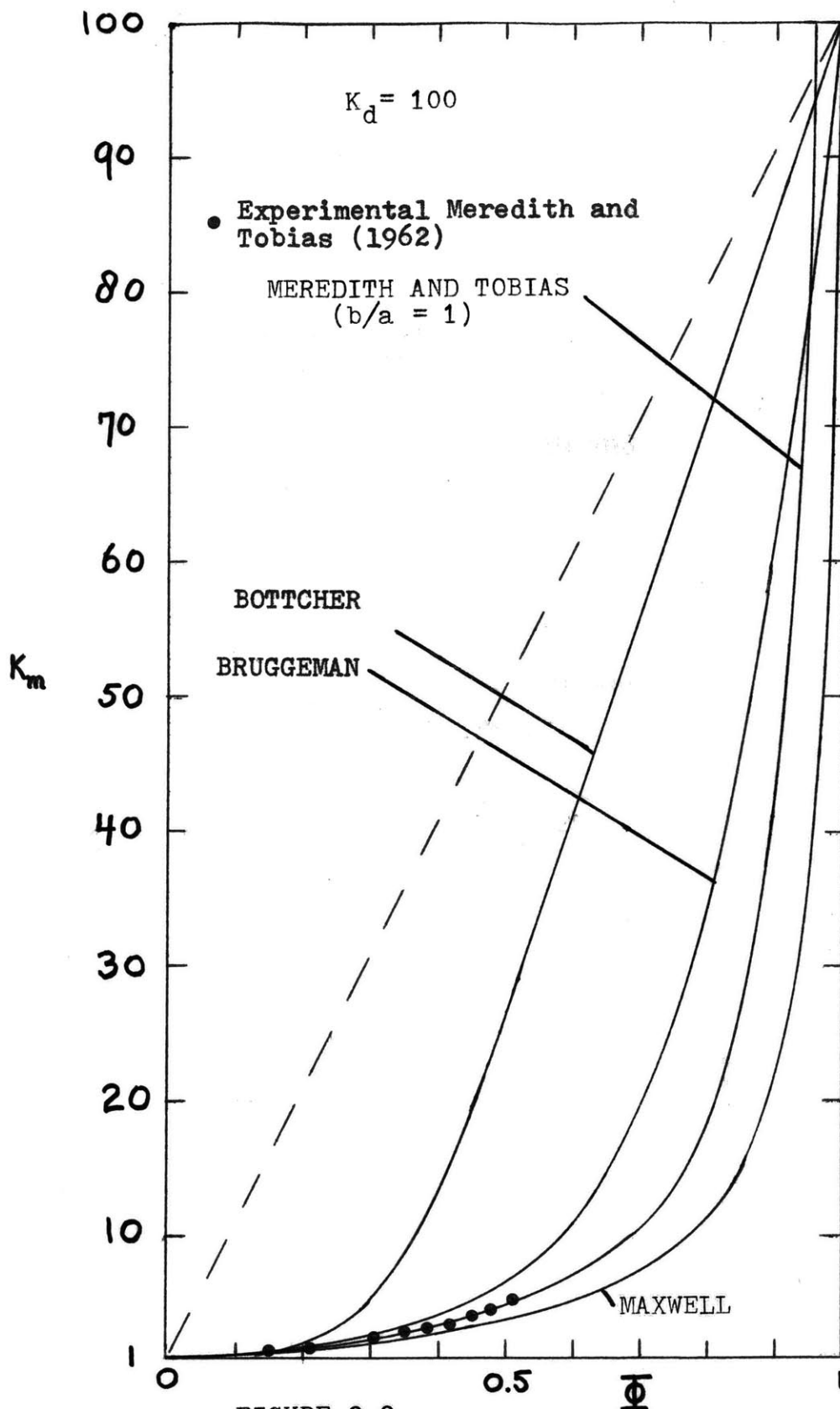


FIGURE 3.3
COMPARISON OF RELATIONSHIPS FOR THE CASE OF $K_d = 100$

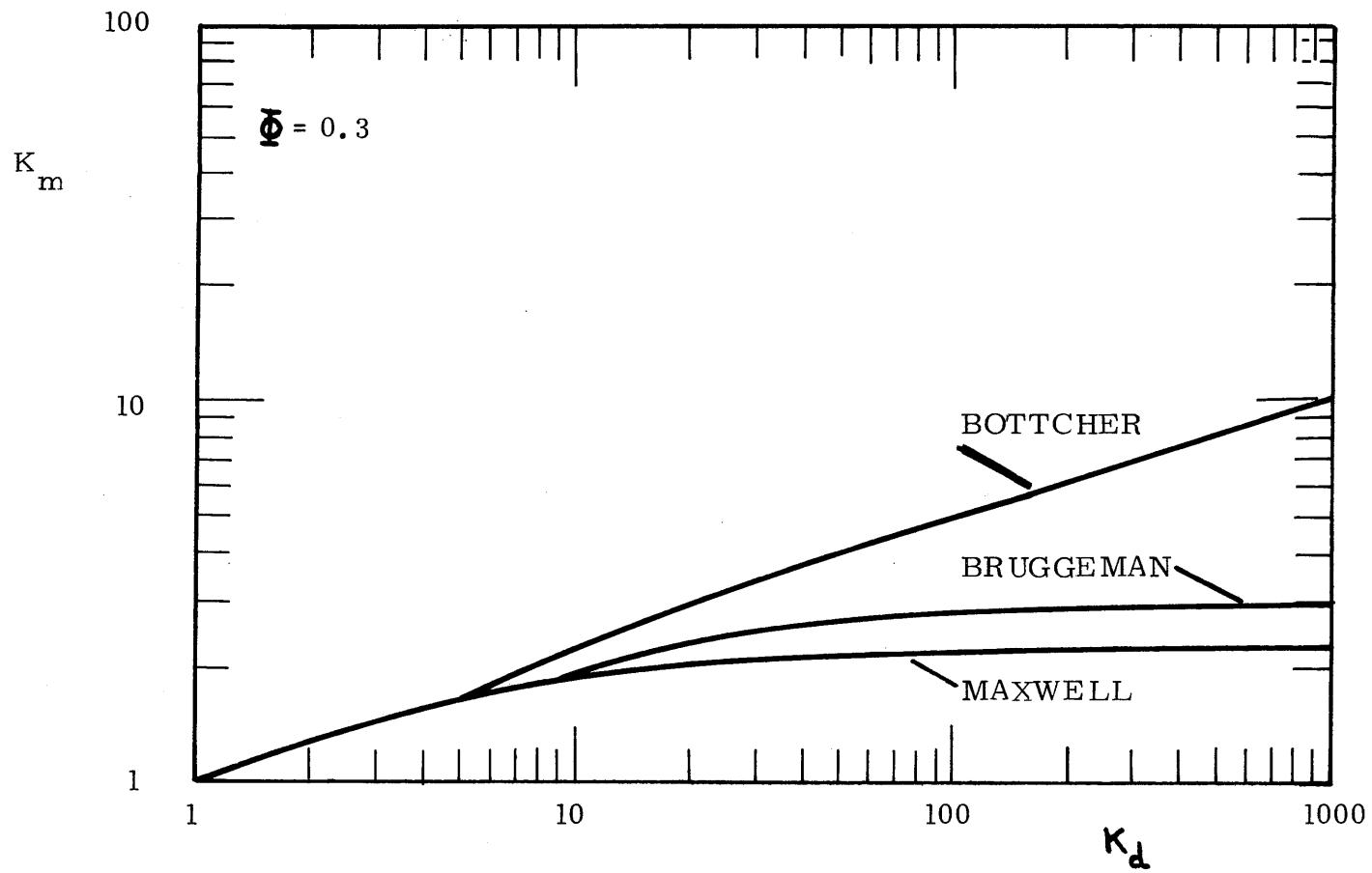


FIGURE 3.4
 K_m AS A FUNCTION OF K_d AT $\phi = 0.3$ FOR VARIOUS RELATIONSHIPS.

TABLE 3.2

MAXIMUM RATIO $\frac{K_m \text{ (author)}}{K_m \text{ (Maxwell)}}$ AND VOLUME

FRACTION AT WHICH IT OCCURS

K_d	Bruggeman ratio	ϕ	Bottcher ratio	ϕ	Fricke* b/a = 4 ratio	ϕ
10^{-5}	0.528	0.860	0.180	0.630	0.788	0.980
0.05	0.790	0.874	0.512	0.773	0.882	0.725
0.1	0.902	0.671	0.717	0.792	0.919	0.675
0.5	0.995	0.697	0.990	0.711	0.995	0.550
1.0	1.0	all ϕ	1.0	all ϕ	1.0	all ϕ
5	1.076	0.670	1.150	0.670	1.066	0.500
10	1.227	0.687	1.472	0.621	1.158	0.525
50	2.200	0.792	4.347	0.618	1.400	0.650
100	3.102	0.825	7.987	0.622	1.476	0.725
500	7.771	0.898	37.15	0.612	1.581	0.850
1000	11.90	0.919	73.62	0.613	1.606	0.900

*Fricke has same physical validity as Maxwell.

Figure 3.4, Bottcher's equation fails when K_d approaches infinity, but the equations of Maxwell and Bruggeman level off to a fixed value for a given value for ϕ when $K_d \rightarrow \infty$. Bottcher's equation increases with no limit, and for $K_d \rightarrow \infty$, the ratio of the effective mass permeability to the mass permeability of the continuous medium, K_m , approaches infinity. This is physically impossible, and therefore Bottcher's equation should not be used for $K_d \gtrsim 0.35$ and for large K_d .

The maximum ratios of K_m predicted by other authors relative to that predicted by Maxwell

$$\frac{K_m \text{ (other author)}}{K_m \text{ (Maxwell)}}$$

are given in Table 2.2 for different values of K_d . Also shown are the approximately volume fractions at which this maximum ratio occurs. The table gives a quick quantitative measure of the maximum possible deviation from Maxwell's equation, and also the spread in predicted values for various models. The shape effect for an oblate spheroid with $b/a = 4$ as predicted by Fricke's equation is significant only when $K_d \rightarrow 0$, and $K_d \gg 1$.

3.1.2 Comparison of Experimental Data

Considerable experimental data have been taken on the effective physical properties of heterogeneous media. The electrical conductivity and thermal conductivity of various materials as a function of the volume fraction of the suspended

phase has been extensively studied. At present there exists considerable disagreement between various authors as to what theoretical model fits the experimental results best. Some authors have obtained data on systems for which the order of magnitude for K_d was one, and then concluded that the data followed a particular model very closely. Since there is little difference between solutions at this point, the same conclusion can therefore be made for the other models. Often the models have been applied to media that do not correspond to the assumptions implicit in the theoretical model. For instance, materials such as porous brick or metallic mixture are usually composed of two continuous phases, not a suspended phase in a continuous phase. Often it is difficult to accurately measure the volume fraction for certain materials. In their review, Meredith and Tobias (1962) have concluded that besides the inaccuracies in actual measurements, the wide disagreement in experimental data can be explained only on the basis of a lack of correspondence between the actual experimental system, and the authors' description of it. They further concluded that data on thermal conductivities is the least reliable.

Most of the reliable information has been obtained on particles in a continuum. Jefferson, Witzell and Sibbitt (1958) measured thermal conductivities of graphite-gelled water ($K_d = 288$) and graphite-silicone oil ($K_d = 1063$) suspensions. The effective thermal conductivity was about 20% higher than Bruggeman's equation. Woodside and Messmer (1961)

measured the thermal conductivities of sands packed in water ($K_d = 13.7$), oil ($K_d = 65$) and air ($K_d = 332$). In all three cases the data fall between that of Maxwell and Bruggeman.

Eichbaum (1959) has measured the dielectric displacement of ground vycor glass in polystyrene ($K_d = 1.68$) and ground window glass in polystyrene ($K_d = 3.12$). The results were in accordance with all the mentioned theoretical models for spheres in a continuum.

Stewart (1899) measured the electrical conductivity of dog's blood for volume fractions of the red blood cell phase from 0.114 to 0.907. His data is in excellent agreement with Fricke's model for the case of oblate spheroids, $b/a = 4.25$, and $K_d = 0$, which suggests that the electrical conductivity of the red blood cell membrane is near zero.

De La Rue and Tobias (1959) measured the electrical conductivity of glass spheres in electrolyte solutions ($K_d = 0$). For a narrow particle size distribution, the data fall between values predicted by the Maxwell and Bruggeman equations (see Figure 3.2). Bruggeman's equation represents the data satisfactorily when the dispersed phase contains a broad range of particle sizes.

Meredith and Tobias (1961, 1962) measured the electrical conductivity of water-propylene carbonate emulsions (both oil in water and water in oil). The conductivity in each phase was adjusted by adding KCl to the aqueous phase and quaternary ammonium iodide salts in the organic phase ($K_d = 0, 0.172, 15.7, 100$). The particle size variation was less than one order of

magnitude. For volume fractions up to 0.5 the data fall between the relationships of Maxwell and Bruggeman (see Figure 3.3) and are represented accurately by the equation of Meredith and Tobias (3.12). Klute (1959) collected various data available on the electrical conductivity of a mixture of spheres ($K_d = 0$) at high volume fractions, and the data again falls between the Maxwell and Bruggeman relations. For spheres in cubical lattices in a continuous medium, Meredith and Tobias (1960) found that their modification of Rayleigh's equation for cubical arrangement of spheres fitted the data well for $K_d = 0$ and $K_d \rightarrow \infty$.

Stein et al. (1971) measured the effective oxygen diffusivity of human red blood cells in Agar gels, and Hershey and Karhan (1968) the oxygen diffusivity in whole sheep's blood. (In this case the solubilities of the dispersed and continuous phases are nearly equal.) This work will be discussed later.

In regards to the experimental work that has been done, the following conclusions may be drawn for spherical particles in a continuum:

- i) Primarily, it has been the electrical conductivity and thermal conductivity of dispersions and emulsions which have been measured. Little work has been done on the effective mass permeability of heterogeneous media.

- ii) For low volume fractions ($\phi < 0.1$) Maxwell's equation is accurate for random or ordered arrangements of spherical particles.
- iii) As the volume fraction increases the data for monodisperse spheres in a continuum scatter between the equations of Maxwell and Bruggeman. Agreement with Bruggeman's equation is closer when there is a wide size distribution of spheres.

In closing, it should be mentioned that there exists a ratio of system dimension to particle dimension below which a particulate composite can no longer be called macroscopically homogeneous. Wyllie and Gregory (1953) experimentally determined this minimum to be 25 for spherical particles in a continuum, and Fidelle and Kirk (1971) reported a ratio of 10 for irregular particles in a continuum.

3.2 Diffusion with Reversible Chemical Reaction in Homogeneous Media

3.2.1 Historical Background

At least since the work of Hatta (1928) and Hill (1928) mass transfer with chemical reaction has received considerable attention from researchers in many disciplines. In the field of chemical engineering, a widely used process is the absorption of a gas by a solution of a substance with which the dissolved gas reacts. This process may be utilized to

remove a component from a mixture of gasses, or to form a useful product from the chemical reaction. Much research has been directed to understanding the effect of chemical reaction upon the mass transport rate, so that chemical engineers can logically design the process. A comprehensive treatment on gas-liquid reactions has been given by Danckwertz (1970). Biologists, on the other hand, are concerned with the diffusion and chemical transformation of physiological important species in organs, tissues, and cells. A knowledge of the effect of chemical reaction on the mass transport rates may not only explain why a living system has evolved as it has, but may also have important implications if these systems fail in case of disease, or environmental stress.

The fundamental phenomenon that occurs for diffusion with chemical reaction in chemical processes or biological systems are of course similar, and Weisz (1973) in an informative paper has pointed out that developments in each field have often been duplicative.

Engineers and biologists have long known that the effect of the chemical reaction is to increase the mass transport rate of the diffusing species above that which can be attributed to purely physical diffusion alone. This increase in the mass transport rate is known in the field of chemical engineering as "enhanced mass transfer". In the field of biology, the increase of mass transfer rate for the case of diffusion with reversible chemical reaction has been

termed "facilitated transport" by Danielli (1954). Facilitated transport is an important phenomenon in the transport of physiologically important species in biological systems. For example, glucose crosses the erythrocyte membrane of man some 10^4 times faster than would be predicted by the assumption that only simple Fickian diffusion of glucose occurs (Stein, 1967). At present it is generally accepted that for many systems the increased mass transfer rate is caused by the diffusive nature of the reactive species, also known as the carrier species. Only in a few well defined systems has the carrier species been identified for a given observed facilitated transport system. Scholander (1960), Hemmingsen and Scholander (1960), and Wittenberg (1959) have reported that oxygen transport in homogeneous solutions of hemoglobin or myoglobin is facilitated. Stein (1968) and Bassett and Schultz (1970) studied the facilitated transport of oxygen in thin films of aqueous solutions of cobaltodihistide, Ward and Robb (1967) reported the facilitated transport of carbon dioxide across thin films of bicarbonate-carbonate solutions, and Ward (1970) showed that nitric oxide transport is facilitated in ferrous chloride solutions. The work cited above is in no way exhaustive, and many other experimental results on well-defined systems have been published. The work of Ward and Robb (1967) is especially fascinating. By adding sodium arsenite to the bicarbonate-carbonate solution to catalyse the reactions and consequently to increase the facilitation rate, a separation factor of 4100 was achieved

in the permeability of carbon dioxide over oxygen. The possible industrial application in separation processes of these "liquid membranes" has created great interest. Before discussing in greater detail the work done on the system of interest, oxygen-hemoglobin, a brief summary on the theoretical developments shall be discussed.

3.2.2 Theoretical Developments

Consider as an example the reaction



occurring in a film of thickness L as shown in Figure 2.2, case 2, and shown in more detail in Figure 2.5. Here A is the transported species and B and AB are the mobile carrier and carrier-complex species which are constrained to remain within the film. The problem is to predict the flux of A , and following Smith et al. (1973) the differential conservation equations for the species within the film are

$$D_A \frac{d^2 C_A}{dx^2} = k_1 C_A C_B - k_2 C_{AB} \quad (3.18)$$

$$D_B \frac{d^2 C_B}{dx^2} = k_1 C_A C_B - k_2 C_{AB} \quad (3.19)$$

$$D_{AB} \frac{d^2 C_{AB}}{dx^2} = -k_1 C_A C_B + k_2 C_{AB} \quad (3.20)$$

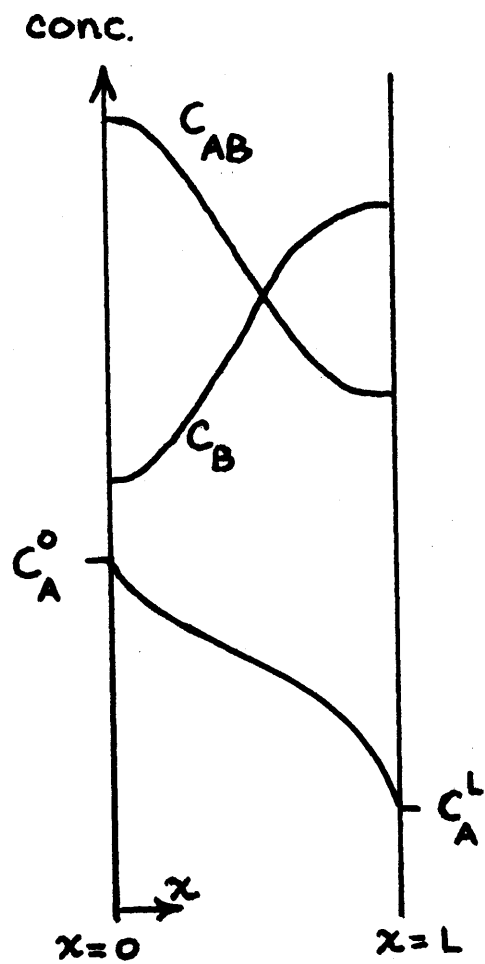


FIGURE 3.5

DIFFUSION WITH REVERSIBLE CHEMICAL REACTION IN A
ONE DIMENSIONAL FILM.

The equations are subject to the following boundary conditions

$$x = 0 \quad C_A = C_A^0 \quad (3.21)$$

$$x = L \quad C_A = C_A^L \quad (3.22)$$

$$x = 0, L \quad \frac{dC_B}{dx} = 0 \quad (3.23)$$

$$x = 0, L \quad \frac{dC_{AB}}{dx} = 0 \quad (3.24)$$

$$\int_0^L (C_B + C_{AB}) dx = C_T L \quad (3.25)$$

Boundary conditions (3.21) and (3.22) are the imposed concentrations of A at the faces of the film; boundary conditions (3.23) and (3.24) maintain the carrier species within the film, and boundary condition (3.25) is a stoichiometric constraint which is necessary because only three of the four boundary conditions given in (3.23) and (3.24) are independent (Goddard et al., 1970).

At this point the problem can be simplified by assuming $D_{AB} = D_B$. This is reasonable because the carrier molecule is generally much larger than the molecule with which it combines. Addition of equations (3.19) and (3.20) and two integrations give

$$C_B + C_{AB} = C_T \quad (3.26)$$

The total carrier concentration is a constant throughout the film when the diffusivities are equal. Substitution of

equation (3.26) into (3.18) and (3.19) gives

$$D_A \frac{d^2 C_A}{dx^2} = k_1 C_A C_B + k_2 C_B - k_2 C_T \quad (3.27)$$

$$D_B \frac{d^2 C_B}{dx^2} = k_1 C_A C_B + k_2 C_B - k_2 C_T \quad (3.28)$$

The constancy of the total flux of A at any point in the film can be utilized by taking the difference of equations (3.27) and (3.28) and integrating

$$N_A^T = -D_A \frac{dC_A}{dx} + D_B \frac{dC_B}{dx} \quad (3.29)$$

Equation (3.29) is equivalent to

$$N_A^T = -D_A \frac{dC_A}{dx} - D_{AB} \frac{dC_{AB}}{dx} \quad (3.30)$$

and the second term of the right hand side of equations (3.29) and (3.30) represents the flux of A due to the carrier species. A second integration of (3.29) yields

$$D_A C_A - D_B C_B = -N_A^T x + a_2 \quad (3.31)$$

In order to solve the problem one can either utilize equations (3.27) and (3.31) or (3.27) and (3.28), with boundary conditions (3.21), (3.22), and (3.23). In the case of thick films (film thickness L approaches infinity), the reaction approaches equilibrium. An order of magnitude analysis shows that the diffusional term of equation (3.27) will vary inversely with L^2 and consequently it will be small compared

to the reaction terms on the right hand side as $L \rightarrow \infty$. In this case the diffusion term can be neglected. Equation (3.27) will then reduce to the equilibrium relationship and use of equation (3.31) will yield the equilibrium solution of Olander (1960)

$$N_A^T = D_A \left(\frac{C_A^0 - C_A^L}{L} \right) + \frac{D_B K C_T}{L} \frac{(C_A^0 - C_A^L)}{(1 + K C_A^0)(1 + K C_A^L)} \quad (3.32)$$

where K is the equilibrium constant and is given by

$$K = \frac{k_1}{k_2}$$

Equation (3.32) can be rewritten as

$$N_A^T = D_A \left(\frac{C_A^0 - C_A^L}{L} \right) (1 + F_{eq}) \quad (3.33)$$

where F is the facilitation factor and is a maximum when the reaction is at equilibrium

$$F_{eq} = \frac{D_B K C_T}{D_A (1 + K C_A^0)(1 + K C_A^L)} \quad (3.34)$$

Equation (3.33) can also be rewritten as Ficks law with a variable effective diffusivity

$$N_A^T = \bar{D} \left(\frac{C_A^0 - C_A^L}{L} \right)$$

where $\bar{D} = D_A (1 + F)_{eq}$

The reaction is therefore to increase the effective diffusivity. In the case of a nonequilibrium reaction the form of equation (3.33) would be

$$N_A^T = D_A (1 + F) \left(\frac{C_A^0 - C_A^L}{L} \right)$$

where the facilitation factor F is the facilitation obtained for nonequilibrium conditions and is smaller than F_{eq} .

When the reaction deviates from equilibrium within the film the solution of equation (3.27) and (3.28) is difficult since the equations are nonlinear. To proceed with a solution the equations must be linearized, and solutions available in the literature differ from each other depending upon what linearization method is used and what assumptions are made. It should be noted here that formally identical problems in heat transfer have been solved earlier by Brokaw (1961). For the mass transfer problem Friedlander and Keller (1965) presented a single point linearization solution valid for small driving forces only. For large driving forces the method of matched asymptotic expansion has proven useful in giving accurate predictions of flux for near equilibrium conditions (Goddard et al., 1970; Kreuzer and Hoofd, 1970, 1972). Recently Smith et al. (1973) have presented approximate analytical solutions corresponding to a perturbation from purely physical diffusion on one hand (thin films), and from reaction equilibrium at each point within the film on the other (thick films). The two cases are developed in such a

manner that, through interpolation, solutions can be obtained for any film thickness with reasonable accuracy.

In essence, the near equilibrium solutions are developed from a perturbation from the equilibrium solution by setting

$$C_A = \bar{C}_A + \Delta C_A \quad (3.35)$$

$$C_B = \bar{C}_B + \Delta C_B \quad (3.36)$$

and substituting into the differential equations. The essential result that is obtained is the facilitation factor F which is a function of F_{eq} and the ratio of the film thickness L to the characteristic length λ . The characteristic length is a ratio of diffusional to chemical reaction effects and is given by

$$\lambda = \left[\frac{k_1 \bar{C}_A + k_2}{D_B} + \frac{k_1 k_2 C_T}{D_A (k_1 \bar{C}_A + k_2)} \right]^{-1/2} \quad (3.37)$$

for the reaction $A + B \rightleftharpoons AB$. The characteristic length also gives a measure of the thickness of the region near the boundaries of the film where departures from chemical equilibrium are largest. The dimensionless ratio L/λ is a dimensionless parameter which is similar to the "Thiele modulus" as has been pointed out by Perelson and Katchalsky (1972), and in a general context by Weisz (1973). As the ratio L/λ increases, nonequilibrium effects become negligible, and the facilitation factor F reaches the asymptotic value F_{eq} as given by

Olander (1960)

$$F \rightarrow F_{eq}, \text{ as } \frac{L}{\lambda} \rightarrow \infty \quad (3.37)$$

As L/λ approaches zero deviations from chemical equilibrium become important and the situation approaches pure Fickian diffusion so that

$$F \rightarrow 0, \text{ as } \frac{L}{\lambda} \rightarrow 0 \quad (3.38)$$

These limits can also be observed qualitatively from equations (3.27) and (3.28) by letting L approach infinity or zero. The Friedlander and Keller solution is an expansion from a single equilibrium value and provides, for $L \rightarrow \infty$, the correct asymptotic value given by (3.37) and (3.38) only for small driving forces. For a reaction of the form of (3.17) they obtained

$$1 + F = \frac{1}{1 - \frac{F_{eq}}{1 + F_{eq}} f\left(\frac{L}{\lambda}\right)} \quad (3.39)$$

where

$$f\left(\frac{L}{\lambda}\right) = 1 - \frac{2}{\left(\frac{L}{\lambda}\right)} \left[\frac{\cosh\left(\frac{L}{\lambda}\right) - 1}{\sinh\left(\frac{L}{\lambda}\right)} \right] \quad (3.40)$$

and F_{eq} , defined for a very small driving force is given by

$$F_{eq} = \frac{D_B K C_T}{D_A (1 + K C_A)^2} \quad (3.41)$$

Although for infinitesimal small driving forces $C_A^0 \approx C_A^L$ any concentration in the film can be used in (3.41) to calculate F_{eq} , the correct concentration is that at the center of the

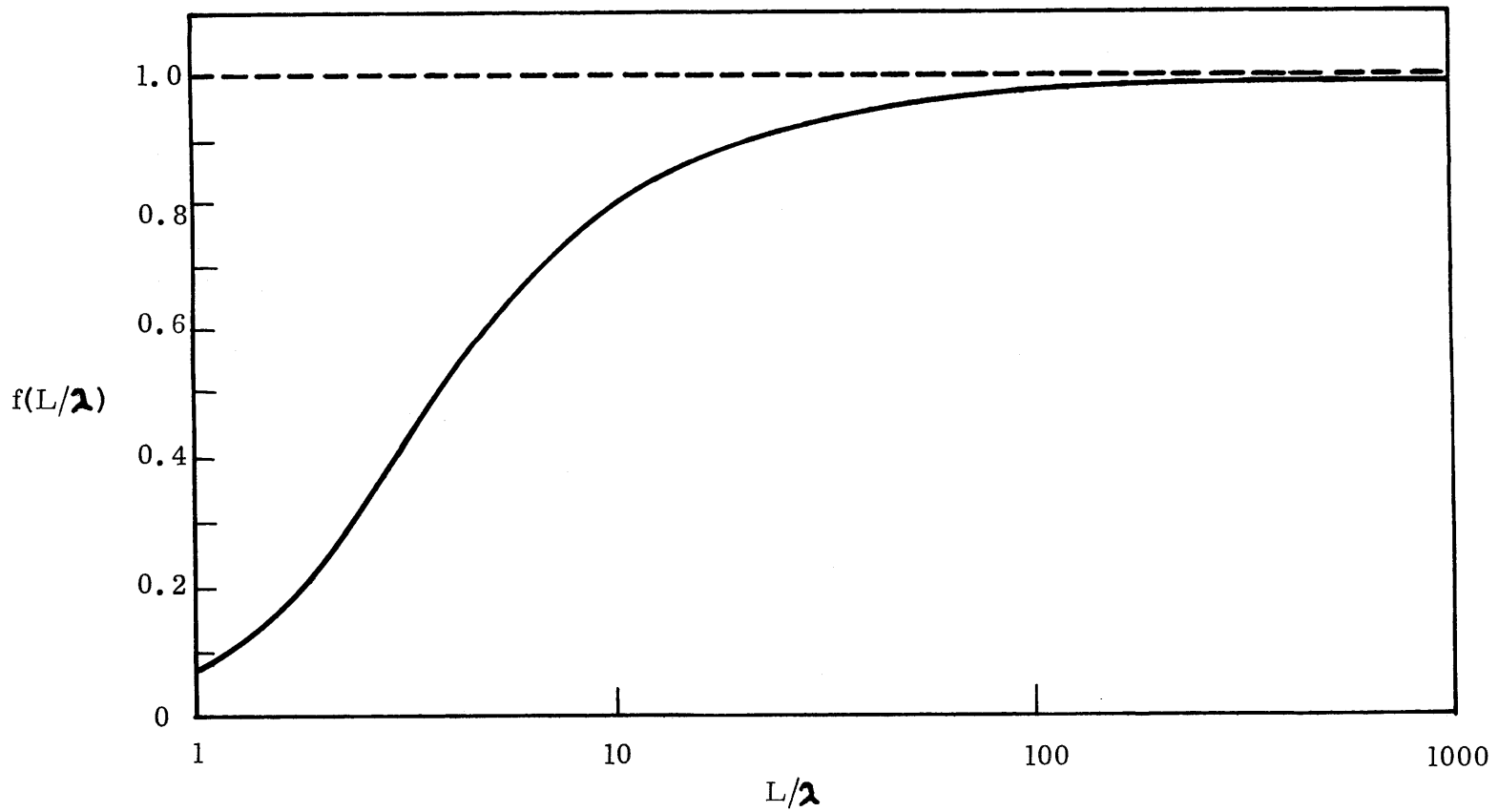


FIGURE 3.6
THE FUNCTION $f(L/\lambda)$ VERSUS L/λ

slab $C_A = (C_A^0 + C_A^L)/2$ where the reaction is at equilibrium. As L/λ varies from zero to infinity $f(L/\lambda)$ varies from zero to one as shown in Figure 3.6. For $L/\lambda > 100$ Figure 3.6 indicates that $f(L/\lambda)$ is near one and consequently from (3.39). F is near F_{eq} implying that the reaction is substantially at equilibrium throughout the film.

As mentioned previously, for large driving forces the Friedlander and Keller single point linearization technique fails to give the correct equilibrium asymptote as given by (3.34). The solutions developed for large driving forces for near equilibrium conditions given by Kreuzer and Hoofd (1970, 1972), Goddard et al. (1970), and Smith et al. (1973) provide the correct equilibrium asymptote. By comparison with numerical solutions of Kutchai et al. (1970) and Meldon (1973), Smith et al. showed that their near equilibrium solutions are of higher accuracy than those previously mentioned. In addition Smith et al. (1973) have given a thin film solution for large departures from chemical equilibrium which approaches the non-reactive asymptote (3.38) in the correct manner.

3.3 The Oxygen-Hemoglobin System

The uptake of oxygen in the lungs, and the subsequent transport to organs and tissue via the bloodstream has been an active and fascinating subject for biologists, chemists, physicists, engineers, and others. A full understanding of the respiratory process in the human body will perhaps never be at hand, but present knowledge about oxygen, and of course

carbon dioxide transport, in the body is already voluminous. Publications appear at a prodigious rate. For example, more than 250 articles per year have appeared on the hemoglobin molecule alone (Buse 1971) in the past few years. No attempt shall be made in this thesis to review the subject exhaustively. Rather selective topics will be discussed which have direct application to the work in this thesis, and even here the reader will be referred to more extensive and authoritative reviews available in the literature. A general introduction to the constituents of blood, and hemoglobin is given in Appendix B and it is assumed that the reader is familiar with the material.

3.3.1 Homogeneous Systems

The effect of hemoglobin on oxygen transport has been considered for a long time (Roughton, 1932; Klug et al., 1956; Roughton, 1959). The current interest in the facilitated transport of oxygen in hemoglobin was initiated by the experiments of Scholander (1960), Hemmingsen and Scholander (1960), and Wittenberg (1959). Scholander (1960) and Hemmingsen and Scholander (1960) reported that for identical pressure differences across a hemoglobin soaked Millipore filter, facilitated transport occurred at low oxygen tensions, where the hemoglobin is partially saturated, while at high oxygen tensions, where the hemoglobin is fully saturated, simple diffusion of oxygen occurred. Scholander (1960), and Enns (1964) proposed a collisional mechanism to explain the

facilitation of oxygen, which is analogous to the well-established phenomenon of surface diffusion of adsorbed gases on solids (Barrer, 1965). Fatt and LaForce (1961), Wang (1961), and Collins (1961) proposed that diffusion of hemoglobin was responsible for the facilitation of oxygen in the experiments of Scholander, Keller and Friedlander (1966a) opposed the collisional mechanism on the grounds that if the collisional mechanism were indeed correct the facilitated mass transfer rate of oxygen should increase as hemoglobin concentration increases because of the increased collision rate, which is contrary to their experimental results. At present the diffusional mechanism of hemoglobin facilitated transport is generally accepted, although a critical test of this mechanism has not been performed.

After the work of Scholander, Keller and Friedlander (1966a) and Wittenberg (1966) reported extensive experimental results on oxygen diffusion in hemoglobin solutions. Keller and Friedlander approximated the oxygen-hemoglobin reaction as (see Appendix B)



and in this case the characteristic length is given by

$$\lambda = \left[\frac{k_1 \bar{C}_{\text{O}_2} + k_2}{D_{\text{Hb}}} + \frac{k_1 k_2 C_{\text{T}}}{D_{\text{O}_2} (k_1 \bar{C}_{\text{O}_2} + k_2)} \right]^{-1/2} \quad (3.43)$$

For the film thickness employed in their studies (0.13 cm) and a calculated maximum characteristic length to be of order 10^{-4} cm they concluded that the use of the Olander's equilibrium approach was justified in order to interpret their data. Coupled with hemoglobin diffusivity data (Keller and Friedlander, 1966b) Keller and Friedlander concluded that they had reasonable agreement of measured oxygen flux with equilibrium facilitation theory. Wittenberg (1966) measured the oxygen facilitated flux in hemoglobin saturated Millipore filters of different thickness. Experimental results indicated that the augmented portion of the oxygen flux was inversely proportional to the length of the diffusion path at least down to a film thickness of 65 μm . For hemoglobin with very high molecular weight such as earthworm hemoglobin (MW = 2.9×10^6), Wittenberg further showed that no facilitated flux of oxygen occurred, suggesting that the diffusional mechanism is indeed correct. All of the previously mentioned work has been reviewed by Kreuzer (1970) in addition to myoglobin facilitated transport of oxygen.

In all of these results on homogeneous systems it has not been resolved what role facilitated transport plays in oxygen transport in red blood cells. The characteristic thickness of a red blood cell is between 2 and 8 μm and homogeneous facilitated transport theory predicts moderate departures from chemical equilibrium. Further it has not been established if physical parameters measured for homogeneous hemoglobin solutions can be applied to intact red blood cells.

3.3.2 Heterogeneous Systems

3.3.2.1 Inert Suspensions

As has been discussed in Appendix B, the oxygen-hemoglobin reaction can be saturated at high oxygen tensions. In order to measure the diffusion of oxygen without any chemical reaction effects in blood suspensions, Hershey and Karhan (1968) saturated thin films of sheep's blood (0.199 cm) with air at one atmosphere prior to exposing one side of the film to 760 mm Hg pressure of oxygen. Diffusion coefficients of oxygen in blood with varying hematocrits were calculated from the transient concentration change with time. Hershey and Karhan obtained for the diffusivity of oxygen in sheep's blood at 25°C

$$D = (1.98 - 0.0085 H) \times 10^{-5} \text{ cm}^2/\text{sec} \quad (3.44)$$

for a hematocrit range of zero to 45 percent. In terms of the nomenclature used for the heterogeneous media theory, the hematocrit is related to the volume fraction of the dispersed phase by

$$H = 100 \phi \quad (3.45)$$

At this point it should be mentioned that 100 percent hematocrit may not be attained for packed red blood cells. Guyton (1968) contends that about 4% of plasma remains in the extracellular space. Most researchers, however, do not correct measured hematocrits since the exact correction factor is not known accurately. The experiments by Hershey and Karhan can be

criticized on at least two points. First the oxygen diffusion studies were made with horizontal films in which case the red blood cell sedimentation in the direction of the oxygen transport may have affected the concentration versus time measurement. Second, prior to experiment, the blood samples were equilibrated by directly bubbling air into the blood sample for one hour. Such a procedure can cause considerable hemolysis of the sample.

Stein et al. (1971) measured the effective steady state diffusion coefficient of oxygen in saturated suspensions of human red blood cells in gelled agar with hematocrits varying from 0 to 100% at 25°C. Utilizing the measurement made for packed red blood cells ($H = 100$), Stein et al. obtained good agreement with Maxwell's equation for $K_d = 0.46$. By working with agar, Stein et al. eliminated the problem of sedimentation. At the same time the introduction of agar and consequent gelling may have affected red blood cell properties.

3.3.2.2 Reactive Suspensions

3.3.2.2.1 Experimental Work

During the course of this thesis several publications appeared on the diffusion of oxygen in unsaturated packed red blood cells. Moll (1969) measured the oxygen transport in human red blood cells smeared into thin sheets of porous nylon or cellulose paper at 37°C in the absence or presence of carbon monoxide. Moll measured higher oxygen transfer rates, on the average 64 percent, in the absence of CO than in the

presence of CO. On assuming equilibrium inside the red blood cell, Moll calculated an average oxyhemoglobin saturation difference of 82%. Substantial hemolysis occurred during these experiments (maximum 25 percent), and the use of nylon or cellulose supports causes the system to be effectively a three component heterogeneous system: red blood cells, plasma, support material. It must therefore be concluded that Moll's experiments are in no sense conclusive with regards to the occurrence of facilitated transport in red blood cells.

Kutchai and Staub (1969) measured oxygen transport rates in films of packed human red blood cells supported on stainless steel screens in the absence and presence of CO at 21.7°C. Facilitated transport of oxygen was measured in the absence of CO over a wide range of driving forces, with minimal hemolysis of the sample (average less than one percent). The amount of hemoglobin facilitated oxygen transport was equivalent to that measured in hemoglobin films of equivalent thickness and total hemoglobin concentration maintained in the same support at 21.2°C. Kutchai and Staub concluded that the reaction inside the red blood cell is at equilibrium. Kutchai and Staub measured hemoglobin concentrations of the packed red bloods of order of 30 gr/100 ml. Since the concentration inside the red blood cell is from 32 to 34 gr/100 ml (Guyton, 1968) as much as 10% of the packed red blood cell samples that Kutchai and Staub used may have been plasma.

Keller (1969) in an article reporting on additional data obtained by Stein (1968) observed no facilitation of

oxygen in red blood cell suspensions. It is believed by this author, however, that these results may be erroneous and they will be discussed further in a later part of this thesis (Results and Discussions).

The effect of the red cell membrane on the mass transfer rate has been investigated for some time and contradictory experimental results have been reported. Roughton (1927) measured the rate of uptake of oxygen and carbon monoxide by flowing red blood cell suspensions, the observations being made by means of the rapid reaction technique (Hartridge and Roughton, 1923). In comparison to dilute hemoglobin solutions of the same total hemoglobin concentration, the rate of oxygen uptake of the red blood cell suspensions was much slower. Roughton (1927, 1932) suggested that the difference in oxygen uptake was due to the red cell membrane resistance. Kreuzer and Yahr (1960) compared the oxyhemoglobin saturation with time of thin films of packed red blood cells and concentrated hemoglobin solutions exposed to oxygen. No differences were observed in the oxygen uptake (saturation) of the stagnant films of red blood cells versus the films of hemoglobin solutions of equal hemoglobin concentrations. Kreuzer and Yahr concluded that the red blood cell membrane offered little resistance to mass transfer in direct contradiction to the suggestion of Roughton. The previous work of Stein et al. (1971) and Kutchai and Staub (1969) support the results of Kreuzer and Yahr, and the present consensus appears to be that membrane resistance is not

significant. This does not mean that the membrane permeability ($P_m = D_m \alpha_m$) is much higher than that of the red blood cell interior. The permeability is probably of the same order of magnitude, but the membrane is very much thinner than RBC radius.

3.3.2.2.2 Theoretical Developments

Little theoretical work has been published on the problem of diffusion with reversible chemical reaction in heterogeneous media. La Force and Fatt (1962) presented a technique to estimate steady state flux of oxygen through whole blood which is developed from the assumption that this flux is greater than that through a system of alternate hemoglobin and plasma layers and less than that through a parallel arrangement of hemoglobin and plasma layers. La Force and Fatt assumed that the oxygen-hemoglobin reaction in the hemoglobin layers (the thickness of order of red blood cell size) was at equilibrium. The theoretical work done on homogeneous solutions suggests that the reaction is in the nonequilibrium regime for these thicknesses so that a better assumption for the lower bound of expected oxygen flux would be a system of alternate inert hemoglobin and plasma layers. Fatt and La Force (1963) also presented an equation that was a modification of the theoretical model for inert heterogeneous media presented by Meredith and Tobias (1962) and is given by equation (3.12). Instead of using the dispersed phase permeability P_d , Fatt and La Force replaced it by the

equilibrium homogeneous theory permeability $P_d(1 + F_{eq})$. Although at equilibrium conditions this is indeed the correct dispersed phase permeability (as will be shown later in the theory), Fatt and La Force gave no proof of the final relationship used. The relationship further does not consider nonequilibrium effects, and in addition, as has been mentioned before, the relationship of Meredith and Tobias fails at high volume fractions of the dispersed phase. (see figure 3.3)

3.3.3 Physico-Chemical Parameters

In order to apply the carrier-facilitated transport theory as developed by such authors as Friedlander and Keller (1965) and Smith et al. (1973) for a particular physico-chemical system, kinetic and thermodynamic parameters need to be known for the system of interest. Such parameters are readily available for the oxygen-hemoglobin system.

3.3.3.1 Oxygen and Hemoglobin Diffusivities

Kreuzer (1970) in his excellent review on facilitated diffusion of oxygen has reviewed the data on oxygen diffusivity and hemoglobin diffusivity in hemoglobin solutions. Kreuzer (1950, 1953), Pircher (1952), Keller and Friedlander (1966a), and Goldstick and Fatt (1970) have reported values for the oxygen diffusivity in hemoglobin solutions from a concentration of 0 gr/100 ml to about 54 gr/100 ml (see Figure 3.7). The data of Goldstick and Fatt (1970) is presently considered to be the most accurate data. From a hemoglobin concentration of

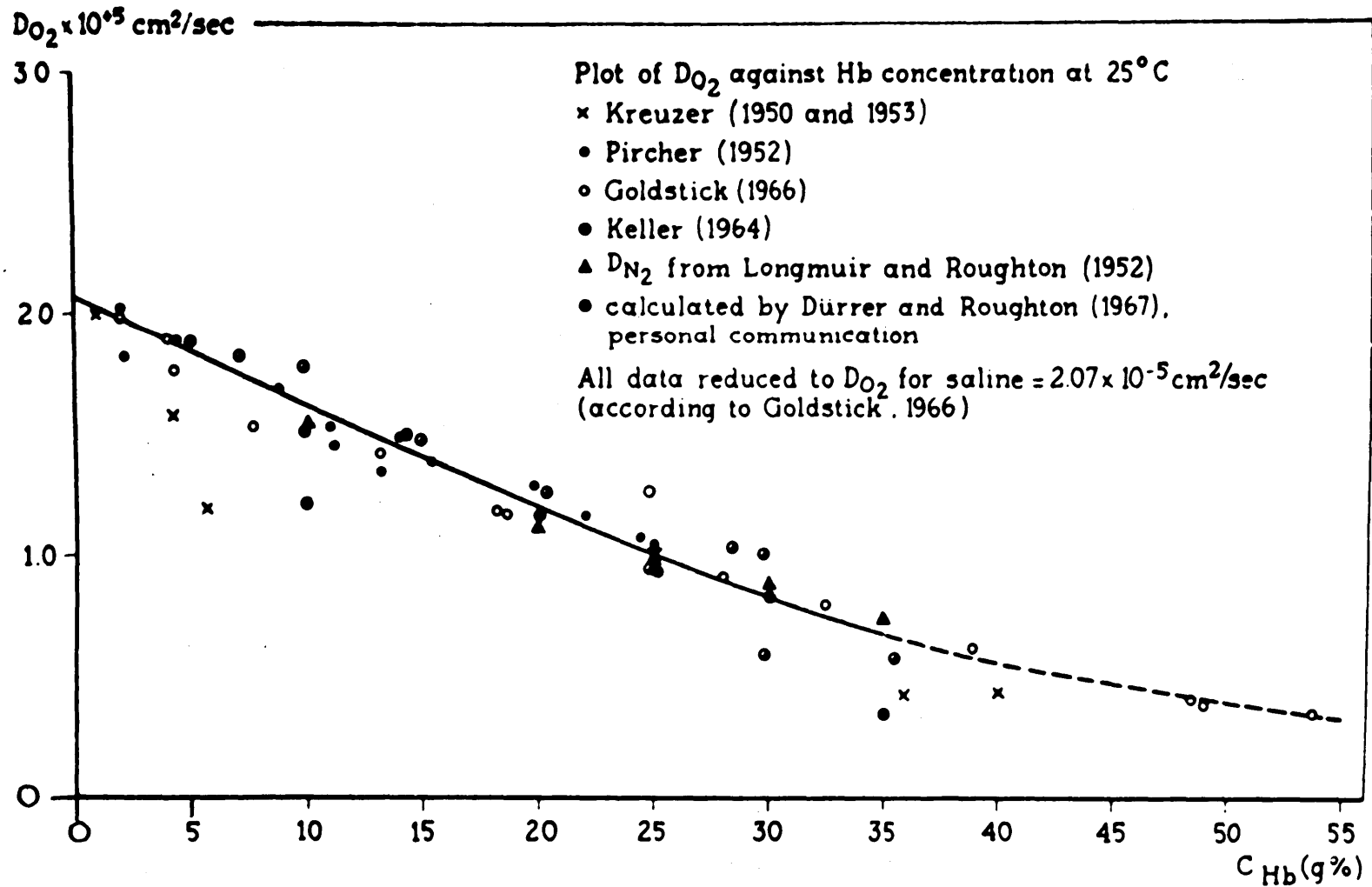


FIGURE 3.7

PLOT OF AVAILABLE DATA FOR O_2 DIFFUSION COEFFICIENT IN Hb SOLUTIONS AT 25 C.

(From Kreuzer 1970, with permission)

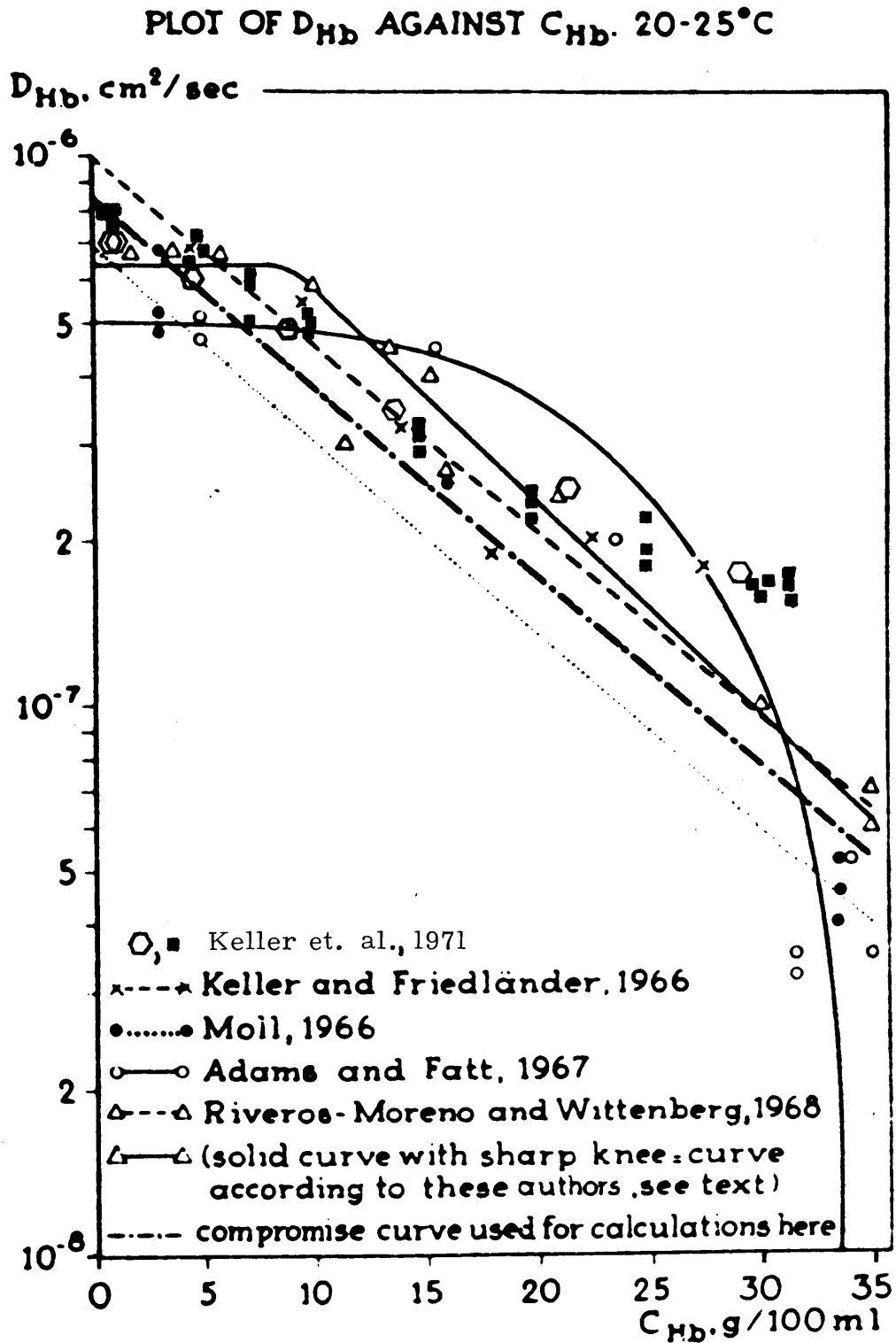


FIGURE 3.8

PLOT OF AVAILABLE DATA FOR Hb DIFFUSION COEFFICIENT IN Hb SOLUTIONS AGAINST Hb CONCENTRATION AT 20-25 C. (Taken in part from Kreuzer (1970))

zero gr/100 ml to physiological concentrations in the red blood cell (32-34 gr/100 ml) the diffusion coefficient of oxygen decreases by approximately a factor of three.

The diffusivity of hemoglobin in hemoglobin solutions versus hemoglobin concentration is shown in Figure 3.8. There appears to be reasonable agreement for concentrations up to 25 gr/100 ml but there is considerable disagreement at higher hemoglobin concentrations. For example the most recent data reported by Riveros-Morenos and Wittenberg (1972) and Keller et al. (1971) shows a variation of approximately 100% at near physiological concentrations. Kreuzer (1970) in his review article proposed a compromise curve which he used in subsequent papers on the theory of facilitated transport (Kreuzer and Hoofd, 1970, 1972).

3.3.3.2 Kinetic Rate Parameters

The reaction rate of hemoglobin ligands has received considerable attention from researchers because they have been able to utilize measured reaction rate parameters to deduce much information about the structure-function behavior of hemoglobin and on the mechanisms of reaction. At present, however, no set of data has correlated in fine detail with any reaction scheme. The early work by Hartridge and Roughton (1925) showed that the combination of oxygen with hemoglobin could be approximated by a second-order reaction, with a rate constant for the overall reaction (k_1) of about 3.0×10^6 moles/l-sec which was not influenced significantly by values

of the pH between 7 and 10. The oxygen dissociation reaction was also studied by Hartridge and Roughton (1923) who used dithione to cause the reaction $\text{HbO}_2 \rightarrow \text{Hb} + \text{O}_2$ to go to completion, and found the dissociation reaction to be first order in HbO_2 ($k_2 \approx 40 \text{ sec}^{-1}$). Later in a series of experiments Gibson and Roughton (1957a,b,c) have attempted to fit the kinetics of oxygen association and dissociation to the four step scheme of Adair (1925). These results have been summarized in a review by Gibson (1959). Recently Gibson (1970) has obtained a set of rate parameters for the four consecutive association and dissociation reaction that also gave an adequate fit of oxygen-hemoglobin saturation curve at pH 7 and at 20-21°C. As has been mentioned in Appendix A the Adair scheme remains an approximation to the true and unknown reaction scheme. It is not surprising, that the simplified one-step scheme still enjoys considerable use because of its simplicity and great utility in mathematical modeling of processes in the oxygen-hemoglobin system.

3.3.3.3 Solubility Coefficient of Oxygen

The solubility coefficient of oxygen in water and various physiological fluids is available at a variety of temperatures. Table 3.3 reports the Bunsen solubility coefficient of oxygen (milliliters of gas at STP dissolved per milliliter of water at 1 atm pressure) for water, isotonic saline, plasma, and whole blood obtained from the tabulations of Altman and Dittmer (1971). It is interesting to note that

the oxygen solubilities in plasma, isotonic saline, and whole blood are virtually the same at a given temperature.

Apparently the introduction of hemoglobin has little effect upon the physical solubility of the total medium, but it increases the solubility of O_2 in water to make up for the excluded volume of hemoglobin. The physical solubility of O_2 in red blood cells can be calculated from Table 3.3 since

$$\alpha_{O_2, \text{blood}} = \phi_{\text{RBC}} \alpha_{O_2, \text{RBC}} + (1 - \phi_{\text{RBC}}) \alpha_{O_2, \text{plasma}}$$

and where

$$\phi_{\text{RBC}} = 0.45$$

For example the Bunsen solubility coefficients of oxygen inside the red blood cells at 25° and 37°C are (cc(STP)/cc/atm)

$$\alpha_{O_2, \text{RBC}} = 0.0276 \quad \text{at } T = 25^\circ\text{C}$$

$$\alpha_{O_2, \text{RBC}} = 0.0236 \quad \text{at } T = 37^\circ\text{C}$$

which is not very different from the oxygen solubility of isotonic saline, and in fact is slightly higher. This is consistent with experimental results obtained by Sendroy et al. (1934) who reported higher oxygen solubility constants for ox blood cells than that for ox plasma at 37°C .

TABLE 3.3
BUNSEN SOLUBILITY COEFFICIENT OF OXYGEN
IN VARIOUS FLUIDS CC(STP)/CC/ATM

Temp °C	Medium			
	Water	Isotonic Saline	Plasma (Human)	Whole Blood (Human)
17	0.03283	0.03170	0.0290	0.0303
21	0.03044	0.02931	0.0273	0.0282
25	0.02831	0.02718	0.0257	0.0265
29	0.02649	0.02536	0.0242	0.0249
33	0.02507	0.02394	0.0226	0.0235
37	0.02386	0.02273	0.0214	0.0223

3.4 Discussion

The previous sections have dealt with theoretical and experimental developments for diffusion with or without reversible chemical reaction in homogeneous and heterogeneous systems. Special emphasis has been placed on the oxygen-hemoglobin system. Several conclusions and comments can be drawn from this review.

- i) Theoretical models for diffusion in inert heterogeneous media appear to be well-developed for moderate permeability differences between dispersed and continuous phases. As far as is known, no extensive data has been obtained on the effective permeability of heterogeneous media.
- ii) Theoretical models for diffusion with reversible chemical reaction in homogeneous media is now well developed.
- iii) Experimental results obtained on the facilitated transport of oxygen in hemoglobin solutions tend to indicate that the diffusive mechanism is responsible for the increased mass transfer rate. Reasonable agreement exists between experimental results and equilibrium facilitated mass transfer theory.
- iv) Experimental data on facilitated mass transfer in heterogeneous media is limited.

- v) No theoretical developments for diffusion with reversible chemical reaction in heterogeneous media have been made that take into account deviations from equilibrium conditions.

The objective of this thesis is to give an improved quantitative understanding of mass transport with and without reversible chemical reaction in heterogeneous media. The program presented in this thesis consists of two phases. First a theoretical model is developed for diffusion with reversible chemical reaction in heterogeneous media. In the second phase experimental results have been obtained on mass transport in reactive and inert systems and the results compared with the developed theory.

4. DEVELOPMENT OF THEORETICAL MODELS

4.1 General Mathematical Formulation of the Problem

- 4.1.1 Outside the Sphere
- 4.1.2 Inside the Sphere

4.2 Impermeable Carrier Model

- 4.2.1 Solution for the Concentrations for the Species Inside and Outside the Sphere
- 4.2.2 Application of the Model to Other Cases
- 4.2.3 Effective Permeability for a Suspension of Spheres
- 4.2.4 Effective Permeability for Other Heterogeneous Media

4.3 Permeable Carrier Model

- 4.3.1 Solution for the Concentrations for the Species Inside and Outside the Sphere
- 4.3.2 Application of the Model to Other Cases
- 4.3.3 Effective Permeability for a Suspension of Spheres
- 4.3.4 Effective Permeability for Other Heterogeneous Systems

4.4 Adair Reaction Scheme Inside the Dispersed Phase - No Reaction in the Continuous Phase

4. DEVELOPMENT OF THEORETICAL MODELS

The types of heterogeneous media considered here are those previously shown in Figure 2.2. The theoretical framework developed here is easily extended to other situations such as, for example, a reactant in a spherical shell. The same approach employed so successfully by Maxwell and later Fricke will be utilized here. First a solution is obtained for the concentration field of diffusing species both inside and outside a single sphere in an infinite medium. With this in hand the average effective permeability of a suspension of spheres may be obtained by utilizing a technique developed by Maxwell. Two models will be considered, the impermeable model and the permeable model. The impermeable carrier model refers to the situation in which the carrier molecules cannot penetrate the continuous-dispersed phase boundary, as is shown by case 6, Figure 2.2. Mobile carrier species are present both in the dispersed and continuous phase, but these species are constrained to remain within their respective phases. For the permeable carrier model, the carrier can diffuse from one phase to the other as is shown in case 7, Figure 2.2. The two cases presented here are for reactions inside and outside the dispersed phase, but it will be shown later that the equations derived here will be applicable to the other cases considered in Figure 2.2. Finally the mathematical technique employed here will be utilized to solve for the problem of an Adair type reaction scheme in the dispersed phase with no reaction in the continuous phase.

4.1 General Mathematical Formulation of the Problem

Because the permeable and impermeable model are similar in mathematical form, the problem will be initially developed in a general way so as to be valid for both models. Consider a single sphere, of radius a and permeability P_d , immersed in an infinite medium, of permeability P_c , which has a constant uniform mass flux of the diffusing species A imposed at large distances from the center of the sphere (see Figure 4.1). A single step reaction with carrier B and B' occurs in the continuous and discontinuous phase respectively



as is shown in Figure 4.1. Primes are used here to denote parameters inside the sphere. Reactions (4.1) and (4.2) are chosen as an example only, and the theoretical development can be extended to other reaction schemes. The steady state differential mass continuity equations in spherical coordinates for species A , B , and AB outside the sphere, and A' , B' , AB' inside the sphere are:

outside the sphere,

$$D_i \left[\frac{1}{r^2} \frac{\partial}{\partial r} \left(r^2 \frac{\partial C_i}{\partial r} \right) + \frac{1}{r^2 \sin \theta} \frac{\partial}{\partial \theta} \left(\sin \theta \frac{\partial C_i}{\partial \theta} \right) \right] = \delta [k_1 C_A C_B - k_2 C_{AB}] \quad (4.3)$$

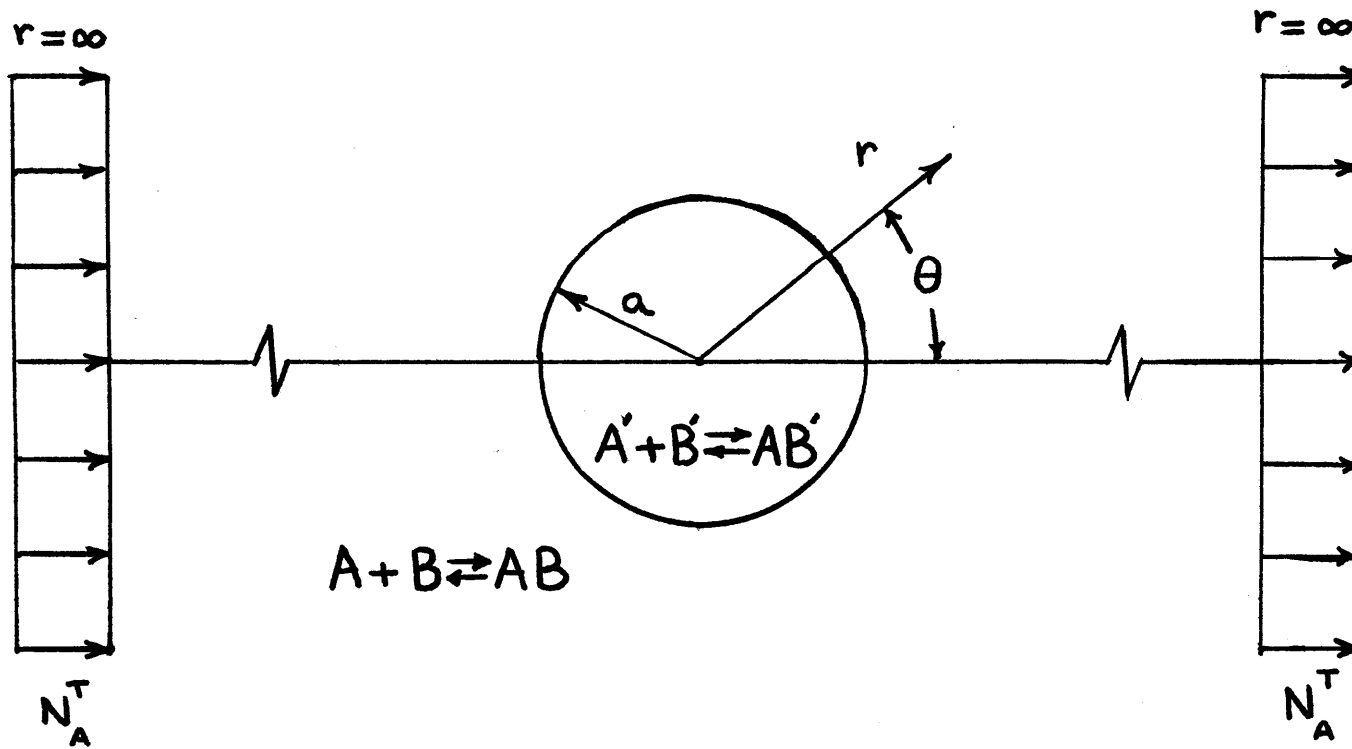


FIGURE 4.1

REACTING SPHERE IN A INFINITE REACTING MEDIUM.

$$\begin{aligned} \text{where: } i = A, B, \quad \delta = +1 \\ i = AB, \quad \delta = -1 \end{aligned} \quad (4.4)$$

inside the sphere,

$$D_i' \left[\frac{1}{r^2} \frac{\partial}{\partial r} \left(r^2 \frac{\partial C_i'}{\partial r} \right) + \frac{1}{r^2 \sin \theta} \frac{\partial}{\partial \theta} \left(\sin \theta \frac{\partial C_i'}{\partial \theta} \right) \right] = \delta [k_1' C_A' C_B' - k_2' C_{AB}'] \quad \dots \dots \dots (4.5)$$

$$\begin{aligned} \text{where: } i = A', B', \quad \delta = +1 \\ i = AB', \quad \delta = -1 \end{aligned} \quad (4.6)$$

The differential mass continuity equations inside and outside the sphere, and the associated boundary conditions for both the permeable and impermeable model are shown in a schematic manner in Figure 4.2. Beside the fact that the permeable and impermeable model have identical mass conservation equations, the boundary conditions at $r = 0$ and $r = \infty$ are the same. The boundary conditions at the phase boundary ($r = a$) are of course different, as expected. The problem will first be developed in a general way utilizing equations (4.3) through (4.6) and the boundary conditions at $r = 0$ and $r = \infty$. Once the problem is formulated the specific boundary conditions at $r = a$ for the specific model will be introduced.

If it is assumed that the diffusivities of the carrier and carrier-complex species within each phase are equal

$$D_{AB} = D_B \quad (4.7a)$$

and

$$D_{AB}' = D_B' \quad (4.7b)$$

Outside Sphere

$$D_i \left[\frac{1}{r^2} \frac{\partial}{\partial r} \left(r^2 \frac{\partial C_i}{\partial r} \right) + \frac{1}{r^2 \sin \theta} \frac{\partial}{\partial \theta} \left(\sin \theta \frac{\partial C_i}{\partial \theta} \right) \right] = [k_1 C_A C_B - k_2 C_{AB}]$$

$$\begin{aligned} \text{where: } i = A, B & \quad \delta = +1 \\ i = AB & \quad \delta = -1 \end{aligned}$$

Inside Sphere

$$D_i' \left[\frac{1}{r^2} \frac{\partial}{\partial r} \left(r^2 \frac{\partial C_i'}{\partial r} \right) + \frac{1}{r^2 \sin \theta} \frac{\partial}{\partial \theta} \left(\sin \theta \frac{\partial C_i'}{\partial \theta} \right) \right] = [k_1' C_A' C_B' - k_2' C_{AB}']$$

$$\begin{aligned} \text{where: } i = A', B' & \quad \delta = +1 \\ i = AB' & \quad \delta = -1 \end{aligned}$$

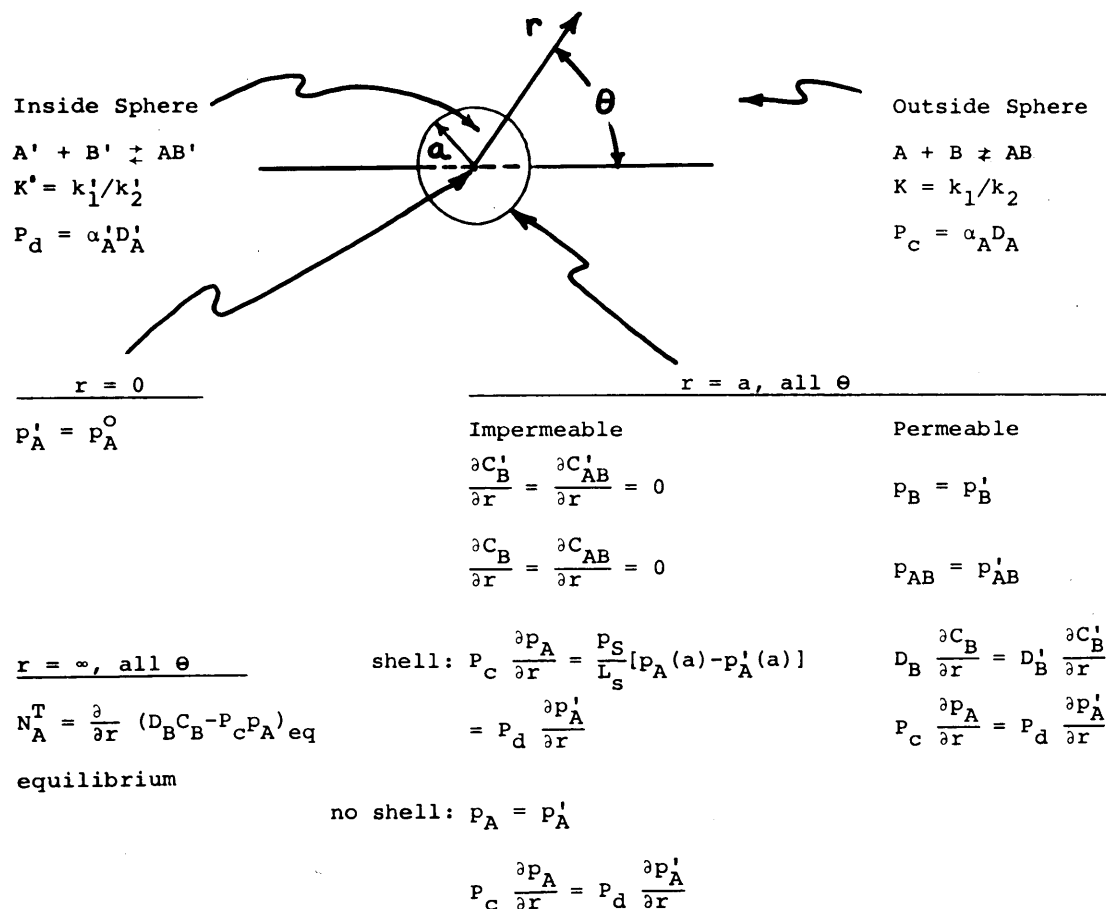


FIGURE 4.2. SINGLE REACTING SPHERE IN A REACTING CONTINUOUS MEDIUM.

it can be shown by a procedure entirely analogous to that by which equation (3.26) was obtained that the total carrier concentration inside and outside the sphere is a constant so that:

outside the sphere,

$$C_B + C_{AB} = C_T \quad (4.8)$$

inside the sphere,

$$C'_B + C'_{AB} = C'_T \quad (4.9)$$

Introduction of equations (4.8) and (4.9) into the mass conservation equations will yield only two independent mass conservation equations in each phase. Retaining the equations for A and B outside the sphere, and A' and B' inside the sphere, and subtraction of the equations for B from A, and B' from A' gives:

outside the sphere,

$$P_c \left[\frac{1}{r^2} \frac{\partial}{\partial r} \left(r^2 \frac{\partial p_A}{\partial r} \right) + \frac{1}{r^2} \frac{1}{\sin \theta} \frac{\partial}{\partial \theta} \left(\sin \theta \frac{\partial p_A}{\partial \theta} \right) \right] = k_1 \alpha_A p_A C_B - k_2 C_T + k_2 C_B \quad \dots \dots \dots (4.10)$$

$$\frac{\partial}{\partial r} \left[r^2 \frac{\partial}{\partial r} (D_B C_B - P_c p_A) \right] + \frac{1}{\sin \theta} \frac{\partial}{\partial \theta} \left[\sin \theta \frac{\partial}{\partial \theta} (D_B C_B - P_c p_A) \right] = 0 \quad \dots \dots \dots (4.11)$$

inside the sphere,

$$P_d \left[\frac{1}{r^2} \frac{\partial}{\partial r} \left(r^2 \frac{\partial p'_A}{\partial r} \right) + \frac{1}{r^2} \frac{1}{\sin \theta} \frac{\partial}{\partial \theta} \left(\sin \theta \frac{\partial p'_A}{\partial \theta} \right) \right] = k'_1 \alpha'_A p'_A C'_B - k'_2 C'_T + k'_2 C'_B \quad \dots \dots \dots (4.12)$$

$$\frac{\partial}{\partial r} \left[r^2 \frac{\partial}{\partial r} (D'_B C'_B - P_d p'_A) \right] + \frac{1}{\sin \theta} \frac{\partial}{\partial \theta} \left[\sin \theta \frac{\partial}{\partial \theta} (D'_B C'_B - P_d p'_A) \right] = 0 \quad \dots \dots \dots (4.13)$$

where the permeability is again the product of diffusivity times the solubility. Since in this work the transferred species A will be a gas the above equations were cast in terms of the partial pressure of A and Henry's law was used

$$C_A = \alpha_A p_A \quad (4.14)$$

$$C'_A = \alpha'_A p'_A \quad (4.15)$$

Henry's law is applicable because the concentration of dissolved gasses under normal physiological conditions is small.

The equations inside the sphere and outside the sphere are nonlinear and must be linearized in order to be solved analytically. For a small sphere in a medium the partial pressure drop of A (driving force) across an individual sphere usually is small so that the single point linearization technique of Friedlander and Keller should be applicable. Like Friedlander and Keller (1965) the equations are linearized about a single point by neglecting second order terms. An obvious choice is the center concentration where the reaction rate is zero and equilibrium exists so that (as a consequence of the technique):

outside the sphere

$$C_B^0 = \frac{k_2 C_T}{k_1 \alpha_A p_A^0 + k_2} \quad (4.16a)$$

inside the sphere

$$C_B^{0'} = \frac{k_2' C_T'}{k_1' \alpha_A' p_A^0 + k_2'} \quad (4.16b)$$

To expand the concentrations as small deviations around the center equilibrium conditions, one defines:

outside the sphere,

$$p_A = p_A^0 + \Delta p_A \quad (4.17)$$

$$C_B = C_B^0 + \Delta C_B \quad (4.18)$$

and inside the sphere,

$$p_A' = p_A^0 + \Delta p_A' \quad (4.19)$$

$$C_B' = C_B^{0'} + \Delta C_B' \quad (4.20)$$

Substitution of equations (4.17)-(4.20) into (4.10) to (4.13), deletion of second order terms, and use of the equilibrium relationships (4.16) yields:

outside the sphere,

$$P_c \left[\frac{1}{r^2} \frac{\partial}{\partial r} \left(r^2 \frac{\partial \Delta p_A}{\partial r} \right) + \frac{1}{r^2 \sin \theta} \frac{\partial}{\partial \theta} \left(\sin \theta \frac{\partial \Delta p_A}{\partial \theta} \right) \right] =$$

$$(k_1 \alpha_A p_A^0 + k_2) \Delta C_B + k_1 \alpha_A C_B^0 \Delta p_A \quad (4.21)$$

$$\frac{\partial}{\partial r} \left[r^2 \frac{\partial}{\partial r} (D_B \Delta C_B - P_c \Delta p_A) \right] + \frac{1}{\sin \theta} \frac{\partial}{\partial \theta} \left[\sin \theta \frac{\partial}{\partial \theta} (D_B \Delta C_B - P_c \Delta p_A) \right] = 0$$

..... (4.22)

and inside the sphere,

$$P_d \left[\frac{1}{r^2} \frac{\partial}{\partial r} \left(r^2 \frac{\partial \Delta p'_A}{\partial r} \right) + \frac{1}{r^2 \sin \theta} \frac{\partial}{\partial \theta} \left(\sin \theta \frac{\partial \Delta p'_A}{\partial \theta} \right) \right] =$$

$$(k'_1 \alpha'_A p_A^0 + k'_2) \Delta C'_B + k'_1 \alpha'_A C_B^0 \Delta p'_A \quad (4.23)$$

$$\frac{\partial}{\partial r} \left[r^2 \frac{\partial}{\partial r} (D'_B \Delta C'_B - P_d \Delta p'_A) \right] + \frac{1}{\sin \theta} \frac{\partial}{\partial \theta} \left[\sin \theta \frac{\partial}{\partial \theta} (D'_B \Delta C'_B - P_d \Delta p'_A) \right] = 0$$

..... (4.24)

Investigation of the physics of the problem suggests a θ dependency of the form of $\cos \theta$ since the problem is symmetric (similar to the Maxwell problem, Appendix A). At large distances away from the sphere the species must approach equilibrium conditions. Noting that $dC_B = d(\Delta C_B)$ the relationship

$$[d \Delta C_B]_{\text{equilibrium}} = - \frac{k_1 k_2 \alpha_A C_T}{(k_1 \alpha_A p_A^0 + k_2)^2} [d \Delta p_A]_{\text{equilibrium}}$$

..... (4.25)

should be satisfied at $r = \infty$ for any solution for Δp_A and ΔC_B .

From equation (3.41) equation (4.25) can conveniently be

rewritten as follows

$$[d \Delta C_B]_{\text{equilibrium}} = - \frac{P_C}{D_B} F_{\text{eq}} [d \Delta p_A]_{\text{equilibrium}} \dots \dots \dots (4.26)$$

where F_{eq} is defined at a point by equation (3.41)

$$F_{\text{eq}} = \frac{D_B k_1 k_2 C_T \alpha_A}{P_C (k_1 + k_2 \alpha p_A^0)^2}$$

In addition as $r \rightarrow \infty$ the flux of A is a constant, N_A^T . From homogeneous facilitation theory the total flux of A is therefore

$$-P_C (1 + F_{\text{eq}}) \frac{\partial \Delta p_A}{\partial r} = N_A^T \cos \theta \text{ as } r \rightarrow \infty \quad (4.27)$$

This suggests a solution for the outside concentrations of the form

$$\Delta p_A = - \frac{N_A^T}{P_C (1 + F_{\text{eq}})} [r - af(r)] \cos \theta \quad (4.28)$$

$$\Delta C_B = \frac{F_{\text{eq}} N_A^T}{D_B (1 + F_{\text{eq}})} [r + ag(r)] \cos \theta \quad (4.29)$$

with the restriction that

$$\begin{aligned} f &\rightarrow 0 && \text{as } r \rightarrow \infty \\ g &\rightarrow 0 && \text{as } r \rightarrow \infty \end{aligned}$$

in order to satisfy (4.25). Inside the sphere let

$$\Delta p_A' = H(r) \cos \theta \quad (4.30)$$

$$D_B \Delta C_B' - P_d \Delta p_A' = G(r) \cos \theta \quad (4.31)$$

with the restriction that

$$\begin{aligned} H(0) &= 0 \\ G(0) &= 0 . \end{aligned}$$

Equations (4.28) through (4.31) are quite general in terms of the dependency on r , but they satisfy symmetry conditions on θ . In addition $\Delta p'_A$ and $\Delta C'_B$ should vanish at $r = 0$ since equilibrium conditions exist at the center of the sphere. Equations for Δp_A and ΔC_B also satisfy the equilibrium condition and the constant flux boundary condition for $r \rightarrow \infty$.

The problem now has been reduced to the solution of four differential equations, two outside the sphere and two inside the sphere, and the mathematical form of these solutions has been deduced. Additional general mathematical formulation can be done before considering specific boundary conditions for each model. In fact the dependency of $f(r)$, $g(r)$, $H(r)$ and $G(r)$ can be obtained exactly, and these will apply to both the impermeable and permeable models.

4.1.1 Outside the Sphere

Outside the sphere we have the differential equations (4.21) and (4.22) and the solutions for these equations given by (4.28) and (4.29). Substitution of the formulas for ΔC_B and Δp_A into (4.22) yields

$$\frac{\partial}{\partial r} [r^2 (F_{eq} g' - f')] - 2(F_{eq} g - f) = 0 \quad (4.32)$$

where $f' = \frac{\partial f}{\partial r}$, $g' = \frac{\partial g}{\partial r}$

The form of (4.32) yields a solution that relates f and g

$$F_{eq}g - f = A \frac{a^2}{r^2} \quad (4.33)$$

where A is a constant whose value will be determined from the boundary conditions at $r = a$. Substitution of (4.28) and (4.29) into (4.21) gives

$$\begin{aligned} \frac{1}{r^2} [r^2 f'' + 2rf' - 2f] = & \left(\frac{k_1 \alpha_A p_A^0 + k_2}{D_B} \right) F_{eq}g + \\ & + \left(\frac{k_1 \alpha_A C_B^0}{P_C} \right) f + \left[\frac{k_1 \alpha_A p_A^0 + k_2}{D_B} F_{eq} - \frac{k_1 \alpha_A C_B^0}{P_C} + \frac{k_2}{D_B} F_{eq} \right] \frac{r}{a} \\ & \dots \dots \dots (4.34) \end{aligned}$$

Substitution of (4.33) into (4.34) yields

$$r^2 f'' + 2rf' - \left[2 + \frac{r^2}{\lambda^2} \right] f = \left(\frac{k_1 \alpha_A p_A^0 + k_2}{D_B} \right) a^2 A \quad (4.35)$$

where the characteristic length λ is again given by

$$\frac{1}{\lambda^2} = \left(\frac{k_1 \alpha_A p_A^0 + k_2}{D_B} \right) + \frac{k_1 \alpha_A k_2 C_T}{P_C (k_1 \alpha_A p_A^0 + k_2)} \quad (4.36)$$

The particular solution for f for equation (4.35) is straightforward

$$f_{part} = - \left(\frac{k_1 \alpha_A p_A^0 + k_2}{D_B} \right) \lambda^2 a^2 A / r^2 \quad (4.37)$$

The homogeneous equation that remains is

$$r^2 f'' + 2rf' - 2 \left[2 + \frac{r^2}{\lambda^2} \right] f = 0 \quad (4.38)$$

Equation (4.38) is a Bessel equation whose solution is (Mickley et al., 1957)

$$f_{\text{homo}} = K_1 r^{-1/2} [C_1 I_{3/2}(\frac{r}{\lambda}) + C_2 I_{-3/2}(\frac{r}{\lambda})] \quad (4.39)$$

where $I_p(Z)$ is a modified Bessel function of the first kind of order p . Since from equation (4.28) $f \rightarrow 0$ as $r \rightarrow \infty$ it follows that

$$C_1 = -C_2$$

so that f becomes

$$f = - \left(\frac{k_1 \alpha_p^0 + k_2}{D_B} \right) \lambda^2 a^2 A / r^2 + K_1 \left(\frac{r}{a} \right)^{-1/2} [I_{3/2}(\frac{r}{\lambda}) - I_{-3/2}(\frac{r}{\lambda})] \dots\dots\dots (4.40)$$

where K_1 is a constant to be determined from the boundary conditions at $r = a$. Since (Abramowitz and Stegun, 1968)

$$I_{3/2}(Z) = \frac{-\frac{1}{Z} \frac{\sinh Z}{Z} + \frac{\cosh Z}{Z}}{\sqrt{\frac{1}{2} \frac{\pi}{Z}}} \quad (4.41)$$

and

$$I_{-3/2}(Z) = \frac{\frac{\sinh Z}{Z} - \frac{1}{Z} \frac{\cosh Z}{Z}}{\sqrt{\frac{1}{2} \frac{\pi}{Z}}}$$

and further

$$\frac{1}{1 + F_{\text{eq}}} = \left(\frac{k_1 \alpha_p^0 + k_2}{D_B} \right) \lambda^2 \quad (4.42)$$

it follows that

$$f = - \frac{a^2 A}{(1 + F_{\text{eq}})} \frac{1}{r^2} + K_1 \left(\frac{r}{a} \right)^{-1/2} \left(\frac{\lambda}{r} \right)^{1/2} \left(1 + \frac{\lambda}{r} \right) [\cosh \frac{r}{\lambda} - \sinh \frac{r}{\lambda}] \dots\dots\dots (4.43)$$

If the constants A and K_1 are known the concentrations p_A and C_B can be determined at any point outside the sphere since

$$p_A = p_A^0 + \Delta p_A = p_A^0 - \frac{N_A^T}{P_c(1 + F_{eq})} [r - af(r)] \cos \theta \quad \dots\dots\dots (4.43a)$$

$$C_B = C_B^0 + \Delta C_B = C_B^0 + \frac{1}{D_B} \frac{F_{eq} N_A^T}{(1 + F_{eq})} [r + ag(r)] \cos \theta \quad \dots\dots\dots (4.43b)$$

where $f(r)$ is given by (4.43) and $g(r)$ by (4.33). Finally

$$(D_B C_B - P_c p_A) = (D_B C_B^0 - P_c p_A^0) + N_A^T r \cos \theta \left\{ 1 + \left(\frac{a}{r}\right)^3 \frac{A}{1 + F_{eq}} \right\} \quad (4.44)$$

is obtained from equations (4.43a and b) and is a useful form in the later use of the boundary conditions at $r = a$, and in the derivation of effective permeabilities.

4.1.2 Inside the Sphere

The differential equations inside the sphere are given by (4.23) and (4.24) with equations (4.30) and (4.31) presenting the respective forms for the solutions. Substitution of (4.30) and (4.31) into (4.24) yields

$$r^2 G'' + 2rG' - 2G = 0 \quad (4.45)$$

which yields a solution of the form

$$G = K_2 r \quad (4.46)$$

and substitution of (4.46) into (4.31) gives

$$D_B \Delta C'_B - P_d \Delta p'_A = K_2 r \cos \theta \quad (4.47)$$

The functional form of (4.47) satisfies the requirement that $\Delta C'_B$ and $\Delta p'_A$ vanish at $r = 0$. The constant K_2 will be determined from the boundary conditions at $r = a$. Substitution of (4.47) and (4.30) into (4.23) yields

$$r^2 H'' + 2rH' - \left(2 + \frac{r^2}{\lambda'^2}\right)H = \frac{K_2}{D_B} \frac{k_1' \alpha_A' p_A^0 + k_2'}{P_d} r^3 \quad (4.48)$$

where λ' is the characteristic length inside the sphere and is defined analogously to (4.36) using parameters appropriate to conditions inside the sphere

$$\frac{1}{\lambda'^2} = \left(\frac{k_1' \alpha_A' p_A^0 + k_2'}{D_B} \right) + \frac{k_1' \alpha_A' k_2' C_T'}{P_d (k_1' \alpha_A' p_A^0 + k_2')} \quad (4.49)$$

The particular solution to (4.48) is

$$H_{\text{part}} = - \frac{K_2}{D_B} \left(\frac{k_1' \alpha_A' p_A^0 + k_2'}{P_d} \right) \lambda'^2 r \quad (4.50)$$

The solution to the homogeneous part to (4.48) is a Bessel function

$$H_{\text{homo}} = r^{-1/2} \left[C_1' I_{3/2} \left(\frac{r}{\lambda'} \right) + C_2' I_{-3/2} \left(\frac{r}{\lambda'} \right) \right] \quad (4.51)$$

Since, from equation (4.30),

$$\Delta p'_A(0) = H(0) = 0$$

it follows that

$$C_2' = 0$$

and the homogeneous solution is

$$H_{\text{homo}} = C_1' r^{-1/2} I_{3/2} \left(\frac{r}{\lambda'} \right) \quad (4.52)$$

Use of (4.41) yields finally for $H(r)$

$$\begin{aligned} H(r) = & - \frac{K_2}{D_B'} \left(\frac{k_1' \alpha_A' p_A^0 + k_2'}{P_d} \right) \lambda'^2 r \\ & + K_4 r^{-1/2} \left[\sqrt{\frac{2}{\pi(r/\lambda')}} \left(\cosh \frac{r}{\lambda'} - \frac{\sinh r/\lambda'}{r/\lambda'} \right) \right] \end{aligned} \quad (4.53)$$

By defining

$$\begin{aligned} K_2' &= \frac{K_2}{N_A^T} \\ K_4' &= \frac{P_c}{N_A^T a \sqrt{\pi a/2}} K_4 \end{aligned}$$

and since

$$\frac{1}{(1 + F_{\text{eq}}')} = \left(\frac{k_1' \alpha_A' p_A^0 + k_2'}{D_B'} \right) \lambda'^2 \quad (4.54)$$

equation (4.53) becomes

$$\begin{aligned} H(r) = & - K_2' \frac{N_A^T}{P_d (1 + F_{\text{eq}}')} r \\ & + \frac{N_A^T a}{P_d} K_4' \left(\frac{a}{r} \right)^{1/2} \left(\frac{\lambda'}{r} \right)^{1/2} \left[\cosh \frac{r}{\lambda'} - \frac{\sinh r/\lambda'}{r/\lambda'} \right] \end{aligned} \quad (4.55)$$

If the constant K_2' and K_4' are known then p_A' and C_B' can be determined at any point within the sphere since

$$p_A' = p_A^0 + \Delta p_A' = p_A^0 + H(r) \cos \theta \quad (4.56)$$

$$C'_B = C_B^{O'} + \Delta C'_B = C_B^{O'} + K'_2 \frac{N_A^T}{D'_B} r \cos \theta + \frac{P_d}{D'_B} H(r) \cos \theta \dots \dots \dots (4.57)$$

where $H(r)$ is given by (4.55). Finally

$$(D'_B C'_B - P_d p'_A) = (D'_B C_B^{O'} - P_d p_A^O) + K'_2 N_A^T r \cos \theta \quad (4.58)$$

The problem that remains now is to evaluate the constants A , K_1 , K'_2 and K'_4 so that the concentrations inside and outside the sphere can be fully specified. At this point the remaining boundary conditions need to be utilized for each model considered here: impermeable and permeable.

4.2 Impermeable Carrier Model

4.2.1 Solution for the Concentrations for the Species Inside and Outside the Sphere

The impermeable carrier model considered here applies specifically to case 6, Figure 2. The constants K_1 , K'_2 , K'_4 , and A can now be solved through use of the boundary conditions at $r = a$ as shown in Figure 4.2. The case considered here will be the case where the sphere is encapsulated by a very thin inert skin (membrane) of finite permeability P_S and thickness L_S . The boundary conditions are as follows:

1. Continuity of flux of A at $r = a$

$$P_c \frac{\partial p'_A}{\partial r} = \frac{P_S}{L_S} [p_A(a) - p'_A(a)] = P_d \frac{\partial p'_A}{\partial r} \quad \text{at } r = a \dots \dots \dots (4.59a,b)$$

Substitution of (4.56) and (4.43a) into (4.59) gives

$$-\frac{N_A^T}{1+F_{eq}} \left[1 - a \frac{df}{dr} \Big|_{r=a} \right] = P_d \frac{dH}{dr} \Big|_{r=a} \quad (4.60a)$$

$$= -\frac{P_s}{L_s} \left\{ -\frac{N_A^T}{P_c(1+F_{eq})} a [1 - f(a)] - H(a) \right\} \quad (4.60b)$$

Use of the definitions for f and H given by equations (4.43) and (4.53) yields after some algebraic work

$$\begin{aligned} & -\frac{1}{1+F_{eq}} \left\{ 1 - \frac{2}{1+F_{eq}} A - K_1 \left(\frac{\lambda}{a} \right)^{\frac{1}{2}} \left[(-2 - 2\frac{\lambda}{a} - \frac{a}{\lambda}) (\cosh \frac{a}{\lambda} - \sinh \frac{a}{\lambda}) \right] \right\} \\ &= \frac{a}{P_c(1+F_{eq})} \frac{P_s}{L_s} \left\{ -1 - \frac{A}{1+F_{eq}} + K_1 \left(\frac{\lambda}{a} \right)^{\frac{1}{2}} (1 + \frac{\lambda}{a}) (\cosh \frac{a}{\lambda} - \sinh \frac{a}{\lambda}) \right. \\ &+ K_2' \frac{1+F_{eq}}{1+F_{eq}'} \frac{P_c}{P_d} - K_4' (1+F_{eq}') \frac{P_c}{P_d} \left(\frac{\lambda'}{a} \right)^{\frac{1}{2}} (\cosh \frac{a}{\lambda'} - \frac{\lambda'}{a} \sinh \frac{a}{\lambda'}) \left. \right\} \quad (4.61a) \end{aligned}$$

$$\begin{aligned} &= -K_2' \left(\frac{1}{1+F_{eq}'} \right) + K_4' \left(\frac{\lambda'}{a} \right)^{\frac{1}{2}} \left[-2 (\cosh \frac{a}{\lambda'} - \frac{\lambda'}{a} \sinh \frac{a}{\lambda'}) + \frac{a}{\lambda'} \sinh \frac{a}{\lambda'} \right] \\ & \dots \dots \dots (4.61b) \end{aligned}$$

2. Skin impermeable to B

$$\frac{\partial C_B}{\partial r} = 0 \quad \text{at } r = a \quad (4.62)$$

Use of equation (4.43b) gives

$$1 + a \frac{dg}{dr} \Big|_{r=a} = 0 \quad (4.63)$$

Substitution of the derivative of g , which is defined by (4.33) and (4.34), yields after rearrangements,

$$K_1 = \frac{-F_{eq} \left(1 - \frac{2A}{1+F_{eq}}\right)}{\left(\frac{\lambda}{a}\right)^{1/2} \left[(-2-2\frac{\lambda}{a} - \frac{a}{\lambda}) \left(\cosh \frac{a}{\lambda} - \sinh \frac{a}{\lambda}\right)\right]} \quad (4.64)$$

3. Skin impermeable to B'

$$\frac{\partial C'_B}{\partial r} = 0 \quad \text{at } r = a \quad (4.65)$$

Use of equation (4.57) gives

$$K'_2 \frac{N_A^T}{D'_B} + \frac{P_c}{D'_B} \left. \frac{dH}{dr} \right|_{r=a} = 0 \quad (4.66)$$

After substitution of (4.55) equation (4.66) becomes

$$K'_2 \left(\frac{F'_{eq}}{1+F'_{eq}}\right) = -K'_4 \left(\frac{\lambda'}{a}\right)^{1/2} \left[-2 \left(\cosh \frac{a}{\lambda'} - \frac{\lambda'}{a} \sinh \frac{a}{\lambda'}\right) + \frac{a}{\lambda'} \sinh \frac{a}{\lambda'}\right] \quad \dots\dots\dots (4.67)$$

Equations (4.61), (4.64), and (4.67) are the necessary relationships to evaluate the unknown constants A, K_1 , K'_2 , and K'_4 . Substitution of (4.64) and (4.67) in the first and last terms of equation (4.61) gives

$$K'_4 = - \frac{\left(\frac{1}{1+F'_{eq}}\right) \left(\frac{F'_{eq}}{1+F'_{eq}}\right) [1 + F_{eq} - 2A]}{\left(\frac{\lambda'}{a}\right)^{1/2} \left[-2 \left(\cosh \frac{a}{\lambda'} - \frac{\lambda'}{a} \sinh \frac{a}{\lambda'}\right) + \frac{a}{\lambda'} \sinh \frac{a}{\lambda'}\right]} \quad \dots\dots\dots (4.68)$$

Substitution of (4.64) and (4.67) into the first and second part of equation (4.61) and substitution of (4.68) gives after algebraic manipulation

$$\frac{A}{1+F_{eq}} = \frac{P_c(1+F_{eq}) - P_d(1+F_d) \left[(1+f_c F_{eq}) - \frac{P_d(1+F_{eq})R_m}{P_c} \right]}{2P_c(1+F_{eq}) + P_d(1+F_d) \left[(1-2f_c F_{eq}) + \frac{2P_d(1+F_{eq})R_m}{P_c} \right]} \quad (4.69)$$

where

$$f_c = - \frac{1 + \frac{\lambda}{a}}{2 + 2 \frac{\lambda}{a} + \frac{a}{\lambda}} \quad (4.70)$$

$$F_d = \frac{F'_{eq} \left[\frac{(3 \frac{\lambda'^2}{a^2} + 1) \tanh \frac{a}{\lambda'} - 3 \frac{\lambda'}{a}}{(2 \frac{\lambda'^2}{a^2} + 1) \tanh \frac{a}{\lambda'} - 2 \frac{\lambda'}{a}} \right]}{1 + F'_{eq} \left[1 - \frac{(3 \frac{\lambda'^2}{a^2} + 1) \tanh \frac{a}{\lambda'} - 3 \frac{\lambda'}{a}}{(2 \frac{\lambda'^2}{a^2} + 1) \tanh \frac{a}{\lambda'} - 2 \frac{\lambda'}{a}} \right]} \quad \dots \dots \dots (4.71)$$

and

$$R_m = \frac{P_{d/a}}{P_{s/L_s}} \quad (4.72)$$

The parameter R_m is the ratio of the membrane mass transfer resistance to the inert particle resistance. The characteristic lengths λ and λ' here give a measure of the thickness of shells outside and inside the sphere where deviations from chemical equilibrium are significant. The factor F_d is called the dispersed phase facilitation factor which will be discussed later.

The constant A is now specified and K_2' can be obtained by substituting (4.68) into (4.67) so that

$$K_2' = 1 - \frac{2A}{1 + F_{eq}} \quad (4.73)$$

Since A is fully specified K_2' can be evaluated from (4.72), K_4' can be evaluated from (4.68), and K_1 can be evaluated from (4.64). The concentration profiles for A, B, and AB are fully specified outside the sphere, and A', B', and AB' are fully specified inside the sphere. For example, equations (4.43a), (4.43) and (4.69) gives the partial pressure profile p_A (or concentration since $C_A = \alpha_A p_A$) outside the sphere.

In the case that the membrane mass transfer resistance is negligible ($R_m \rightarrow 0$) the constant A as presented by (4.69) reduces to

$$\frac{A}{1+F_{eq}} = \frac{P_c(1+F_{eq}) - P_d(1+F_d)(1+f_c F_{eq})}{2P_c(1+F_{eq}) + P_d(1+F_d)(1-2f_c F_{eq})} \quad (4.74)$$

while the expressions for K_1 , K_2' , and K_4' remain the same. Equation (4.74) can also be derived by using the no shell boundary conditions as shown in Figure 4.2.

4.2.2 Application of the Model to Other Cases

For the potential ϕ of species A outside the sphere, Maxwell derived the following relationship (see Appendix A):

$$\phi = p_A - p_A^o = - \left(\frac{N_A}{P_c} \right) r \cos\theta \left\{ 1 + \left(\frac{a}{r} \right)^3 A \right\} \quad (4.75)$$

where A is defined as

$$A = \frac{P_c - P_d}{2P_c + P_d} \quad (4.76)$$

The above relationship is valid for an inert sphere in an inert continuum. In the case of a sphere in a reacting medium the potential must be appropriately re-defined to include the contribution to the potential by the carrier species,

$$\phi = (p_A - \frac{D_B}{P_c} C_B) - (p_A^o - \frac{D_B}{P_c} C_B^o) \quad (4.77)$$

From the previous section the potential outside a reacting sphere in a reacting medium is given by

$$\phi = - \left(\frac{N_A^T}{P_c} \right) r \cos \theta \left\{ 1 + \left(\frac{a}{r} \right)^3 \frac{A}{1 + F_{eq}} \right\} \quad (4.78)$$

where $A/(1+F_{eq})$ is given by (4.74) for the case of negligible membrane resistance

$$\frac{A}{1+F_{eq}} = \frac{P_c(1+F_{eq}) - P_d(1+F_d)(1+f_c F_{eq})}{2P_c(1+F_{eq}) + P_d(1+F_d)(1-2f_c F_{eq})} \quad (4.74)$$

Comparison with Maxwell's equation shows that in the case of a reactive continuous medium the constant $A/(1+F_{eq})$ is similar to Maxwell's A. The effective continuous phase permeability is given by

$$P_c(1 + F_{eq})$$

and the dispersed phase permeability is increased by a factor $(1+F_d)$ times a factor that is a function of f_c and F_{eq} . The dispersed phase facilitation factor F_d has the following properties

$$F_d = F'_{eq} \quad \text{as } \frac{a}{\lambda} \rightarrow \infty \quad (4.79)$$

$$F_d = 0 \quad \text{as } \frac{a}{\lambda} \rightarrow 0 \quad (4.80)$$

and therefore exhibits the same properties as the homogeneous systems' facilitation factor as discussed in the Literature Survey. In the case that a/λ approaches zero the reactive sphere becomes "inert" and equation (4.74) reduces to

$$\frac{A}{1+F_{eq}} = \frac{P_c(1+F_{eq}) - P_d(1+f_c F_{eq})}{2P_c(1+F_{eq}) + P_d(1-2f_c F_{eq})} \quad (4.81)$$

which is the solution for the case of an inert sphere in a reactive continuum as presented by Figure 2, case 5.

Unlike the dispersed phase, the continuous phase cannot be made unreactive by letting a/λ approach zero. The parameter f_c is a function of a/λ as is shown by equation (4.70) and its effect is solely on the effective permeability of the dispersed phase as is shown by equation (4.74). The limits on f_c are as follows

$$f_c = 0 \quad \frac{a}{\lambda} \rightarrow \infty \quad (4.82)$$

$$f_c = -\frac{1}{2} \quad \frac{a}{\lambda} \rightarrow 0 \quad (4.83)$$

and in no way, either from (4.82) and (4.83) or (4.74), can the effective permeability of the continuous phase be made to approach the value P_c as a/λ approaches zero in the case of a finite F_{eq} . Regardless of how large λ is relative to a , equilibrium conditions have been imposed at $r \rightarrow \infty$ by boundary condition (4.27). In a qualitative sense, nonequilibrium conditions in the continuous phase, as indicated by small values of a/λ , exist only locally near the sphere while the total reactive continuous medium remains at equilibrium. The only way that the reactive continuous medium can be made inert is by making the effect of the chemical reaction negligible. This requires that F_{eq} is much smaller than one. Since F_{eq} is defined by

$$F_{eq} = \frac{D_B k_1 k_2 \alpha_A C_T}{P_c (k_2 + k_1 \alpha_A P_A^0)^2}$$

it can be made to approach zero by letting D_B or C_T approach zero. By the appropriate choice of various parameters equation (4.74) can now be reduced to various models.

1. Maxwell's relationship for an inert sphere in an inert medium; case 2, Figure 2.

By letting $F_{eq} \rightarrow 0$ and either $a/\lambda' \rightarrow 0$ or $F'_{eq} \rightarrow 0$, equation (4.74) becomes

$$A = \frac{P_c - P_d}{2P_c + P_d} \quad (4.84)$$

and the potential ϕ is from (4.78)

$$\phi = - \left(\frac{N_A^T}{P_C} \right) r \cos \theta \left\{ 1 + \left(\frac{a}{r} \right)^3 A \right\} \quad (4.85)$$

Since $N_A^T = N_A$ when F_{eq} is zero, equations (4.84) and (4.85) contain the correct solutions for the Maxwell problem as given by (4.76) and (4.75).

2. Reactive sphere in an inert continuum; case 4,
Figure 2.

By letting $F_{eq} \rightarrow 0$, equation (4.74) becomes

$$A = \frac{P_C - P_d(1 + F_d)}{2P_C + P_d(1 + F_d)} \quad (4.86)$$

and the potential ϕ is from (4.78)

$$\phi = - \left(\frac{N_A}{P_C} \right) r \cos \theta \left\{ 1 + \left(\frac{a}{r} \right)^3 A \right\} \quad (4.87)$$

In the nonreactive continuous medium the effective permeability of the reactive dispersed phase is given by $P_d(1+F_d)$ by comparison with Maxwell's equation.

3. Inert sphere in a reactive medium; case 5,
Figure 2.

By letting $F'_{eq} \rightarrow 0$, or $a/\lambda' \rightarrow 0$, equation (4.74) reduces to

$$\frac{A}{1+F_{eq}} = \frac{P_C(1+F_{eq}) - P_d(1+f_c F_{eq})}{2P_C(1+F_{eq}) + P_d(1-2f_c F_{eq})} \quad (4.89)$$

and the potential ϕ outside the sphere is from (4.78)

$$\phi = - \left(\frac{N_A}{P_c} \right) r \cos \theta \left\{ 1 + \left(\frac{a}{r} \right)^3 \frac{A}{1+F_{eq}} \right\} \quad (4.90)$$

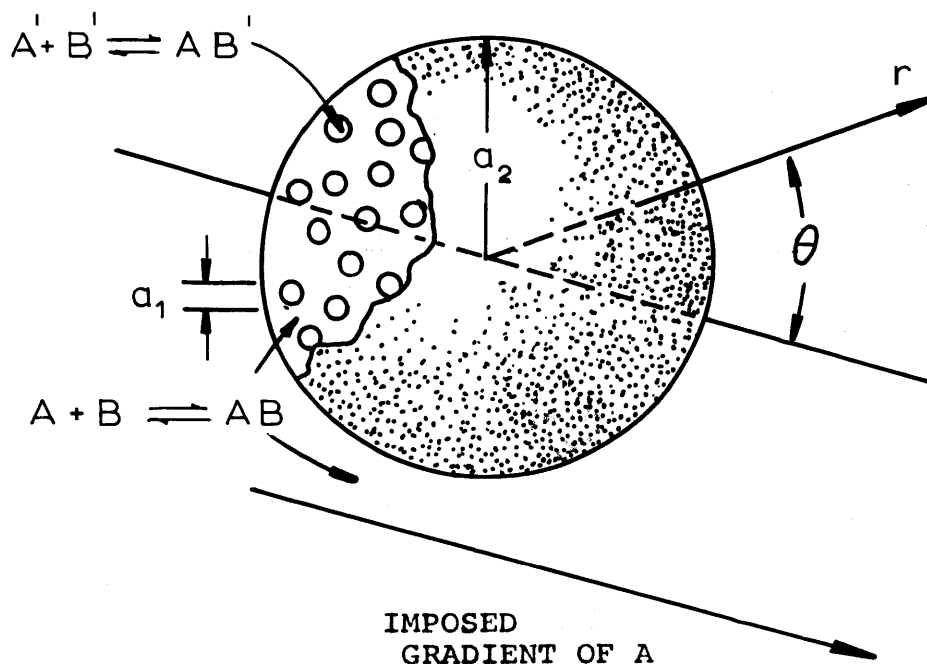
It is obvious that the impermeable reaction outside-reaction inside model derived in the previous section is quite versatile in that it can be applied successfully to the other systems of interest.

4.2.3 Effective Permeability for a Suspension of Spheres

Consider a suspension of n reactive spheres, of radius a_1 , suspended in a spherical volume of reactive continuous medium, with radius a_2 , which is suspended in an infinite bath of the reactive medium. A unidirectional constant mass flux of A is imposed on the infinite reactive medium at very large distances from the spherical cluster (see Figure 4.3). The suspension is sufficiently dilute that interactions between spheres may be neglected. The potential at a point which is located a large distance R from the center of the spherical cluster ($R \gg a_2$) is given by

$$\phi = - \left(\frac{N_A}{P_c} \right) R \cos \theta \left\{ 1 + \frac{na_1^3}{R^3} \frac{A}{1+F_{eq}} \right\} \quad (4.91)$$

Equation (4.91) is obtained from (4.78) and the second term in the brackets accounts for the disturbance on the potential caused by the presence of the spheres. The constant $A/(1+F_{eq})$ is that defined for either an inert or reactive sphere in a reactive medium. The potential can be equated to one derived for the spherical cluster with an effective permeability \bar{P}



$$\frac{\bar{p}}{P_c (1+F_{eq})} = \left| \frac{(1+F_{eq}) - 2\phi A}{(1+F_{eq}) - \phi A} \right|$$

A = function (p_A° , -----)

$$\bar{p}_{AVE} = \frac{1}{p_A^{(2)} - p_A^{(1)}} \int_{p_A^{(1)}}^{p_A^{(2)}} \bar{p} dp_A$$

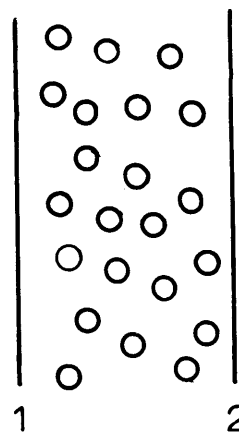


FIGURE 4.3

SPHERICAL CLUSTER OF REACTIVE SPHERES IN A REACTIVE CONTINUUM

$$\phi = - \left(\frac{N_A}{P_c} \right) R \cos \theta \left\{ 1 + \frac{a_2^3}{R^3} \frac{A^*}{1 + F_{eq}} \right\} \quad (4.92)$$

where the constant $A^*/(1+F_{eq})$ is that defined for an inert sphere with permeability \bar{P} in the reactive medium

$$\frac{A^*}{1+F_{eq}} = \frac{P_c(1+F_{eq}) - \bar{P}(1+f_c^*F_{eq})}{2P_c(1+F_{eq}) + \bar{P}(1-2f_c^*F_{eq})} \quad (4.93)$$

Now f_c^* is given by equation (4.70) with a equal to a_2 . However, since $a_2 \gg a_1$ and the spheres do not interact with each other it follows that a_2/λ is sufficiently large so that f_c^* is zero. The general relationship for the effective permeability, \bar{P} , of a suspension of spheres in a reactive medium is then

$$\frac{\bar{P}}{P_c(1+F_{eq})} = \left[\frac{(1+F_{eq}) - 2\Phi A}{(1+F_{eq}) + \Phi A} \right] \quad (4.94)$$

Equation (4.94) is similar to that derived for the Maxwell problem given by equation (A.15) but the factor A is dependent upon many factors, including the partial pressure of species A at the center of an individual sphere. Thus, the effective permeability is defined only at a local point within the suspension, or for the total suspension when the driving force across the total physical system is extremely small. If one considers a slab composed of such a suspension which has imposed upon it a large partial pressure gradient of A , then the average permeability of the slab may be calculated by integrating the local expression as presented by (4.94) over

the thickness of the film

$$\bar{P}_{AVE} = \frac{\int_{p_A^{x=0}}^{p_A^{x=L}} \bar{P} dp_A}{(p_A^{x=L} - p_A^{x=0})} \quad (4.95)$$

This expression for the average effective permeability is valid if the expression for \bar{P} is valid: the partial pressure difference across each sphere must be small compared to the local value of the partial pressure at the center of the sphere, and the reaction in the continuous phase must be near equilibrium.

The local effective permeability for a suspension of reactive medium can be obtained from equations (4.94) and (4.74)

$$\frac{\bar{P}}{P_c(1+F_{eq})} = \frac{2P_c(1+F_{eq}) + P_d(1+F_d)(1-2F_{eq}^f) - 2\phi[P_c(1+F_{eq}) - P_d(1+F_d)(1+F_{eq}^f)]}{2P_c(1+F_{eq}) + P_d(1+F_d)(1-2F_{eq}^f) + \phi[P_c(1+F_{eq}) - P_d(1+F_d)(1+F_{eq}^f)]} \quad (4.96)$$

Again the form of (4.96) is quite similar to that derived by Maxwell. In order to obtain the average effective permeability, \bar{P} must be integrated as shown by (4.95).

4.2.4 Effective Permeability for Other Heterogeneous Media

As has been stated in the previous section equation (4.94) is the general relationship for the effective permeability

for a suspension of spheres in a reactive medium. The general relationship for a suspension of spheres in an inert medium ($F_{eq} = 0$) is

$$\frac{\bar{P}}{P_c} = \left[\frac{1 - 2\phi A}{1 + \phi A} \right] \quad (4.97)$$

where A is the constant for either a reactive or inert sphere in an inert continuum. Equations (4.97) and (4.94) can be applied to derive local effective permeabilities for specific systems, or the very same equations can be derived by inspection from the local effective permeability equation for the impermeable model as presented by (4.96).

1. Maxwell's relationship for a suspension of inert spheres in an inert continuum.

By letting $F_{eq} = 0$, and $a/\lambda' \rightarrow 0$ or $F'_{eq} \rightarrow 0$, equation (4.96) reduces to

$$\frac{\bar{P}}{P_c} = \frac{2P_c + P_d - 2\phi[P_c - P_d]}{2P_c + P_d + \phi[P_c - P_d]} \quad (4.98)$$

2. Suspension of reactive spheres in an inert continuum; case 4, Figure 2.

By letting $F_{eq} \rightarrow 0$, equation (4.96) becomes

$$\frac{\bar{P}}{P_c} = \frac{2P_c + P_d(1+F_d) - 2\phi[P_c - P_d(1+F_d)]}{2P_c + P_d(1+F_d) + \phi[P_c - P_d(1+F_d)]} \quad (4.99)$$

3. Inert sphere in a reactive medium; case 5,
Figure 2.

By letting $F'_{eq} \rightarrow 0$, or $a/\lambda' \rightarrow 0$, equation (4.96)

reduces to

$$\frac{\bar{P}}{P_c(1+F_{eq})} = \frac{2P_c(1+F_{eq}) + P_d(1-2F_{eq}f_c) - 2\phi[P_c(1+F_{eq}) - P_d(1+F_{eq}f_c)]}{2P_c(1+F_{eq}) + P_d(1-2F_{eq}f_c) + \phi[P_c(1+F_{eq}) - P_d(1+F_{eq}f_c)]} \dots\dots\dots (4.100)$$

4.3 Permeable Carrier Model

The permeable carrier model refers to case 7, Figure 2.2 where a mobile carrier species is present in each phase, continuous and dispersed, and the carrier and carrier-complex species can diffuse from one phase into another. Whereas in the impermeable carrier model B, AB and B', AB' can be entirely different species, for the permeable carrier model these species are the same. However, the kinetic reaction rate constants and activity coefficients are permitted to be different in each phase. The boundary conditions at $r = a$ are shown in Figure 4.2 and these are utilized to determine the constants A, K_1 , K_2' and K_4' . For convenience the equations derived in Section 4.1 are summarized outside the sphere:

$$P_A - P_A^O = - \frac{N_A^T}{P_c(1+F_{eq})} [r - af(r)] \cos \theta \quad (4.101)$$

$$C_B - C_B^O = \frac{1}{D_B} \frac{F_{eq} N_A^T}{(1+F_{eq})} [r + ag(r)] \cos \theta \quad (4.102)$$

$$\phi = - \frac{N_A^T a}{P_c} \frac{r}{a} \cos \theta \left\{ 1 + \left(\frac{a}{r}\right)^3 \frac{A}{1+F_{eq}} \right\} \quad (4.103)$$

where

$$f(r) = -\frac{A}{1+F_{eq}} \left(\frac{a}{r}\right)^2 + K_1 \left(\frac{r}{a}\right)^{-1/2} \left(\frac{\lambda}{r}\right)^{1/2} \left(1 + \frac{\lambda}{r}\right) \left[\cosh \frac{r}{\lambda} - \sinh \frac{r}{\lambda}\right] \quad (4.104)$$

$$g(r) = \frac{A}{F_{eq}} \left(\frac{a}{r}\right)^2 + \frac{f(r)}{F_{eq}} \quad (4.105)$$

inside the sphere,

$$p'_A - p_A^O = H(r) \cos \theta \quad (4.106)$$

$$C'_B - C_B^O = \frac{K'_2 N_A^T a}{D'_B} \frac{r}{a} \cos \theta + \frac{P_d}{D'_B} H(r) \cos \theta \quad (4.107)$$

$$\phi' = -\frac{K'_2 N_A^T a}{P_d} \frac{r}{a} \cos \theta \quad (4.108)$$

where

$$H(r) = -K'_2 \frac{N_A^T a}{P_d (1+F'_{eq})} \frac{r}{a} + \frac{N_A^T a}{P_d} K'_4 \left(\frac{a}{r}\right)^{1/2} \left(\frac{\lambda'}{r}\right)^{1/2} \left[\cosh \frac{r}{\lambda'} - \frac{\sinh \frac{r}{\lambda'}}{\frac{r}{\lambda'}}\right] \quad \dots\dots\dots (4.109)$$

4.3.1 Solution for the Concentrations for the Species Inside and Outside the Sphere

From Figure 4.2 the boundary conditions at $r = a$ are as follows:

1. Continuity of total flux of A at $r = a$.

$$\frac{\partial}{\partial r} (D_B C_B - P_c p_A) = \frac{\partial}{\partial r} (D'_B C'_B - P_d p'_A) \quad \text{at } r = a \quad \dots\dots\dots (4.110)$$

If equations (4.103) and (4.108) are utilized, equation (4.110) becomes,

$$K'_2 = 1 - \frac{2A}{1 + F_{eq}} \quad (4.111)$$

which relates K'_2 to A.

2. Continuity of the potential species A at $r = a$

$$p_A = p'_A \quad \text{at } r = a \quad (4.112)$$

Substitution of equation (4.101) and (4.106) yields

$$\frac{-N_A^T}{P_c(1 + F_{eq})} a [1 - f(a)] = H(a) \quad (4.113)$$

The definitions of $f(r)$ and $H(r)$ are given by (4.104) and (4.109) so that

$$1 + \frac{A}{1 + F_{eq}} - K_1 \left(\frac{\lambda}{a}\right)^{1/2} \left(1 + \frac{\lambda}{a}\right) \left(\cosh \frac{a}{\lambda} - \sinh \frac{a}{\lambda}\right) =$$

$$K'_2 \frac{P_c(1 + F_{eq})}{P_d(1 + F'_{eq})} - K'_4(1 + F_{eq}) \frac{P_c}{P_d} \left(\frac{\lambda'}{a}\right)^{1/2} \left[\cosh \frac{a}{\lambda'} - \frac{\lambda'}{a} \sinh \frac{a}{\lambda'}\right] \quad (4.114)$$

3. Continuity of the potential of B at $r = a$

$$p_B = p'_B \quad \text{at } r = a \quad (4.115)$$

or

$$\left(\frac{C_B}{\alpha_B}\right) = \left(\frac{C'_B}{\alpha'_B}\right) \quad \text{at } r = a \quad (4.116)$$

where p_B is the activity. This boundary condition is analogous to the second boundary condition that specifies that the potential of A (or activity) is continuous across the phase boundary. Substitution of (4.102) and (4.107) into (4.116) and use of the relationship

$$\frac{C_B^O}{\alpha_B} = \frac{C_B'^O}{\alpha_B'} \quad (4.117)$$

gives

$$\begin{aligned} & \frac{1}{\alpha_B} \left\{ \frac{1}{D_B} \frac{F_{eq}}{1+F_{eq}} N_A^T a \left[1 + \frac{A}{F_{eq}} + \frac{f(a)}{F_{eq}} \right] \right\} \\ &= \frac{1}{\alpha_B'} \left\{ K_2' \frac{N_A^T}{D_B'} a + \frac{P_d}{D_B'} H(a) \right\} \end{aligned} \quad (4.118)$$

Substitution of the functional forms of $f(r)$ and $H(r)$ as given by (4.104) and (4.109) yields

$$\begin{aligned} & \frac{F_{eq}}{1+F_{eq}} \left\{ 1 + \frac{A}{F_{eq}} - \frac{1}{1+F_{eq}} \frac{A}{F_{eq}} + \frac{K_1}{F_{eq}} \left(\frac{\lambda}{a} \right)^{1/2} \left(1 + \frac{\lambda}{a} \right) \left[\cosh \frac{a}{\lambda} - \sinh \frac{a}{\lambda} \right] \right\} \\ &= \frac{\alpha_B^D D_B}{\alpha_B' D_B'} \left\{ K_2' - K_2' \frac{1}{1+F_{eq}'} + K_4' \left(\frac{\lambda'}{a} \right)^{1/2} \left[\cosh \frac{a}{\lambda'} - \frac{\lambda'}{a} \sinh \frac{a}{\lambda'} \right] \right\} \end{aligned}$$

4. Continuity of the dissolved species flux on $r = a$

$$P_c \frac{\partial p_A}{\partial r} = P_d \frac{\partial p_A'}{\partial r} \quad \text{at } r = a \quad (4.120)$$

Use of equations (4.101) and (4.106) gives

$$-\frac{N_A^T}{1+F_{eq}} \left[1 - a \frac{df}{dr} \Big|_{r=a} \right] = P_d \frac{dH}{dr} \Big|_{r=a} \quad (4.121)$$

which becomes

$$\begin{aligned} & -\frac{1}{1+F_{eq}} \left\{ 1 - \frac{2A}{1+F_{eq}} - K_1 \left(\frac{\lambda}{a}\right)^{1/2} \left[(-2 - 2\frac{\lambda}{a} - \frac{a}{\lambda}) (\cosh \frac{a}{\lambda} - \sinh \frac{a}{\lambda}) \right] \right\} \\ & = -K_2' \frac{1}{1+F_{eq}} + K_4' \left(\frac{\lambda'}{a}\right)^{1/2} \left[-2 (\cosh \frac{a}{\lambda'} - \frac{\lambda'}{a} \sinh \frac{a}{\lambda'}) + \frac{a}{\lambda'} \sinh \frac{a}{\lambda'} \right] \\ & \dots\dots\dots (4.122) \end{aligned}$$

The resulting four equations (4.111), (4.114), (4.119), and (4.122) are the necessary relationships to completely specify the constants K_1 , K_2' , K_4' , and A . The use of equation (4.111) in (4.114), (4.119), and (4.122) will eliminate K_2' . Solution for K_1 , K_4' and A is straightforward and the final results are

$$K_4' = \frac{(1 + F_{eq} - 2A) \left[\frac{P_c (1+F_{eq})}{P_d (1+F_{eq}') } \right] - (1 + F_{eq} + A)}{(1+F_{eq}') \frac{P_c}{P_d} \left[1 - \frac{F_{eq}}{F_{eq}'} \right] \left(\frac{\lambda'}{a}\right)^{1/2} \left[\cosh \frac{a}{\lambda'} - \frac{\lambda'}{a} \sinh \frac{a}{\lambda'} \right]} \quad (4.123)$$

$$\begin{aligned} K_1 &= \frac{1}{\left(\frac{\lambda}{a}\right)^{1/2} \left(1 + \frac{\lambda}{a}\right) (\cosh \frac{a}{\lambda} - \sinh \frac{a}{\lambda})} \left\{ \left(1 + \frac{A}{1+F_{eq}}\right) \right. \\ & \quad - \left. \left(1 - \frac{2A}{1+F_{eq}}\right) \left[\frac{P_c (1+F_{eq})}{P_d (1+F_{eq}') } \right] \right. \\ & \quad \left. + \frac{(1 + F_{eq} - 2A) \left[\frac{P_c (1+F_{eq})}{P_d (1+F_{eq}') } \right] - (1 + F_{eq} + A)}{\left[1 - \frac{F_{eq}}{F_{eq}'} \right]} \right\} \quad (4.124) \end{aligned}$$

$$\frac{A}{1+F_{eq}} = \frac{P_c(1+F_{eq}) - P_d(1+F'_{eq}) \left[\frac{1}{1-Q} \right]}{2P_c(1+F_{eq}) + P_d(1+F'_{eq}) \left[\frac{1}{1-Q} \right]} \quad (4.125)$$

where

$$Q = \frac{\frac{f_c}{F'_{eq}} \left[\frac{F'_{eq} - F_{eq}}{1 + F_{eq}} \right]^2}{\frac{P_c(1+F'_{eq})(F_{eq})}{P_d(1+F_{eq})(F'_{eq})} + f_c \left[\frac{2 - \tanh \frac{a}{\lambda'} \left(2 \frac{\lambda'}{a} + \frac{a}{\lambda'} \right)}{1 - \frac{\lambda'}{a} \tanh \frac{a}{\lambda'}} \right]} \quad (4.126)$$

and f_c is again defined by (4.70). The constants K_1 , K'_2 , K'_4 , and A are now completely specified by equations (4.124), (4.111), (4.123) and (4.125). In arriving at the relationship for A use was made of the relationship

$$\frac{\alpha_B^D}{\alpha_B^I} = \frac{P_c F_{eq}}{P_d F'_{eq}} \quad (4.127)$$

Equation (4.127) is a thermodynamic constraint, and is equivalent to maintaining the equilibrium constant, based on activity, the same in each phase

$$K_a = K'_a \quad (4.128)$$

where

$$K_a = \frac{P_{AB}}{P_A P_B} \quad (4.129)$$

Equation (4.127) can be derived from (4.128) in a straightforward manner. Since the total carrier concentration inside and outside the sphere is constant,

$$C_T = C_B^O + C_{AB}^O = \alpha_B p_B^O + \alpha_{AB} p_{AB}^O$$

$$C'_T = C_B^{O'} + C_{AB}^{O'} = \alpha'_B p_B^O + \alpha'_{AB} p_{AB}^O$$

If in addition it is assumed that

$$\alpha_B = \alpha_{AB} \quad (4.130)$$

and

$$\alpha'_B = \alpha'_{AB} \quad (4.131)$$

then the thermodynamic constraint in terms of equilibrium constants based on concentration is

$$K\alpha_A = K'\alpha'_A \quad (4.132)$$

where

$$K = \frac{C_{AB}}{C_A C_B} = \frac{C_{AB}}{\alpha_A p_A C_B}$$

It follows from equation (4.132) that the following relationship is also valid

$$\frac{\left[\frac{K\alpha_A}{(K\alpha_A p_A^O + 1)^2} \right]}{\left[\frac{K'\alpha'_A}{(K'\alpha'_A p_A^O + 1)^2} \right]} = 1 \quad (4.133)$$

Since F_{eq} and F'_{eq} are defined as

$$F_{eq} = \frac{D_B K \alpha_A C_T}{P_C (K \alpha_A p_A^O + 1)^2} \quad (4.134)$$

$$F'_{eq} = \frac{D'_B K' \alpha'_A C'_T}{P'_d (K' \alpha'_A p_A^O + 1)^2} \quad (4.135)$$

substitution of equations (4.134) and (4.135) yields equation (4.127).

Equations (4.130) and (4.131) are reasonable assumptions if the carrier does not undergo major physical changes upon binding the solute A. In the case that equation (4.130) and (4.131) are physically untrue the theory can be appropriately modified in a straightforward manner.

4.3.2 Application of the Model to Other Cases

The relationship (4.125) derived for the permeable carrier model can be reduced so that it gives valid solutions for other systems of interest. Investigation of (4.125) shows that some similarity exists between it and Maxwell's model. Again some of the comments made in section 4.2.2 are valid here.

1. The equation derived is valid for a sphere in a reactive medium that is virtually everywhere at equilibrium. Nonequilibrium conditions can exist in shells of thickness λ and λ' outside and inside the sphere.
2. As a/λ approaches zero the reactive continuous medium does not approach inert conditions throughout. At distances much larger than λ equilibrium must be attained because of mathematical constraint (boundary condition) as $r \rightarrow \infty$. In order to reduce the general relationship to continuous inert problems F_{eq} must be set to zero in order not to violate boundary condition (4.27).

Application of (4.125) under the specific constraints will yield valid expressions for the following heterogeneous systems of interest.

1. Inert sphere in an inert medium: the Maxwell problem.

Setting F_{eq} equal to zero, and letting $a/\lambda \rightarrow 0$, or setting $F'_{eq} = 0$, equation (4.125) reduces to Maxwell's relationship. It should be emphasized here that "permeable" and "impermeable" models become indistinguishable for the inert continuous medium. If F_{eq} is zero, this implies that the carrier concentration is zero in the continuous phase (it cannot exist) or the diffusivity of the carrier is zero so that it can neither diffuse in or out.

2. Reactive sphere in an inert medium.

By setting F_{eq} equal to zero, equation (4.125) reduces to that given by (4.86).

3. Inert sphere in a reactive medium.

For this particular situation the "permeable" and "impermeable" model will give different results. Even if no reaction occurs inside the sphere the permeable carrier model allows the carrier to diffuse through the inert particle, while in the impermeable model the carrier must diffuse around the particle. By letting a/λ' approach zero so that the sphere is essentially nonreactive. Q in equation (4.126) becomes

$$Q^* = \frac{\frac{f_c}{F'_{eq}} \left[\frac{F'_{eq} - F_{eq}}{1 + F_{eq}} \right]^2}{\frac{P_c (1 + F'_{eq}) F_{eq}}{P_d (1 + F_{eq}) F'_{eq}} - 2 f_c} \quad (4.136)$$

It should be noticed from equation (4.136) and (4.125) that $A/(1+F_{eq})$ is still a function of F'_{eq} even though the reaction is negligible inside the sphere. The relationships can be expressed solely in terms of F_{eq} since the thermodynamic constraint given by (4.127) still holds. If in addition F'_{eq} is set equal to zero equation (4.125) gives the equivalent result that is obtained from the nonpermeable model as given by equation (4.89). By setting F'_{eq} zero the carrier either does not exist inside the sphere, or its mobility is zero, and the permeable model is essentially reduced to the nonpermeable model.

4.3.3 Effective Permeability for a Suspension of Spheres.

The derivation of the effective permeability for a suspension of spheres in a reactive medium has been given in section 4.2.3. From equations (4.94) and (4.125) the local effective permeability for the permeable model is

$$\frac{\bar{P}}{P_c (1 + F_{eq})} = \frac{2P_c (1 + F_{eq}) + P_d (1 + F'_{eq}) \left[\frac{1}{1 - Q} \right] - 2\phi \{ P_c (1 + F_{eq}) - P_d (1 + F'_{eq}) \left[\frac{1}{1 - Q} \right] \}}{2P_c (1 + F_{eq}) + P_d (1 + F'_{eq}) \left[\frac{1}{1 - Q} \right] + \phi \{ P_c (1 + F_{eq}) - P_d (1 + F'_{eq}) \left[\frac{1}{1 - Q} \right] \}} \quad \dots \dots \dots (4.137)$$

The average effective permeability is again

$$\bar{P}_{AVE} = \int_{P_A^O}^{P_A^L} \bar{P} dp_A / (P_A^L - P_A^O)$$

4.3.4 Effective Permeability for Other Heterogeneous Systems

The relationship for the local effective permeability obtained for the permeable model as presented by equation (4.137) can be used to derive analogous relationships for the other heterogeneous media of interest.

1. Effective local permeability of an inert suspension of spheres in an inert medium.

By letting $F_{eq} = 0$, and $a/\lambda' \rightarrow 0$ and/or $F'_{eq} = 0$, equation (4.137) reduces to Maxwell's equation.

2. Effective local permeability of a reactive suspension of spheres in an inert medium.

By letting $F_{eq} = 0$, equation (4.137) reduces to that given by (4.99).

3. Effective local permeability of a suspension of inert spheres in a reactive medium.

- a. Permeable carrier.

By letting a/λ' approach zero, equation (4.137) reduces to

$$\frac{\bar{P}}{P_c(1+F_{eq})} = \frac{2P_c(1+F_{eq}) + P_d(1+F'_{eq}) \left(\frac{1}{1-Q^*}\right) - 2\phi [P_c(1+F_{eq}) - P_d(1+F'_{eq}) \left(\frac{1}{1-Q^*}\right)]}{2P_c(1+F_{eq}) + P_d(1+F'_{eq}) \left(\frac{1}{1-Q^*}\right) + \phi [P_c(1+F_{eq}) - P_d(1+F'_{eq}) \left(\frac{1}{1-Q^*}\right)]} \dots\dots\dots (4.138)$$

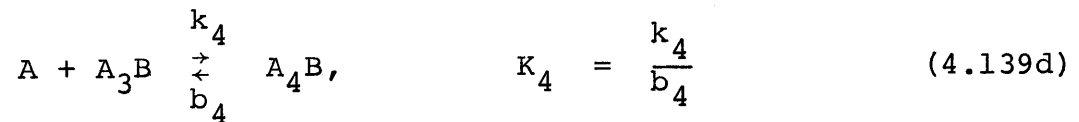
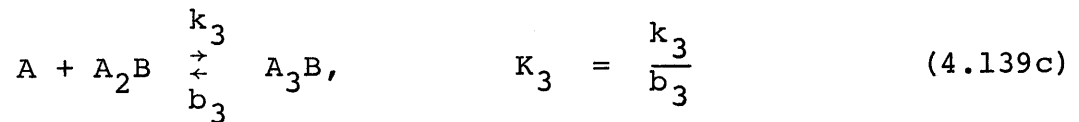
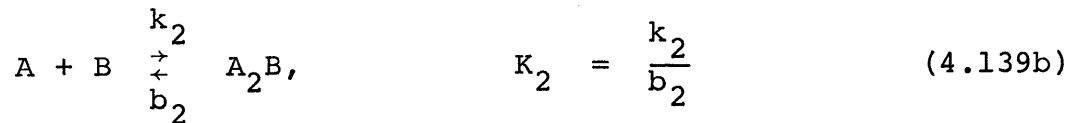
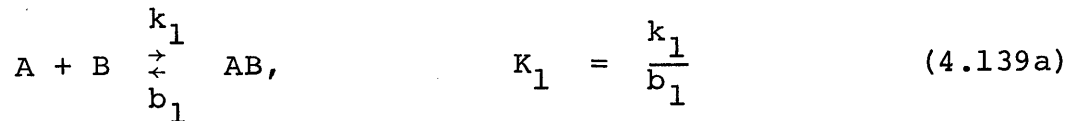
b. Impermeable carrier.

By letting $F'_{eq} = 0$ and $a/\lambda' \rightarrow 0$, equation (4.137) reduces to that given by (4.100).

4.4 Adair Reaction Scheme Inside the Dispersed Phase - No Reaction in the Continuous Phase

The two models developed in the previous sections have been shown to be quite versatile in that they can be reduced to the various cases shown in Figure 2.2. The models were developed for a second order reversible reaction, as an example only, and the theoretical procedure can be utilized to arrive at solutions for different reaction schemes (in identical or other types of media). In this section a solution will be discussed for a four-step reversible reaction scheme involving the diffusing species A inside the dispersed phase with no reaction in the continuous phase (see case 4, Figure 2.2). The four-step reaction scheme was proposed by Adair (1925) to model the reaction of oxygen with hemoglobin and this reaction scheme has been discussed in Appendix B.

Consider a single sphere, of radius a and permeability P_d , immersed in an infinite liquid medium of permeability P_c . A constant mass flux N_A is imposed at large distances from the sphere (as shown in Figure A.1). Inside the sphere the species A reacts with the carrier species B (which is constrained to remain within the sphere) in a four-step reaction scheme



Here k_j is the forward rate constant, b_j is the reverse rate constant, and K_j is the corresponding equilibrium constant. The mass conservation equations inside the sphere are of the form

$$\nabla^2(D_i C_i) = R_i \quad (4.139)$$

where ∇^2 is the Laplacian in spherical coordinates, which (for azimuthal symmetry) is

$$\nabla u^2 = \frac{1}{r^2} \frac{\partial}{\partial r} \left(r^2 \frac{\partial u}{\partial r} \right) + \frac{1}{r^2 \sin \theta} \frac{\partial}{\partial \theta} \left(\sin \theta \frac{\partial u}{\partial \theta} \right) \quad (4.140)$$

and R_i is the rate per unit volume of the depletion of species i . Mass conservation equations of the form of (4.139) apply to the species C_A , C_B , C_{AB} , C_{A_2B} , C_{A_3B} , and C_{A_4B} inside the sphere. In this section the primes have been omitted to denote conditions inside the sphere, and the asterisk will be used to denote

conditions outside the sphere. Outside the sphere the sole species is A and the mass conservation equation in spherical coordinates is

$$\nabla^2 (D_A^* C_A^*) = 0$$

or

$$\nabla^2 (p_A^*) = 0 \quad (4.141)$$

The boundary conditions for this problem are;

inside the sphere,

$$p_A = p_A^o \quad \text{at } r = 0 \quad (4.142)$$

at the sphere boundary,

$$P_d \frac{\partial p_A}{\partial r} = P_c \frac{\partial p_A^*}{\partial r} \quad \text{at } r = a \quad (4.143)$$

$$p_A = p_A^* \quad \text{at } r = a \quad (4.144)$$

$$\frac{\partial C_B}{\partial r} = \frac{\partial C_{AB}}{\partial r} = \frac{\partial C_{A_2B}}{\partial r} = \frac{\partial C_{A_3B}}{\partial r} = \frac{\partial C_{A_4B}}{\partial r} = 0$$

$$\text{at } r = a \quad (4.145)$$

and far away from the sphere,

$$P_c \frac{\partial p_A^*}{\partial r} = -N_A \cos \theta \quad \text{as } r \rightarrow \infty \quad (4.146)$$

The solution for the partial pressure variation of A outside the sphere is of the form

$$p_A^* - p_A^o = -\frac{N_A}{P_c} r \cos \theta \left\{ 1 + A \left(\frac{a}{r} \right)^3 \right\} \quad (4.147)$$

The potential outside the sphere is given by $(p_A^* - p_A^0)$ so that

$$\phi = -\frac{N_A}{P_C} r \cos \theta \left\{ 1 + A \left(\frac{a}{r} \right)^3 \right\} \quad (4.148)$$

The solution of the equations inside the sphere is obtained by a linearized perturbation analysis similar to that described earlier. Before proceeding it will be assumed here that the diffusivities of the carrier species are equal

$$D_B = D_{AB} = D_{A_2B} = D_{A_3B} = D_{A_4B} \quad (4.149)$$

It can then be shown (Appendix C) that the total carrier concentration is a constant throughout the sphere

$$C_B + C_{AB} + C_{A_2B} + C_{A_3B} + C_{A_4B} = C_T \quad (4.150)$$

from which the concentration C_{A_4B} can be eliminated. The concentration of the other species are expanded as small deviations from conditions at the center of the sphere

$$p_A = p_A^0 + \Delta p_A = p_A^0 + f(r) \cos \theta \quad (4.151a)$$

$$C_B = C_B^0 + \Delta C_B = C_B^0 + g(r) \cos \theta \quad (4.151b)$$

$$C_{AB} = C_{AB}^0 + \Delta C_{AB} = C_{AB}^0 + h(r) \cos \theta \quad (4.151c)$$

$$C_{A_2B} = C_{A_2B}^0 + \Delta C_{A_2B} = C_{A_2B}^0 + i(r) \cos \theta \quad (4.151d)$$

$$C_{A_3B} = C_{A_3B}^0 + \Delta C_{A_3B} = C_{A_3B}^0 + j(r) \cos \theta \quad (4.151e)$$

After substitution of these equations in the conservation equations inside the sphere, and elimination of second order terms, one arrives at five differential equations in f , g , h , i , and j . Appendix C gives the solution in detail. Once the constant A has been determined, the effective permeability can be obtained (utilizing Maxwell's technique) from

$$\frac{\bar{P}}{P_c} = \frac{1 - 2\phi A}{1 + \phi A} \quad (4.152)$$

As shown in Appendix C, if the reactions (4.139) are at equilibrium throughout the sphere, the constant A is given by

$$A = \frac{P_c - P_d [1 + F_{eq}^{Adair}]}{2P_c + P_d [1 + F_{eq}^{Adair}]} \quad (4.153)$$

where the equilibrium facilitation factor for the Adair four-step model is given by

$$F_{eq}^{Adair} = \frac{4D_B C_T \left(\frac{dy}{dp_A} \right)^0}{P_d} \quad (4.154)$$

The term dy/dp_A is the slope of the hemoglobin saturation curve.

The effective permeability can therefore be obtained from

$$\frac{\bar{P}}{P_c} = \frac{P_d (1 + F_{eq}^{Adair}) + 2P_c - 2\phi [P_c - P_d (1 + F_{eq}^{Adair})]}{P_d (1 + F_{eq}^{Adair}) + 2P_c + \phi [P_c - P_d (1 + F_{eq}^{Adair})]} \quad (4.155)$$

Equation (4.153) and (4.155) show that the dispersed phase permeability of A is increased by a factor $(1 + F_{eq}^{Adair})$.

In the case that the reaction is not at equilibrium, it is shown in Appendix C that the solution for A depends on

four eigenvalues. The four eigenvalues, β_j , for the four-step model correspond to the characteristic length λ of the one-step model. Although in the Adair four-step model there are four reactions and four β_j , there is not an one-to-one correspondence between a specific reaction and any of the β_j . Changing the rate constants for an individual reaction will change all β_j as they are each dependent on all the rate parameters. Each β_j represents a solution to the differential equations governing the four-step reaction scheme.

In the case of nonequilibrium conditions inside the sphere the constant A is obtained by solving (see Appendix E) a system of ten equations containing ten unknowns (including A). Since the effect of a reversible chemical reaction involving mobile carrier species is to increase the steady state mass transfer flux of the diffusing species it can be shown that the constant A must be of the form

$$A = \frac{P_c - P_d(1 + F^{\text{Adair}})}{2P_c + P_d(1 + F^{\text{Adair}})} \quad (4.156)$$

where F^{Adair} is the nonequilibrium facilitation factor. The effective (relative) permeability of the heterogeneous medium can be obtained from (4.152) by substitution of equation (4.156) for A, which yields

$$\frac{\bar{P}}{P_c} = \frac{P_d(1 + F^{\text{Adair}}) + 2P_c - 2\phi[P_c - P_d(1 + F^{\text{Adair}})]}{P_d(1 + F^{\text{Adair}}) + 2P_c + \phi[P_c - P_d(1 + F^{\text{Adair}})]} \quad (4.157)$$

If F^{Adair} is near zero equation (4.157) reduces to Maxwell's

equation. The average effective permeability over a large driving force is obtained by integrating the local effective permeability \bar{P} over the total partial pressure range

$$\bar{P}_{AVE} = \frac{\int_{p_A^{x=0}}^{p_A^{x=L}} \bar{P} dp_A}{(p_A^{x=L} - p_A^{x=0})} \quad (4.158)$$

Note that once \bar{P}_{AVE} has been determined the flux can be calculated from Fick's law.

5. ANALYSIS AND APPLICATION OF THEORY

5.1 Reaction in the Dispersed Phase Only

5.1.1 One-Step Model

5.1.1.1 Single Sphere in a Continuum

5.1.1.2 Permeability of a Suspension of Spheres: Application to the Oxygen-Hemoglobin System

5.1.1.3 A Note on Kinetic Parameters

5.1.2 Four-Step Model

5.1.3 Comparison of One-Step and Four-Step Model

5.2 Reaction in the Dispersed and Continuous Phase. The Impermeable and Permeable Model

5.2.1 Single Sphere in a Continuum

5.2.2 Effective Permeability of a Suspension of Spheres

5.2.3 A Note on the Impermeable Model

5. ANALYSIS AND APPLICATION OF THEORY

In the reduction of the impermeable carrier model and the permeable carrier model to other systems of interest, it was shown that the two models give the same predictions for the case of a reaction inside the dispersed phase, but no reaction inside the continuous phase. The case of reaction inside only is of interest because it is the model for oxygen diffusion in whole blood. In addition to the one-step reaction in the dispersed phase, a four-step reaction scheme in the dispersed phase was developed in chapter four. These will be referred to as the one-step and the four-step model. These two reaction models will be discussed and applied to oxygen transport before considering the general impermeable and permeable models.

5.1 Reaction in the Dispersed Phase Only

5.1.1 One-Step Model

5.1.1.1 Single Sphere in a Continuum

In order to reduce the general model (permeable or impermeable) to the case of reaction inside the dispersed phase only, it was shown earlier that F_{eq} must be set equal to zero. The partial pressure p_A' inside the sphere is given by equations (4.56), (4.55), (4.68), (4.73), and (4.86) and is

$$p_A' = p_A^o - \frac{N_A^T a}{P_c} \left(\frac{r}{a}\right) \left[\frac{3P_c}{2P_c + P_d(1+F_d)} \right]$$

$$\left\{ \left(\frac{1}{1+F_{eq}'} \right) + \frac{F_{eq}' \left(\frac{a}{r}\right)^{3/2} \left(\frac{\lambda'}{r}\right)^{1/2} \left[\cosh \frac{r}{\lambda'} - \frac{\sinh(r/\lambda')}{r/\lambda'} \right]}{(1+F_{eq}') \left(\frac{\lambda'}{a}\right)^{1/2} \left[-2 \left(\cosh \frac{a}{\lambda'} - \frac{\lambda'}{a} \sinh \frac{a}{\lambda'} \right) + \frac{a}{\lambda'} \sinh \frac{a}{\lambda'} \right]} \right\} \cos \theta$$

.....(5.1)

The partial pressure p_A outside the sphere is obtained from equations (4.43), (4.43a), (4.64), and (4.68) and is

$$p_A = p_A^o - \frac{N_A^T a}{P_c} \left(\frac{r}{a}\right) \left\{ 1 + \left(\frac{a}{r}\right)^3 \left[\frac{P_c - P_d(1 + F_d)}{2P_c + P_d(1 + F_d)} \right] \right\} \cos \theta \quad (5.2)$$

(Subscript d or superscript prime refers to the dispersed phase.)

As discussed earlier the partial pressure of species A outside the sphere is given by the imposed potential field plus a term accounting for the presence of the sphere. The relative effect of the disturbance term decays with the cube of the distance from the center of the sphere. The dispersed phase facilitation factor F_d is the relative amount by which permeation of species A across the sphere is increased by carrier-facilitated transport. Insofar as the concentration field outside the sphere is concerned, the effect of chemical reaction is simply to increase the apparent permeability of the sphere which is given by $P_d(1 + F_d)$. When no reaction occurs, or the reaction effect is insignificant with respect to diffusive transport, F_d is zero and the problem reduces to that of an inert sphere in a continuum (Maxwell Problem).

The facilitation factor F_d was derived by utilizing a single-point linearization similar to the approximation employed by Friedlander and Keller (1965), and the functionality

of F_d is given by equation (4.71). In Figure 5.1 a comparison is given between the facilitation factor F_d derived by Friedlander and Keller for a slab, given by equation (3.39), and the facilitation factor derived here for a single sphere (Note: the subscript d and superscript prime are irrelevant in this comparison). The facilitation factor depends only upon F'_{eq} and a/λ' (or L/λ') and the case chosen here is consistent with parameters (listed in Table 5.1) occurring inside the red blood cell at 25°C. At large a/λ' , F_d approaches its maximum value which is characteristic of chemical reaction equilibrium throughout the sphere. As a/λ' decreases, F_d decreases as the chemical reaction departs from equilibrium within a boundary layer at the sphere surface, the thickness of which is of order λ' . Note that the Friedlander and Keller facilitation factor, for permeation through a one dimensional slab, approaches F'_{eq} in the same way as the solution for a sphere. That is to say, when λ' is very much smaller than the size of the sphere, the boundary layer is a spherical shell which is essentially one dimensional in character. The influence of spherical geometry begins to have an effect when λ' is greater than 20% of the sphere radius.

In Figure 5.2 radial profiles are shown for species A (partial pressure) and B (concentration) at the axis of symmetry. The profile of B inside the sphere can be obtained from equations (4.57), (4.55), (4.73), and (4.86) and is

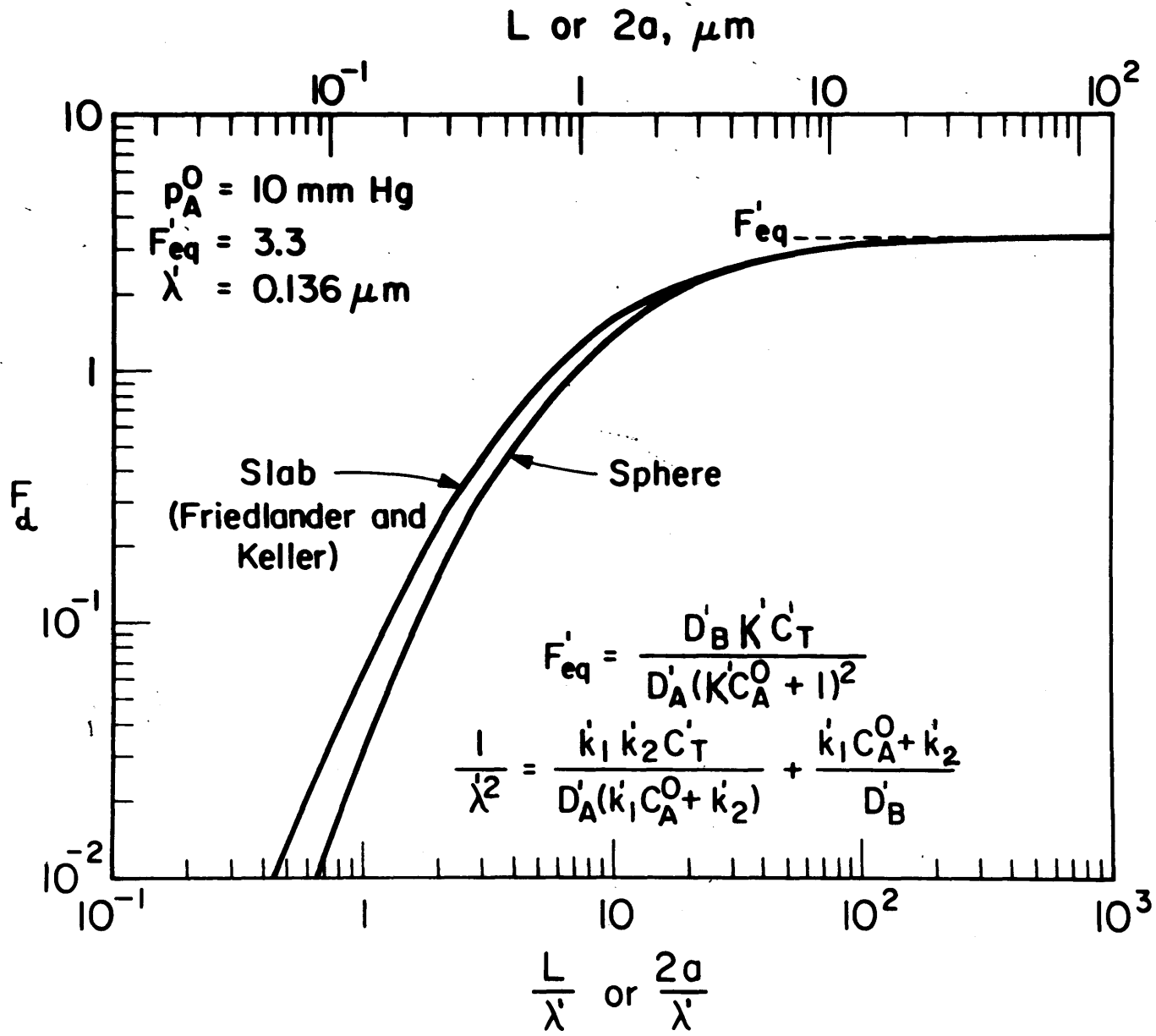


FIGURE 5.1. COMPARISON OF THE FACILITATION FACTOR FOR SPHERE AND SLAB.

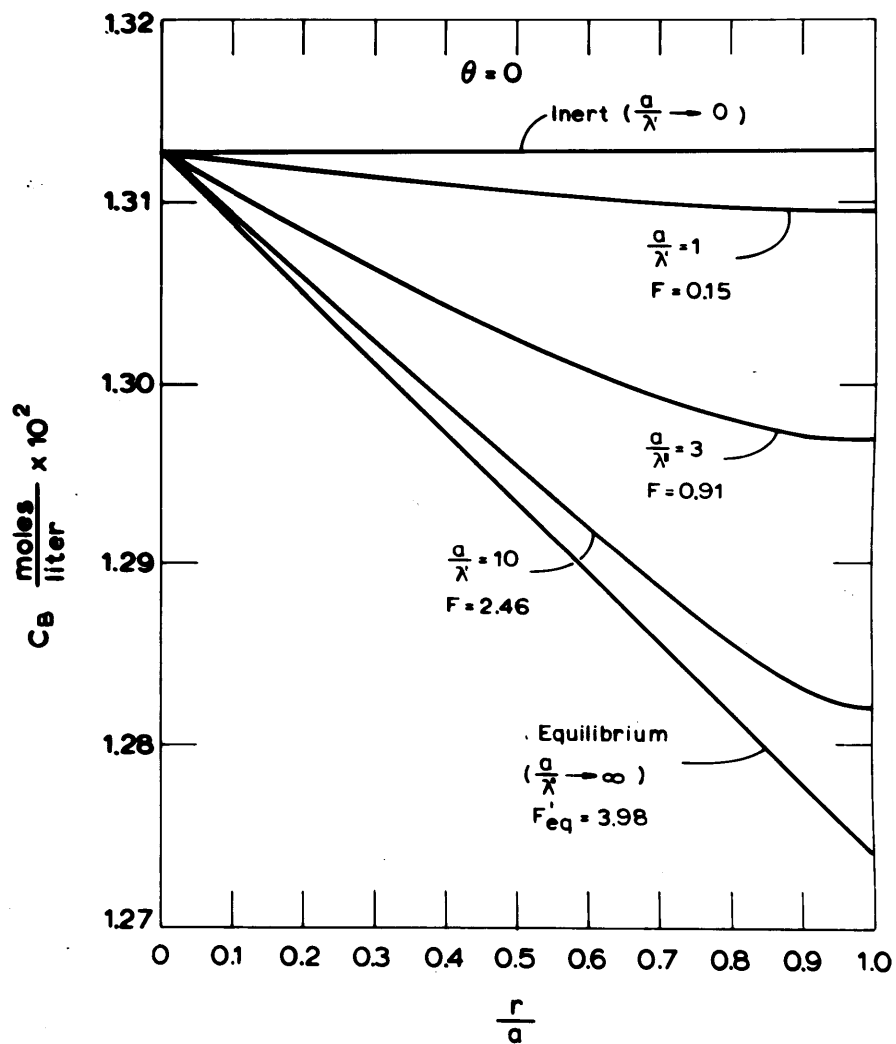
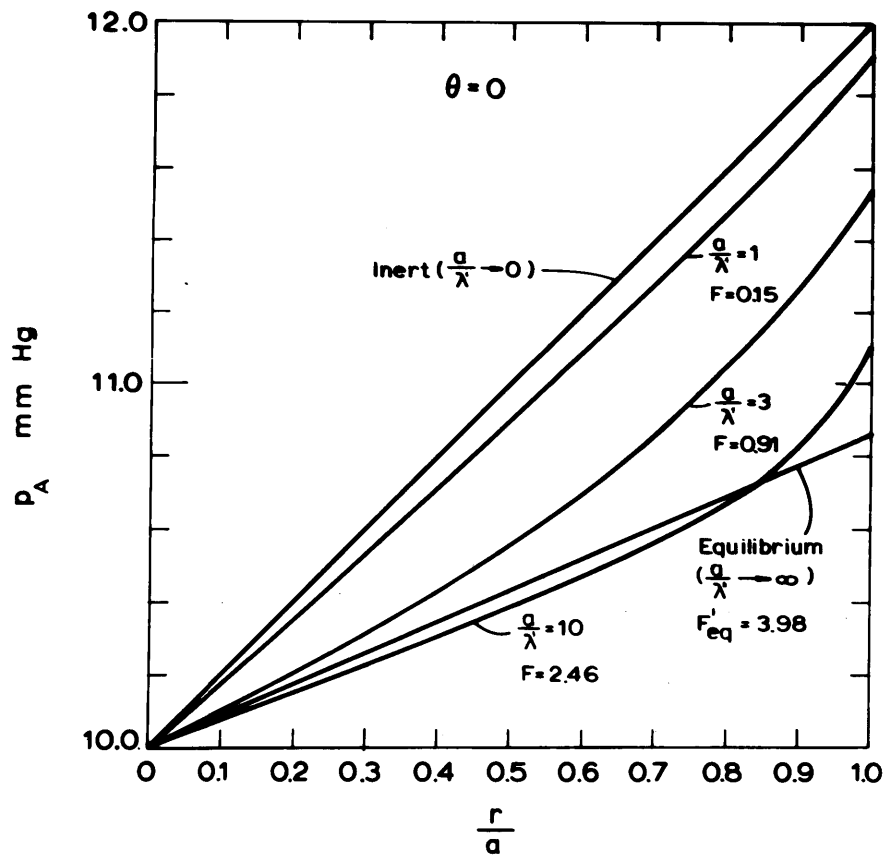


FIGURE 5.2

CONCENTRATION PROFILES INSIDE THE SPHERE FOR THE SPECIES A AND B FOR DIFFERENT VALUES OF a/λ' .

$$C'_B = C'_B{}^O + \frac{N_A^T a}{D'_B} (1 - 2A) \left(\frac{r}{a}\right) \left\{ \frac{F'_{eq}}{1 + F'_{eq}} - \frac{F'_{eq} \left(\frac{a}{r}\right)^{3/2} \left(\frac{\lambda'}{r}\right)^{1/2} \left[\cosh \frac{r}{\lambda'} - \frac{\sinh(r/\lambda')}{r/\lambda'} \right]}{(1 + F'_{eq}) \left(\frac{\lambda'}{a}\right)^{1/2} \left[-2 \left(\cosh \frac{a}{\lambda'} - \frac{\lambda'}{a} \sinh \frac{a}{\lambda'} \right) + \frac{a}{\lambda'} \sinh \frac{a}{\lambda'} \right]} \right\} \cos \theta$$

..... (5.3)

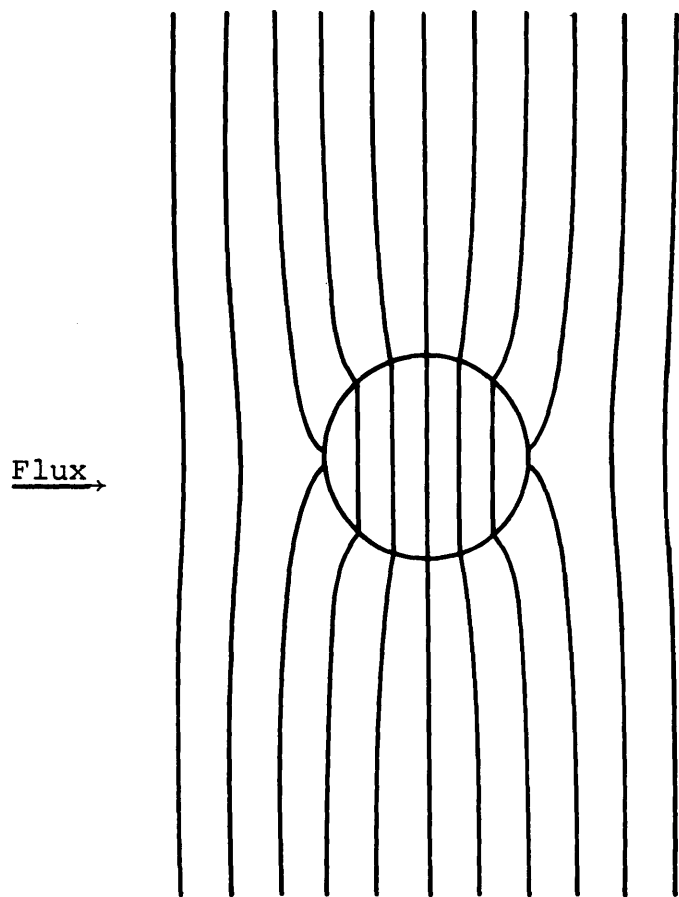
The curves in Figure 5.2 are plotted for a case where the permeabilities of the dispersed and continuous phases are equal. They show qualitatively the effects of increasing facilitation factor as a/λ' increases. For the inert case ($a/\lambda' = 0$), the partial pressure of A is linear in r across the entire sphere. When reaction occurs, the profile is curved over a region comparable in length to λ' . As F_d increases towards its equilibrium value F'_{eq} , the apparent permeability of the sphere increases and the partial pressure of A at the surface of the sphere decreases. As a consequence, the concentration or partial pressure differences across the sphere are less than those imposed over an equivalent dimension in the free stream far from the sphere. This reinforces the validity of the key assumption in the analysis that is, the grounds on which the second order terms in the reaction rate expression are dropped.* The concentration profiles of B behave in a qualitatively similar fashion except that the gradient at the surface is zero. The concentration profile of B becomes successively steeper as a/λ' increases and equilibrium conditions are attained throughout the sphere. Note that for $a/\lambda' = 10$ the reaction is close to equilibrium near the center of the sphere, and since C_B for $a/\lambda' = 10$ is greater than the equilibrium value of C_B at $a/\lambda' \rightarrow \infty$,

* It also reinforces the use of single point linearization.

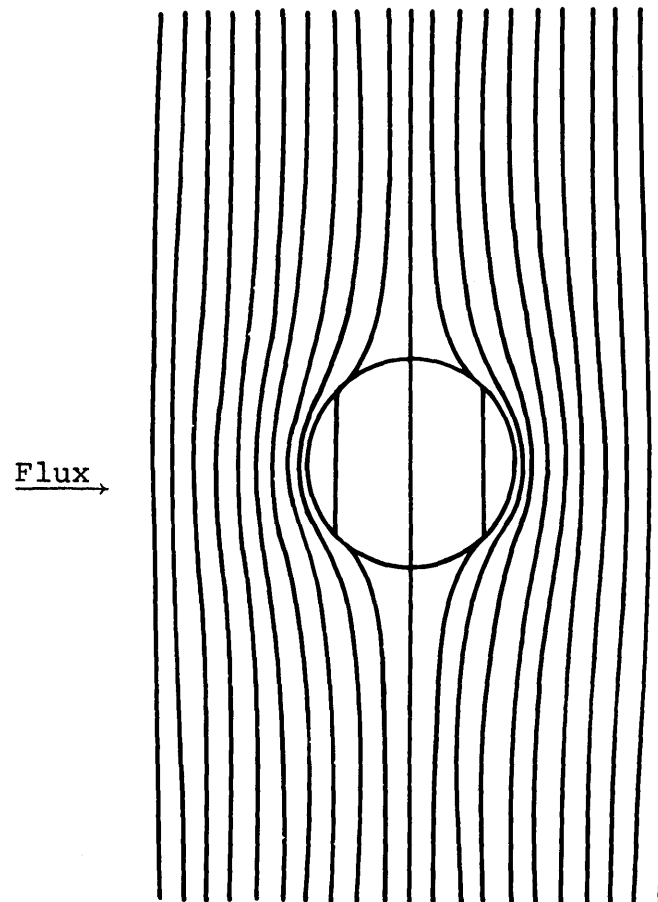
the profile of A (Figure 5.2) will dip below the equilibrium p_A profile near the center of the sphere.

Figure 5.3 shows qualitatively the local partial pressure field (potential) when the permeability of the sphere is either less than or greater than the surroundings for the case of no reaction inside the sphere (Maxwell's problem). As expected, curves of constant potential outside the sphere (p_A) tend to bend away from the region of higher permeability, but within the sphere (p'_A) they are straight lines. Notice that the disturbance on the potential outside the sphere decays rapidly as the distance from the periphery of the sphere increases. When a chemical reaction occurs inside the sphere, the interior loci of constant partial pressure, p'_A , become curved as shown in Figure 5.4. Figure 5.4 has been drawn so that the field outside the sphere does not change by making the apparent permeability of the sphere the same, with or without reaction. As has been discussed before, the partial pressure of A is equivalent to the potential ϕ in the case of an inert continuum. For the case of a reactive sphere in an inert continuum p_A still represents the potential outside the sphere, but p'_A no longer is the potential inside the sphere. The potential must be appropriately defined to include the effect of the chemical reaction, so as to satisfy Laplace's equation and can be taken as

$$\phi' = (p'_A - p_A^0) - \frac{D'_B}{P_d} C'_B + D_1 + D_2 \cos \theta \quad (5.4)$$



$P_{\text{Sphere}} < P_{\text{Surroundings}}$



$P_{\text{Sphere}} > P_{\text{Surroundings}}$

FIGURE 5.3
 POTENTIAL FIELD (LOCI OF CONSTANT PARTIAL PRESSURE OF A) AROUND
 INERT SPHERES.

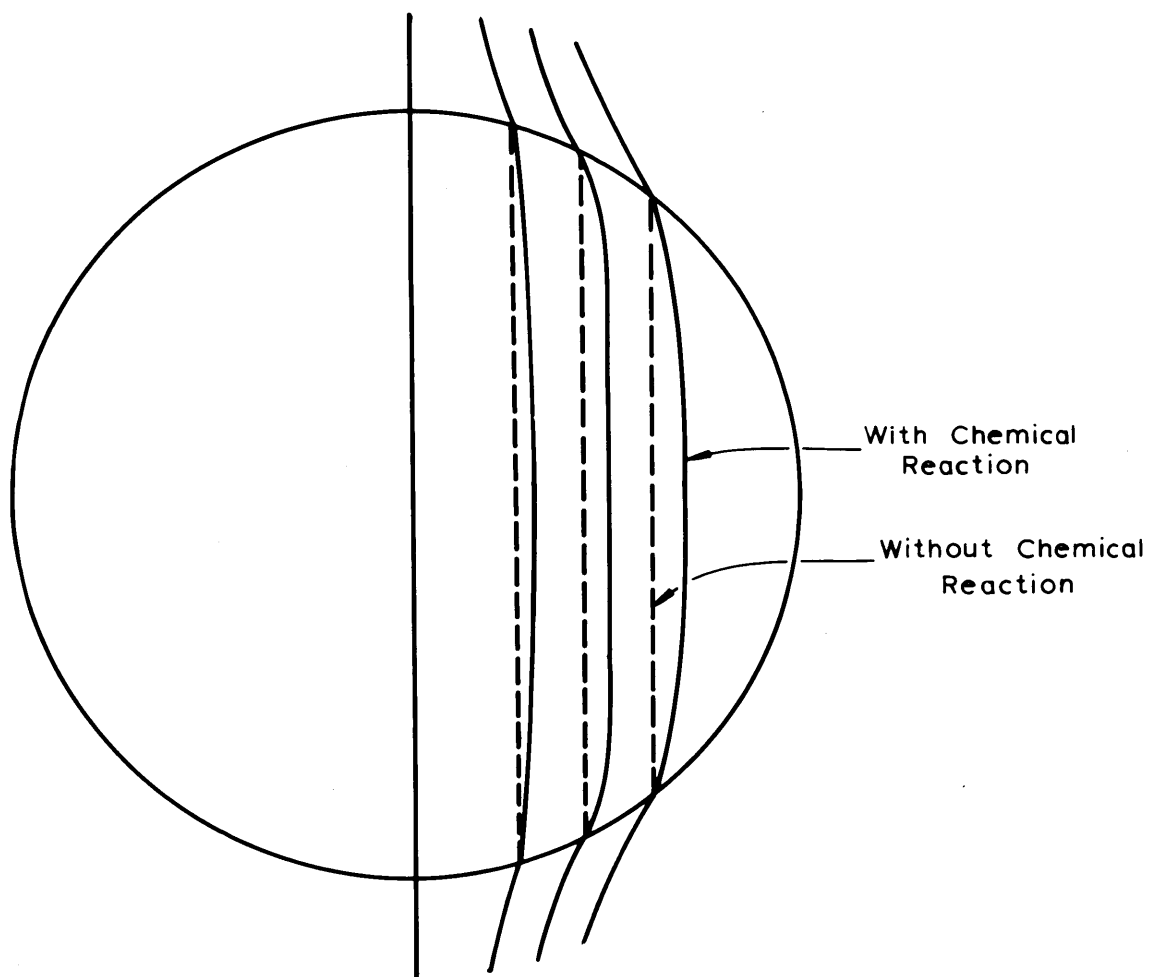


FIGURE 5.4
LOCI OF CONSTANT PARTIAL PRESSURE OF SPECIES
A INSIDE AND OUTSIDE THE SPHERE.

inside the sphere and

$$\phi = p_A - p_A^0 \quad (5.5)$$

outside the sphere. The constants D_1 and D_2 can be evaluated by requiring

$$\phi' = \phi \quad \text{at } r = a \quad (5.6)$$

$$p_A' = p_A \quad \text{at } r = a \quad (5.7)$$

so that

$$D_1 = \frac{D_B'}{P_d} C_B^0 \quad (5.8)$$

and

$$D_2 = \frac{N_A^T a}{P_c} [-(1 + A) + \frac{P_c}{P_d} (1 - 2A)] \quad (5.9)$$

where A is given by equation (4.86). The form of the potential is somewhat arbitrary in terms of the constants because as defined by equations (5.4) and (5.5) and boundary condition (5.6) the potential has been made arbitrarily continuous across the sphere boundary. Once the potential has been defined the flux can be calculated by

$$(\psi_2 - \psi_1) = \int_1^2 r^2 \sin \theta \frac{d\phi}{dr} d\theta \quad (5.10)$$

The flux outside and inside the sphere is therefore given respectively by

$$(\psi_2 - \psi_1) = \frac{N_A^T a^2}{P_d} \frac{\sin^2 \theta}{2} \left[\frac{A}{(r/a)} - \frac{(r/a)^2}{2} \right] \quad (5.11)$$

(where the limits of integration are from zero to θ).

and
$$(\psi_2' - \psi_1') = - \frac{N_A^T a^2}{P_d} \left(\frac{r}{a}\right)^2 \left(\frac{1 - 2A}{2}\right) \frac{\sin^2 \theta}{2} \quad (5.12)$$

Complete flux, potential, and partial pressure plots, are shown in Figure 5.5 . Here predominantly vertical curves are loci of constant potential or partial pressure, and the predominantly horizontal lines are streamlines or lines of constant flux difference. In the absence of reactions inside the sphere, these two sets of curves are, of course, mutually orthogonal and are calculated so that they form curvilinear squares outside the sphere. For reference, the case of equal permeabilities in the dispersed and continuous phases is shown in the left hand figure. Lines of constant potential are all vertical and lines of constant mass flux difference are all parallel to the imposed potential gradient.

On the right hand side are figures for three sets of conditions involving a sphere exposed to the same imposed potential gradient (or mass flux). At the bottom, the permeability of the sphere is less than that of the surroundings for the case of no reaction. Constant potential lines bend into the sphere (as they do for the left hand side of Figure 5.3) while the streamlines bend away from the sphere as most of the mass diffuses around it. In the center figure on the right the reaction has been turned on, and lines of constant partial pressure are plotted. Inside the sphere, of course, these two sets of lines are no longer orthogonal. When the potential function is appropriately defined to include the effect of chemical reaction as given by equation (5.12) the isopotential lines and streamlines will again be orthogonal, as shown in

Outside Sphere.

$$\phi = p_A' - p_A^0$$

$$\psi = \frac{P_c}{P_d} \int_0^\theta r^2 \sin \theta \frac{\partial \phi}{\partial r} d\theta$$

Inside Sphere.

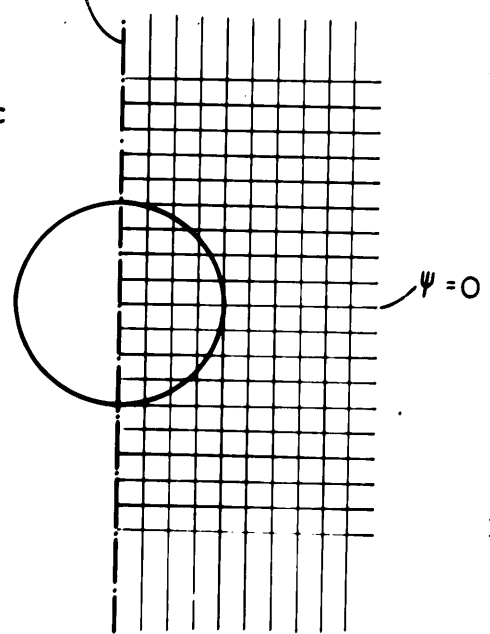
$$\phi' = p_A' + \frac{D_B' C'_{AB}}{P_d} + (\text{const}) \cos \theta$$

$$+ \text{const.}$$

$$\psi' = \int_0^\theta r^2 \sin \theta \frac{\partial \phi'}{\partial r} d\theta$$

$$\phi = 0$$

$P_d = P_c$



(No) Reaction

$$P_d \equiv P_d, (1+F) > P_c$$

Reaction

$$P_d, (1+F) > P_c$$

$$\frac{a}{\lambda} = 20$$

$$F = 11$$

Inside Sphere

$$\phi = p_A$$

No Reaction

$$P_d = P_d, < P_c$$

$$\frac{P_d}{P_c} \equiv 0.3$$

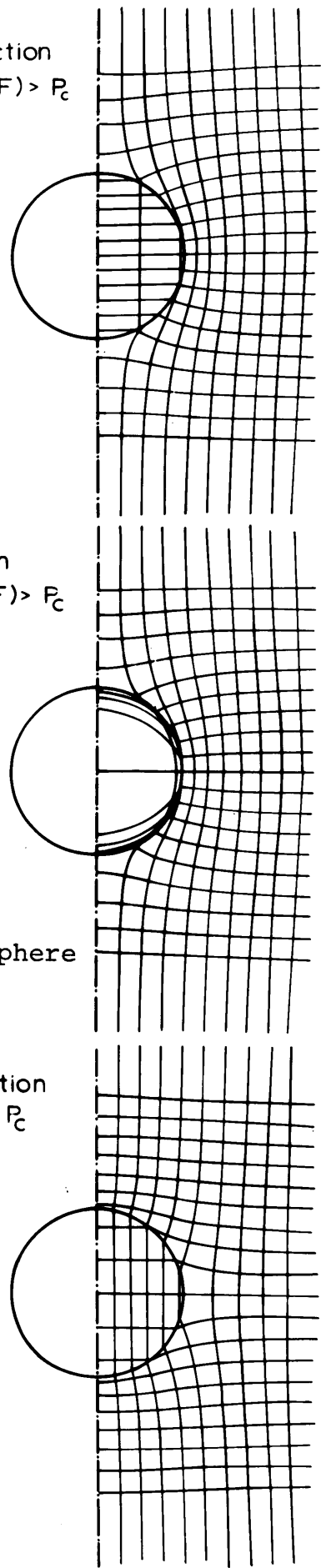


FIGURE 5.5

COMPLETE FLUX AND POTENTIAL PLOTS.

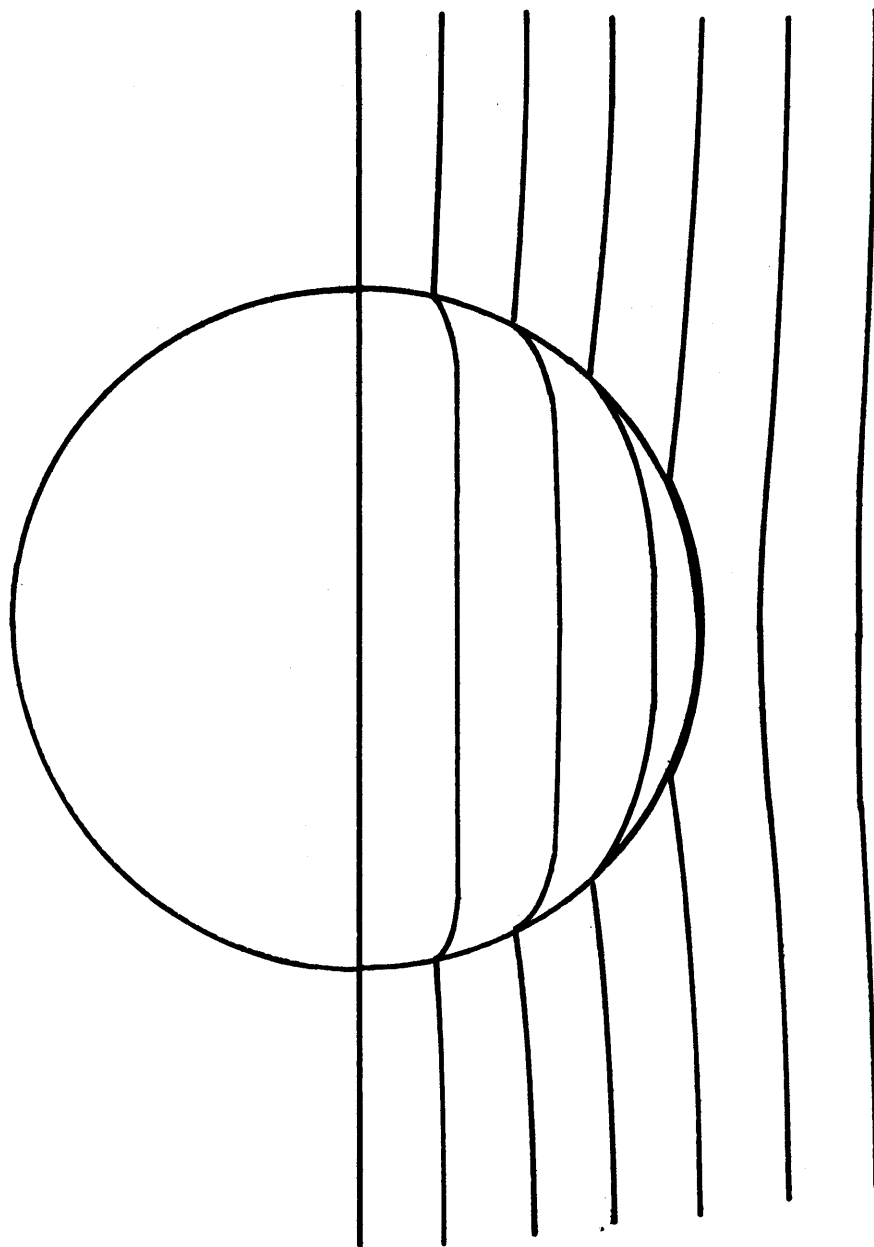


FIGURE 5.5a

LOCI OF CONSTANT PARTIAL PRESSURE OF SPECIES A
INSIDE AND OUTSIDE THE SPHERE.

the figure in the upper right. The lines of constant flux difference for both figures bend towards the sphere as most of the mass near the sphere diffuses through the sphere. The partial pressure loci (in the right hand middle figure) are severely curved near the periphery of the inside of the sphere because the carrier species concentration gradient near the periphery must approach zero so that most of the flux (near the periphery) is by diffusion of A which requires a large gradient in A.

The top figure can also represent an inert sphere in an inert continuum for the case

$$P_d(\text{no reaction}) = P_d(1 + F)$$

The potential and flux definitions are valid generally since the term in equation (5.4) due to the presence of the carrier species reduces to zero as a/λ' approaches zero.

Finally an interesting graphical result is obtained when $P_d(1 + F_d)$ is smaller than P_c . In this case partial pressure profiles outside the sphere bend towards the sphere, and the partial pressure profiles inside the sphere bend towards the periphery of the sphere as shown in Figure 5.5a, reversing curvature.

5.1.1.2 Permeability of a Suspension of Spheres:

Application to the Oxygen-Hemoglobin System

Once the outside potential is fully described as a function of r and θ , an effective permeability can be obtained

for a dilute suspension of spheres. From the previous chapter the effective permeability is given by equation (4.99)

$$\frac{\bar{P}}{P_c} = \frac{2P_c + P_d(1 + F_d) - 2\phi[P_c - P_d(1 + F_d)]}{2P_c + P_d(1 + F_d) + \phi[P_c - P_d(1 + F_d)]} \quad (5.13)$$

It is interesting to analyze the behaviour of the above relationship in terms of criteria similar to those given by equations (3.2) and (3.3)

$$\phi = 0 \quad \bar{P} = P_c \quad (5.14)$$

$$\phi = 1 \quad \bar{P} = P_d(1 + F_d) \quad (5.15)$$

Equation (5.13) exhibits the correct behaviour. Notice that, for a "homogeneous" medium of the dispersed phase, the permeability would be

$$\bar{P} = P_d(1 + F'_{eq}) \quad (5.16)$$

if the film thickness L should be of such a magnitude that L/λ' is large enough so that equilibrium is established throughout the film. In the case of a "heterogeneous" medium of the dispersed phase (at maximum volume fraction $\phi = 1$), one still has boundaries between adjoining particles that require the gradients of the carrier species to reduce to zero at each interface. This situation may be approached by packed red blood cells where volume fractions near one may be attained since the red blood cells are deformable. Even though in this case the particles are not spherical, equation (5.13) through (5.15) still will give a reasonable quantitative approximation

of the real situation. Notice that if the reaction is at equilibrium inside the sphere, the carrier concentration gradient inside the sphere adjusts to zero in an infinitely thin boundary layer at the periphery of the sphere so that in this case (5.15) reduces in that case to (5.16).

Equation (5.13) will now be applied to the problem of oxygen transport in red blood cell suspensions. The oxygen-hemoglobin saturation curve has been discussed in Appendix B and was shown to be sigmoidal in nature. The one-step reaction scheme leads to a hyperbolic saturation curve. Figure 5.6 compares the hyperbolic saturation curves for various equilibrium constant with a sigmoidal saturation curve with a p_{50} of 10 mm Hg. The p_{50} here is the partial pressure at 50 per cent saturation, and a p_{50} of approximately 10 mm Hg is consistent with human blood in the presence of 2,3 DPG at 25°C. It should be obvious from Figure 5.6 that a sigmoidal saturation curve cannot be fitted with a one-step saturation curve regardless of what equilibrium constant is used. The one-step approach therefore is an approximation to the real physical situation, but as has been discussed in Chapter 3, it remains a reasonable model in light of the results of the kinetic experiments performed by Roughton and others. The analysis performed here can be extended to the four-step scheme (see next section) that more closely models the sigmoidal saturation curve. However, as has been pointed out in Appendix B, the Adair scheme too is still an approximation (of higher accuracy than the one-step model) as has been indicated from experimental results obtained

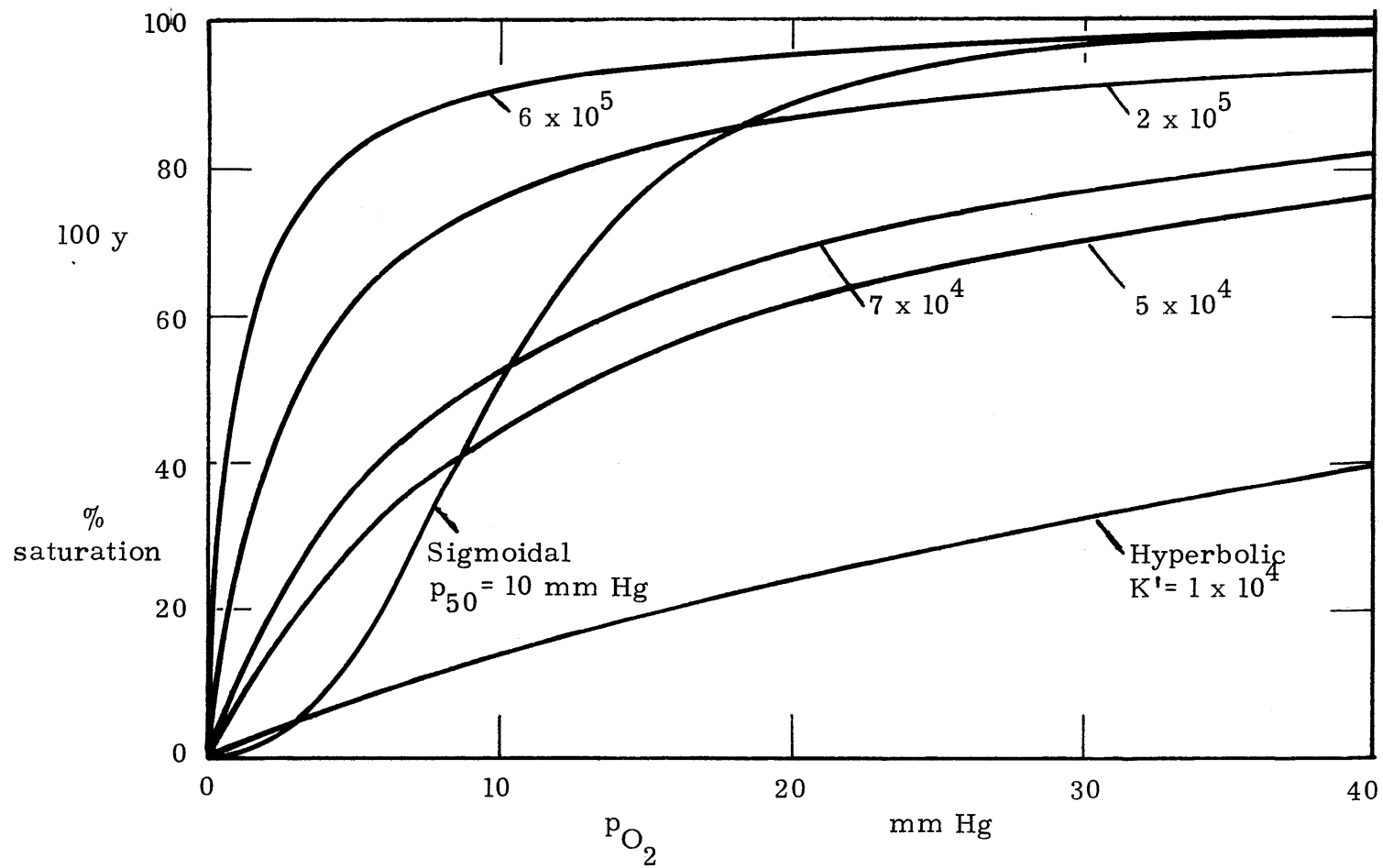


FIGURE 5.6
COMPARISON OF SIGMOIDAL SATURATION CURVE WITH HYPERBOLIC CURVES.

by Roughton et al. (1971) and Gibson (1973). The kinetic rate parameters chosen here are those given by Gibson (1959) and are equal to those used by Kreuzer and Hoofd (1970, 1972).

Figure 5.7 shows the characteristic length λ calculated as a function of oxygen partial pressure inside the red cell at 25°C for the one-step model. Oxygen and hemoglobin diffusion coefficients were taken from Kreuzer's review (shown in Figures 3.7 and 5.8) at red blood cell concentrations, and the oxygen solubility from Table 3.3. The parameters are consistent for whole blood at 25°C (red blood cells in plasma) and are tabulated in Table 5.1. The hemoglobin concentration is given in terms of the total heme concentration (four times the hemoglobin concentration).

The characteristic length λ' varies from 0.1 to 0.15 μm and reaches a maximum at about 24 mm Hg. The facilitation factor F_d calculated from these parameters is shown in Figure 5.8. F_d is plotted as a function of sphere radius for various values of oxygen partial pressure. The upper and lower bounds for the equivalent radius of the red blood cell treated as a sphere are given, first, on the low side by the smallest half-thickness of the red blood cell, taken as 1 μm , and second on the high side by the largest half axis of the red cell, taken to be 4 μm . Within these bounds, the facilitation factor varies from 40 to 80% of its equilibrium value. The curves depend markedly upon partial pressure primarily because of its effect on the equilibrium facilitation factor F'_{eq} and only secondarily because of the dependence of λ' in partial pressure. For a

TABLE 5.1
PARAMETERS EMPLOYED IN CALCULATIONS

$C_{Hm,T}$	=	0.020 moles/liter (one step model)
C_T	=	0.005 moles/liter
α_{O_2}	= α_A	= 1.75×10^{-6} gr-mole/liter/mmHg
D_{O_2}	= D_A	= 0.65×10^{-5} cm ² /sec
D_{Hb}	= D_B	= 0.76×10^{-7} cm ² /sec

KINETIC PARAMETERS

One-Step Model:

$$k_1' = 3.0 \times 10^6 \text{ liter/mole/sec}$$

$$k_2' = 42.8 \text{ sec}^{-1}$$

Four-Step Model:

<u>With 2,3 DPG*</u>	<u>Stripped of 2,3 DPG**</u>
$k_1 = 1.77 \times 10^6$	1.47×10^6 liter/mole/sec
$b_1 = 1900$	136 sec ⁻¹
$k_2 = 3.32 \times 10^6$	3.52×10^6 liter/mole/sec
$b_2 = 158$	15.7 sec ⁻¹
$k_3 = 4.89 \times 10^5$	1.58×10^6 liter/mole/sec
$b_3 = 539$	138 sec ⁻¹
$k_4 = 3.30 \times 10^6$	3.30×10^6 liter/mole/sec
$b_4 = 50$	50 sec ⁻¹

* Exact concentration of 2,3 DPG not known (probably 1 mole DPG: 1 mole Hb). T = 21.5°C, pH = 7.0.

** T = 20°C, pH = 7.0.

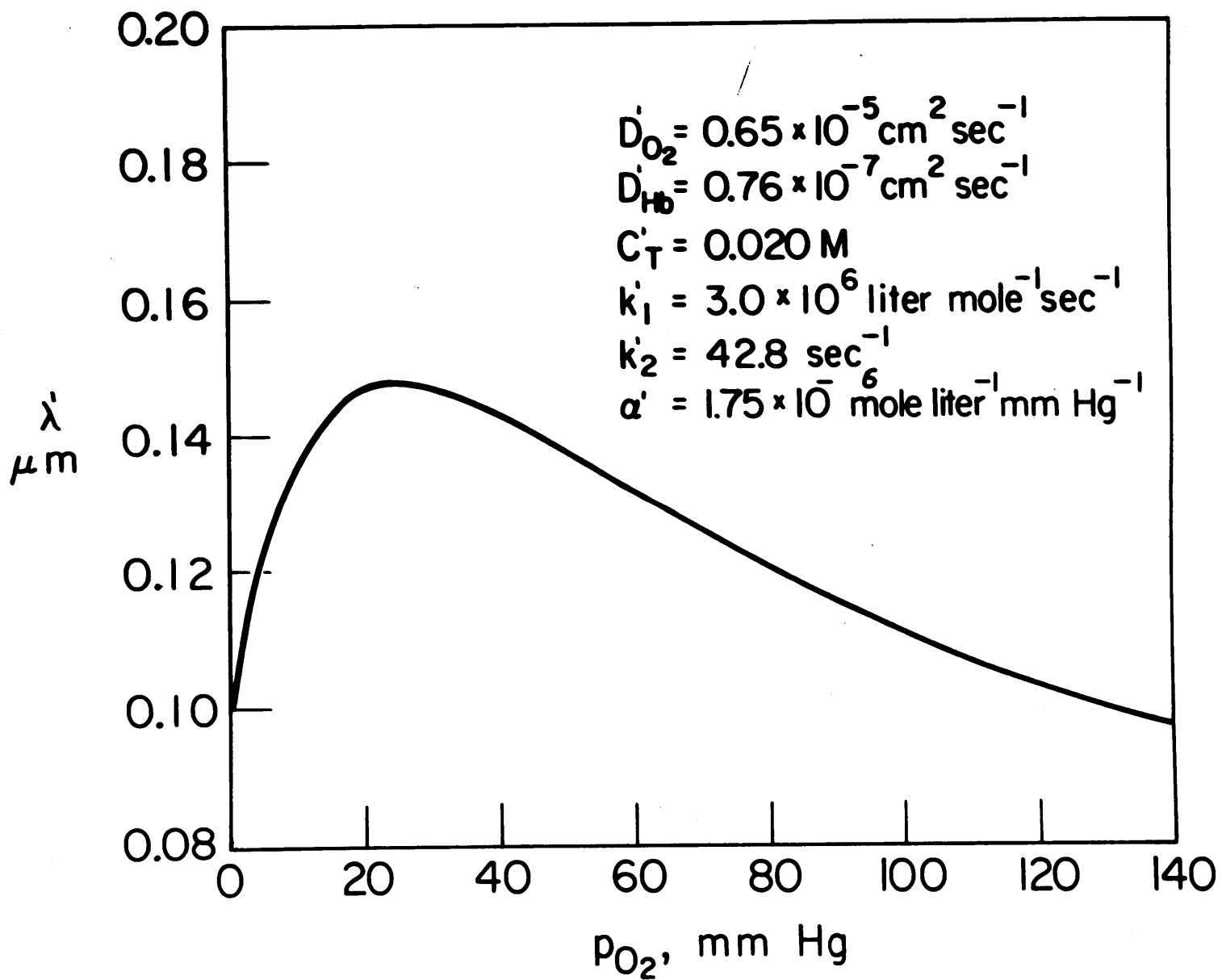


FIGURE 5.7. CHARACTERISTIC LENGTH FOR RED BLOOD CELL CONDITIONS.

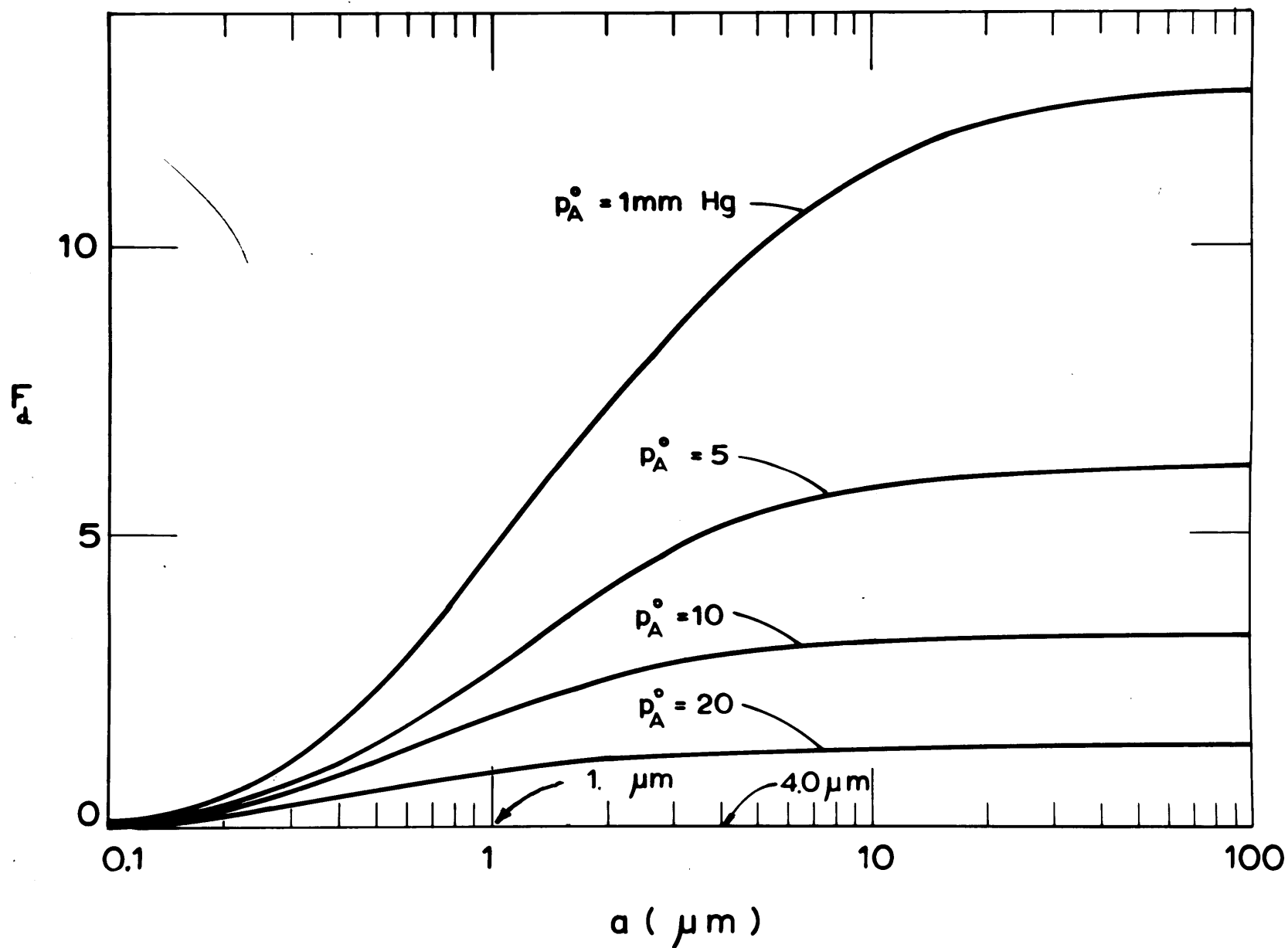


FIGURE 5.8. THE FACILITATION FACTOR AS A FUNCTION OF OXYGEN PARTIAL PRESSURE AND EQUIVALENT SPHERE RADIUS.

one-step reaction and at fixed a , F_d attains a maximum value as partial pressure approaches zero.

The local effective permeability values consistent with these facilitation factors for whole blood as a function of oxygen partial pressure are shown in Figure 5.9. The curves are plotted for the bounding estimates of the red cell equivalent sphere radius, for a sphere with equivalent red cell area, $1.6 \mu\text{m}$, and for the inert and equilibrium limiting conditions. For large partial pressures of oxygen all curves approach the inert situation since F_d continuously decreases with increasing partial pressure. At high oxygen concentrations the reaction saturates and the effect of the chemical reaction is negligible. It is noteworthy that the effective permeability is somewhat less sensitive to a departure from chemical equilibrium than is the facilitation factor itself. For example, in the limit of zero partial pressure, the permeability for a suspension of spheres with a $1.6 \mu\text{m}$ radius is only about 24% lower than the comparable value for reaction equilibrium, whereas the facilitation factor is about half of its equilibrium value. This is due in part to the fact that plasma, which constitutes 55 per cent of the total volume, has a significantly higher permeability than the red blood cells so that the chemical reaction effects are somewhat "dampened" by the continuous phase volume.

The average effective permeability over a specified partial pressure range is proportional to the area under the curve

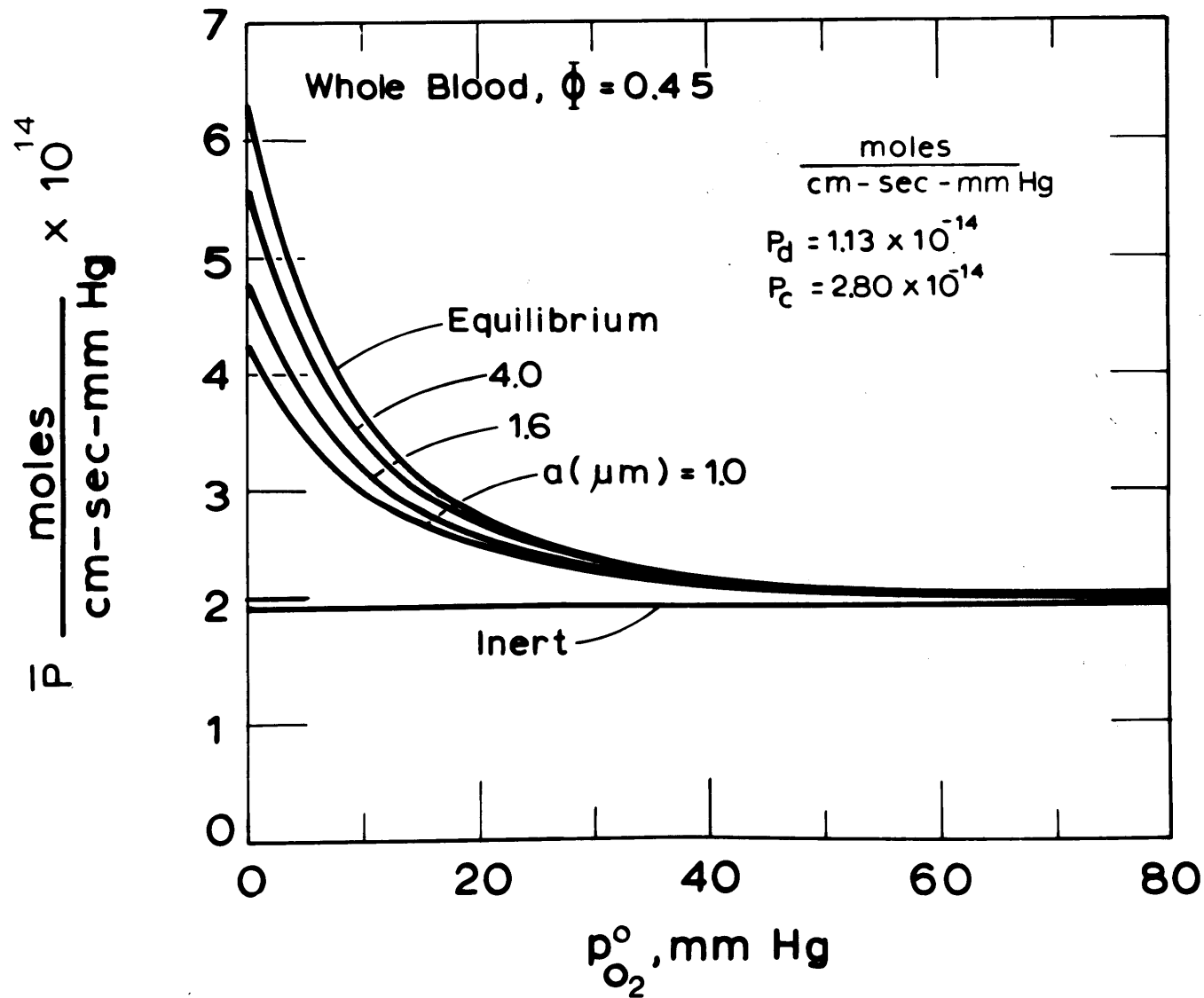


FIGURE 5.9. LOCAL EFFECTIVE PERMEABILITY FOR WHOLE BLOOD AT 25 °C.

$$\bar{P}_A = \frac{\int_{P_A^{(1)}}^{P_A^{(2)}} \bar{P} dp_A}{P_A^{(2)} - P_A^{(1)}} \quad (5.17)$$

For the equilibrium case the integral in equation (5.17) can be obtained in closed form

$$\bar{P}_{AVE} = P_c \left\{ \frac{s}{q} + \frac{t - \frac{rs}{q}}{K' \alpha_A' \sqrt{qr}} \left[\frac{\tan^{-1} \frac{q}{r} (K' \alpha_A' p_A^{(1)}) - \tan^{-1} \frac{q}{r} (K' \alpha_A' p_A^{(2)} + 1)}{p_a^{(1)} - p_A^{(2)}} \right] \right\} \quad (5.18)$$

where

$$q = \left(\frac{D'_A}{D'_B K'_T C'_T} \right) \left[\frac{P_d}{P_c} (1 - \phi) + 2 + \phi \right] \quad (5.19)$$

$$r = \frac{P_d}{P_c} (1 - \phi) \quad (5.20)$$

$$s = \left(\frac{D'_A}{D'_B K'_T C'_T} \right) \left[\frac{P_d}{P_c} (1 + 2\phi) + 2(1 - \phi) \right] \quad (5.21)$$

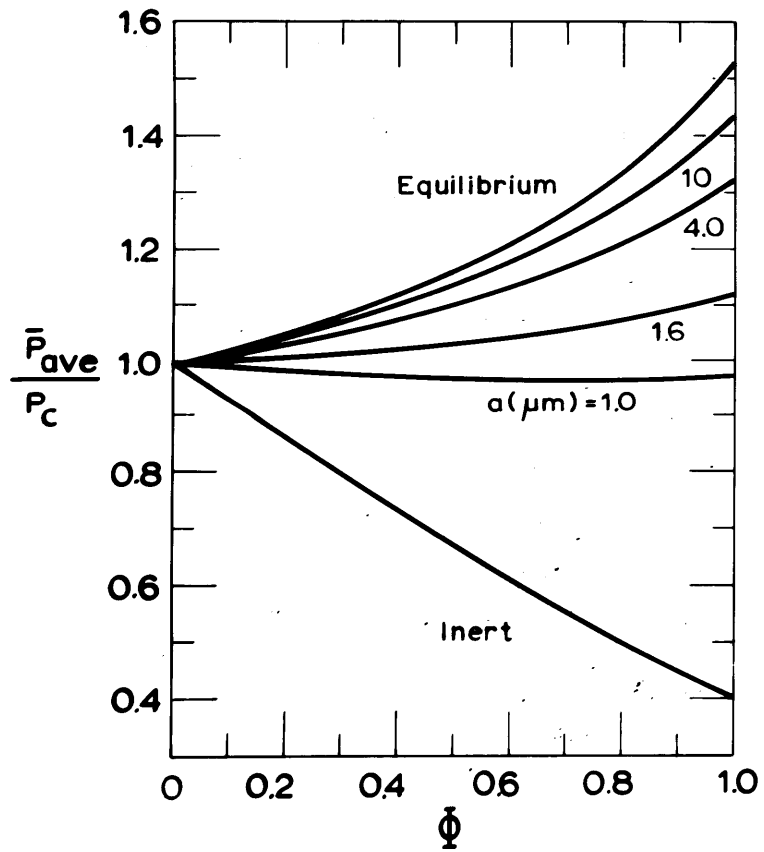
$$t = \frac{P_d}{P_c} (1 + 2\phi) \quad (5.22)$$

For the nonequilibrium case equation (5.13) cannot be integrated in closed form and a computer program was written that integrated the area numerically using the trapezoidal rule (see Appendix E). By comparison with equation (5.18) for the equilibrium case it was found that 250 incremental divisions were sufficient to give accurate average effective permeabilities (to four significant figures) for any partial pressure variation between 0 and 150 mm Hg.

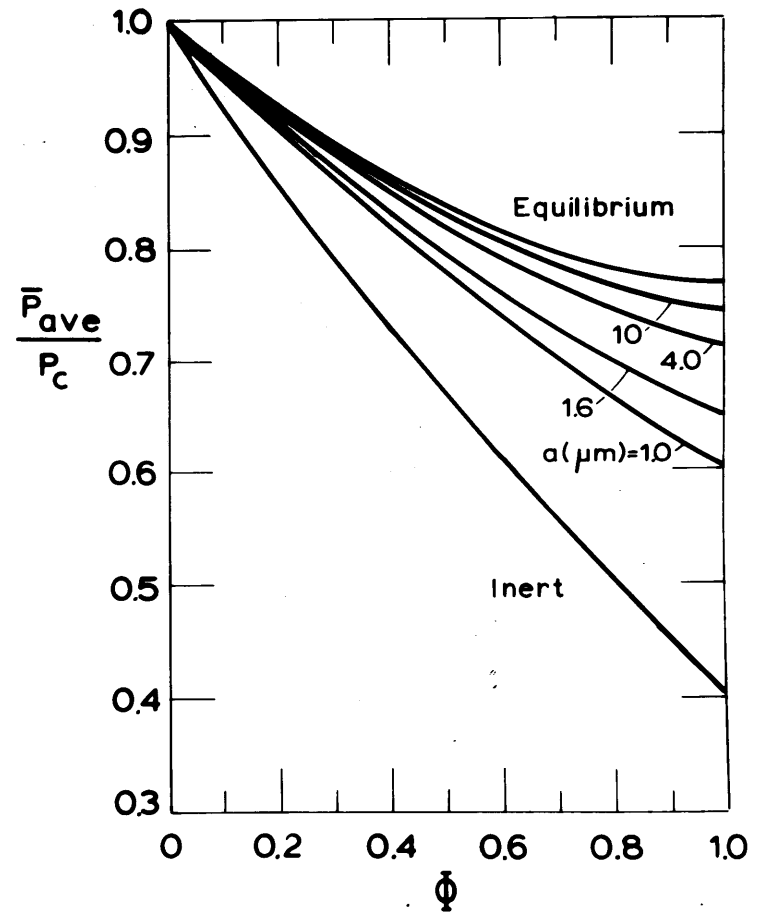
Figure 5.10 shows the ratio of the average effective permeability of blood to that of plasma as a function of sphere

$p_{O_2}^{(1)} = 40 \text{ mm Hg}$
 $p_{O_2}^{(2)} = 0 \text{ mm Hg}$

$$\frac{P_d}{P_c} = 0.40$$



$p_{O_2}^{(1)} = 140 \text{ mm Hg}$
 $p_{O_2}^{(2)} = 0 \text{ mm Hg}$



RED CELLS IN PLASMA

FIGURE 5.10. AVERAGE EFFECTIVE PERMEABILITY RATIO.

radius and volume fraction of suspended red blood cell in plasma. The two conditions shown correspond to a situation in which the downstream partial pressure of oxygen for a thin film of blood is maintained at zero, and the upstream partial pressure is maintained at 40 or 140 mm Hg. The intercept at a volume fraction of unity for the inert case corresponds to the permeability ratio of the dispersed and continuous phases. As anticipated, the average effective permeability is increased by facilitation within the red cell. The magnitude of this effect increases as the facilitation factor increases with decreasing oxygen partial pressure. At sufficiently low values of the upstream partial pressure, the addition of red cells to plasma can actually increase the average effective permeability above that of plasma alone. Note again the relatively small effect to be expected from the departure of the reaction within the red cells from equilibrium for whole blood conditions, especially for large driving forces. For very small sphere sizes the facilitation effect is negligible and the results reduce to that predicted by Maxwell's equation (inert).

A common method of presenting experimental data for the facilitated diffusion through a thin one dimensional film or slab is a plot of species flux versus applied upstream pressure, with the downstream pressure fixed as shown in Figure 5.11. Predicted curves are shown for permeation across 800 μm films of whole blood for the situation where the downstream partial pressure of oxygen is maintained at zero. Above about 50 mm Hg, all the curves asymptote into straight lines and become

$$N_{O_2} = \frac{P_{AVE}}{L} (p_{O_2}^{x=0} - p_{O_2}^{x=L})$$

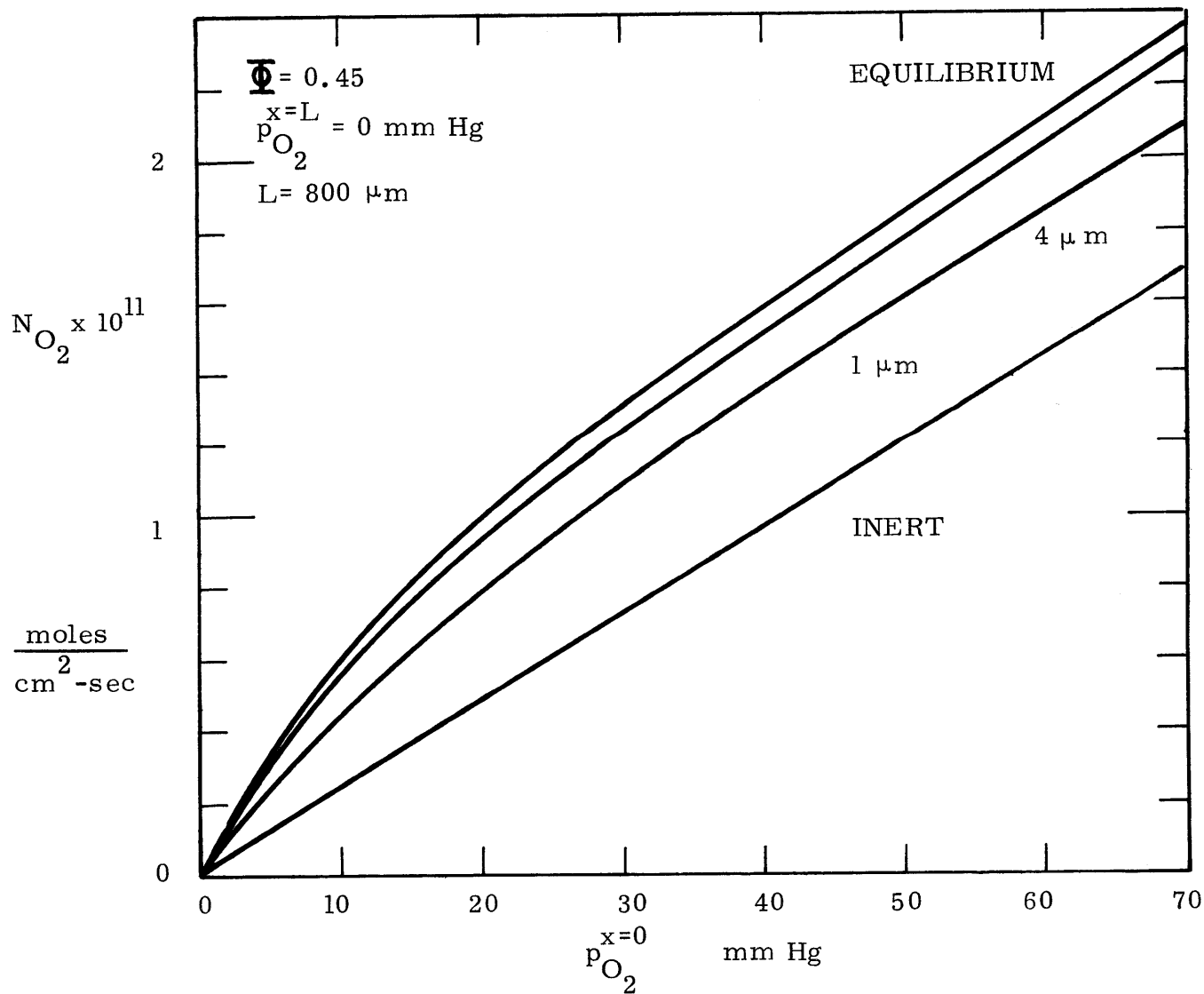


FIGURE 5.11
 FLUX VERSUS DRIVING FORCE PLOT WITH $p_{O_2}^{x=L} = 0 \text{ mm Hg}$.

virtually parallel to the inert case. Again note the relative insensitivity to a moderate departure from reaction equilibrium for whole blood by comparison of the 1 μm , 4 μm , and equilibrium curves. Note that the flux is given by

$$N_{\text{O}_2} = \bar{P}_{\text{AVE}} \left(\frac{p_{\text{O}_2}^{x=0} - p_{\text{O}_2}^{x=L}}{L} \right)$$

5.1.1.3 A Note on Kinetic Parameters

In the use of the one-step model to predict effective permeabilities and mass fluxes, a question arises regarding what backward rate constant should be used. The forward rate constant here is considered fixed and taken from Gibson (1959). A particular choice of the backward rate constant will fix the equilibrium constant and consequently a particular hyperbolic saturation curve as is shown in Figure 5.6 ($K' = k_1'/k_2'$). From Figure 5.6, if the whole equilibrium curve is considered, a K' of 7.0×10^4 would be a better approximation of the sigmoidal saturation curve than a K' of 1.0×10^4 . For different saturation curves a question arises as to what the most appropriate one-step approximation might be. Unfortunately, as far as is known, no extensive experimental comparison of measured kinetic rate constants with the oxygen-hemoglobin saturation curves has been developed. The only relevant work known to this author is that done by Bauer (1971). Bauer measured both forward and backward rate constants, and the p_{50} for hemoglobin solutions with or without 2,3 DPG at 10°C . In

comparing the calculated p_{50} obtained from the one-step saturation with the measured p_{50} , Bauer showed that these were virtually identical over the pH range from 5.8 to 8.2. This suggests that a suitable base approximation would be to choose a backward rate such that the p_{50} obtained from the one-step hyperbolic saturation curve is the same as that given by the sigmoidal saturation curve.

5.1.2 Four-Step Model

The four-step model or Adair reaction scheme in heterogeneous media was developed in section 4.4. The theoretical developments will be utilized to predict oxygen transport in red blood cell suspensions. To date the only complete set of kinetic parameters for the Adair reaction scheme has been given by Gibson (1970) for hemoglobin solutions in the presence of and "stripped" of normal blood 2,3 DPG. These kinetic parameters are listed in Table 5.1 and will be used here in the theoretical calculations as an example (note that primes will not be used in the four-step model to denote conditions in the sphere). In comparing the two sets of constants for "stripped" and "unstripped" hemoglobin it is interesting to note that the fourth reaction is unaffected by DPG. The greatest differences are found in the reverse rate constants for the first three reactions, these being substantially lower in the absence of DPG. The effect of the absence of DPG is to produce a significantly higher oxygen affinity. The reason is that 2,3 DPG binds deoxy- and

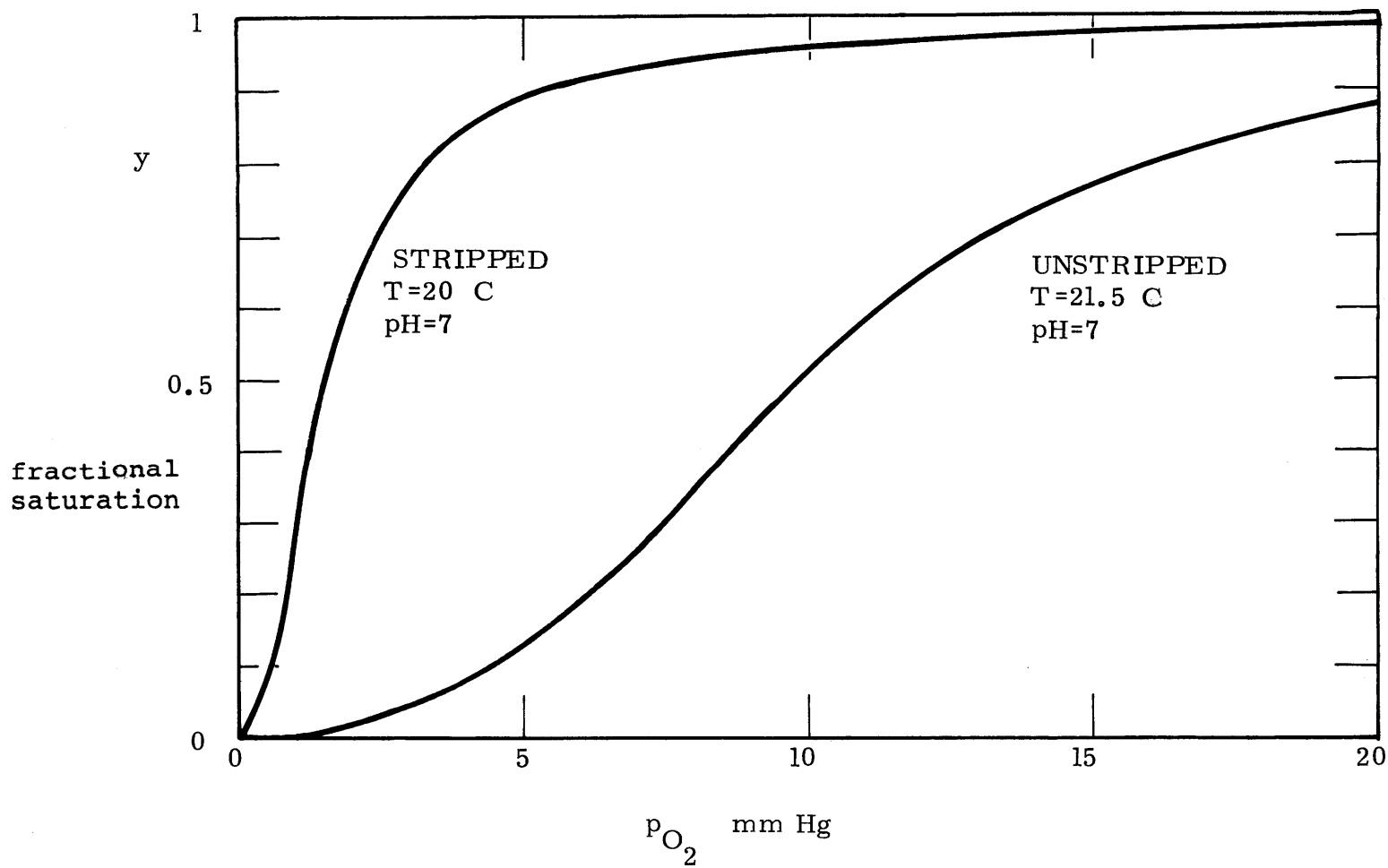


FIGURE 5.12

ADAIR SATURATION CURVES FOR STRIPPED AND UNSTRIPPED HEMOGLOBIN

oxy-hemoglobin but is released after the third oxygen molecule reacts with the Hb molecule (see Appendix B). Before proceeding with a discussion of the theoretical computations with the four-step model, the reader is reminded that the Adair reaction scheme remains an approximation to a very complex reaction mechanism. However, it should be an improved model over the one-step version. On the other hand kinetic data for the one step model are more readily available than that of the Adair mechanism.

Figure 5.12 shows the oxygen hemoglobin saturation curves, obtained from Adair's equation, for stripped and unstripped conditions utilizing Gibson's rate constants as tabulated in Table 5.1. It should be noted here that the data for stripped hemoglobin were reported at 20°C, and the unstripped kinetic rate data were reported at 21.5°C. The 1.5°C temperature difference lessens the comparability of the two sets of data. However, the differences in reaction rates due to 2,3 DPG are much greater than that which can be attributed to temperature.

The Adair reaction scheme in heterogeneous media presents an eigenvalue problem, and in Figure 5.13 the four eigenvalues β_1 , β_2 , β_3 , and β_4 are shown (for the unstripped case). The eigenvalues were obtained from equation (C.54). The eigenvalues are physically comparable to the characteristic length λ in the one step problem. (Note that in this discussion primes are not used to denote conditions inside the dispersed phase). Figure 5.13 shows that the numerical values of the

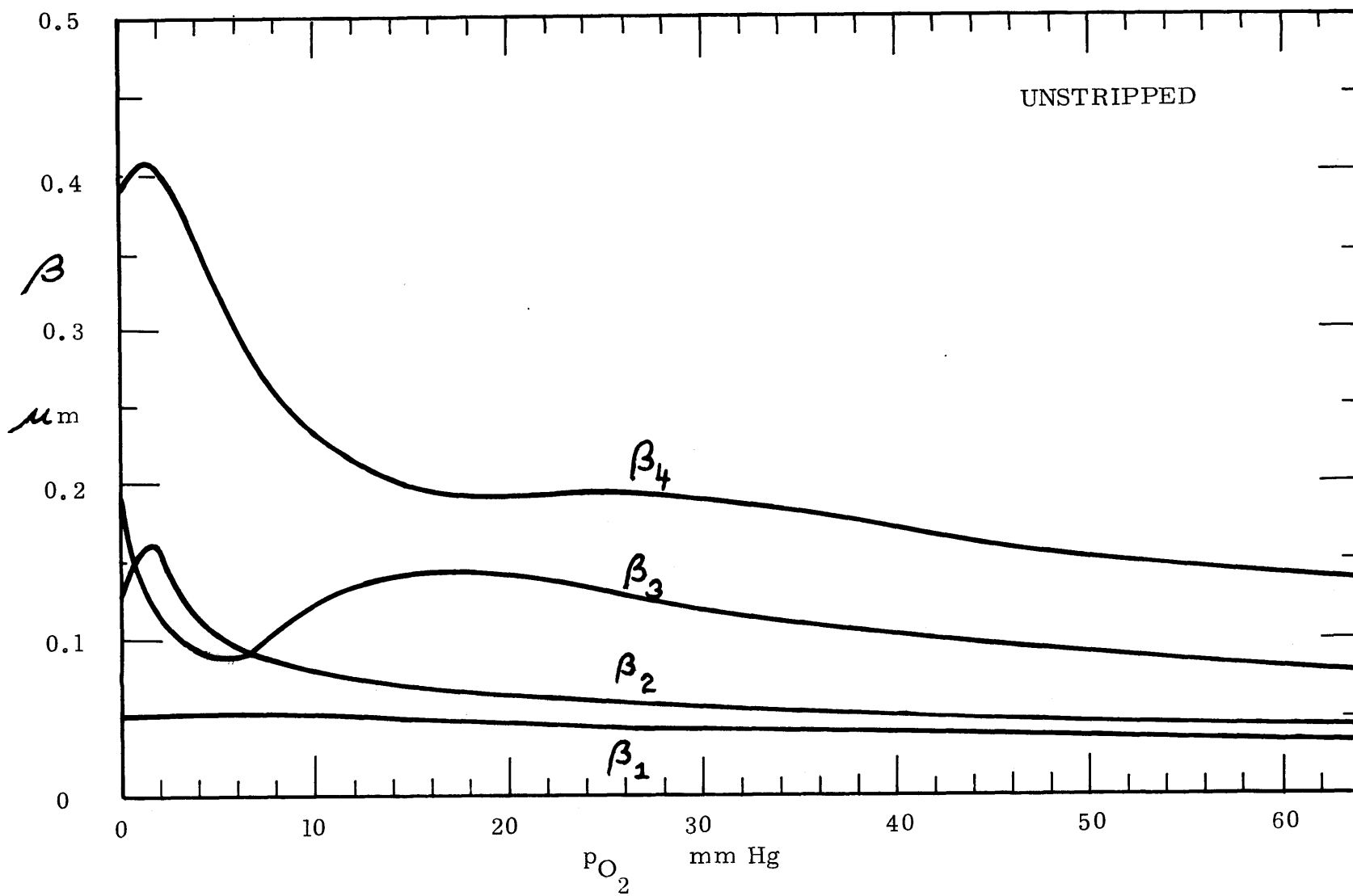


FIGURE 5.13

THEORETICAL EIGENVALUES FOR THE ADAIR FOUR-STEP MODEL.

eigenvalues are of the same order of magnitude. For the case of unstripped hemoglobin, the eigenvalues are weak functions of oxygen partial pressure beyond a p_{O_2} of 25 mm Hg. Once the eigenvalues are determined, the constant A can be obtained as described in Appendix C. Once A has been determined the Adair facilitation factor F^{Adair} , can be calculated from equation (4.156) and F_{eq}^{Adair} is obtained from (4.154). The computer programs for the Adair four-step model are listed in Appendix E.

Figure 5.14 gives a comparison of the Adair facilitation factor for a sphere and for a slab. The facilitation factor for a slab was obtained from a Friedlander and Keller type analysis for a four-step reaction scheme in a homogeneous slab as outlined in Appendix C.3. At large sphere diameters or slab thicknesses, F^{Adair} approaches its maximum value, F_{eq}^{Adair} , which is characteristic of chemical reaction equilibrium throughout the sphere. Note that the facilitation factor for the slab and the sphere approach F_{eq}^{Adair} in the same manner. As the sphere diameter or slab thickness decreases ($2a/\beta_j$ decreases) F^{Adair} decreases as the chemical reactions depart from equilibrium within a boundary layer at the sphere surface. The influence of spherical geometry begins to have an effect at a dimension of about 5 μm . Note that the behaviour of the Adair facilitation factor is very similar to that of the one-step model presented in Figure 5.1.

The facilitation factor dependence upon the partial pressure of oxygen is shown in Figure 5.15 and 5.16 for stripped and unstripped hemoglobin. As expected, the

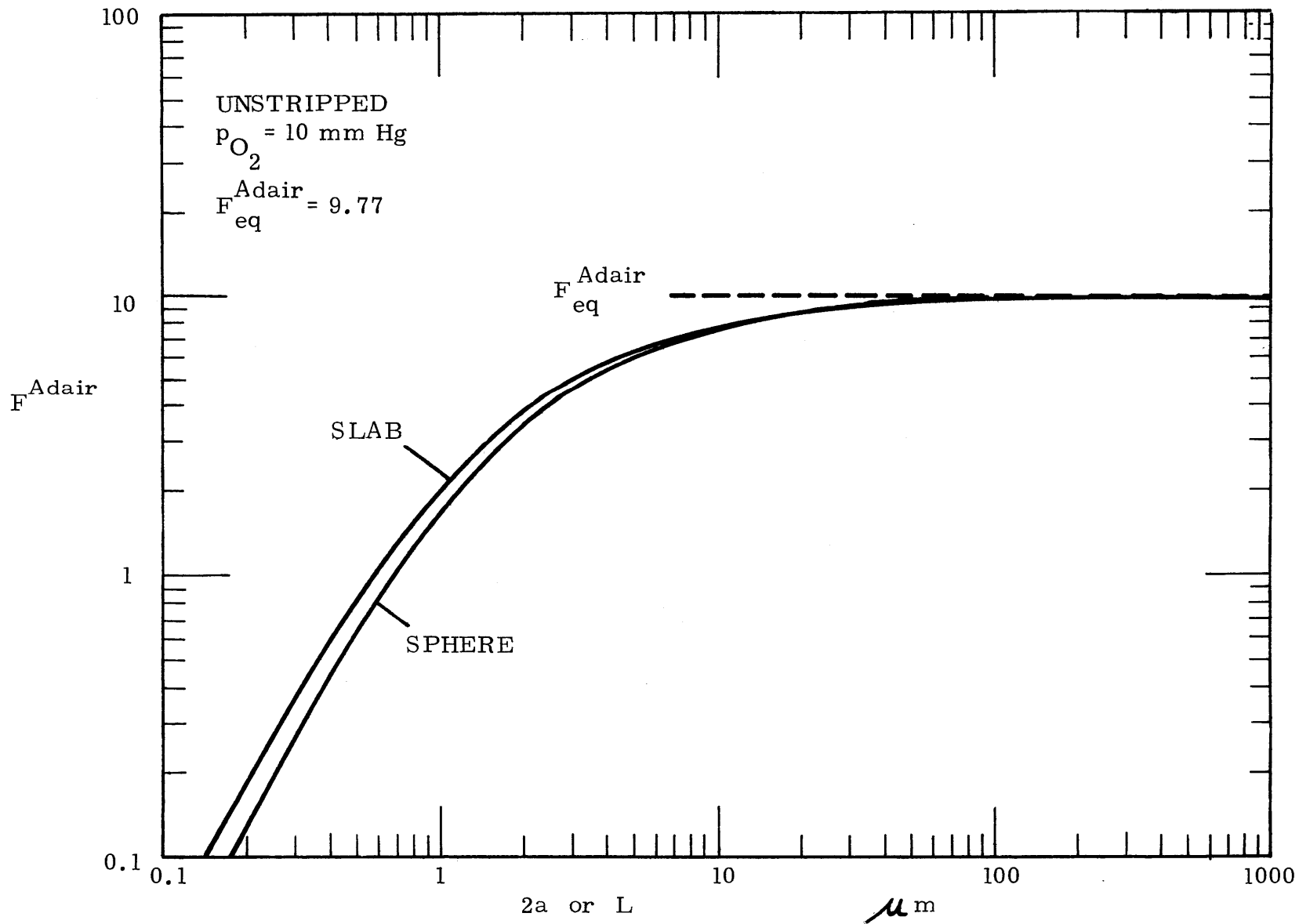


FIGURE 5.14. ADAIR FACILITATION FACTOR FOR SPHERE AND SLAB

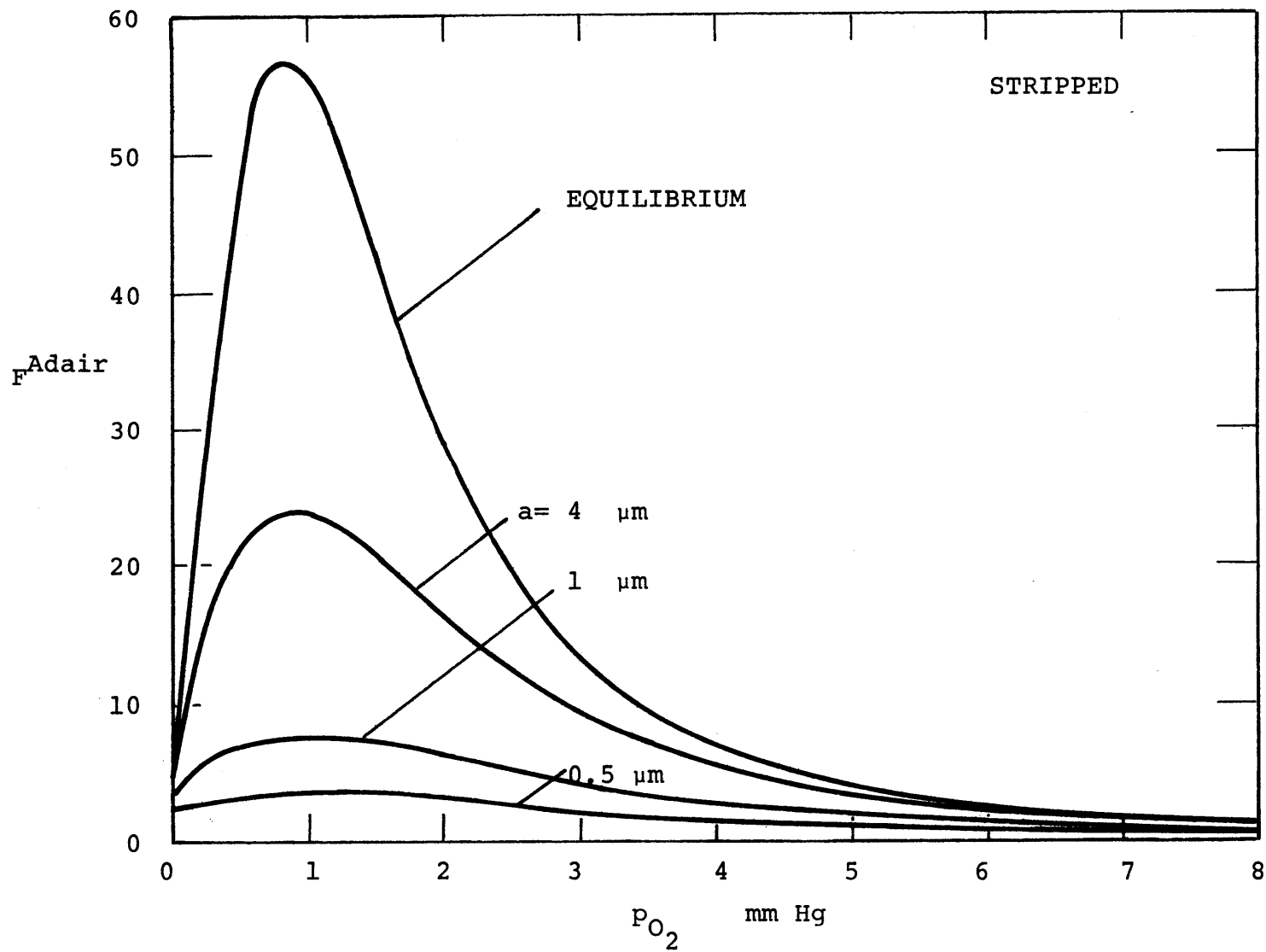


FIGURE 5.15. ADAIR FACILITATION FACTOR FOR STRIPPED HEMOGLOBIN.

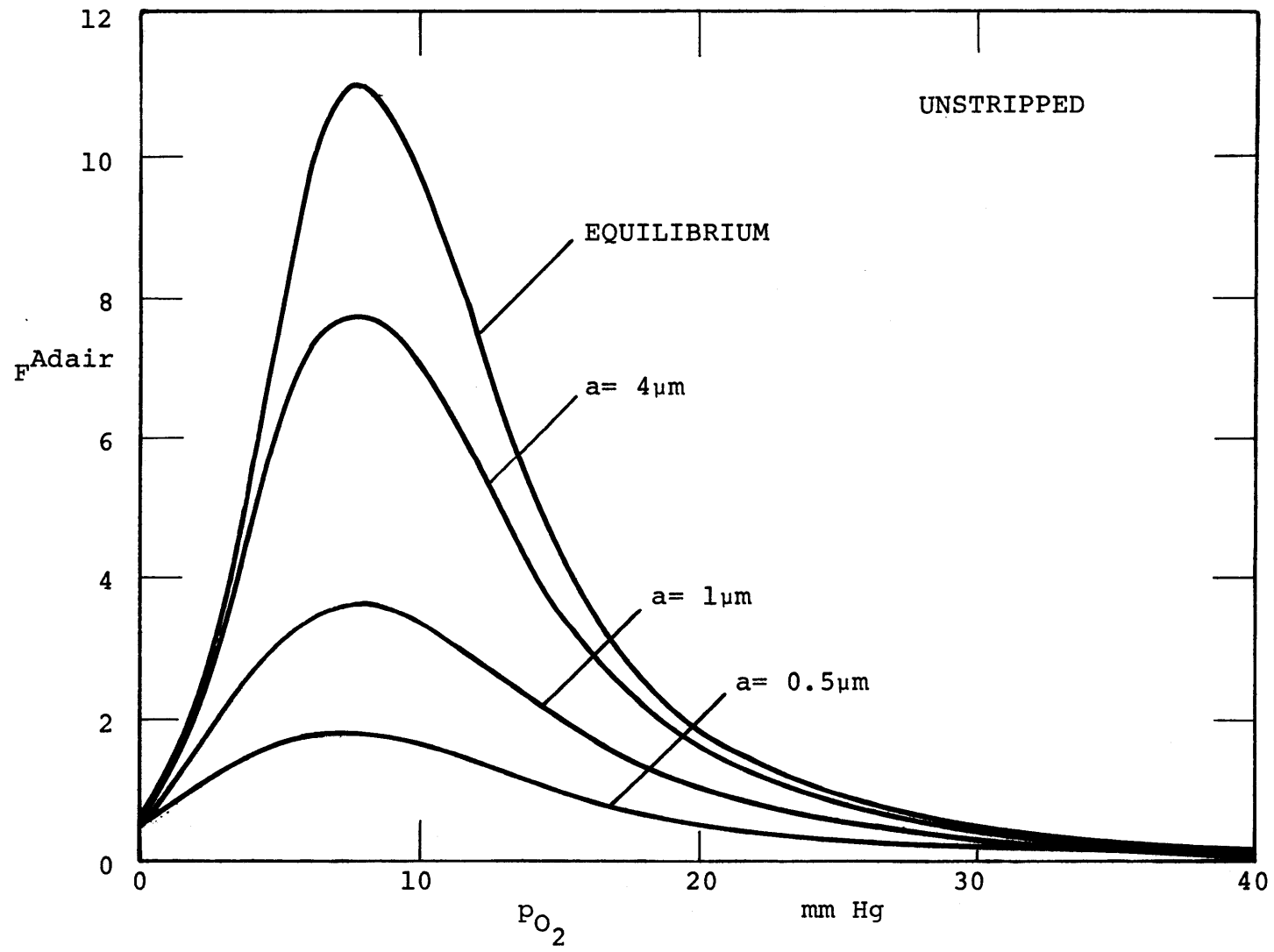


FIGURE 5.16. ADAIR FACILITATION FACTOR FOR UNSTRIPPED HEMOGLOBIN.

facilitation factor is strongly dependent on sphere radius and oxygen partial pressure. The Adair equilibrium facilitation factor, F_{eq}^{Adair} , has a maximum at the partial pressure for which the slope of the Adair saturation curve is steepest (as indicated by equation 4.154). For the nonequilibrium facilitation factors, the maximum occurs at nearly the same oxygen pressure as for the equilibrium facilitation factor (there is a slight but negligible shift). An important qualitative conclusion can therefore be made: The behaviour of the nonequilibrium facilitation factor is similar to the equilibrium facilitation factor. The numerical value of the nonequilibrium facilitation factor is of course always less than the equilibrium value and is dependent upon the sphere radius. Note that the nonequilibrium facilitation factor for the stripped hemoglobin (for a fixed radius) is less attenuated in comparison to the unstripped curves, each relative to their respective equilibrium facilitation factors. This is due to the lower kinetic parameters for the stripped case (compared to the unstripped case). The facilitation factors for the stripped case, however, are numerically larger at very low pressures because the stripped saturation curve is much steeper in this region than the unstripped saturation curve. The stripped facilitation factor increases and decreases rapidly as saturated conditions are attained for relatively low oxygen partial pressures.

The local effective permeability for whole blood, stripped and unstripped, is shown in Figures 5.17 and 5.18 as

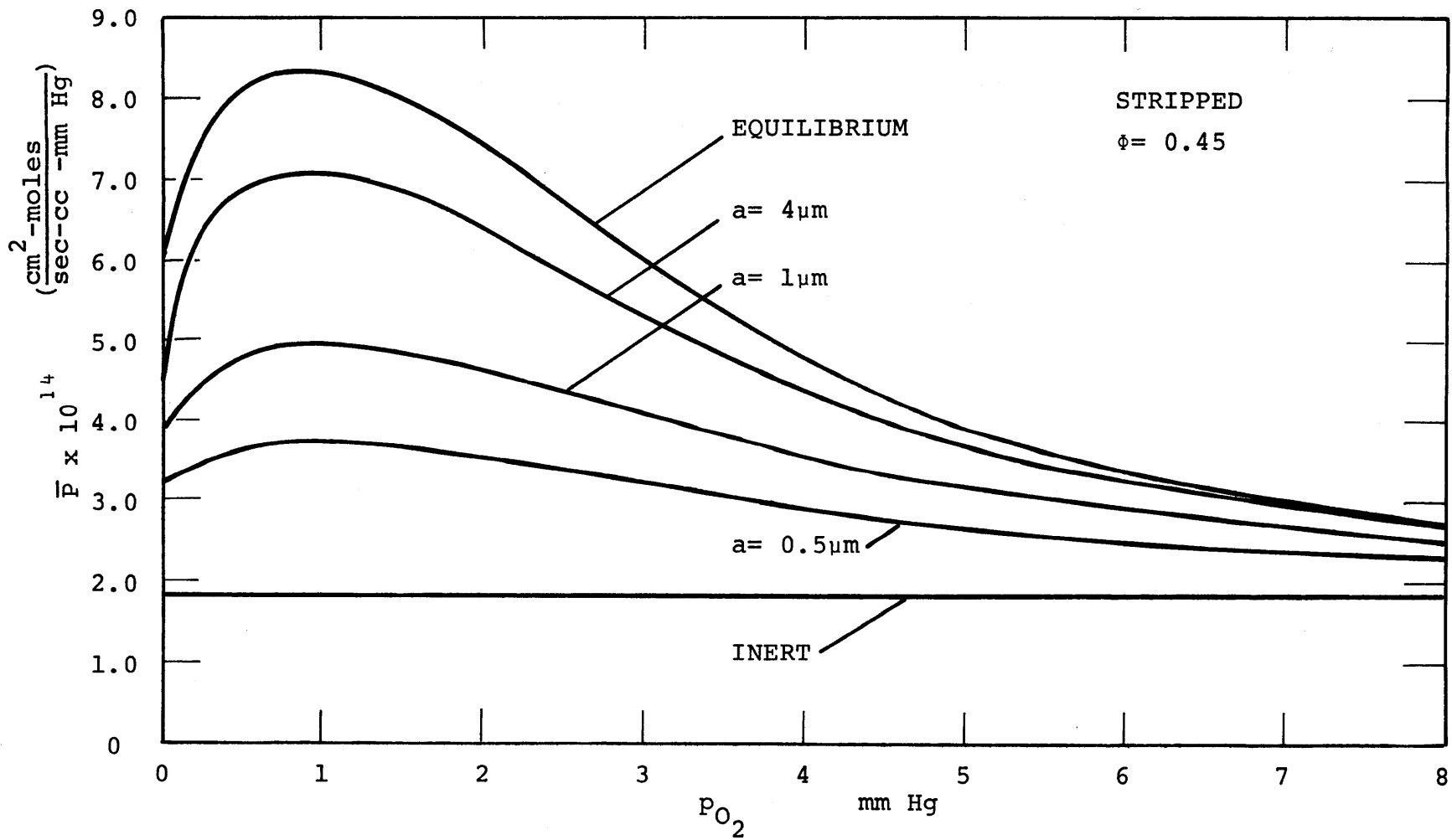


FIGURE 5.17. EFFECTIVE LOCAL PERMEABILITY FOR STRIPPED WHOLE BLOOD.

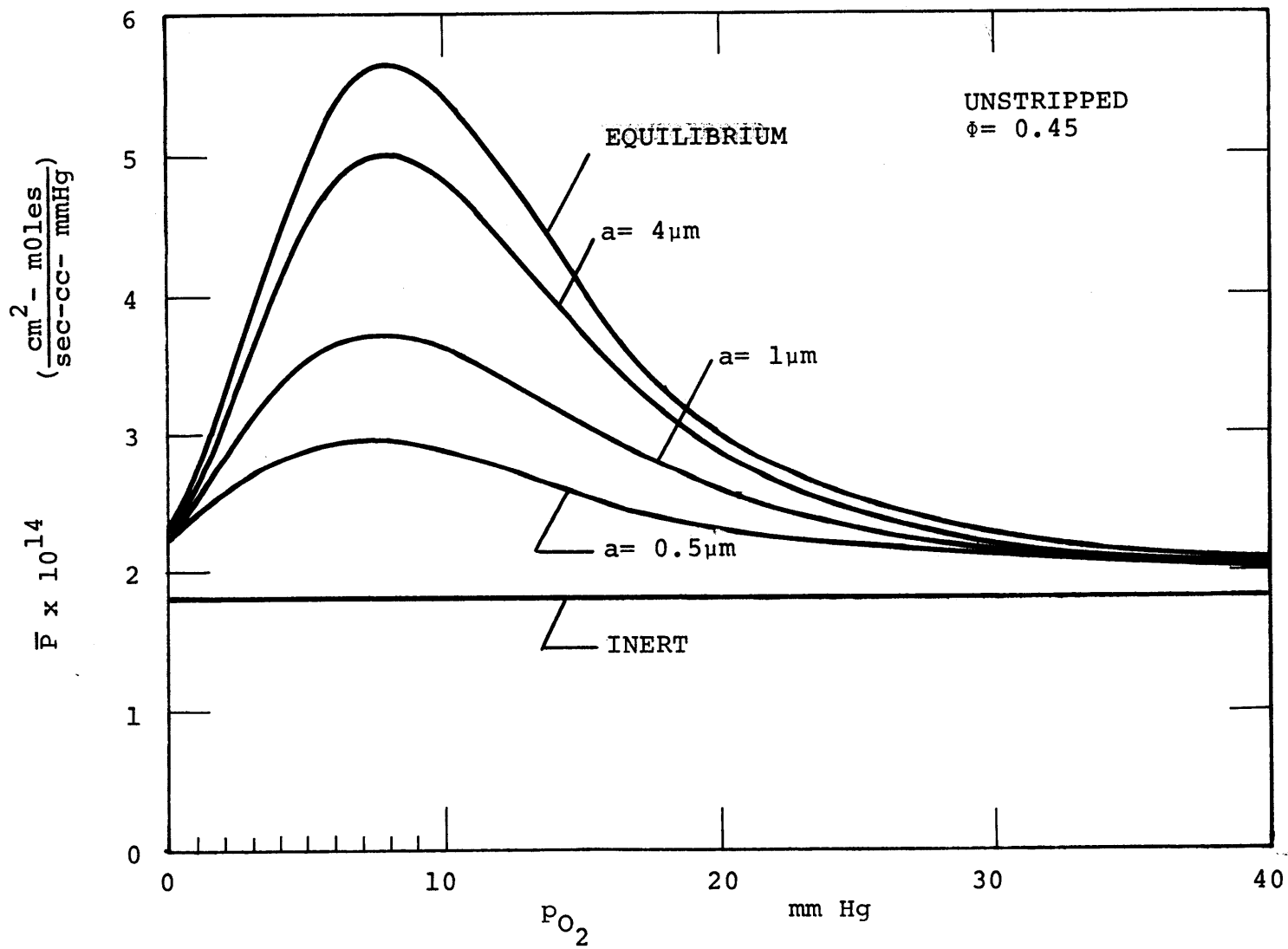


FIGURE 5.18. EFFECTIVE PERMEABILITY FOR UNSTRIPPED WHOLE BLOOD.

a function of oxygen partial pressure. Since the local effective permeability is dependent on the facilitation as shown by equation (4.157) the curves in Figures 5.17 and 5.18 show somewhat similar behaviour as the two preceding figures. Like the local effective permeability obtained by the one step model, the Adair local effective permeability maximizes at the point where the equilibrium curve has the steepest slope, but for the one-step model this occurs at zero partial pressure.

Once the local effective permeability has been determined, the average effective permeability for a given driving force can be obtained by integration as given by equation (4.158). Figure 5.19 shows the average effective permeability ratio of red cells in plasma as a function of sphere radius and volume fraction for both stripped and unstripped blood. The conditions shown are an upstream oxygen partial pressure of 20 mm Hg and a downstream pressure of 0 mm Hg. For those particular conditions the stripped suspension has a slightly higher equilibrium effective permeability than the unstripped suspension. This is because at equilibrium a larger saturation difference exists for the stripped than the unstripped hemoglobin as can be seen from Figure 5.12. For the nonequilibrium case, however, the converse is true. For the 1 μm and 4 μm sphere radius the effective (relative) permeability for the stripped red blood cells is lower than that of the unstripped case because of the lower kinetic rates associated with the former system. As the sphere radius decreases, the facilitation factor will approach zero and

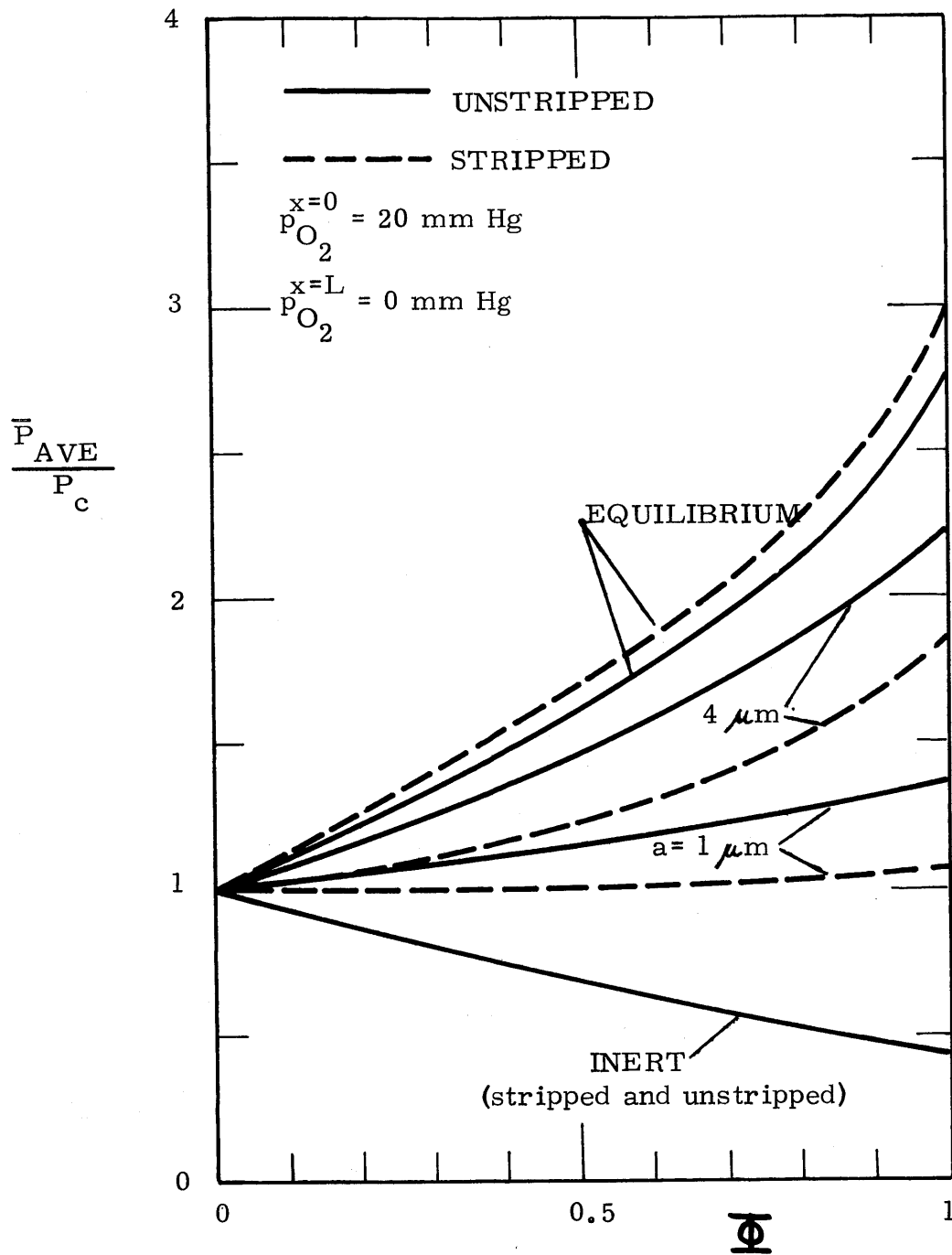


FIGURE 5.19
EFFECTIVE AVERAGE PERMEABILITY RATIO
FOR STRIPPED AND UNSTRIPPED RED BLOOD
CELL SUSPENSIONS; ZERO BACKPRESSURE.

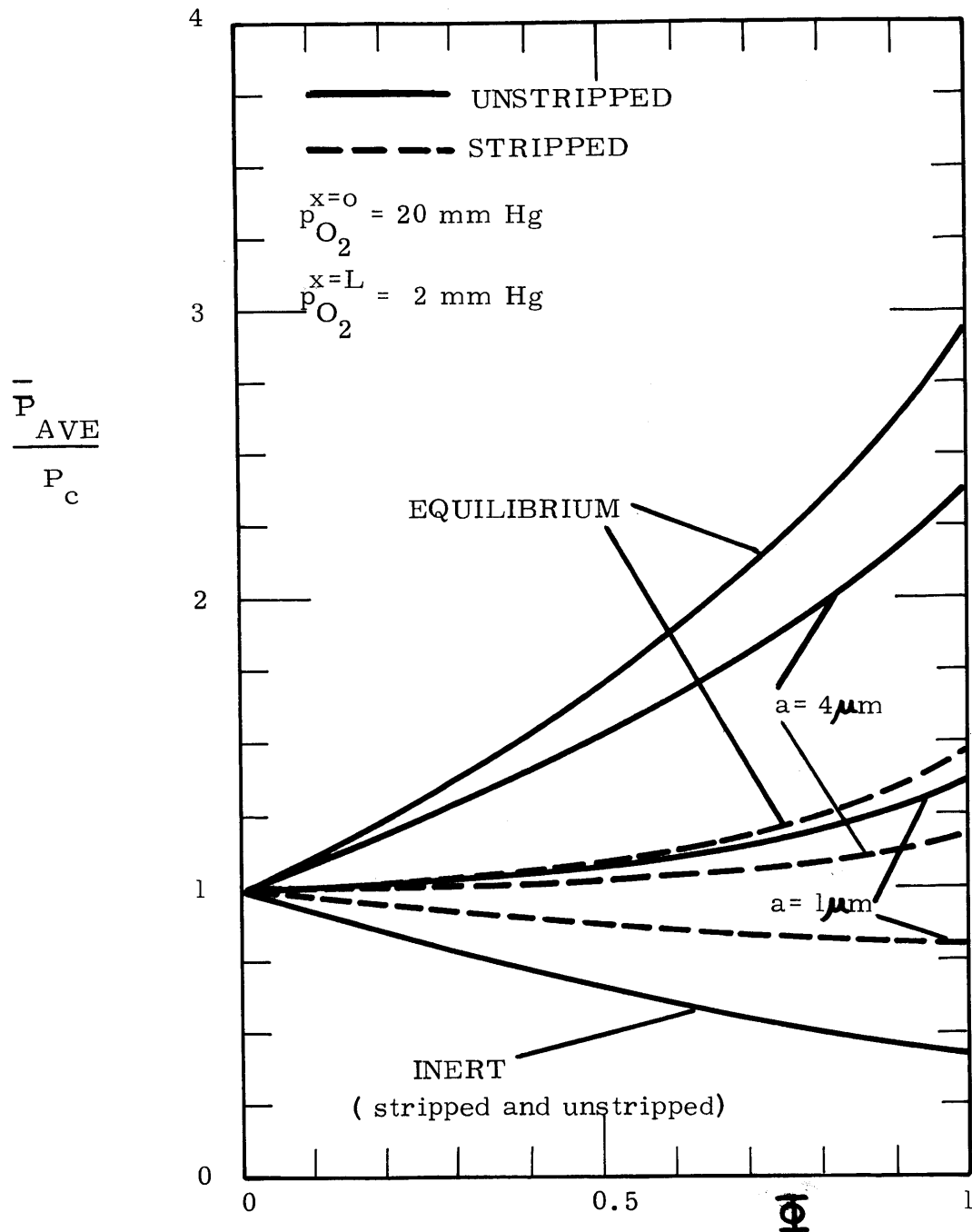


FIGURE 5.20
 AVERAGE EFFECTIVE PERMEABILITY RATIO
 FOR STRIPPED AND UNSTRIPPED RED BLOOD
 CELL SUSPENSIONS; 2 mm Hg BACKPRESSURE.

the effective (relative) average permeability reduces to that which is given by Maxwell's solution.

In Figure 5.20 the downstream pressure (back pressure) has been raised from zero mm Hg to 2 mm Hg. As can be seen from Figure 5.20, the average effective permeability for the unstripped suspensions is barely affected, in fact, it is slightly higher. In terms of equilibrium conditions, the saturation difference from a driving force from 20 to zero mm Hg or 20 to 2 mm Hg has barely decreased for the unstripped system. The driving force has been decreased by 10% so that the "amount of facilitation per unit driving force", which is a function of the saturation difference, is greater. A slight increase in the back pressure has a significant affect on the average effective permeability ratio of the stripped red blood cell suspensions. In the case of equilibrium, a 2 mm back pressure raises the downstream saturation from zero to 61%. The resulting drop in saturation difference across the suspension causes a drop in the facilitation factor and consequently the dispersed phase permeability is reduced. It should be noted that explanations offered here in terms of the equilibrium situation are also valid for the nonequilibrium cases.

5.1.3 Comparison of One-Step and Four-Step Model

Some of the results presented in sections 5.1.1 and 5.1.2 have already indicated similarities and differences between the one-step and four-step model. In making a

comparison between the one-step model and the four-step model, the obvious question arises: When does the one-step model fail to predict accurate permeabilities? That answer can be qualitatively answered from an inspection of the behavior of the one-step and four-step saturation curves.

Consider the saturation curves presented in Figure 5.6. The sigmoidal saturation curve is identical with the saturation curve obtained from Gibson's kinetic parameters for unstripped hemoglobin. It has been suggested in Section 5.1.1.3, that a base case for comparison of the one-step and the four-step model should be agreement between the p'_{50} of the two models. The hyperbolic saturation curve with $K' = 7.0 \times 10^4$ l/mole gives virtually the same p_{50} as the sigmoidal Adair curve in Figure 5.6 and this particular value of K will be considered the base case. It is also the value employed in the theoretical calculations in Section 5.1.1.2. The discussion that follows will be in terms of the equilibrium situation, but it is assumed that the same qualitative conclusions apply to the nonequilibrium results (assuming comparable kinetic rate parameters between the two models). The discussion will be followed with a few examples.

As an example, consider a thin film of blood which has an oxygen driving force imposed upon it. The following general remarks can be made for various driving forces in the unsaturated portion of the equilibrium curves:

1. Large oxygen driving force across the film.

For this particular case the one-step and the

four-step model should give close agreement in predicting the average effective permeability, because both predict large differences in hemoglobin saturation across the film.

2. Small or moderate oxygen driving force across the film.

In this case the one-step model is expected to fail if the oxygen partial pressure change in the film occurs in the region where the saturation curve is steepest. If the partial pressure drop of oxygen across the film occurs at the top or bottom of the curve, the one-step model should give good agreement with the four-step model, if a hyperbolic saturation curve is employed that closely matches the Adair saturation curve over the region of interest.

A few examples follow:

Figure 5.2la and 5.2lb give the average effective permeability ratio for the four-step model for the following driving force conditions

$$(1) \quad p_{O_2}^{x=0} = 140 \text{ mm Hg}, \quad p_{O_2}^{x=L} = 0 \text{ mm Hg}$$

$$(2) \quad p_{O_2}^{x=0} = 40 \text{ mm Hg}, \quad p_{O_2}^{x=L} = 0 \text{ mm Hg}$$

Parameters as reported in Table 5.1 were employed. It can be seen, in comparison with Figure 5.10, that the one-step model and the four-step model give excellent agreement. This was

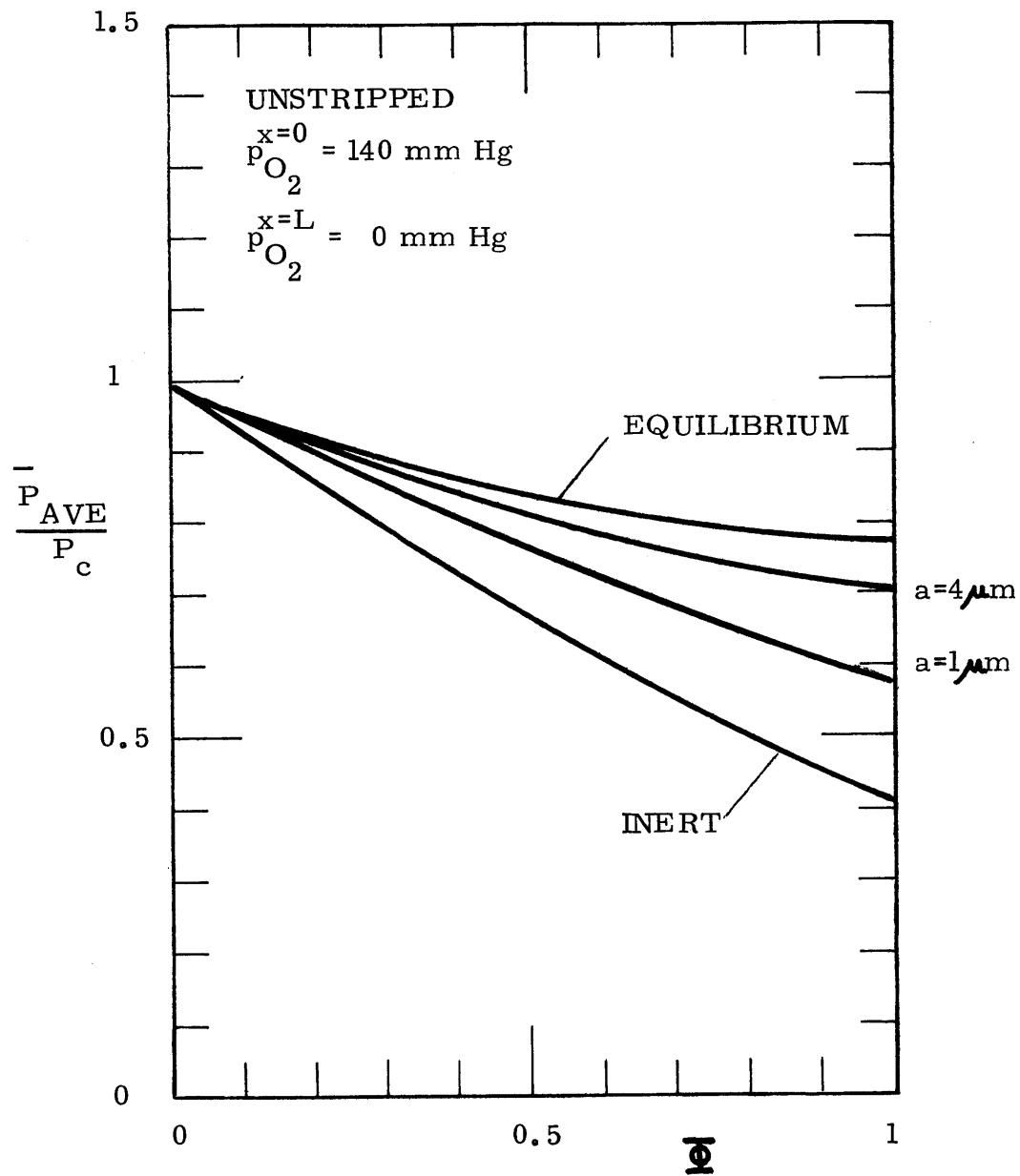


FIGURE 5.21a
 AVERAGE EFFECTIVE PERMEABILITY RATIO
 FOR THE FOUR-STEP MODEL FOR THE
 CONDITIONS SHOWN.

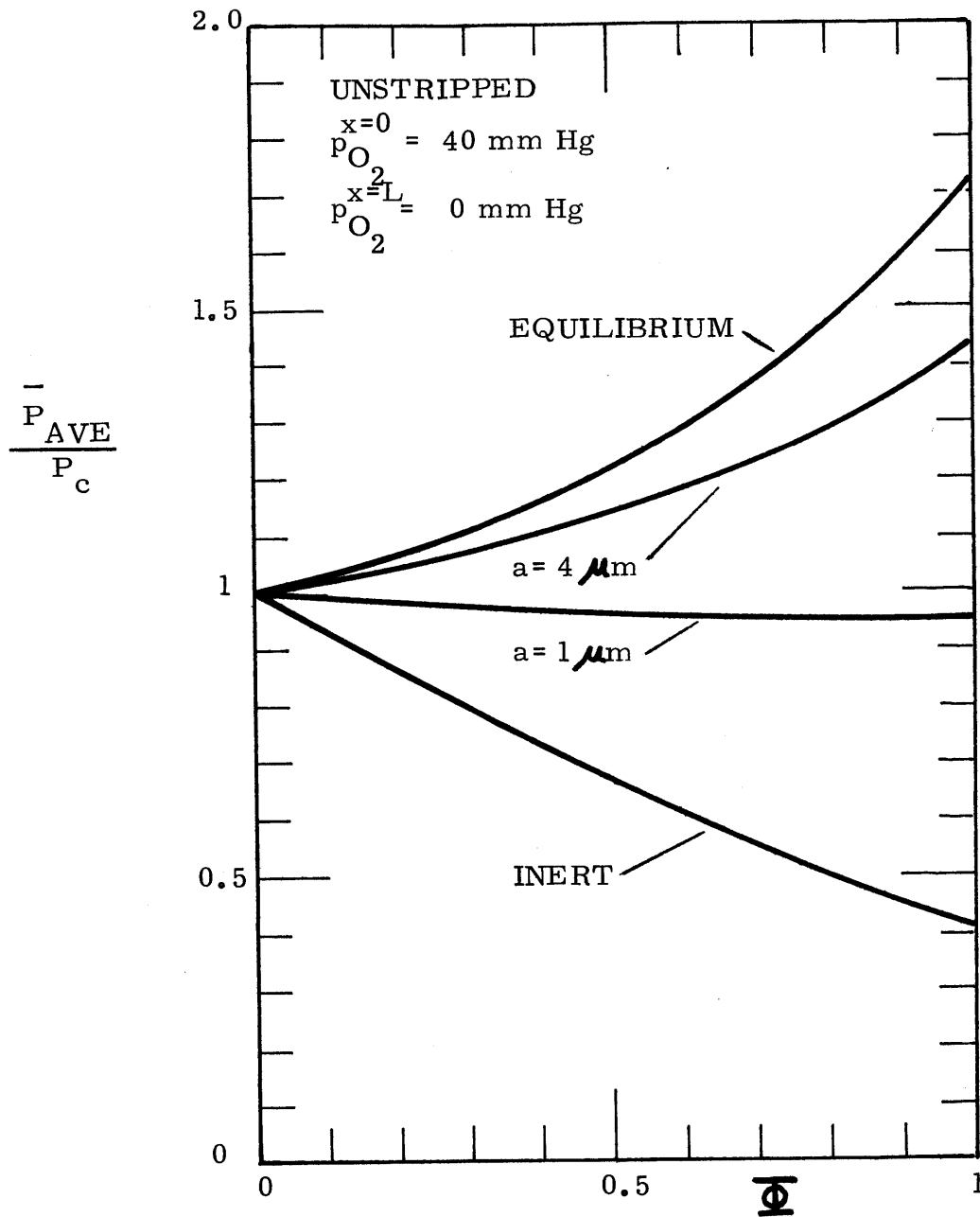


FIGURE 5.21b
 AVERAGE EFFECTIVE PERMEABILITY RATIO
 FOR THE FOUR-STEP MODEL FOR CONDITIONS
 SHOWN.

anticipated in view of: (1) the large driving force across the film (with a large equilibrium saturation difference across the film); (2) the close agreement of the numerical values between the characteristic length and the four eigenvalues as presented in Figures 5.7 and 5.13. An improved fit is obtained if a larger K' than 7.0×10^4 is employed (with k_1' fixed at 3.0×10^6 1/mole/sec, k_2' must be lowered). The change is not significant. Finally note from Figures 5.21 the relative small effect to be expected from a departure of the reaction within the red cells from equilibrium, especially for whole blood conditions ($\phi = 0.45$). This is consistent with similar observations made for the one-step model, particularly for large driving force conditions.

Figure 5.22 shows a comparison of the average effective permeabilities between the one-step and four-step model for the case of a small driving force in the region of the steeper part of the sigmoidal saturation curve. The one-step model deviates considerably from the four-step model and predicts much lower permeabilities. Besides the base case of $K' = 7.0 \times 10^4$, results were also generated for the cases of $K' = 2 \times 10^5$, 3×10^4 , and 2×10^4 . In each case the effective permeabilities were lower than those predicted by the base case. It is obvious that for this particular driving force the one-step model is not satisfactory.

Figure 5.23 shows the average effective permeability ratio for the driving force of $p_{O_2}^{x=0} = 5$ mm Hg and $p_{O_2}^{x=L} = 0$ mm Hg. The "base" one-step model fails to agree with the four-step model

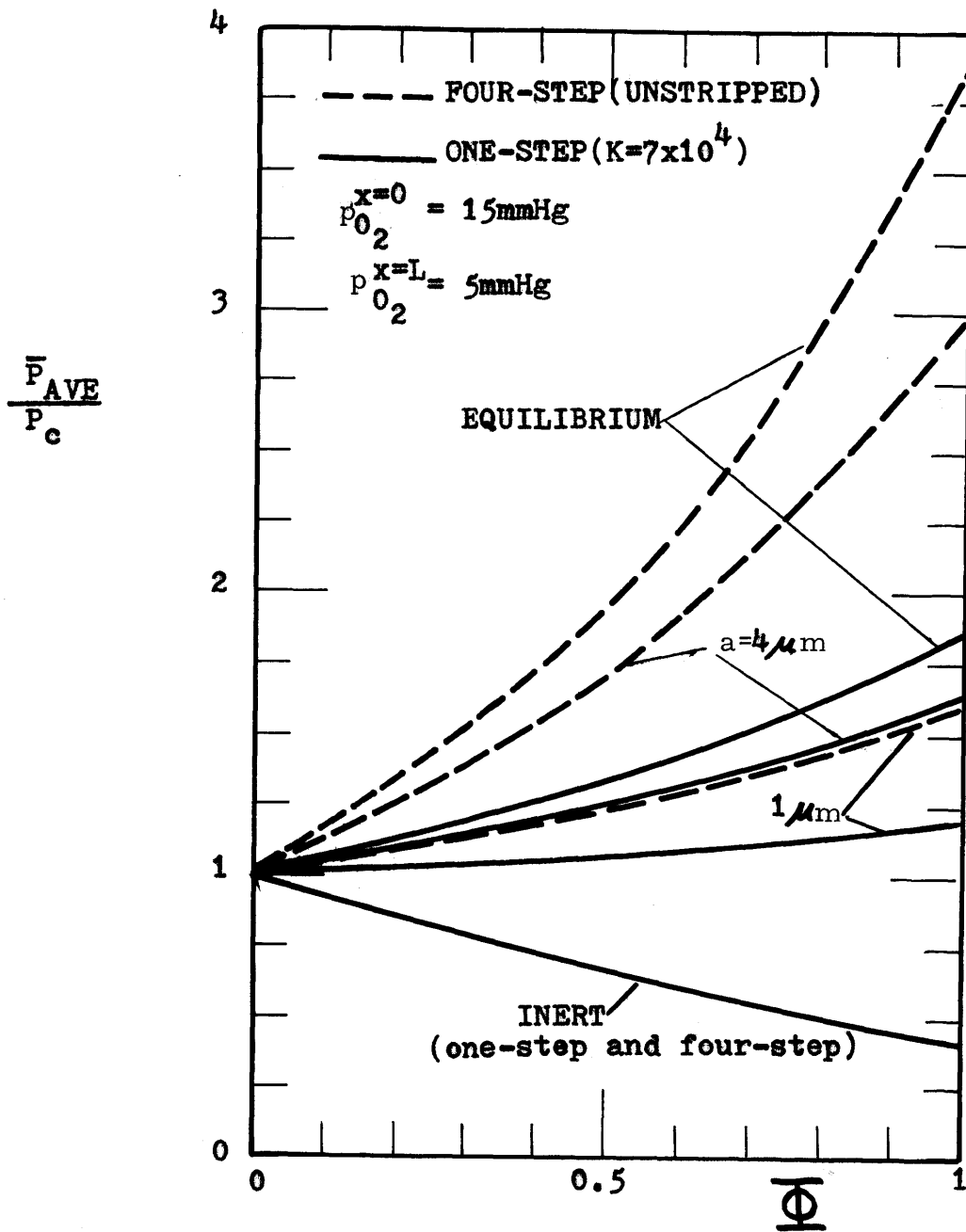


FIGURE 5.22
AVERAGE EFFECTIVE PERMEABILITY RATIO FOR
A DRIVING FORCE OF

$$p_{O_2}^{x=0} = 15\text{mmHg} \quad \text{AND} \quad p_{O_2}^{x=L} = 5\text{mmHg}$$

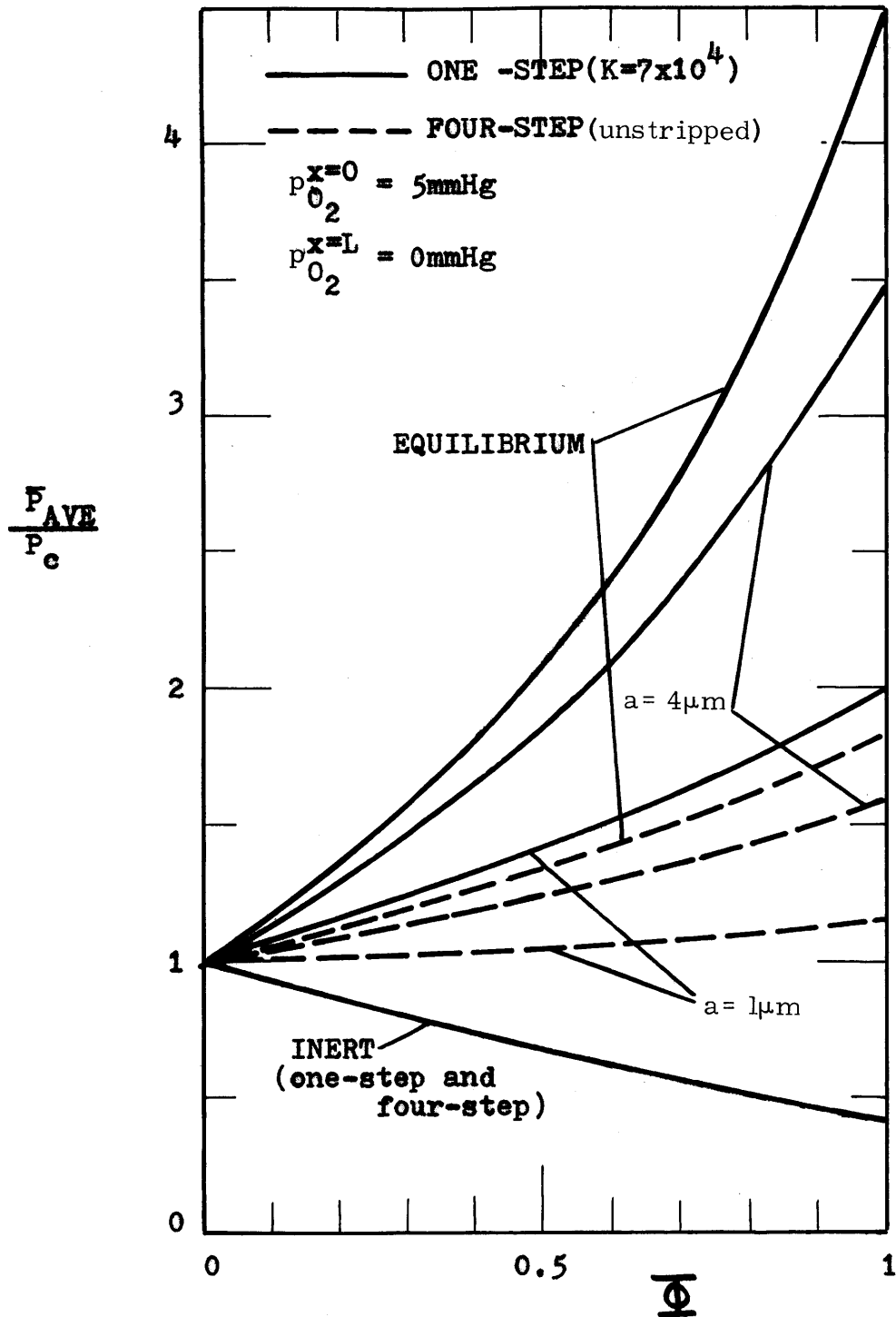


FIGURE 5.23
 AVERAGE EFFECTIVE PERMEABILITY RATIO FOR
 A DRIVING FORCE OF $x=0$ AND
 $p_{O_2} = 5 \text{ mmHg}$
 $p_{O_2}^{x=L} = 0 \text{ mmHg}$

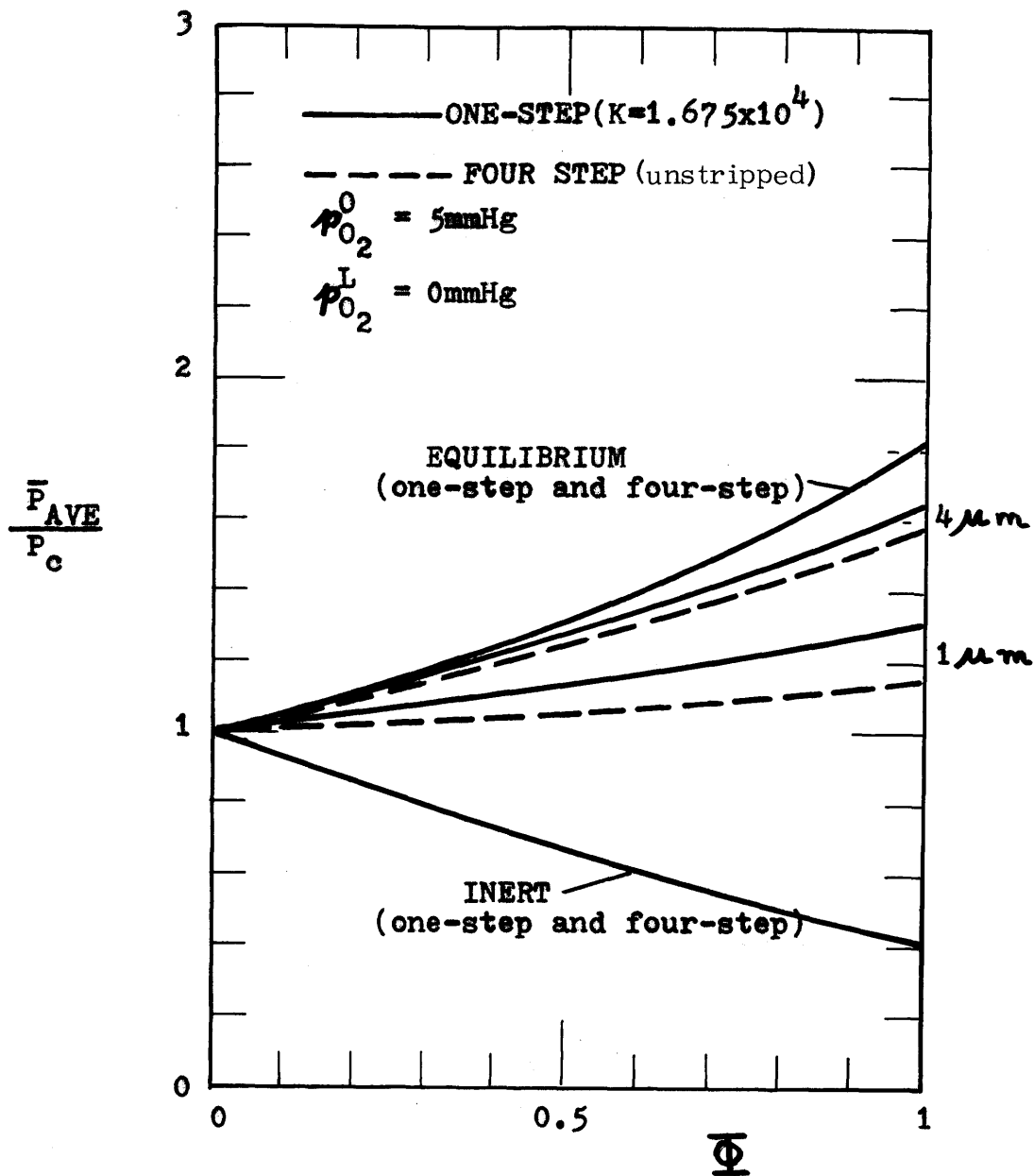


FIGURE 5.24
 ATTEMPTED FIT OF FOUR-STEP MODEL WITH
 ONE-STEP MODEL FOR WHICH $K=1.675 \times 10^4$
 l/mole.

and in this situation it predicts much larger permeabilities. This behaviour can be understood from the behaviour of the saturation curves in Figure 5.6. For a K' of 7.0×10^4 l/mole the hyperbolic saturation curve does not match the sigmoidal Adair curve in the low saturation range. A K' can be chosen however that will give a better fit. If k_2' is adjusted such that

$$K' = \frac{k_1'}{k_2'} = 1.675 \times 10^4 \text{ l/mole}$$

so that $k_2' = 179 \text{ sec}^{-1}$, a better fit is obtained as can be seen from Figure 5.24. This particular value for K' matches the saturation value given by the hyperbolic saturation curve at 5 mm Hg.

The nonequilibrium response of the average effective permeability for the 1 μm and 4 μm show qualitatively the same behaviour at that exhibited at equilibrium. The nonequilibrium response depends to a major part on the magnitude of the numerical value of the facilitation factor inside the dispersed phase. Figure 5.25 compares the normalized facilitation factor F/F_{eq} for the one-step and four-step model versus the sphere radius a . Two conditions are shown: a partial pressure of 10 mm Hg where the equilibrium facilitation factors are large, and a partial pressure of 40 mm Hg where the equilibrium facilitation factors are smaller (for the chosen parameters). The four-step model and one-step model show close agreement at a p_{O_2} of 40 mm Hg (small F_{eq} , all a), but difference exists where the equilibrium facilitation factor is relatively large. The results

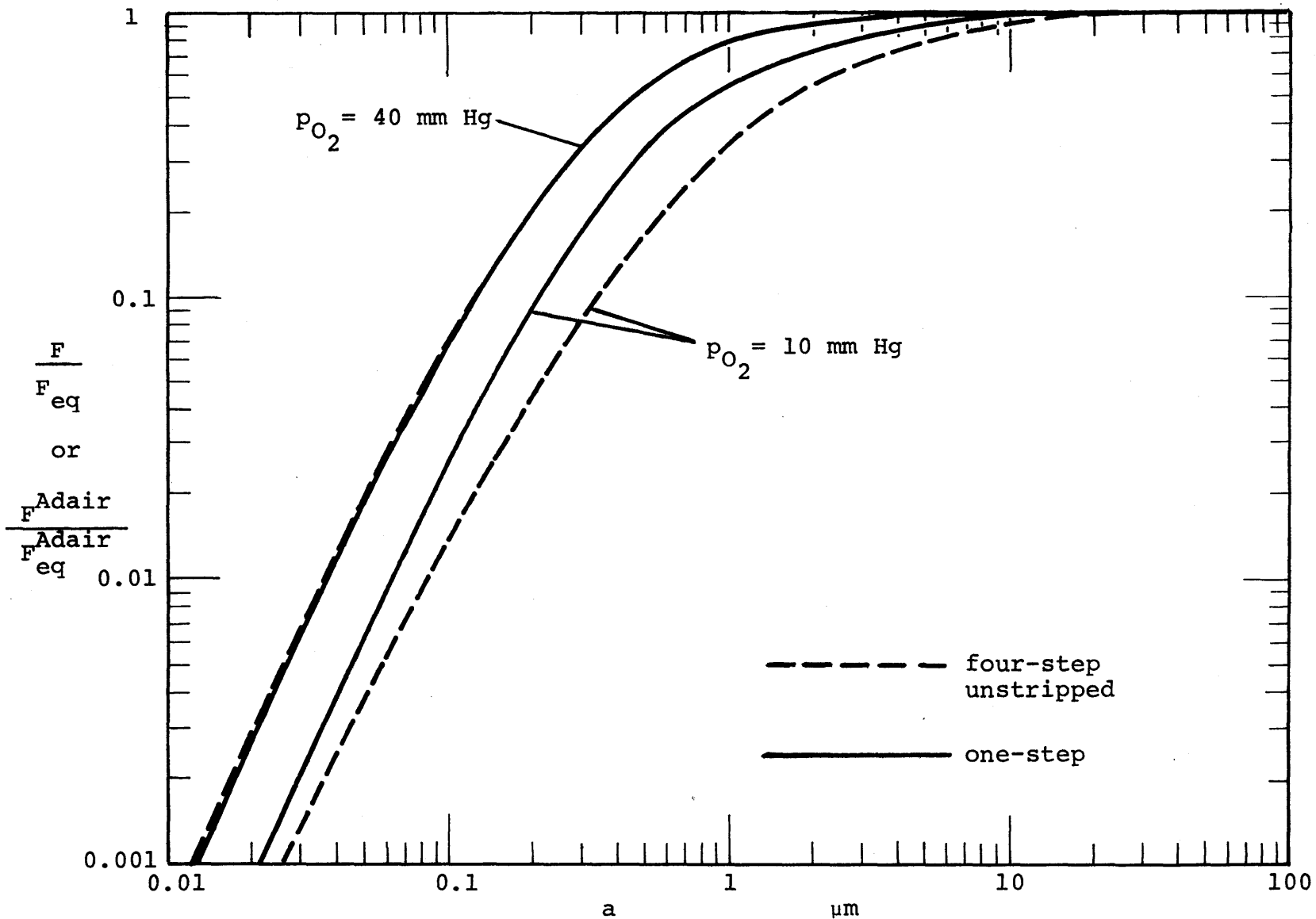


FIGURE 5.25. COMPARISON OF THE FOUR-STEP AND ONE-STEP NORMALIZED FACILITATION FACTORS AS A FUNCTION OF SPHERE RADIUS AND PARTIAL PRESSURE.

in Figure 5.25 are qualitatively similar to the behaviour of the nonequilibrium curves for the one-step and four-step model shown in Figures 5.22, 5.23, and 5.24.

From the above examples it can be concluded that the one-step model can give close agreement with the four-step model if the equilibrium saturation curves can predict approximately the same hemoglobin saturation drop across the film (Figure 5.26 summarizes the regions of the sigmoidal curve where hyperbolic saturation curves are expected to give close fits for a driving force in that region). For the nonequilibrium regime one-step model should give reasonable results if the above is satisfied, and in addition the kinetic rate parameters for both models are of comparable value. If these conditions are not met, the one-step model is expected to give incorrect results with the deviation from the four-step model a function of the amount of facilitation. An implicit assumption here is that the Adair model is correct.

Finally in Figure 5.27 a plot of flux versus p_{O_2} for the four-step model is shown for whole blood conditions ($\phi = 0.45$). The thickness for blood film is identical to that of Figure 5.11. Note the sigmoidal behaviour of the flux curves in the low oxygen partial pressure range. The theory predicts correctly the behaviour observed experimentally by Kutchai and Staub (1969) who measured oxygen flux as a function of upstream oxygen pressure (with $p_{O_2}^{x=0} = 0$ mm Hg) for packed red blood cells.

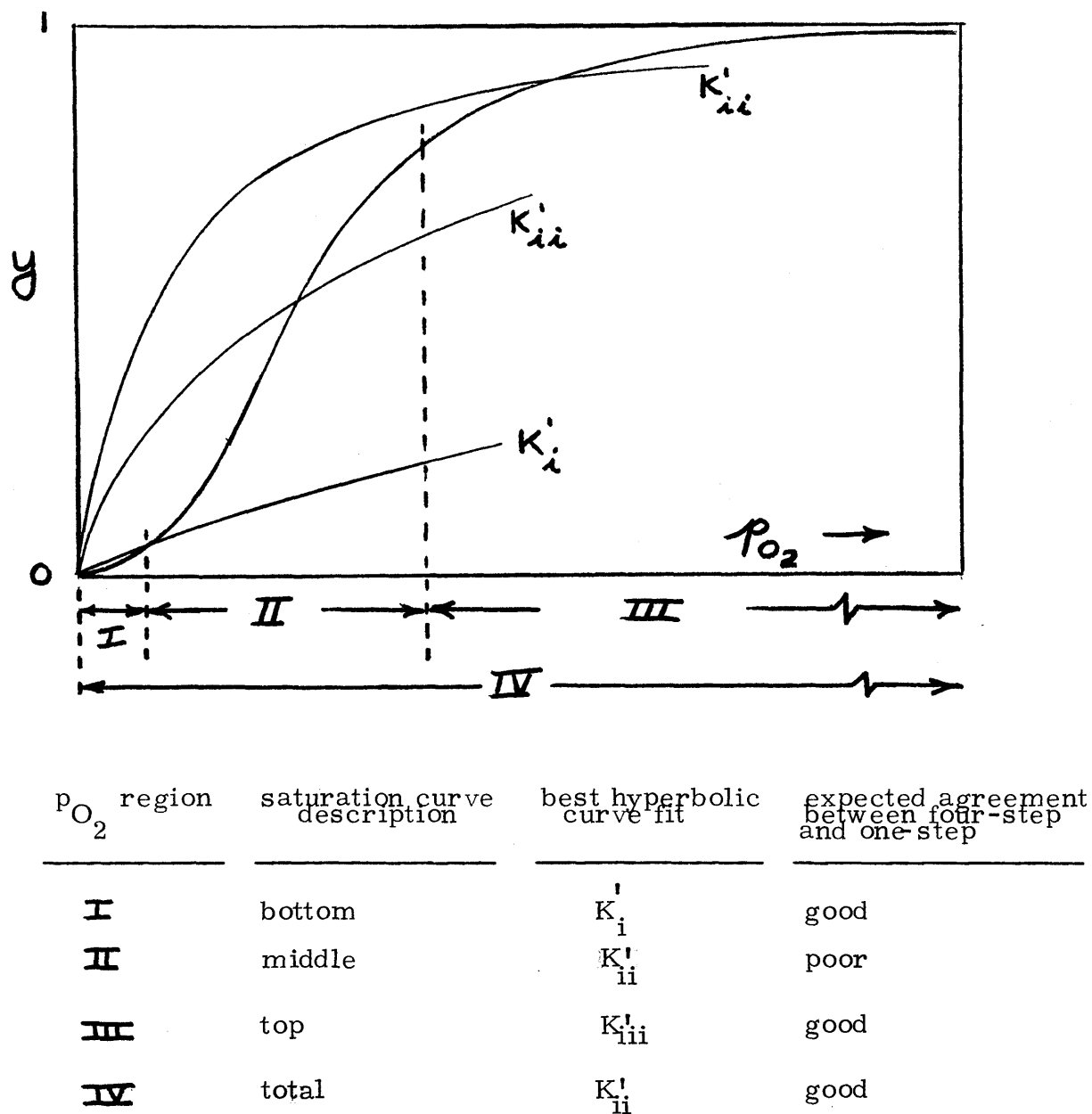


FIGURE 5.26

COMPARISON OF THE ONE-STEP AND FOUR-STEP MODEL IN TERMS OF THE EQUILIBRIUM SATURATION CURVES.

$$N_{O_2} = \frac{\bar{P}_{AVE}}{L} (p_{O_2}^{x=0} - p_{O_2}^{x=L})$$

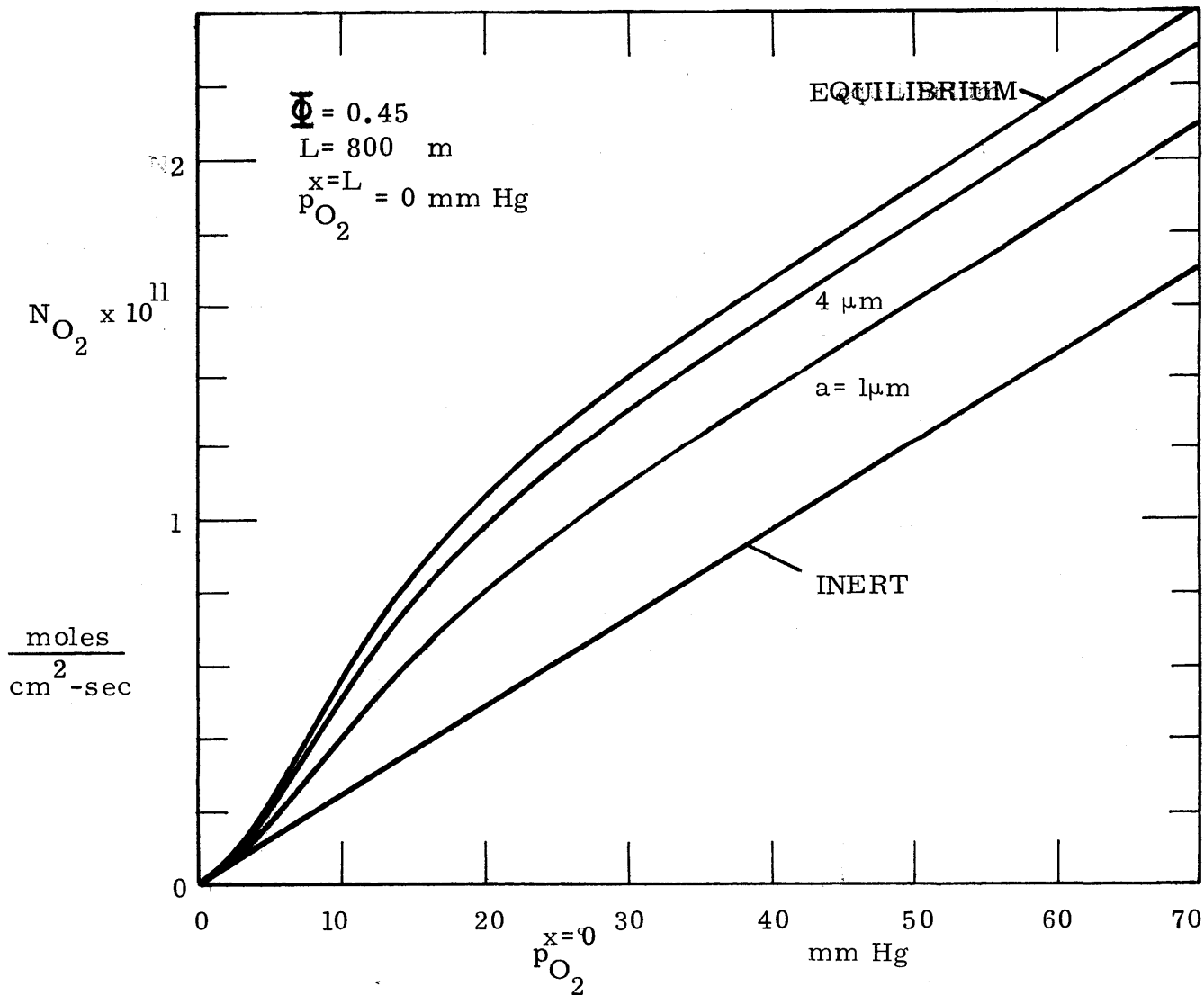


FIGURE 5.27. FLUX PLOT FOR THE FOUR-STEP MODEL.

5.2 Reaction in the Dispersed and Continuous Phase. The Impermeable and Permeable Model

In this section the behaviour of the two general models - impermeable and permeable - will be compared and discussed. As a logical basis of comparison all parameters for both models must be the same. As a consequence, the parameters must be of such values that the thermodynamic constraint, required for the permeable model, is not violated. Recall that the constraint requires that

$$K'_{\alpha'_A} = K_{\alpha_A} \quad (5.23)$$

of in terms of the kinetic rate parameters the relationship becomes

$$\frac{k'_{1\alpha'_A}}{k'_2} = \frac{k_{1\alpha_A}}{k_2} \quad (5.24)$$

Table 5.2 lists the parameters used in this section. The values of the parameters were chosen as an example only. Although equation (5.24) is satisfied, this is not a necessary constraint for the impermeable model. Computer programs for all the theoretical calculations are listed in Appendix E.

5.2.1 Single Sphere in a Continuum

For a single sphere in an infinite medium, concentration profiles and lines of constant total flux differences can be calculated from the equations developed in Chapter 4. The partial pressure of A inside the sphere is given by

TABLE 5.2
 PARAMETERS USED FOR THE COMPARISON
 OF THE IMPERMEABLE AND PERMEABLE MODEL

forward rate constants:	$k_1' = 4 \times 10^6$ l/mole/sec
	$k_1 = 4 \times 10^7$ l/mole/sec
backward rate constants:	$k_2' = 80$ sec ⁻¹
	$k_2 = 400$ sec ⁻¹
concentration of carrier:	$C_T' = 0.10$ moles/l
	$C_T = 0.02$ moles/l
solubility rate of A in the two phases:	$\alpha_A' = 2 \times 10^{-6}$ moles/l/mm Hg
	$\alpha_A = 1 \times 10^{-6}$ moles/l/mm Hg
permeabilities and diffusivities:	$P_d = 1 \times 10^{-11}$ cm ² -moles/sec/l/mm Hg
	$P_c = 2 \times 10^{-11}$ cm ² -moles/sec/l/mm Hg
	$D_B' = 4 \times 10^{-8}$ cm ² /sec
	$D_B = 1 \times 10^{-7}$ cm ² /sec

$$p'_A = p_A^O + H(r) \cos \theta \quad (5.25)$$

where $H(r)$ is given by equation (4.55) (or (4.109)). Outside the sphere, the partial pressure of A is given by

$$p = p_A^O - \frac{N_A^T}{P_c(1 + F_{eq})} [r - af(r)] \cos \theta \quad (5.26)$$

where the function $f(r)$ is given by equation (4.43) (or (4.104)). Equations (5.25) and (5.26) are general and apply to both the impermeable and the permeable model. The models differ in respect to the numerical values of the mutually similar constants that appear in the functional forms of $H(r)$ and $f(r)$. The iso-partial pressure lines of A inside and outside the sphere are given in Figure 5.28 for the impermeable model, and in Figure 5.29 for the permeable model. Note that the iso-partial pressure lines are bent inside the sphere. This is consistent with the behaviour of the iso-partial pressure lines for a single reacting sphere in a inert medium as presented by Figures 5.4 and 5.5a. Outside the sphere the iso-partial pressure lines bend away from the sphere into linear lines (at very large distances away from the sphere). The iso-partial pressure lines for the impermeable model show significantly more curvature than the iso-partial pressure lines for the permeable model. The latter are considerably smoother than the former.

The potential inside and outside the sphere is:

IMPERMEABLE
 $a/\lambda = 16.7, a/\lambda' = 20.9$
 $p_A^o = 10 \text{ mm Hg}$
 $F'_{eq} = 10, F_{eq} = 2.5$

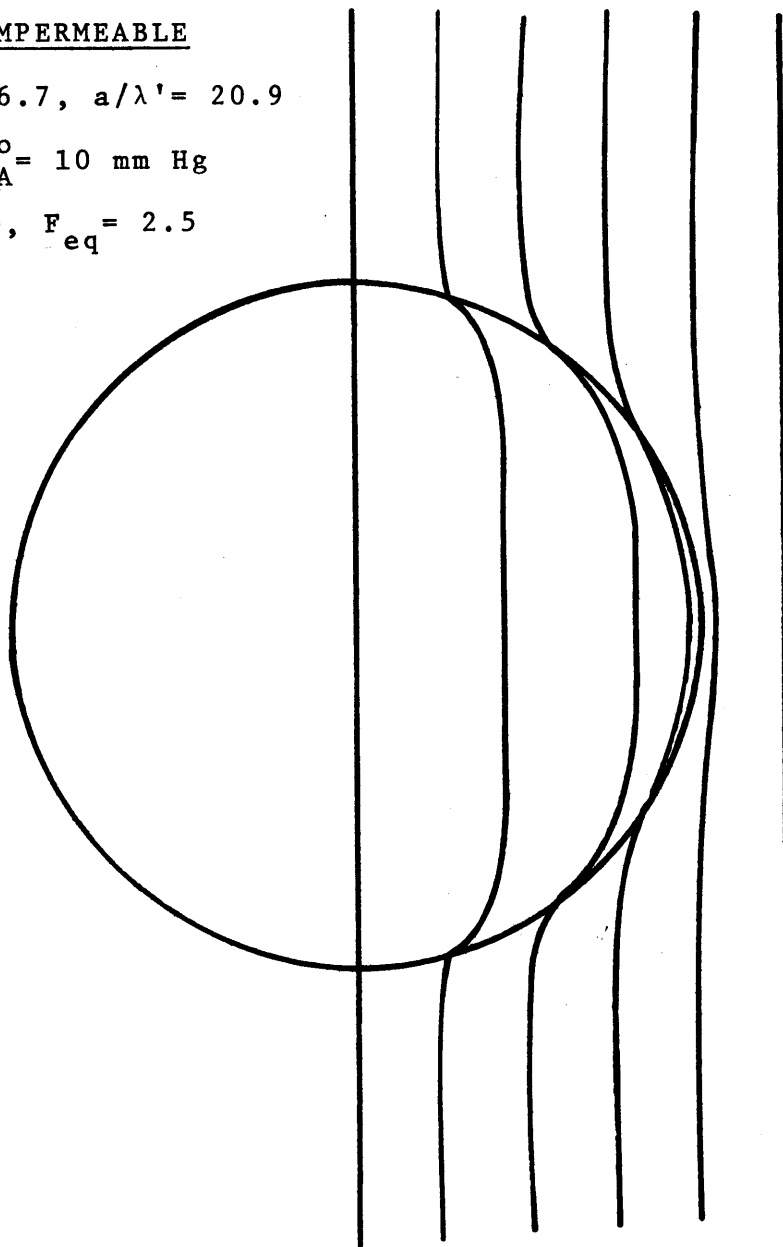


FIGURE 5.28

ISO-PARTIAL PRESSURE LINES FOR A REACTING SPHERE
IN A REACTING CONTINUUM. IMPERMEABLE CASE.

PERMEABLE
 $a/\lambda = 16.7, a/\lambda' = 20.9$
 $p_A^o = 10 \text{ mm Hg}$
 $F'_{eq} = 10, F_{eq} = 2.5$

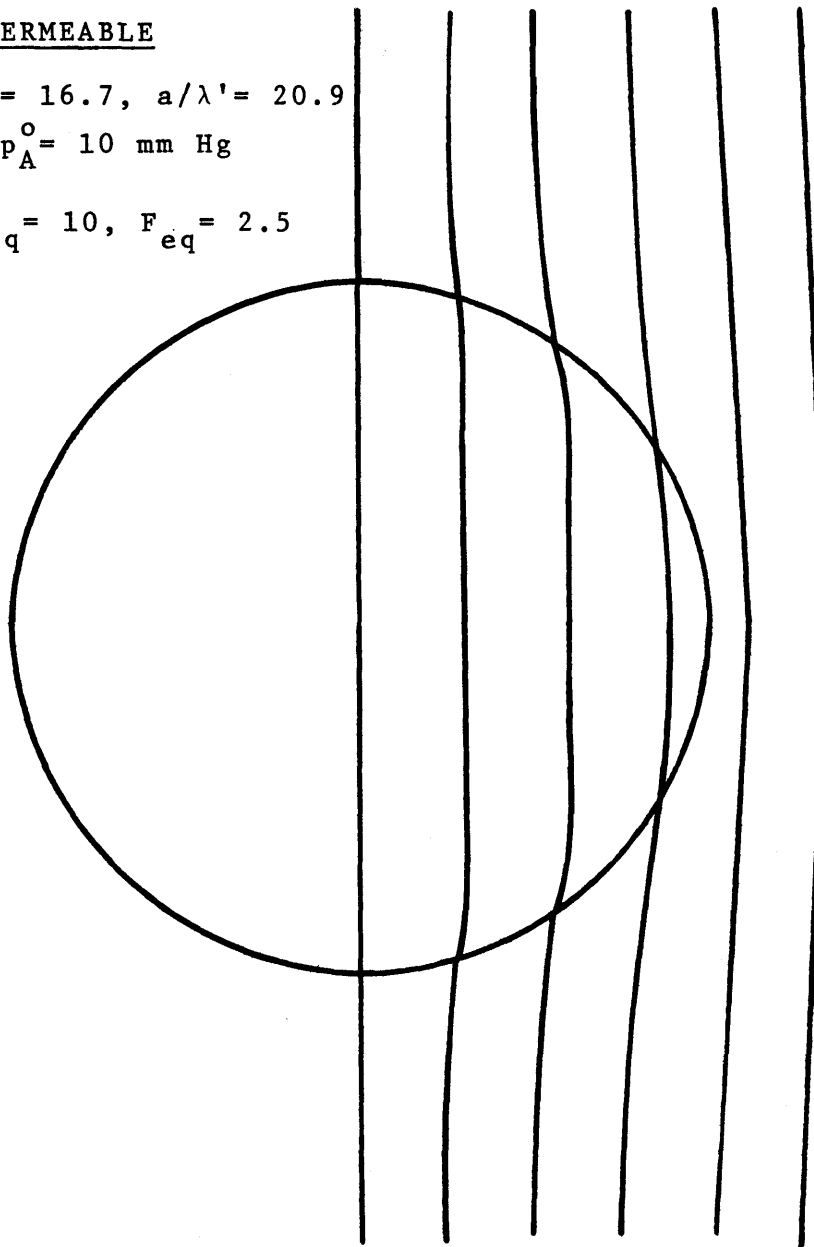


FIGURE 5.29

ISO-PARTIAL PRESSURE LINES FOR A REACTING SPHERE
IN A REACTING CONTINUUM. PERMEABLE CASE.

Inside the sphere:

$$\phi' = \left(p_A' - \frac{D_B'}{P_d} C_B'\right) - \left(p_A^o - \frac{D_B'}{P_d} C_B^{o'}\right) + E \cos \theta \quad \dots\dots\dots (5.27)$$

$$= \frac{k_2' N_A^T}{P_d} r \cos \theta + E \cos \theta \quad (5.28)$$

Outside the sphere:

$$\phi = \left(p_A - \frac{D_B}{P_c} C_B\right) - \left(p_A^o - \frac{D_B}{P_c} C_B^o\right) \quad (5.29)$$

$$= - \left(\frac{N_A^T}{P_c}\right) r \cos \theta \left\{1 + \left(\frac{a}{r}\right)^3 \left[\frac{A}{1+F_{eq}}\right]\right\} \quad (5.30)$$

The constant E can be evaluated by requiring

$$\phi' = \phi \quad \text{at } r = a \quad (5.31)$$

from which

$$E = - N_A^T a \left(\frac{3A}{1 + F_{eq}}\right) \quad (5.32)$$

Once the potential has been defined, the total flux can be calculated by

$$(\psi_2 - \psi_1) = \int_1^2 r^2 \sin \theta \frac{d\phi}{dr} d\theta \quad (5.33)$$

The flux difference inside and outside the sphere is therefore given by:

Inside the sphere,

$$(\psi_2' - \psi_1') = - \frac{N_A^T a^2}{2} \left(\frac{r}{a}\right)^2 \sin^2 \theta \left(1 - \frac{2A}{1+F_{eq}}\right) \quad \dots\dots\dots (5.34)$$

Outside the sphere:

$$(\psi_2 - \psi_1) = - \frac{N_A^T a^2}{2} \left(\frac{r}{a}\right)^2 \sin \theta \left[1 - \frac{2A}{1+F_{eq}} \left(\frac{a}{r}\right)^3\right] \dots\dots\dots (5.35)$$

where the limits of integration are from zero to θ radians.

Note that the definition of the potential satisfies Laplace's equation

$$\nabla^2 \phi' = 0 \quad (5.36)$$

$$\nabla^2 \phi = 0 \quad (5.37)$$

which can also be obtained from subtraction of the differential mass conservation equations for species B from A as was done in equations (4.13) and (4.11). As a consequence one can expect that lines of constant potential and lines of constant flux difference are mutually orthogonal. In addition such plots would behave in a similar manner as the isopotential and isoflux difference plots given earlier in Section 5.1.1.1 (see Figure 5.5). Since the flux plots are symmetrical along the $0^\circ - 180^\circ$ axis and a mirror image along the $90^\circ - 270^\circ$ axis only one quarter of a circle will be shown (the 0 to 90° quarter). This way several conditions can be shown on the same figure. Figure 5.30 shows lines of constant flux difference for the impermeable model for three conditions:

1. equilibrium
2. $a/\lambda = 16.7, a/\lambda' = 20.9$
3. $a/\lambda = 1.67, a/\lambda' = 2.09$

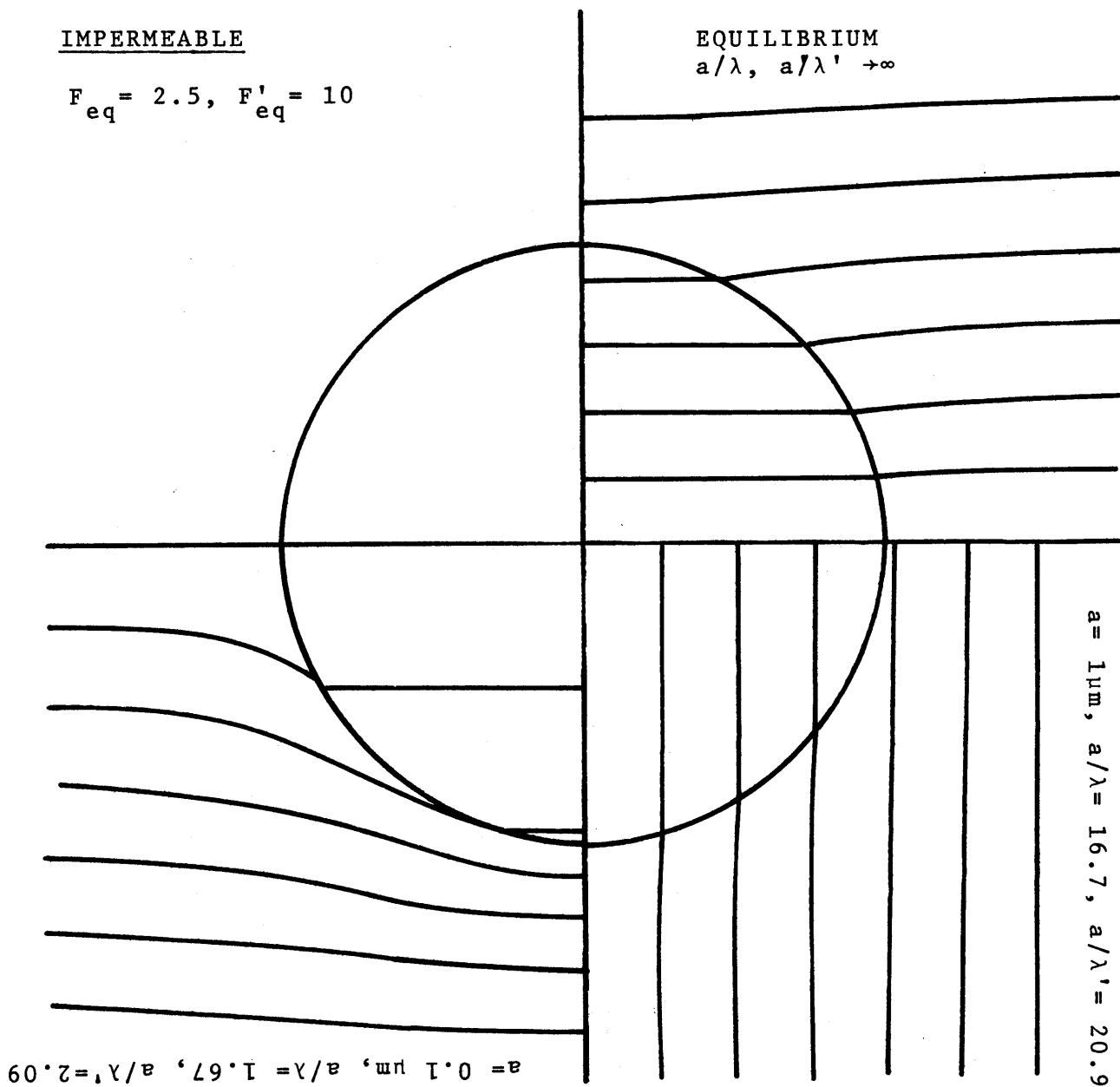


FIGURE 5.30

LOCI OF CONSTANT TOTAL FLUX DIFFERENCE FOR THREE VALUES OF THE CHARACTERISTIC LENGTHS. IMPERMEABLE MODEL.

By appropriate rotation of the figure each subfigure can be viewed. For equilibrium conditions inside and outside the sphere, the effective permeability inside the sphere is greater than the effective permeability outside the sphere, and lines of constant flux difference bend towards the sphere. As the reaction deviates from equilibrium in boundary layers inside and outside the sphere periphery, the effective permeability inside the sphere becomes less than the effective permeability of the continuum and lines of constant flux difference bend away from the sphere. This is due (besides the particular choice of variables) to the fact that nonequilibrium conditions can reduce facilitation effects inside the sphere to be negligible, but since the mathematical model requires the continuous medium to be at equilibrium throughout the medium, except locally very near the sphere, the facilitation effects are always a maximum in the continuous phase. Therefore reduction of sphere radius and consequently the reduction of a/λ (and a/λ') has little effect on the effective permeability of the surrounding reacting medium. This of course is a mathematical result and has been discussed to some extent in Chapter 4. The only manner (mathematically) in which the reacting continuous medium can be made to be inert is by setting F_{eq} equal to zero.

Flux plots for the permeable model are shown in Figure 5.31 for identical conditions as those shown in Figure 5.30. Notice that there is little change in the plots as a/λ and a/λ' are decreased. This is due to the fact that

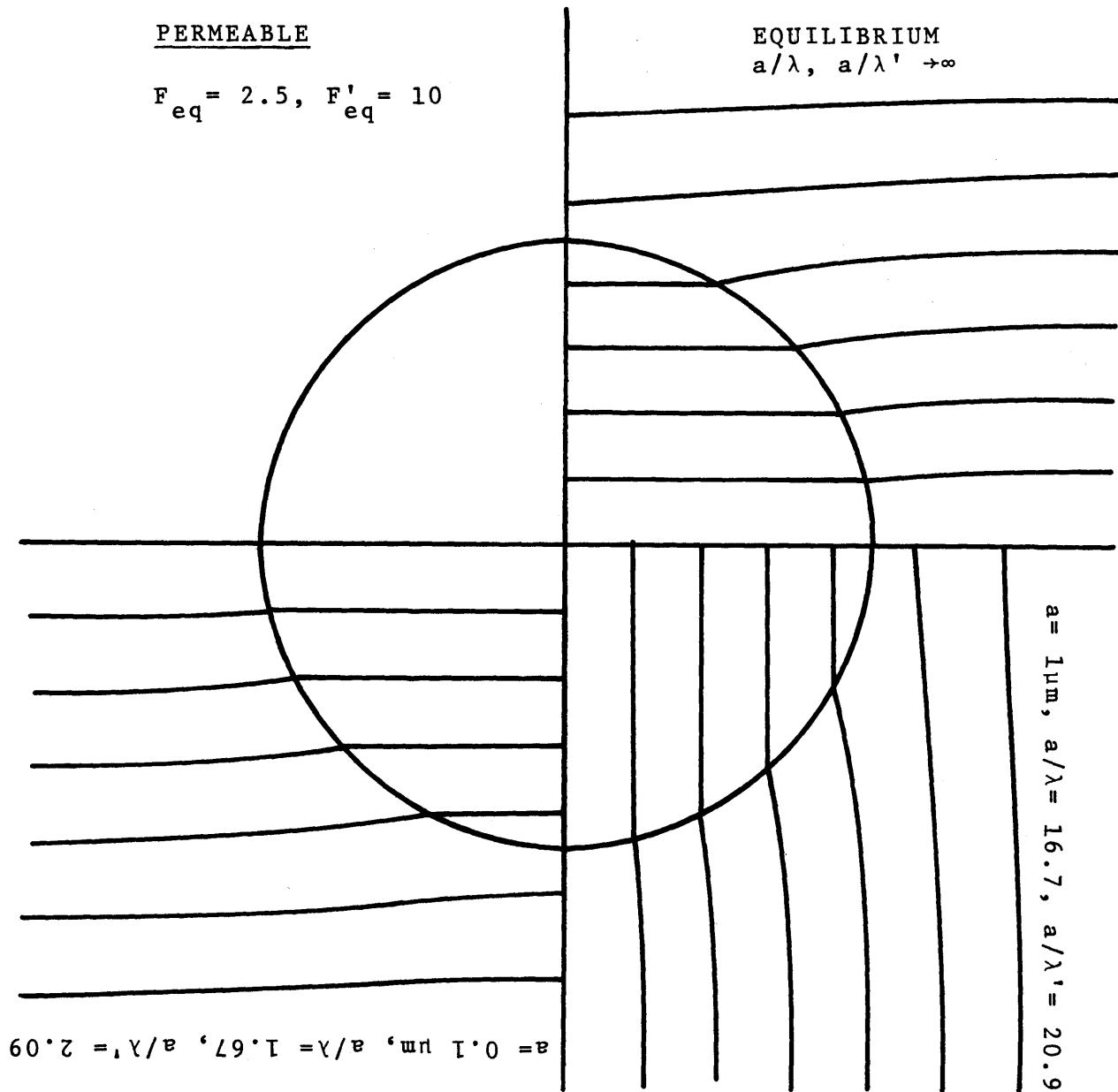


FIGURE 5.31

LOCI OF CONSTANT TOTAL FLUX DIFFERENCE FOR THREE VALUES OF THE CHARACTERISTIC LENGTHS. PERMEABLE MODEL.

the carrier species can still diffuse through (and facilitate transport of species A) the sphere. Note that for equilibrium conditions the two models, permeable and impermeable give identical iso-flux difference plots.

5.2.2 Effective Permeability of a Suspension of Spheres

The general equation for the effective permeability for the impermeable model has been given by equation (4.96) and is

$$\frac{\bar{P}}{P_c(1+F_{eq})} = \frac{2P_c(1+F_{eq})+P_d(1+F_d)(1-2F_{eq}f_c)-2\phi\{P_c(1+F_{eq})-P_d(1+F_d)(1+F_{eq}f_c)\}}{2P_c(1+F_{eq})+P_d(1+F_d)(1-2F_{eq}f_c)+\phi\{P_c(1+F_{eq})-P_d(1+F_d)(1+F_{eq}f_c)\}} \dots\dots\dots (5.39)$$

where

$$f_c = - \frac{1 + \frac{\lambda}{a}}{2 + 2 \frac{\lambda}{a} + \frac{a}{\lambda}} \quad (5.40)$$

For the permeable model the effective permeability is given by equation (4.137) which is

$$\frac{\bar{P}}{P_c(1+F_{eq})} = \frac{2P_c(1+F_{eq})+P_d(1+F'_{eq})\left[\frac{1}{1-Q}\right]-2\phi\{P_c(1+F_{eq})-P_d(1+F'_{eq})\left[\frac{1}{1-Q}\right]\}}{2P_c(1+F_{eq})+P_d(1+F'_{eq})\left[\frac{1}{1-Q}\right]+\phi\{P_c(1+F_{eq})-P_d(1+F'_{eq})\left[\frac{1}{1-Q}\right]\}} \quad (5.41)$$

where the factor Q is given by

$$Q = \frac{\frac{f_c}{F'_{eq}} \left[\frac{F'_{eq} - F_{eq}}{1 + F'_{eq}} \right]^2}{\frac{P_c (1 + F'_{eq}) F_{eq}}{P_d (1 + F'_{eq}) F'_{eq}} + f_c \left[\frac{2 - \tanh \frac{a}{\lambda'} \left(2 \frac{\lambda'}{a} + \frac{a}{\lambda'} \right)}{1 - \frac{\lambda'}{a} \tanh \frac{a}{\lambda'}} \right]} \quad (5.42)$$

and f_c is given by equation (5.40). As has been pointed out, the relationships are valid for reacting spheres in a continuous reacting fluid that is everywhere at equilibrium except locally near the sphere. On letting a/λ approach zero, which implies that the nonequilibrium region around each sphere is very large, at distances sufficiently far from all spheres, the medium must be at equilibrium as specified by the boundary conditions for $r \rightarrow \infty$ (see Figure 4.2). Therefore one would expect that for small a/λ the relationships are no longer valid if the distances between each sphere in the suspension is of order λ . This will put a constraint on the maximum volume fraction for a given a/λ that the relationship can be used for. This constraint will be developed a little later.

First it is of interest to investigate additional mathematical behaviour of the effective permeability relationships of the two models. Some limiting cases will be analyzed.

For the case that the reactions inside and outside are completely at equilibrium, which can be attained by letting a/λ and a/λ' approach infinity, the effective permeability for both the impermeable and permeable model becomes

$$\frac{\bar{P}}{P_c(1+F_{eq})} = \frac{2P_c(1+F_{eq})+P_d(1+F'_{eq})-2\phi\{P_c(1+F_{eq})-P_d(1+F'_{eq})\}}{2P_c(1+F_{eq})+P_d(1+F'_{eq})+\phi\{P_c(1+F_{eq})-P_d(1+F'_{eq})\}} \quad (5.43)$$

At equilibrium, and for identical physical parameters, the permeable model and impermeable model are indistinguishable. Equation (5.43) indicates that at equilibrium the dispersed phase permeability is increased by the factor $(1+F'_{eq})$, and the continuous phase permeability is increased by the factor $(1+F_{eq})$. Equation (5.43) also has the appropriate limits for $\phi = 0$ and $\phi = 1$ which are

$$\bar{P} = P_c(1 + F_{eq}) \quad \phi = 0 \quad (5.44)$$

$$\bar{P} = P_d(1 + F'_{eq}) \quad \phi = 1 \quad (5.45)$$

For the case that the continuous medium is at equilibrium ($a/\lambda \rightarrow \infty$) and the parameter a/λ' is allowed to approach zero the impermeable model reduces to

$$\frac{\bar{P}}{P_c(1+F_{eq})} = \frac{2P_c(1+F_{eq})+P_d-2\phi\{P_c(1+F_{eq})-P_d\}}{2P_c(1+F_{eq})+P_d+\phi\{P_c(1+F_{eq})-P_d\}} \quad (5.46)$$

Equation (5.36) is the relationship for a suspension of inert spheres in a reacting fluid that is at equilibrium. The limits for $\phi = 0$ and $\phi = 1$ are

$$\bar{P} = P_c(1+F_{eq}) \quad \phi = 0 \quad (5.47)$$

$$\bar{P} = P_d \quad \phi = 1 \quad (5.48)$$

For the case $a/\lambda \rightarrow \infty$, $a/\lambda' \rightarrow 0$ (same as above) the permeable model yields the relationship

$$\frac{\bar{P}}{P_c(1+F_{eq})} = \frac{2P_c(1+F_{eq}) + P_d(1+F'_{eq}) - 2\phi\{P_c(1+F_{eq}) - P_d(1+F'_{eq})\}}{2P_c(1+F_{eq}) + P_d(1+F'_{eq}) + \phi\{P_c(1+F_{eq}) - P_d(1+F'_{eq})\}} \quad (5.49)$$

which is identical to equation (5.43) for equilibrium in both phases. This is not so surprising if one recalls the boundary conditions for the permeable model that specify that the activity of the species are continuous across the phase boundary (see Figure 4.2). If the carrier species A, B and AB are at equilibrium at the phase boundary, it follows that species A', B' and AB' are at equilibrium at the phase boundary. Since equilibrium conditions exist also at the center of the sphere it follows that equilibrium conditions exist throughout the sphere. Therefore equation (5.49) is consistent. The same equation is also obtained when $a/\lambda' \rightarrow \infty$ and $a/\lambda \rightarrow 0$ and a similar explanation as given above explains the result. In that case equilibrium conditions everywhere inside the sphere impose equilibrium conditions locally outside the sphere. As a consequence, one would expect from the above discussion and those in the previous section, that equation (5.4) is fairly insensitive to what the value of a/λ and a/λ' are.

Before presenting some graphical results on how the average effective permeability behaves, a volume fraction constraint on the solutions will be developed. The "flip-flop" or "on-off" nature of the theory has already been pointed out with regards to the reaction in the continuous phase. There is no smooth transition from equilibrium to inert conditions

in the continuous phase if a/λ is allowed to change from infinity to zero. In fact there is no transition whatsoever because of the constraints imposed by the mathematical approach in the solution. The only way that the continuous phase can be made inert is by setting the continuous phase equilibrium facilitation factor, F_{eq} , equal to zero. Since reduction of a/λ implies increase of the thickness of the nonequilibrium zone around a particle the equations are valid only for suspensions for which the distance of separation between pairs of particles is adequate for an approach to equilibrium conditions at the midway point. As a consequence, there is a maximum volume fraction beyond which the equations are expected to fail.

A criterion must therefore be set up to arrive at some minimum distance, away from the center of the sphere, at which equilibrium conditions start to prevail. Once this minimum distance has been determined, the maximum volume fraction for which the models are still valid can be determined since it is a function of the minimum distance. For both models the concentration variation for A and B outside the sphere is given by

$$p_A = p_A^o - \frac{N_T^A}{P_c(1+F_{eq})} [r - af(r)] \cos \theta \quad (5.52)$$

$$c_B = c_B^o + \frac{1}{D_B} \frac{F_{eq} N_T^A}{1+F_{eq}} [r + ag(r)] \cos \theta \quad (5.51)$$

where f and g are given by

$$f(r) = -\frac{A}{1+F_{eq}} \left(\frac{a}{r}\right)^2 + K_1 \left(\frac{r}{a}\right)^{-1/2} \left(\frac{\lambda}{r}\right)^{1/2} \left(1 + \frac{\lambda}{r}\right) \left[\cosh \frac{r}{\lambda} - \sinh \frac{r}{\lambda}\right] \dots\dots\dots (5.52)$$

$$g(r) = \frac{A}{F_{eq}} \left(\frac{a}{r}\right)^2 + \frac{f(r)}{F_{eq}} \quad (5.53)$$

The function $f(r)$ is composed of two parts $f_1(r)$ and $f_2(r)$ which are

$$f_1(r) = -\frac{A}{1+F_{eq}} \left(\frac{a}{r}\right)^2 \quad \text{and,} \quad (5.54)$$

$$f_2(r) = K_1 \left(\frac{r}{a}\right)^{-1/2} \left(\frac{\lambda}{r}\right)^{1/2} \left(1 + \frac{\lambda}{r}\right) \left[\cosh \frac{r}{\lambda} - \sinh \frac{r}{\lambda}\right] \quad (5.55)$$

so that $f(r)$ can be restated as

$$f(r) = f_1(r) + f_2(r) \quad (5.56)$$

For equilibrium conditions throughout the continuous medium ($a/\lambda \rightarrow \infty$) the function $f_2(r)$ approaches zero while $f_1(r)$ remains finite (since A remains finite). Therefore the equilibrium profile is given by

$$p_A = p_A^o - \frac{N_T^A}{P_c(1+F_{eq})} [r - af_1(r)] \cos \theta \quad (5.57)$$

In addition, the function $f(r)$ must approach zero as r/a approaches ∞ . As a consequence, the function $f_2(r)$ accounts for the nonequilibrium conditions near the sphere, and it decays rapidly for values greater than $r/a = 1$. Therefore the relative value of $f_2(r)$ to $f_1(r)$ will determine how closely the concentrations of species A and B approach their equilibrium values. Since, if

$$\left| \frac{f_2(r)}{f_1(r)} \right| = 0, \quad (5.58)$$

the concentrations are near equilibrium, two criteria are adopted below to determine at what value (r/a) the ratio $f_2(r)/f_1(r)$ is small enough so one can assume equilibrium conditions have been attained (this value of (r/a) is then the minimum (r/a)). The criteria are:

1. "10% away from equilibrium" when

$$\left| \frac{f_2(r)}{f_1(r)} \right| = 0.1 \quad \text{then } r = r_{\text{minimum}} \quad (5.59)$$

and

2. "1% away from equilibrium" when

$$\left| \frac{f_2(r)}{f_1(r)} \right| = 0.01 \quad \text{then } r = r_{\text{minimum}} \quad (5.60)$$

The value of the ratio $f_2(r)/f_1(r)$ is shown in Figures 5.32a-b as a function of (r/a) and a . The parameters utilized are listed in Table 5.2. As expected the ratio decays rapidly - for large a/λ but more slowly for small a/λ . When r_{minimum} has been determined, the maximum volume fraction can be determined from

$$\phi_{\text{maximum}} \cong \frac{1}{\left[\left(\frac{r}{a} \right)_{\text{minimum}} \right]^3} \quad (5.61)$$

which assumes that the volume fraction can be determined from a sphere (the dispersed sphere) in a sphere (the sphere of surrounding nonequilibrium fluid) model.

Now the average effective permeability can be calculated and the maximum volume fraction can be determined.

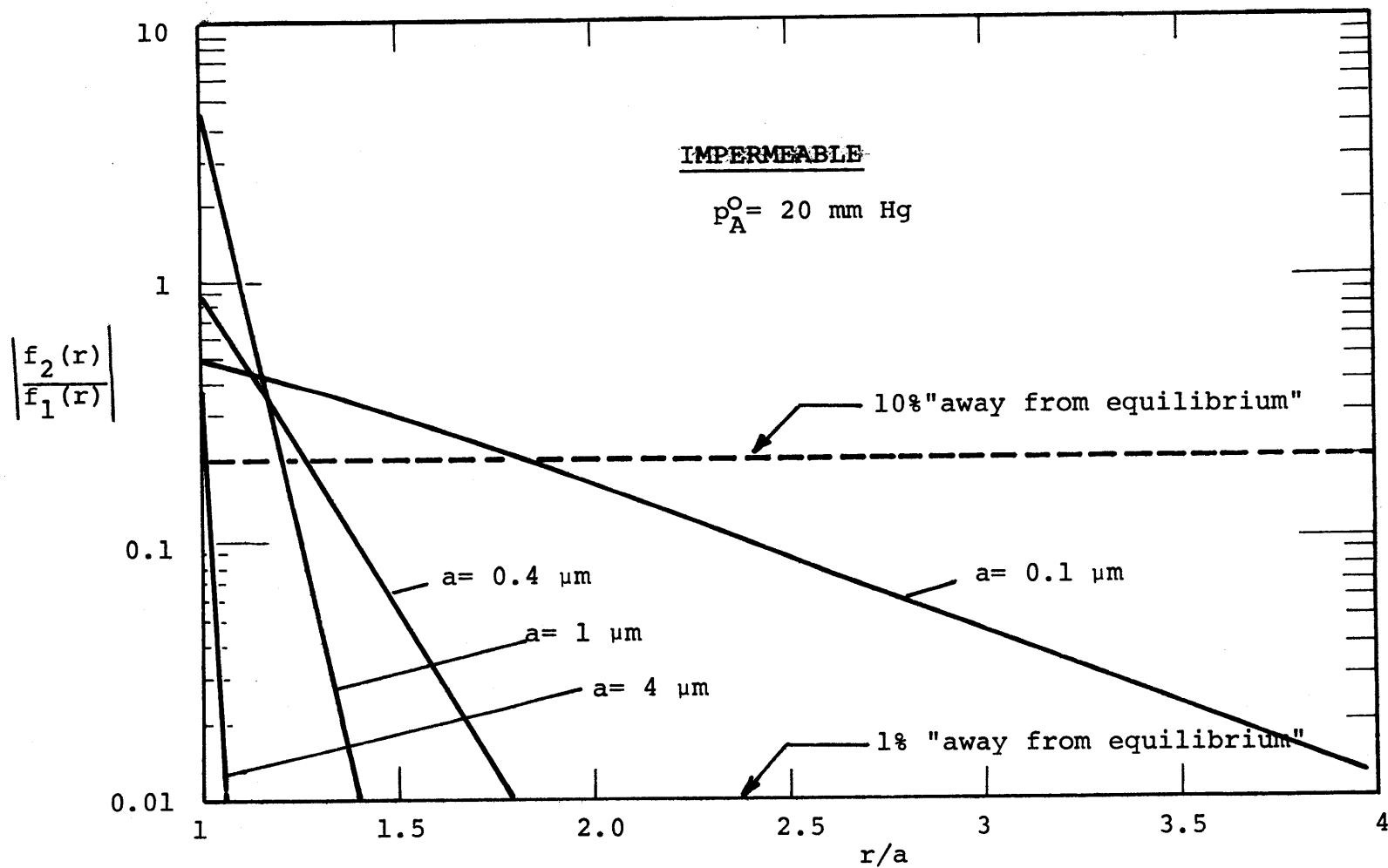


FIGURE 5.32a. THE FUNCTION $|f_2(r)/f_1(r)|$ AS A FUNCTION OF r/a AND SPHERE RADIUS. IMPERMEABLE MODEL

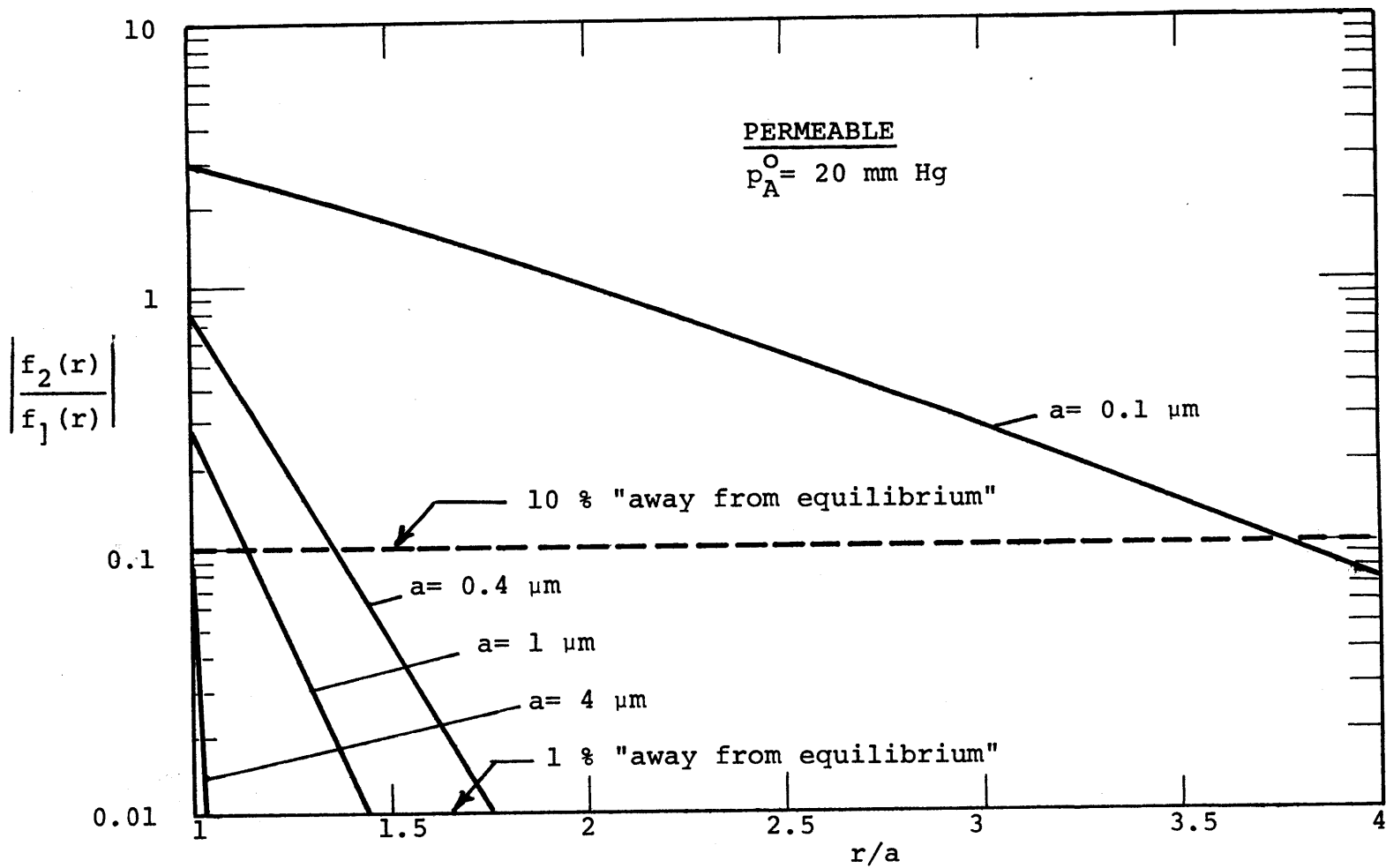


FIGURE 5.32b. THE FUNCTION $\left| \frac{f_2(r)}{f_1(r)} \right|$ AS A FUNCTION OF r/a AND SPHERE RADIUS. PERMEABLE MODEL.

It should be pointed out, that for a particular driving force range and a fixed radius a , the parameter a/λ is not constant since it is a function of the species concentration. In this work the minimum local a/λ for a given driving force was selected as the parameter to determine r_{minimum} and ϕ_{maximum} . Figures 5.33 and 5.34 show the average effective permeability for a suspension of spheres calculated for the indicated driving force and the physical parameters listed in Table 5.2. As expected, for the impermeable model, the average effective permeability decreases as the sphere radius decreases (see Figure 5.33). The equilibrium curve is obtained when a/λ and a/λ' both are larger than 100. The dashed lines indicated the region above which one expects the impermeable relationship to be valid. The "10% away from equilibrium" criterion is a less restrictive constraint than the 1% criterion and therefore allows a greater region of validity. Table 5.3 summarizes the minimum radius ratios and maximum volume fractions as a function of the sphere radius.

The permeable model predicts little change of the average effective permeability as a function of sphere radius. No envelopes of regions of validity have been constructed on the figure because of a limitation of space. Table 5.4 lists the respective minimum volume fractions as a function of sphere radius. Note that for comparison the average relative effective permeability of a completely inert suspension is given in Figures 5.33 and 5.34. This curve is of course consistent with Maxwell's equation and can be obtained by setting $F_{\text{eq}} = 0$ and letting a/λ' approach zero.

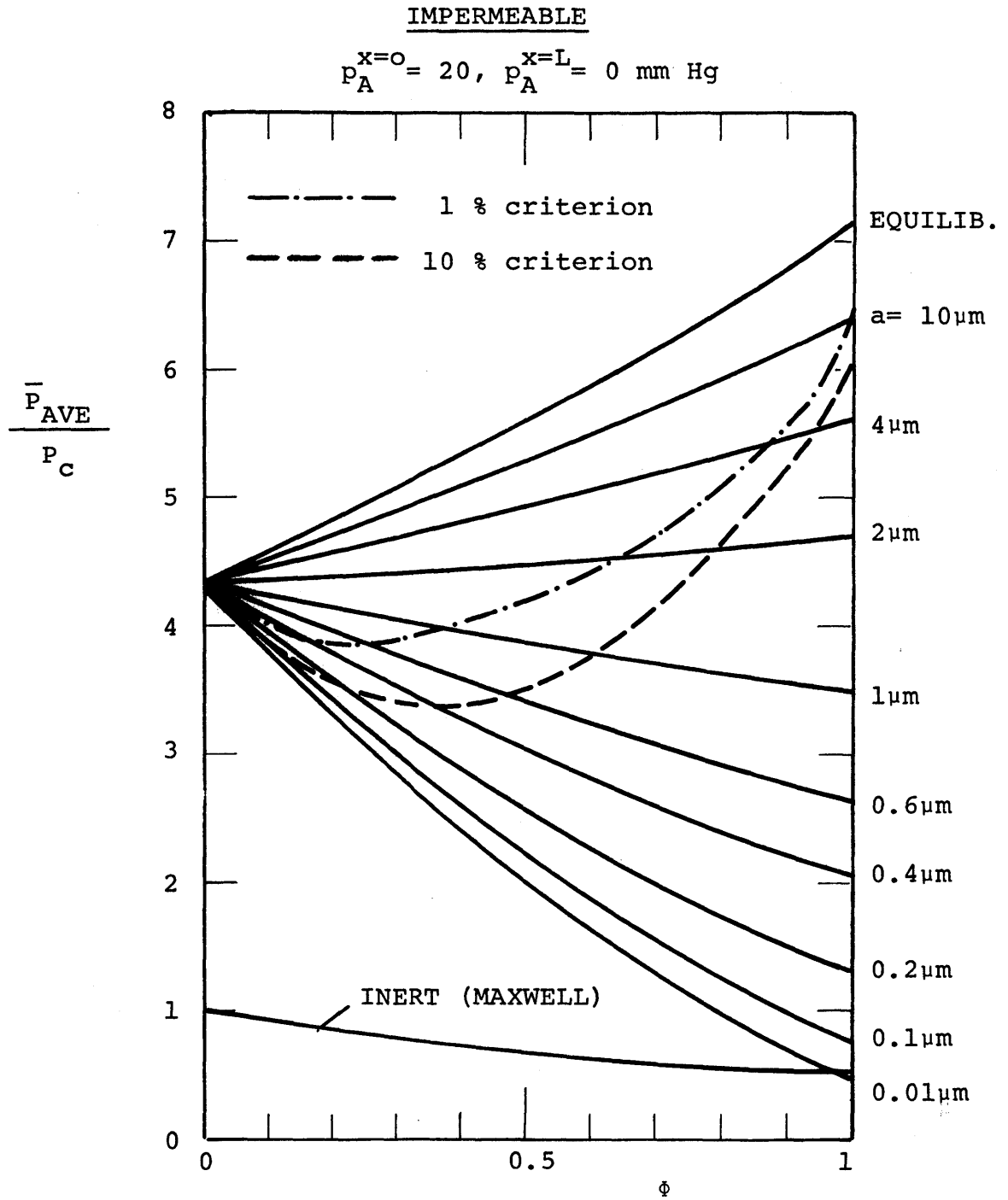


FIGURE 5.33

AVERAGE EFFECTIVE PERMEABILITY RATIO FOR THE IMPERMEABLE MODEL (FOR CONDITIONS SHOWN)

TABLE 5.3
 MAXIMUM ALLOWABLE VOLUME FRACTION
 FOR IMPERMEABLE MODEL AS A FUNCTION
 OF SPHERE RADIUS

sphere radius a (μm)	<u>10% equilibrium</u>		<u>1% equilibrium</u>	
	$\left(\frac{r}{a}\right)$ min	ϕ max	$\left(\frac{r}{a}\right)$ min	ϕ max
6	~1	~1	~1	~1
5	1.01	0.97	1.04	0.89
4	1.02	0.95	1.05	0.85
3	1.04	0.90	1.08	0.79
2	1.08	0.80	1.15	0.65
1.5	1.14	0.66	1.24	0.53
1	1.20	0.58	1.41	0.36
0.6	1.30	0.36	1.56	0.26
0.4	1.71	0.20	1.80	0.17
0.1	2.4	0.073	4.10	0.0145
0.06	3.4	0.032	6.30	0.004

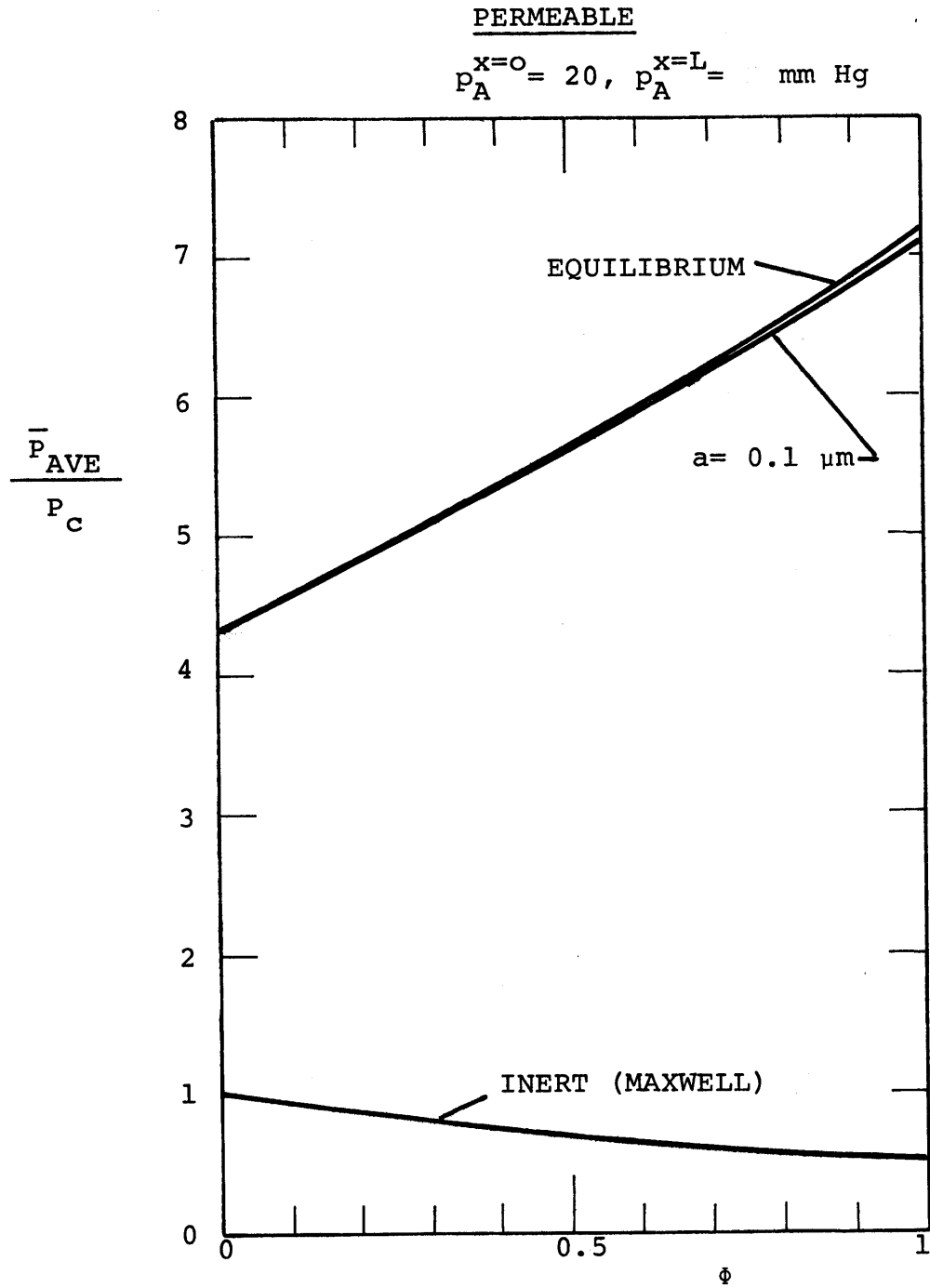


FIGURE 5.34
AVERAGE EFFECTIVE PERMEABILITY RATIO FOR
THE PERMEABLE MODEL. (FOR CONDITIONS SHOWN)

TABLE 5.4
 MAXIMUM ALLOWABLE VOLUME FRACTION
 FOR PERMEABLE MODEL AS A FUNCTION
 OF SPHERE RADIUS

sphere radius a (μm)	<u>10% equilibrium</u>		<u>1% equilibrium</u>	
	$(\frac{r}{a})$ min	ϕ_{max}	$(\frac{r}{a})$ min	ϕ_{max}
6	~1	~1	~1	~1
5	~1	~1	1.02	0.94
4	~1	~1	1.03	0.92
3	~1	~1	1.05	0.86
2	1.01	0.97	1.09	0.77
1.5	1.03	0.92	1.13	0.69
1	1.07	0.82	1.22	0.55
0.6	1.18	0.67	1.44	0.35
0.4	1.38	0.38	1.76	0.18
0.1	3.8	0.019	5.4	0.007

5.2.3 A Note on the Impermeable Model

A common method of observing facilitated transport in a biological sample is to measure the mass transport rate across a thin film of the sample as a function of the driving force. Figure 5.35 shows, for the impermeable case, a typical mass flux versus upstream partial pressure plot, where the downstream pressure is maintained near zero. Physico-chemical parameters are listed in Table 5.5. In this case the thermodynamic constraint has not been imposed. It is of interest to note that the behaviour of the mass transport curves is similar to that calculated for a medium in which a reversible reaction occurred only in the dispersed phase. This similarity points out the hazards of using mass transport data (of the above kind) to deduce information about the physical characteristics inside the sample. The models discussed and developed in this thesis could be reasonable models of reactive heterogeneous biological media that have physical structures similar to those shown in Figure 2.2. However, a mass transport experiment on such a medium may not necessarily indicate what, where, and how many kinds of biological carriers are present in the sample.

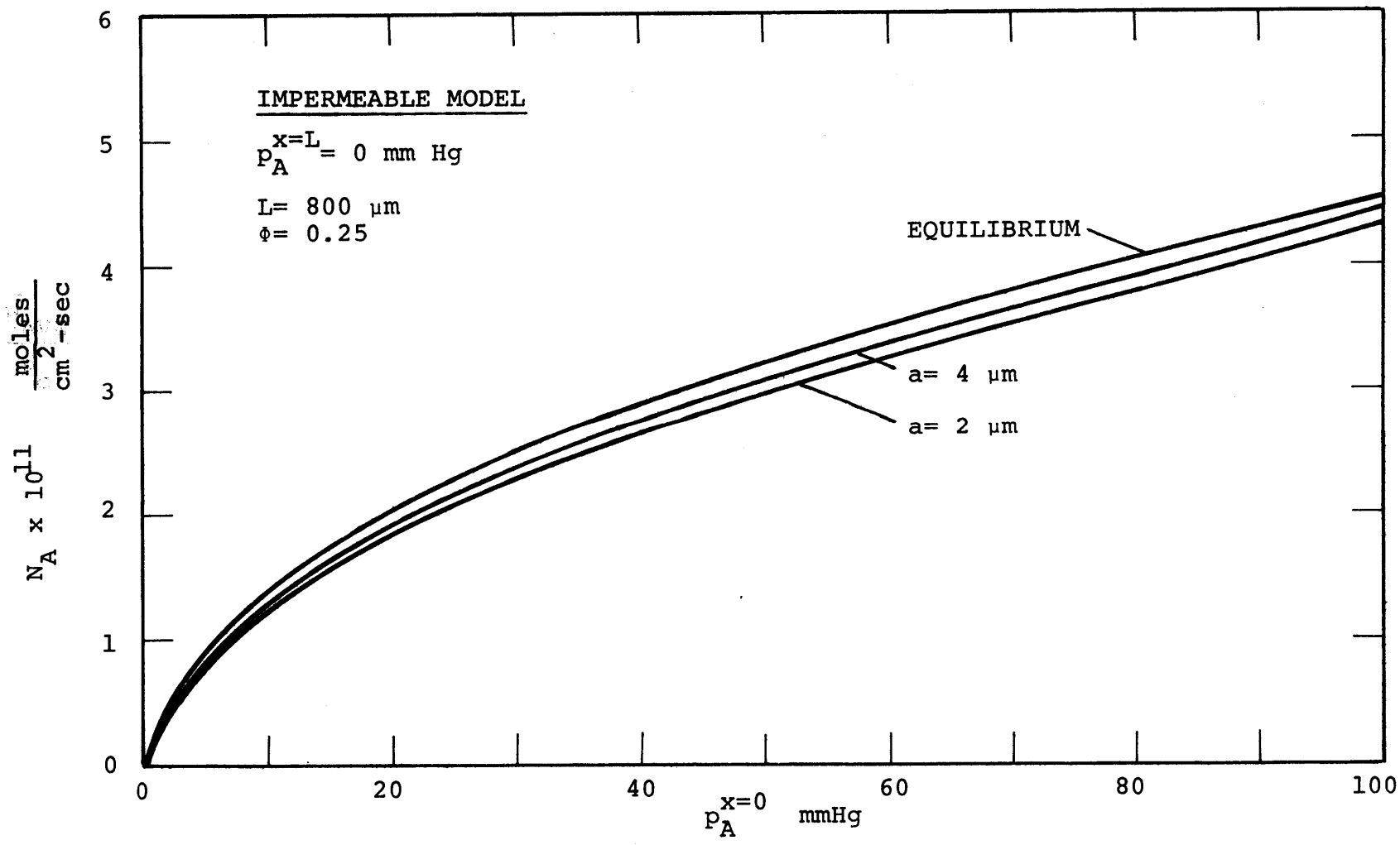


FIGURE 5.35
FLUX VERSUS DRIVING FORCE PLOT FOR THE IMPERMEABLE MODEL.

TABLE 5.5
 PHYSICO-CHEMICAL PARAMETERS USED IN SECTION 5.2.3
 FOR THE IMPERMEABLE MODEL

foward rate constants:	$k_1' = 4 \times 10^6$ l/mole
	$k_1 = 4 \times 10^7$ l/mole
backward rate constants:	$k_2' = 80$ sec ⁻¹
	$k_2 = 400$ sec ⁻¹
concentration of carrier:	$C_T' = 0.10$ mole/l
	$C_T = 0.02$ mole/l
solubility of A in the two phases:	$\alpha_A' = 1 \times 10^{-6}$ mole/l/mm Hg
	$\alpha_A = 1 \times 10^{-6}$ mole/l/mm Hg
permeabilities and diffusivities:	$P_d = 1 \times 10^{-11}$ cm ² -mole/sec/ l/mm Hg
	$P_c = 2 \times 10^{-11}$ cm ² -mole/sec/ l/mm Hg
	$D_B' = 4 \times 10^{-8}$ cm ² /sec
	$D_B = 8 \times 10^{-8}$ cm ² /sec

6. EXPERIMENTAL PROGRAM, METHODS, AND APPARATUS

6.1 Introduction

6.2 Inert Systems

6.2.1 Dispersions

6.2.2 Emulsions

6.3 Reactive Systems

6.3.1 Immobilized Hemoglobin Films

6.3.2 Hemoglobin Solutions

6.3.2.1 Preparation of Hemoglobin Solutions

6.3.3 Red Blood Cell Suspensions

6.3.3.1 Preparation and Analysis of Red Blood Cell Suspensions

6.3.3.2 Equilibrium Saturation Curve Considerations

6.3.3.3 Equilibrium Saturation Curve Measurements

6.3.4 Model Systems

6.3.4.1 Motivation for Working with a Model System

6.3.4.2 Methods of Encapsulation

6.4 Gas Permeation Experiments

6.4.1 Experimental Apparatus

6.4.2 Experimental Procedure

6.4.3 Game Plan and Analysis of Experimental Results

6. EXPERIMENTAL PROGRAM, METHODS, AND APPARATUS

6.1 Introduction

In the literature survey it was pointed out that, excluding theoretical developments on inert heterogeneous media, little theoretical and experimental work has been performed on mass transport in heterogeneous media. With the theoretical models proposed in this thesis the theoretical gap has now largely been closed. An experimental program will be described in this chapter and the results reported in the next chapter, the aim of which was to significantly improve present understanding of the problem. Since the problem of diffusion in inert heterogeneous media became a subproblem of the general theory for reactive heterogeneous media and since in addition little experimental work has been performed on inert heterogeneous media it seemed logical to perform experiments first on inert heterogeneous media. It was expected that if the experimental results showed good agreement with Maxwell's equation, then further experimental results could be obtained with confidence on reactive heterogeneous media. Inert heterogeneous media utilized in this thesis were dispersions and emulsions with a broad spectrum of permeabilities. The work on reactive heterogeneous media focused on the system of interest, namely the oxygen-hemoglobin system, and utilized red blood cell suspensions and one model system. In addition, experiments were carried out to elucidate the augmentation mechanism of human hemoglobin, in particular to determine if any site-to-site diffusion occurs.

In general the experimental procedure utilized in this thesis was to measure mass transfer rates of gas (usually oxygen) across one-dimensional liquid slabs of the system of interest with a known driving force, thickness of the liquid film, and total mass transfer area. The sample was held in a sample holder and the oxygen flux was measured with a modified time lag apparatus (Barrer and Skirrow, 1948). A full description of the apparatus and sample holder will be given at the end of this chapter. The permeability obtained from the experimental measurements

$$\bar{P} = \frac{N_{O_2} L}{A_E (p_{O_2}^{x=0} - p_{O_2}^{x=L})} \quad (6.1)$$

was compared with the predicted permeability obtained from the heterogeneous media theory. In the case of a reactive suspension \bar{P} in equation (6.1) is of course \bar{P}_{AVE} or in the case of a reactive homogeneous film of liquid it is P_{AVE} .

The chapter will outline the experimental program in this thesis, the methods utilized in the preparation of the heterogeneous media employed, and the apparatus utilized to analyze these media.

6.2 Inert Systems

6.2.1 Dispersions

A dispersion is a suspension of solid particles in a liquid continuum. The dispersions utilized in this thesis consist of colloidal polymer particles suspended in an aqueous medium. The

three dispersions used are as follows

- i) Teflon 120 FEP-fluorocarbon resin (Du Pont).
Teflon 120 FEP-fluorocarbon resin is a dispersion of fluorinated ethylene-propylene (FEP) in an aqueous medium. The particle size ranges from approximately 0.10 μm to 0.25 μm .
- ii) Teflon 30 TFE-fluorocarbon resin (Du Pont).
Teflon 30 TFE-fluorocarbon resin is a dispersion of tetrafluoroethylene (TFE) in an aqueous medium. The colloid particles are 0.05 to 0.5 μm in size.
- iii) Polystyrene latex dispersion.

The Teflon fluorocarbon dispersions were received from the Du Pont Company in one quart containers. The dispersions are stabilized with 5-7% of surfactants. The specific gravity for the dispersions and the continuous aqueous phase were determined from the weighings of calibrated volumes of the liquids. The aqueous phase was obtained from the dispersion by centrifuging out the solid particles at 16,000 rpm for 40 minutes in a centrifuge (Servall, Model RC-2). (To insure that all solid content was removed from the aqueous media the color intensity of the centrifuged "solid-free" liquids were compared to mixtures of small aliquots of the respective dispersions in large known volumes of water. It was determined that the solid content of the aqueous media so obtained was less than 0.004 volume percent.) Specific gravities determined in this manner compared well with those reported in the Du Pont data sheets for 120 FEP and 30 TFE dispersions as is shown

in Table 6.1 and 6.2. Once the specific gravities were determined the volume fraction of the solids was calculated and compared to the percent obtained solely from Du Pont data. These numbers compared quite well as is shown in Tables 6.1 and 6.2 (the maximum difference is about 1 volume percent). It was assumed that the Du Pont data was correct. Dispersions of smaller volume fractions than those reported in the tables were obtained by pipetting calibrated volumes of dispersions and solid free liquid. In one case a higher volume fraction was obtained by centrifuging a weighed amount of dispersion, removing some of the solid free liquid, weighing the remaining amount and then gently redispersing the solid material with a glass rod until the solution was homogeneous in appearance.

The polystyrene latex dispersion was prepared by emulsion polymerization of styrene monomer in an aqueous media. Through proper control of additives in the water phase (anionic and nonionic surfactants, free radical initiator), and control of reaction temperature and stirring rate, virtually monodisperse polystyrene beads can be grown according to the methods of Woods et al. (1968). The basic procedure is to place known amounts of styrene monomer (Eastman), distilled water, Siponate DS-10 (disodium dodecyl diphenyl ether disulfonate from Alcolac Chemical Co.), the nonionic surfactant Triton X-100 (a polyoxyethylene isooctylphenyl ether from Rohm and Haas), and the radical initiator $K_2S_2O_8$ (potassium peroxydisulfate from Fischer Scientific) into a closed container and to then react the contents with gentle agitation at $65^{\circ}C$ for 24 hours. After the 24 hour period

TABLE 6.1
 PHYSICAL PROPERTIES OF 120 FEP DISPERSIONS
 (Blend 283)

	<u>Du Pont data sheets</u>	<u>Experimental</u>
% solid by weight	53.7 ¹	-
Specific gravity of dispersion	1.43 ²	1.426
Specific gravity of solids	2.12-2.17 ²	-
Specific gravity of liquid	-	1.003
% solid by volume	35.4-36.2 ³	34.2 ⁴
pH	-	9.18

1 Data from packing slip data sheet

2 Data from Du Pont data sheet A-21458

3 Calculated from 1 and 2

4 Calculated from 1 and experimental data (can also utilize
 ρ_{solid})

TABLE 6.2
 PHYSICAL PROPERTIES OF 30 TFE DISPERSION
 (Blend 2400)

	<u>Du Pont data sheets</u>	<u>Experimental</u>
% solid by weight	59.7 ¹	-
Specific gravity of dispersion	1.50 ²	1.498
Specific gravity of solids	2.18-2.26 ²	-
Specific gravity of liquid	-	1.003
% solid by volume	39.4-42.0 ³	39.8 ⁴
pH	-	8.71

1 Data from packing slip data sheet

2 Data from Du Pont data sheet A-46473

3 Calculated from 1 and 2

4 Calculated from 1 and experimental data

the reaction vessel is maintained at 80°C for an additional five hours in order to complete the reaction. Woods et al. investigated various recipes of reactants and reported the effect of varying surfactant contents upon the particle size distribution of the polystyrene latex, and they have given various recipes that can produce monodisperse particles. The theory of emulsion polymerization will not be reviewed here since it is incidental to the real problem in this thesis. It should be pointed out however that the polystyrene polymer does not grow in the monomer styrene droplets but rather in the micelles created by the surfactants, and that both free radical initiator and styrene monomer must diffuse through the water phase into the micelle (or later to the growing polymer particle).

In this thesis the basic recipe given by Woods et al. in their table 1 was utilized. The reactants were placed in a glass bottle containing some glass beads, capped, and then tied to the blade of an inclined electric stirrer. The inclined stirrer was placed in a water bath maintained at 65°C by a Tempunit temperature controller (Cole-Parmer) and was rotated end over end at approximately 30 rpm. After 24 hours the temperature was increased to 80°C for an additional 5 hours. Several latexes were produced in this manner until a suitable sample was prepared (both in homogeneity and particle size) with the recipe as reported in Table 6.3 for sample S-6. A small amount of the latex dispersion was centrifuged for one hour at 16,000 rpm but no clean separation of solids and continuous phase was observed. This was probably due to the following: the relatively small specific

TABLE 6.3

RECIPE FOR MONODISPERSE POLYSTYRENE LATEX (S-6)

<u>Ingredient</u>	<u>Amount (gr)</u>
Water	54.863
Triton X-100	2.149
Siponate	0.740
$K_2S_2O_8$	0.333
Styrene	66.287

gravity difference between polystyrene and aqueous medium; the high volume fraction of solid; and electrostatic repulsion between particles. Woods et al. (1968) reported a density for polystyrene beads of 1.05 gr/cc. In order to obtain additional latex samples with different solid volume fractions it was decided to make up aqueous solutions with the same proportion of water and water soluble components (surfactants but no $K_2S_2O_8$) as that reported in Table 6.3. This surfactant solution was then used to dilute the original sample (S-6) to obtain samples with smaller solid volume fractions. The density of the polystyrene latex sample (S-6) and the surfactant solution was determined by weighing calibrated volumes of the liquids. The density of the surfactant solution was found to be 1.003 gr/cc and that of the dispersion for sample S-6 as 1.027 gr/cc as reported in Table 6.4.

The volume fraction or volume per cent of solids for sample S-6 can now be calculated by two independent methods. By

TABLE 6.4

PROPERTIES OF POLYSTYRENE LATEX SAMPLE S-6

Specific gravity of dispersion	1.027
Specific gravity of liquid	1.003
Specific gravity of solids	1.05 (Woods et al.)
Volume per cent of solids	52.4
Volume per cent of liquid	47.6

utilizing data from Table 6.3 and the two measured densities the specific gravity of the solid and the volume per cent solids for S-6 can be determined. For example;

$$\begin{aligned} \text{total volume dispersion} &= \frac{\text{total weight}}{\rho_{\text{dispersion}}} \\ &= \frac{124.372 \text{ gr}}{1.027 \text{ gr/cc}} = 121.1 \text{ cc} \end{aligned}$$

$$\begin{aligned} \text{volume water} &= \frac{\text{weight water + surfactants}}{\rho_{\text{aqueous phase}}} \\ &= \frac{57.753 \text{ gr}}{1.003 \text{ gr/cc}} = 57.6 \text{ cc} \end{aligned}$$

$$\begin{aligned} \text{volume \% solids} &= \frac{\text{volume solids}}{\text{total volume}} 100 \\ &= \frac{121.1 \text{ cc} - 57.6 \text{ cc}}{121.1 \text{ cc}} 100 = 52.4 \end{aligned}$$

On the other hand one can utilize the density data for the aqueous solution and the density data for the solids as reported by Woods

et al. and arrive at a density of the dispersion and the volume percent of the solids for sample S-6. Either method yields exactly the same numbers.

The fluorocarbon and polystyrene dispersions showed good stability characteristics. The fluorocarbon dispersion would only show some phase separation after standing on the shelf for several weeks. No noticeable phase separation occurred for the polystyrene sample after several months storage.

The particle size and particle size distribution of the latex particles for both the fluorocarbon dispersions and the polystyrene dispersion was measured by electron photomicrography. The electron microscope used is a Phillips EM-2000 Electron Microscope. The technique involved was to place a drop of diluted dispersion on a ultrathin collodion film supported on a fine circular screen. After allowing the drop to evaporate the screen was placed into the microscope and analyzed.

6.2.2 Emulsions

An emulsion is a dispersion of one liquid dispersed in a second liquid. Emulsions can be formed if appropriate emulsifying agents are used to stabilize the suspension. Since the oxygen permeation measurements made in this thesis took roughly six hours, the emulsion employed had to be stable for at least this time span. The term stability is used somewhat loosely in the literature and may have different connotations

depending on what property of the emulsion one is interested in. In this work an emulsion was considered stable if the emulsion did not show gross separation (creaming or sedimentation) over a six hour period while particle size remained reasonably constant. The stability of an emulsion is a function of the chemical nature of the materials, the density difference between the immiscible phases, the particle size of the emulsion, and the emulsifying agents used. If no emulsifying agent is used emulsions are generally unstable even though a double layer is often present. The charge density without the presence of a surfactant is usually low; however, upon addition of a surface active agent it will adsorb at the oil/water interface and may provide sufficient repulsion to overcome van der Waals attraction and consequently stabilize the emulsion. Another method of stabilization is so called "pickering" where small solid particles are allowed to adsorb at the oil/water interface and act as a mechanical buffer. Further, long chain surfactant molecules may exhibit an entropic repulsion effect when the tails of the adsorbed molecules meet upon collision of two particles. Although the stability of lyophobic colloids is physically well understood in terms of double layer phenomena and van der Waals attractive forces, and the theory based on these physical phenomena (DLVO theory for Derjaguin, Landau, Verwey and Overbeek) has been successfully applied to understanding stability phenomena in colloidal dispersions, one can not yet predict the ideal surfactants to give an emulsion a particular desirable property. A useful semi-theoretical

semi-empirical method for selecting a surfactant is the numerical classification based on the H.L.B. scale; this refers to the hydrophilic-lipophilic balance of the emulsifier molecule (Griffin, 1949, 1954). The numerical H.L.B. values for many emulsifiers have been found by experimental tests, and the characteristic application of the emulsifier has been correlated relative to the H.L.B. value. Table 6.5 classifies the H.L.B. value according to the application of the emulsifier and Table 6.6 gives the experimentally determined H.L.B. value for some specific surfactants (Davies and Rideal, 1963). By choosing a surface active agent with the appropriate H.L.B. value, either O/W (oil dispersed in water) or W/O (water dispersed in oil) emulsions can be generated.

TABLE 6.5

CLASSIFICATION OF EMULSIFIERS ACCORDING TO H.L.B. VALUES¹

<u>Range of H.L.B. Values</u>	<u>Application</u>
3.5 - 6	W/O emulsifier
7 - 9	Wetting agent
8 - 18	O/W emulsifier
13 - 15	Detergent
15 - 18	Solubilizing agent

¹ From Davies and Rideal (1963).

TABLE 6.6
H.L.B. VALUES FOR SOME SURFACE ACTIVE AGENTS^{1,2}

<u>Surface Active Agent</u>	<u>H.L.B. Value</u>
Na Oleate	18
Tween 40 (polyoxyethelene (20) sorbitan monoplamate)	15.6
Alkyl aryl sulphonate	11.7
Tween 80 (polyoxyethylene (20) sorbitan monooleate)	10.0
Span 20 (sorbitan monolaurate)	8.6
Ethanol	7.9
Span 80 (sorbitan monooleate)	4.3
Glycerol Monostearate	3.8

1 From Davies and Rideal (1963).

2. Atlas Chemical Industries publication LG-60.

Note: The Span and Tween surfactants are commercial trade names of Atlas Chemical Industries (now ICI America Inc.).

Two researchers collaborated with the author in order to select emulsion systems and methods of preparation that would be suitable for oxygen transport studies (Stricoff, 1971; El-Twaty, 1972). Many types of emulsions were analyzed; both O/W and W/O emulsions. It should be mentioned here that good

stability is not the sole requirement to determine if a particular oil-water emulsion system is acceptable in this work. In addition the chemical nature of the system must be such that it is inert in regards to the materials of construction of the sample holder. As will be shown later in the discussion of the apparatus, the liquid slab (emulsion slab) is isolated by two thin silicone membranes in a sample holder constructed of plexiglass, so the organic liquid used as the oil phase should not attack either the silicone membranes or the plexiglass. Unfortunately silicone polymers are soluble in many organic liquids. In addition another requirement is that the vapor pressure of the organic must be about the same as that of water at 25°C or less (see discussion on apparatus). The final emulsion systems used in this thesis are given in Table 6.7, and these systems gave a wide range of permeabilities, as will be shown in the next chapter. The physical properties and description of the organics are given in Table 6.8.

The fluorocarbon was selected because it is known that certain fluorinated organic liquids have a higher oxygen solubility than whole blood at 1 atm oxygen pressure. Because of numerous clinical transplantations now attempted, various fluorocarbons such as PID have been studied as possible organ preservatives (Malchesky and Nose, 1970). The principal function of the fluorocarbon liquids is to supply the perfused organ with oxygen and to remove carbon dioxide from the organ. In actual use the fluorocarbon is often emulsified into an aqueous phase, through use of the surface active agent Pluronic F-68

TABLE 6.7
EMULSION SYSTEMS STUDIED

<u>Emulsion System</u>	<u>Composition Oil Phase</u>	<u>Composition Aqueous Phase</u>
Castor oil in water	Castor oil	90 vol% water 10 vol% Tween 40
Castor oil in water	90 vol% Castor oil 10 vol% Span 80	90 vol% water 10 vol% Tween 40
Wesson vegetable oil in water	Wesson vegetable oil	90 vol% water 10 vol% Tween 40
Fluorocarbon PID	Fluorocarbon PID	50 gr of Pluronic F68 per 1 liter water

(BASF Wyandotte Corporation), and is used in emulsion form to perfuse the organs. Fluorocarbon emulsions have also been used as blood substitutes in intact animals (Sloviter et al. 1969). Pluronic F-68 is a high molecular weight polyoxypropylene-polyoxyethylene block polymer with a molecular weight of 1,750 that appears to have a low toxicity level (Schmolka, 1970; Malchesky and Nose, 1970).

The method of emulsification chosen in this thesis was mechanical agitation, and the device used was the Brown emulsator. The device is essentially a homogenizer consisting of two 15 ml hypodermic syringes connected by a double hubbed needle. The two syringes are held in a cradle while an air-actuated ram forces the liquid mixture to be emulsified back and forth through the needle orifice. Becher (1967) made a six-parameter statistical study of the effect of various parameters on the initial size distribution function of oil in water emulsions. The following parameters studied for the

TABLE 6.8

PHYSICAL PROPERTIES AND DESCRIPTION OF ORGANICS AT 25°C

<u>Organic</u>	<u>Density</u> <u>gr/cc</u>	<u>Viscosity</u> <u>C_p</u>	<u>Vapor</u> <u>Pressure</u> <u>mm Hg</u>	<u>Commercial</u> <u>Source</u>	<u>Composition</u>
Castor oil ¹	0.960	986	-	Fisher Chemical	87% ricinoleic acid 7% oleic acid 3% linoleic acid 3% saturated fatty acids
Wesson Vegetable oil ²	0.92	60	-	Hunt- ⁴ Wesson	45% linoleic acid 36% oleic acid 11% palmitic acid 5% stearic acid 3% linolenic acid
PID fluorocarbon ³	1.75	1.2	6	Allied Chemical	$[(CF_3)_2CF-O-CF_2CF_2]_2$ perfluoro-1,4- diisopropoxybutane 99.9% pure

1 Data from Handbook of Chemistry and Physics, 49th Edition (1968).

2 Personal Communication Hunt-Wesson Foods, Inc.

3 Mears, W. H. and R. L. Bearers, Fed. Proc. 29, 1819 (1970).

4 Purchased off the shelf in single bottle.

emulsion system of a 57/43 mixture of chlorobenzene and light mineral oil in water:

1. Number of passes through needle orifice
2. Orifice area of needle
3. Air pressure on ram
4. Phase volume fraction
5. Concentration of emulsifying agent
6. Hydrophilic-lipophilic balance (H.L.B.).

The distribution functions were determined photomicrographically, and the data analyzed in terms of the average size. Becher found that the primary parameters that determine particle size are the number of passes, and the air pressure. Becher claimed that (at least for his emulsion system) narrow particle size distributions can be achieved. El-Twaty (1972) found that the particle size distribution was a function of the emulsion system studied, and further that not only air ram pressure and number of passes were of primary importance in determining particle-size but also emulsifier concentration. El-Twaty experimentally determined that emulsions generated by the Brown emulsator were reproducible for a fixed set of parameters. For more information, the reader is referred to El-Twaty's thesis. In this thesis, emulsions of different volume fractions were made by mixing appropriate volumes of the aqueous and the organic phase. Volumes of liquids were determined by calibrating the syringes in the Brown emulsator. The number of passes was 60 and the air ram pressure used was 40 psi for all emulsions.

Particle size of the emulsion was analyzed with either a Coulter Counter or a Microscope. Particle size analysis was used here both as a method of quality control (to insure that the particle size was reasonable in comparison to emulsions of the same type) and as a check to see if an emulsion failed to obey Maxwell's equation because of possible particle size variations.

6.3 Reactive Systems

The heading "reactive systems" is somewhat restrictive here because experiments are conducted in certain cases where the chemical reaction is completely saturated (inactivated) and consequently is of no importance in the mass transfer phenomena. In addition some experiments have been performed on some homogeneous systems.

6.3.1 Immobilized Hemoglobin Films

As has been discussed in the literature survey, the augmentation of oxygen transport in hemoglobin solutions has been explained by the mobile carrier facilitation hypothesis. In collaboration with Zahka (1971) a study was made to determine if any oxygen transport augmentation occurs in the absence of significant hemoglobin translational mobility.

If the overall oxygenation process is presented by a single step reaction



where A, B, and AB are oxygen, hemoglobin, and oxyhemoglobin respectively, then the steady-state oxygen flux through a one-dimensional system, according to the mobile carrier hypothesis, is given by

$$N_A^T = -D_A \frac{dC_A}{dx} - D_{AB} \frac{dC_A}{dx} \quad (6.3)$$

For the asymptotic case where the reaction is at equilibrium throughout a film of thickness L the above equation is easily integrated giving Olander's equilibrium solution as presented by equation (3.32)

$$N_A^T = \frac{D_A (C_A^O - C_A^L)}{L} \left[1 + \frac{D_B K C_T}{D_A (1 + K C_A^O) (1 + K C_A^L)} \right] \quad (6.4)$$

Alternatively, another mechanism may be responsible for a portion of the observed facilitation, such as site-to-site migration of oxygen across the hemoglobin molecule as suggested by Scholander. Within the framework of a site-to-site surface diffusion mechanism, equation (6.3) retains its validity, but now C_{AB} is the surface concentration of oxygen associated with hemoglobin and D_{AB} is the effective steady-state surface diffusion coefficient of this species times the surface area of the hemoglobin molecules per unit volume of solution. In the concentrated solutions of interest here, the hemoglobin molecules are in very close proximity, but long-range order does not exist (Perutz, 1948). Since continuous arrays of hemoglobin molecules are unlikely, the effective diffusion coefficient would be expected to be a complex function of

hemoglobin concentration (Barrer, 1965). Integration of equation (6.3) yields a result identical in form to equation (6.4). Whether the "carrier" is mobile or fixed the mathematics remain essentially the same, as has been previously shown in other contexts (Hill and Kedem, 1969). Because of the similarity in functional form between the two models, an experiment with a mobile carrier cannot conclusively demonstrate that another mechanism is not simultaneously operative. By greatly reducing the mobility of the hemoglobin carrier without affecting its reactivity towards oxygen an unequivocal test can be made to differentiate between these mechanisms.

Hemoglobin or any other large protein molecule can be immobilized (or insolubilized) by four principal methods:

- i) physical adsorption to an inert carrier (such as glass beads, charcoal, or collodion)
- ii) entrapment inside the lattice of a polymeric matrix
- iii) covalent binding of the protein to a suitable water-insoluble carrier
- iv) covalent cross-linking of the protein by a suitable bifunctional reagent.

The immobilization of proteins is currently an active scientific topic, and excellent reviews are available that have compared the various techniques involved in the various methods (Silman and Katchalski, 1966; Goldman et al., 1972; Weetal and Messing, 1972). Zahka (1971) investigated the immobilization of hemoglobin by physical adsorption into

collodion films, and the crosslinking of hemoglobin into films with glutaraldehyde and benzidine diazonium salt. The crosslinking agents deactivated the hemoglobin molecules and could not be used in the test. The hemoglobin immobilized by sorption into collodion membranes remained fully active, and these membranes were used for the oxygen permeation experiments.

The collodion membranes were prepared from nitrocellulose (U.S.P., J. T. Baker Chemicals Co.) by standard techniques but were not further oxidized (Carr and Sollner, 1944; Gregor and Sollner, 1946). The films were about 300 μ thick, contained 85 to 90 per cent by volume water, and have been shown to have an effective pore diameter of about 0.3 μ (Goldman, et al., 1968). Hemoglobin solutions were prepared by standard methods, the description of which will appear in a later section of this chapter. Methemoglobin solutions were prepared by addition of potassium ferricyanide to the hemoglobin in solution. Collodion membranes, which were stored in buffer prior to use, were equilibrated with hemoglobin or methemoglobin solutions for 14 days. To make sure that the hemoglobin used in this study did indeed facilitate oxygen transport, experiments were conducted similar in nature to those of Scholander (1960). Millipore HA fillers (approximate thickness 150 μ , porosity 0.79, average pore diameter 0.45 μ , according to the Millipore Corp.) were first filled with the same hemoglobin solution by capillary action and then equilibrated for 12 hours. Membrane thickness measurements were made before each oxygen permeation determination with a sensitive micrometer (Ames dial comparator, Model 412).

It was anticipated that some of the hemoglobin would be irreversibly sorbed by the nitrocellulose, as has been observed with various enzymes which retained their activity in hydrophilic collagen membranes (Vieth et al., 1972), and that mobility of the retaining hemoglobin would be severely restricted. This was analyzed by immersion of a hemoglobin-saturated film of known thickness and area, the surface of which was first wiped dry, into a large volume of agitated buffer. Effective diffusivity of the free hemoglobin was calculated from the amount eluted at known times and at equilibrium by use of the solution for diffusion from a slab into a well-stirred finite bath (Crank, 1964).

Oxygen affinity of hemoglobin was measured by equilibrium uptake experiments. Measured amounts of hemoglobin or of pieces of saturated membranes were placed in agitated phosphate buffer, degassed, and then exposed to a specified mass of oxygen in the presence of saturated water vapor. Oxygen partial pressure in the gas space above the liquid was followed manometrically (MKS Baratron) until there was no change with time. Dissolved oxygen at the equilibrium partial pressure was calculated from the known solubility (Altman and Dittmer, 1971), and hemoglobin-bound oxygen was determined by material balance through use of the ideal gas law. Additional points on the oxyhemoglobin saturation curve were obtained by varying the initial mass of oxygen.

All solutions were stored, and membrane equilibration with hemoglobin solutions was carried out, at 4°C. All other

experiments were conducted at $25 \pm 0.5^{\circ}\text{C}$. Additional details are available (Zahka, 1971).

6.3.2 Hemoglobin Solutions

Oxygen permeability data was obtained on "inactivated" hemoglobin solution in order to compare measured permeabilities with literature values of hemoglobin solutions diffusivity and also to obtain some results at temperatures other than 25°C . The oxygen-hemoglobin reaction can be inactivated by several methods. In the presence of 0.7 mm Hg carbon monoxide (lethal concentration) the heme sites are completely blocked and unavailable for the reaction with oxygen. Another method is to convert the hemoglobin to the inactive methemoglobin form by addition of potassium ferricyanide. A third method is to saturate the hemoglobin completely with oxygen so that the reaction is completed and no longer participates in the mass transfer process. In each of these three cases, the oxygen mass flux is solely a diffuse flux. Oxygen permeabilities were measured in hemoglobin solutions where the hemoglobin reaction was inactivated by each of the three mentioned methods. Permeabilities obtained should of course be independent of the inactivation manner chosen. Oxygen permeabilities were obtained on hemoglobin concentrations from zero to 32 gr/100 ml at 25°C . Oxygen permeabilities were also obtained over a range of temperatures for a fixed hemoglobin concentrations.

6.3.2.1 Preparation of Hemoglobin Solutions

Outdated or fresh whole human blood (O positive) was obtained either from the Red Cross Blood Bank, or the Massachusetts General Hospital Blood Bank both in Boston, Massachusetts. It was centrifuged at 7,500 rpm for 15 min at 4°C in a centrifuge (Servall, Model RC-2) and the plasma and buffy coat were discarded. The red cells were washed three times with pH 7.2 isotonic phosphate buffer (7.67 gr of NaCl, 1.36 gr Na₂HPO₄, 0.51 gr of KH₂PO₄ per liter of water) and recentrifuged. Complete hemolysis of the packed red cells was obtained by three cycles of freeze-thawing in a salt-ice slush at -10°C. The concentrated hemoglobin solution was centrifuged at 16,000 rpm for 30 minutes in order to remove the red cell stroma. The concentrated hemoglobin solution was diluted as needed with the isotonic phosphate buffer (pH = 7.2) or isotonic saline. Methemoglobin was prepared by the addition of 1.05 mole of potassium ferricyanide per mole of heme. The five percent excess is necessary to insure that the hemoglobin is fully reduced to methemoglobin (Antonini and Brunor; 1971). Total hemoglobin concentration of solution was quantitated by the cyanmethemoglobin method (Richerich, 1969). The adsorption at 540 mμ was measured (using a Bausch and Lomb 505 spectrophotometer) of a .02 ml sample of hemoglobin solution diluted with 5.0 ml of standard cyanmethemoglobin stable reagent (Hycel Inc., catalog no. 116C). The adsorption was related to hemoglobin concentration through use of the Hycel certified

cyanmethemoglobin standard (Hycel Inc., catalog no. 117). The calibration curve was prepared by Emmer (1972).

6.3.3 Red Blood Cell Suspensions

The reactive heterogeneous media of interest was red blood cell suspensions in buffered isotonic saline. Whole blood was not used for a variety of reasons. Whole blood is usually collected in 67.5 ml of ACD solution (Anticoagulant Citrate Dextrose Solution U.S.P.) for the total collection of 450 ml of blood. The ACD solution is acidic and causes the blood pH to drop. Upon storage of whole human blood at 4°C additional physiological changes take place most of which are not understood. However it is known that blood pH becomes more acidic with time, and that some hemolysis of red blood cells may take place. Small microsize clots may form in the suspension. In this study, in order to be assured of reasonably consistent samples, red blood cells obtained from whole blood were washed and suspended in buffered isotonic saline at a pH of 7.0.

6.3.3.1 Preparation and Analysis of Red Blood Cell Suspensions

Freshly collected whole human blood was purchased from the Massachusetts General Hospital Blood Bank and stored at 4°C in a refrigerator. Red blood cells were obtained from the stored whole blood for oxygen permeation experiments and saturation curve measurements. Red blood cells (RBC) were prepared by a technique analogous to the method for preparation

of hemoglobin solution (but of course not hemolyzed). RBC suspensions of various hematocrits were obtained by diluting the packed red blood cells. The samples prepared were used immediately for oxygen permeation experiments. The usual time span of preparation, from removal from the blood collection bag to insertion into sample holder, was of the order of one to two hours. All blood was handled in plastic containers and maintained at about 4°C. The packed red blood cells were diluted with the phosphate buffer at 25°C and the red blood cells resuspended with gentle stirring with a teflon-covered magnetic stirring bar and a magnetic stirrer at approximately 30 rpm for a few minutes. In order to prevent bacterial growth, the plastic containers used were rinsed (and sample holder was flushed) with dilute formaldehyde solution (10 ml/liter distilled water) and then rinsed thoroughly with distilled water and finally rinsed one more time with buffered isotonic saline prior to use in the red blood cell preparation. Small amounts of streptomycin sulfate (1 mg/10 ml) were added to some of the red blood cell suspension to inhibit bacterial growth (Richterich, 1969).

The hematocrit of the red blood cell suspension was determined by filling five heparinized glass capillary tubes, 5 cm long and 1.3 mm in diameter, with the suspension, sealing the bottom with a white vinyl clay compound (Critoseal, Sherwood Medical Industries) and centrifuging at 17,000 g for 7 minutes in a microcapillary centrifuge (International Equipment Co., Model MB). Hematocrit was calculated as the

percentage ratio of the red cell pack to the total sample length through use of a calibrated card reader (Critocap tube reader, Sherwood Medical Industries). Hematocrit was also analyzed after the experiments in order to determine the amount of hemolysis.

Once the red blood cell suspension was prepared, a small sample was introduced into the sample holder for mass transfer analysis, and the remaining amount was used for equilibrium saturation curve measurements. Experiments were conducted either at 25°C or 37°C.

6.3.3.2 Equilibrium Saturation Curve Considerations

To assure that RBC suspensions are similar from run to run, a necessary requirement is that the oxygen-hemoglobin saturation curve is fairly constant from run to run. From the discussion in Chapter 5 on nonequilibrium mass transport in red blood cell suspensions, it seems reasonable that if there is no correspondence of samples under equilibrium conditions, one should not expect a correspondence in case of nonequilibrium transport. The best way to control the saturation curve is to control temperature, partial pressure of carbon dioxide, pH, and organic phosphates such as 2,3-DPG (see Appendix B). Since temperature is fixed (25° or 37°C) and the partial pressure of carbon dioxide in the permeation experiments is zero mm Hg, the other parameters that need to be controlled are pH and organic phosphate concentrations. The dilution and washing of red blood cells with pH 7.2

buffer leaves the final RBC suspension near a pH of 7.0, which gives a reasonable equilibrium saturation curve in that, if the reaction were indeed at equilibrium, reasonable saturation differences could be attained in actual experiments. A pH of 7.4, which is a physiological pH, was not chosen because the equilibrium saturation curve is fairly steep so that the reaction is readily saturated for small oxygen concentrations at the low concentration side of the liquid slab. Control of pH for the RBC suspensions in the case of dilute suspensions (of red blood cells) was attained by diluting the suspension partly with pH 7.0 isotonic phosphate buffer. The procedures guaranteed that the pH of all samples was near 7.0. For all samples the pH was measured with a Radiometer BMS 3 pH meter, and the pH range in the experiments was from 6.90 to 7.00. Addition of 2,3-DPG to the suspension is ineffective because organic phosphates cannot penetrate the red blood cell membrane (Chanutin, 1971). A possible way to adjust 2,3-DPG is to control metabolic processes within the red blood cell through proper addition of nutrients. This was beyond the scope of this thesis. The saturation data obtained here was mainly used to ascertain the uniformity of the blood from sample to sample. In order to utilize these results theoretically for an Adair type transport model or any other model, kinetic rate constants compatible with the model need to be obtained. For all runs the saturation at near fifty per cent saturation (p_{50}) was measured or several points on the equilibrium saturation curve were obtained.

6.3.3.3 Equilibrium Saturation Curve Measurements

In order to obtain the hemoglobin saturation curve the fraction of total hemoglobin in oxyhemoglobin form (or per cent saturation) must be measured as a function of partial pressure of oxygen. The oxygen hemoglobin saturation curve is properly defined only at fixed temperature, partial pressure of carbon dioxide, pH and other variables that affect the saturation curve. The pH and free organic phosphate concentrations do change somewhat due to structural changes in the hemoglobin molecule upon oxygenation (Appendix B). The pH changes are small but common convention defines the pH of a saturation curve at the fifty per cent value.

Various methods are available for the measurement of the oxyhemoglobin saturation or total oxygen content (from which oxyhemoglobin saturation can be calculated if the dissolved oxygen content is subtracted). Gasometric (Van Slyke and Neill, 1924), gas chromatography (Lenfant and Aucutt, 1966), spectrophotometry (Gordy and Drabkin, 1957), a mixing technique (Edwards and Martin, 1966), and dynamic methods (Duvelleroy et al., 1969) have been reviewed in detail by Cole and Hawkins (1967) and by Duc and Engel (1970). The gasometric technique developed by Van Slyke and Neill is still considered to be the standard method, and usually other methods are analyzed by comparing results with the gasometric method known as the Van Slyke method. The Van Slyke method is somewhat laborious and requires appropriate training to perform the

method accurately. It is not surprising therefore that many commercial devices have become available that can determine oxyhemoglobin saturation quickly and accurately. In this study, oxyhemoglobin saturation was determined with an IL 182 CO-Oximeter (Instrumentation Laboratory Inc.). The IL 182 CO-Oximeter utilizes the spectrophotometric method and total hemoglobin content automatically upon introduction of a 0.5 ml sample. The accuracy of the device is ± 1 oxyhemoglobin saturation percentage. The partial pressure of oxygen and of carbon dioxide, and the pH of the blood samples (or hemoglobin solution) was measured with the BMS 3 blood micro system (Radiometer). The Radiometer BMS 3 has a p_{O_2} range from 0 to 800 mm Hg (accuracy ± 0.1 mm Hg), a p_{CO_2} range of 8 to 400 mm Hg (accuracy ± 0.1 mm Hg) and a pH range of 0 to 14 (accuracy ± 0.005). The three electrodes (oxygen, carbondioxide, and pH) are situated in a temperature bath controlled by a built-in temperature controller that controls the temperature to within $\pm 0.02^\circ\text{C}$ variation.

The basic procedure for obtaining points on the saturation curve was to tonometer two samples with known gas of fixed oxygen concentration; one with humidified nitrogen gas ($p_{O_2} = 0$ mm Hg) and the other with humidified air ($p_{O_2} \approx 150$ mm Hg). The volumes of red blood cell suspensions (about 20 cc each) were each placed in an Erlenmeyer flask, stoppered with a two hole rubber stopper (containing one tube for gas inlet and one for gas outlet) and the humidified gas (nitrogen or air) was then blown on the surface of the liquid

while the flasks were gently agitated (at temperature of interest). After about two hours the flask tonometered with nitrogen was virtually at zero per cent oxyhemoglobin saturation, and the air tonometered flask at complete saturation. By mixing two small volumes (one each out of each flask) in certain ratios, any saturation per cent between 0 and 100 per cent saturation can be obtained. Samples out of the flasks were withdrawn through a small sampling port at the bottom side of the flask (making sure that no gas was present in the sample) with a 2-1/2 ml plastic syringe (Plastipak; Becton, Dickinson and Company) and the two syringes (one zero per cent HbO_2) were connected with a plastic three way stopcock (Pharmaceal Laboratories). The two volumes were thoroughly mixed by reciprocal movement of the plungers of the syringes, and then the mixed sample was analyzed for oxyhemoglobin saturation, pH, and partial pressure of oxygen. The partial pressure of carbon dioxide was checked to insure that it was near zero, and total hemoglobin concentration measured in order to compare it with the more exact value obtained from the cyanmethemoglobin method.

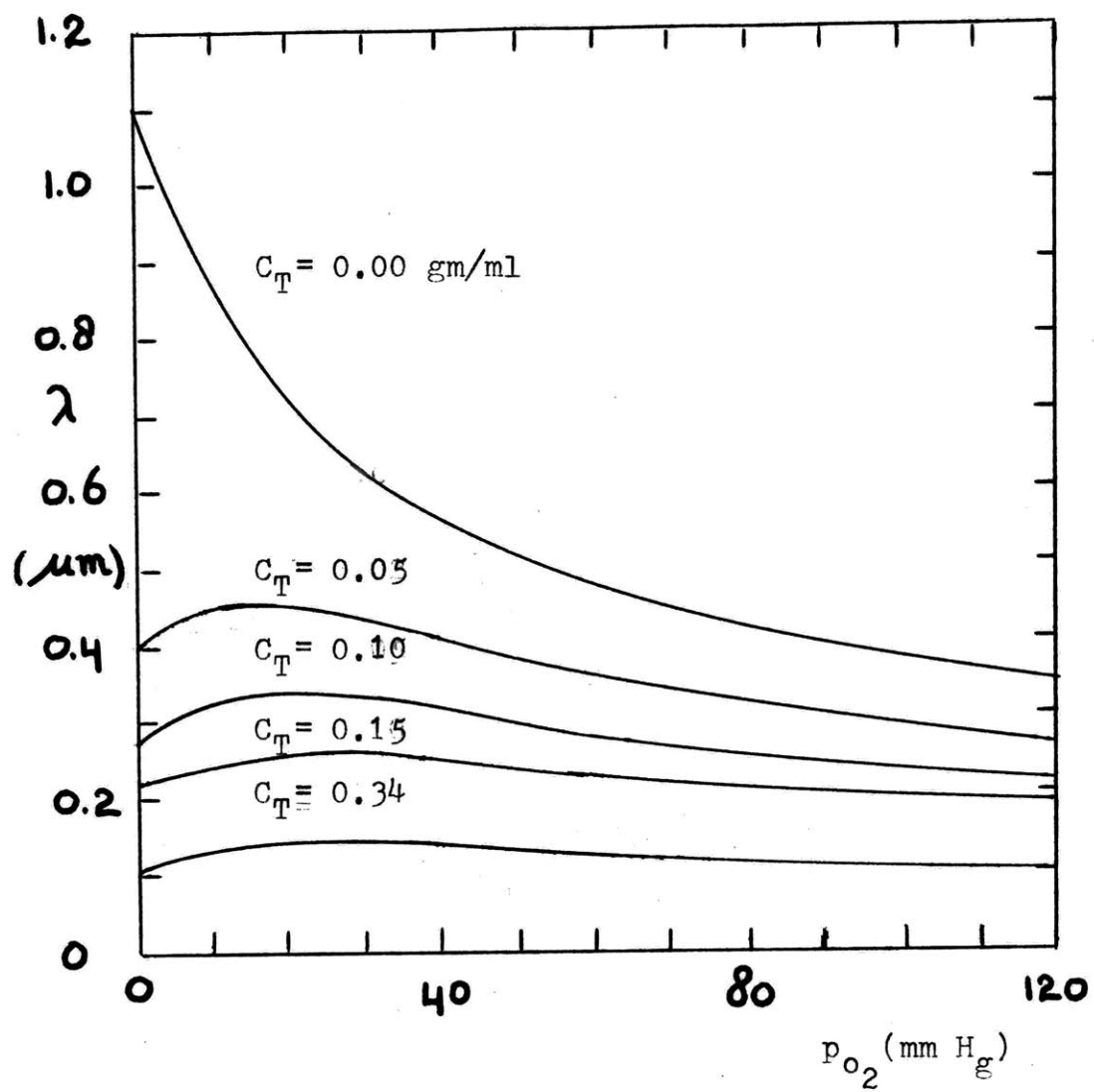
Prior to the analysis of the equilibrium saturation curve of a red blood cell suspension, the sample was stored at 25°C (or 37°C) for the same time period as another sample was maintained inside the sample holder of the permeation apparatus prior to measurement of the steady state oxygen flux through that sample.

6.3.4 Model Systems

6.3.4.1 Motivation for Working with a Model System

In the literature review chapter it was indicated that the hemoglobin diffusivity was not known with great accuracy at hemoglobin concentrations comparable to those inside the red blood cell. In addition hemoglobin diffusivities inside the red blood cell has not been measured. It can be assumed however that the hemoglobin diffusivity inside the red blood cell is of the same order as that measured at comparable hemoglobin concentrations in homogeneous solutions because long-range order does not exist inside the red blood cell (Perutz, 1948). The comparison of experimentally obtained permeabilities with those predicted by theory is open to some question in regards to what the hemoglobin diffusivity should be. In absence of an exact value of the hemoglobin diffusivity inside the red blood cell, a logical procedure would be to compare the experimental results with theoretical predictions utilizing the maximum, the minimum, and an average value of the reported hemoglobin diffusivities. On the other hand, the hemoglobin diffusivity is known more precisely at concentrations below 25 gr/100 ml (see Figure 3.8). If a hemoglobin solution of a concentration below 25 gr/100 ml can be encapsulated inside a spherical particle, so that one has a model red blood cell, a suspension of such particles could give a more precise test of the theoretical model developed in this study. In addition, the particle would be in spherical form as was assumed in the derivation of the model.

In this work four methods were investigated to encapsulate hemoglobin solution in spherical form. Before considering these methods in detail, some additional considerations should be discussed. In the analysis of the theory it was shown that at a hemoglobin diffusivity of 0.70×10^{-7} cm^2/sec (an average value) the oxygen-hemoglobin reaction is not completely at equilibrium even if the maximum allowable red blood cell radius ($4 \mu\text{m}$) is used (see Section 5.1.2). At a lower hemoglobin concentration, the oxygen permeability and hemoglobin diffusivity will increase, so that the value of a/λ' will be shifted more in the nonequilibrium regime. By performing permeation experiments with model red blood cells of one size, lets say with average particle diameter about $2 \mu\text{m}$, and permeation experiments with a suspension of larger size, lets say with average particle diameter of about $10 \mu\text{m}$, one should be able to show experimentally that the average effective permeability for the "large size suspension" must be greater because it would be nearer chemical equilibrium. The characteristic length of the oxygen-hemoglobin reaction is not a strong function of hemoglobin concentration, as is shown in Figure 6.1, so that the two suggested sizes are of a reasonable value since the transition from inert to equilibrium regimes occurs in the particle size range of about 0.5 to about $10 \mu\text{m}$ particle diameter (see Figure 5.8). The large size suspension can of course contain even larger particles as long as particle size is at least $1/10$ of the liquid film thickness (see Section 3.1.2).

**FIGURE 6.1**

CHARACTERISTIC LENGTH AS A FUNCTION OF HEMOGLOBIN CONCENTRATION

6.3.4.2 Methods of Encapsulation

As far as could be determined, four methods are available to encapsulate a liquid inside a spherical particle and these methods are:

1. Encapsulation of liquid with a thin polymeric membrane.
2. Encapsulation of liquid with a thin liquid hydrocarbon phase (liquid membrane).
3. Encapsulation of liquid with a lipid bimolecular layer (lipid membrane).
4. Emulsification of the liquid into an organic liquid such that a W/O emulsion is formed.

Publications have appeared in the open literature that describe various techniques for each of the methods. A fifth possible method which was not considered would be the adjustment of the tonicity of the medium around the red blood cell to hypotonic conditions so that the red blood cell would swell in volume accompanied with a reduction in hemoglobin concentration. This method was not used because it would be impossible to get a "large size suspension" with the same hemoglobin concentration as a "small size suspension" since the total hemoglobin inside the red blood cell is fixed. A possible modification of this technique would be the controlled rupture of the red blood cell membrane by adjusting osmotic pressure and allowing some of the hemoglobin to escape, and then by readjusting osmotic pressure allow the red blood cell membrane to "repair" itself. This

technique could also be used to encapsulate another liquid into the ruptured red blood cell ghost, and subsequent adjustment of osmotic pressure to repair the membrane. However it was felt that to develop such a technique was beyond the scope of this thesis.

For all of the four methods the initial step is to form a W/O emulsion of the aqueous fluid to be emulsified in an appropriate organic liquid. Once the emulsion is formed and the suspended particles are of the desirable particle size, the next step is to form a "skin" around the particles in order to be able to isolate them (not for method 4 of course). In the case of the first method, polymer skins are formed either through interfacial condensation or interfacial coarcervation. The techniques for these methods have been established by Chang and co-workers at Mc Gill University (Chang et al., 1964, 1966, 1968, 1968a, 1972), and have been successfully applied to the encapsulation of a variety of enzymes. The next step, after polymer skin formation is complete (≈ 200 A thickness), is to quench the reaction (by diluting the reactant concentrations). The particles are then suspended in an aqueous solution by removing the organic liquid through repeated centrifugation and washing.

Alternatively, the W/O emulsion is directly added into a stirred aqueous phase (isotonic saline). If the organic oil is properly tailored, the final result will be a multiple emulsion, i.e. oil droplets containing droplets of hemoglobin solution (or other liquid of interest) suspended in a

continuous aqueous phase. (Li and Shrier, 1972, May and Li, 1972) An organic oil developed for this purpose is a mixture of Span 80, ENJ-3029 and S100N. ENJ-3029 is a high molecular weight amine with an average molecular weight of 2000 manufactured by ENJAY Additives Laboratories, and SIOON (ENJAY) is a mixture of organic compounds (28.8% Paraffins-mostly iso-, 57.2% Napthenes, 9.2% Aromatics, and 4.8% Polar compounds) with an average molecular weight of 386.5, and a specific gravity of 0.8597 (Li, personal communication). The resulting beads of hemoglobin are surrounded by the liquid organics which have been termed liquid membranes.

The third method utilizes the tendency of phospholipids to form bimolecular lipid layers in an aqueous solution or at a water-oil interface. Cell membranes are at present considered to be partially made up of bimolecular lipid layers, and extensive research in the physical characteristic of bimolecular lipid layers is currently in progress (see reviews by Tien, 1972; Szabo et al., 1970; Finkelstein, 1972). Previously small spherical vesicles have been produced which were surrounded by bimolecular lipid layers, but the size of the vesicles were of a diameter of approximately 500 A, too small to be of interest in this study (Seufert, 1970; Hauser et al., 1972). No attempt was made in those studies to encapsulate a specific protein or enzyme solution inside the phospholipid vesicles (just water). Recently Chowhan et al. (1972) reported the preparation of large size (1-2 μm) lecithin spherules (particles bounded by

a bimolecular layer of lecithin) containing a 5.14% glucose solution. The initial step is to emulsify the glucose solution into a volatile organic solution (chloroform) containing lecithin and dicetyl phosphate. The chloroform is then removed slowly from the W/O emulsion by using a partial vacuum and continuous stirring of the emulsion. After removal of chloroform the result is a high volume fraction ($\phi \approx 1$) dispersion of spherical liposomes.

In each of the four methods, common problems are particle size control and deactivation of the hemoglobin. The particle size can be controlled through the proper control of emulsification parameters such as time of emulsification and stirring speed. Because large quantities of emulsions were needed in the process of encapsulation, the Brown emulsator was not used. Instead in the first step emulsions were made with magnetic stirrers, electric blade stirrers, and a Waring blender. Another problem encountered with the Brown emulsator was the inversion of the W/O emulsion and relatively low volume fraction of the aqueous phase. Deactivation of hemoglobin occurs in all phases of the encapsulation process.

A major problem with the liquid membrane technique was that a dispersion of single hemoglobin droplets in oil droplets suspended in saline could not be obtained. Instead the oil droplets would contain many hemoglobin particles as is shown in Figure 6.2. The oil droplets would be of order 100 to 1000 μm while the hemoglobin droplets were of order of 2 to 10 μm . No method of stirring or adjustment of surfactant

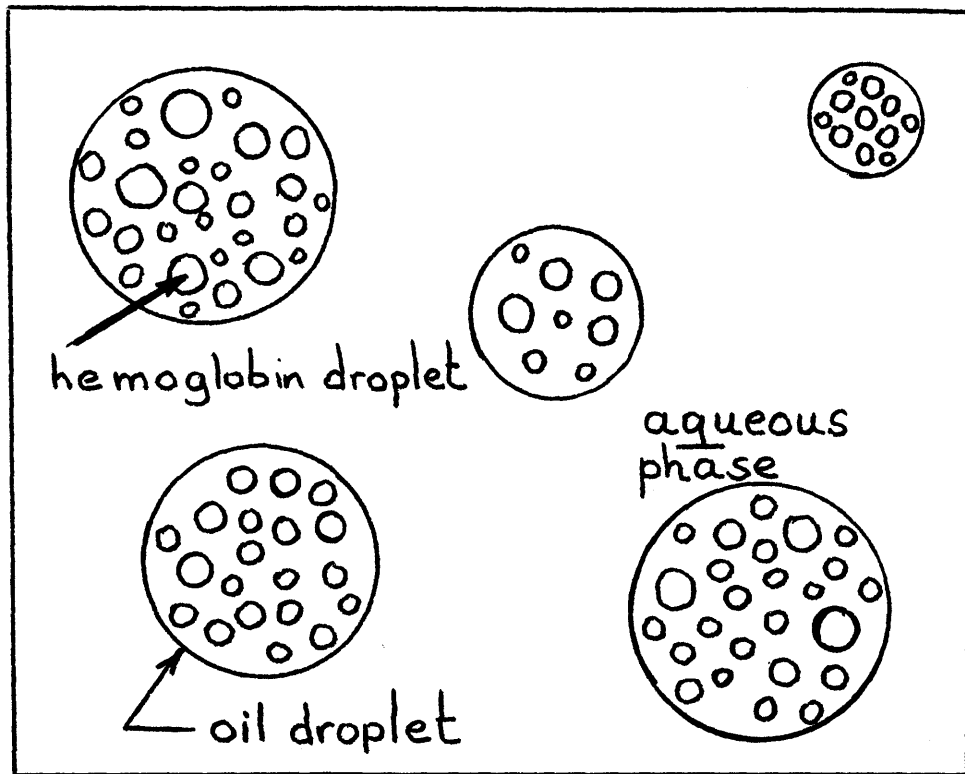


FIGURE 6.2

MULTIPLE EMULSION OBTAINED IN METHODS 2 AND 3
(SEE TEXT).

concentrations could isolate single hemoglobin particles.

No successes were obtained with the bimolecular lipid membrane technique as described by Chowan et al. (1972) because upon evaporation of the oil phase the hemoglobin particles coalesced rapidly. An attempt was made to prepare the particles similar to the liquid membrane technique, but a multiple emulsion with many hemoglobin solution particles in the oil droplets was the result as shown in Figure 6.2. As a consequence method 2 and 3 were abandoned.

In collaboration with Tuntunjian (1973), method 1 and 2 were extensively investigated. In method 1 hemoglobin solution was encapsulated with either collodion or nylon membranes of order 200 Å thickness, and suspensions were formed with an average particle diameter as small as 4 μm. The oxygen uptake of hemoglobin at full saturation was checked through the Van Slyke technique which was performed at the Massachusetts General Hospital Blood Gas Laboratory. It was found that for the particle size range of interest hemoglobin was approximately 90 percent deactivated (Tuntunjian, 1973). This amount of deactivation is so great that these suspensions would be of little use in permeation experiments, and consequently this model system was abandoned.

A problem with the water in oil emulsion system is that it is relatively difficult to obtain emulsions of high aqueous phase volume fraction without inversion and with good stability. As has been discussed previously the presence of a strong double layer stabilizes an emulsion because it imparts

repulsive forces that counteract particle coalescence. Usually the electrical conductivity in oils is poor so that the electrical double layer is extended, and as a consequence dilute W/O emulsions are favored. An appropriate volume fraction of the hemoglobin phase would be of order of $\phi \geq 0.40$ in order that the facilitated transport effect upon oxygen transport could be investigated. Of many oils investigated only a S100N mixture was found to give high volume fractions of aqueous hemoglobin solutions in oil emulsions. Volume fractions as high as $\phi \approx 0.7$ could be attained before inversion of the emulsion resulted. This high volume fraction suggests that ion permeabilities are relatively large in the S100N mixture. The S100N mixture was 90 volume per cent S100N, 5% ENJ-3029, and 5% Span 80.

Emulsions (W/O) were made with a Fisher Jumbo Magnetic Stirrer (Fisher Scientific) yielding particles with approximately 9 μm particle size (stirring speed of Teflon stirring bar is 400 rpm), and emulsions with a particle size of about 3 μm were obtained with an electric blade stirrer (1000 rpm). The hemoglobin solution was prepared from freshly collected blood (purchased from the Massachusetts General Hospital Blood Bank, type O positive) as previously described. To prevent bacterial growth 1 mg of streptomycin sulfate per 10 ml red blood cell suspension was added. Additional details are available elsewhere (Tuntunjian, 1973).

The S100N W/O emulsion system was used as the model system for permeation experiments. Since the oil is the

continuous phase, the permeability of the oil phase should not be very large compared to the permeability of the hemoglobin solution, otherwise facilitation effects will not be apparent due to the high mass flux in the continuous oil phase. Experimentally the permeability of the S100N mixture was found to be about 15 per cent higher than that of isotonic saline. The permeability and the facilitation factor are a function of the hemoglobin concentration and as a consequence an appropriate hemoglobin concentration must be found that gives a reasonable high facilitated flux. Tuntunjian (1973) has performed many computer calculations utilizing the theory developed for dispersed phase reaction only in order to analyze what concentration range of hemoglobin should be used. A concentration range of 14 to 18 gr/100 ml was found to be most suitable to give maximum facilitation effects.

6.4 Gas Permeation Experiments

6.4.1 Experimental Apparatus

The gas permeation apparatus is a modification of Barrer's classic, vacuum, time-log apparatus (Barrer and Skirrow, 1948) and is shown in Figure 6.3. The thin liquid film of the system of interest (such as an emulsion, dispersion, red blood cell suspension, hemoglobin solution, etc.) is held vertically between two silicone support membranes within the sample holder. A schematic cross-sectional view of the sample holder is shown in Figure 6.4. The sample holder is situated

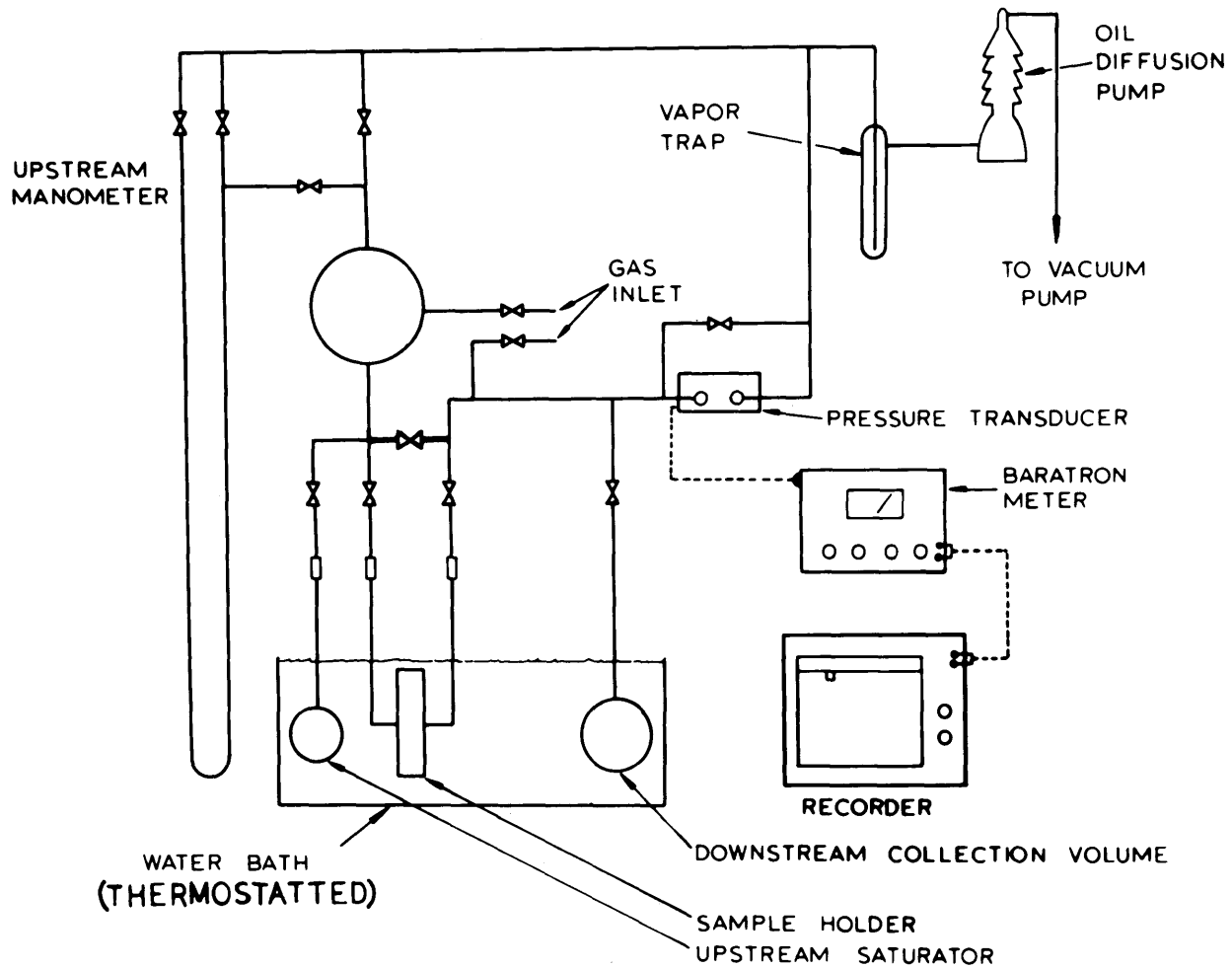
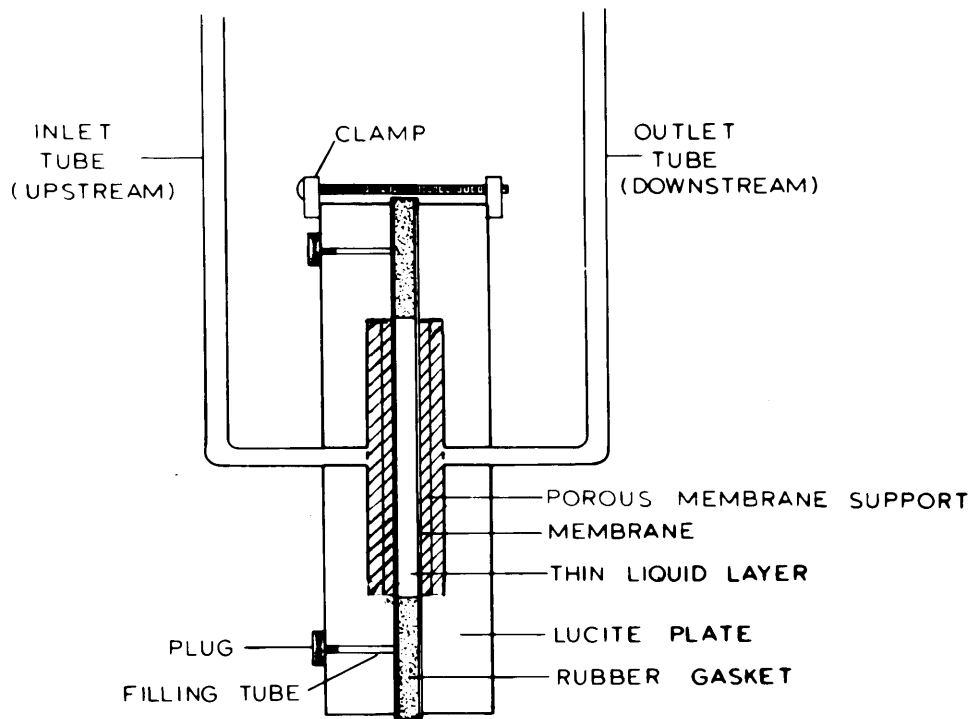
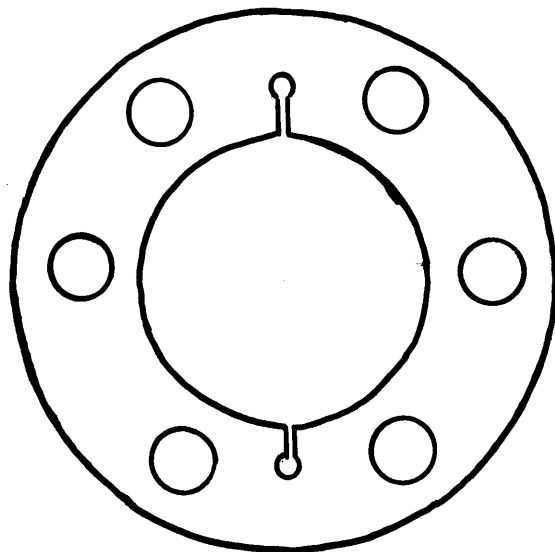


FIGURE 6.3. SCHEMATIC DIAGRAM OF EXPERIMENTAL APPARATUS



SAMPLE HOLDER DETAIL
(NOT TO SCALE)



PLANE VIEW OF RUBBER GASKET

FIGURE 6.4

DETAIL OF THE SAMPLE HOLDER AND THE RUBBER GASKET.

in a constant temperature bath controlled by a Yellow Stone Instruments Model 72 proportional temperature controller (distributed by Cole-Parmer). The YSI model 72 has a set point repeatability of $\pm 0.01^{\circ}\text{C}$ and a stability of $\pm 0.001^{\circ}\text{C}$. Such precise temperature control is necessary to assure negligible interference in downstream pressure readings as a result in fluctuations in the liquid sample vapor pressure. Temperature changes are measured to within 0.001°C with a Beckman Differential Thermometer.

The sample holder is connected with Cajon ultra-torr fittings (stainless steel) to a large upstream gas volume and a small downstream gas volume such that the liquid slab is in a vertical position. The face of the upstream slab is then exposed to the upstream gas volume, and the downstream face of the liquid slab is exposed to the downstream gas volume.

The whole permeation apparatus can be evacuated by means of a vacuum pump. Prior to beginning an experiment the previously evacuated upstream and downstream volumes are equilibrated to the vapor pressure of the liquid system of interest through use of the saturator. The gas volumes upstream and downstream of the liquid slab need to be saturated in order to be certain that no liquid evaporates from the sample. Next the gas of interest is introduced into the upstream volume and the downstream volume pressure change is recorded with time. The experiments are run at partial vacuum in order to reduce gas phase resistance to mass transfer. The gas on the upstream side diffuses through the liquid slab and emerges in

the gas phase of the downstream volume. The pressure change with time can be converted to moles of gas transferred per unit time through use of the ideal gas law. During the course of an experiment, the upstream pressure decreases minimally as gas diffuses through the film because of low mass transfer ratio and the large upstream volume (≈ 3000 cc). Because of the low flux the downstream pressure change is also small, so that a quasi steady state situation arises after the initial transient period.

In order to measure the downstream volume a calibrated bulb was connected to the downstream volume. The bulb volume was measured by repeated filling with water and weighing the contents. Through use of the calibrated bulb the downstream volume could be increased by approximately a factor of eight.

The downstream pressure was measured by means of a Baratron Type 77 Capacitance manometer (MKS Instruments). The sensitivity of the Baratron was such that pressure changes as low as $1 \mu\text{m Hg}$ could be measured accurately and recorded on a Sargent MR or a Heath model EVW-20A recorder. The upstream pressure is read to within 0.02 mm Hg from a mercury manometer through the use of a cathometer.

Most of the vacuum apparatus is enclosed by a large wooden box to minimize the effects of variations in room temperature. The interior of the box was maintained approximately 3°C above the water bath temperature and held constant within $\pm 0.02^\circ\text{C}$, by means of a YSI Model 2156 proportional temperature controller (Cole-Parmer). The purpose of keeping

the air above the water bath several degrees higher than water bath temperature is to avoid any condensation of the liquid in the apparatus, especially in the Baratron pressure sensing head. Any evaporation and recondensation can result in erratic downstream pressure variations.

The liquid film in the sample holder is bounded at each side by two thin support membranes (MEM-213, General Electric Co.). These silicone membranes are nominally 25 and 50 μm thick and have a high gas permeability. Since the liquid films used in this study varied from approximately 450 to 2200 μm the mass transfer resistance of these membranes was usually only a few percent of the total resistance. The three layer sandwich of polymer-liquid film-polymer is enclosed by two plexiglas plates, 5 cm in diameter and 1.9 cm thick. A thin rubber sheet (the thickness of which corresponds to that of the liquid film) serves as a gasket and the use of silicone grease (Dow Corning) provides the seals between plexiglas, membrane, and gasket. As shown in Figure 6.4, circular holes are cut in the rubber gasket in which small metal disc spacers fit with a thickness approximately 20 μm less than the gasket. These spacers define the actual thickness of the liquid film once the whole sample holder is tightly clamped. At the inside of each plexiglas plate is a cylindrical cavity which defines the membrane area exposed to gas transfer (25.5 cm^2). The membrane areas exposed to gas transfer are supported by a disc of very porous nickel "foammetal" (General Electric Co.) which fits smoothly into the cavity (its thickness is exactly the same as

the depth of the cavity) and has an area of about 24 cm^2 to give a loose fit. The foammatal has an open pore structure that constitutes 91 percent of the total volume. Because of its porosity, the effect of the foammatal on total mass transfer area and mass transfer resistance is negligible (also indicated by experiment). The sample holder is tightly clamped by two brackets to insure a vacuum tight seal and the correct film thickness. Two filling ports are arranged in such a manner inside the sample holder that, once the holder is assembled, samples can be introduced with the aid of a syringe.

Once the sample holder is hooked up to the apparatus the liquid slab is in a vertical position. If any sedimentation or creaming of the dispersed phase occurs inside the liquid slab, the direction of sedimentation or creaming is normal to the direction of mass flux so that it should have little effect. The sample holder is connected in such a manner that it can be rotated (a half turn at a time) so that any separated system can be redispersed prior to starting the actual mass flux experiment. After an experiment was finished, and the sample holder was disconnected from the apparatus, the degree of creaming or sedimentation was checked. In none of the experiments was the height of the clear separated continuous phase more than one-ninth of the total liquid slab height (diameter of transfer area). A dummy sample holder, containing the same sample, and the same film thickness, was utilized to decide how many times per unit time the sample holder needed to be rotated. One half turn every two hours was deemed sufficient for all systems that exhibited separation.

6.4.2 Experimental Procedure

The sample holder is assembled as follows:

1. An extremely thin film of vacuum grease is spread over the flat inner faces of the plexiglas plates.

2. Silicone membranes are stretched taut over each plate.

3. A rubber gasket is placed on top of one of the plates along with spacers of appropriate thickness. The filling grooves of the gasket are placed over the filling ports.

4. The second plexiglas plate is placed on top of the rubber gasket and the plates are then securely clamped.

5. The liquid sample is introduced into one of the filling ports after the membrane over the port openings has been punctured with a needle. The sample holder is placed in an upright position with the filling ports in a vertical direction and the liquid is introduced through the bottom filling port through use of a syringe and a plastic tube. Special care must be taken that no gas bubbles are introduced during the filling procedure. After the liquid has been introduced, the filling ports are sealed (small glass rods are plugged in the Teflon Cajon ultra-torr male connectors).

6. The sample holder is placed in the water bath and hooked up to the apparatus with Cajon ultra-torr unions. Note that the assembled sample holder could be used over and over again as long as there were no leaks in the support membranes.

The following procedure was followed during the course of all runs, prior to introduction of the gas of interest, to insure that the sample and apparatus are degassed from all unwanted gasses, and that the up and downstream gas phases and the liquid film are equilibrated at the vapor pressure of the sample.

1. Prior to connection of the liquid film holder, the apparatus is evacuated to an absolute pressure $<30 \mu\text{m Hg}$ as read by a thermocouple vacuum gauge (No. 94178), Cenco Instruments).

2. Upstream and downstream volumes are saturated with the sample's vapor (some of the sample is present in the saturator).

3. Nitrogen is introduced into the system until the pressure in the upstream and downstream volumes is about 720 to 740 mm Hg.

4. The sample holder is connected to the apparatus and exposed to the up and downstream volumes.

5. The sample holder is isolated and the pressure in the volumes is reduced 20 to 40 mm Hg. The sample holder is again exposed to the up and downstream volumes for about 30 seconds. Step 5 is repeated until the system pressure has been reduced to the vapor pressure of the sample. (For each 200 mm Hg reduction in pressure an additional waiting time of about 10 minutes is imposed.) The saturator is open at all times.

6. Once the sample holder pressure is near the vapor pressure of the sample steps (1) and (2) are repeated twice and

each time the sample holder is exposed to the up and downstream volumes after the second step. Note that the pressure in the up and downstream volumes in this procedure are the same by using a common saturator and a connecting line.

7. The up and downstream volumes, the sample holder, and the saturator are now equilibrated for approximately 1 - 2 hours until the pressure is stable.

8. The saturator valve and the connecting line valve are closed and the downstream pressure is monitored until the pressure variation with time is of order $+1 \mu\text{m}$ per minute or less than 5 per cent of the expected rate of pressure rise during the permeation experiment. This time period is usually another 1 - 2 hours. After this period, the downstream pressure is recorded for about 30 minutes to 2 hours to ensure that pressure increase with time is constant. This pressure increase is usually due to extremely small leakages and is subtracted from the measured pressure rise with time observed during the mass transfer experiment.

9. The system is now ready for a mass transfer experiment and at time zero the appropriate pressure of gas is introduced into the upstream volume, and the downstream pressure is recorded with time.

In case that an additional gas (such as carbon dioxide) needs to be introduced, this is done right at the end of step 6).

6.4.3 Game Plan and Analysis of Experimental Results

Since there are a number of systems of interest in this thesis each with increasing complexity, the simpler systems were analyzed first before more complexity was introduced. Permeability runs were first performed on water in order to characterize the experimental apparatus. The diffusivity and solubility of oxygen in water is known with greater certainty than for any other liquid. The oxygen diffusivity values measured by Goldstick (1966) were assumed to be the most accurate and these were used to compare with experimental results. The next systems considered were the inert heterogeneous media and the hemoglobin solutions. The effect of creaming and sedimentation upon the mass transfer rate could be ascertained by investigations different volume fractions of dispersed phase. The reactive systems were analyzed last.

The experimental data obtained consisted of the recorded variation of downstream pressure with time, the partial pressure of oxygen upstream ($p_{O_2}^{up}$) and downstream ($p_{O_2}^{down}$), the liquid film thickness the liquid film thickness L , the membrane thickness L_m , the cross-sectional area A_E , downstream volume V_d , and system temperature T . The flux through the three layer sandwich in terms of moles per unit time is

$$\frac{dn}{dt} = \frac{(p_{O_2}^{up} - p_{O_2}^{down}) A_E}{\frac{2L_m}{P_m} + \frac{L}{P_{AVE}}} \quad (6.5)$$

The membranes have the same thickness L_m (measured while stretched with the Ames dial comparator, Model 412), and the membrane permeability P_m of oxygen through the MEM-213 is 1.214×10^{-6} (cm^2/sec) ($\text{cc}(\text{STP})/\text{cc-atm}$) (General Electric Co., pamphlet no. GEA-8685A and confirmed by experiment). The flux at steady state is given by

$$\frac{dQ}{dt} = \frac{(D\alpha) A_E \Delta P_{O_2}}{L} \quad (6.6)$$

where

$(D\alpha)$ is the permeability in (cm^2/sec) ($\text{cc}(\text{STP})/\text{cc-atm}$)

A_E is the area in cm^2

Δp_{O_2} is the partial pressure driving force in atm

L is the thickness in cm

dQ/dt is mass flux in cc/O_2 (STP)/sec

Through use of the ideal gas law the mass flux in $\text{cc}(O_2)\text{STP}/\text{sec}$ can be converted into moles/sec

$$\frac{dn}{dt} = \left(\frac{P}{RT}\right)_{\text{STP}} \frac{(D\alpha) A_E \Delta p_{O_2}}{L} \quad (6.7)$$

where

dn/dt is mass flux in moles/sec

Since the actual experimental measurement is a pressure rise with time (at the conditions of the experiment) it is more convenient to express equation (6.7) in terms of dp/dt so that

$$\frac{dp}{dt} = \left(\frac{T + 273}{273}\right) \frac{(D\alpha) A_E \Delta p_{O_2}}{V_d L} \quad (6.8)$$

where dp/dt is the downstream pressure increase with time
in atm/sec

and V_d is downstream volume in cm^3 .

Equation (6.8) can be further modified so that all parameters will have units that are measured experimentally. The final "working equation" becomes

$$\frac{dp}{dt} = \left(\frac{T + 273}{273} \right) \frac{60 P A_E \Delta P_{O_2} (10^3)}{V_d L} \quad (6.9)$$

where

P is the permeability in $(cm^2/sec)(cc(STP)/cc-atm)$

T is the temperature in $^{\circ}C$

A_E is in cm^2

ΔP_{O_2} is in mm Hg

V_d is in cm^3

L is in cm

dp/dt is in $\mu m Hg/minute$ ($1000 \mu m Hg = 1 mm Hg$)

The pressure drop through the membranes can now be calculated through use of equation (6.9) and is

$$\Delta P_m = \frac{dp}{dt} \left(\frac{273}{T + 273} \right) \frac{V_d L_m}{60 A_E P_m 10^3} \quad (6.10)$$

The partial pressure at the upstream side of the liquid slab (between upstream membrane and liquid slab) and downstream side of the liquid slab (between downstream membrane and liquid slab) is

$$p_{O_2}^{x=0} = p_{O_2}^{up} - \Delta P_m \quad (6.11)$$

$$p_{O_2}^{x=L} = p_{O_2}^{down} + \Delta P_m \quad (6.12)$$

Finally the average effective permeability of the liquid system is obtained from

$$\bar{P}_{AVE} = \frac{dp}{dt} \left(\frac{273}{T + 273} \right) \frac{V_d L}{60 A_E (p_{O_2}^{x=0} - p_{O_2}^{x=L}) 10^3} \quad (6.9)$$

7. EXPERIMENTAL RESULTS AND DISCUSSION

7.1 Characterization of the Permeation Apparatus

7.1.1 Permeability of Support Membranes

7.1.2 Oxygen-Water Runs

7.1.2.1 Effect of Support Material

7.1.2.2 Assemblage of Sample Holder

7.1.2.3 Permeability of Other Gases in Water

7.1.2.4 Oxygen Permeability at Different Temperatures

7.2 Inert Systems

7.2.1 Dispersions

7.2.2 Inert Emulsions

7.3 "Reactive" Systems

7.3.1 Immobilized (Reactive) Hemoglobin Films

7.3.2 Inert Hemoglobin Solutions

7.3.3 Red Blood Cell Suspensions

7.3.3.1 Inert Red Blood Cell Suspension

7.3.3.2 Reactive Red Blood Cell Suspension

7.3.3.2.1 Details on the Oxygen Permeation Experiments on Reactive Red Blood Cell Suspensions

7.3.4 Model System

7. EXPERIMENTAL RESULTS AND DISCUSSION

Experimental results are discussed in this chapter in the same order as the experimental program presented in Chapter 6. Permeation experiments were analyzed as described in Section 6.4. Results for permeabilities are reported in the following units

$$\frac{\text{cm}^2 - \text{cc (STP)}}{\text{sec} - \text{cc} - \text{atm}}$$

these can be converted to the units

$$\frac{\text{moles}}{\text{cm} - \text{sec} - \text{mm Hg}}$$

by multiplying the permeabilities by the conversion factor 5.875×10^{-8} .

7.1 Characterization of the Permeation Apparatus

7.1.1 Permeability of Support Membranes

The oxygen permeability of the MEM-213 support membranes was measured for the 25 μm and 50 μm nominal thickness membranes. In addition, the oxygen permeability of two membranes as assembled in the sample holder was measured. In all runs but one, the upstream and downstream volumes were completely evacuated to about 20 μm Hg absolute pressure. In one experiment the volumes were allowed to equilibrate with water present in the saturator. The presence of water vapor did not affect the permeability of the MEM-213 membranes, indicating that gas phase resistance is negligible even in the case of a

film of low mass transfer resistance (at those experimental conditions). The average oxygen permeability obtained from all the runs at 25°C is

$$P_{O_2, MEM-213} = 12.0 \times 10^{-7} \frac{\text{cm}^2 - \text{cc (STP)}}{\text{sec} - \text{cc} - \text{atm}}$$

which compares favorably with the value reported by General Electric as

$$P_{O_2, MEM-213} = 12.14 \times 10^{-7} \frac{\text{cm}^2 - \text{cc (STP)}}{\text{sec} - \text{cc} - \text{atm}}$$

In all permeation runs with thin liquid films, the thicknesses of the support membranes were measured. Liquid permeabilities were calculated as described in Section 6.4 taking into account the membrane mass transfer resistance. For most of the oxygen permeation runs, the membrane resistance was approximately 3 to 6 per cent of total mass transfer resistance.

7.1.2 Oxygen Water Runs

In order to characterize the gas permeation apparatus, experiments were conducted with the diffusion of oxygen through slabs of water because for no other gas-liquid system are the diffusivity and solubility known with better accuracy.

Although reported values of the oxygen diffusivity vary from $1.87 \times 10^{-5} \text{ cm}^2/\text{sec}$ (Kreuzer, 1950) to $2.44 \times 10^{-5} \text{ cm}^2/\text{sec}$ (Davidson and Cullen, 1957) the most precise determination to date of the oxygen diffusivity appears to be that of Goldstick (1966) who reported a value for D_{O_2, H_2O} of $2.13 \times 10^{-5} \text{ cm}^2/\text{sec}$. The oxygen solubility is known with good accuracy and the value

for α_{O_2, H_2O} is 0.02831 $\frac{cc(STP)}{cc-atm}$ at 25°C as reported in Table 3.3.

The conventional time lag experiment for the diffusion of a gas across a thin slab yields two independent measurements. The transient period yields a diffusivity and from the pseudo-steady state period (during which the downstream partial pressure builds up linearly with time and driving force changes very little) the permeability is obtained. From a plot of downstream pressure versus time, a straight line extrapolation of the linear steady state portion of the curve yields an intercept, θ , on the time coordinate. Barrer (1939) has shown that this "time lag" is related to the diffusivity as follows

$$D = \frac{L^2}{6\theta} \quad (7.1)$$

Unfortunately the sudden introduction of gas into the upstream volume appeared to cause some fluid movement in the liquid film, which in turn appeared to cause an initially anomalously high transient flux as is shown in Figure 7.1. Intercept times obtained from the anomalously high flux portion (θ') gave reasonable diffusivities while intercepts with the final steady state portion of the flux line often gave negative intercept times. If the gas was introduced very slowly, so as not to disturb the liquid layer, the anomalously high portion of the curve disappeared. Intercept times were in this case too long and gave small diffusivities (because of long introduction time). The transient analysis of the experiments were abandoned because

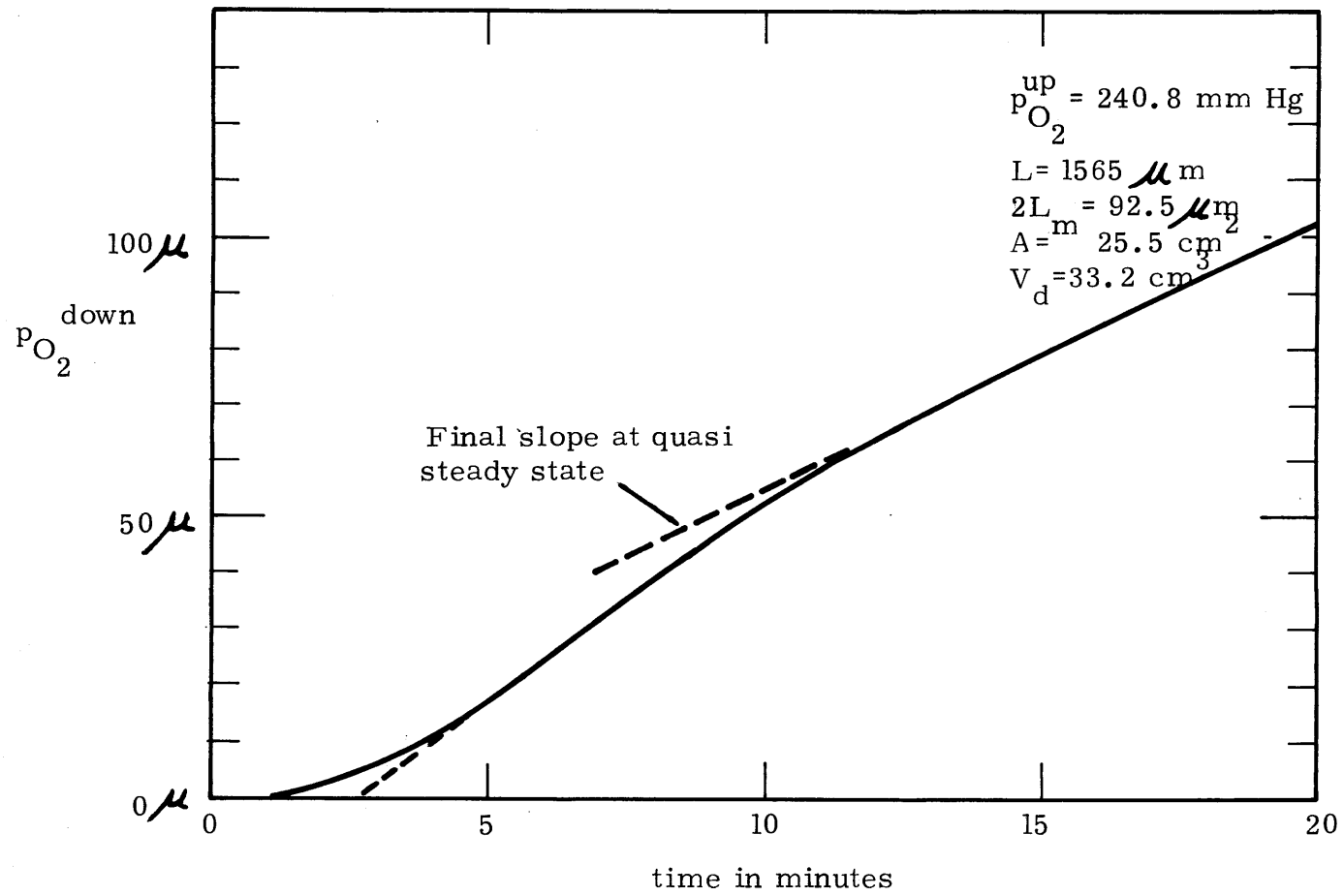


FIGURE 7.1
 UNSTEADY STATE AND STEADY STATE RESPONSE OF OXYGEN
 DIFFUSION IN WATER

of the doubtful values obtained from such an analysis in these experiments and only steady state results are reported here.

An alternate anomalously high flux was observed by Meldon (1973) in his study of the diffusion of carbon dioxide through thin vertical films of alkaline solutions (same experimental apparatus). In the case of carbon dioxide, which has a significantly larger solubility than oxygen, convection flows may be induced due to small density gradients in the film for large driving force differences. The density differences are caused by the variation of the CO_2 concentration across the film. Meldon (1973) experimentally determined the per cent of flux due to the natural convection as a function of the Rayleigh number

$$N_{\text{Ra}} = N_{\text{Gr}} N_{\text{Sc}}$$

where the Grashof number and Schmidt number are defined as

$$N_{\text{Sc}} = \frac{\nu}{D}$$

$$N_{\text{Gr}} = \frac{gL^3}{\nu^2} \left(\frac{\Delta\rho}{\rho} \right)$$

Here the relative density difference is given by

$$\left(\frac{\Delta\rho}{\rho} \right) .$$

In Meldon's work the maximum per cent contribution for a film thickness of 1564 μm was approximately 10 per cent with a Rayleigh number of approximately 6000. For oxygen transport in water with a driving force of 200 mm Hg the Rayleigh number is approximately 10 so that contributions due to density driven

natural convection is virtually zero.

The permeability obtained from a steady state experiment can still be used to calculate a diffusivity when the gas solubility in a non-reacting system is known so that

$$D_{\text{calculated}} = \frac{P_{\text{experimental}}}{\alpha_{\text{literature}}} \quad (7.2)$$

The diffusion so obtained will be referred to as calculated diffusivities to remind the reader that these were obtained from the experimentally measured permeabilities. Table 7.1 reports the oxygen permeabilities obtained for water films of six different thicknesses. The average permeability for 34 experiments is

$$P_{\text{H}_2\text{O}} = 6.27 \times 10^{-7} \frac{\text{cm}^2\text{-cc (STP)}}{\text{sec-cc-atm}}$$

with a standard deviation of

$$\text{S.D.} = \pm 0.18 \times 10^{-7} \frac{\text{cm}^2\text{-cc (STP)}}{\text{sec-cc-atm}}$$

and yields an oxygen diffusivity of

$$D_{\text{H}_2\text{O}} = 2.22(\pm 0.06) \times 10^{-5} \frac{\text{cm}^2}{\text{sec}}$$

This value is in very reasonable agreement with that obtained by Goldstick. The standard deviation is approximately +3% of the average permeability. Investigation of Table 7.1 shows that the permeability is independent of film thickness and clearly suggests that gas phase resistance is negligible. Figure 7.2 shows a single experimental run for a 752 μm thick

TABLE 7.1

TABULATION OF OXYGEN PERMEATION IN DISTILLED WATER RUNS

Liquid Slab Thickness L μm	Average Measured Permeability $P \times 10^7$ $\text{cm}^2\text{-cc O}_2\text{(STP)}$ <u>sec-cc-atm</u>	Calculated Diffusivity $D \times 10^5$ $\frac{\text{cm}^2}{\text{sec}}$	Number of Experiments
655	6.22	2.20	1
676	6.32	2.23	3
752	6.26	2.21	10
803	6.22	2.20	10
1563	6.31	2.23	9
2332	6.38	2.26	1
Average	6.27 ± 0.18	2.22 ± 0.006	Total 34

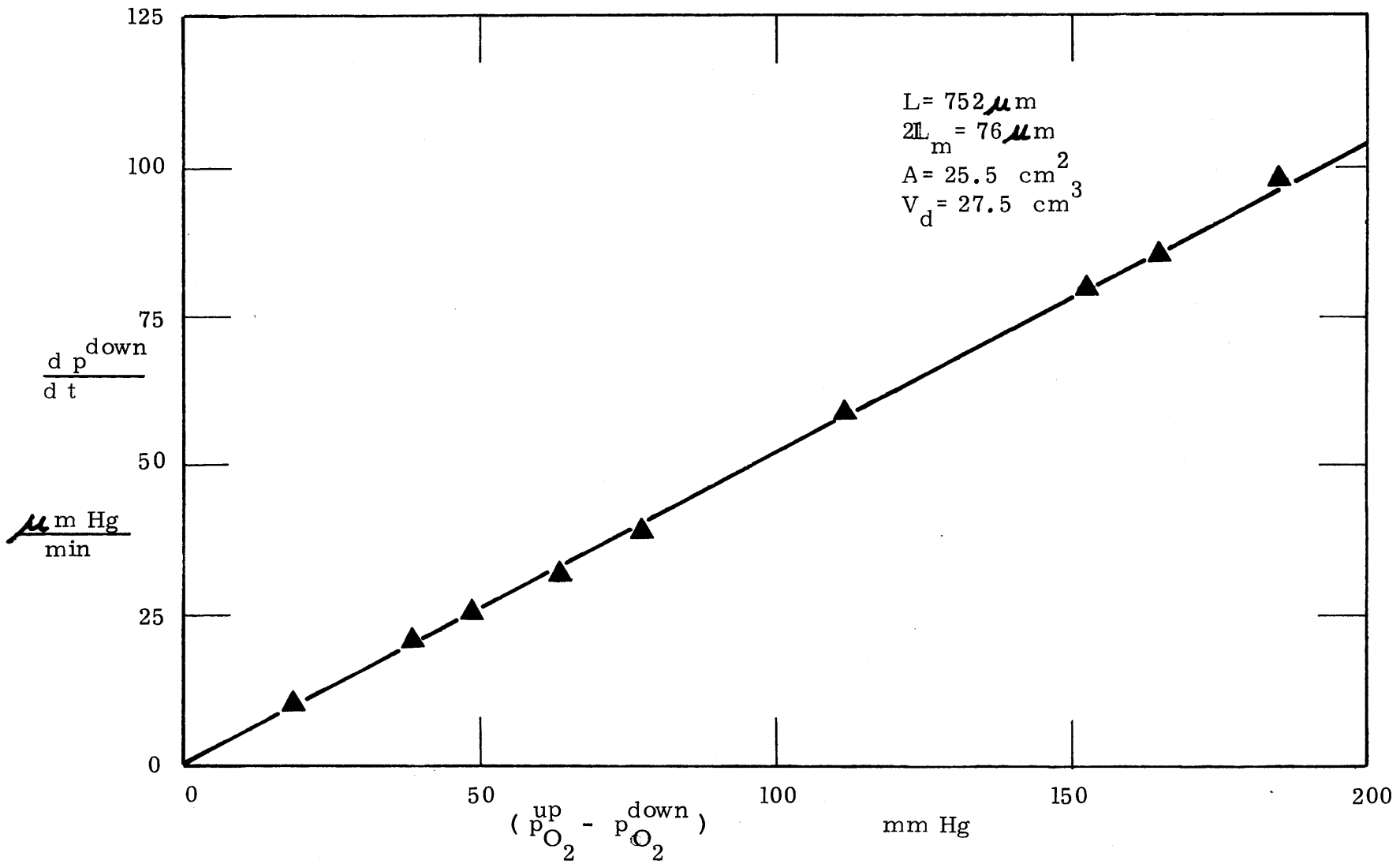


FIGURE 7.2
DIFFUSION OF OXYGEN IN DISTILLED WATER

liquid film. According to Fick's law, the flux (here in pressure increase per unit time) is proportional to the driving force (in mm Hg of oxygen) and Figure 7.2 shows excellent experimental agreement. Figure 7.2 also suggests that gas phase resistance is negligible as no negative deviation is apparent in the high pressure range where gas phase resistance becomes larger. The linearity of Figure 7.2 also suggests that no change in liquid film thickness occurred with increasing pressure. In some cases, the experiment was left on overnite, and the flux and driving force were measured the next day. Inspection of Appendix D shows that in all cases agreement with Fick's law was excellent and the experiment showed good stability over long times.

In addition to measuring the average oxygen permeability and comparing it to literature values, a number of other observations and experiments were made and are summarized below.

7.1.2.1 Effect of Support Material

In order to ascertain the blockage effect upon total mass transfer area by the 9% nickel supports (91% open void space) the supports were replaced by 20% nickel supports (80% open void space). In the one experimental run which was performed, the measured permeability was

$$P_{O_2, \text{water}} = 5.83 \times 10^{-7} \frac{\text{cm}^2\text{-cc (STP)}}{\text{sec-cc-atm}}$$

some 7 per cent below the average value. Although the standard deviation of the average oxygen permeability measured in water is approximately 3 per cent, a conservative estimate would attribute the 7 per cent decrease to the 11 per cent increase of the nickel content of the support material, so that a conservative estimate of the total area blocked for mass transfer by the 9% nickel support material would be approximately 6 per cent. However, the average oxygen diffusivity in water is already some 4 per cent above the value given by Goldstick. In addition the 9% nickel support is a light open structured material which allows light to pass through. The 20% nickel support, although porous, is a dense material and is optically opaque. In addition, it is estimated that the size of the contact points of the 9% support material (on the membranes) is

$$d_c \approx .005 \text{ cm}$$

so that the relative size of contact point to film thickness

$$\frac{d_c}{L} \ll 1 .$$

In this case no effect of support material is anticipated, irrespective of what the solid content of the material is.

7.1.2.2 Assemblage of Sample Holder

In assembly the sample holder the amount of silicone grease used was critical. A slight excess of grease used would cause seepage of the grease onto the open transfer

area, decreasing the latter below the normal value of 25.5 cm^2 (area without grease). In the case that seepage occurred, which could be visually observed, a planimeter was used to measure the area not covered by the grease. The uncertainty in these measurement to quantify the area was $\pm 5\%$. These runs were not used to obtain the average oxygen permeability of water.

7.1.2.3 Permeability of Other Gasses in Water

The permeability of nitrogen and carbon dioxide in distilled water was measured in two experiments each and is reported in Table 7.2. The calculated diffusivities compare well with values reported by Himmelblan (1964) for nitrogen, $D_{\text{N}_2, \text{water}} = 2.10 \times 10^{-5} \text{ cm}^2/\text{sec}$, and carbon dioxide, $D_{\text{CO}_2, \text{water}} = 1.92 \times 10^{-5} \text{ cm}^2/\text{sec}$.

TABLE 7.2

PERMEABILITY OF NITROGEN AND CARBON DIOXIDE
IN DISTILLED WATER

Gas	Permeability	Solubility ¹	Calculated Diffusivities
	$\frac{\text{cm}^2}{\text{sec}} \frac{\text{cc (STP)}}{\text{cc-atm}}$	$\frac{\text{cc (STP)}}{\text{cc-atm}}$	$\frac{\text{cm}^2}{\text{sec}}$
N ₂	3.28×10^{-7}	0.01434	2.28×10^{-5}
CO ₂	151.9×10^{-7}	0.759	2.00×10^{-5}

1 Altman and Dittmer (1971).

7.1.2.4 Oxygen Permeability and Different Temperatures

The oxygen permeability in distilled water was also measured at several temperatures in a set of experiments in order to test the equipment at a variety of temperatures. According to the Stokes-Einstein relationship, the diffusivity of species in a liquid is directly proportional to the absolute temperature and inversely proportional to the viscosity

$$D = \text{constant} \frac{T}{\mu} \quad (7.3)$$

The experimental results are tabulated in Table 7.3 and the calculated diffusivities are plotted versus the parameter T/μ . A straight line has been drawn with a slope equal to

$$\text{constant} = 6.92 \times 10^{-10} \frac{\text{gr-cm}}{\text{°K-sec}}$$

and through the diffusivity value of $2.13 \times 10^{-5} \text{ cm}^2/\text{sec}$ at $T = 25^\circ\text{C}$. This slope was obtained from St-Denis and Fell (1971) who compared the measured oxygen diffusivities in water of a number of investigators over the temperature interval of 10 to 60°C . Their slope was obtained by a least squares fit to the data. The dashed line is the Stokes Einstein equation. The results show fairly good agreement with the two straight lines.

7.2 Inert Systems

7.2.1 Dispersions

The inert dispersions used here are polystyrene, 30 TFE, and 120 FEP dispersions and their characteristics have been

TABLE 7.3
 EXPERIMENTAL OXYGEN PERMEABILITIES AT
 A VARIETY OF TEMPERATURES

Temperature °C	Permeability $\frac{\text{cm}^2\text{-cc (STP)}}{\text{sec-cc-atm}}$	Solubility ¹ $\frac{\text{cc (STP)}}{\text{cc-atm}}$	Diffusivity $\frac{\text{cm}^2}{\text{sec}}$	Viscosity ² Centipoise
17	5.78×10^{-7}	0.03283	1.77×10^{-5}	1.081
21	6.02×10^{-7}	0.03044	1.98×10^{-5}	0.9779
25	6.01×10^{-7}	0.02831	2.13×10^{-5}	0.8904
29	6.05×10^{-7}	0.02649	2.28×10^{-5}	0.8148
33	5.97×10^{-7}	0.02386	2.50×10^{-5}	0.7491

1 Altman and Dittmer (1971).

2 Handbook of Physics and Chemistry, 49th edition (1968).

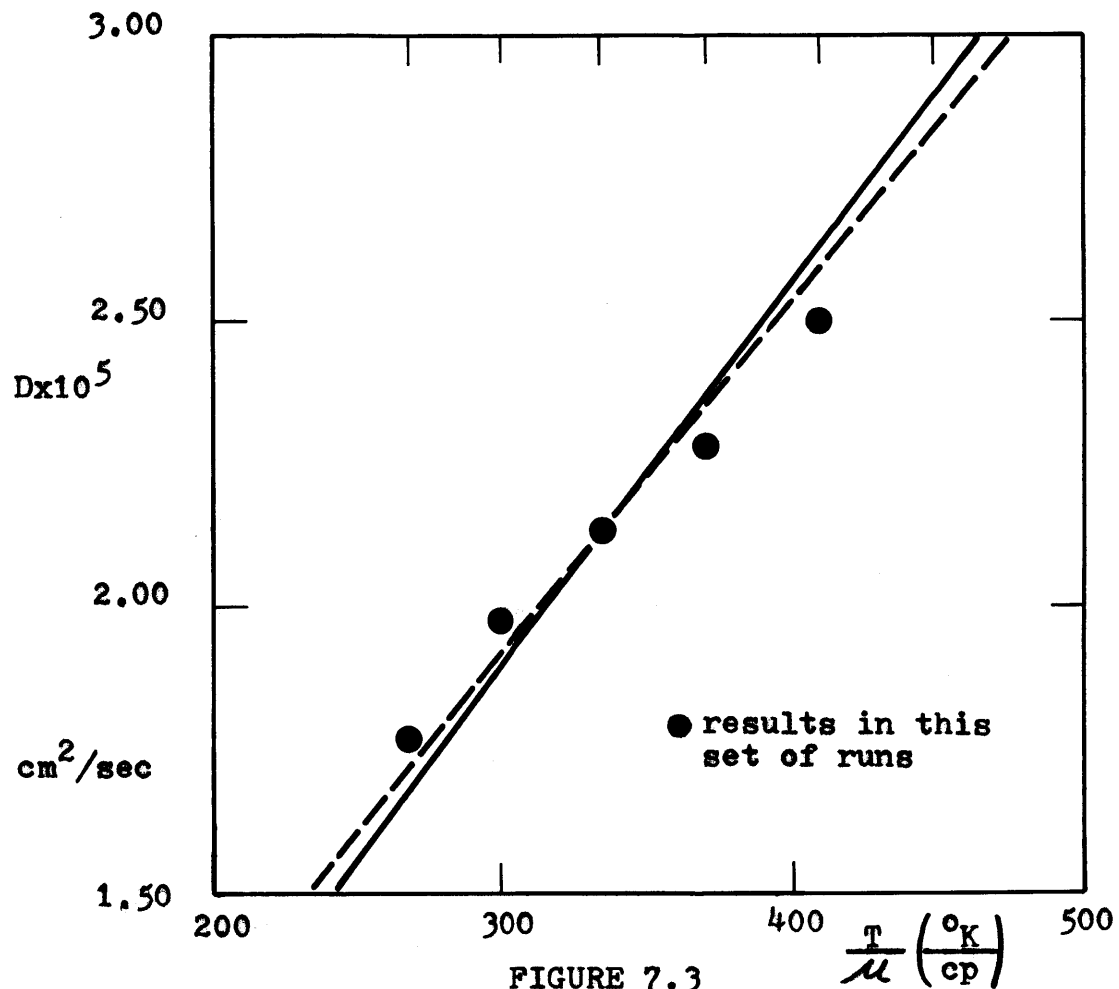


FIGURE 7.3

DIFFUSIVITIES OF OXYGEN IN WATER PLOTTED
VERSUS THE PARAMETER T/μ .

described in Chapter 6. For each of the dispersions, the permeability of the solid phase is orders of magnitude smaller than the permeability of the continuous phase so that the parameter K_d defined as

$$K_d = \frac{P_d}{P_c},$$

is near zero for Maxwell's equation.

The results of the oxygen permeability of polystyrene dispersions of different volume fractions of the dispersed phase is shown in Figure 7.4. The experimental points show good agreement with Maxwell's equation: the maximum deviation from the theoretical line is 5% at a volume fraction of 0.261. The polystyrene dispersions were fairly viscous at high volume fractions and, when charged into the sample holder, caused the rupture of the support membranes. Therefore no data points were obtained beyond a volume fraction of 0.261. The permeability of oxygen in polystyrene is

$$P_d = 9.13 \times 10^{-9} \frac{\text{cm}^2\text{-cc (STP)}}{\text{sec-cc-atm}}$$

as given by Robb (1971), so that the ratio of dispersed to continuous phase permeability is

$$K_d = 0.015$$

because in this case

$$P_c = 6.02 \times 10^{-7} \frac{\text{cm}^2\text{-cc (STP)}}{\text{sec-cc-atm}}$$

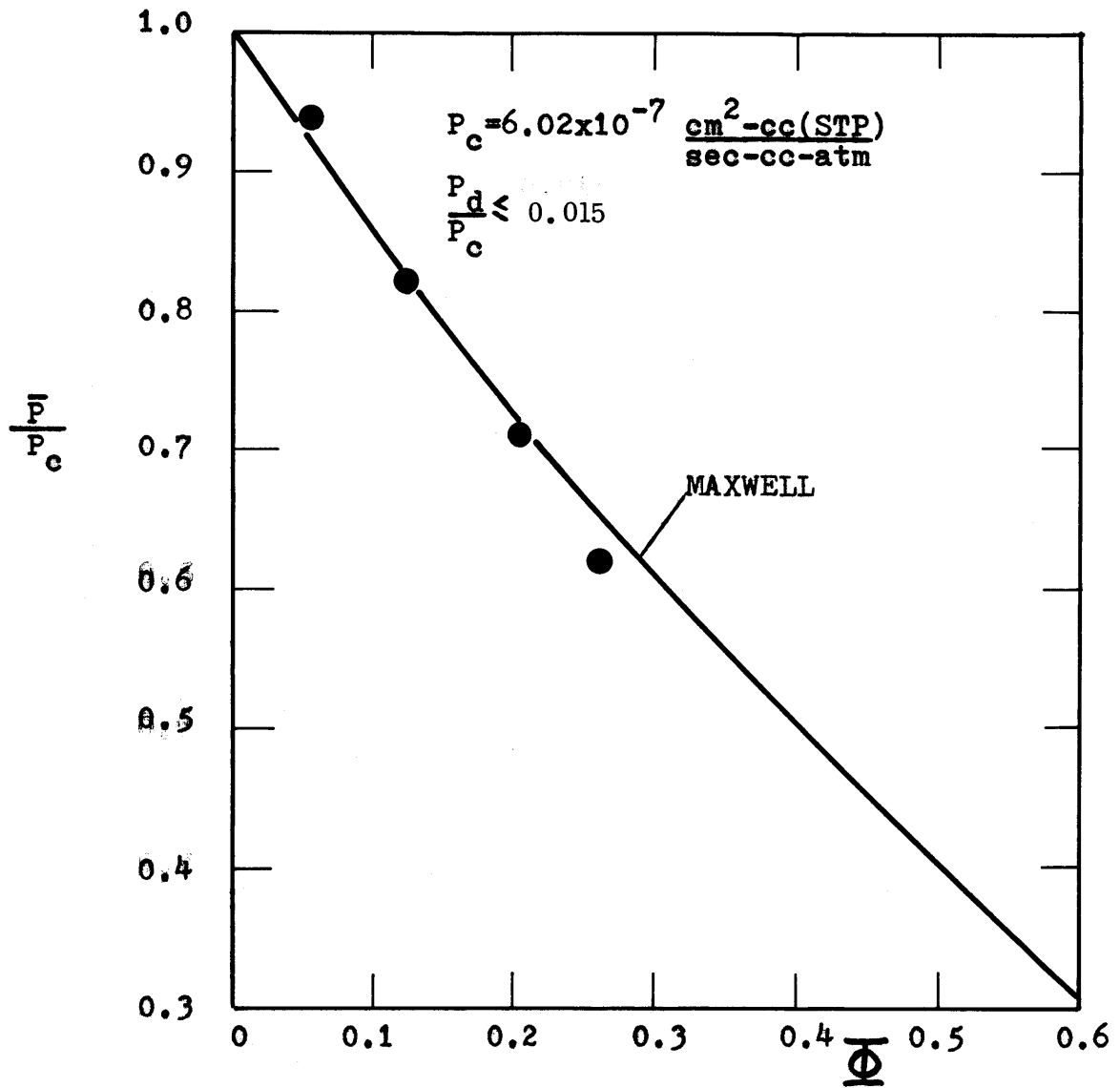


FIGURE 7.4

PERMEATION OF OXYGEN IN POLYSTYRENE DISPERSIONS.

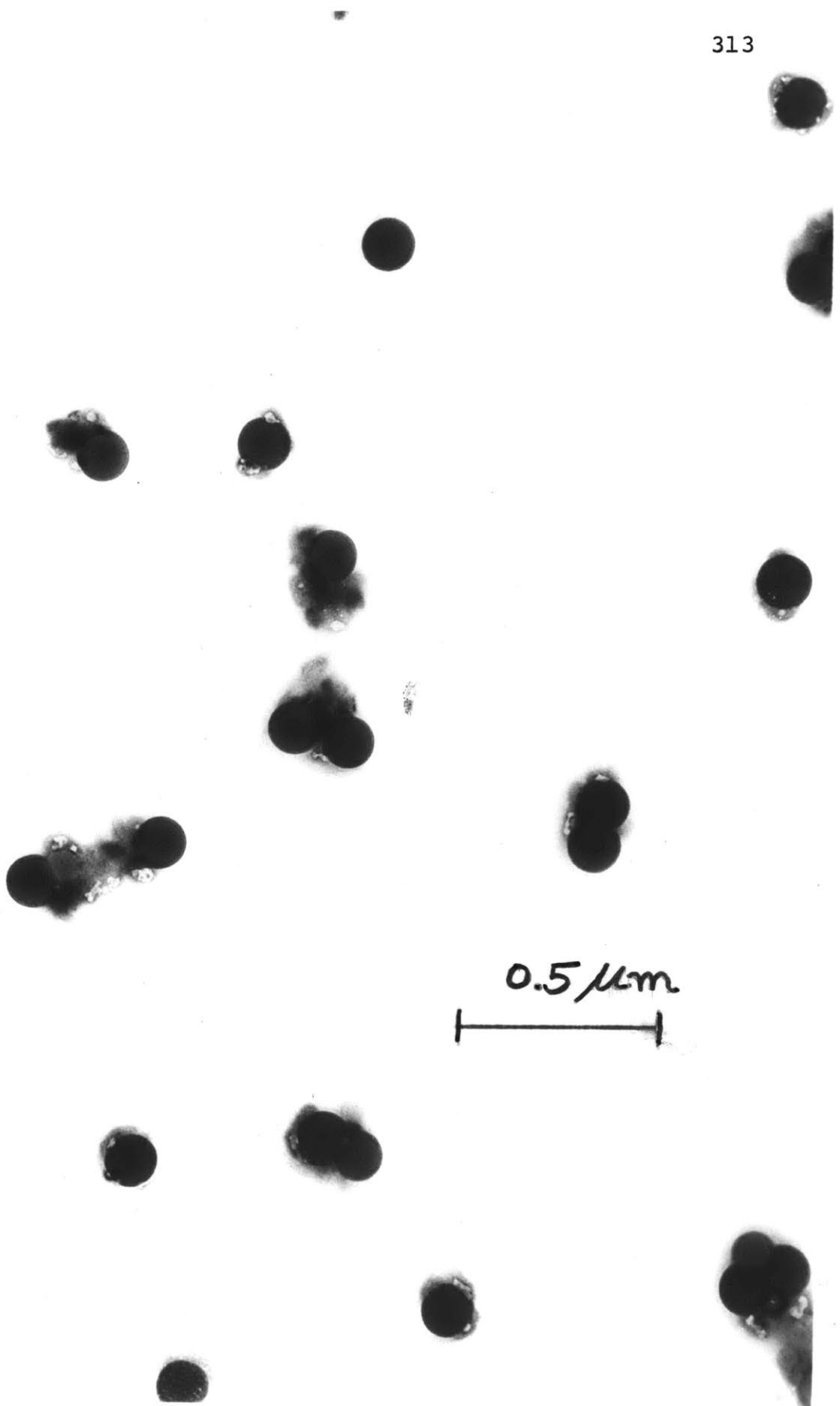


FIGURE 7.5
ELECTRON MICROGRAPH OF STYRENE DISPERSION

The polystyrene particles were nearly mono-dispersed. Figure 7.5 shows an electronphotomicrograph of the particles (prepared as described in Chapter 6). The volume mean diameter defined as

$$\bar{d}_v = \frac{\sum_i n_i v_i d_i}{\sum_i n_i v_i} \quad (7.4)$$

was $\bar{d}_v = 0.120 \mu\text{m}$,

and the volume mean diameter standard deviation defined as

$$\sigma_v = \frac{\sum_i n_i v_i (d_i - \bar{d}_v)^2}{\sum_i n_i v_i} \quad (7.5)$$

was $\sigma_v = 0.008 \mu\text{m}$

for a total number of 400 measured particles.

Figure 7.6 shows the permeability of carbon dioxide in FEP 120 dispersions of various solid volume fractions. The experimental points show good agreement with a theoretical line calculated from Maxwell's equation. Maximum deviation is eight per cent at a volume fraction of 0.411. This concentration dispersion was obtained by centrifugation of the original FEP 120 dispersion ($\phi = 0.357$). The continuous phase permeability was measured as

$$P_c = 11.2 \times 10^{-6} \frac{\text{cm}^2\text{-cc(STP)}}{\text{sec-cc-atm}}$$

and the solid phase permeability has been reported as

$$P_d = 9.67 \times 10^{-8} \frac{\text{cm}^2\text{-cc(STP)}}{\text{sec-cc-atm}}$$

for solid films of FEP (Pasternak et al, 1971), so that K_d is

$$K_d = 0.00863 \quad .$$

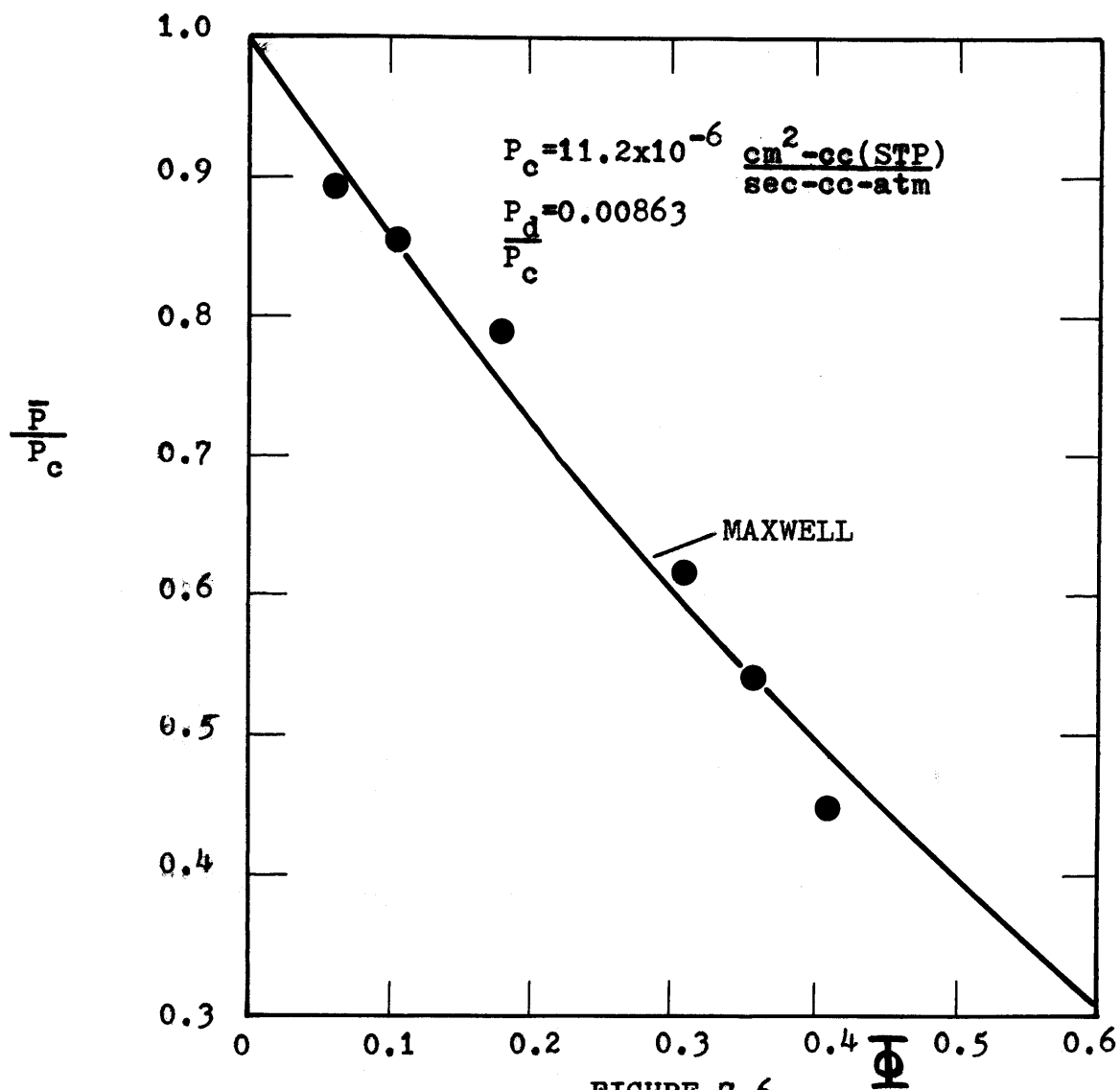


FIGURE 7.6

PERMEATION OF CARBON DIOXIDE IN FEP 120
DISPERSIONS.

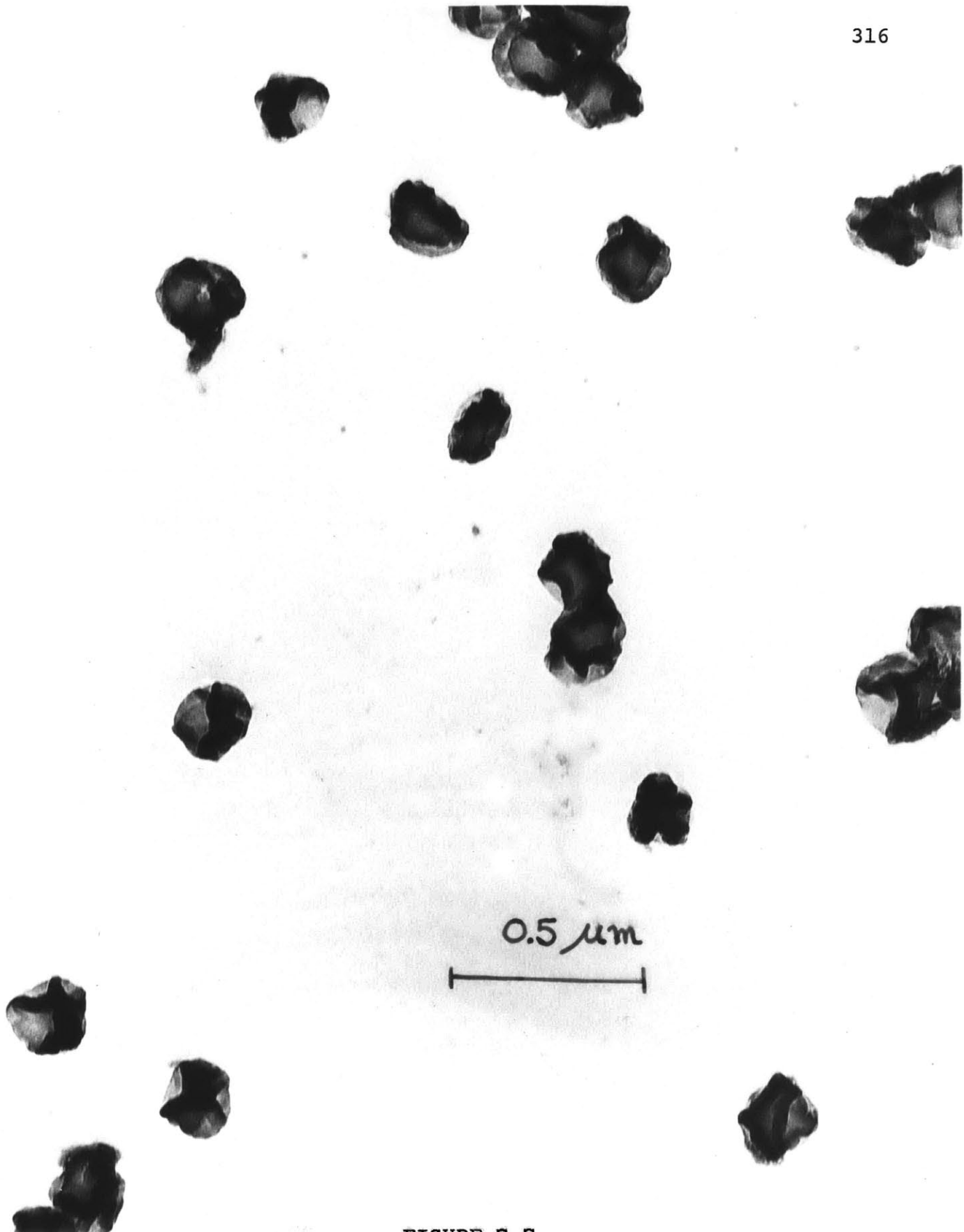


FIGURE 7.7
ELECTRON MICROGRAPH OF FEP 120 DISPERSION

Figure 7.7 shows an electronphotomicrograph of the FEP 120 particles. The particles appear to have a slightly "crumpled" look, but are fairly spherical. The particles were virtually monodisperse and had a volume mean diameter and standard deviation of

$$\bar{d}_v = 0.199 \mu\text{m}$$

$$\sigma_v = 0.016 \mu\text{m}$$

for a total of 200 measured particles.

Figure 7.8 shows the comparison of experimental results obtained on the permeation of carbon dioxide in 30 TFE dispersions with Maxwell's equation. The experimental points are from five to ten per cent below values predicted by Maxwell. The continuous phase permeability was measured as

$$P_c = 13.0 \times 10^{-6} \frac{\text{cm}^2\text{-cc (STP)}}{\text{sec-cc-atm}}$$

and the solid phase permeability was reported by Pasternak et al. (1970, 1971) as

$$P_d = 8.90 \times 10^{-8} \frac{\text{cm}^2\text{-cc (STP)}}{\text{sec-cc-atm}}$$

for TFE films. Pasternak et al. (1971) suggested that the TFE films most likely contain micropores so that the dispersed to continuous phase permeability ratio is properly stated as

$$\frac{P_d}{P_c} \geq 0.00685$$

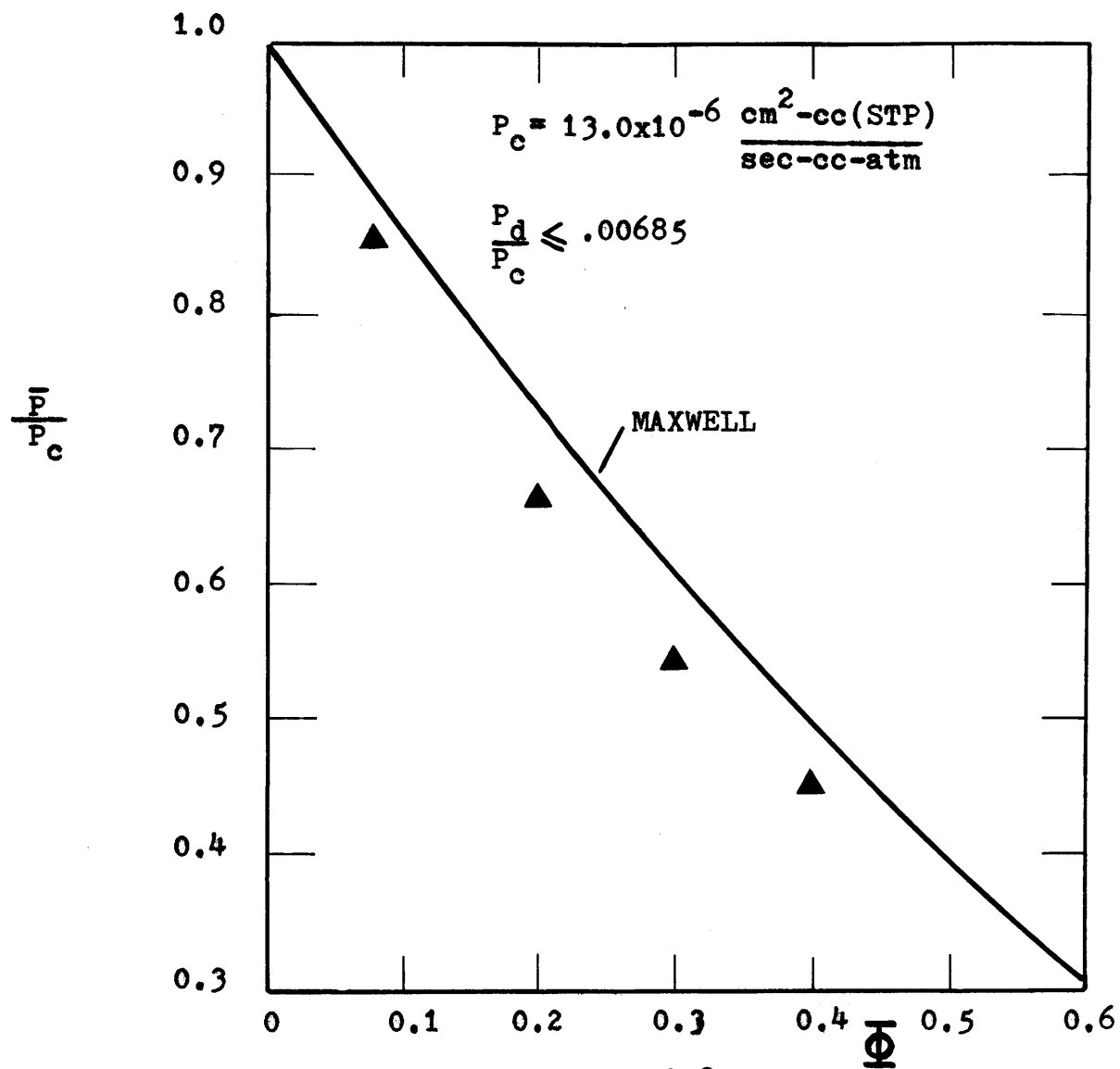


FIGURE 7.8

PERMEATION OF CARBON DIOXIDE IN TFE 30
DISPERSIONS.

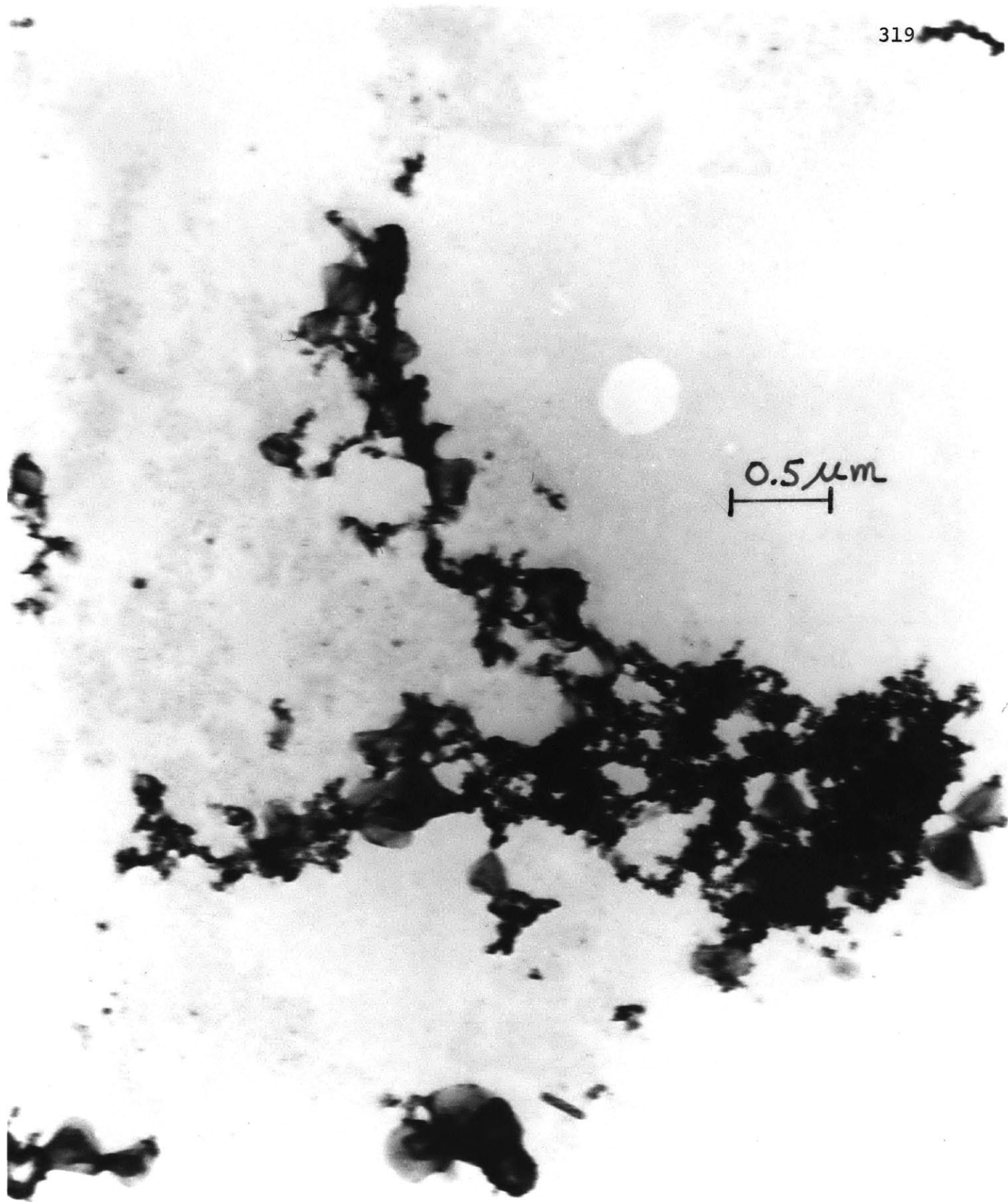


FIGURE 7.8a
ELECTRONMICROGRAPH OF TFE 30 DISPERSION

Figure 7.8a is an electronphotomicrograph of a TFE 30 particle. The particle appears to be an agglomeration of small (about $0.05 \mu\text{m}$) and larger particles (about $0.5 \mu\text{m}$). No particle size measurement of the agglomerated particles or the individual particles could be made as detail in other photographs was very poor. If the particles exist in solution as irregular agglomerates it should not be surprising that the data on Figure 7.8 deviates from Maxwell's equation. Maxwell's equation applies to spherical-like particles, while the agglomerated TFE 30 particles were anything but spherical and were often flake-like in appearance. If the particles are assumed disc-like and modeled as an oblate spheroid, then Fricke's equation predicts the correct deviation (see Figure 3.1) from Maxwell's equation.

7.2.2 Inert Emulsion

The emulsions used here were castor oil, vegetable oil, and fluorocarbon in water; they have been described in the previous chapter. Oxygen permeabilities were measured for a variety of dispersed phase volume fractions up to approximately 0.75, and the dispersed phase to continuous phase permeability varied from 0.471 to 33.4. All experimental runs are listed in Appendix D .

The aqueous phase for the two castor oil emulsion systems and the vegetable oil emulsion system was 10% Tween 40 surfactant and 90% water by volume. The surfactant solution used for the fluorocarbon emulsions was 50 gr of Pluronic F-68 per liter of water. Table 8.8 in Appendix D reports the

oxygen permeability of these surfactant solutions.

Figure 7.9 shows the comparison of the experimental oxygen permeability for castor oil in water emulsions (O/W) with Maxwell's equation. The dispersed phase and continuous phase permeabilities were measured as

$$P_d = 2.55 \times 10^{-7} \frac{\text{cm}^2\text{-cc (STP)}}{\text{sec-cc-atm}}$$

$$P_c = 5.42 \times 10^{-7} \frac{\text{cm}^2\text{-cc (STP)}}{\text{sec-cc-atm}}$$

so that the dispersed phase to continuous phase permeability ratio is 0.471. Although there is some scatter of the experimental points, the results seem to correlate reasonably with Maxwell's equation even at the highest volume fraction. At a volume fraction of 0.750 the emulsion had the consistency of a cream.

The emulsions had a broad range of particle sizes (and were of course spherical) from about 1 μm to 15 μm with an average volume mean diameter of $\bar{d}_v = 10.0 \mu\text{m}$. A typical size distribution for a castor oil emulsion is shown in Appendix D.

The experimental oxygen permeabilities measured in castor oil - Span 80 (10% by volume of Span 80 oil soluble surfactant) in water emulsions are compared with Maxwell's equation in Figure 7.10. The dispersed phase permeability was measured as

$$P_d = 2.76 \times 10^{-7} \frac{\text{cm}^2\text{-cc (STP)}}{\text{sec-cc-atm}}$$

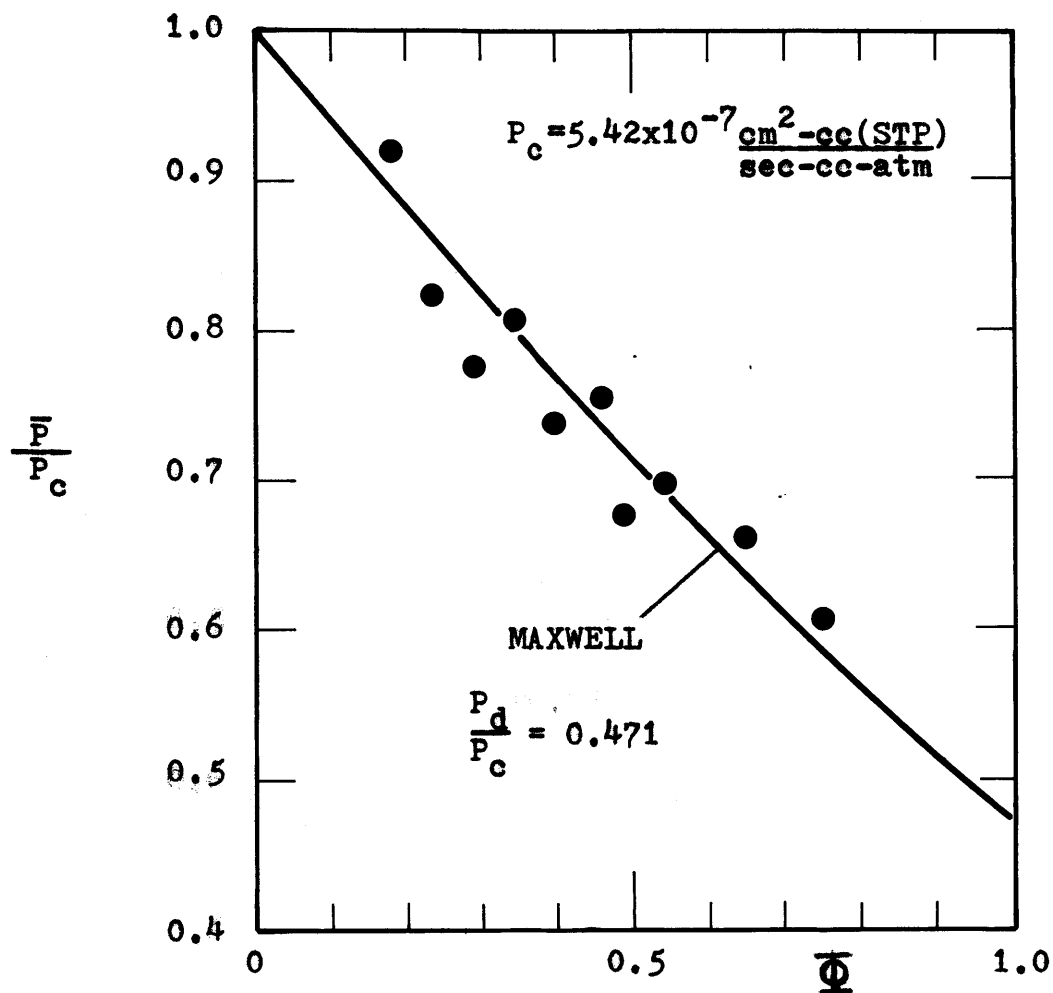


FIGURE 7.9

PERMEABILITY OF OXYGEN IN CASTOR OIL EMULSIONS (O/W).

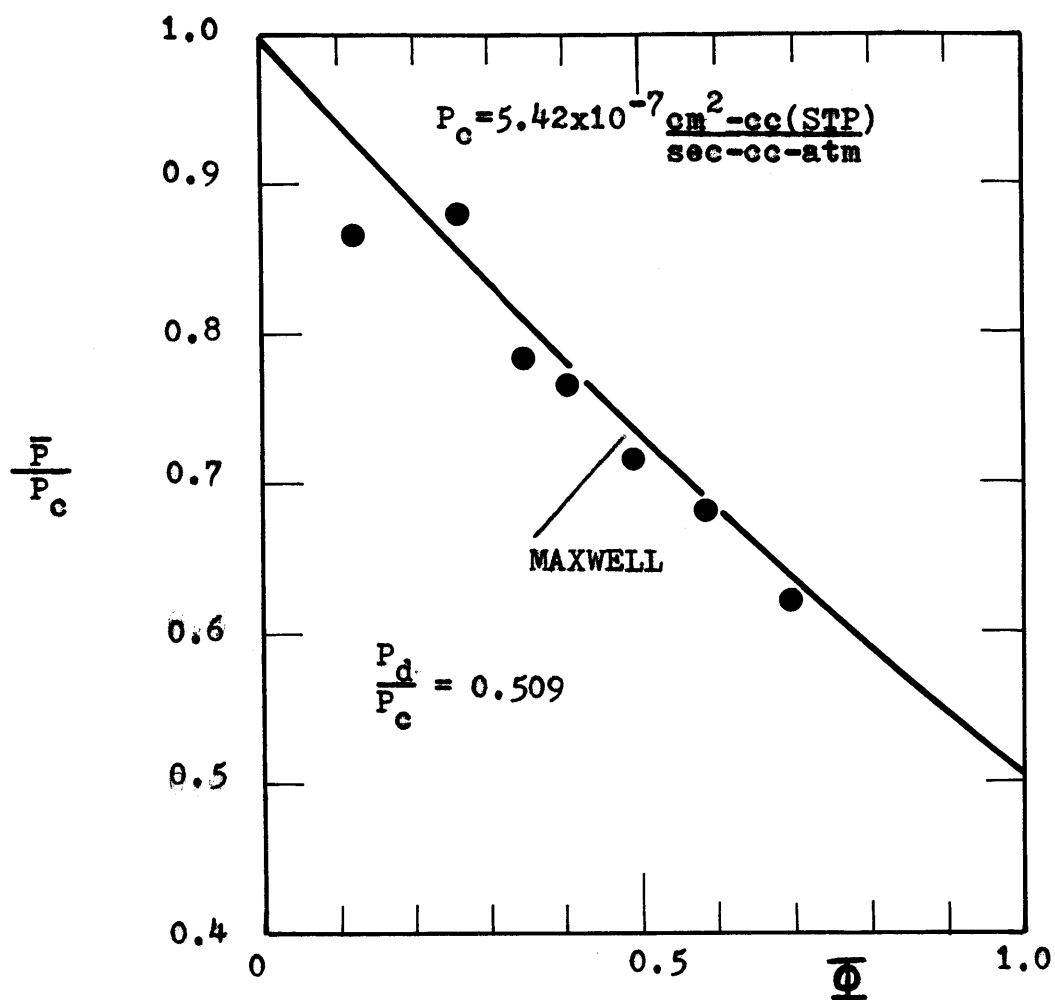


FIGURE 7.10

PERMEABILITY OF OXYGEN IN CASTOR OIL
(10% SPAN 80) EMULSIONS (O/W).

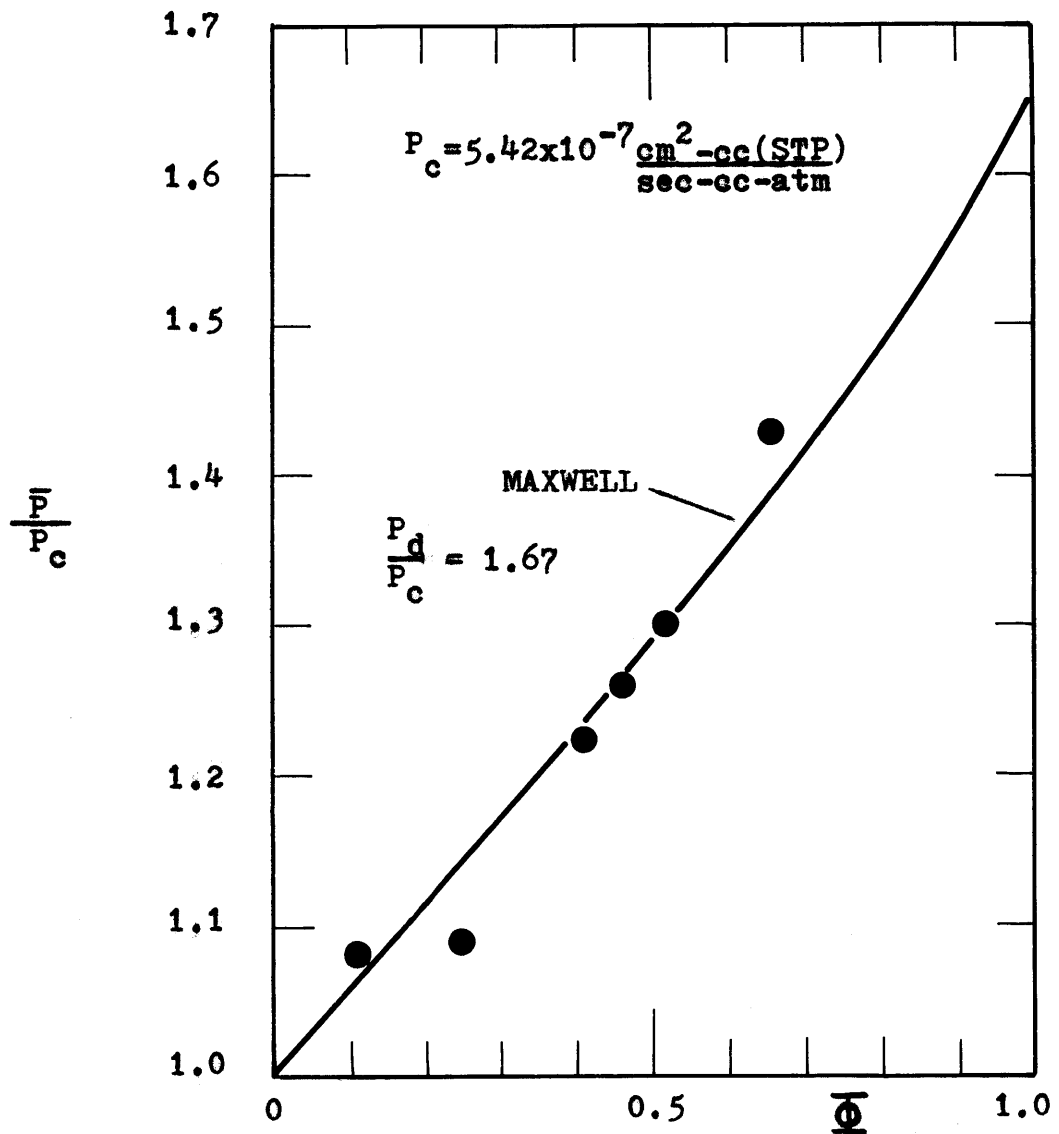


FIGURE 7.11

PERMEABILITY OF OXYGEN IN WESSON
VEGETABLE OIL EMULSIONS (O/W).

so that in this case the dispersed phase to continuous phase permeability is equal to 0.509. Except for one experimental point, the agreement with Maxwell's equation is very good. The particle size distribution was quite similar to the previous system. The volume mean diameter was about $\bar{d}_v = 9.0 \mu\text{m}$ with a standard deviation of $\pm 4.0 \mu\text{m}$.

Another system investigated was the vegetable oil in water emulsion. The dispersed phase permeability for the vegetable oil is

$$P_d = 9.09 \times 10^{-7} \text{ cm}^2\text{-cc (STP) / (sec-cc-atm)}$$

so that the dispersed phase to continuous phase permeability is 1.67 as is shown in Figure 7.11. The particle size of the vegetable oil emulsion varied from 1 to 20 μm and the mean diameter was approximately 10 μm with a standard deviation of 4 μm . Again the experimental points show reasonable agreement with the theory.

Some phase separation was observed after the permeation experiment was terminated for volume fractions below $\phi = 0.3$, but at no time was the separated layer more than 1/9 of the total height of the liquid slab (for the previously mentioned emulsion systems). Since the experimental agreement with Maxwell's equation is quite good, the results suggest that for these three emulsion systems interfacial resistance, caused by the adsorption of the Tween 40 surfactant at the oil-water interface, is negligible. It is surprising that the oxygen permeability for the castor oil is one half that of water. In

general the oxygen solubility of organics is much larger than that of water. For instance, the oxygen solubility of olive oil at 25°C is given as 0.116 cc(STP)/cc/atm (Battino et al., 1968). Unfortunately (as far as is known) the oxygen solubility in Castor oil has not been determined, but if indeed it is larger than that of water, it follows that the diffusivity is much smaller than that of water. This was partially confirmed by experiment because the lag time θ' for castor oil was approximately six times as long as that of water suggesting that the diffusivity is approximately 4.0×10^{-6} cm²/sec.

Before proceeding to a discussion of the PID fluorocarbon emulsion, it should be mentioned that the permeabilities of the three oils studied have only moderate departures from that of the aqueous phase. In the reactive red blood cell suspension the theoretically predicted effective permeabilities also show only moderate departures from the permeability of the continuous phase. It is therefore gratifying that at least in this range of permeabilities Maxwell's equation gives an adequate prediction of the effective permeability even at high volume fractions.

Some trouble was encountered in accurately measuring the oxygen permeability of the PID fluorocarbon. In the case of a highly permeable liquid the membrane resistance becomes a significant part of the total mass transfer resistance. In the case of the PID fluorocarbon for a film thickness of approximately 0.16 mm and total membrane thickness of 93 μ m the membrane resistance accounts for about 50% of total resistance.

Therefore the measured permeability was more variable from run to run. The average oxygen permeability in PID fluorocarbon was measured as

$$P_d = (2.02 \pm 0.28) \times 10^{-5} \frac{\text{cm}^2\text{-cc (STP)}}{\text{sec-cc-atm}}$$

The permeability of the aqueous phase is

$$P_c = 6.02 \times 10^{-7} \frac{\text{cm}^2\text{-cc (STP)}}{\text{sec-cc-atm}}$$

so that the dispersed phase to continuous phase ratio is

$$\frac{P_d}{P_c} = 33.4 \pm 4.7$$

As indicated by Table 6.8 the specific gravity of PID fluorocarbon is much higher than that of water. Because of sedimentation problems it was decided to measure oxygen permeabilities only for emulsions with a concentrated particle size where particles were packed so tightly that no sedimentation could occur. Figure 7.12 shows the comparison of the experimental results for the effective permeability (of the PID emulsions) with that predicted with Maxwell's and Bruggeman's equation. The data points fall in a region between Bruggeman's and Maxwell's equation, some 20% above the values predicted by Maxwell. This behavior is quite similar to that encountered by other investigators when K_d is much larger than one. These permeability differences are not encountered in the physiological system of interest, but for other systems with a large K_d Maxwell's relationship can be rigorously applied only for dilute suspensions. The average volume mean diameter for the

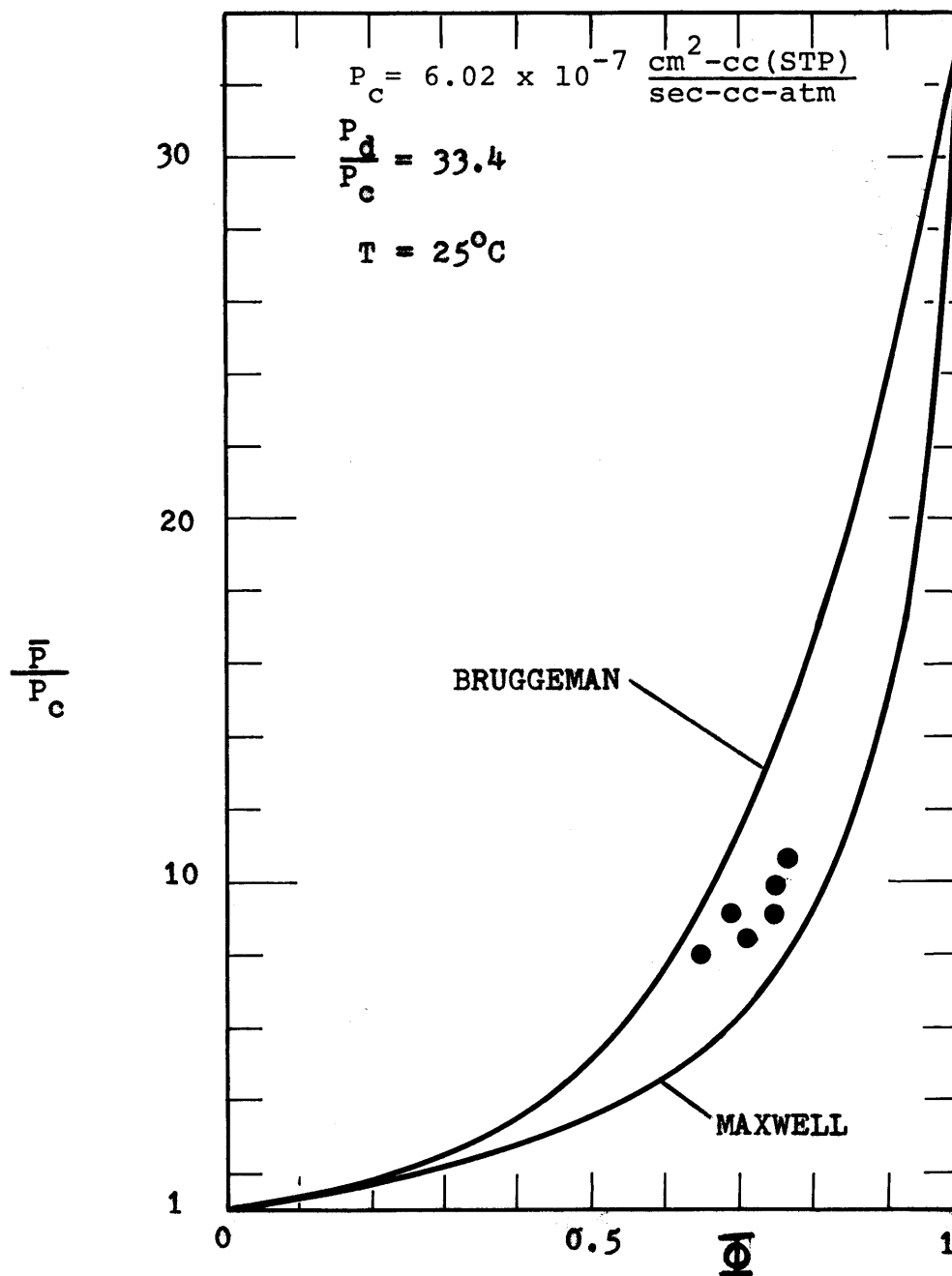


FIGURE 7.12

OXYGEN PERMEABILITY IN FLUORCARBON EMULSIONS.

fluorocarbon emulsion was 11 μm with a standard deviation of 4 μm .

In addition to the PID fluorocarbon the oxygen permeability of the fluorocarbon FC 80 was measured. Fluorocarbon FC 80 is composed predominantly of perfluorobutyltetrahydrofuran (obtained from the 3M Company) and has an oxygen solubility which is almost identical to that of PID. The oxygen permeability for this compound is (two measurements)

$$P_{\text{FC 80}} = 1.83 \times 10^{-5} \frac{\text{cm}^2\text{-cc (STP)}}{\text{sec-cc-atm}}$$

which is of comparable value to that of PID fluorocarbon.

7.3 "Reactive" Systems

The reactive system of interest is the oxygen-hemoglobin system. First the experiments on films of partially immobilized hemoglobin will be discussed. Then data will be presented on the diffusion of oxygen in inert films of hemoglobin solution and inert red blood cell suspensions prior to the discussion on heterogeneous reactive systems.

7.3.1 Immobilized (Reactive) Hemoglobin Films

In collaboration with Zahka (1971) hemoglobin was immobilized by sorption into a swollen hydrophilic gel (collodion) as has been described in the previous chapter. The relative immobility of hemoglobin within the collodion film was demonstrated by desorption experiments. Effective hemoglobin diffusivities, calculated as a function of time during the

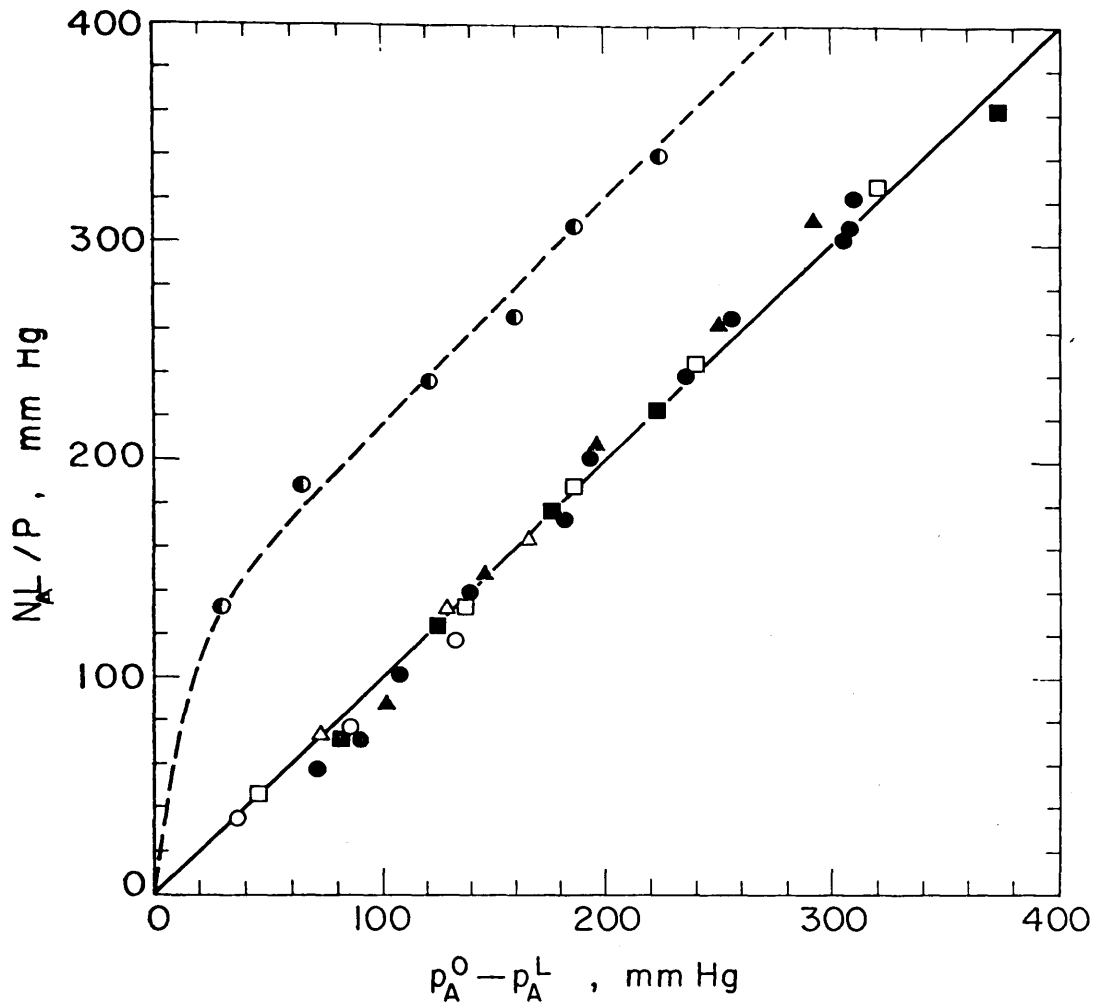
desorption experiments, increased as the mean concentration in the membrane decreased. This is consistent with the observed dependence of hemoglobin diffusivity on hemoglobin as shown in Figure 3.8. The initial value, when the free hemoglobin concentration in aqueous solution within the membrane was maximal (34.4 and 25.0 gr/100 ml in two experiments) averaged 3×10^{-9} cm²/sec. At equilibrium, about 12 gr hemoglobin/100 gr collodion (wet weight) remained permanently sorbed to the membrane and did not leach out after several weeks. Roughly one-third to one-fourth of the hemoglobin within the film was therefore irreversibly adsorbed, and it was assumed in the diffusion calculations that this strongly adsorbed component was immobilized and did not contribute to the observed diffusive flux of hemoglobin. Immobilization in the hydrophilic gel may result from hydrogen bonds and van der Waals and electrostatic interactions between hemoglobin and the polymer. With regard to electrostatic effects, it is well known (Carr and Sollner, 1944) that collodion membranes have a net negative charge which arises from the presence of dissociable acidic groups. The remainder of the hemoglobin was clearly mobile, but its diffusivity was reduced from its value in free solution by a factor of about 25 (see Figure 7.8). This diffusivity reduction factor is consistent with previous results with hydrophilic films of similar water content (Colton et al., 1971a). All hemoglobin in the collodion films was found to reversibly bind oxygen in a manner similar to hemoglobin in free solution. In pH 7.4 phosphate buffer at 25°C, the p_{50} was 10 mm Hg, and the

total oxygen uptake was approximately equal to that expected if all the hemoglobin in the film were active.

Oxygen permeation rates through the immobilized hemoglobin films were compared with those for similar films containing only water or methemoglobin as well as microporous Millipore filters containing hemoglobin solution, the latter having been shown to augment oxygen transport (Scholander, 1960). The membranes were clamped into the sample holder without the presence of the support membranes.

Normalized oxygen permeation rates as a function of partial pressure driving force are plotted in Figure 7.13 in a manner such that all experimental data are shown on one graph. Data points lying on a straight line which passes through the origin conform to normal Fickian diffusion, whereas points lying above that line indicate augmented transport. Oxygen permeability (defined as $P = D\alpha$), was first calculated from the slope of the best straight line fitting the data for large driving forces from a plot of permeation rate versus driving force. Permeability values so calculated are tabulated in the legend to Figure 7.13 and range from about one-fifth to two-thirds of the value expected for a film of pure water. Minor corrections (less than 10 per cent) were made to put all data in Figure 1 on a uniform basis of zero downstream partial pressure.

Augmentation of oxygen transport occurred only through hemoglobin-filled Millipore filters. The dotted curve in Figure 7.13 was calculated from equation (6.4), with



Membrane and Solution Contained Therein	L μ	C_T g/100 ml	P $\frac{\text{g mole}}{\text{cm-sec-mm Hg}} \times 10^{15}$
● Collodion - Hb	330	25.0	10.6
▲ Collodion - Hb	275	34.4	8.6
■ Collodion - Hb	345	34.4	8.6
○ Collodion - MetHb	345	34.4	8.6
△ Collodion - Water	291	0	24.7
□ Millipore - Water	150	0	21.3
◐ Millipore - Hb	150	25.0	7.5

FIGURE 7.13

NORMALIZED STEADY-STATE OXYGEN PERMEATION RATE AS A FUNCTION OF IMPOSED PARTIAL PRESSURE DRIVING FORCE.

$K = 7.0 \times 10^7 \text{ cm}^3/\text{mole}$ (Gibson, 1959), and $D_B = 6.5 \times 10^{-8} \text{ cm}^2/\text{sec}$. Equation (6.4) is a valid approximation for flux prediction since for the thicknesses of the membranes employed the reaction was at equilibrium (Wittenberg, 1966). The hemoglobin diffusivity, treated here as a fitting parameter, is within the range reported in Figure 7.8 when corrected for the porosity and the tortuosity (1.45). These data therefore conform to a mobile carrier mechanism.

All other data, including that for collodion containing immobilized hemoglobin, are statistically indistinguishable and fall on a straight line which passes through the origin, as would be expected from equation (6.4) if no augmentation mechanism of any kind were operative. These results clearly demonstrate that mobility of human hemoglobin was a prerequisite for measurable oxygen transport augmentation in the system studied.

7.3.2 Inert Hemoglobin Solutions

Oxygen permeabilities were measured in inert liquid films of hemoglobin solutions (methemoglobin) of various hemoglobin concentrations. Since oxygen solubilities in hemoglobin solutions can be estimated accurately from data presented in Table 3.3, the oxygen diffusivities can be calculated from the experimentally measured permeabilities.

Figure 7.14 gives the experimentally determined oxygen permeabilities in hemoglobin solutions at 25°C . At a zero hemoglobin concentration the oxygen permeability is the

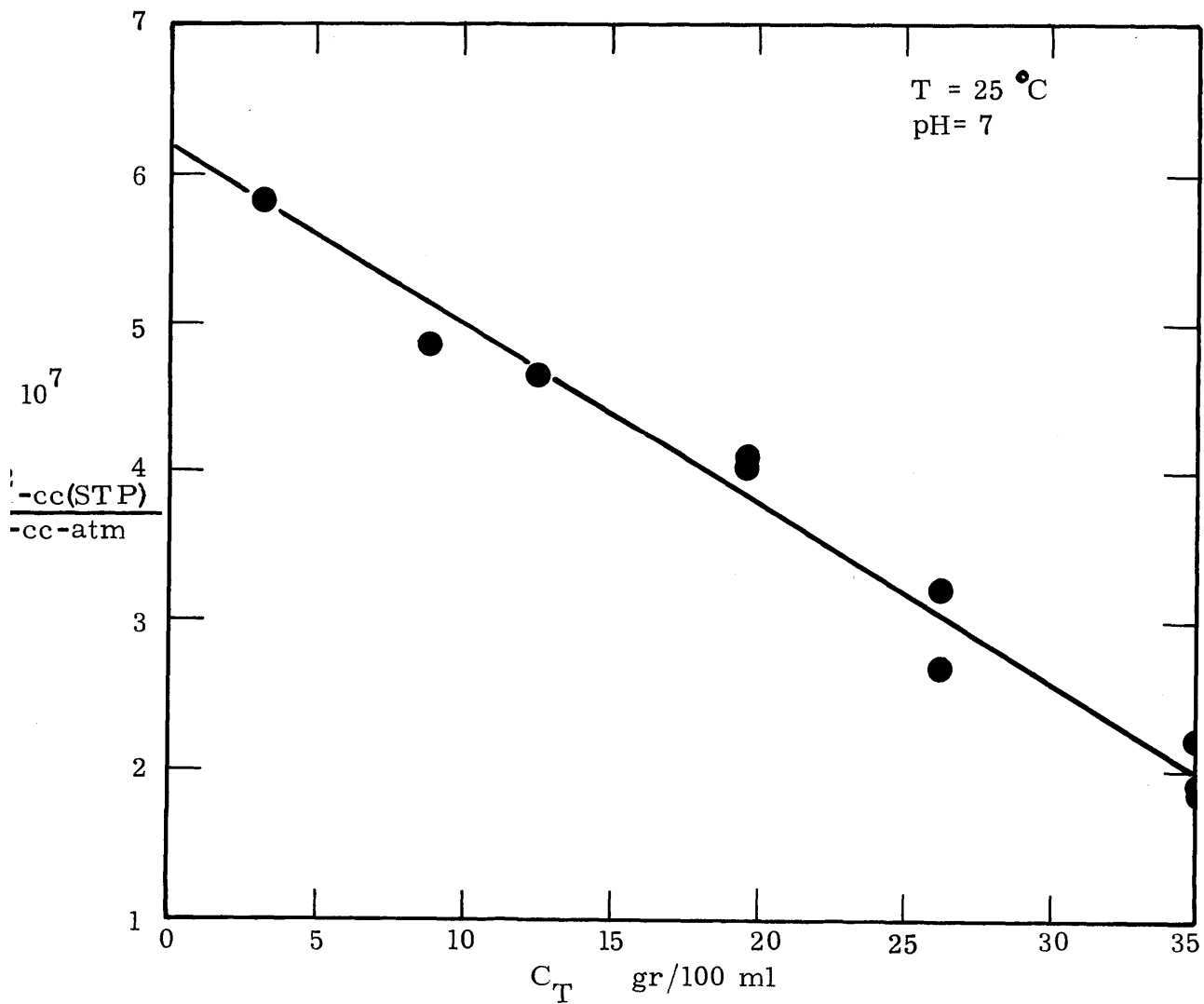


FIGURE 7.14
 OXYGEN PERMEABILITY IN HEMOGLOBIN SOLUTIONS.

permeability of the buffered isotonic saline and was measured as

$$P_{O_2, \text{isotonic saline}} = 6.00 \times 10^{-7} \frac{\text{cm}^2\text{-cc (STP)}}{\text{sec-cc-atm}}$$

As the hemoglobin concentration increases to red blood cell concentrations the oxygen permeability decreases by about a factor of three. The decrease is virtually linear with concentration. The data presented in Figure 7.14 is tabulated in Table 7.4 in addition to the estimated oxygen solubility coefficients and the calculated diffusivities. It was assumed that the oxygen solubility coefficient for concentrated hemoglobin solutions (33 gr/100 ml) is equal to that of packed red blood cells. A linear estimate was made between the values of the oxygen hemoglobin solubility for isotonic saline and concentrated hemoglobin solution in order to arrive at oxygen solubility coefficients for hemoglobin solutions with intermediate hemoglobin concentrations. Since the oxygen solubility coefficient varies by only 1.5% the values in Table 7.4 should be quite accurate. The estimated oxygen diffusivity is compared with the Kreuzer correlation for all published values of the oxygen diffusion coefficient in hemoglobin solutions (see Figure 3.7). Kreuzer (1970) reduced all data relative to the D_{O_2} for saline which was taken as $2.07 \times 10^{-5} \text{ cm}^2/\text{sec}$ (according to Goldstick, 1966). The calculated diffusivities fall somewhat above Kreuzer's correlation. However if the line is replotted so that the D_{O_2} for saline is $2.22 \times 10^{-5} \text{ cm}^2/\text{sec}$ by multiplying the plot by the factor $(\frac{2.22}{2.07})$

TABLE 7.4
 OXYGEN PERMEABILITIES AND CALCULATED
 OXYGEN DIFFUSIVITIES IN INERT
 HEMOGLOBIN SOLUTIONS (T = 25°C)

C_T gr/100 ml	P $\frac{\text{cm}^2\text{-cc (STP)}}{\text{sec-cc-atm}}$	α $\frac{\text{cc (STP)}}{\text{cc-atm}}$	D $\frac{\text{cm}^2}{\text{sec}}$
0	6.00×10^{-7}	0.0272	2.20×10^{-5}
8.78	5.30×10^{-7}	0.0273	1.94×10^{-5}
8.78	4.78×10^{-7}	0.0273	1.76×10^{-5}
15.4	3.96×10^{-7}	0.0274	1.44×10^{-5}
15.4	3.93×10^{-7}	0.0274	1.43×10^{-5}
22.3	3.35×10^{-7}	0.0275	1.29×10^{-5}
26.2	3.14×10^{-7}	0.0275	1.14×10^{-5}
31.8	2.20×10^{-7}	0.0276	0.80×10^{-5}

(All experimental runs are listed in Appendix D.)

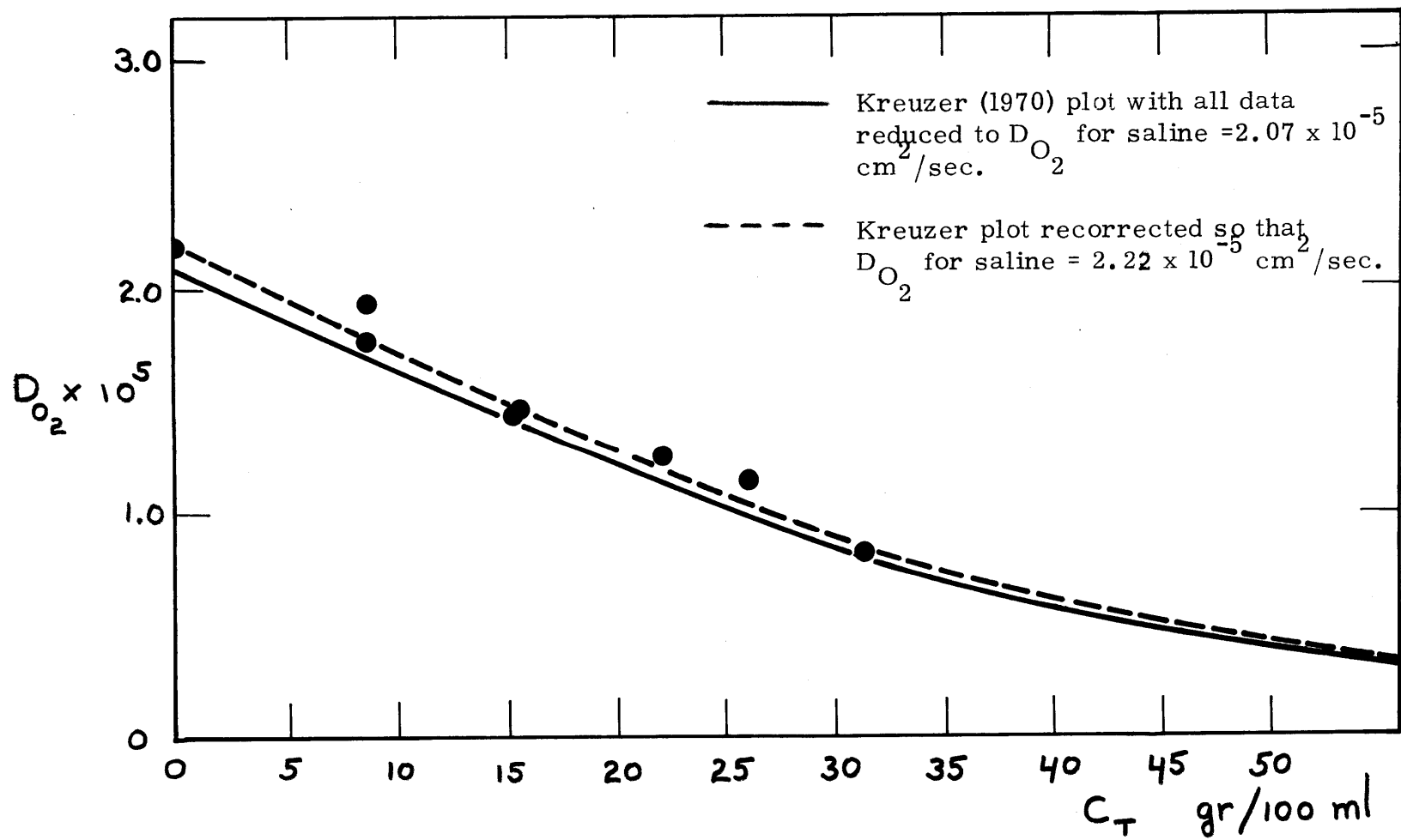


FIGURE 7.15
 COMPARISON OF THE CALCULATED OXYGEN DIFFUSIVITIES WITH KREUZER'S PLOT FOR ALL PREVIOUS DATA.

the calculated diffusivities scatter around the corrected line. It should be mentioned here that even if the Kreuzer plot is not corrected the scatter of the data points is no worse than those shown in Figure 3.7. It can be concluded that the data obtained here is consistent with other literature values.

Oxygen permeabilities were also measured for a hemoglobin solution of fixed hemoglobin concentration (15.4 gr/100 ml) at a variety of temperatures. Table 7.5 shows the oxygen permeability and calculated diffusivity for a hemoglobin solution with a concentration of 15.4 gr/100 ml over the temperature range of 17-33°C. Oxygen solubilities were estimated as described earlier. The oxygen permeability appears to be quite insensitive to temperature changes over this range. According to the Stokes-Einstein equation, the diffusivities (at two temperatures) for a gas-liquid system are related by

$$\frac{D_2}{D_1} = \frac{T_2}{T_1} \frac{\mu_1}{\mu_2} \quad (7.6)$$

Unfortunately viscosity data is scarce for hemoglobin solutions so that a rigorous comparison of equation (7.6) with the calculated diffusivities presented in Table 7.5 is not possible. One could assume however that the viscosity ratio (μ_1/μ_2) is approximately the same as that of pure water. Figure 7.16 shows a comparison of the oxygen diffusivities from Table 7.5. The experimentally obtained diffusivities appear to deviate somewhat from equation (7.6) if the viscosity data of pure water is used. The hemoglobin concentration of 15.4 gr per 100 ml was

TABLE 7.5
 OXYGEN PERMEABILITY IN INERT HEMOGLOBIN SOLUTION
 (15.4 gr/100 ml) AS A FUNCTION OF TEMPERATURE

T	α^1	P x 10 ⁷	D (calculated) x10 ⁵
<u>°C</u>	<u>$\frac{\text{cc (STP)}}{\text{cc-atm}}$</u>	<u>$\frac{\text{cm}^2\text{-cc (STP)}}{\text{cc-atm}}$</u>	<u>$\frac{\text{cm}^2}{\text{sec}}$</u>
17	.0318	3.99	1.25
21	.0295	3.96	1.35
25	.0274	4.02	1.47
29	.0256	-	-
33	.0243	3.90	1.61
37	.0228	-	-

(All experimental runs are listed in Appendix D.)

-
- 1 Estimated from the oxygen solubility of concentrated hemoglobin solutions (equal to O₂ solubility in red blood cells which was calculated from Table 3.3 as described in Section 3.3.3.3) and the oxygen solubility of isotonic saline. A linear estimate was made between the two values at each temperature assuming that C_T in red blood cells is 33 gr/100 ml and in that in saline is 0 gr/100 ml (see Table 3.3).

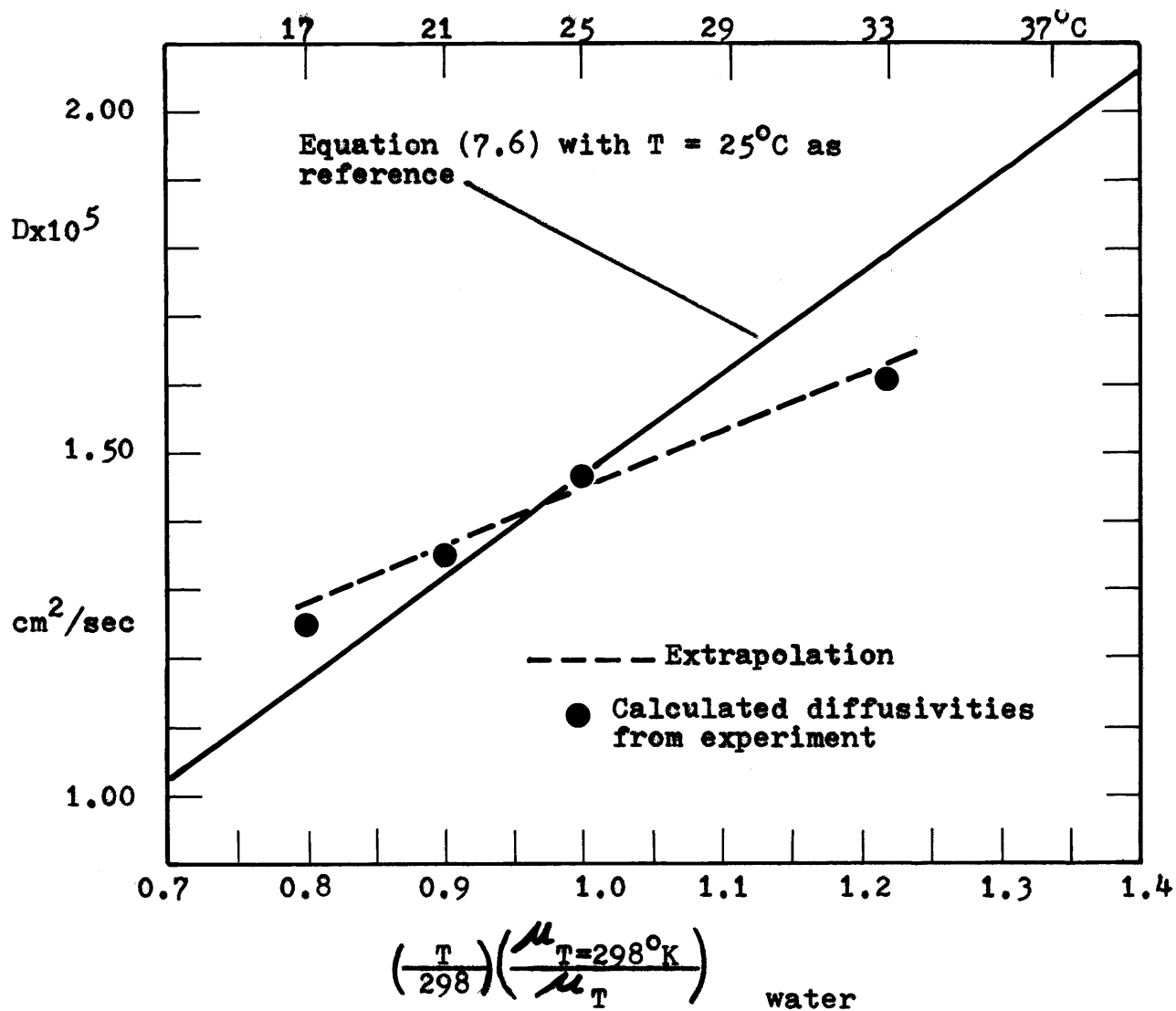


FIGURE 7.16

COMPARISON OF CALCULATED OXYGEN DIFFUSIVITIES WITH EQUATION (7.6).

chosen because it is approximately equal to the hemoglobin concentration of normal whole human blood.

7.3.3 Red Blood Cell Suspensions

Oxygen permeabilities were measured for red blood suspensions with a volume fraction variation from zero to 0.98 and at different driving force conditions. As has been shown in Chapter 5, facilitation effects are a maximum at low partial pressures where the hemoglobin is largely unsaturated throughout the liquid film. As the partial pressure is increased at both sides of the film, the hemoglobin becomes more saturated throughout the film and facilitation effects become negligible. This then becomes a case of pure Fickian diffusion through the suspension. Experimental results were obtained for both the inert case and the reactive case.

The red blood cell suspensions were prepared as described in Section 6.3.3.1 and suspended in buffered isotonic saline. The pH of the suspensions was near 7.0, and the temperature was 25°C. Two experiments were also performed at physiological temperatures (37°C).

7.3.3.1 Inert Red Blood Cell Suspensions

At conditions of pH = 7.0 and T = 25°C, the oxygen-hemoglobin saturation curve is nearly fully saturated at about 40 mm Hg at pH = 7 and T = 25°C (with or without 2,3 DPG). In order to measure the oxygen permeability in inert suspensions, the samples were equilibrated at approximately 50 mm Hg partial

pressure of oxygen prior to the permeation experiment. This procedure guaranteed that the hemoglobin inside the red blood cells was fully saturated, and that the reaction did not affect the diffusion of oxygen through the suspension. In Table 7.7 the experimental results are tabulated, with the calculated diffusivities. In the case of red blood cells suspended in saline the oxygen solubility is virtually a constant, because the solubilities for saline and the red blood cell differ by only 1.5 per cent. To obtain oxygen solubilities for red blood cell suspensions of various volume fractions, a linear estimate was made between values for saline and red blood cells. If the red blood cell membrane resistance to oxygen transport is negligible, it follows that the oxygen permeability for red blood cells should be equal to that for concentrated hemoglobin solutions of 33 gr/100 ml (red blood cell hemoglobin concentration). From Figure 7.14 the oxygen permeability for a hemoglobin solution of 33 gr/100 ml is 2.05×10^{-7} cm²-cc(STP)/sec/cc/atm. Figure 7.17 shows a comparison of the data from Table 7.6 which Maxwell's equation with a dispersed phase to continuous phase permeability ratio given as

$$\frac{P_d}{P_c} = \frac{P_{RBC}}{P_{saline}} = \frac{2.05 \times 10^{-7}}{6.00 \times 10^{-7}} = 0.342$$

The data agree quite well with the theoretical line (maximum deviation 10 per cent) and no consistent deviation from the theoretical equation is apparent. These results are in agreement with previous authors' work that suggested that membrane

TABLE 7.6
 OXYGEN PERMEABILITIES IN INERT¹ RED BLOOD CELL SUSPENSIONS
 AT 25°C and pH = 7.0

ϕ	\bar{P}	$\frac{\bar{P}}{P_c}$	$\bar{\alpha}$ (estimated)	\bar{D} (calculated)
	$\frac{\text{cm}^2\text{-cc (STP)}}{\text{sec-cc-atm}}$		$\frac{\text{cc (STP)}}{\text{cc-atm}}$	$\frac{\text{cm}^2}{\text{sec}}$
0	6.00×10^{-7}	1	0.272	2.20×10^{-5}
0.214	5.18×10^{-7}	0.865	0.273	1.40×10^{-5}
0.417	3.93×10^{-7}	0.655	0.274	1.43×10^{-5}
0.585	3.58×10^{-7}	0.596	0.274	1.31×10^{-5}
0.715	3.05×10^{-7}	0.509	0.275	1.11×10^{-5}
0.828	2.90×10^{-7}	0.483	0.275	1.05×10^{-5}
0.866	2.26×10^{-7}	0.377	0.275	0.823×10^{-5}
0.974	2.08×10^{-7}	0.347	0.276	0.755×10^{-5}
0.985	2.07×10^{-7}	0.345	0.276	0.752×10^{-5}

(All experimental runs are tabulated in Appendix D.)

1 Partial pressure downstream was about 50 mm Hg and the upstream partial pressure was about 200 mm Hg (see Appendix D).

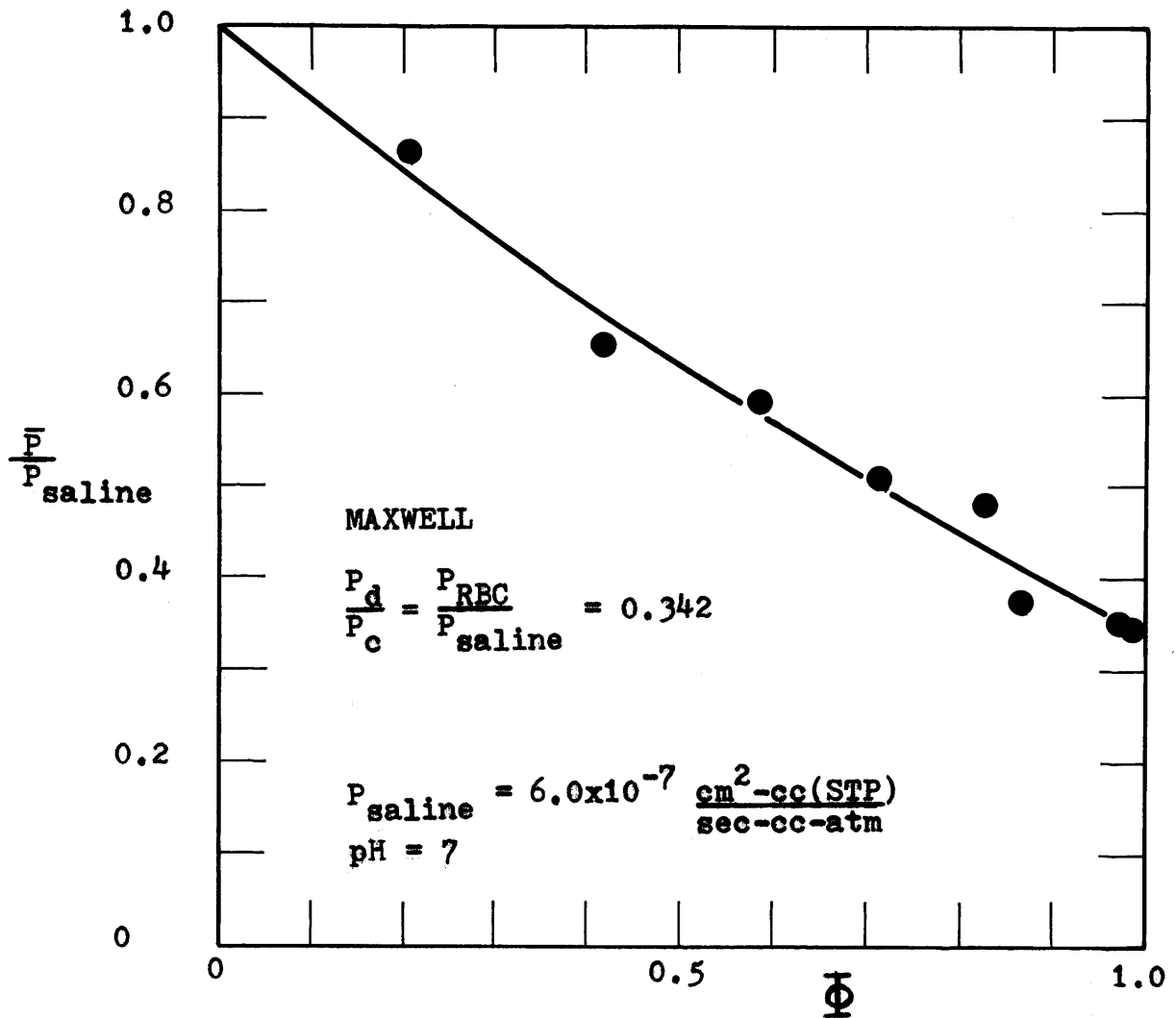


FIGURE 7.17

OXYGEN PERMEATION THROUGH INERT RED BLOOD CELL
SUSPENSIONS AT 25°C.

resistance is not significant (Kreuzer and Yahr, 1960; Kutchai and Staub, 1969; Stein et al., 1971).

At this point it is of interest to compare the data obtained by Hershey and Karhan (1968) on oxygen diffusion in red blood cells suspended in plasma with Maxwell's equation. Hershey and Karhan reported an oxygen diffusivity of 1.98×10^{-5} cm^2/sec in plasma. From Table 3.3 the oxygen solubility coefficient in plasma has a value of $.0257 \text{ cc(STP)/cc/atm}$ so that the permeability of oxygen in plasma is 5.10×10^{-7} $\frac{\text{cm}^2\text{-cc(STP)}}{\text{sec-cc-atm}}$. The oxygen permeability of the red blood cell is 2.05×10^{-7} . The dispersed phase to continuous phase ratio is therefore 0.402. Figure 7.17 compares Hershey and Karhan's data with Maxwell's equation. The data scatters above the theoretical line. The dashed line is equivalent to equation (3.44) after converting diffusivities into permeabilities by multiplication of the appropriate solubility (Table 3.3). For a volume fraction of 0.45 the Hershey and Karhan correlation predicts permeabilities approximately 20 per cent higher than that given by Maxwell's equation. It should be recognized that Hershey and Karhan's data is for sheep's blood not human blood, but the dispersed phase permeability would have to be as much as 50 per cent higher if the data is to correlate with Maxwell's equation ($K_d \cong 0.6$). Since it is unlikely that the oxygen permeability in sheep's red blood cells is that much larger than that in human red blood cells, a possible explanation of the high data is sedimentation of the red blood cells which in Hershey and Karhan's experimental system was in the direction of oxygen transport (see discussion

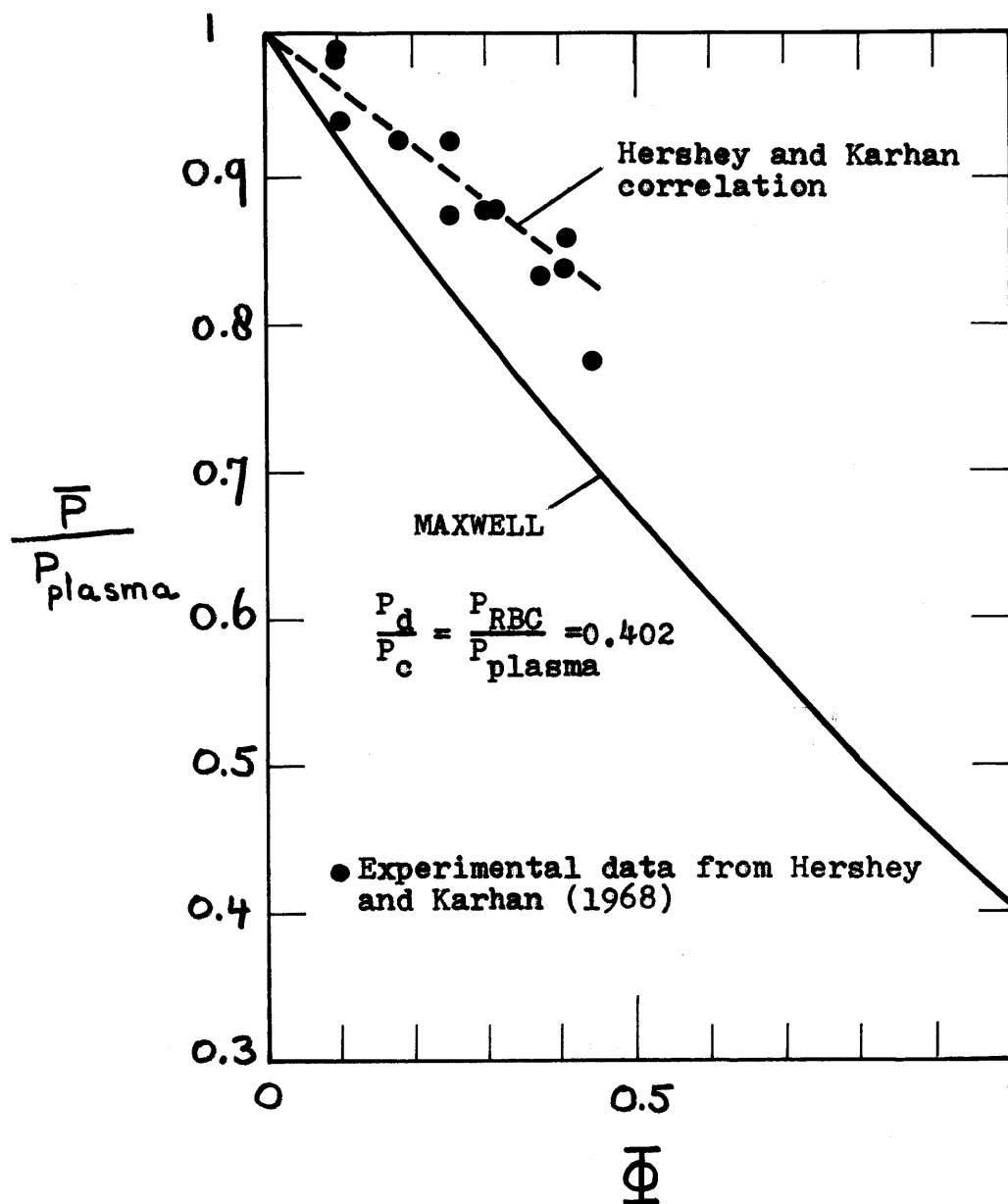


FIGURE 7.18

COMPARISON OF HERSHEY AND KARHAN'S DATA (RBC IN PLASMA) WITH MAXWELL'S EQUATION.

in Section 3.3.2.1). In this work the liquid film was in a vertical position so that red blood cell sedimentation was normal to oxygen transport and therefore should have considerably less effect on the mass transfer rate. This was confirmed by experiment (both on the emulsion systems and the red blood cell suspension) where in certain cases some phase separation occurred but where no increase of the mass transfer rate was observed. For the red blood cell suspensions some phase separation due to sedimentation occurred only for volume fractions below 0.45 (separated phase height less than 1/9 of total height). For concentrated volume fractions little sedimentation should occur as the red blood cells are in physical contact with each other and interfere with each others motions. It should be noted here that for the red blood cell suspensions in saline no rouleaux formation (stacking of individual red blood cells) was observed by microscopic examination both before and after experiments.

7.3.3.2 Reactive Red Blood Cell Suspension

Oxygen permeabilities of red blood cell suspensions were measured for cases in which the downstream oxygen partial pressure was low. Experiments were conducted at 25°C, and the pH of the red blood cell suspension in saline was near 7. Experiments were also conducted at 37°C with physiological driving force conditions. For the experiments at 25°C, runs were performed at three different driving force conditions as reported in Table 7.7. These conditions were such that large

TABLE 7.7

AVERAGE EFFECTIVE PERMEABILITIES OF OXYGEN IN REACTIVE RED
BLOOD CELL SUSPENSION FOR THREE DIFFERENT DRIVING
FORCE CONDITIONS

ϕ	$\bar{P}_{AVE} \times 10^7$ <u>cm²-cc (STP)</u> <u>sec-cc-atm</u>	$\frac{\bar{P}_{AVE}}{P_{saline}}$
$p_{O_2}^{x=0} = 24.3, p_{O_2}^{x=L} = 2.0$ mm Hg		
0.384	6.28	1.05
0.536	5.96	0.995
0.732	6.29	1.05
$p_{O_2}^{x=0} = 50.0, p_{O_2}^{x=L} = 3.3$ mm Hg		
0.210	5.83	0.972
0.387	5.02	0.837
0.492	5.01	0.836
0.785	4.42	0.737
0.852	4.39	0.731
0.911	4.57	0.762
0.916	4.40	0.733
0.920	4.02	0.670
$p_{O_2}^{x=0} = 89.7, p_{O_2}^{x=L} = 4.8$ mm Hg		
0.225	5.45	0.908
0.394	4.68	0.781
0.518	4.45	0.742
0.765	3.77	0.629
0.908	4.00	0.667
0.909	3.96	0.660
0.932	3.21	0.535
0.941	4.08	0.680
0.963	3.66	0.610

saturation differences should exist across the film.

The red blood cell suspensions were prepared as described in Chapter 6. Hemolysis encountered at the termination of the oxygen permeation experiments was usually one per cent or less of the initial volume fraction of red blood cells. Saturation curves and p_{50} 's were measured utilizing the techniques described in Chapter 6. All experimental results are tabulated in Appendix D. Additional details about the experiments will be given in the next section.

Figures 7.19a,b, 7.20a,b, and 7.21a,b give a comparison of the experimental results tabulated in Table 7.7 with theoretical curves predicted by the one-step model. The hemoglobin diffusivity in Figures 7.19a, 7.20a, and 7.21a is $7.0 \times 10^{-8} \text{ cm}^2/\text{sec}$ and is consistent with Kreuzer's compromise curve. The hemoglobin diffusivity in Figures 7.19b, 7.20b, and 7.21b is $6.0 \times 10^{-8} \text{ cm}^2/\text{sec}$ and is given as a comparison. The other physical parameters employed here are consistent either with experimental data reported in earlier sections or with values reported previously in the literature. These are tabulated in Table 7.8. The backward reaction rate (k_2') was chosen such that the hyperbolic saturation curve would give the same p_{50} as that measured experimentally (the base case). Inspection of Figures 7.19a, 7.20a, and 7.21a or Table 7.7 indicates that, for the reported conditions, oxygen transport is facilitated in red blood cell suspensions. For sufficiently low driving forces the average effective permeability becomes greater than the permeability of the continuous phase. The

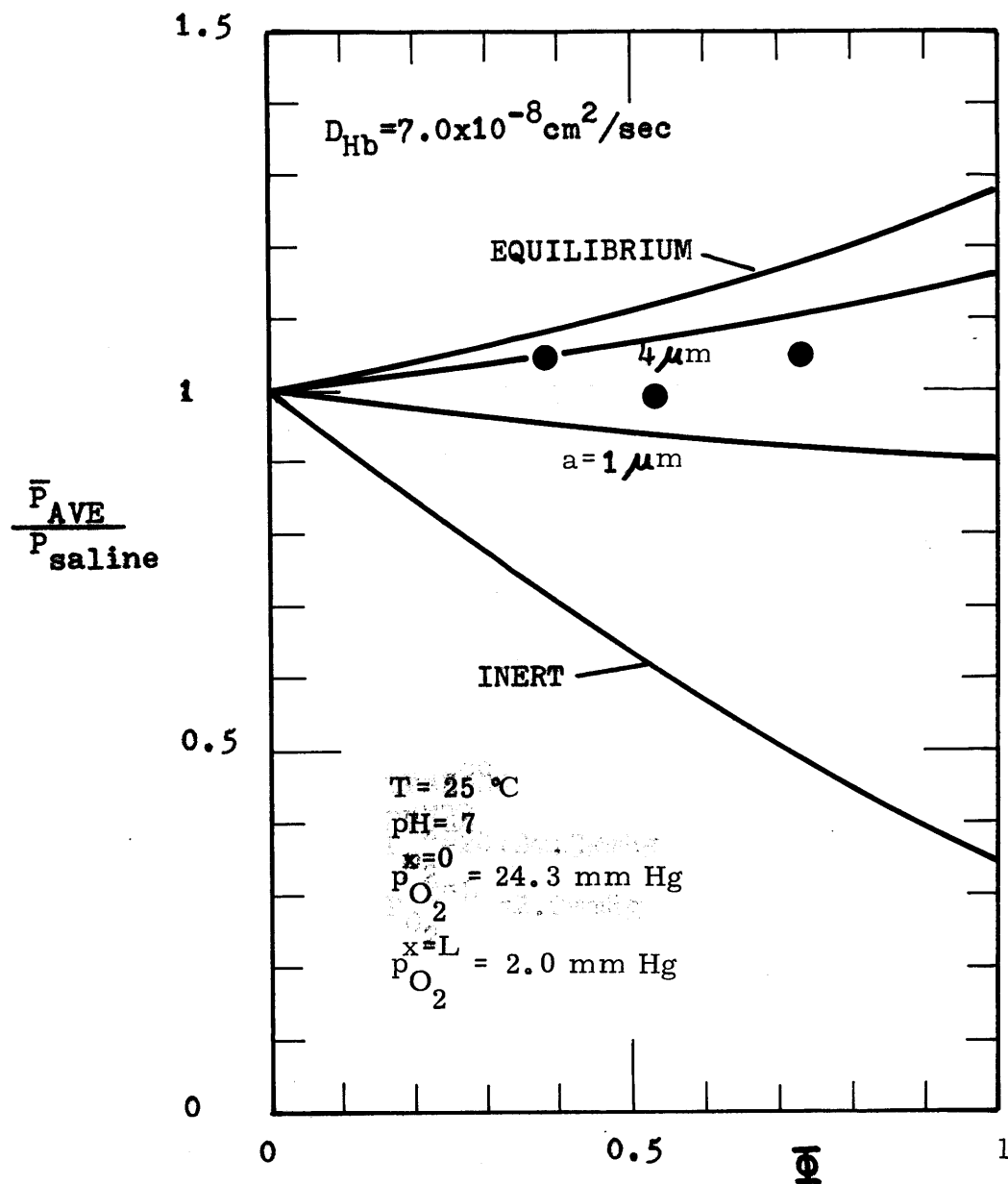


FIGURE 7.19a
 AVERAGE EFFECTIVE OXYGEN PERMEABILITY
 IN REACTIVE RED BLOOD CELL SUSPENSIONS
 FOR CONDITIONS AS SHOWN. COMPARISON
 WITH ONE STEP MODEL. ($D_{Hb} = 7.0 \times 10^{-8} \text{ cm}^2/\text{sec}$)

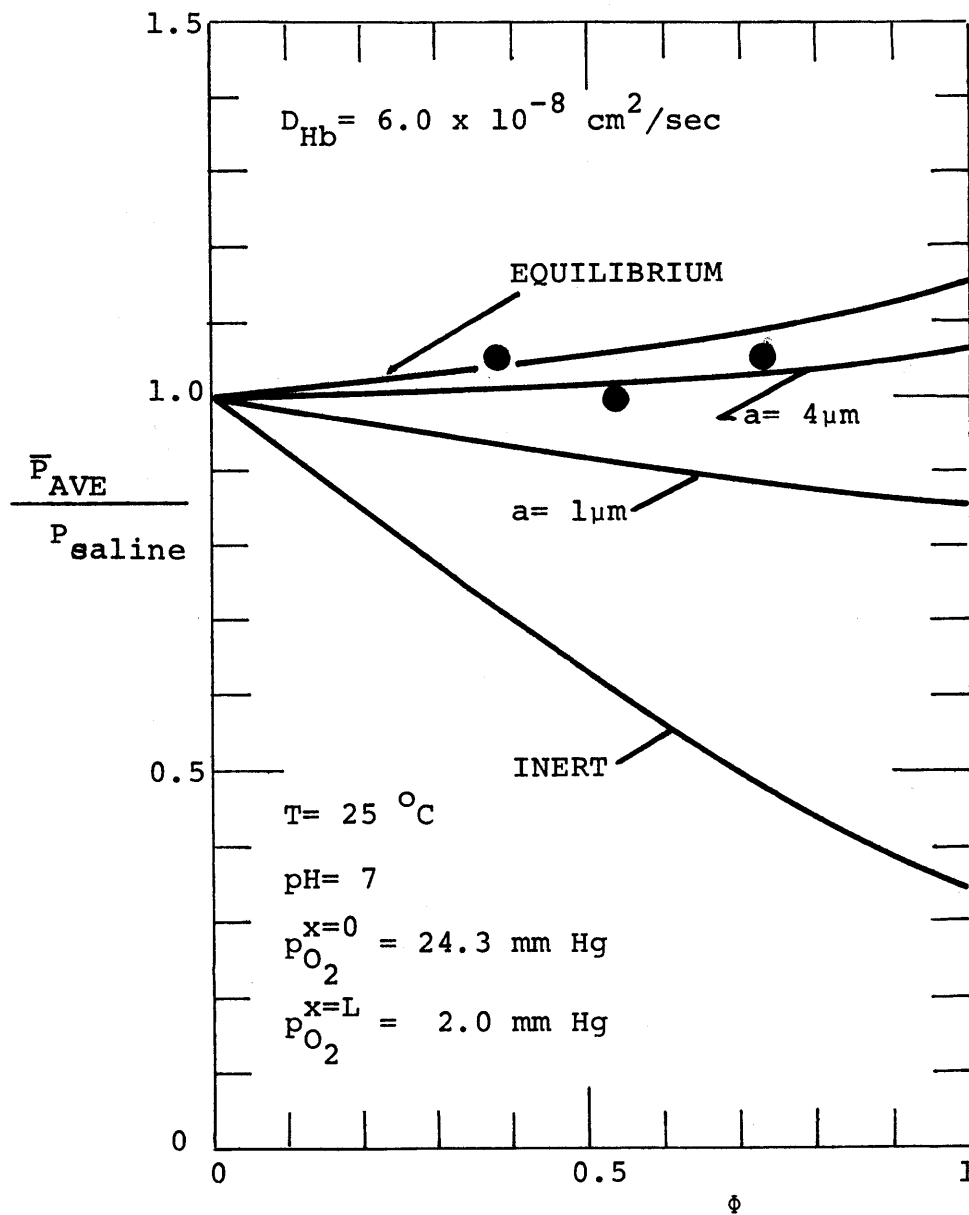


FIGURE 7.19b

AVERAGE EFFECTIVE OXYGEN PERMEABILITY IN REACTIVE RED BLOOD CELL SUSPENSIONS FOR CONDITIONS AS SHOWN. COMPARISONS WITH ONE-STEP MODEL. ($D_{Hb} = 6 \times 10^{-8} \text{ cm}^2/\text{sec}$)

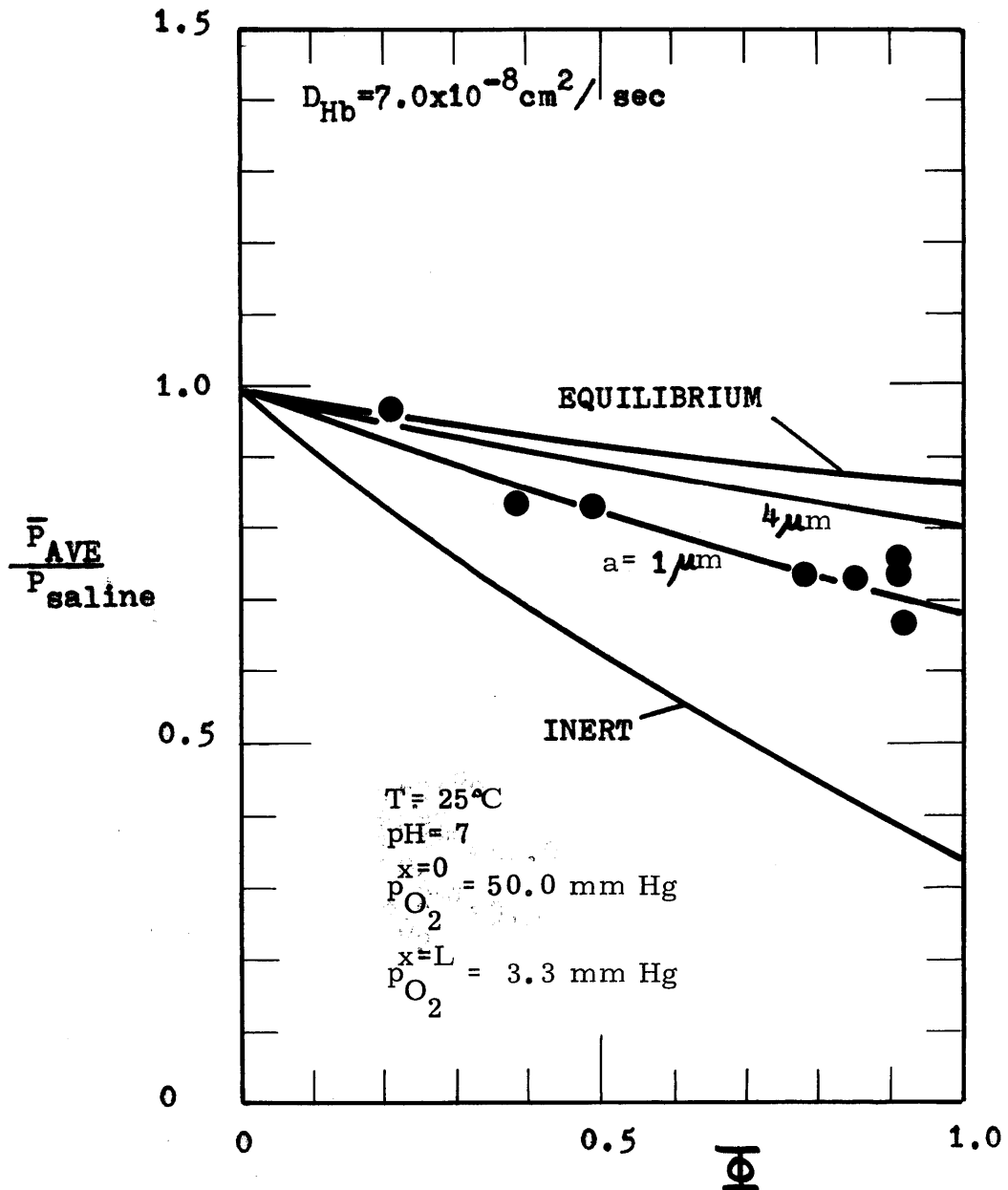


FIGURE 7.20a
 AVERAGE EFFECTIVE OXYGEN PERMEABILITY
 IN REACTIVE RED BLOOD CELL SUSPENSIONS
 FOR CONDITIONS AS SHOWN. COMPARISON
 WITH ONE STEP MODEL. ($D_{Hb} = 7 \times 10^{-8} \text{ cm}^2 / \text{sec}$)

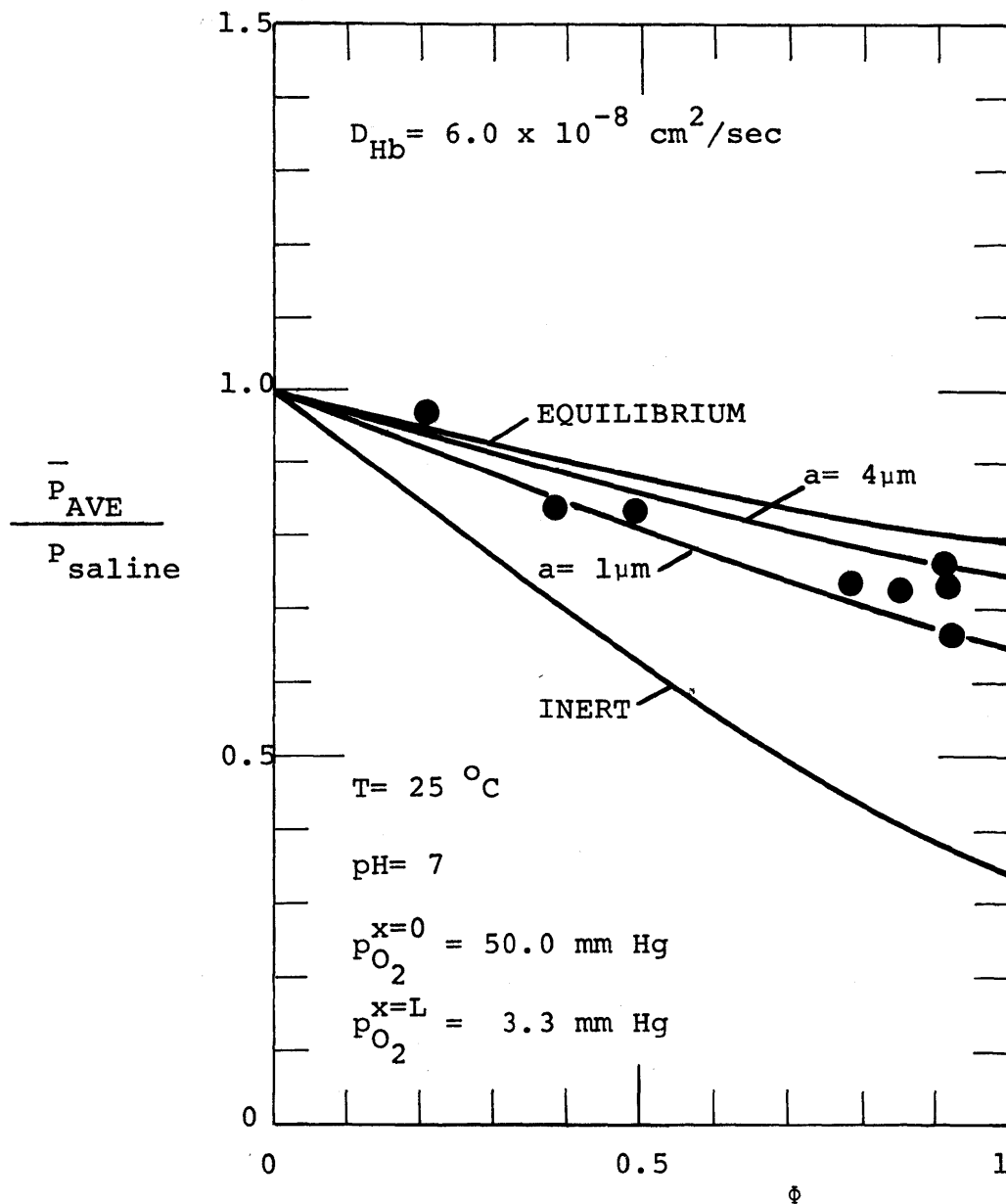


FIGURE 7.20b

AVERAGE EFFECTIVE OXYGEN PERMEABILITY IN REACTIVE RED BLOOD CELL SUSPENSIONS FOR CONDITIONS AS SHOWN. COMPARISON WITH ONE-STEP MODEL. ($D_{Hb} = 6 \times 10^{-8} \text{ cm}^2/\text{sec}$)

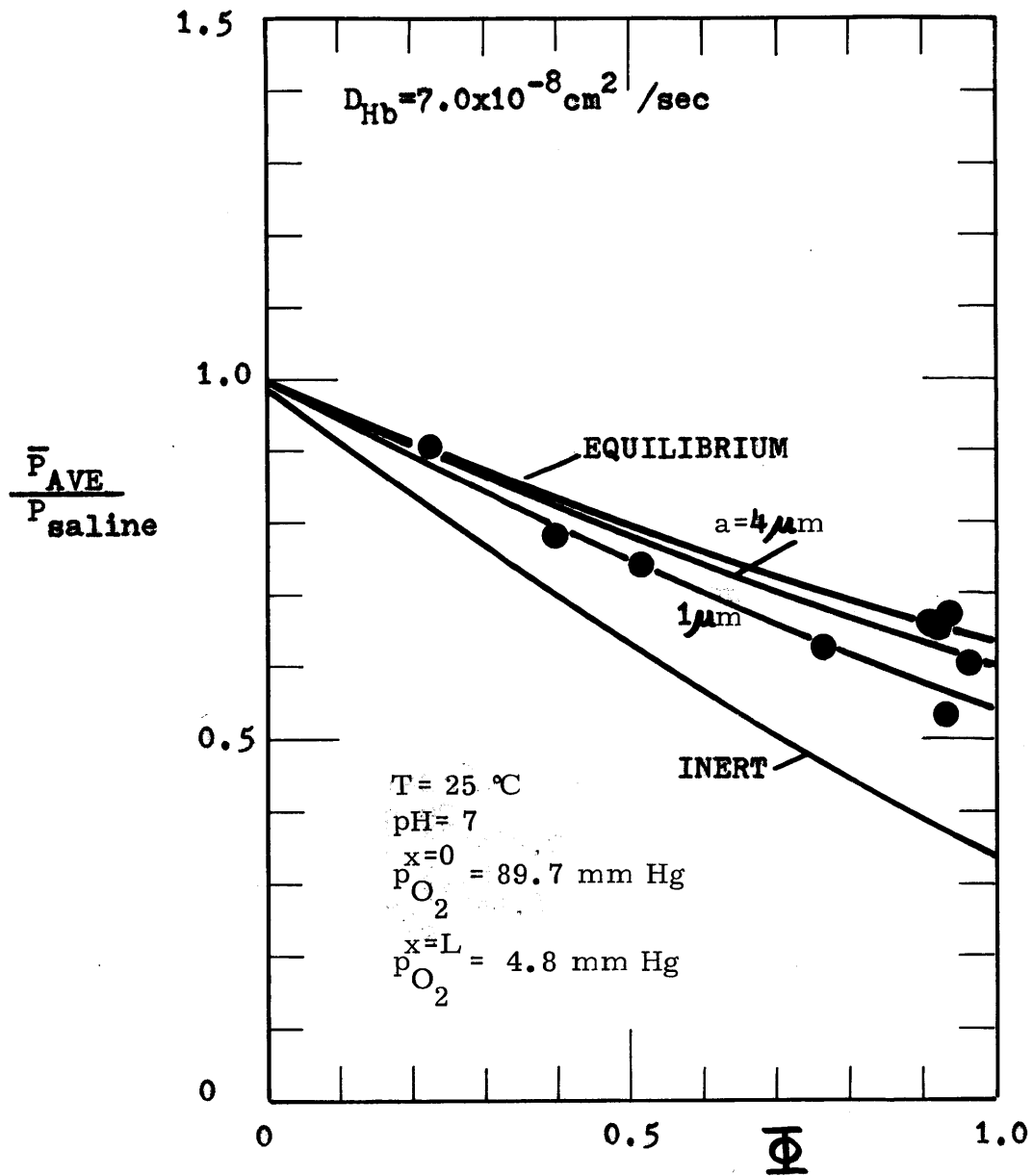


FIGURE 7.21a
 AVERAGE EFFECTIVE OXYGEN PERMEABILITY
 IN REACTIVE RED BLOOD CELL SUSPENSIONS
 FOR CONDITIONS AS SHOWN. COMPARISON
 WITH ONE STEP MODEL. ($D_{Hb} = 7 \times 10^{-8} \text{ cm}^2 / \text{sec}$)

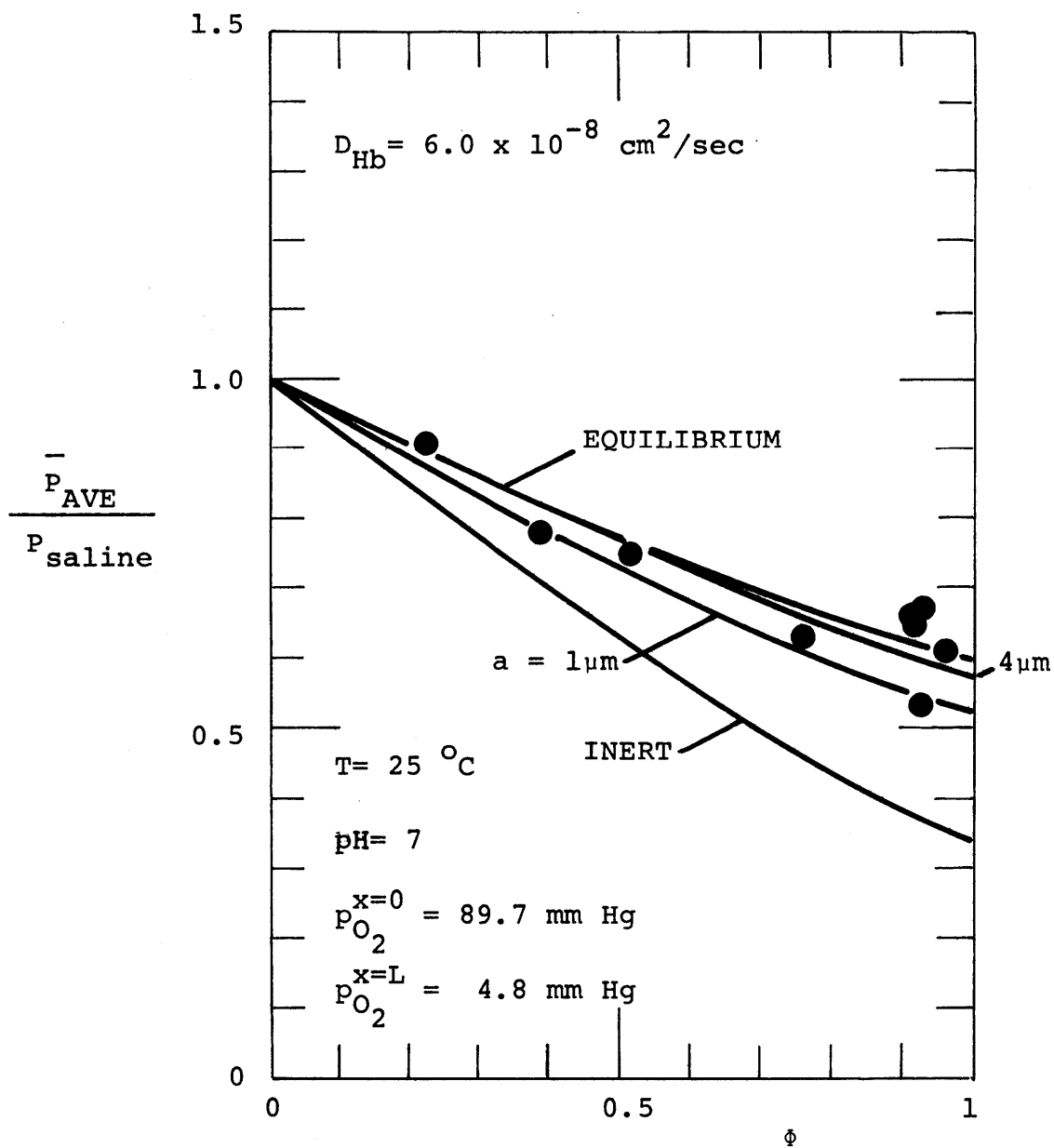


FIGURE 7.21b

AVERAGE EFFECTIVE PERMEABILITY FOR OXYGEN IN REACTIVE RED BLOOD CELL SUSPENSIONS FOR CONDITIONS AS SHOWN. COMPARISON WITH ONE-STEP MODEL. ($D_{Hb} = 6 \times 10^{-8} \text{ cm}^2/\text{sec}$)

TABLE 7.8
PARAMETERS USED IN THEORETICAL CALCULATIONS

$$P_c = P_{\text{saline}} = 6.00 \times 10^{-7} \frac{\text{cm}^2\text{-cc(STP)}}{\text{sec-cc-atm}}, \text{ from Figure 7.14}$$

$$P_d = P_{\text{RBC}} = 2.05 \times 10^{-7} \frac{\text{cm}^2\text{-cc(STP)}}{\text{sec-cc-atm}}, \text{ from Figure 7.14}$$

$$\alpha'_{\text{O}_2} = .02718 \frac{\text{cc(STP)}}{\text{cc-atm}}, \text{ from Table 3.3}$$

$$C_{\text{T,Heme}}' = .02045 \text{ moles/liter}$$

$$C_{\text{T}} = .00509 \text{ moles/liter}$$

KINETIC RATE PARAMETERS

One-step Model:

$$k_1' = 3.0 \times 10^6 \text{ l/mole/sec}$$

$$k_2' = 68.5 \text{ sec}^{-1}$$

Four-step Model:

$$k_1 = 1.77 \times 10^6 \quad \text{liter/mole/sec}$$

$$b_1 = 2280 \quad \text{sec}^{-1}$$

$$k_2 = 3.32 \times 10^6 \quad \text{liter/mole/sec}$$

$$b_2 = 190 \quad \text{sec}^{-1}$$

$$k_3 = 4.89 \times 10^6 \quad \text{liter/mole/sec}$$

$$b_3 = 647 \quad \text{sec}^{-1}$$

$$k_4 = 3.30 \times 10^6 \quad \text{liter/mole/sec}$$

$$b_4 = 60 \quad \text{sec}^{-1}$$

experimental results scatter between the minimum red blood cell radius, which is 1 μm , and the maximum radius, which is 4 μm , in comparison with the theoretical results, if a hemoglobin diffusivity of $7.0 \times 10^7 \text{ cm}^2/\text{sec}$ is used. The inert line is the theoretical result for very small radii ($a \gg 1 \mu\text{m}$) or for inactive hemoglobin. This curve is of course identical to that shown in Figure 7.17, and is equivalent to Maxwell's equation.

The data was also compared with theoretical calculations employing hemoglobin diffusivities consistent with the maximum and minimum values of the reported hemoglobin diffusivities at the hemoglobin concentration inside the red blood cell of 33 gr/100 ml. This concentration is consistent with experimentally measured values (in this work) to within ± 1 gr/100 ml. From the data of Keller et al. (1971) the maximum plausible diffusivity is approximately

$$D_{\text{Hb}} = 1.5 \times 10^{-7} \text{ cm}^2/\text{sec}$$

and from the data of Adams and Fatt (1967) the minimum value is

$$D_{\text{Hb}} = 3.0 \times 10^{-8} \text{ cm}^2/\text{sec}$$

As an example Figures 7.22 and 7.23 compare the data for the driving force conditions

$$p_{\text{O}_2}^{x=0} = 50 \text{ mm Hg}, p_{\text{O}_2}^{x=L} = 3.3 \text{ mm Hg}$$

For the one-step model neither of these particular diffusivity values correlate with the data, assuming that the latter should fall in the 1 μm to 4 μm range. The same conclusion was drawn

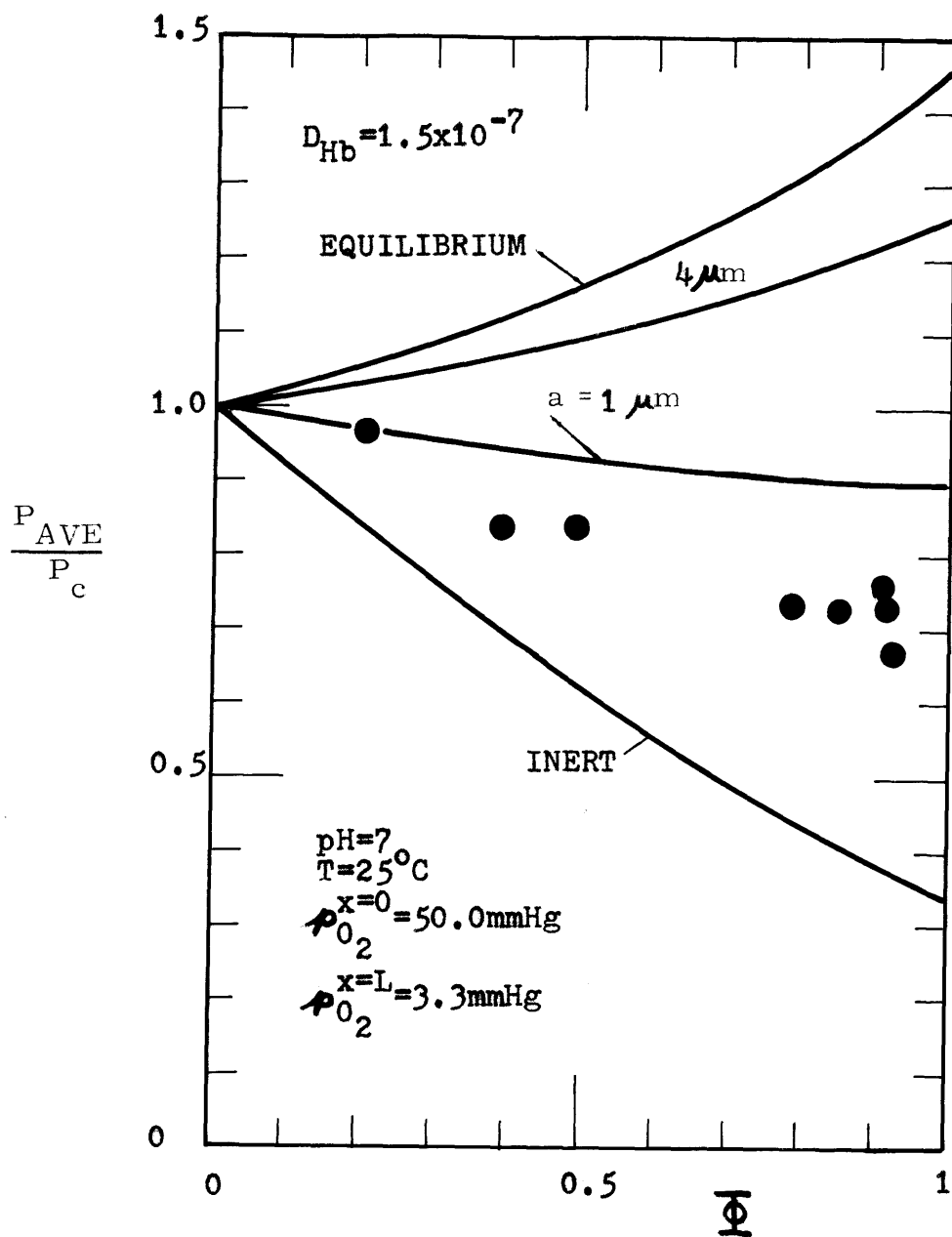


FIGURE 7.22
 COMPARISON OF EXPERIMENTAL DATA AND ONE-
 STEP MODEL WITH
 $D_{Hb} = 1.5 \times 10^{-7} \text{ cm}^2/\text{sec}$

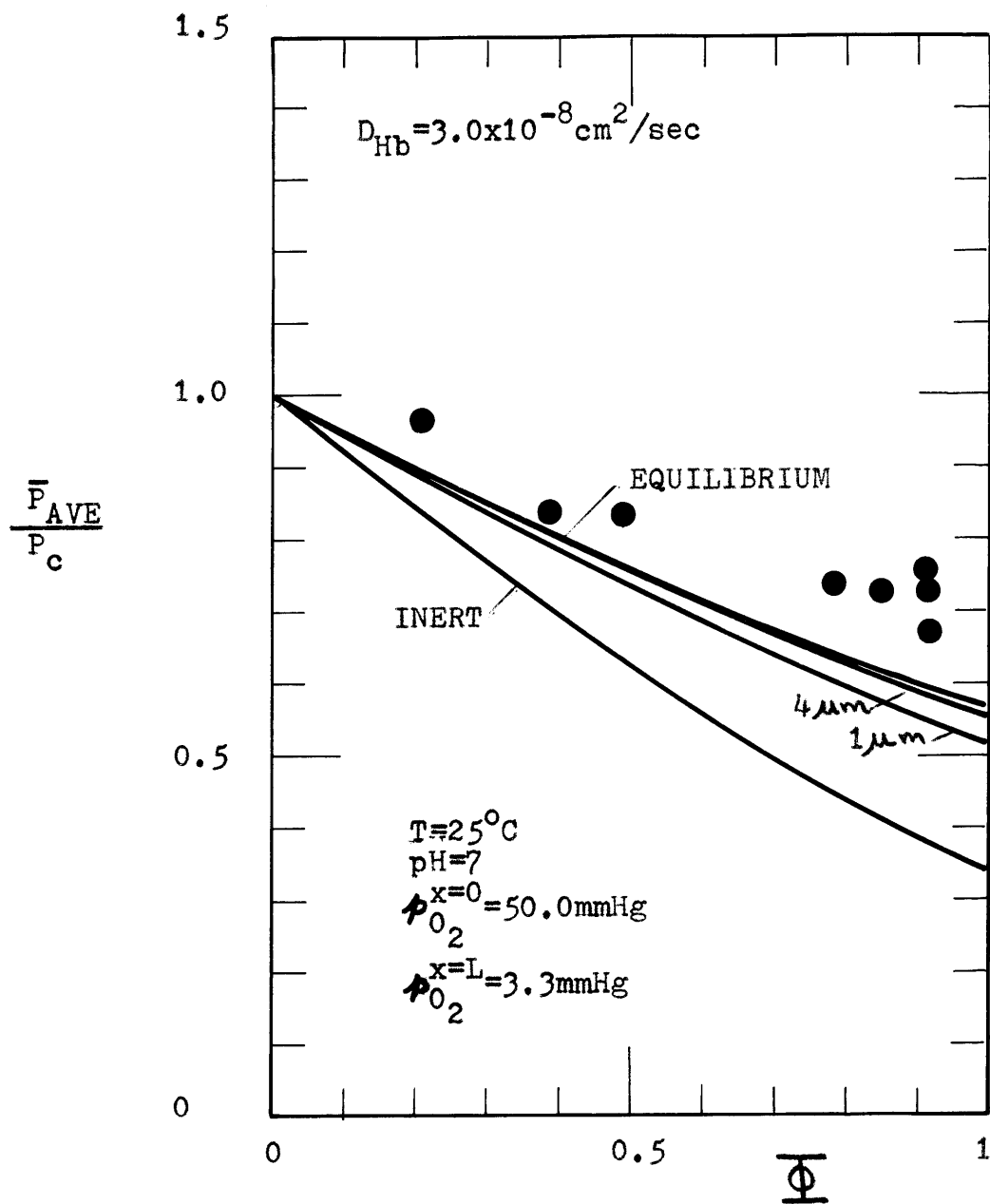


FIGURE 7.23
 COMPARISON OF EXPERIMENTAL DATA AND
 ONE-STEP MODEL WITH

$D_{Hb} = 3.0 \times 10^{-8} \text{ cm}^2/\text{sec}$

for the other two driving force conditions. Since the one-step model is expected to underestimate \bar{P}_{AVE} to some extent, it appears that an appropriate fit between data and the one-step theory is a hemoglobin diffusivity of order 7.0×10^{-7} or somewhat smaller (see Discussion in Section 5.1.3).

Saturation measurements on all of the samples used for permeation experiments are reported in Figure 7.24. It appears that the red blood cell preparation procedure, as described, insured reasonable consistency of the equilibrium saturation behaviour of the red blood cell suspensions.

It would be of interest to compare the four-step model with the experimental data. However, no Adair kinetic rate parameters have been reported for the conditions of these experiments. The data reported by Gibson (1970) for hemoglobin solutions at $T = 21.5^{\circ}\text{C}$, $\text{pH} = 7$, and physiological 2,3 DPG is sufficiently similar to conditions in this work that one might be tempted to use those parameters for comparison. Unfortunately, these parameters predict a p_{50} of approximately 10 mm Hg which is inconsistent with the p_{50} in Figure 7.24 (which is approximately 13.5 mm Hg). Gibson states that the accuracy of the numerical values of the kinetic parameters is approximately ± 20 per cent. By increasing all reverse rate constants by 20 per cent and leaving the forward rates unchanged a saturation curve is obtained which has a p_{50} of about 13 mm and gives a reasonable fit of the data as is shown in Figure 7.24 (ignoring the 3.5°C increase). Utilizing these particular values, reasonable agreement between the experimental

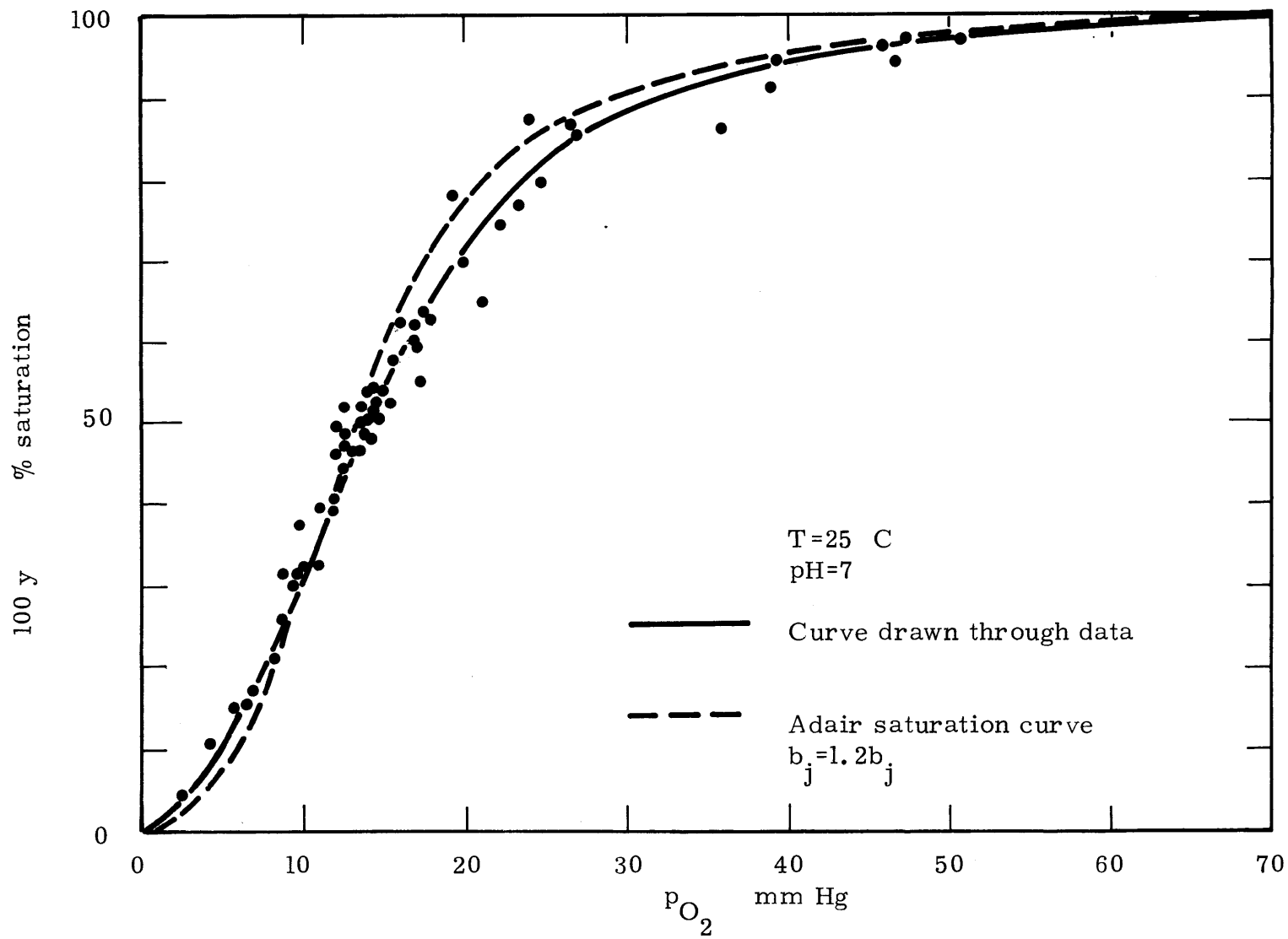


FIGURE 7.24
 SATURATION CURVE FOR RED BLOOD CELL SUSPENSIONS -

data and the four-step model was obtained for a hemoglobin diffusivity of $D_B = 6.0 \times 10^{-8} \text{ cm}^2/\text{sec}$ as is shown in Figures 7.25, 7.26, and 7.27. If the assumptions made in regards to the parameters employed in these calculations are justified, it appears that the hemoglobin diffusivity in red blood cells is in the lower range of experimentally reported values. At this point, an exact value of the hemoglobin diffusivity inside the red blood cell must await precise experimental measurement.

The driving forces employed in the experiments with reactive red blood cell suspensions were chosen to give maximum saturation differences. Under actual physiological conditions, or in the operation of artificial oxygenators the oxygen partial pressures are such that the blood is nearly fully saturated. Since the facilitation factor is dependent on the slope of the saturation curve, facilitation effects will be reduced if conditions are such that one "operates on the top of the saturation curve." Typically, in an artificial oxygenator such as a membrane oxygenator, the reduced blood would flow into the device at a p_{O_2} near 45 mm Hg. It would then be contacted with pure oxygen at one atmosphere pressure. From Figure B.3, which shows the oxygen-hemoglobin saturation curve at physiological conditions, the hemoglobin saturation change for the above conditions would be from approximately 75 to 100 per cent saturation.

This saturation change is considerably less than that encountered in the experimental work in this thesis, and as a consequence the amount of facilitated transport should be

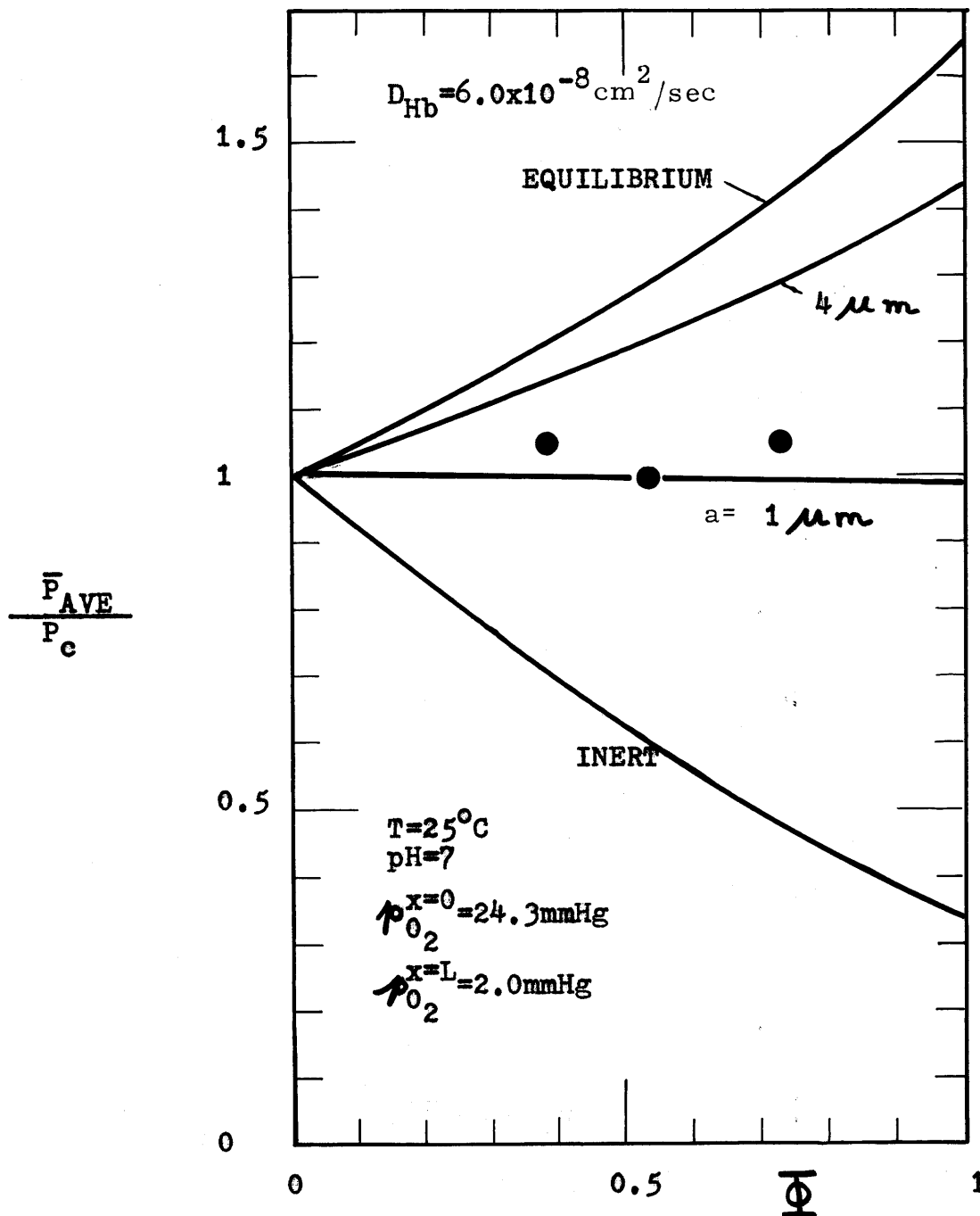


FIGURE 7.25
 COMPARISON OF EXPERIMENTAL DATA AND
 FOUR-STEP MODEL WITH
 $D_{Hb} = 6.0 \times 10^{-8} \text{ cm}^2/\text{sec}$

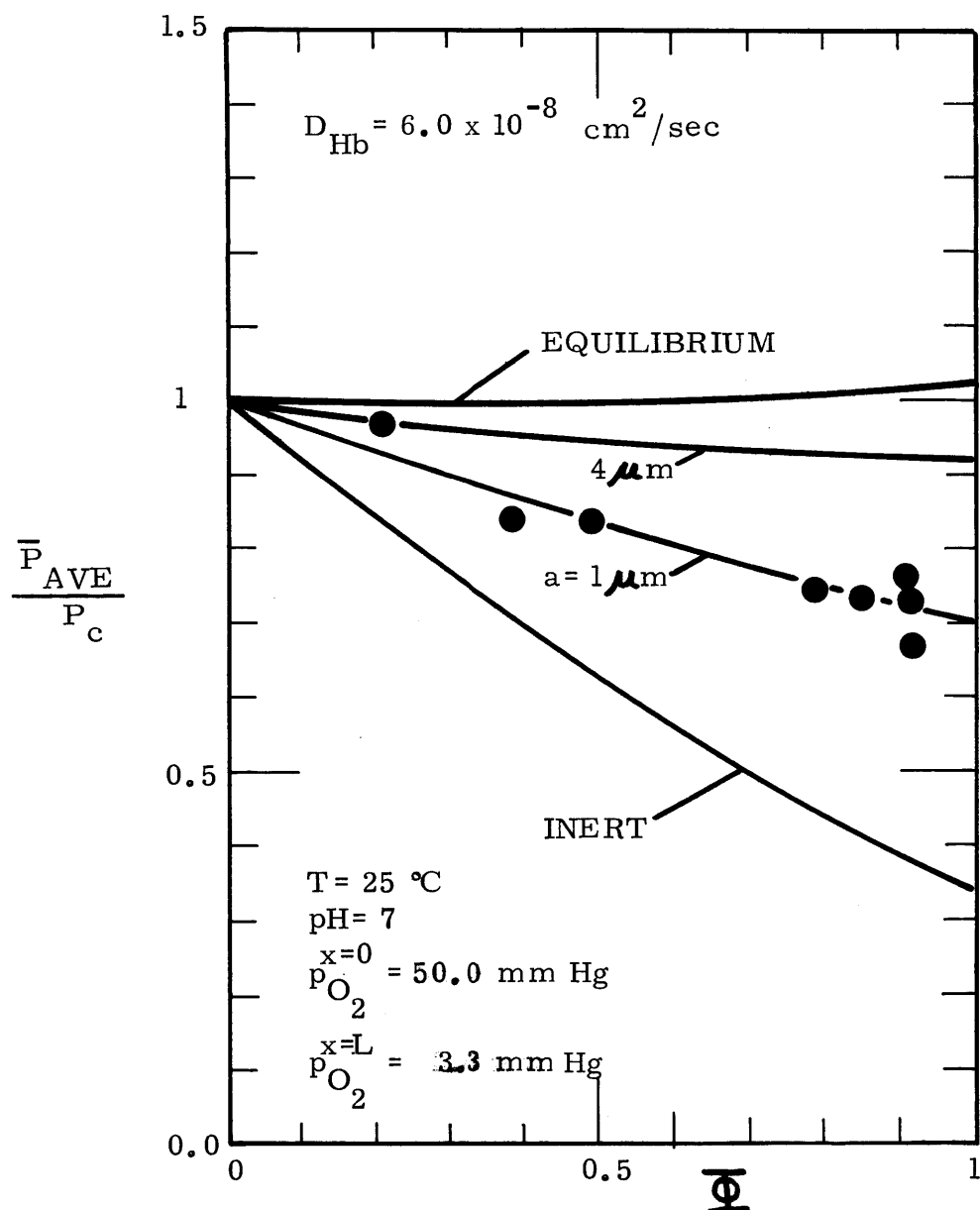


FIGURE 7.26
 COMPARISON OF EXPERIMENTAL DATA AND
 FOUR-STEP MODEL WITH

$$D_{Hb} = 6.0 \times 10^{-8} \text{ cm}^2/\text{sec}$$

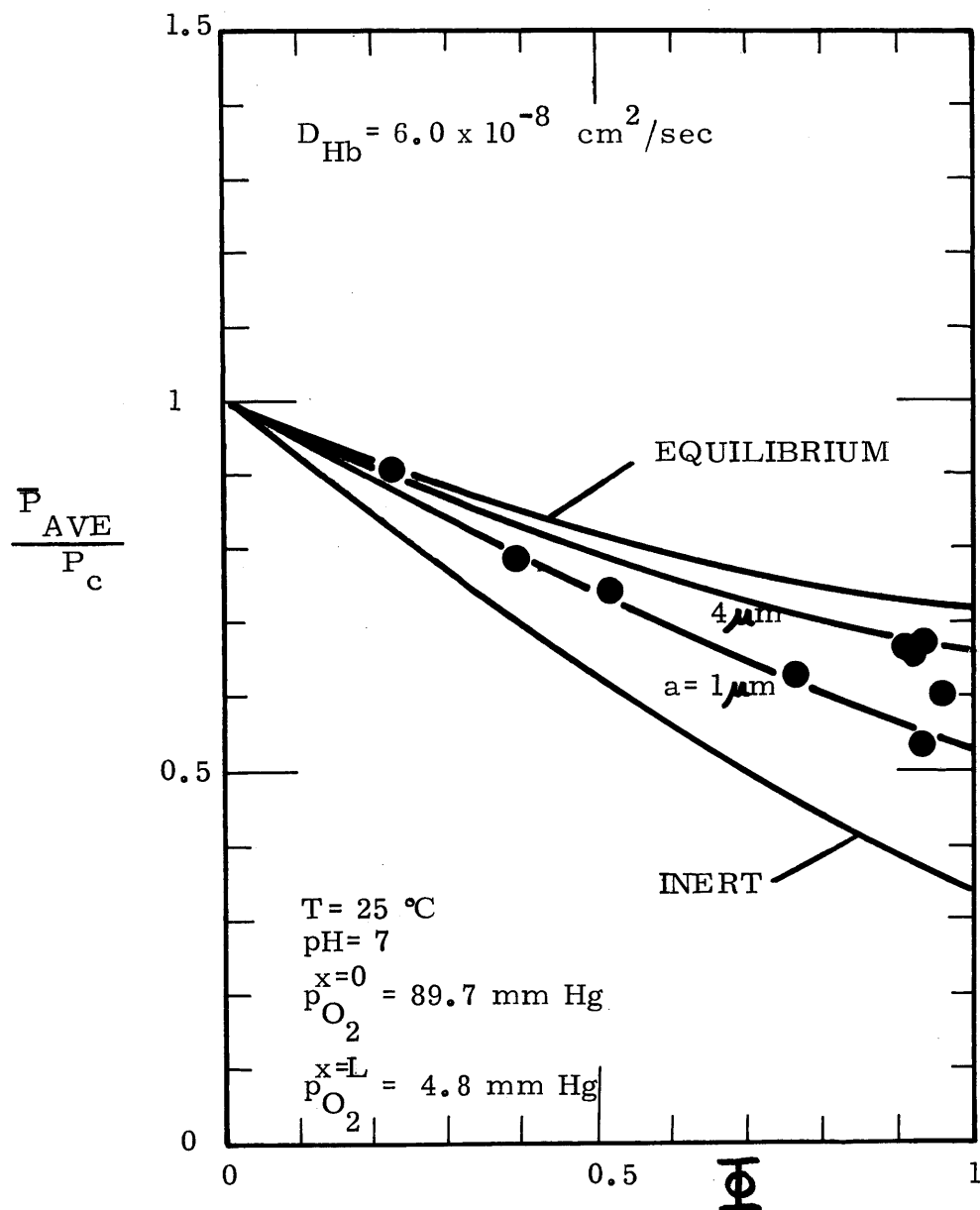


FIGURE 7.27
 COMPARISON OF EXPERIMENTAL DATA AND
 FOUR-STEP MODEL WITH

$$D_{Hb} = 6.0 \times 10^{-8} \text{ cm}^2/\text{sec}$$

considerably less. In fact, from theory presented here, it would appear that hemoglobin facilitated transport is only a fraction of total oxygen transport in an artificial oxygenator. In the human lungs p_{O_2} changes are encountered from about 100 mm Hg to 45 mm Hg. It would appear that hemoglobin facilitated transport in the lungs is not the major transport mechanism. It should be pointed out however that the theory developed here is good for steady state transport in films thick enough that red blood cell dimensions are much smaller than the characteristic dimension of the film. Oxygen transport in the lungs and tissues is an unsteady state process which occurs in thin capillaries of the same thickness of the red blood cell. Therefore one must be careful in applying the derived model to these systems. However the theory can be used to give an educated quantitative guess of the amount of facilitated transport in an artificial oxygenator. Here, blood films are encountered which are substantially thicker than those in the body, so that the blood can be treated as a homogeneous fluid.

In order to measure the amount of facilitation for physiological driving force conditions, two experiments were carried out at 37°C with a volume fraction of red cells of 0.45. In one experiment, the hemoglobin inside the red blood cell was inactivated by introduction of 20 mm Hg of carbon monoxide. In the second experiment the hemoglobin was active. The driving forces were: upstream oxygen partial pressure of 100 mm Hg, and a downstream pressure of 35 mm Hg. The physiological conditions of a temperature of 37°C, a pH of 7.4

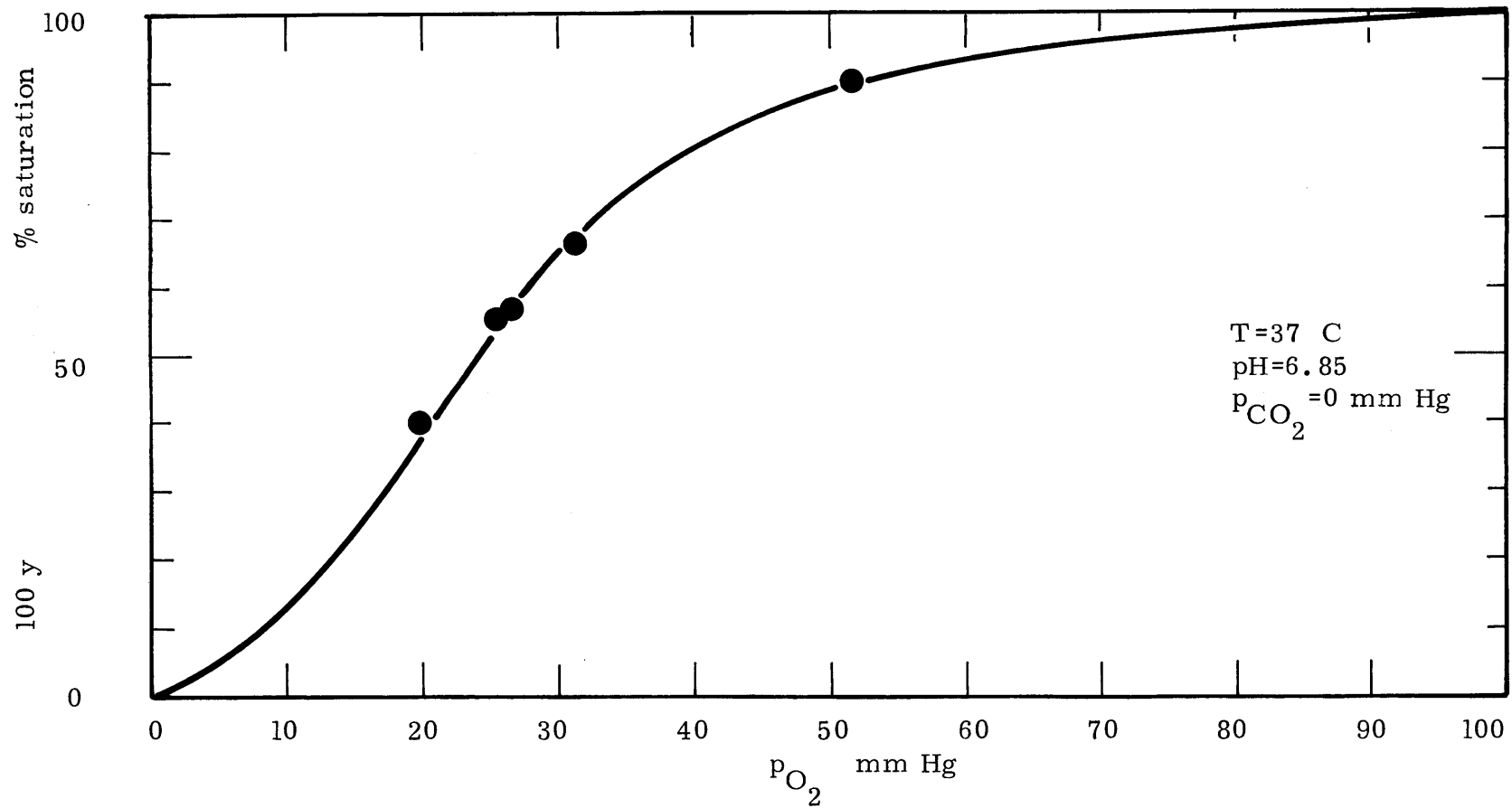


FIGURE 7.28
HEMOGLOBIN SATURATION CURVE FOR RED BLOOD CELL SUSPENSIONS AT CONDITIONS SHOWN

and a pressure of about 40 mm Hg give a p_{50} of about 26.5 mm Hg. For a pH of 6.85 at 37°C the p_{50} is approximately 25 mm Hg as shown in Figure 7.28. For the driving force conditions chosen, the saturation differences would be 25% across the film for equilibrium conditions. These were the conditions employed for the two runs. For the inert run the permeability measured was

$$\bar{P} = 3.85 \times 10^{-7} \frac{\text{cm}^2\text{-cc (STP)}}{\text{sec-cc-atm}}$$

at a volume fraction of

$$\phi = 0.45$$

This can be compared with an effective permeability at 25°C of

$$\bar{P} = 3.99 \times 10^{-7} \frac{\text{cm}^2\text{-cc (STP)}}{\text{sec-cc-atm}}$$

which can be obtained from Figure 7.17 (for a volume fraction of $\phi = 0.45$). The change in temperature affects the permeability little because, while the diffusivity increases, the solubility decreases as temperature increases. For the run with the reactive red blood suspension the average effective permeability was

$$\bar{P}_{\text{AVE}} = 4.05 \times 10^{-7} \frac{\text{cm}^2\text{-cc (STP)}}{\text{sec-cc-atm}}$$

for a volume fraction 0.45. Compared with the inert run the permeability is only 5.2% above that of the inert run.

In order to make a comparison between theory and the two data points, one needs to know the necessary physical parameters at 37°C. From the permeability data on water,

hemoglobin solutions, and the red blood cell suspension versus temperature it can be assumed that P_{saline} and P_{RBC} remain virtually unchanged. From Bauer's work (1971) the forward reaction rate is

$$k_1' = 5.0 \times 10^6 \text{ l/mole/sec}$$

and choosing the p_{50} as a match between the hyperbolic saturation curve and the sigmoidal curve presented in Figure 7.28 it follows that the backward reaction rate constant is

$$k_2' = 163.5 \text{ sec}^{-1}$$

The oxygen solubility in the dispersed phase is (from Table 3.3)

$$\alpha_{\text{O}_2}' = .02273 \frac{\text{cc (STP)}}{\text{cc-atm}}$$

Taking the hemoglobin diffusivity at 37°C to be approximately

$$D_{\text{Hb}}' = 7.0 \times 10^{-8} \text{ cm}^2/\text{sec}$$

than theoretical predictions can be made for the driving forces

$$p_{\text{O}_2}^{x=0} = 100 \text{ mm Hg}$$

$$p_{\text{O}_2}^{x=L} = 35 \text{ mm Hg}$$

Figure 7.29 gives the theoretical curves predicted by the one-step model for the conditions shown. At a volume of $\phi = 0.45$ the predicted increase of the effective permeability over the inert permeability is about eight per cent for the $1 \mu\text{m}$ radius. This is in close agreement (within experimental error) with the experimentally measured increased indicating that at physiological

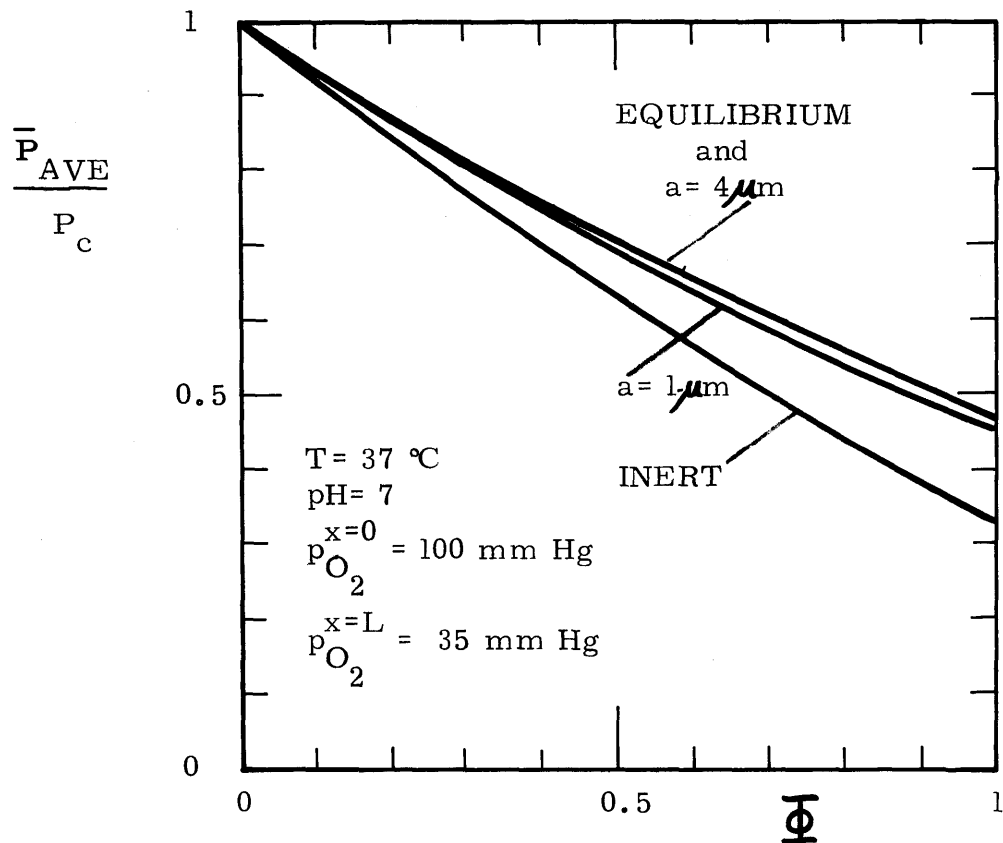


FIGURE 7.29
 AVERAGE EFFECTIVE PERMEABILITY RATIO
 FOR PHYSIOLOGICAL DRIVING FORCE CON-
 DITIONS

driving forces the facilitated flux contributes only a minor fraction of the total flux (if above mentioned restrictions are met). The above conclusion is consistent with the conclusion made by Schroeder and Holmquist (1968). Through approximate calculations, Schroeder and Holmquist compared the diffusive oxygen transport and the hemoglobin facilitated oxygen transport at normal physiological conditions and concluded that at those conditions "facilitated transport may contribute approximately 6 per cent of the total flux of oxygen into the erythrocyte." It has already been mentioned that one must be careful not to extend the theory for the average effective permeability to situations where the characteristic dimension is of the same order as the red blood cell radius. A reconsideration of the problem of a single sphere in an infinite medium would also predict low facilitation factors at physiological conditions (average p_{O_2} equal 70 mm Hg) as can be seen from Figure 5.8. It appears therefore that Schroeder and Holmquist's conclusion is probably correct. On the other hand, if indeed the contribution of facilitated flux is only a fraction of total flux, it does not mean that facilitated flux is not important. In the uptake of oxygen in the lungs six per cent may be important. Further in strenuous exercise, the p_{O_2} in muscle tissues may drop as low as 10 mm Hg, in which case facilitated transport would become very significant as saturation changes inside the red blood cell would occur in the steep portion of the saturation curve (where the facilitation factor is a maximum).

7.3.3.2.1 Details and Comments on the Oxygen Permeation Experiments on Reactive Red Blood Cell Suspensions

The liquid film thickness of the red blood cell suspensions in Figures 5.19a,b was 4.57 μm , and those in Figures 5.20a,b and 5.21a,b was 803 μm . The transient period in these experiments prior to the establishment of the steady state flux was from approximately a half to two hours depending on film thickness and red blood cell volume fraction. No anomalously high flux was observed during the unsteady state portion of the experiment. For the 457 μm thick films no sedimentation of the red blood cell phase was observed, indicating that wall effects reduces sedimentation. For the 803 μm thick films some phase separation occurred for volume fractions below $\phi = 0.45$, but at no time was the separated layer more than one-ninth of total liquid height.

Hemolysis was less than one per cent in the reported experiments. Hemolysis as defined here, is the per cent of red blood cells that lysed during the course of an experiment given by

$$\% \text{ Hemolysis} = 100 \frac{\phi_{\text{before}} - \phi_{\text{after}}}{\phi_{\text{before}}} \quad (7.7)$$

Hemolysis can affect the mass transport significantly. If red blood cells lyse, they will release the hemoglobin into the continuous saline phase. Although the presence of the hemoglobin may decrease the oxygen permeability in the continuous

phase, the hemoglobin will have a large diffusivity since total hemoglobin concentration will be low (true unless the volume fraction, $\phi = 1.0$). In addition, if indeed the oxygen-hemoglobin reaction is not at equilibrium inside the red blood cell, upon release into the continuous phase, the released hemoglobin would be at chemical equilibrium in the continuous phase. This then becomes a problem of reaction inside the dispersed phase and within the continuous phase and is compatible with the impermeable carrier model developed in Chapter 4. Figure 7.30 gives theoretical comparisons for the average effective permeability ratio obtained for zero per cent hemolysis (reaction inside the dispersed phase only) and three per cent hemolysis. Figure 7.31 gives the theoretical calculations for ten per cent hemolysis. The calculations were made by first computing the amount of hemoglobin in the continuous phase and the new volume fraction upon hemolysis. Second, the hemoglobin diffusivity in the continuous phase was determined through use of Kreuzer's compromise curve (see Figure 3.8), and third, the oxygen permeability in the continuous phase was determined from Figure 7.14. The calculated average effective relative permeability is plotted versus the initial volume fraction of red blood cells. The same parameters as listed in Table 7.8 were employed (for the dispersed phase), and the kinetic rate constants for the hemoglobin in the continuous phase were taken to be the same as those in the dispersed phase.

It is obvious from Figures 7.30 and 7.31 that small amounts of hemolysis can have a significant effect on the

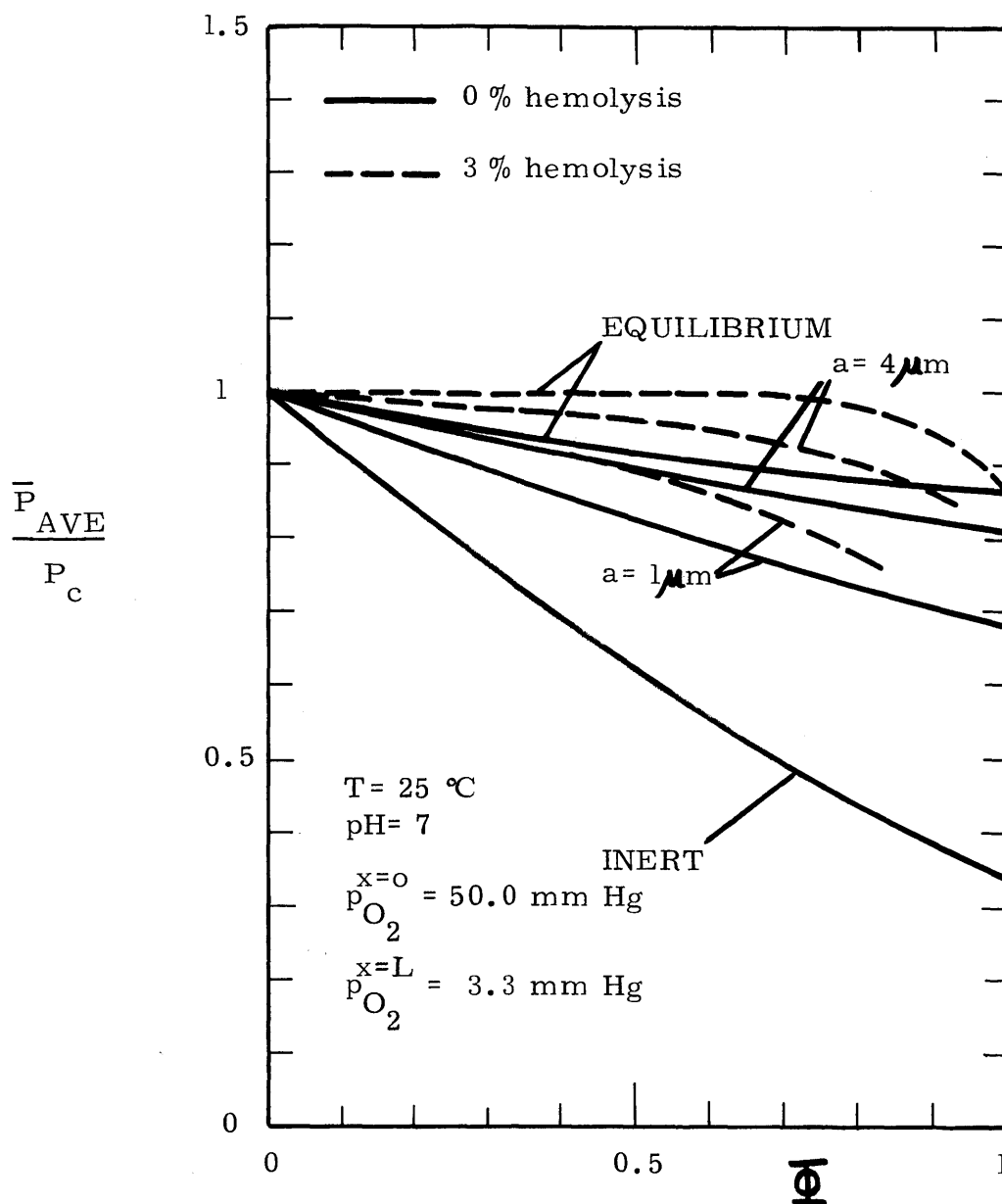


FIGURE 7.30
 EFFECT OF HEMOLYSIS ON THE AVERAGE
 EFFECTIVE PERMEABILITY RATIO.

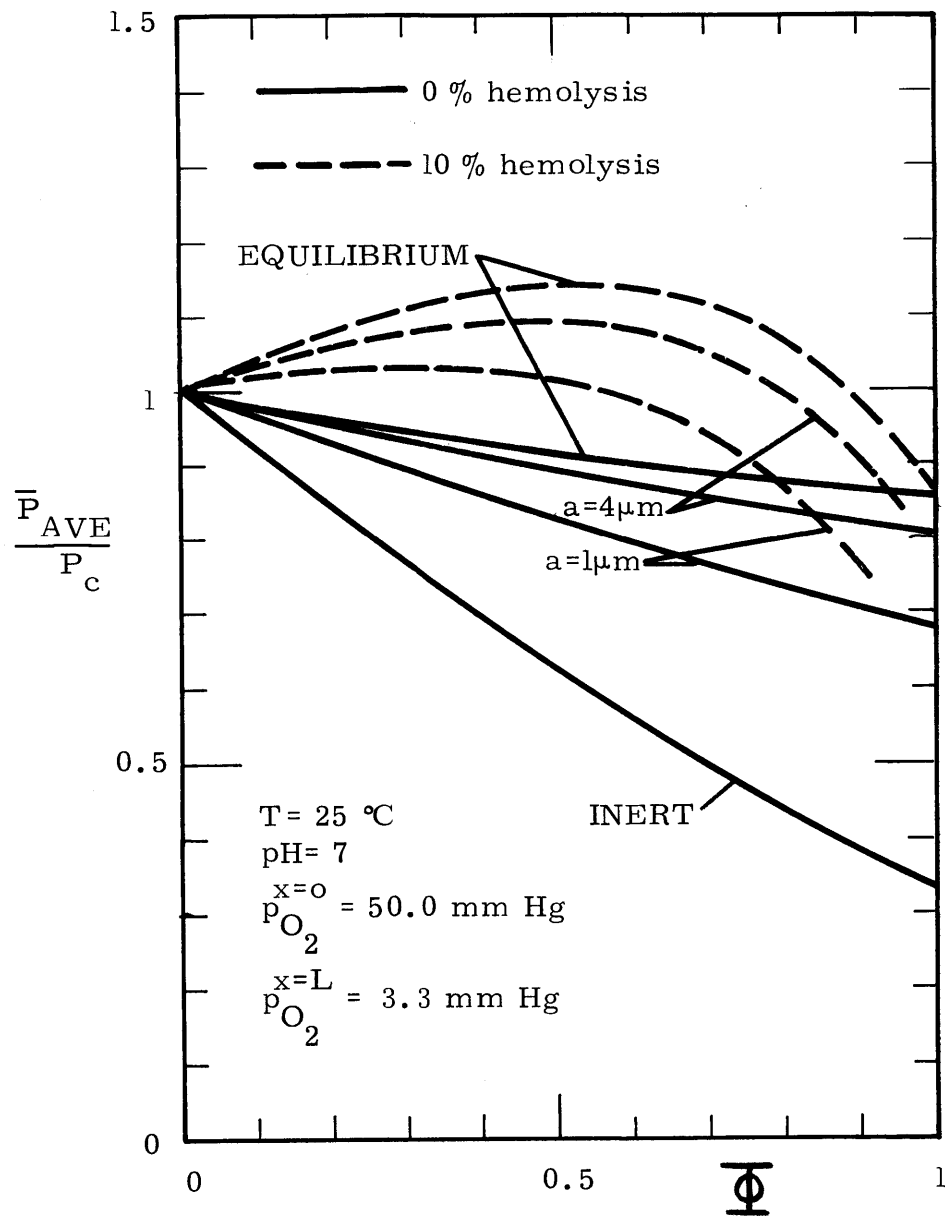


FIGURE 7.31

EFFECT OF HEMOLYSIS ON THE AVERAGE EFFECTIVE PERMEABILITY RATIO.

average effective permeability and must be avoided. This was confirmed in experiments where hemolysis was larger than one percent. These experiments were discarded. Hemolysis appears to be a function of the age of the blood; it increases as the age of the blood increases. (Age is defined here as the time after actual withdrawal from a donor.)

Another phenomenon that was observed was that the oxygen consumption rate of red blood cell suspensions increased with the age of the red blood cells. This effect was encountered in some initial exploratory experiments with outdated blood. In oxygen permeation experiments it was found that the average effective permeability was less for outdated reactive suspensions than those observed for fresh inert suspensions. In order to check that this effect was indeed due to "oxygen consumption" by the suspension, independent consumption experiments were performed. Saline red blood cell suspensions in saline of different ages, and initially fully saturated with air, were placed in sealed plastic syringes and the per cent saturation was measured as a function of time. To inhibit bacterial growth, 1 mg of streptomycin sulfate per 10 ml suspension was added to some of the samples (Richterich, 1969). Some typical results are shown in Figure 7.32 for outdated blood (age = 25 days) and relatively fresh blood (age = 5 days). (Human blood is considered outdated 21 days after withdrawal from donor). The common result is that initially the blood remains at 100 per cent saturation. After some time has passed the saturation drops slowly and then will drop rapidly. The

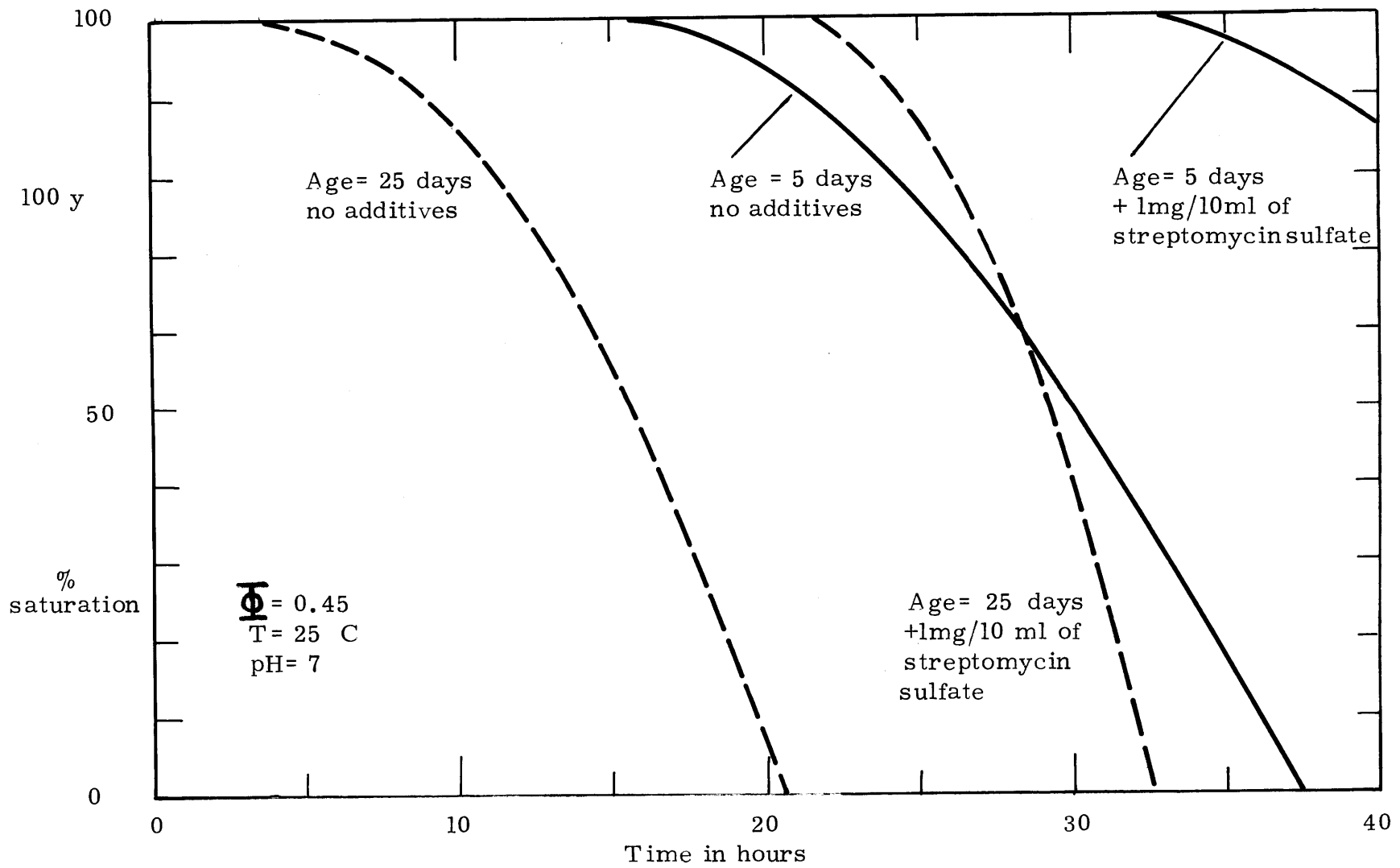


FIGURE 7.32
 DEOXYGENATION OF RED BLOOD CELL SUSPENSIONS IN SEALED SYRINGES.

older the blood the sooner the desaturation process would initiate. Addition of streptomycin sulfate (an antibiotic) delays but does not stop the desaturation process. Another additive added to the blood samples was potassium cyanide (1 gr/10 ml). Tyuma and Ueda (1971), who observed similar deoxygenation rates in hemoglobin solutions, have suggested that there are "oxygen consuming factors" present in hemoglobin (as yet undetermined) and they showed that addition of cyanide inhibited the deoxygenation process in hemoglobin solutions. In this work, the addition of KCN gave approximately the same result as the addition of streptomycin sulfate. As far as the author could determine, this process (which is reversible) is as yet not understood (is it oxygen consumption or bacterial growth?). It does point out the need to work with fresh blood as was done in this thesis. In some permeation experiments streptomycin sulfate (1 mg/10 ml) was added to the fresh blood, but no effect was observed (see Appendix D). From these results and Figure 7.32 it appears that "oxygen consumption" (the most appropriate word) is negligible in fresh red blood cell suspensions. It should be noted here that streptomycin sulfate was added for the experiments at 37°C. Finally, it should be mentioned that Stein (1968), who did not observe facilitated mass transfer in red blood cell suspensions (see Chapter 3), used outdated whole blood in his experiments. A possible explanation of his results is that in his experiments the oxygen consumption was responsible for a reduction of the observed oxygen mass transfer rate.

7.3.4 Model System

In the preceding sections on reactive red blood cell suspensions, it was shown that the theory correctly predicts the experimental behaviour of the permeability data. It was pointed out however that the exact hemoglobin diffusivity is at present not known, so that a precise comparison with the theory is not possible. This is due to the fact that the experimentally measured hemoglobin diffusivity at red blood cell concentrations varies from approximately 3.0×10^{-8} cm^2/sec to 1.5×10^{-7} cm^2/sec . At lower hemoglobin concentrations there exists less disagreement between the various reported values for the hemoglobin diffusivity. In collaboration with Tuntunjian (1973), oxygen permeability experiments were conducted utilizing a model system chosen to lessen this uncertainty. The model system consisted of a fresh hemoglobin solution ($C_T = 16.3$ gr/100 ml) emulsified into a continuous oil phase as described in Chapter 6. Emulsions (W/O) were made that had either a large particle size or a small particle size by appropriate control of the emulsification procedure. The emulsification process caused some denaturation of the hemoglobin, and the remaining activity of the hemoglobin was measured through the Van Slyke technique. Appropriate details of the experiments have been given by Tuntunjian (1973). It was found that the large size emulsions had a number average particle size of

$$\bar{d}_n = 9.30 \text{ } \mu\text{m}$$

with a standard deviation of

$$\sigma_n = 8.77 \text{ } \mu\text{m}$$

and a hemoglobin activity of 58% of the original hemoglobin.

The volume mean diameter and standard deviation was calculated as:

$$\bar{d}_v = 16.3 \text{ } \mu\text{m}$$

$$\sigma_v = 24.5 \text{ } \mu\text{m}$$

The small emulsion had a number average particle size of

$$\bar{d}_n = 2.54 \text{ } \mu\text{m}$$

a standard deviation of

$$\sigma_n = 0.95 \text{ } \mu\text{m}$$

and a hemoglobin activity of 46%. The volume mean diameter was calculated as

$$\bar{d}_v = 2.90 \text{ } \mu\text{m}$$

and the standard deviation was

$$\sigma_v = 3.26 \text{ } \mu\text{m}$$

The particle size was measured with the aid of a microscope and a total of 500 particles were measured for each emulsion. Figure 7.33 shows a comparison of the measured permeability data with the theoretical curves obtained from the one-step model. Parameters used in the calculations are listed in

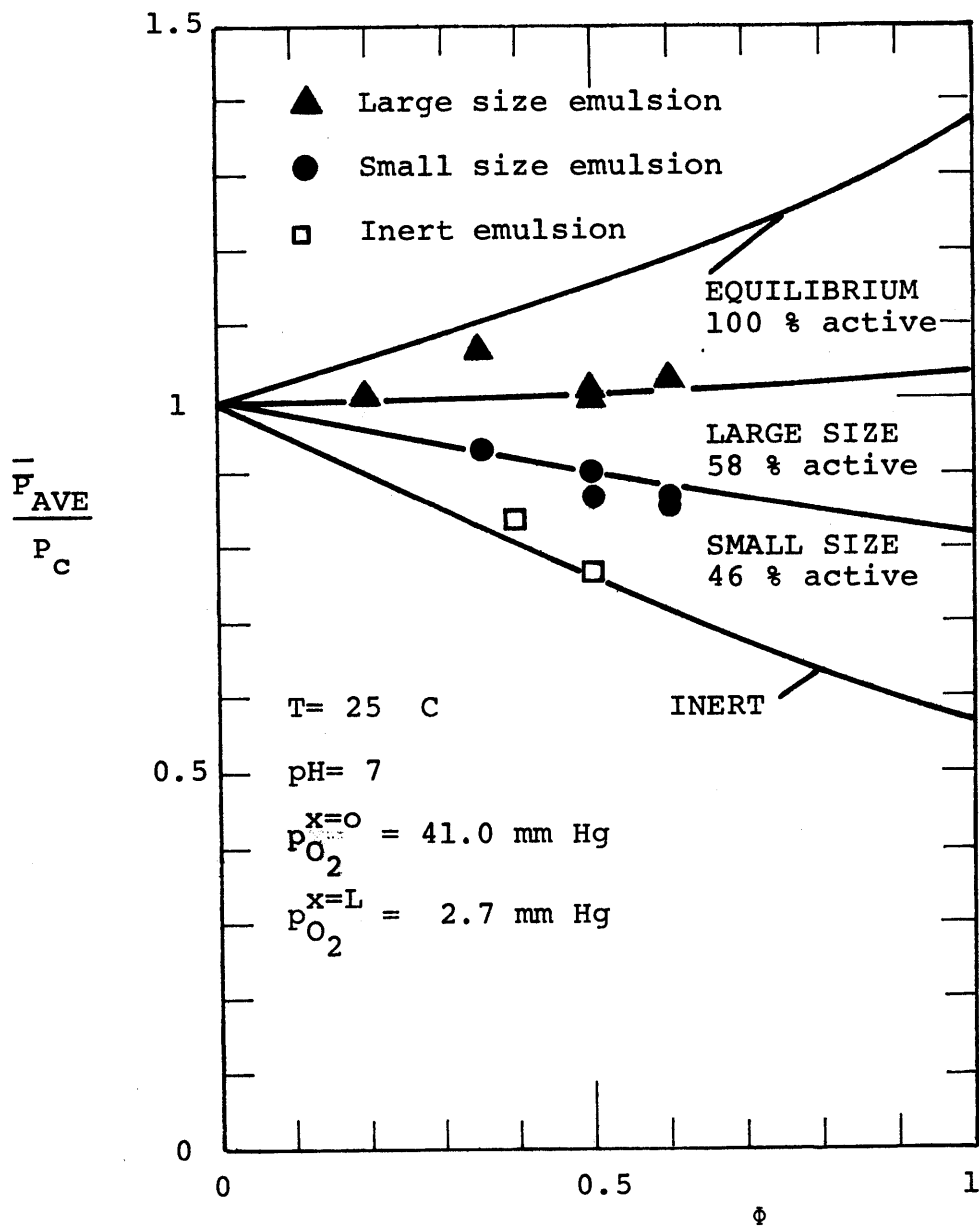


FIGURE 7.33

COMPARISON OF EXPERIMENTAL RESULTS WITH
 THEORETICAL PREDICTIONS FOR THE ONE-STEP
 MODEL FOR THE REACTIVE EMULSIONS.

Table 7.9 and these were either measured or they are consistent with previously discussed values. The deactivation of the hemoglobin inside the hemoglobin solution droplets was accounted for in the calculations by reducing the hemoglobin concentration in proportion to deactivation, but leaving diffusion coefficients unchanged. The size distribution of the emulsions was taken into account by integrating over the volume particle size distribution. The oxygen-hemoglobin saturation curve of the hemoglobin solution was measured and it was found to be virtually identical to that shown in Figure 7.24; the p_{50} was 13 mm Hg (Tuntunjian, 1973).

Figure 7.33 clearly indicates the effect of particle size upon the mass transfer rate. The reaction inside the large emulsion ($\bar{a}_v = 8.1 \mu\text{m}$) is nearly at equilibrium. (If not corrected for the 42% deactivation the line will fall just slightly below the equilibrium curve.) The reaction inside the small emulsions ($\bar{a}_v = 1.45 \mu\text{m}$) is not at equilibrium. The theory shows quite reasonable agreement with the experimentally measured values. The inert runs were obtained by introduction of carbon monoxide into the upstream and downstream volumes.

TABLE 7.9
PARAMETERS EMPLOYED IN CALCULATIONS
FOR THE MODEL SYSTEM

<u>Parameter</u>	<u>Source</u>
$C_T = 16.3 \text{ gr/100 ml}$	measured
$\therefore C_{T,Hm} = 0.0101 \text{ mole/l}$	
$D_{Hb} = 2.25 \times 10^{-7} \text{ cm}^2/\text{sec}$	Kreuzer compromise, Figure 3.8
$\alpha_{O_2} = .0272 \text{ cc(STP)/cc/atm}$	Table 3.3
$P_c = P_{oil} = 7.05 \times 10^{-7} \frac{\text{cm}^2\text{-cc(STP)}}{\text{sec-cc-atm}}$	Appendix D
$P_d = 4.03 \times 10^{-7} \frac{\text{cm}^2\text{-cc(STP)}}{\text{sec-cc-atm}}$	Figure 7.17
$k_1' = 3.0 \times 10^6 \text{ l/mole/sec}$	Table 7.8
$k_2' = 62.5 \text{ sec}^{-1}$	Table 7.8
$p_{O_2}^{x=0} = 41.0 \text{ mm Hg}$	Appendix D
$p_{O_2}^{x=L} = 2.7 \text{ mm Hg}$	Appendix D

8. CONCLUSIONS AND RECOMMENDATIONS

A theoretical framework has been developed that models diffusion with reversible chemical reaction in heterogeneous media. The theoretical framework incorporates general aspects of previously published work on mass transport phenomena in inert heterogeneous media, and diffusion with reversible chemical reaction in homogeneous media. As an example, several models have been developed for various types of heterogeneous media and reaction schemes. Effective permeabilities were derived which show that the effect of reversible chemical reactions is to facilitate the transport of the diffusing species in heterogeneous media. The effective permeability is a maximum when the chemical reactions are at equilibrium. In the case that the reaction departs sufficiently far from equilibrium facilitated transport becomes negligible and the theoretical equations reduce to Maxwell's equation for inert heterogeneous media.

Coupled with the theoretical developments, an experimental program was undertaken to investigate mass transport phenomena in both inert and reactive media. Experimentally measured oxygen permeabilities in thin liquid films of inert dispersions, inert emulsions, reactive red blood cell suspensions, and reactive emulsions showed reasonable agreement with the theoretical predictions. It was concluded that in the operation of an artificial oxygenator at normal physiological conditions, hemoglobin-facilitated oxygen transport contributes only a fraction of the total mass transport

rate. This same conclusion appears to be valid for oxygen uptake in the lung, but in the tissues and muscles, where the partial pressure of oxygen can be low, hemoglobin facilitated oxygen transport may become significant. In regards to the theoretical modeling of oxygen transport in the lungs or an artificial oxygenator at physiological conditions, the assumption that the oxygen-hemoglobin reaction is at equilibrium appears to be a reasonable approximation for whole blood.

The theoretical framework presented here can be used to model and predict mass transport phenomena in a variety of other reactive heterogeneous media. Shape effects can be incorporated as has been done for example by Fricke (1924) for inert heterogeneous media. Important biological problems such as the diffusion of carbon dioxide in blood, transport of nutrients and metabolites through tissues, and the absorbance of drugs through the skin should be amenable to analyses similar to those presented in this thesis if the necessary physico-chemical parameters are known for the system of interest. In addition, similar processes of chemical engineering interest, such as, for example, absorption and reversible reaction into emulsions, slurries, and dispersions, can be analyzed.

9. APPENDICES

- A. MAXWELL PROBLEM
 - A.1 Single Sphere in a Continuum
 - A.2 Effective Permeability for an Ensemble of Spheres

- B. THE NATURE OF BLOOD AND HEMOGLOBIN
 - B.1 Constituents of Blood
 - B.2 The Hemoglobin Molecule
 - B.3 Reaction of Hemoglobin with Oxygen

- C. DETAILS OF THE ADAIR DIFFUSION-REACTION SCHEME.
 THE FOUR-STEP MODEL
 - C.1 Equilibrium Solution
 - C.2 Nonequilibrium Solution
 - C.3 Single Point Linearization Technique for Slab Geometry

- D. COMPILATION OF EXPERIMENTAL RESULTS

- E. LISTING OF THE COMPUTER PROGRAMS

- F. SAMPLE CALCULATION FOR DATA REDUCTION

- G. NOMENCLATURE

- H. LITERATURE CITATIONS

APPENDIX A: MAXWELL PROBLEM

A.1 Single Sphere in a Continuum

Consider a single sphere, of radius a and permeability P_d , immersed in an infinite liquid medium of permeability P_c . A constant mass flux N_A is imposed at large distances from the sphere as shown in Figure A.1. Note that maintaining either the mass flux or the driving force gradient $\Delta p/L$ (or potential gradient) constant is equivalent since at large distances from the sphere ($\theta = 0$)

$$N_A = P_c \frac{\Delta p}{\Delta r}$$

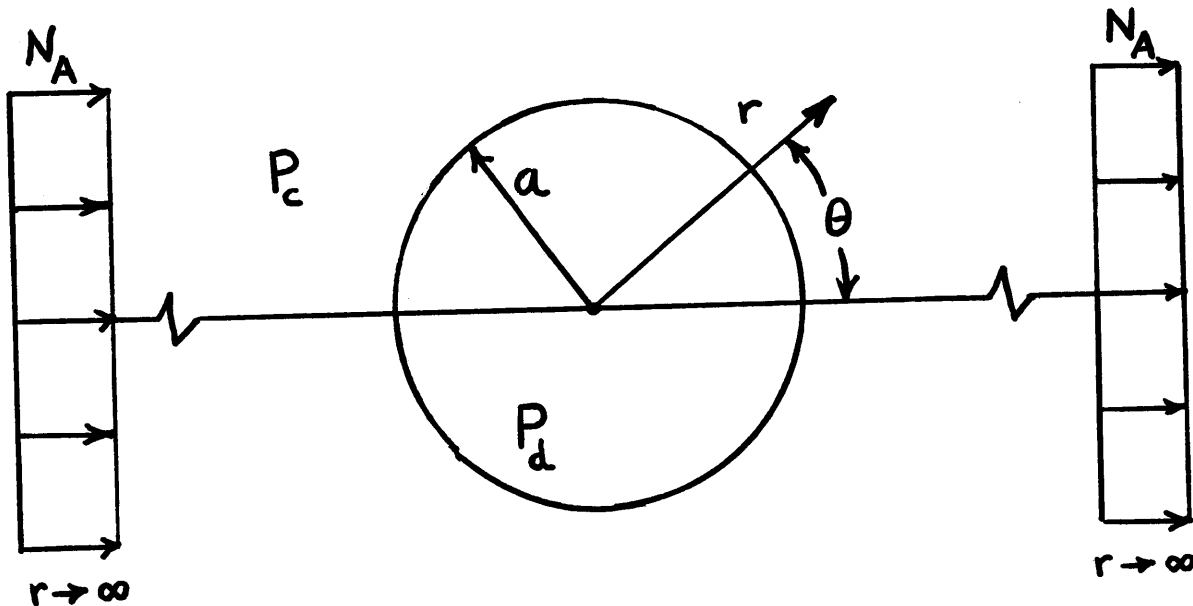


FIGURE A.1. SINGLE SPHERE IN INFINITE MEDIUM.

The mass conservation equations for A inside and outside the sphere are:

outside sphere,

$$P_c \left[\frac{1}{r^2} \frac{\partial}{\partial r} \left(r^2 \frac{\partial p_A}{\partial r} \right) + \frac{1}{r^2 \sin \theta} \frac{\partial}{\partial \theta} \left(\sin \theta \frac{\partial p_A}{\partial \theta} \right) \right] = 0 \quad (\text{A.1})$$

inside sphere,

$$P_d \left[\frac{1}{r^2} \frac{\partial}{\partial r} \left(r^2 \frac{\partial p'_A}{\partial r} \right) + \frac{1}{r^2 \sin \theta} \frac{\partial}{\partial \theta} \left(\sin \theta \frac{\partial p'_A}{\partial \theta} \right) \right] = 0 \quad (\text{A.2})$$

In deriving equations (A.1) and (A.2), it was assumed that Henry's Law is applicable,

$$C_A = \alpha_A p_A$$

which is a reasonable assumption for sparingly soluble gasses such as oxygen. The permeability is therefore defined as the diffusivity D_A times the solubility α_A of A in the medium. The boundary conditions are as follows:

1. Continuity of the potential p_A at the phase boundary

$$p_A = p'_A \text{ at } r = a, \text{ all } \theta \quad (\text{A.3})$$

2. Continuity of the mass flux of A at the phase boundary

$$P_c \frac{\partial p_A}{\partial r} = P_d \frac{\partial p'_A}{\partial r} \text{ at } r = a, \text{ all } \theta \quad (\text{A.4})$$

3. Concentration at the center of the sphere is fixed

$$p'_A = p_A^0 \text{ at } r = 0 \quad (\text{A.5})$$

4. Constant mass flux of A at large distances from the sphere

$$P_c \frac{\partial p_A}{\partial r} = - N_A \cos \theta \text{ as } r \rightarrow \infty, \text{ all } \theta \quad (\text{A.6})$$

The last boundary condition also imposes the condition of symmetry on the solution of equation (A.1) and (A.2). The solution of (A.1) and (A.2) is straightforward (Panofsky and Phillips, 1962) and is attained through the method of the separation of variables by letting (for the inside potential or the outside potential)

$$p = R(r) \theta(\theta)$$

The separated equations are of the form

$$\frac{\partial}{\partial r} (r^2 \frac{\partial R}{\partial r}) - n(n+1) R = 0$$

$$\frac{1}{\sin \theta} \frac{\partial}{\partial \theta} (\sin \theta \frac{\partial \theta}{\partial \theta}) + \frac{1}{\sin^2 \theta} + n(n+1) \theta = 0$$

The general solution of the differential equation $R(r)$ is

$$R(r) = A_n r^n + B_n r^{-n-1}$$

and the general solution for $\theta(\theta)$ is

$$\theta = E_m P_n^m(\cos \theta) + D_M Q_n^m(\cos \theta)$$

The functions $P_n^m(\cos \theta)$ and $Q_n^m(\cos \theta)$ are the associated Legendre functions of the first and second kind, respectively. Application of the boundary conditions (A.3) through (A.6) yields:

outside the sphere

$$(p_A - p_A^O) = -\left(\frac{N_A}{P_C}\right) r \cos \theta \left\{ 1 - \left(\frac{a}{r}\right)^3 \left[\frac{P_d - P_c}{P_d + 2P_c} \right] \right\} \quad (\text{A.7})$$

inside the sphere,

$$p_A' - p_A^O = -\left(\frac{N_A}{P_C}\right) r \cos \theta \left[\frac{3P_c}{2P_c + P_d} \right] \quad (\text{A.8})$$

Outside the sphere, the partial pressure of A (or potential field of A, $(p_A' - p_A^O)$) is given by the imposed potential gradient,

$$\frac{N_A}{P_C} = \frac{\Delta p_A}{\Delta r} \quad \text{at } r \rightarrow \infty \quad (\text{A.9})$$

plus a term accounting for the disturbance arising from the presence of the sphere. The relative effect of this disturbance term decays with the cube of the distance from the center of the sphere.

A.2 Effective Permeability for an Ensemble of Spheres

Consider a dilute suspension of n spheres, with permeability P_d and radius a_1 , located in a spherical volume of the continuous medium, with radius a_2 , which itself is located in an infinite bath of the continuous medium which has

a constant mass flux (or potential gradient) imposed on it (see Figure A.2). The suspension is assumed to be sufficiently dilute that the interactions between spheres may be neglected.

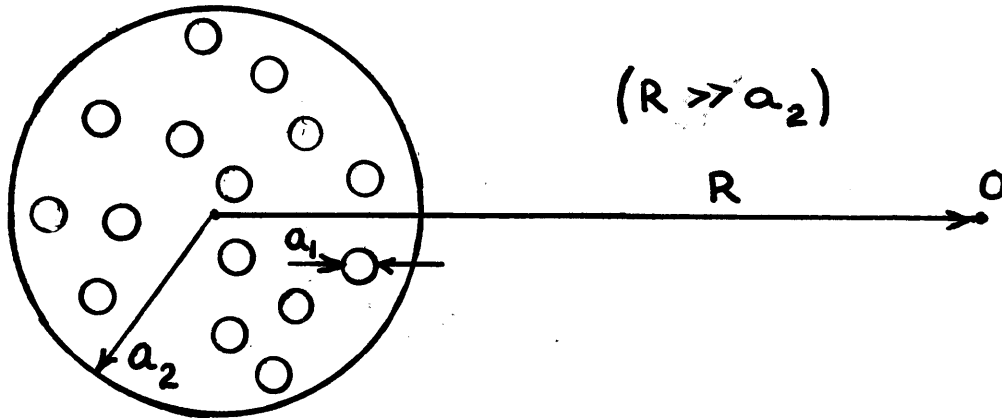


FIGURE A.2

SPHERICAL SUSPENSION OF SPHERES.

Under these conditions the disturbance in the potential field at large distances from the center of the spherical cluster arising from the presence of the n spheres is simply the sum of the disturbances resulting from each sphere individually. From equation (A.7) it follows that

$$p_A - p_A^o = -\left(\frac{N_A}{P_C}\right) r \cos \theta \left\{ 1 - \frac{na_1^3}{R^3} \left[\frac{P_d - P_C}{P_d + 2P_C} \right] \right\} \quad (\text{A.10})$$

The disturbance at such a point may also be written in terms of an effective permeability of the spherical cluster as a whole, \bar{P} ,

$$p_A - p_A^o = -\left(\frac{N_A}{P_C}\right) r \cos \theta \left\{ 1 - \frac{a_2^3}{R^3} \left(\frac{\bar{P} - P_C}{\bar{P} + 2P_C} \right) \right\} \quad (\text{A.11})$$

By equating the two expressions (A.10) and (A.11) and use of the volume fraction ϕ of the dispersed phase

$$\phi = \frac{na_1^3}{a_2^3} \quad (\text{A.12})$$

one arrives at Maxwell's expression

$$\frac{\bar{P}}{P_c} = \frac{P_d + 2P_c - 2\phi[P_c - P_d]}{P_d + 2P_c + \phi[P_c - P_d]} \quad (\text{A.13})$$

or in the nomenclature of Section 3.1

$$K_m = \frac{K_d + 2 - 2\phi[1 - K_d]}{K_d + 2 + \phi[1 - K_d]} \quad (\text{A.14})$$

Reviewing the procedure of obtaining the solution of equation (A.14) the first step is to obtain the potential outside the sphere which is of the form

$$(p_A - p_A^0) = -\left(\frac{N_A}{P_c}\right)r \cos \theta \left\{1 + \left(\frac{a}{r}\right)^3 A\right\}$$

where A is obtained from the boundary conditions and is from equation (A.7)

$$A = -\frac{P_d - P_c}{P_d + 2P_c} \quad (\text{A.15})$$

Once the constant A is in hand, Maxwell's technique for obtaining the average permeability of a suspension of spheres yields, in terms of A

$$\frac{\bar{P}}{P_c} = \left[\frac{1 - 2\phi A}{1 + \phi A} \right] \quad (\text{A.16})$$

APPENDIX B: THE NATURE OF BLOOD AND HEMOGLOBIN

B.1 Constituents of Blood

Blood is a complex suspension composed of two primary components, the plasma and the blood cells. The red blood cells (erythrocytes) make up the major volume of the blood cells, approximately 98 to 99 per cent, and the remaining is contributed by white blood cells and platelets. As a reasonable approximation, blood can be considered to be a two phase heterogeneous system, plasma and erythrocytes, where the erythrocyte membrane demarcates the phase boundary between the two. Both phases are aqueous, where at 25°C the plasma phase has a specific gravity of 1.0239 and the erythrocytes a specific gravity of 1.098.

A short discussion will be given here of the properties of plasma and the red blood cells, and for more complete details the reader is referred to extensive reviews and tabulations available in the literature (Bishop and Surgenor, 1964; Mc Farlane and Robb-Smith, 1961; Altman and Dittmer, 1971).

Plasma

Plasma is a buffered, straw yellow liquid consisting of a complex mixture of electrolytes, inorganics, organics and proteins in solution in water. Many of the compounds present in plasma have been identified and Altman and Dittmer (1971) have tabulated presently available information. The protein content of plasma is approximately 7 per cent by weight and

consists of globulins, albumin and fibrinogen. One of the primary functions of albumin (and to some extent the other proteins) is to exert osmotic pressure at the capillary membrane, in order to prevent the fluid of the plasma from leaking out of the capillaries in the interstitial spaces (Guyton, 1968). The globulins are divided into three major types: alpha, beta, and gamma globulins. The gamma globulins, and to a lesser extent the beta globulins, are the antibodies that resist infection and toxicity, and thus are responsible for providing the body with immunity. The alpha and beta globulins (as well as albumin) play an important role in transporting nutrients and metabolites in the blood stream through reversible combinations with the species and subsequent release in another part of the body.

The Red Blood Cells

The red blood cell has several major functions, of which the most important one is the transport of hemoglobin, which in turn carries oxygen from the lungs to the tissues. The red blood cell also contains carbonic anhydrase, an enzyme which catalyzes the hydration reaction of carbon dioxide, and at the same time CO_2 can reversibly combine with hemoglobin. Consequently the red blood cell is a very important mediator of CO_2 transport. Another important aspect of the red blood cells is that the hemoglobin inside the cells is an excellent acid-base buffer and the blood cells therefore are responsible for approximately 70 per cent of all the buffering power of the blood (Guyton, 1968).

The red blood cell is a biconcave disc with a mean diameter of approximately 8 micrometers, a thickness of 2 μm at the peripheral region and a thickness of 1 μm in the middle. Recently Evans and Fung (1972) have reported geometric dimensions of the red cell to within 0.02 μm through use of interference microscope. Table B.1 shows the statistics for various dimensions, surface area and the volume of the red blood cell obtained from the measurement of 50 cells at physiological conditions as reported in their paper. Under

TABLE B.1

DIMENSIONS OF THE HUMAN RED CELL

Diameter	$7.82 \pm 0.62 \mu\text{m}$
Maximum thickness	$2.58 \pm 0.27 \mu\text{m}$
Minimum thickness	$0.81 \pm 0.35 \mu\text{m}$
Surface area	$135 \pm 16 (\mu\text{m})^2$
Volume	$94 \pm 14 (\mu\text{m})^3$

certain conditions the shape of the red blood cell can be deformed. The membrane is quite flexible and shape variations can be induced by pH, osmotic pressure, and the flow field of the fluid.

The red blood cells usually comprise about 45 per cent of the total blood volume. In flowing blood the cells are individually dispersed, but in stagnant blood the red cells may form clusters. These clusters are known as rouleaux because

the red cells are stacked in rolls, and the rouleaux will break up when the shear rate of the fluid is above 1 sec^{-1} (Meyer, 1967). The hemoglobin inside the red cell is in a concentrated aqueous solution with an average concentration of 32 to 34 gr/100 ml, so that the blood of a normal person contains approximately 15 grams of hemoglobin in each 100 ml of blood. Since each hemoglobin molecule (MW = 64,500) can react with 4 oxygen molecules, on the average, 100 ml of blood can combine with a total of about 20 ml of oxygen (STP). Compared to the physical solubility of oxygen in blood, the presence of hemoglobin increases the oxygen capacity of whole blood about fifty times.

B.2 The Hemoglobin Molecule

Hemoglobin and its cousin myoglobin have enjoyed a special relationship with researchers from many disciplines since the beginning of the twentieth century. If one considers the functions of hemoglobin, its universal occurrence in vertebrates and many lower forms of life, and its ready availability it should not be surprising that hemoglobin and myoglobin are likely candidates for the devoted attention of molecular biologists, chemists, physicists, engineers, and even philosophers. In terms of scientific motivation, hemoglobin has such a versatility of biological, chemical, and physical functions and behavior that the study of hemoglobin has nearly become an academic discipline by itself and the term hemoglobinologists has been coined for those scientists active in

the field. Since the author does not belong to that select group, any attempt on his part to give a concise review of published work that pertains to developments in this thesis would be fruitless. For an up to date account of a significant portion of work performed on hemoglobin, the recent book by Antonini and Brunori (1971) and the review by Buse (1971) is recommended.

Hemoglobin is a very complex molecule that consists of about 10,000 atoms with a molecular weight of 64,500. Each hemoglobin molecule is composed of four subunits each of which in turn consists of a heme group, an iron atom surrounded by a porphyrin ring, and a globin, a polypeptide chain. The iron atom is in the divalent or ferrous state and each atom can combine with one molecule of oxygen. The capacity of the ferrous ion to bind reversibly with molecular oxygen is acquired only through the combination of the heme group and the globin. The heme alone will not bind oxygen. Further the globin subunits allow each of the four hemes to interact in a physiologically advantageous manner. Four major globins that occur in humans have been identified: α , β , γ and δ polypeptide. The normal adult hemoglobin (hemoglobin A or Hb A) is composed of two α and two β chains and is often written α_2^A/β_2^A . The superscript A shows that the molecule is of the genetically normal, adult type. The normal human adult also has a minor hemoglobin component (hemoglobin A₂) consisting of two α chains and two δ chains. The γ polypeptide chains occur in the fetal hemoglobin (Hb F) which is written as α_2^A/γ_2^F (Ingram, 1963).

Considerable progress has been made in elucidating the primary, secondary, tertiary, and quaternary structure of hemoglobin. The amino acid sequence, or primary structure, of the α , β , and γ -chains of human adult hemoglobin has been identified (Braunitzer et al., 1961, 1964; Koningsberg et al., 1961, 1962, 1963; Schroeder, 1963). In addition over 100 mutant hemoglobins have been discovered and the variations in the amino acid sequence have since been identified, and the modification in properties due to amino acid substitution has been useful in analyzing the relationship between structure and function in the hemoglobin molecule.

The α chain and the β chain have 141 and 146 amino acids respectively. The secondary structure, or the regular arrangement in space of the polypeptide chain, has been identified for hemoglobin of several species. Portions of the chains have helical twists, as shown in Figure B.1, and by convention have been numbered A through H. The three-dimensional arrangement (tertiary structure) of the chain for myoglobin and hemoglobin, and the location of the four subunits in space (quaternary structure) for hemoglobin has been under intensive investigation by Kendrew, Perutz and co-workers at the University of Cambridge. A three-dimensional model of sperm whale myoglobin showing the arrangements of the amino acids in the helical and non-helical regions and the heme group has been given by Watson and Kendrew (1961) through use of x-ray analysis. Myoglobin may be taken to represent a simpler type of respiratory protein (one subunit per molecule instead of four)

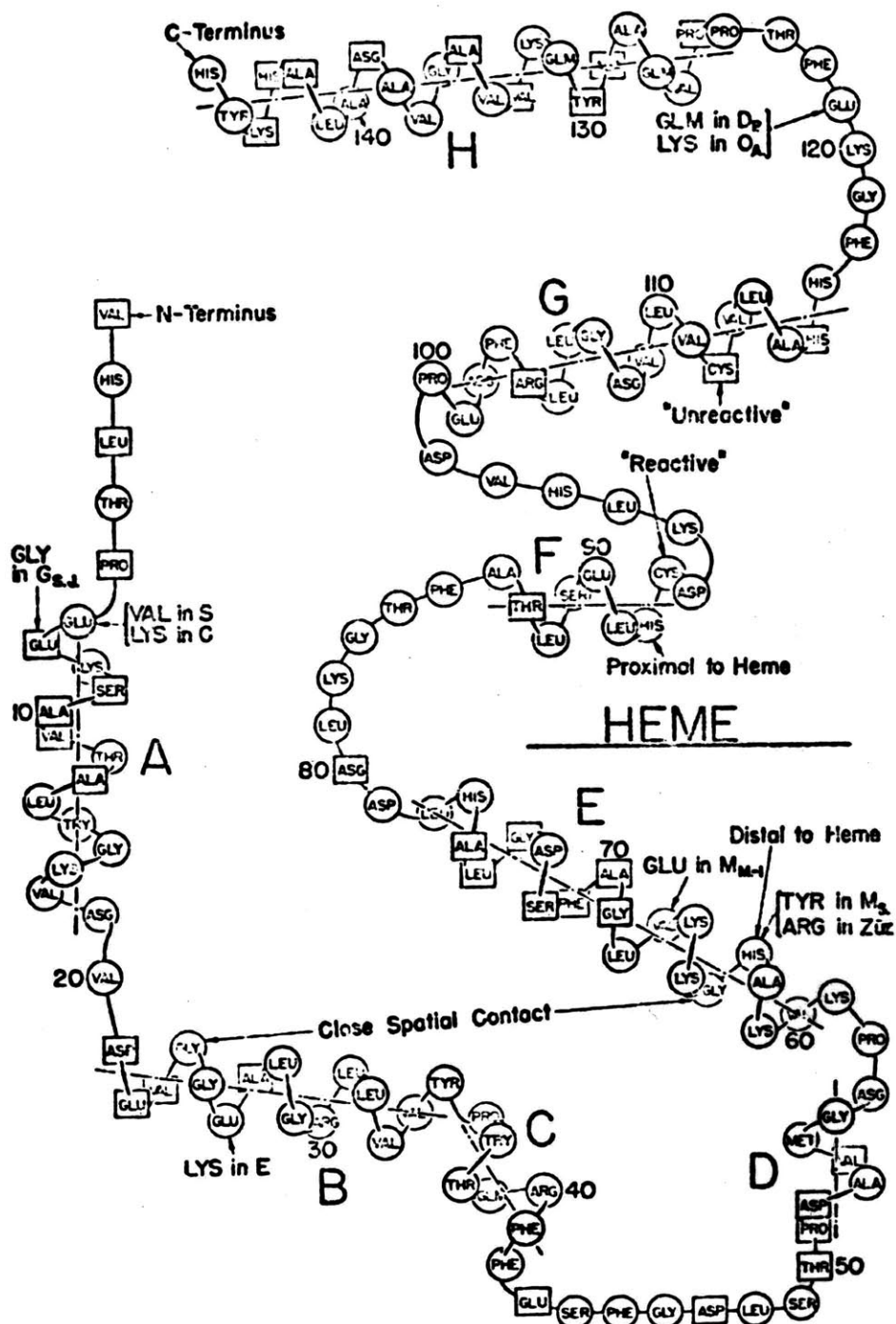


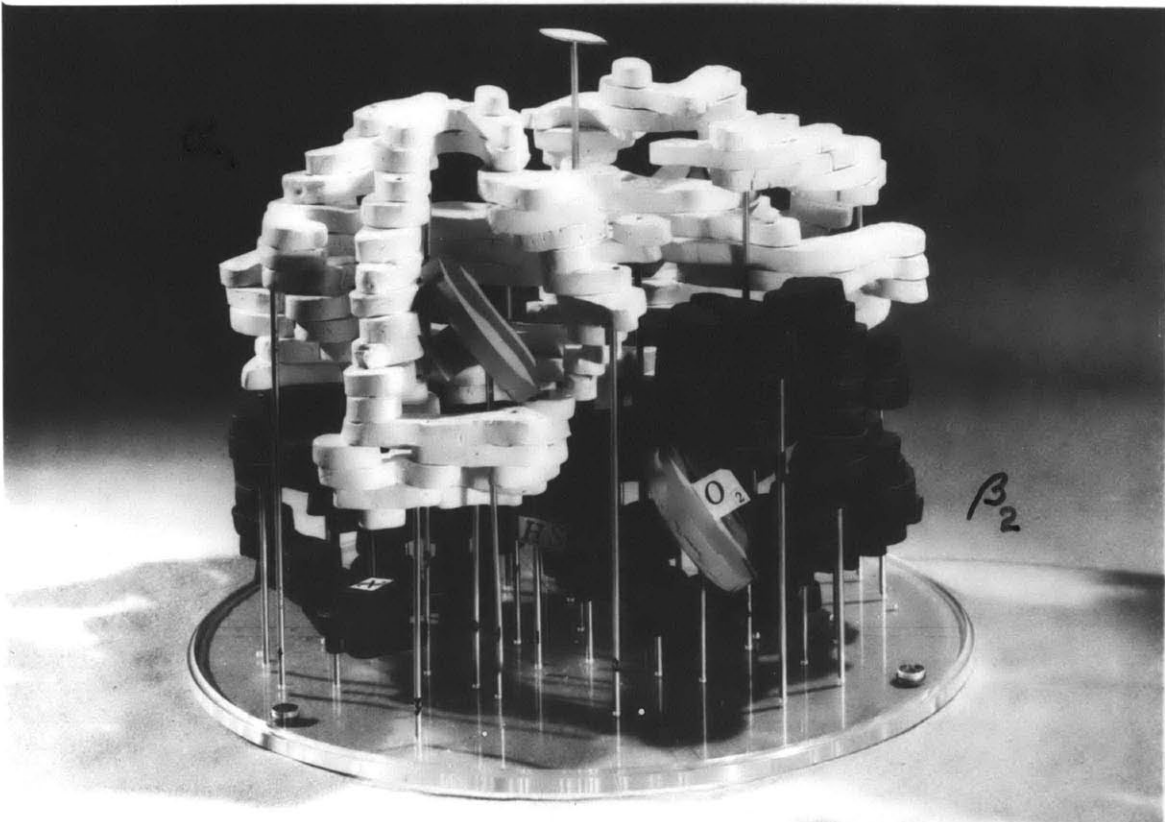
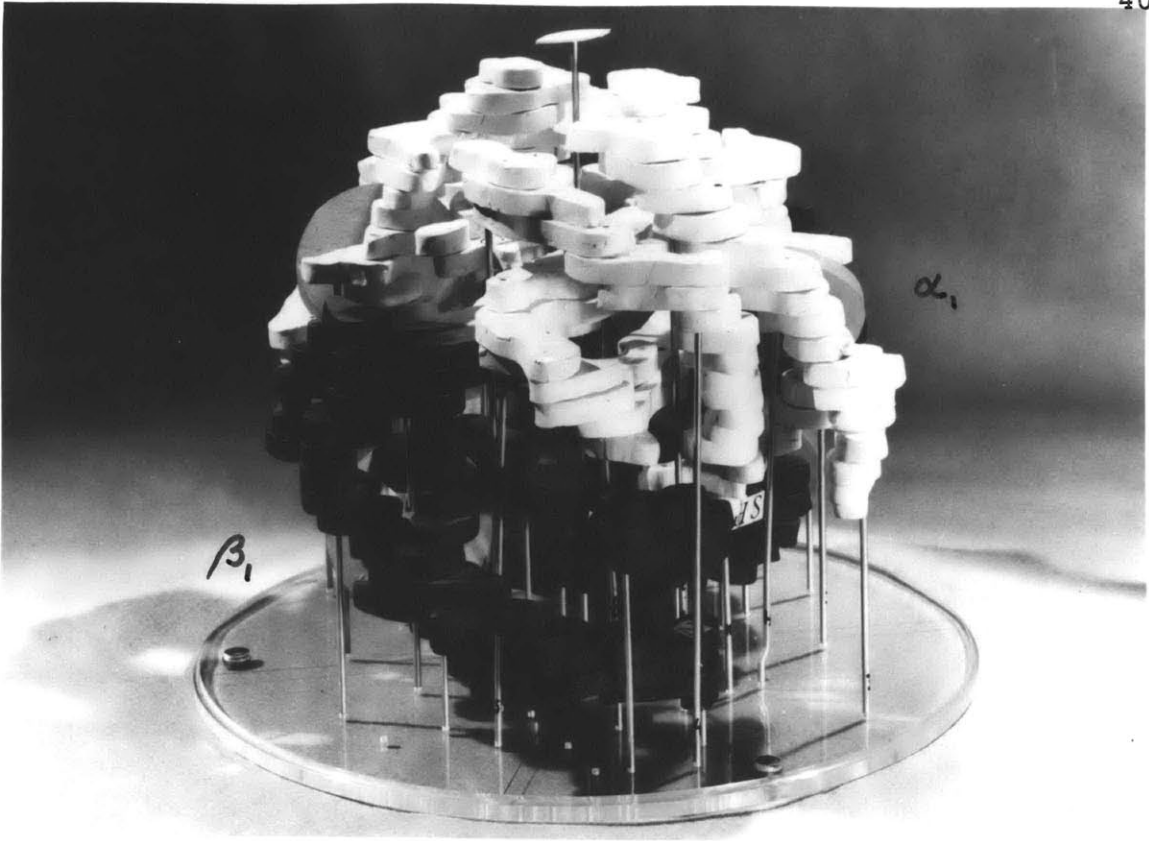
FIGURE B.1
 A REPRESENTATION OF THE β CHAIN OF HUMAN HEMOGLOBIN
 SHOWING THE LOCATION OF THE AMINO ACIDS. (reproduced
 with permission of Prof. Schroeder)

from which hemoglobin has evolved. Subsequent analysis of horse hemoglobin has shown large architectural similarities between the subunits of hemoglobin and the myoglobin molecule and the arrangement of the α and β subunits in space (Cullis, et al., 1962). The heme in the subunits of hemoglobin is tucked in a cleft made up by the polypeptide chain of each subunits as shown in Figure B.2. The molecular interactions between the heme and the protein are very complex and involve about 90 Van der Waals contacts (Antonini and Brunori, 1971). As shown in Figure B.2 the hemoglobin molecule consists of two α and β chains. Contacts between the different hemoglobin chains are of such a nature that dissociation gives two $\alpha\beta$ dimers.

Considerable evidence has been obtained on conformational changes associated with the binding of ligands in hemoglobin. It is generally accepted that in hemoglobin, conformational changes in ligand-binding are responsible for the functional interaction of the molecule (Antonini and Brunori, 1971). Extensive experimental results indicate that oxy- and deoxyhemoglobin are in different conformational states, but at present the precise influences of the conformational changes upon hemoglobin function has not yet been determined.

FIGURE B.2

THREE DIMENSIONAL MODEL OF THE HORSE HEMOGLOBIN MOLECULE. TOP FIGURE SHOWS SEGMENTS INVOLVED IN THE CONTACT $\alpha_1\beta_1$. LOWER FIGURE SHOWS SEGMENTS INVOLVED IN THE CONTACT $\alpha_1\beta_2$.
(Courtesy of Prof. Perutz)



B.3 Reaction of Hemoglobin with Oxygen

As discussed in the previous section the hemoglobin molecule consists of four subunits, each of which can react with one molecule of oxygen. The heme also reacts with other ligands such as carbon monoxide and nitric oxide, while carbon monoxide combines with the hemoglobin polypeptide chains. The study of the equilibria and kinetics of the ligand binding of hemoglobin has progressed since the beginning of the century. Development of theoretical treatments on the behavior of hemoglobin have developed virtually in parallel with experimental results obtained on ligand binding and information gained on hemoglobin structure.

Hufner (1903) proposed the first model for the reaction of oxygen with hemoglobin



Based on reaction (B.1) the fractional saturation of hemoglobin with the ligand, defined as

$$Y = \frac{C_{\text{HbO}_2}}{C_{\text{Hb}} + C_{\text{HbO}_2}} \quad (\text{B.2})$$

is as follows

$$Y = \frac{K\alpha p_{\text{O}_2}}{1 + K\alpha p_{\text{O}_2}} \quad (\text{B.3})$$

where K is the equilibrium constant

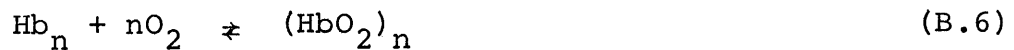
$$K = \frac{k_1}{k_2} \quad (\text{B.4})$$

and p_{O_2} is the partial pressure of oxygen which is related to the oxygen concentration by the solubility constant

$$c_{O_2} = \alpha p_{O_2} \quad (\text{B.5})$$

It was soon recognized that the oxygen-hemoglobin equilibrium curve, plotted as hemoglobin saturation versus oxygen partial pressure, was of a sigmoidal shape as shown in Figure B.3. The hyperbolic saturation curve given by equation (B.3) has been shown to give correct behavior for myoglobin but could not give a correct fit for hemoglobin. The interaction of the subunits in hemoglobin is responsible for the sigmoidal behaviour of the saturation curve, and "cooperative phenomena" of this nature occurs in many biological species.

Hill (1910) proposed that each hemoglobin molecule contained n active sites for binding oxygen and that the reaction could be treated as n -th order



The saturation of hemoglobin according to equation (B.6) is

$$y = \frac{K(\alpha p_{O_2})^n}{1 + K(\alpha p_{O_2})^n} \quad (\text{B.7})$$

Hill's equation has no physical significance because it was shown that: (i) the experimentally determined value for n for hemoglobin at physiological conditions was not an integer value

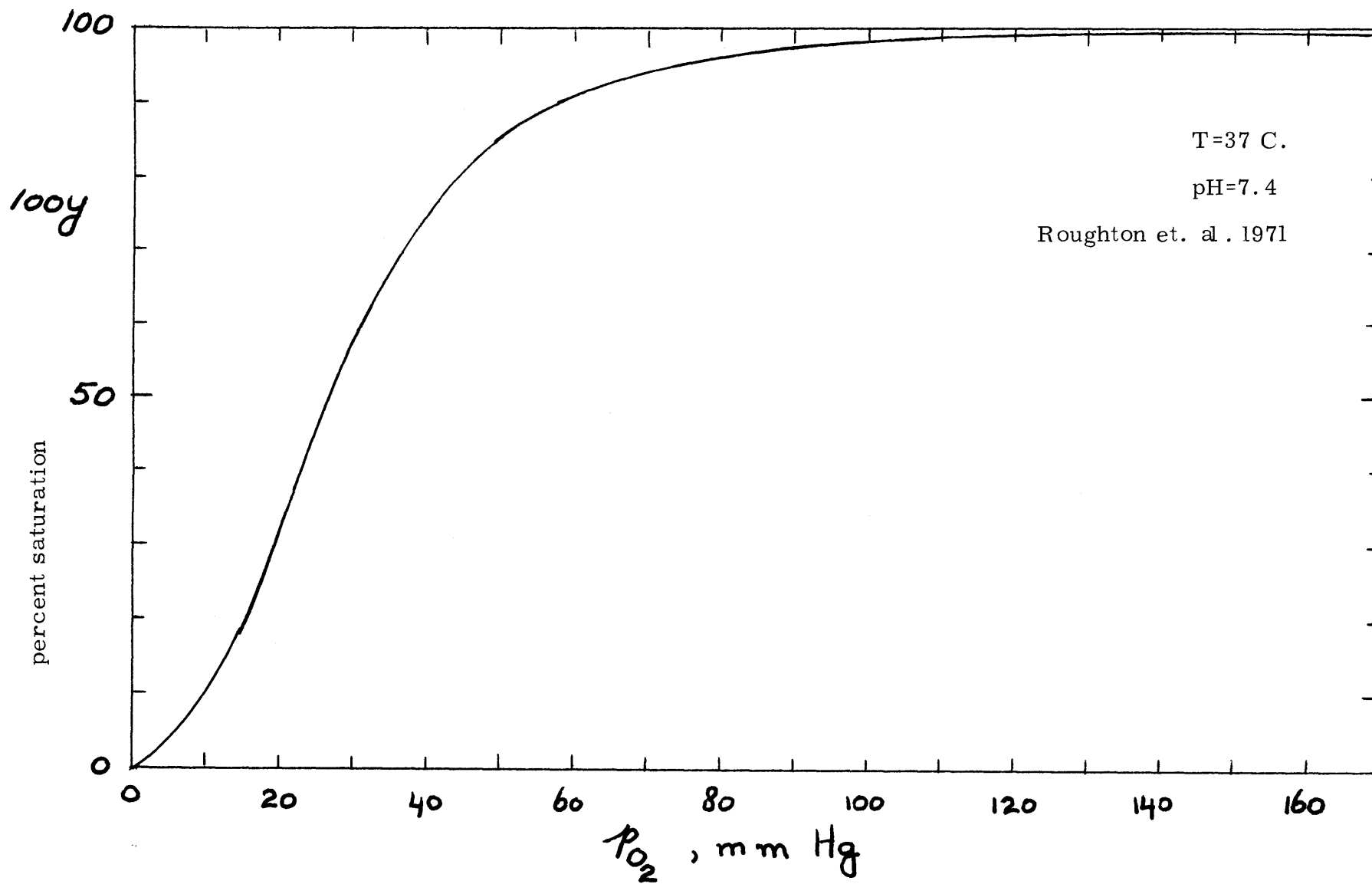
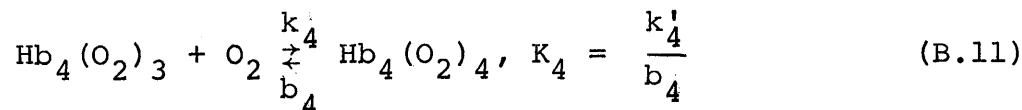
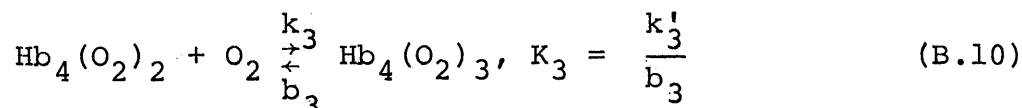
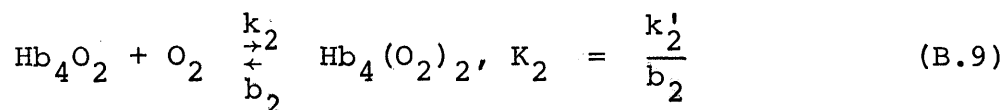
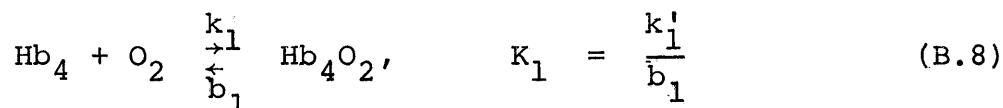


FIGURE B.3

OXYGEN-HEMOGLOBIN SATURATION CURVE AT PHYSIOLOGICAL CONDITIONS:

($n = 2.8$); (ii) by kinetic measurements the oxygen-hemoglobin is a second order reaction (Hartridge and Roughton, 1925); (iii) through molecular weight determinations it was determined that hemoglobin was a tetramer (Adair, 1923). However, the Hill equation has enjoyed considerable success as an empirical relationship to describe equilibrium data.

Adair in 1925 proposed a four step mechanism to account for the sigmoidal shape of the oxygen-hemoglobin equilibrium curve and the knowledge that there are four active sites in each molecule because of the presence of the four subunits



The Adair reaction scheme yields for the fractional hemoglobin saturation (Adair, 1925)

$$y = \frac{K_1 \alpha p_{\text{O}_2} + 2K_1 K_2 (\alpha p_{\text{O}_2})^2 + 3K_1 K_2 K_3 (\alpha p_{\text{O}_2})^3 + 4K_1 K_2 K_3 K_4 (\alpha p_{\text{O}_2})^4}{4[1 + K_1 \alpha p_{\text{O}_2} + K_1 K_2 (\alpha p_{\text{O}_2})^2 + K_1 K_2 K_3 (\alpha p_{\text{O}_2})^3 + K_1 K_2 K_3 K_4 (\alpha p_{\text{O}_2})^4]} \quad \dots \dots \dots (\text{B.12})$$

The equilibrium constants are macroscopic constants, and when the intrinsic constants (K_i) for the sites are the same it can be shown from statistical reasons that (Antonini and Brunori, 1971)

$$K_1:K_2:K_3:K_4 = 1:\frac{3}{8}:\frac{1}{6}:\frac{1}{16}$$

Any deviation from these statistically determined ratios, as implied from the sigmoidal shape of the hemoglobin curve, indicates heme-heme interactions. In the latter case Adair's equation remains valid as the relationship does not imply any particular values for the equilibrium constants. Considerable effort has been undertaken by Roughton and Gibson to quantify the kinetic rate constants and equilibrium constants from kinetic and equilibrium measurements (Roughton, 1949; Gibson and Roughton, 1957; Gibson, 1959, 1970). Recent accurate experiments by Roughton et al. (1971) at the top part of the saturation curve has shown that the Adair scheme cannot accurately fit the equilibrium curve in the 98.50 to 99.50 per cent range. This is not surprising considering that the Adair scheme is extremely simplified relative to the complexity of the molecular reactions. First of all many other reactions occur on the oxygenation of hemoglobin. For instance, recent interest has been centered on the different attraction of 2,3 diphosphoglycerate (DPG) towards deoxy- and oxyhemoglobin. DPG has been shown to be an important affector of oxygen affinity, its presence decreasing the overall hemoglobin affinity (Benesch and Benesch, 1967; Chanutin and Curnish, 1967). Benesh

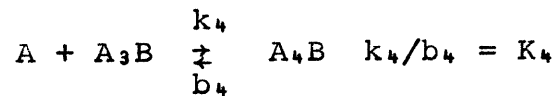
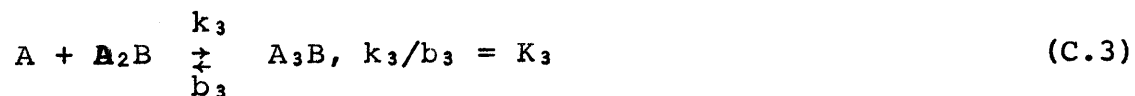
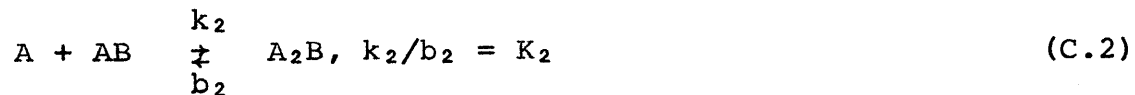
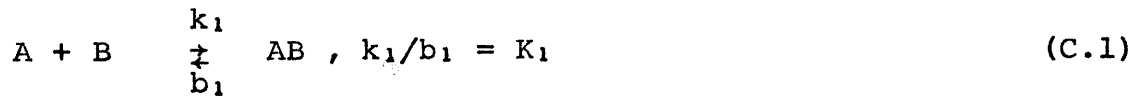
and his co-workers (1967, 1968, 1969) have reported that deoxyhemoglobin binds DPG strongly, but that oxyhemoglobin does not bind DPG to any appreciable extent. Further, the conformational states of deoxy- and oxyhemoglobin affect the reactivity of the ligands towards the hemes of hemoglobin. Therefore the Adair scheme is at best an approximation to the real physical, but as yet unknown, situation. Various models have recently been proposed that take into account the transformational transitions in order to explain the heme-heme interactions (homotropic interactions) and the interaction effects on ligand binding caused by other molecules (heterotropic interaction). Such allosteric models have been proposed by Monod et al. (1965), Koshland et al. (1966) and Perutz (1970). Modifications of these models will most likely occur as more information and insight is gained on the structure and function relationship in hemoglobin.

APPENDIX C

DETAILS OF THE ADAIR DIFFUSION-REACTION SCHEME

The Four-Step Model

Adair (1925) proposed the following kinetic scheme for the reaction of oxygen (A) with hemoglobin (B)



where k_j is the forward rate of reaction (C.j) and b_j is the corresponding reverse reaction rate constant.

Consider a single sphere, of radius a and permeability P_d , immersed in an infinite liquid medium of permeability P_c , which has a constant mass flux N_A imposed at a large distance away from the sphere as shown in Figure A1. With azimuthal symmetry the Laplacian in spherical coordinates is

$$\nabla^2 u = \frac{1}{r^2} \frac{\partial}{\partial r} \left(r^2 \frac{\partial u}{\partial r} \right) + \frac{1}{r^2 \sin \theta} \frac{\partial}{\partial \theta} \left(\sin \theta \frac{\partial u}{\partial \theta} \right)$$

so the steady state conservation mass equations for species A, B, AB, A₂B, A₃B, A₄B inside the sphere, and for species A

outside the sphere are:

Inside the sphere,

$$D_A \nabla^2 C_A = k_1 C_A C_B + k_2 C_A C_{AB} + k_3 C_A C_{A_2 B} + k_4 C_A C_{A_3 B} - b_1 C_{A_3 B} - b_2 C_{A_2 B} - b_3 C_{A_3 B} - b_4 C_{A_4 B} \quad (C.5)$$

$$D_B \nabla^2 C_B = k_1 C_A C_B - b_1 C_{AB} \quad (C.6)$$

$$D_{AB} \nabla^2 C_{AB} = k_2 C_A C_{AB} + b_1 C_{AB} - k_1 C_A C_B - b_2 C_{A_2 B} \quad (C.7)$$

$$D_{A_2 B} \nabla^2 C_{A_2 B} = k_3 C_A C_{A_2 B} + b_2 C_{A_2 B} - k_2 C_A C_{AB} - b_3 C_{A_3 B} \quad (C.8)$$

$$D_{A_3 B} \nabla^2 C_{A_3 B} = k_4 C_A C_{A_3 B} + b_3 C_{A_3 B} - k_3 C_A C_{A_2 B} - b_4 C_{A_4 B} \quad (C.9)$$

$$D_{A_4 B} \nabla^2 C_{A_4 B} = b_4 C_{A_4 B} - k_4 C_A C_{A_3 B} \quad (C.10)$$

Outside sphere,

$$\nabla^2 C_A^* = 0 \quad (C.11)$$

Note that the primes which previously denoted conditions inside the sphere have been omitted and that the asterisk now denotes conditions outside the sphere. The boundary conditions for the problem are:

Inside the sphere,

$$p_A = p_A^\circ \quad \text{at} \quad r = 0 \quad (C.12)$$

(again note that $C_A = \alpha_A P_A$ (C.13)).

Sphere boundary,

$$P_d \frac{\partial P_A}{\partial r} = P_c \frac{\partial P_A^*}{\partial r} \quad \text{at } r = a \quad (\text{C.14})$$

$$P_A = P_A^* \quad \text{at } r = a \quad (\text{C.15})$$

$$\frac{\partial C_B}{\partial r} = \frac{\partial C_{AB}}{\partial r} = \frac{\partial C_{A_2B}}{\partial r} = \frac{\partial C_{A_3B}}{\partial r} = \frac{\partial C_{A_4B}}{\partial r} = 0 \quad \text{at } r = a \quad (\text{C.16})$$

Far away from the sphere,

$$P_c \frac{\partial P_A^*}{\partial r} = - N_A \cos \theta \quad \text{as } r \rightarrow \infty \quad (\text{C.17})$$

The solution for the partial pressure variation of A ($C_A^* = \alpha_A^* P_A^*$) outside the sphere is again of the form (see Appendix A, or section 4.2.3 for the case of a single reacting sphere in a continuum).

$$P_A^* - P_A^o = - \frac{N_A}{P_c} r \cos \theta \left\{ 1 + A \left(\frac{a}{r} \right)^3 \right\} \quad (\text{C.18})$$

The remaining problem is to find suitable solutions for equation (C.5) through (C.10) and to determine the appropriate constants in these solutions and that of equation (C.18) through use of the appropriate boundary conditions.

C.1 Equilibrium Solution

For cases of spheres so large that chemical equilibrium is attained throughout the film, an equilibrium solution can be derived. By adding equations (C.6) through (C.10), integrating twice and utilizing boundary conditions (C.13) and (C.16), it

can be shown that the total carrier concentration is a constant throughout the sphere.

$$C_B + C_{AB} + C_{A_2B} + C_{A_3B} + C_{A_4B} = C_T \quad , \quad (C.19)$$

if the carrier diffusivities are equal.

By utilizing equations (C.5) and (C.7) through (C.10), one obtains

$$\nabla^2 [P_d p_A + D_B (C_{AB} + 2C_{A_2B} + 3C_{A_3B} + 4C_{A_4B})] = 0 \quad (C.20)$$

where

$$p_A = \frac{C_A}{\alpha_A}$$

Upon integrating equation (C.20) twice, the result becomes

$$P_d p_A + D_B (C_{AB} + 2C_{A_2B} + 3C_{A_3B} + 4C_{A_4B}) = B r \cos \theta + E \quad (C.21)$$

The equilibrium fractional saturation is defined

$$y = \frac{C_{AB} + 2C_{A_2B} + 3C_{A_3B} + 4C_{A_4B}}{4 C_T}$$

Since the fractional saturation value at the center of the sphere is y° , for a small driving force of A across the sphere the saturation change through the sphere can be related to the center saturation concentration by

$$y = y^\circ + \left. \frac{dy}{dp_A} \right|^\circ \Delta p_A \quad (C.22)$$

(provided that the reactions are everywhere at equilibrium).

So the total concentration of oxygenated hemes can be related by

$$(C_{AB} + 2C_{A_2B} + 3C_{A_3B} + 4C_{A_4B}) = 4C_T y^\circ + 4C_T \left(\frac{dy}{dp_A} \right)^\circ \Delta p_A \quad (C.23)$$

Substitution of (C.23) into (C.21) yields

$$P_d p_A + D_B [4C_T y^\circ + 4C_T \left(\frac{dy}{dp_A} \right)^\circ \Delta p_A] = Br \cos \theta + E \quad (C.24)$$

Equations (C.18) and (C.24) can now be utilized when coupled with the boundary conditions to solve for the constant A. Application of boundary condition (C.15) yields

$$\begin{aligned} & P_d \left\{ p_A^\circ - \frac{N_A}{P_c} a \cos \theta (1+A) \right\} + \\ & D_B \left\{ 4y^\circ C_T + 4C_T \left(\frac{dy}{dp_A} \right)^\circ \left| - \frac{N_A a}{P_c} \cos \theta (1+A) \right| \right\} \\ & = Ba \cos \theta + E \end{aligned} \quad (C.25)$$

If one then equates powers of $(\cos \theta)$, equation (C.25) yields

$$E = P_d p_A^\circ + 4D_B C_T y^\circ \quad (C.26)$$

and

$$\begin{aligned} & - \frac{P_d}{P_c} N_A a - \frac{P_d}{P_c} N_A A a - \frac{4D_B C_T}{P_d} \left(\frac{dy}{dp_A} \right)^\circ \frac{N_A P_d}{P_c} \\ & - \frac{4D_B C_T}{P_d} \left(\frac{dy}{dp_A} \right)^\circ \frac{N_A P_d}{P_c} A a = Ba \end{aligned} \quad (C.27)$$

Further at $r=a$

$$P_d \frac{\partial p_A}{\partial r} + D_B \frac{\partial (C_{AB} + 2C_{A_2B} + 3C_{A_3B} + 4C_{A_4B})}{\partial r} = P_c \frac{\partial p_A^*}{\partial r} \quad (C.28)$$

from which

$$B = - N_A (1-2A) \quad (C.29)$$

Substitution of equation (C.29) into (C.27) yields a solution for A which is

$$A = \frac{P_c - P_d \left| 1 + \frac{4D_B C_T \frac{dy}{dp_A}^\circ}{P_d} \right|}{2P_c + P_d \left| 1 + \frac{4D_B C_T \frac{dy}{dp_A}^\circ}{P_d} \right|} \quad (C.30)$$

Defining

$$F_{eq}^{Adair} = \frac{4D_B C_T \frac{dy}{dp_A}^\circ}{P_d}, \quad (C.31)$$

equation (C.30) can be rewritten as

$$A = \frac{P_c - P_d (1 + F_{eq}^{Adair})}{2P_c + P_d (1 + F_{eq}^{Adair})} \quad (C.32)$$

Substitution of A into (C.18) gives for the outside partial pressure

$$p_A^* - p_A^\circ = - \frac{N_A}{P_c} r \cos \theta \left\{ 1 + \left(\frac{a}{r}\right)^3 \frac{P_c - P_d (1 + F_{eq}^{Adair})}{2P_c + P_d (1 + F_{eq}^{Adair})} \right\} \quad (C.33)$$

Maxwell's technique can now be utilized to obtain the effective

permeability as described in Appendix A so that

$$\frac{\bar{P}}{P_c} = \frac{P_d(1+F_{eq}^{Adair}) + 2P_c - 2\phi[P_c - P_d(1+F_{eq}^{Adair})]}{P_d(1+F_{eq}^{Adair}) + 2P_c + \phi[P_c - P_d(1+F_{eq}^{Adair})]} \quad (C.34)$$

Equation (C.34) gives the effective (relative) permeability for a suspension of spheres in a continuum where a four step reversible reaction which is completely at equilibrium occurs inside the spheres. The fractional saturation y is given by Adair's equilibrium relationship. This relationship can be obtained from the equilibrium conditions of the four step reaction scheme which are

$$C_{AB}^{\circ} = K_1 \alpha p_A^{\circ} C_B^{\circ}$$

$$C_{A_2B}^{\circ} = K_2 \alpha p_A^{\circ} C_{AB}^{\circ} = K_1 K_2 (\alpha p_A^{\circ})^2 C_B^{\circ}$$

$$C_{A_3B}^{\circ} = K_3 \alpha p_A^{\circ} C_{A_2B}^{\circ} = K_1 K_2 K_3 (\alpha p_A^{\circ})^3 C_B^{\circ}$$

$$C_{A_4B}^{\circ} = K_4 \alpha p_A^{\circ} C_{A_3B}^{\circ} = K_1 K_2 K_3 K_4 (\alpha p_A^{\circ})^4 C_B^{\circ}$$

From equation (C.19) and the above relationships the concentration of C_B° is given by

$$C_B^{\circ} = \frac{C_T}{1 + K_1 \alpha p_A^{\circ} + K_1 K_2 (\alpha p_A^{\circ})^2 + K_1 K_2 K_3 (\alpha p_A^{\circ})^3 + K_1 K_2 K_3 K_4 (\alpha p_A^{\circ})^4}$$

so that the fractional saturation is given by

$$y^{\circ} = \frac{K_1 \alpha p_A^{\circ} + 2K_1 K_2 (\alpha p_A^{\circ})^2 + 3K_1 K_2 K_3 (\alpha p_A^{\circ})^3 + 4K_1 K_2 K_3 K_4 (\alpha p_A^{\circ})^4}{4[1 + K_1 \alpha p_A^{\circ} + K_1 K_2 (\alpha p_A^{\circ})^2 + K_1 K_2 K_3 (\alpha p_A^{\circ})^3 + K_1 K_2 K_3 K_4 (\alpha p_A^{\circ})^4]}$$

C.2 Nonequilibrium Solution

The nonequilibrium solution is obtained from a linearized perturbation analysis which is similar to that as described in Chapter 4. First the number of differential equations can be reduced through use of equation (C.19) and (C.21) which are not dependent on the equilibrium assumption. Elimination of C_{AB_4} gives:

$$P_d p_A + D_B (-4C_B - 3C_{AB} - 2C_{A_2B} - C_{A_3B}) = E + B r \cos \theta \quad (C.35)$$

In order to expand the concentrations as small deviations around the conditions at $r=0$, one defines:

$$P_A = P_A^\circ + \Delta P_A = P_A^\circ + f(r) \cos \theta \quad (C.36a)$$

$$C_B = C_B^\circ + \Delta C_B = C_B^\circ + g(r) \cos \theta \quad (C.36b)$$

$$C_{AB} = C_{AB}^\circ + \Delta C_{AB} = C_{AB}^\circ + h(r) \cos \theta \quad (C.36c)$$

$$C_{A_2B} = C_{A_2B}^\circ + \Delta C_{A_2B} = C_{A_2B}^\circ + i(r) \cos \theta \quad (C.36d)$$

$$C_{A_3B} = C_{A_3B}^\circ + \Delta C_{A_3B} = C_{A_3B}^\circ + j(r) \cos \theta \quad (C.36e)$$

Consider first equation (C.5). Substitution of equation (C.36a) through (C.36e) and (C.19), elimination of second order terms, and requiring to zeroth order the perturbations quantities are equal, which requires

$$0 = k_1 \alpha P_A^\circ C_B^\circ - b_1 C_{AB}^\circ \quad (C.37a)$$

$$0 = k_2 \alpha p_A^\circ C_{AB}^\circ - b_2 C_{A_2B}^\circ \quad (\text{C.37b})$$

$$0 = k_3 \alpha p_A^\circ C_{A_2B}^\circ - b_3 C_{A_3B}^\circ \quad (\text{C.37c})$$

$$0 = k_4 \alpha p_A^\circ C_{A_3B}^\circ - b_4 [C_{\text{F}}^\circ - C_B^\circ - C_{AB}^\circ - C_{A_2B}^\circ - C_{A_3B}^\circ] \quad (\text{C.37d})$$

one obtains

$$P_d \left[\frac{d^2 f}{dr^2} + \frac{2}{r} \frac{df}{dr} - \frac{2f}{r^2} \right] =$$

$$\alpha (k_1 C_B^\circ + k_2 C_{AB}^\circ + k_3 C_{A_3B}^\circ + k_4 C_{A_3B}^\circ) f$$

$$+ (\alpha p_A^\circ k_1 + b_4) g$$

$$+ (\alpha p_A^\circ k_2 - b_1 + b_4) h$$

$$+ (\alpha p_A^\circ k_3 - b_2 + b_4) i$$

$$+ (\alpha p_A^\circ k_4 - b_3 + b_4) j \quad (\text{C.38})$$

A consequence of (C.37) is that the concentrations at $r=0$ are at equilibrium. A similar treatment of equations (C.6), (C.7), and (C.8) yields

$$D_B \left[\frac{d^2 g}{dr^2} + \frac{2}{r} \frac{dg}{dr} - \frac{2g}{r^2} \right] = \alpha k_1 C_B^\circ f + \alpha p_A^\circ k_1 g - b_1 h, \quad (\text{C.39})$$

$$D_B \left[\frac{d^2 h}{dr^2} + \frac{2}{r} \frac{dh}{dr} - \frac{2h}{r^2} \right] = \alpha (k_2 C_{AB}^\circ - k_1 C_B^\circ) f$$

$$- \alpha p_A^\circ k_1 g$$

$$+ (\alpha p_A^\circ k_2 + b_1) h$$

$$- b_2 i, \quad (\text{C.40})$$

and

$$\begin{aligned}
 D_B \left[\frac{d^2 i}{dr^2} + \frac{2}{r} \frac{di}{dr} - \frac{2i}{r^2} \right] &= \alpha (k_3 C_{A_2 B}^\circ - k_2 C_{AB}^\circ) f \\
 &- \alpha p_A^\circ k_2 h \\
 &+ (\alpha p_A^\circ k_3 + b_2) i \\
 &- b_3 j
 \end{aligned} \tag{C.41}$$

Also from equation (C.35) one obtains through a similar procedure

$$\alpha D_A f - D_B (4g + 3h + 2i + j) = Br \tag{C.42}$$

Equations (C.38) through (C.42) must be solved for f , g , h , i , and j . As suggested by the one-step solution given in Chapter 4 a trial solution for f can be assumed to be of the form

$$f = F_1 \left(\frac{r}{a} \right) + F_2 \left(\frac{r}{a} \right)^{-2} \left(\frac{a}{\beta} \right)^{-3/2} \sinh \frac{r}{\beta} + F_3 \left(\frac{r}{a} \right)^{-1} \cosh \frac{r}{\beta} \tag{C.43}$$

Since from boundary condition (C.12) the function f at $r=0$ must be zero

$$f(0) = 0$$

it follows that

$$F_3 = - F_2 \frac{a}{\beta}$$

As a consequence the function f becomes

$$f = F_1 \left(\frac{r}{a} \right) + F_2 \left(\frac{r}{a} \right)^{-2} \sinh \frac{r}{\beta} - F_2 \left(\frac{a}{\beta} \right) \left(\frac{r}{a} \right)^{-1} \cosh \frac{r}{\beta} \tag{C.44a}$$

Similarly for g, h, i, j assume a solution of the form

$$g = G_1 \left(\frac{r}{a}\right) + G_2 \left(\frac{r}{a}\right)^{-2} \sinh \frac{r}{\beta} - G_2 \left(\frac{a}{\beta}\right) \left(\frac{r}{a}\right)^{-1} \cosh \frac{r}{\beta} \quad (\text{C.44b})$$

$$h = H_1 \left(\frac{r}{a}\right) + H_2 \left(\frac{r}{a}\right)^{-2} \sinh \frac{r}{\beta} - H_2 \left(\frac{a}{\beta}\right) \left(\frac{r}{a}\right)^{-1} \cosh \frac{r}{\beta} \quad (\text{C.44c})$$

$$i = I_1 \left(\frac{r}{a}\right) + I_2 \left(\frac{r}{a}\right)^{-2} \sinh \frac{r}{\beta} - I_2 \left(\frac{a}{\beta}\right) \left(\frac{r}{a}\right)^{-1} \cosh \frac{r}{\beta} \quad (\text{C.44d})$$

$$j = J_1 \left(\frac{r}{a}\right) + J_2 \left(\frac{r}{a}\right)^{-2} \sinh \frac{r}{\beta} - J_2 \left(\frac{a}{\beta}\right) \left(\frac{r}{a}\right)^{-1} \cosh \frac{r}{\beta} \quad (\text{C.44e})$$

Equations (C.44a) through (C.44e) can now be substituted into equation (C.38) and two equations can be obtained (from the r/a part and hyperbolic part) which are

$$\begin{aligned} 0 &= \frac{1}{D_A} (k_1 C_B^\circ + k_2 C_{AB}^\circ + k_3 C_{A_2B}^\circ + k_4 C_{A_3B}^\circ) F_1 \\ &+ \frac{1}{P_d} (\alpha p_A^\circ k_1 + b_4) G_1 \\ &+ \frac{1}{P_d} (\alpha p_A^\circ k_2 - b_1 + b_4) H_1 \\ &+ \frac{1}{P_d} (\alpha p_A^\circ k_3 - b_2 + b_4) I_1 \\ &+ \frac{1}{P_d} (\alpha p_A^\circ k_4 - b_3 + b_4) J_1 \end{aligned} \quad (\text{C.45})$$

and

$$\begin{aligned}
\frac{1}{\beta^2} F_2 &= \frac{1}{D_A} (k_1 C_{\mathbf{N}}^{\circ} + k_2 C_{AB}^{\circ} + k_3 C_{A_2 B}^{\circ} + k_4 C_{A_4 B}^{\circ}) F_2 \\
&+ \frac{1}{P_d} (\alpha p_A^{\circ} k_1 + b_4) G_2 \\
&+ \frac{1}{P_d} (\alpha p_A^{\circ} k_2 - b_1 + b_4) H_2 \\
&+ \frac{1}{P_d} (\alpha p_A^{\circ} k_3 - b_2 + b_4) I_2 \\
&+ \frac{1}{P_d} (\alpha p_A^{\circ} k_4 - b_3 + b_4) J_2
\end{aligned} \tag{C.46}$$

Similarly from equations (C.39), (C.40), and (C.41), one obtains three additional sets of relationships for F_2 , G_2 , H_2 , I_2 , J_2 , and for F_1 , G_1 , H_1 , I_1 , J_1 . In addition by substituting equations (C.44a) through (C.44e) into (C.42) one can show that F_1, G_1, H_1, I_1, J_1 satisfy equations (C.42) automatically but for the other constants one obtains

$$P_d F_2 - D_B (4G_2 + 3H_2 + 2I_2 + J_2) = 0 \tag{C.47}$$

Eliminating J_2 and substituting into the four relationships for F_2 , G_2 , H_2 , I_2 (and J_2) one obtains for homogeneous equations for F_2 , G_2 , H_2 , and I_2 of the form

$$\begin{aligned}
(\alpha_{11} - \Lambda) F_2 + \alpha_{12} G_2 + \alpha_{13} H_2 + \alpha_{14} I_2 &= 0 \\
\alpha_{21} F_2 + (\alpha_{22} - \Lambda) G_2 + \alpha_{23} H_2 + \alpha_{24} I_2 &= 0 \\
\alpha_{31} F_2 + \alpha_{32} G_2 + (\alpha_{33} - \Lambda) H_2 + \alpha_{34} I_2 &= 0 \\
\alpha_{41} F_2 + \alpha_{42} G_2 + \alpha_{43} H_2 + (\alpha_{44} - \Lambda) I_2 &= 0
\end{aligned} \tag{C.48}$$

$$\text{where } \Lambda = \frac{1}{\beta_2} \quad (\text{C.49})$$

and the specific coefficients are

$$\begin{aligned} \alpha_{11} &= \frac{1}{D_A} [k_1 C_B^\circ + k_2 C_{AB}^\circ + k_3 C_{A_2B}^\circ + k_4 (C_{A_3B}^\circ + \alpha_{P_A}^\circ \frac{D_A}{D_B}) + \frac{D_A}{D_B} (b_4 - b_3)] \\ \alpha_{12} &= \frac{1}{P_d} [k_1 \alpha_{P_A}^\circ + 4b_3 - 3b_4 - 4k_4 \alpha_{P_A}^\circ] \\ \alpha_{13} &= \frac{1}{P_d} [(k_2 - 3k_4) \alpha_{P_A}^\circ - b_1 + 3b_3 - 2b_4] \\ \alpha_{14} &= \frac{1}{P_d} [(k_3 - 2k_4) \alpha_{P_A}^\circ - b_2 + 2b_3 - b_4] \end{aligned} \quad (\text{C.50})$$

(The above were obtained from (C.46))

$$\begin{aligned} \alpha_{21} &= \frac{1}{D_B} [k_1 \alpha_{C_B}^\circ] \\ \alpha_{22} &= \frac{1}{D_B} [k_1 \alpha_{P_A}^\circ] \\ \alpha_{23} &= - \frac{1}{D_B} [b_1] \\ \alpha_{24} &= 0 \end{aligned} \quad (\text{C.51})$$

(obtained from equation (C.39))

$$\begin{aligned} \alpha_{31} &= \frac{1}{D_B} [k_2 \alpha_{C_{AB}}^\circ - k_1 \alpha_{C_B}^\circ] \\ \alpha_{32} &= - \frac{1}{D_B} [k_1 \alpha_{P_A}^\circ] \\ \alpha_{33} &= \frac{1}{D_B} [k_2 \alpha_{P_A}^\circ + b_1] \\ \alpha_{34} &= - \frac{1}{D_B} [b_2] \end{aligned} \quad (\text{C.52})$$

(obtained from equation (C.40))

$$\alpha_{41} = \frac{1}{D_B} [k_3 \alpha_{A_2B}^{\circ} - k_2 \alpha_{AB}^{\circ} - b_3 \frac{\alpha_A^D}{D_B}]$$

$$\alpha_{42} = \frac{1}{D_B} [4b_3]$$

$$\alpha_{43} = \frac{1}{D_B} [3b_3 - k_2 \alpha_A^{\circ}] \quad (C.53)$$

$$\alpha_{44} = \frac{1}{D_B} [k_3 \alpha_A^{\circ} + b_2 + 2b_3]$$

(obtained from equation (C.41))

The coefficients are constants and are defined in terms of equilibrium concentrations which can be determined from the four equilibrium relationships that can be obtained from equations (C.1) through (C.2).

Equation (C.48) can be satisfied only if the coefficient matrix vanishes

$$\begin{vmatrix} \alpha_{11} - \Lambda & \alpha_{12} & \alpha_{13} & \alpha_{14} \\ \alpha_{21} & \alpha_{22} - \Lambda & \alpha_{23} & \alpha_{24} \\ \alpha_{31} & \alpha_{32} & \alpha_{33} - \Lambda & \alpha_{34} \\ \alpha_{41} & \alpha_{42} & \alpha_{43} & \alpha_{44} - \Lambda \end{vmatrix} = 0 \quad (C.54)$$

The characteristic equation for Λ (actually β^2) is solved to give the four eigenvalues $\beta_1, \beta_2, \beta_3$ and β_4 . (A similar problem was considered by Meldon (1973) who solved the problem of the Adair reaction scheme in a homogeneous slab.)

For each value of β_k , the values of $F_2^{(k)}$, $G_2^{(k)}$, $H_2^{(k)}$, and $I_2^{(k)}$ are given to within a multiplicative constant. One therefore arrives at the solution for f , g , etc. as

$$\begin{aligned}
 f = & F_1\left(\frac{r}{a}\right) + F_2^{(1)}\left(\frac{r}{a}\right)^{-2} \sinh \frac{r}{\beta_1} - F_2^{(1)} \frac{a}{\beta_1} \left(\frac{r}{a}\right)^{-1} \cosh \frac{r}{\beta_1} \\
 & F_2^{(2)}\left(\frac{r}{a}\right)^{-2} \sinh \frac{r}{\beta_2} - F_2^{(2)} \frac{a}{\beta_2} \left(\frac{r}{a}\right)^{-1} \cosh \frac{r}{\beta_2} \\
 & F_2^{(3)}\left(\frac{r}{a}\right)^{-2} \sinh \frac{r}{\beta_3} - F_2^{(3)} \frac{a}{\beta_3} \left(\frac{r}{a}\right)^{-1} \cosh \frac{r}{\beta_3} \\
 & F_2^{(4)}\left(\frac{r}{a}\right)^{-2} \sinh \frac{r}{\beta_4} - F_2^{(4)} \frac{a}{\beta_4} \left(\frac{r}{a}\right)^{-1} \cosh \frac{r}{\beta_4}
 \end{aligned}
 \tag{C.54a}$$

$$\begin{aligned}
 g = & G_1\left(\frac{r}{a}\right) + G_2^{(1)}\left(\frac{r}{a}\right)^{-2} \sinh \frac{r}{\beta_1} - G_2^{(1)} \frac{a}{\beta_1} \left(\frac{r}{a}\right)^{-1} \cosh \frac{r}{\beta_1} \\
 & \quad \quad \quad | \quad \quad \quad | \\
 & \quad \quad \quad | \quad \quad \quad | \\
 & + G_2^{(4)}\left(\frac{r}{a}\right)^{-2} \sinh \frac{r}{\beta_4} - G_2^{(4)} \frac{a}{\beta_4} \left(\frac{r}{a}\right)^{-1} \cosh \frac{r}{\beta_4}
 \end{aligned}
 \tag{C.55}$$

etc.

where the constants $G_2^{(k)}$, $H_2^{(k)}$, $I_2^{(k)}$ are known in terms of $F_2^{(k)}$

$$\begin{aligned}
 G_2^{(k)} &= e_2^{(k)} F_2^{(k)} \\
 H_2^{(k)} &= e_3^{(k)} F_2^{(k)} \\
 I_2^{(k)} &= e_4^{(k)} F_2^{(k)} \quad \quad \quad k=1,2,3,4
 \end{aligned}$$

At this point there are 10 unknowns and these are

$F_1, G_1, H_1, I_1, J_1,$ and

$F_2^{(1)}, F_2^{(2)}, F_2^{(3)}, F_2^{(4)}$ and

A .

Ten relationships are needed in order to solve for the ten constants. So far 4 relationships can be obtained relating the constants F_1, G_1, H_1, I_1, J_1 as has been described earlier. The first relationship is given by equation (C.45) and can be rewritten as

$$\gamma_{11}F_1 + \gamma_{12}G_1 + \gamma_{13}H_1 + \gamma_{14}I_1 + \gamma_{15}J_1 = 0 \quad (\text{C.56})$$

where:

$$\gamma_{11} = \frac{1}{D_A} [k_1 C_B^\circ + k_2 C_{AB}^\circ + k_3 C_{A_2B}^\circ + k_4 C_{A_3B}^\circ]$$

$$\gamma_{12} = \frac{1}{P_d} [k_1 \alpha_{P_A}^\circ + b_4]$$

$$\gamma_{13} = \frac{1}{P_d} [k_2 \alpha_{P_A}^\circ - b_1 + b_4]$$

$$\gamma_{14} = \frac{1}{P_d} [k_3 \alpha_{P_A}^\circ - b_2 + b_4]$$

$$\gamma_{15} = \frac{1}{P_d} [k_4 \alpha_{P_A}^\circ - b_3 + b_4] \quad (\text{C.57})$$

The other three relationships dealing with F_1, G_1, H_1, I_1, J_1 are derived in a manner analogous to that by which equation (C.45) was obtained (as described previously). From (C.39) one obtains

$$\gamma_{21}F_1 + \gamma_{22}G_1 + \gamma_{23}H_1 + \gamma_{24}I_1 + \gamma_{25}J_1 = 0 \quad (\text{C.58})$$

where

$$\gamma_{21} = \frac{1}{D_B} [\alpha k_1 C_B^\circ]$$

$$\gamma_{22} = \frac{1}{D_B} [\alpha k_1 p_A^\circ]$$

$$\gamma_{23} = -\frac{1}{D_B} [b_1]$$

$$\gamma_{24} = \gamma_{25} = 0 \quad (\text{C.59})$$

From (C.40) one obtains

$$\gamma_{31}F_1 + \gamma_{32}G_1 + \gamma_{33}H_1 + \gamma_{34}I_1 + \gamma_{35}J_1 = 0 \quad (\text{C.60})$$

where

$$\gamma_{31} = \frac{1}{D_B} [k_2 \alpha C_{AB}^\circ - k_1 \alpha C_B^\circ]$$

$$\gamma_{32} = -\frac{1}{D_B} [k_1 \alpha p_A^\circ]$$

$$\gamma_{33} = \frac{1}{D_B} [k_2 \alpha p_A^\circ + b_1]$$

$$\gamma_{34} = -\frac{1}{D_B} [b_2]$$

$$\gamma_{35} = 0 \quad (\text{C.61})$$

And from (C.41) one obtains

$$\gamma_{41}F_1 + \gamma_{42}G_1 + \gamma_{43}H_1 + \gamma_{44}I_1 + \gamma_{45}J_1 = 0 \quad (\text{C.62})$$

where

$$\begin{aligned}\gamma_{41} &= \frac{1}{D_B} [k_3 \alpha C_{A_2 B}^\circ - k_2 \alpha C_{AB}^\circ] \\ \gamma_{42} &= 0 \\ \gamma_{43} &= -\frac{1}{D_B} [k_2 \alpha p_A^\circ] \\ \gamma_{44} &= \frac{1}{D_B} [k_3 \alpha p_A^\circ + b_2] \\ \gamma_{45} &= -\frac{1}{D_B} [b_3] \end{aligned} \tag{C.63}$$

Six more relationships are needed which are obtained from the boundary condition at $r=a$. Four relationships are obtained from (C.16) which requires that

$$\frac{\partial g}{\partial r} = 0 \quad r=a \tag{C.64a}$$

$$\frac{\partial h}{\partial r} = 0 \quad r=a \tag{C.64b}$$

$$\frac{\partial i}{\partial r} = 0 \quad r=a \tag{C.64c}$$

$$\frac{\partial j}{\partial r} = 0 \quad r=a \tag{C.64d}$$

Substitution of equations (C.44b) through (C.44e) into equations (C.64a-d) yields

$$G_1 = \sum_{k=1}^4 2F_2(k) e_2^k \left\{ \left[1 + \left(\frac{a}{\beta_k} \right)^2 \frac{1}{2} \right] \sinh \frac{a}{\beta_k} - \frac{a}{\beta_k} \cosh \frac{a}{\beta_k} \right\} \tag{C.67}$$

$$H_1 = \sum_{k=1}^4 2F_2^{(k)} e_3^{(k)} \left\{ \left[1 + \left(\frac{a}{\beta_k} \right)^2 \frac{1}{2} \right] \sinh \frac{a}{\beta_k} - \frac{a}{\beta_k} \cosh \frac{a}{\beta_k} \right\} \quad (\text{C.68})$$

$$I_1 = \sum_{k=1}^4 2F_2^{(k)} e_4^{(k)} \left\{ \left[1 + \left(\frac{a}{\beta_k} \right)^2 \frac{1}{2} \right] \sinh \frac{a}{\beta_k} - \frac{a}{\beta_k} \cosh \frac{a}{\beta_k} \right\} \quad (\text{C.69})$$

$$J_1 = \sum_{k=1}^4 2F_2^{(k)} e_5^{(k)} \left\{ \left[1 + \left(\frac{a}{\beta_k} \right)^2 \frac{1}{2} \right] \sinh \frac{a}{\beta_k} - \frac{a}{\beta_k} \cosh \frac{a}{\beta_k} \right\} \quad (\text{C.70})$$

where $e_5^{(k)}$ is defined as

$$e_5^{(k)} = \left| \frac{P_d}{D_B} - (4e_2^{(k)} + 3e_3^{(k)} + 2e_4^{(k)}) \right| \quad (\text{C.71})$$

The final two equations are obtained from boundary conditions (C.12) and (C.14) which yields

$$F_1 + \sum_{k=1}^4 F_2^{(k)} \left[\sinh \frac{a}{\beta_k} - \frac{a}{\beta_k} \cosh \frac{a}{\beta_k} \right] + \frac{N_A a}{P_c} A = -\frac{N_A a}{P_c} \quad (\text{C.72})$$

$$\begin{aligned} \frac{P_d}{a} \left\{ F_1 - \sum_{k=1}^4 2F_2^{(k)} \left[\sinh \frac{a}{\beta_k} \left(1 + \frac{1}{2} \left(\frac{a}{\beta_k} \right)^2 \right) - \frac{a}{\beta_k} \cosh \frac{a}{\beta_k} \right] \right\} \\ - \frac{2N_A a}{P_d} A = -\frac{N_A a}{P_d} \quad (\text{C.73}) \end{aligned}$$

Equations (C.56), (C.58), (C.60), (C.62), (C.67) through (C.70), (C.72) and (C.73) can now be used to solve for the ten constants. This is of course done on a computer. Once the values of the constants are known the effective permeability can again be obtained using Maxwell's method so

that

$$\frac{\bar{P}}{P_C} = \left| \frac{1-2\phi_A}{1+\phi_A} \right| \quad (C.74)$$

Again the average effective permeability is given by

$$\bar{P}_{AVE} = \frac{\int_{P_A^0}^{P_A^L} \bar{P} dp_A}{P_A^0 - P_A^L} \quad (C.75)$$

C.3 Single Point Linearization Technique for Slab Geometry

A similar analysis as presented in the preceding sections can be carried out for the Adair four step mechanism in a homogeneous medium. For a slab geometry such that variations occur only in the x-direction, the Laplacian is given as

$$\nabla^2 u = \frac{\partial^2 u}{\partial x^2} \quad (C.76)$$

and equations (C.5) through (C.10) still apply if the above Laplacian is used. The boundary conditions for a homogeneous slab are

$$C_A = C_A^0 \quad ; \quad \text{at } x = 0 \quad (C.76)$$

$$C_A = C_A^L \quad ; \quad \text{at } x = L \quad (C.77)$$

$$\frac{dC_B}{dx} = \frac{dC_{AB}}{dx} = \frac{dC_{A_2B}}{dx} = \frac{dC_{A_3B}}{dx} = \frac{dC_{A_4B}}{dx} = 0; \quad \text{at } x=0, L \quad (C.78)$$

$$\int_0^L (C_B + C_{AB} + C_{A_2B} + C_{A_3B} + C_{A_4B}) dx = C_T \quad (C.88)$$

If the diffusivities of the carrier species are the same it can be shown that the carrier concentration is a constant throughout the slab

$$C_B + C_{AB} + C_{A_2B} + C_{A_3B} + C_{A_4B} = C_T \quad (C.89)$$

In addition one can arrive at an equation similar to (C.20) so that

$$\nabla^2 [D_A C_A + D_B (C_{AB} + 2C_{A_2B} + 3C_{A_3B} + 4C_{A_4B})] = 0 \quad (C.90)$$

In the special case that the reaction is at equilibrium throughout the slab it can be shown from equation (C.90) that the flux of A through the slab

$$N_A = + D_A [1 + F_{eq}^{Adair}] \frac{C_A^{\circ} - C_A^L}{L} \quad (C.91)$$

where F_{eq}^{Adair} is defined by (C.31). In the case that the reaction is near but not at equilibrium and for the case that the driving force across the slab is small ($C_A^{\circ} \approx C_A^L$) the concentrations can be expanded as small perturbations from concentration \bar{C}_A where

$$\bar{C}_A = \frac{C_A^{\circ} + C_A^L}{2} \quad (C.92)$$

in the center of the slab.

Therefore

$$C_A = \bar{C}_A + \Delta C_A \quad (C.93a)$$

$$C_B = \bar{C}_B + \Delta C_B \quad (C.93b)$$

$$C_{AB} = \bar{C}_{AB} + \Delta C_{AB} \quad (\text{C.94b})$$

$$C_{A_2B} = \bar{C}_{A_2B} + \Delta C_{A_2B} \quad (\text{C.95b})$$

$$C_{A_3B} = \bar{C}_{A_3B} + \Delta C_{A_3B} \quad (\text{C.96b})$$

$$C_{A_4B} = \bar{C}_{A_4B} + \Delta C_{A_4B} \quad (\text{C.97b})$$

Substitution of equations (C.97) into (C.5) through (C.10) and the elimination of C_{A_4B} through use of equation (C.89) yields a set of equations somewhat similar to those given by (C.38) through (C.41). These are of the form

$$\frac{d^2 \Delta C_A}{dx^2} = \alpha_{11} \Delta C_A + \alpha_{12} \Delta C_B + \alpha_{13} \Delta C_{AB} + \alpha_{14} \Delta C_{A_2B} \quad (\text{C.98a})$$

$$\frac{d^2 \Delta C_B}{dx^2} = \alpha_{21} \Delta C_A + \alpha_{22} \Delta C_B + \alpha_{23} \Delta C_{AB} + \alpha_{24} \Delta C_{A_2B} \quad (\text{C.98b})$$

$$\frac{d^2 \Delta C_{AB}}{dx^2} = \alpha_{31} \Delta C_A + \alpha_{32} \Delta C_B + \alpha_{33} \Delta C_{AB} + \alpha_{34} \Delta C_{A_2B} \quad (\text{C.98c})$$

$$\frac{d^2 \Delta C_{A_2B}}{dx^2} = \alpha_{41} \Delta C_A + \alpha_{42} \Delta C_B + \alpha_{43} \Delta C_{AB} + \alpha_{44} \Delta C_{A_2B} \quad (\text{C.99d})$$

Again the requirement that to zeroth order the perturbation quantities are equal requires that the center concentrations are at equilibrium.

The specific coefficients are similar to those reported in (C.48) through (C.53). These coefficients are:

$$\alpha_{11} = \frac{1}{D_A} [k_1 C_B^\circ + k_2 C_{AB}^\circ + k_3 C_{A_2B}^\circ + k_4 (C_{A_3B}^\circ + \frac{D_A}{D_B} C_A^\circ) + \frac{D_A}{D_B} (b_4 - b_3)]$$

$$\alpha_{12} = \frac{1}{D_A} [k_1 C_A^\circ + 4b_3 - 3b_4 - 4k_4 C_A^\circ]$$

$$\alpha_{13} = \frac{1}{D_A} [(k_2 - 3k_4) C_A^\circ - b_1 + 3b_3 - 2b_4]$$

$$\alpha_{14} = \frac{1}{D_A} [(k_3 - 2k_4) C_A^\circ - b_2 + 2b_3 - b_4]$$

$$\alpha_{21} = \frac{1}{D_B} [k_1 C_B^\circ]$$

$$\alpha_{22} = \frac{1}{D_B} [k_1 C_A^\circ]$$

$$\alpha_{23} = -\frac{1}{D_B} [b_1]$$

$$\alpha_{24} = 0$$

$$\alpha_{31} = \frac{1}{D_B} [k_2 C_{AB}^\circ - k_1 C_B^\circ]$$

$$\alpha_{32} = -\frac{1}{D_B} [k_1 C_A^\circ]$$

$$\alpha_{33} = \frac{1}{D_B} [k_2 C_A^\circ + b_1]$$

$$\alpha_{34} = -\frac{1}{D_B} [b_2]$$

$$\alpha_{41} = \frac{1}{D_B} [k_3 C_{A_2B}^{\circ} - k_2 C_{AB}^{\circ} - b_3 \frac{D_A}{D_B}]$$

$$\alpha_{42} = \frac{1}{D_B} [4b_3]$$

$$\alpha_{43} = \frac{1}{D_B} [3b_3 - k_2 C_A^{\circ}]$$

$$\alpha_{44} = \frac{1}{D_B} [k_3 C_A^{\circ} + b_2 + 2b_3]$$

The general solution for equations (C.99) are

$$\Delta C_A = C_{11} e^{x/\beta} + C_{12} e^{-x/\beta} \quad (\text{C.100a})$$

$$\Delta C_B = C_{21} e^{x/\beta} + C_{22} e^{-x/\beta} \quad (\text{C.100b})$$

$$\Delta C_{AB} = C_{31} e^{x/\beta} + C_{32} e^{-x/\beta} \quad (\text{C.100c})$$

$$\Delta C_{A_2B} = C_{41} e^{x/\beta} + C_{42} e^{-x/\beta} \quad (\text{C.100d})$$

Upon substitution of equations (C.100) into (C.99) one arrives at two sets of relationships analogous to that given in (C.48) except that F_2 , G_2 , H_2 , and I_2 are replaced by C_{11} , C_{21} , C_{31} , and C_{41} or C_{12} , C_{22} , C_{32} , and C_{42} . These are

$$\sum_{j=1}^4 (\alpha_{ij} - \delta_{ij} \Lambda) C_{j1} = 0 \quad i = 1, 2, 3, 4$$

$$\sum_{j=1}^4 (\alpha_{ij} - \delta_{ij} \Lambda) C_{j2} = 0 \quad i = 1, 2, 3, 4$$

where

$$\begin{aligned} \delta_{ij} &= 1 && \text{for } i=j \\ \delta_{ij} &= 0 && \text{for } i \neq j \end{aligned}$$

As with equation (C.54), the eigenvalues Λ (where $\Lambda = 1/\beta_2$) are obtained from the coefficient matrix.

$$\begin{vmatrix} \alpha_{11} - \Lambda & \alpha_{12} & \alpha_{13} & \alpha_{14} \\ \alpha_{21} & \alpha_{22} - \Lambda & \alpha_{23} & \alpha_{24} \\ \alpha_{31} & \alpha_{32} & \alpha_{33} - \Lambda & \alpha_{34} \\ \alpha_{41} & \alpha_{42} & \alpha_{43} & \alpha_{44} - \Lambda \end{vmatrix} = 0 \quad (\text{C.101})$$

The above 4x4 matrix yields the four eigenvalues $\Lambda^{(k)}$ from which $\beta_1, \beta_2, \beta_3,$ and β_4 can be determined. For the same concentrations and physical parameters, the eigenvalues determined from equations (C.54) are equal to those determined from (C.101). For each value of β_k the values of $C_{31}^{(k)}, C_{21}^{(k)}, C_{31}^{(k)}, C_{41}^{(k)}$ or $C_{12}^{(k)}, C_{22}^{(k)}, C_{32}^{(k)}, C_{42}^{(k)}$ can be determined within a multiplicative constant. Expressing all constants in terms of $C_{11}^{(k)}$ and $C_{12}^{(k)}$ one can obtain

$$\begin{aligned} C_{j1}^{(k)} &= e_j^{(k)} C_{11}^{(k)} && j = 2, 3, 4 \\ C_{j2}^{(k)} &= e_j^{(k)} C_{12}^{(k)} && j = 2, 3, 4 \end{aligned}$$

At this point the unknowns are

$$C_{11}^{(1)}, C_{11}^{(2)}, C_{11}^{(3)}, C_{11}^{(4)} \quad \text{and}$$

$$C_{12}^{(2)}, C_{12}^{(3)}, C_{12}^{(4)}$$

and eight relationships are needed. These can be obtained from the boundary conditions. The first two boundary conditions are obtained from (C.76) and (C.77) which require that

$$\Delta C_A = \Delta C_A^\circ \quad \text{at } x=0 \quad (\text{C.102})$$

$$\Delta C_A = \Delta C_A^\circ \quad \text{at } x=L \quad (\text{C.103})$$

where

$$\Delta C_A^\circ = \frac{C_A^\circ - C_A^L}{2}$$

Substitution of the solution of ΔC_A , which is of the form

$$\Delta C_A = \sum_{k=1}^4 [C_{11}^{(k)} e^{x/\beta_k} + C_{12}^{(k)} e^{-x/\beta_k}] \quad (\text{C.104})$$

into equation (C.102) and (C.103) yields

$$\Delta C_A^\circ = \sum_{k=1}^4 (C_{11}^{(k)} + C_{12}^{(k)}) \quad (\text{C.105})$$

$$-\Delta C_A^\circ = \sum_{k=1}^4 (C_{11}^{(k)} e^{L/\beta_k} + C_{12}^{(k)} e^{-L/\beta_k}) \quad (\text{C.106})$$

Also from boundary condition (C.78) for ΔC_B , ΔC_{AB} , and ΔC_{A_2B}

which gives

$$\frac{d\Delta C_B}{dx} = \frac{d\Delta C_{AB}}{dx} = \frac{d\Delta C_{A_2B}}{dx} = 0; \quad x=0, L \quad (C.107)$$

the remaining six equations are obtained which are

$$\sum_{k=1}^4 \left[\frac{e_i^{(k)}}{\beta_k} (C_{11}^{(k)} - C_{12}^{(k)}) \right] = 0, \quad i = 2, 3, 4 \quad (C.108)$$

$$\sum_{k=1}^4 \left[\frac{e_i^{(k)}}{\beta_k} (C_{11}^{(k)} e^{L/\beta_k} - C_{12}^{(k)} e^{-L/\beta_k}) \right] = 0, \quad i=2, 3, 4 \quad (C.109)$$

Now the eight constants $C_{11}^{(k)}$, $C_{12}^{(k)}$ ($k=1, 2, 3, 4$) can be solved from the eight equations (C.105), (C.106), (C.107) and (C.108). The facilitation factor F can be obtained by calculating the flux at $x=0$ or $x=L$. Since

$$D_A \frac{dC_A}{dx} = -N_A^T = -(1+F^{\text{Adair}})N_A \quad (C.110)$$

(at $x=0$, or $x=L$)

The facilitation factor is

$$F^{\text{Adair}} = \frac{1}{2} \frac{\sum_{k=1}^4 \left[\frac{1}{\beta_k} (C_{11}^{(k)} - C_{12}^{(k)}) \right]}{\frac{\Delta C_A^0}{L}} - 1 \quad (C.111)$$

The outlined derivation can be used to calculate facilitation factors for the single point linearization technique. Due to time limitations the actual technique was not used. Instead the methods described by Meldon (1973), who considered the same problem but performed a matched asymptotic technique,

were utilized to predict facilitation factors. Meldon (1973) has shown that for small driving forces the method of matched asymptotic expansion gives equivalent results when compared to the single point linearization technique.

TABLE D.1

OXYGEN PERMEABILITY IN MEM-213 MEMBRANES

Expt #	L_m	$p_{O_2}^{up}$ mm Hg	$p_{O_2}^{down}$ mm Hg	Flux dp/dt $\mu/m \text{ in}$	V_d cm^3	Permeability $\frac{cm^2-cc(STP)}{sec-cc-atm}$
1	48.3	66.2	0.3	98.8	255.5	12.2×10^{-7}
2	48.3	66.0	0.3	93.8	255.5	11.7×10^{-7}
3	25.4	36.3	0.2	106.8	256.2	11.5×10^{-7}
	25.4	48.9	0.9	143.0	256.2	11.6×10^{-7}
4*	25.4	63.5	36.3	80.7	256.2	11.5×10^{-7}
5	88.0	50.4	1.1	46.2	256.2	12.6×10^{-7}
	88.0	83.9	2.5	74.9	256.2	12.4×10^{-7}

$$T = 25^\circ C, A = 25.5 \text{ cm}^2$$

* Plus $p_{H_2O} = 23.8 \text{ mm Hg}$ upstream and downstream.

TABLE D.2

OXYGEN PERMEATION THROUGH THIN LIQUID SLABS OF WATER

(For all runs $T = 25^{\circ}\text{C}$, $A = 25.5 \text{ cm}^2$)

L μm	$2L_m$ μm	V_d cm^3	$p_{\text{O}_2}^{\text{up}}$ mm Hg	$p_{\text{O}_2}^{\text{down}}$ mm Hg	Flux dp/dt μ/min	$\Delta p_{\text{O}_2}^{\text{liq}}$ mm Hg	Δp_m mm Hg	Permeability $\frac{\text{cm}^2\text{-cc(STP)}}{\text{sec-cc-atm}}$
655	2.10	33.20	103.4	2.2	45.7	97.2	4.0	6.22×10^{-7}
676	76.2	27.5	19.1	0.15	10.3	17.9	1.0	6.40×10^{-7}
			39.3	0.45	20.6	36.7	2.1	6.25×10^{-7}
			49.7	0.8	25.3	46.3	2.6	6.08×10^{-7}
			65.2	1.3	31.7	60.6	3.3	5.81×10^{-7}
			79.6	2.1	39.1	73.5	4.0	5.92×10^{-7}
			114.7	3.5	58.8	105.1	6.1	6.22×10^{-7}
			156.6	4.3	80.0	152.3	8.2	6.17×10^{-7}
			170.5	5.6	86.0	156.1	8.8	6.13×10^{-7}
191.7	6.7	97.8	174.9	10.1	6.23×10^{-7}			
676	76.2	27.5	61.7	1.2	32.1	57.2	3.3	6.24×10^{-7}
			97.5	2.0	53.9	89.9	5.6	6.67×10^{-7}
			176.6	4.7	88.8	162.7	9.2	6.07×10^{-7}
			214.6	5.9	108.9	197.5	11.2	6.12×10^{-7}
			238.7	7.7	121.5	218.5	12.5	6.19×10^{-7}
676	76.2	27.5	94.1	1.5	51.7	87.3	5.3	6.59×10^{-7}
			133.6	4.8	71.2	121.4	7.4	6.55×10^{-7}
752	75.2	33.20	96.4	2.2	36.9	89.7	4.5	5.98×10^{-7}
			148.7	2.8	56.0	139.0	6.9	6.02×10^{-7}

TABLE D.2 (cont'd)

L	L _m	V _d ₃	p _{O₂} ^{up}	p _{O₂} ^{down}	Flux dp/dt	Δp _{O₂} ^{liq}	Δp _m	Permeability
<u>μm</u>	<u>μm</u>	<u>cm³</u>	<u>mm Hg</u>	<u>mm Hg</u>	<u>μ/min</u>	<u>mm Hg</u>	<u>mm Hg</u>	<u>cm²-cc (STP) sec-cc-atm</u>
676	93.0	33.20	124.2	1.5	46.0	115.7	7.0	5.95x10 ⁻⁷
	53.3	33.20	100.5	10.7	36.2	86.6	3.2	6.23x10 ⁻⁷
	71.9	33.20	104.7	3.0	40.6	97.0	4.7	6.26x10 ⁻⁷
	71.9	33.20	104.1	2.0	41.9	97.2	4.9	6.42x10 ⁻⁷
	97.0	33.20	111.3	5.6	42.0	99.0	6.7	6.33x10 ⁻⁷
	98.1	33.20	130.2	3.2	49.1	119.2	7.8	6.15x10 ⁻⁷
	96.6	33.20	103.2	2.3	40.1	94.5	6.4	6.35x10 ⁻⁷
	97.0	33.20	108.1	8.5	41.7	93.0	6.6	6.69x10 ⁻⁷
	96.6	34.31	222.6	49.7	66.7	169.0	10.9	6.35x10 ⁻⁷
803	98.1	33.20	103.6	2.7	36.2	95.1	5.8	6.07x10 ⁻⁷
	98.1	33.20	100.5	2.2	35.8	92.6	5.7	6.16x10 ⁻⁷
	98.1	33.20	117.8	1.6	41.3	109.6	6.6	6.01x10 ⁻⁷
	96.6	33.20	173.1	3.0	63.7	160.0	10.1	6.35x10 ⁻⁷
	93.0	34.31	92.9	3.0	31.8	84.8	5.1	5.98x10 ⁻⁷
	94.5	34.31	93.8	4.1	33.7	84.3	5.4	6.38x10 ⁻⁷
	94.5	34.31	49.9	1.0	17.7	46.1	2.8	6.13x10 ⁻⁷
	93.0	30.48	92.3	2.0	36.7	84.9	5.4	6.35x10 ⁻⁷
	93.0	30.48	51.7	1.7	20.3	47.0	3.0	6.33x10 ⁻⁷
	86.4	30.48	91.3	1.5	37.2	84.7	5.1	6.43x10 ⁻⁷
1563	93.0	33.20	213.1	2.4	40.8	204.5	6.2	6.24x10 ⁻⁷
	93.0	33.20	199.1	3.4	40.1	189.6	6.1	6.57x10 ⁻⁷
	93.0	33.20	200.9	3.1	38.9	191.9	5.9	6.28x10 ⁻⁷
	93.0	33.20	196.5	2.7	38.3	188.0	5.8	6.32x10 ⁻⁷
			243.9	4.7	46.8	232.1	7.1	6.25x10 ⁻⁷
1563	92.5	33.20	240.8	4.7	47.3	228.9	7.2	6.40x10 ⁻⁷
	93.5	33.20	295.9	3.9	54.7	283.7	8.3	6.00x10 ⁻⁷
	93.0	33.20	206.3	5.2	39.1	195.2	5.9	6.22x10 ⁻⁷
	92.0	33.20	206.0	4.7	39.0	195.4	5.9	6.19x10 ⁻⁷
	93.0	33.20	202.7	10.1	39.5	186.6	6.0	6.57x10 ⁻⁷
2332	93.0	33.20	240.5	3.0	32.0	232.6	4.9	6.38x10 ⁻⁷

TABLE D.3

MISCELLANEOUS GAS (O_2 , N_2 , CO_2) PERMEATION RUNS THROUGH
THIN LIQUID SLABS OF WATER ($T = 25^\circ C$)

<u>L</u>	<u>2L_m</u>	<u>A</u>	<u>V_d</u>	<u>P_{O₂}^{up}</u>	<u>P_{O₂}^{down}</u>	<u>Flux</u> <u>dp/dt</u>	<u>Permeability</u> <u>$\frac{cm^2-cc(STP)}{sec-cc-atm}$</u>
<u>μm</u>	<u>μm</u>	<u>cm²</u>	<u>cm³</u>	<u>mm Hg</u>	<u>mm Hg</u>	<u>μ/min</u>	
OXYGEN ($P_m = 1.214 \times 10^{-6} \text{ cm}^2\text{-cc(STP)/sec/cc/atm}$)							
1563	93.0	23.1	30.56	135.7 186.7 265.7	2.1 8.0 12.7	26.3 34.7 51.0	6.39×10^{-7} 6.31×10^{-7} 6.55×10^{-7}
1563	93.0	20.1	30.56	154.8 199.7	1.5 3.6	24.1 31.6	5.87×10^{-7} 6.00×10^{-7}
1563	93.0	19.0	30.56	235.8 261.2 261.1	3.2 5.3 31.1	37.2 39.8 36.6	6.34×10^{-7} 6.15×10^{-7} 6.30×10^{-7}
1563	93.0	23.9	33.20	176.5	2.0	31.4	6.14×10^{-7}
(20% support material)							
1563	93.0	25.5	30.48	100.0	1.0	37.4	5.83×10^{-7}
NITROGEN ($P_m = 5.32 \times 10^{-7} \text{ cm}^2\text{-cc(STP)/sec/cc/atm}$)							
676	76.2	25.5	27.5	53.2 98.1	0.6 1.5	15.4 26.8	3.50×10^{-7} 3.29×10^{-7}
676	76.2	25.5	27.5	57.2	1.3	14.4	3.06×10^{-7}

TABLE D.3 (cont'd)

L	$2L_m$	A	V_d	$P_{O_2}^{up}$	$P_{O_2}^{down}$	Flux dp/dt	Permeability
μm	μm	cm^2	cm^3	mm Hg	mm Hg	μ/min	$\frac{cm^2-cc(STP)}{sec-cc-atm}$
CARBON DIOXIDE ($P_m = 7.38 \times 10^{-6} cm^2-cc(STP)/sec/cc/atm$)							
1563	93.0	20.1	257.7	101.6	1.8	43.0	1.49×10^{-5}
1563	93.0	20.1	257.7	106.3 183.7	4.1 10.1	43.6 79.3	1.48×10^{-5} 1.59×10^{-5}
1563	93.0	19.0	257.7	114.8 138.4	3.5 6.9	42.7 51.9	1.40×10^{-5} 1.52×10^{-5}

OXYGEN PERMEABILITY AT DIFFERENT TEMPERATURES

T	L	$2L_m$	$P_{O_2}^{up}$	$P_{O_2}^{down}$	Flux dp/dt	$\Delta P_{O_2}^{liq}$	Δp_m	Permeability
$^{\circ}C$	μm	μm	mm Hg	mm Hg	μ/min			$\frac{cm^2-cc(STP)}{sec-cc-atm}$
17	803	98.1	102.1	2.6	32.9	93.3	6.2	5.78×10^{-7}
21	803	98.1	102.3	3.4	34.7	93.0	5.9	6.02×10^{-7}
25	803	98.1	117.8	1.6	41.3	109.6	6.6	6.01×10^{-7}
29	803	98.1	146.0	6.4	50.7	132.0	7.6	6.05×10^{-7}
33	803	98.1	115.3	2.7	41.0	106.6	6.0	5.97×10^{-7}

(For all experiments $A = 25.5 cm^2$.)

TABLE D.4

PERMEATION OF OXYGEN THROUGH THIN LIQUID SLABS
OF POLYSTYRENE DISPERSIONS

System	Flux $\frac{dp}{dt}$	$p_{O_2}^{up}$	$p_{O_2}^{down}$	ϕ_{solid}	\bar{P}	$\frac{\bar{P}}{P_c}$
	μ/min	mm Hg	mm Hg		$\frac{cm^2-cc(STP)}{sec-cc-atm}$	
Surfactant solution	37.4	99.7	2.6	0.0	6.02×10^{-7}	1
Polystyrene dispersion	35.1	98.9	1.2	0.055	5.65×10^{-7}	0.939
Polystyrene dispersion	35.7	115.3	2.1	0.123	4.93×10^{-7}	0.820
Polystyrene dispersion	32.1	120.8	2.9	0.205	4.27×10^{-7}	0.710
Polystyrene dispersion	35.4	148.5	2.2	0.261	3.73×10^{-7}	0.619

$T = 25^\circ C$ $V_d = 33.20 \text{ cm}^3$ $A = 25.5 \text{ cm}^2$ $L = 752 \text{ } \mu\text{m}$
 $2L_m = 75.2 \text{ } \mu\text{m}$

D.5

TABLE D.5

PERMEATION OF CARBON DIOXIDE THROUGH THIN LIQUID SLABS
OF 120 FEP DISPERSIONS

System	Flux dp/dt <u>μ/min</u>	^{up} P _{O₂}	^{down} P _{O₂}	A	φ _{solid}	\bar{P} <u>cm²-cc (STP) sec-cc-atm</u>	$\frac{\bar{P}}{P_c}$
120 FEP liquid	56.2	173.0	2.7	19.0	0.000	11.6x10 ⁻⁶	1
120 FEP liquid	53.0	160.9	3.8	19.0	0.000	10.8x10 ⁻⁶	1
120 FEP dispersion	31.6	181.4	2.0	19.0	0.357	6.02x10 ⁻⁶	0.540
120 FEP dispersion	48.8 60.9	193.6 242.7	1.9 8.2	19.0	0.178	8.84x10 ⁻⁶ 8.99x10 ⁻⁶	0.790
120 FEP dispersion	35.4	162.1	2.0	21.1	0.309	6.93x10 ⁻⁶	0.618
120 FEP dispersion	49.2	165.4	2.4	21.1	0.106	9.55x10 ⁻⁶	0.855
120 FEP dispersion	53.0	170.5	3.2	21.1	0.060	10.0x10 ⁻⁶	0.893
120 FEP dispersion	31.8	193.0	1.7	21.1	0.411	5.02x10 ⁻⁶	0.448

T = 25°C, V_d = 257.7, L = 1565 μm, 2L_m = 93.0 μm, P_m = 7.38x10⁻⁶ cm²-cc (STP)
sec-cc-atm

TABLE D.6

PERMEATION OF CARBON DIOXIDE THROUGH THIN LIQUID SLABS
OF 30 TFE DISPERSIONS

System	Flux dp/dt μ/min	$P_{O_2}^{\text{up}}$	$P_{O_2}^{\text{down}}$	ϕ_{solid}	\bar{P} $\frac{\text{cm}^2\text{-cc (STP)}}{\text{sec-cc-atm}}$	$\frac{\bar{P}}{P_c}$
30 TFE liquid	38.9	107.3	1.3	0	13.0×10^{-6}	1
30 TFE liquid	60.0	169.9	1.5	0	13.0×10^{-6}	1
30 TFE dispersion	23.0	137.2	1.2	0.398	5.85×10^{-6}	0.450
30 TFE dispersion	37.8	122.4	2.3	0.80	11.0×10^{-6}	0.855
	54.0	180.2	5.1		11.0×10^{-6}	
	63.7	213.9	10.0		11.2×10^{-6}	
	53.5	213.7	43.3		11.3×10^{-6}	
30 TFE dispersion	42.8	173.6	1.3	0.199	8.60×10^{-6}	0.660
30 TFE dispersion	32.8	160.4	1.3	0.299	7.10×10^{-6}	0.543

$T = 25^\circ\text{C}$, $A = 19.0 \text{ cm}^2$, $V_d = 257.7 \text{ cm}^3$, $L = 1565 \text{ }\mu\text{m}$, $2L_m = 93.0 \text{ }\mu\text{m}$,

$P_m = 7.38 \times 10^{-6} \text{ cm}^2\text{-cc (STP)/sec/cc/atm}$

TABLE D.7
 PERMEATION OF OXYGEN IN THIN LIQUID SLABS OF
 SURFACTANT SOLUTIONS USED FOR EMULSIONS

Surfactant Solution	Flux dp/dt <u>μ/min</u>	$p_{O_2}^{up}$ <u>mm Hg</u>	$p_{O_2}^{down}$ <u>mm² Hg</u>	P <u>cm²-cc (STP) sec-cc-atm</u>
10% Tween 40 90% Water	34.3	197.0	2.2	5.60×10^{-7}
"	48.1	286.6	3.3	5.42×10^{-7}
"	33.9	207.7	2.6	5.27×10^{-7}
"	41.2	246.5	2.6	5.39×10^{-7}
50 gr F-68 per liter water	54.8	296.7	3.1	5.96×10^{-7}
"	63.5	337.4	4.0	6.08×10^{-7}

$T = 25^{\circ}C$, $V_d = 33.20$, $L = 1563 \mu m$, $L = 93.0 \mu m$, $A = 25.5 \text{ cm}^2$

TABLE D.8
 PERMEATION OF OXYGEN THROUGH THIN LIQUID SLABS
 OF CASTOR OIL EMULSIONS (O/W)

<u>System</u>	<u>Flux dp/dt μ/min</u>	<u>p_{O₂}^{up}</u>	<u>p_{O₂}^{down}</u>	<u>A</u>	<u>φ_{oil}</u>	<u>cm²-cc (STP) sec-cc-atm</u>	<u>$\frac{\bar{P}}{P_c}$</u>
Castor oil emulsion	50.3	324.1	3.2	25.5	0.180	4.97 x 10 ⁻⁷	0.918
"	42.6	305.1	2.4	25.5	0.234	4.46 x 10 ⁻⁷	0.825
"	37.9	288.4	3.0	25.5	0.291	4.20 x 10 ⁻⁷	0.775
"	41.0	302.0	4.8	25.5	0.347	4.37 x 10 ⁻⁷	0.806
"	35.9	268.4	1.8	25.5	0.394	3.99 x 10 ⁻⁷	0.736
"	44.5	347.5	5.2	25.5	0.460	4.09 x 10 ⁻⁷	0.755
"	36.9	321.7	2.8	25.5	0.487	3.66 x 10 ⁻⁷	0.675
"	40.6	342.7	2.3	25.5	0.542	3.78 x 10 ⁻⁷	0.698
"	42.2	371.6	2.0	25.5	0.648	3.59 x 10 ⁻⁷	0.662
"	38.8	383.3	4.7	25.5	0.750	3.29 x 10 ⁻⁷	0.608
Castor Oil	28.2	375.0	2.0	23.9	1.0	2.54 x 10 ⁻⁷	0.470
"	28.7	378.4	3.3	23.9	1.0	2.55 x 10 ⁻⁷	0.471

T = 25°C, V_d = 33.20, L = 1565 μm, 2L_m = 93.0 μm.

TABLE D.9

TYPICAL SIZE DISTRIBUTION DATA FOR EMULSIONS

<u>CASTOR OIL EMULSION</u>		<u>VEGETABLE OIL EMULSION</u>	
<u>Diameter</u>	<u>Number</u>	<u>Diameter</u>	<u>Number</u>
<u>μm</u>	<u>of</u>	<u>μm</u>	<u>of</u>
	<u>Particles</u>		<u>Particles</u>
0 - 1	344	0 - 1	34
1 - 2	365	1 - 2	605
2 - 3	120	2 - 3	45
3 - 4	66	3 - 4	42
4 - 5	36	4 - 5	31
5 - 6	17	5 - 6	14
6 - 7	13	6 - 7	14
7 - 8	7	7 - 8	23
8 - 9	5	8 - 9	13
9 - 10	2	9 - 10	9
10 - 11	2	10 - 11	4
11 - 12	1	11 - 12	1
12 - 13	0	12 - 13	0
13 - 14	0	13 - 14	0
14 - 15	0	14 - 15	1

All counts were made by microscope (American Optical) at 1000X magnification.

TABLE D.10

PERMEATION OF OXYGEN THROUGH THIN LIQUID SLABS OF
CASTOR OIL (10% SPAN 80) EMULSIONS (O/W)

System	Flux dp/dt μ/min	$p_{\text{O}_2}^{\text{up}}$	$p_{\text{O}_2}^{\text{down}}$	A	ϕ_{oil}	\bar{P}	$\frac{\bar{P}}{P_c}$
						$\frac{\text{cm}^2\text{-cc (STP)}}{\text{sec-cc-atm}}$	
Castor oil emulsion	38.0	259.5	3.3	25.5	0.122	4.68×10^{-7}	0.865
"	32.3	229.6	1.7	23.9	0.260	4.77×10^{-7}	0.880
"	36.5	274.2	1.9	25.5	0.348	4.24×10^{-7}	0.783
"	36.1	294.1	1.1	23.9	0.403	4.17×10^{-7}	0.768
"	35.2	317.0	1.9	23.9	0.490	3.88×10^{-7}	0.717
"	35.5	326.5	2.5	23.9	0.586	3.70×10^{-7}	0.683
"	38.7	367.2	5.3	25.5	0.694	3.36×10^{-7}	0.620
90% Castor oil 10% Span 80	30.9	381.3	3.4	23.9	1.0	2.76×10^{-7}	0.509

$T = 25^\circ\text{C}$, $V_d = 33.20$, $L = 1565 \mu\text{m}$, $2L_m = 93.0 \mu\text{m}$.

TABLE D.11

PERMEATION OF OXYGEN THROUGH THIN LIQUID SLABS OF
WESSON VEGETABLE OIL EMULSIONS (O/W)

<u>System</u>	Flux dp/dt μ/min	$p_{\text{O}_2}^{\text{up}}$	$p_{\text{O}_2}^{\text{down}}$	ϕ_{oil}	\bar{P} $\frac{\text{cm}^2\text{-cc(STP)}}{\text{sec-cc-atm}}$	$\frac{\bar{P}}{P_c}$
Wesson vegetable oil emulsion	42.5	234.9	3.6	0.122	5.87×10^{-7}	1.08
"	41.9	230.1	2.7	0.248	5.89×10^{-7}	1.09
"	38.0	186.2	2.6	0.403	6.64×10^{-7}	1.22
"	45.0	216.8	5.8	0.460	6.83×10^{-7}	1.26
"	45.1	209.6	4.7	0.515	7.06×10^{-7}	1.30
"	46.8	198.8	3.4	0.655	7.75×10^{-7}	1.43
Wesson vegetable oil	97.4	370.7	6.7	1.0	8.68×10^{-7}	1.60
"	99.9	343.5	5.8	1.0	9.50×10^{-7}	1.75

$T = 25^\circ\text{C}$, $A = 25.5$, $L = 1565 \mu\text{m}$, $V_d = 33.20$, $2L_m = 93.0 \mu\text{m}$.

TABLE D.12

PERMEATION OF OXYGEN THROUGH THIN LIQUID SLABS OF FLUOROCARBON

<u>Fluorocarbon</u>	<u>Flux dp/dt</u> μ/min	$p_{\text{O}_2}^{\text{up}}$ <u>mm Hg</u>	$p_{\text{O}_2}^{\text{down}}$ <u>mm Hg</u>	$2L_m$ <u>μm</u>	Δp_m <u>mm Hg</u>	$p_{\text{O}_2}^{\text{O}} - p_{\text{O}_2}^{\text{L}}$ <u>mm Hg</u>	P <u>$\frac{\text{cm}^2\text{-cc (STP)}{\text{sec-cc-atm}}$</u>
PID	151.7	372.4	12.6	93.0	190.5	169.3	$*2.29 \times 10^{-5}$
PID	145.9	377.8	24.8	93.0	171.8	180.7	1.93×10^{-5}
PID	58.8	151.9	52.3	45.8	34.1	65.5	2.16×10^{-5}
PID	59.9	167.1	15.9	84.8	64.5	86.7	1.66×10^{-5}
FC 80	45.5	108.9	2.5	84.8	49.0	57.4	1.91×10^{-5}
FC 80	39.4	104.4	5.3	84.8	42.4	56.4	1.66×10^{-5}

$T = 25^\circ\text{C}$, $V_d = 257.2 \text{ cm}^3$, $A = 25.5$, $L = 1565 \text{ }\mu\text{m}$ ($A^* = 23.9 \text{ cm}^2$).

TABLE D.13

PERMEATION OF OXYGEN THROUGH THIN LIQUID SLABS OF
PID EMULSIONS (O/W)

<u>System</u>	<u>Flux dp/dt</u> μ/min	<u>$p_{\text{O}_2}^{\text{up}}$</u> mm Hg	<u>$p_{\text{O}_2}^{\text{down}}$</u> mm Hg	<u>V_d</u> cm^3	<u>ϕ_{oil}</u>	<u>\bar{P}</u> $\frac{\text{cm}^2\text{-cc (STP)}}{\text{sec-cc-atm}}$	<u>$\frac{\bar{P}}{P_c}$</u>
PID emulsion	434.0	293.0	3.1	33.20	0.750	6.00×10^{-6}	9.97
"	118.4	94.7	10.6	33.20	0.750	5.53×10^{-6}	9.18
"	53.0	300.5	8.5	257.2	0.692	5.54×10^{-6}	9.19
"	62.6	387.8	8.3	257.2	0.710	5.05×10^{-6}	8.39
"	48.2	297.6	7.4	257.2	0.648	4.85×10^{-6}	8.05
"	74.7	376.3	7.8	257.2	0.765	6.41×10^{-6}	10.65

$A = 25.5 \text{ cm}^2$, $2L_m = 93.0 \text{ }\mu\text{m}$, $T = 25^\circ\text{C}$.

TABLE D.14

PERMEATION OF OXYGEN THROUGH THIN LIQUID SLABS OF
INERT HEMOGLOBIN SOLUTION (pH 7.0) ISOTONIC RESULTS

<u>System</u>	<u>C_T</u> gr/100 ml	<u>L</u> μm	<u>2L_m</u> μm	<u>p_{O₂}^{up}</u> mm Hg	<u>p_{O₂}^{down}</u> mm Hg	<u>Flux</u> μ/min	<u>Permeability</u> $\frac{\text{cm}^2\text{-cc (STP)}}{\text{sec-cc-atm}}$
Buffered isotonic saline pH 7.2	0	752	97.0	103.9	3.4	36.7	5.80x10 ⁻⁷
"	0	752	97.0	108.0	3.6	40.3	6.13x10 ⁻⁷
"	0	752	93.0	185.0	2.0	69.9	6.06x10 ⁻⁷
Methemoglobin	8.78	752	97.0	130.1	5.3	41.9	5.30x10 ⁻⁷
"	8.78	803	93.0	133.7	8.9	35.6	4.78x10 ⁻⁷
"	15.4	752	97.0	154.2	8.2	37.2	3.96x10 ⁻⁷
"	15.4	803	93.0	142.0	3.2	33.6	3.93x10 ⁻⁷
"	22.3	752	97.0	99.9	3.3	20.9	3.35x10 ⁻⁷
"	26.2	665	53.3	153.4	2.7	35.6	3.14x10 ⁻⁷
Hemoglobin (saturated)	31.8	752	97.0	166.1	33.5	18.8	2.16x10 ⁻⁷

T = 25°C, A = 25.5 cm², V_d = 33.20 cm³.

TABLE D.15

OXYGEN PERMEABILITY IN THIN LIQUID FILMS OF RED BLOOD CELL SUSPENSIONS
 UNDER INERT CONDITIONS AT T = 25°C

ϕ_{RBC}	$p_{\text{O}_2}^{\text{up}}$ mm Hg	$p_{\text{O}_2}^{\text{down}}$ mm Hg	Flux $\frac{dp}{dt}$ μ/min	$p_{\text{O}_2}^{\text{O}}$	$p_{\text{O}_2}^{\text{L}}$	Permeability $\frac{\text{cm}^2\text{-cc (STP)}}{\text{sec-cc-atm}}$	$\frac{\bar{P}}{P_c}$	pH
0.204	229.8	50.4	57.1	225.1	55.0	5.18×10^{-7}	0.865	7.02
0.417	222.5	45.1	45.2	218.8	48.8	3.93×10^{-7}	0.655	-
0.585	237.0	62.7	39.0	233.8	65.9	3.58×10^{-7}	0.596	7.00
0.715	224.0	48.1	33.7	221.2	50.8	3.05×10^{-7}	0.509	6.94
*0.828	202.4	64.9	26.6	200.6	66.7	2.90×10^{-7}	0.483	6.97
0.866	178.0	40.0	19.8	176.4	41.6	2.26×10^{-7}	0.377	-
0.979	231.2	50.6	23.9	229.2	52.5	2.08×10^{-7}	0.347	6.91
0.985	226.5	52.5	22.9	224.7	54.4	2.07×10^{-7}	0.345	6.89

$$V_d = 34.31 \text{ cm}^3, A = 25.5 \text{ cm}^2, L = 752 \text{ } \mu\text{m}, 2L_m = 96.7 \text{ } \mu\text{m}.$$

$$*V_d = 30.48 \text{ cm}^3, L_m = 86.9 \text{ } \mu\text{m}.$$

TABLE D.16
 OXYGEN PERMEATION EXPERIMENTS IN
 "REACTIVE" RED BLOOD CELL SUSPENSIONS

ϕ	$p_{O_2}^{up}$ mm Hg	$p_{O_2}^{down}$ mm Hg	Flux dp/dt μ/min	$p_{O_2}^{x=0}$ mm Hg	$p_{O_2}^{x=L}$ mm Hg	Permeability $\frac{cm^2-cc(STP)}{sec-cc-atm}$	% Hemo- lysis	pH	P_{50} mm Hg
0.536	24.8	1.3	16.1	24.1	2.0	5.96×10^{-7}	1.3	7.00	14.8
0.384	25.1	1.3	16.7	24.4	2.0	6.28×10^{-7}	0.8	7.00	14.0
0.732	25.1	1.3	16.7	24.3	2.0	6.29×10^{-7}	1.3	6.95	-

$L = 457 \mu m$, $2L_m = 55.9 \mu m$, $A = 25.5 cm^2$, $V_d = 30.48 cm^3$, $T = 25^\circ C$.

For all runs 1 mg/10 ml streptomycin sulfate added.

average $p_{O_2}^{x=L} = 2.0$, average $p_{O_2}^{x=0} = 24.3$ mm Hg.

(Note: For this thickness no phase separation observed.)

TABLE D.17

OXYGEN PERMEATION EXPERIMENTS IN "REACTIVE" RED BLOOD CELL SUSPENSIONS

ϕ	V_d cm ³	$p_{O_2}^{up}$ mm Hg	$p_{O_2}^{down}$ mm Hg	Flux dp/dt μ /min	$p_{O_2}^{x=0}$ mm Hg	$p_{O_2}^{x=L}$ mm Hg	Permeability $\frac{cm^2-cc(STP)}{sec-cc-atm}$	% Hemo- lysis	pH	P_{50} mm Hg
0.852	34.31	50.8	2.6	12.7	49.8	3.6	4.39×10^{-7}	0.4	6.90	13.3
0.387	34.31	52.3	2.3	15.0	51.1	3.5	5.02×10^{-7}	0.2	6.91	-
0.920	34.31	50.8	2.0	12.3	49.8	3.0	4.02×10^{-7}	1.3	6.93	14.1
0.607	30.48	50.3	2.1	17.7	48.8	3.4	5.83×10^{-7}	14.1	6.90	12.2
0.916	30.48	52.6	3.0	14.3	51.3	4.0	4.40×10^{-7}	0.0	6.92	14.0
0.492*	30.48	52.0	2.0	16.3	51.6	3.2	5.01×10^{-7}	0.8	6.97	13.5
0.210	30.48	51.1	2.0	18.3	48.8	3.3	5.83×10^{-7}	0.7	7.06	-
0.785	30.48	50.5	2.0	14.0	49.4	3.1	4.42×10^{-7}	1.0	6.89	14.9
0.911	30.48	50.0	2.0	14.3	49.0	3.0	4.57×10^{-7}	0.5	6.95	-

* added 1 mg/10 ml of streptomycin sulfate added.

$A = 25.5 \text{ cm}^2$, $L = 803 \text{ } \mu\text{m}$, $2L_m = 94.5 \text{ } \mu\text{m}$, $T = 25^\circ\text{C}$, average $p_{O_2}^{x=L} = 3.3$, average $p_{O_2}^{x=0} = 50.0$.

TABLE D.18

OXYGEN PERMEATION EXPERIMENTS IN "REACTIVE" RED BLOOD CELL SUSPENSIONS

ϕ	V_d cm ³	$p_{O_2}^{up}$ mm Hg	$p_{O_2}^{down}$ mm Hg	Flux dp/dt μ /min	$p_{O_2}^{x=0}$ mm Hg	$p_{O_2}^{x=L}$ mm Hg	Permeability $\frac{cm^2-cc(STP)}{sec-cc-atm}$	% Hemo- lysis	pH	P_{50} mm Hg
0.776	34.31	91.0	3.0	23.4	88.2	4.8	4.43×10^{-7}	1.3	6.93	13.5
0.932	34.31	92.4	3.0	17.4	91.0	4.4	3.21×10^{-7}	1.0	6.91	14.2
0.963	30.48	93.3	3.0	21.8	91.7	4.6	3.66×10^{-7}	0.4	6.97	13.3
0.941	30.48	93.3	3.0	24.2	91.7	4.8	4.08×10^{-7}	0.0	6.95	13.3
0.905	30.48	91.6	3.0	24.5	89.8	4.8	4.20×10^{-7}	0.1	7.00	-
0.394	30.48	90.7	3.0	26.8	88.8	5.0	4.68×10^{-7}	0.6	7.00	-
0.225	30.48	91.2	3.0	31.1	88.9	5.3	5.45×10^{-7}	0.9	6.90	14.1
0.518	30.48	91.3	3.0	25.8	89.5	4.7	4.45×10^{-7}	0.0	6.92	14.0
0.909	30.48	91.1	3.0	22.9	89.4	4.7	3.96×10^{-7}	0.2	6.94	12.5
0.908	30.48	89.2	3.0	22.7	87.7	4.6	4.00×10^{-7}	1.1	6.90	13.1
0.765	34.31	92.3	3.0	20.3	90.7	4.6	3.77×10^{-7}	1.1	7.03	-

$A = 25.5 \text{ cm}^2$, $T = 25^\circ\text{C}$, $L = 803 \text{ }\mu\text{m}$, $2L_m = 94.5 \text{ }\mu\text{m}$,
 average $p_{O_2}^{x=0} = 4.8$, $p_{O_2}^{x=L} = 89.7 \text{ mm Hg}$

TABLE D.19
 OXYGEN PERMEATION EXPERIMENTS THROUGH
 RED BLOOD CELL SUSPENSIONS AT 37°C

ϕ	P_{CO} mm Hg	Calculated		Flux $(\frac{\mu}{\text{min}})$	\bar{P}_{AVE} $\frac{\text{cm}^2\text{-cc (STP)}}{\text{sec-cc-atm}}$	%
		$P_{O_2}^{x=0}$ mm Hg	$P_{O_2}^{x=L}$ mm Hg			
0.447	0	35.1	98.2	17.8	4.05×10^{-7}	1.3
0.446	20	38.0	99.6	16.3	3.85×10^{-7}	0

For both experiments: $V_d = 30.48 \text{ cm}^3 + 1 \text{ mg/10 ml streptomycine sulfate}$
 $A = 25.5 \text{ cm}^2$
 $L = 803 \text{ }\mu\text{m}$
 $2L_m = 87 \text{ }\mu\text{m}$

TABLE D.20

OXYGEN PERMEATION EXPERIMENTS ON THE MODEL SYSTEM

Type of Emulsion	Run Number	ϕ	$P_{O_2}^{up}$ mm Hg	$P_{O_2}^{down}$ mm Hg	Flux μ/min	$P_{O_2}^{x=0}$ mm Hg	$P_{O_2}^{x=L}$ mm Hg	\bar{P}_{AVE} $\frac{cm^2-cc(STP)}{sec-cc-atm}$	$\frac{\bar{P}_{AVE}}{P_{OIL}}$
<u>LARGE:</u> $\bar{a}=4.56$ m 58% active	R _x E2	0.50	41.9	1.7	18.6	40.7	2.9	7.18×10^{-7}	1.02
	R _x E6	0.60	42.9	1.6	19.2	41.6	2.9	7.25×10^{-7}	1.03
	R _x E9	0.50	41.9	1.5	18.3	40.7	2.7	7.07×10^{-7}	1.00
	R _x E10	0.35	44.4	1.5	20.6	43.0	2.9	7.53×10^{-7}	1.07
	R _x E12	0.20	42.6	0.7	19.0	41.3	2.0	7.08×10^{-7}	1.00
<u>SMALL:</u> $\bar{a}=1.27$ m 46% active	R _x E1	0.50	40.1	1.5	15.3	39.0	2.6	6.14×10^{-7}	0.870
	R _x E2	0.35	42.7	1.5	17.9	41.4	2.7	6.60×10^{-7}	0.937
	R _x E5	0.60	42.6	1.5	16.5	41.4	2.6	6.08×10^{-7}	0.863
	R _x E13	0.50	43.5	1.5	17.2	42.1	2.7	6.35×10^{-7}	0.903
	R _x E14	0.60	43.5	1.5	16.2	42.0	2.6	6.02×10^{-7}	0.853
<u>INERT:</u> 0% active	R _x E11	0.40	107.6	1.5	41.3	104.7	4.4	5.93×10^{-7}	0.841
	R _x E13	0.50	167.4	32.1	47.5	164.1	35.3	5.36×10^{-7}	0.761
<u>OIL:</u>	--	0	40.7	2.5	17.0	39.5	3.6	6.93×10^{-7}	1
	--	0	46.1	3.0	19.9	44.7	4.3	7.19×10^{-7}	1

$V_d = 30.48 \text{ cm}^3$, $A = 25.5 \text{ cm}^2$, $L = 803 \text{ } \mu\text{m}$, $2L_m = 87 \text{ } \mu\text{m}$, $T = 25^\circ\text{C}$,

$P_{O_2}^{x=0} = 41.0 \text{ mm Hg}$, $P_{O_2}^{x=L} = 2.7 \text{ mm Hg}$.

APPENDIX E

LISTING OF THE COMPUTER PROGRAMS

The following computer programs are listed in this appendix:

1. General Impermeable Model Program
2. General Permeable Model Program
3. Four-Step Reaction Scheme Program (Nonequilibrium)
4. Four-Step Reaction Scheme Equilibrium Program
5. Potential Concentration, and Flux Difference Program for One-Step Reaction in the Dispersed Phase Only
6. General Program for Pressure and Constant Flux Difference Profiles for a Reacting Sphere in a Reacting Medium.

The first four programs calculate the average effective permeability for a given driving force sphere radius, and volume fraction of the dispersed phase. The average effective permeability is obtained by numerical integration of the effective permeability over the partial pressure and division by the driving force. The first three programs were run on the IBM 370 and the latter three on the IBM 1130 computer. Programs 1, 2 and 6 can be used for any type of media discussed.

IMPERMEABLE MODEL

THIS PROGRAM IS THE GENERAL IMPERMEABLE PROGRAM.
 THE PROGRAM CALCULATES THE AVERAGE EFFECTIVE PERMEABILITY
 BY NUMERICAL INTEGRATION FOR A GIVEN DRIVING FORCE.
 THE PROGRAM CAN BE USED FOR OTHER SYSTEMS SHOWN IN
 FIGURE 2.2. A MODIFICATION OF THE PROGRAM WAS UTILIZED
 FOR DETERMINING THE EFFECT OF HEMOLYSIS UPON THE MASS
 TRANSFER RATE OF OXYGEN IN RED BLOOD CELL SUSPENSIONS.
 PHYSICO-CHEMICAL PARAMETERS IN THE DISPERSED PHASE ARE
 USUALLY DENOTED BY THE LETTER P.
 CK1, CK2, ARE THE KINETIC RATE PARAMETERS. ALPHA IS THE
 SOLUBILITY. CT IS THE TOTAL CARRIER CONCENTRATION. PERM
 IS THE PERMEABILITY AND DB IS THE CARRIER DIFFUSIVITY.
 PHI IS THE VOLUME FRACTION OF THE DISPERSED PHASE
 A - RADIUS OF SPHERE. AK- THE CONSTANT A. PEFF- EFFECTIVE
 PERMEABILITY. PAVE(1) AVERAGE EFFECTIVE PERMEABILITY.
 R IS THE DISPERSED TO MEMBRANE PHASE RESISTANCE

```

IMPLICIT REAL*8 (A-H,O-Z)
DOUBLE PRECISION DSINH,DCOSH,DSQRT ,DTANH
DIMENSION PAVE(10)
NITER=0

```

PARAMETERS ARE READ IN

```

READ(5,501) CK1P,CK2P,CK1,CK2
READ(5,501) CTP,CT,ALPHP,      ALPH
READ(5,501) PERMP,PERM,DBP,DB
WRITE(6,601) CK1P,CK2P,CK1,CK2
WRITE(6,603) CTP,CT,ALPHP,ALPH
WRITE(6,605) PERMP,PERM,DBP,DB
5 NITER=NITER+1
READ(5,501) A, RM, THICK
PHI=.25
THICK=.0803
DO 800 KJI=1,1
RM=.1D+19
WRITE(6,621)
WRITE(6,607) A, RM, THICK, PHI
PO2=0.
KJI=1
IF(KJI.GT.0) GO TO 777

```

LOCAL VALUES OF FEQ, PEFF, AND AK CAN BE DETERMINED IF DESIRED

```

DO 20 IK=1,11

```

```

FEQ=(DB *CK1 *ALPH *CK2 *CT )/(PERM *(CK1 *ALPH *PO2 +CK2)**2)
TAMD=(CK1*      ALPH*PO2+CK2)/DB+(CK1*CK2*ALPH*CT)/(PERM*(CK1*ALPH
1*PO2+CK2))
GAM=1./DSQRT(TAMD)
ALAM=A/GAM
GAMA=GAM/A
TAMDP=( CK1P*ALPHP*PO2+CK2P)/DBP+(CK1P*CK2P*ALPHP*CTP)/(PERMP*
1 (CK1P*ALPHP*PO2+CK2P))
FEQP=(DBP*CK1P*ALPHP*CK2P*CTP)/(PERMP*(CK1P*ALPHP*PO2+CK2P)**2)
GAMP=1./DSQRT(TAMDP)
ALAMP=A/GAMP
GAMAP= GAMP/A
IF(ALAMP.GT.100) GO TO 101
GO TO 102
101 TP=1.
GO TO 103
102 TP=DTANH(ALAMP)
103 R=PERMP/PERM*RM
SGAMA=-2.-2.*GAMA-ALAM
UVP=1.-GAMAP*TP
QUVP=-2.*UVP+ALAMP*TP
RFAC=PERM/PERMP*(1.+FEQ)/(1.+FEQP)
TERM2=FEQ*R*(1.+GAMA)*QUVP
TERM3=RFAC*FEQP*R*UVP*SGAMA
TOP=QUVP*SGAMA*((1.+FEQ)-R+RFAC*R)-TERM2+TERM3
BOT=QUVP*SGAMA*((1.+FEQ)+ R/2+RFAC*R) -TERM2+TERM3
AK=(1.+FEQ)/2*TOP/BOT
PEFF=PERM*(1.+FEQ)*((1.+FEQ)-2.*PHI*AK)/((1.+FEQ)+PHI*AK)
WRITE(6,300) FEQ,FEQP,ALAM,ALAMP
WRITE(6,301) AK,PEFF,PO2
PO2=PO2+10
IF(PO2.GT.51) GO TO 104
GO TO 20
104 PO2=PO2+5
20 CONTINUE

```

C
C
C

DRIVING FORCE CONDITIONS SPECIFIED.

```

777 PAO=0
N=120
PAL=5
DO 400 NNN=1,20
J=1
WRITE(6,304)
11 J=J+1
TOTAL=0.
N=N*(J-1)
IF(PAL.GT.41.) GO TO 21
GO TO 22
21 N=300
22 DELPO=(PAL-PAO)/N
SUM=0
DO 75 I=1,N
PO22=PAO+I*DELPO

```

```

PO21=PO22-DELPO
KKK=0
PO2=PO22

```

C
C
C
C

```

PARAMETERS FOR IMPERMEABLE MODEL DETERMINED FOR FIXED PO2.
REPEATED N TIMES IN ORDER TO OBTAIN PAVE(1)

```

```

12 FEQ=(DB *CK1 *ALPH *CK2 *CT )/(PERM *(CK1 *ALPH *PO2 +CK2)**2)
TAMD=(CK1* ALPH*PO2+CK2)/DB+(CK1*CK2*ALPH*CT)/(PERM*(CK1*ALPH
1*PO2+CK2))
GAM=1./DSQRT(TAMD)
ALAM=A/GAM
GAMA=GAM/A
TAMDP=( CK1P*ALPHP*PO2+CK2P)/DBP+(CK1P*CK2P*ALPHP*CTP)/(PERMP*
1 (CK1P*ALPHP*PO2+CK2P))
FEQP=(DBP*CK1P*ALPHP*CK2P*CTP)/(PERMP*(CK1P*ALPHP*PO2+CK2P)**2)
GAMP=1./DSQRT(TAMDP)
ALAMP=A/GAMP
GAMAP= GAMP/A
IF(ALAMP.GT.100) GO TO 201
GO TO 202
201 TP=1.
GO TO 203
202 TP=DTANH(ALAMP)
203 R=PERMP/PERM*RM
SGAMA=-2.-2.*GAMA-ALAM
UVP=1.-GAMAP*TP
QUVP=-2.*UVP+ALAMP*TP
RFAC=PERM/PERMP*(1.+FEQ)/(1.+FEQP)
TERM2=FEQ*R*(1.+GAMA)*QUVP
TERM3=RFAC*FEQP*R*UVP*SGAMA
TOP=QUVP*SGAMA*((1.+FEQ)-R+RFAC*R)-TERM2+TERM3
BOT=QUVP*SGAMA*((1.+FEQ)+ R/2+RFAC*R) -TERM2+TERM3
AK=(1.+FEQ)/2*TOP/BOT
PEFF=PERM*(1.+FEQ)*((1.+FEQ)-2.*PHI*AK)/((1.+FEQ)+PHI*AK)
IF(KKK)24,24,30
24 PEFF2=PEFF
KKK=KKK+1
PO2=PO21
GO TO 12
30 PEFF1=PEFF
AREA=(PO22-PO21)*(PEFF1+PEFF2)/2
SUM=SUM+AREA
75 CONTINUE
FAVE=TOTAL/(PAL-PAO)
FLUXL=SUM/THICK
PAVE(J)=SUM/(PAL-PAO)
RATIO =PAVE(J)/PERM
WRITE(6,305) PAO,PAL, PAVE(J), FLUXL , RATIO,N
400 PAL=PAL+5
800 CONTINUE
IF(NITER.LT.4 ) GO TO 5
300 FORMAT(10X,' FEQ=',D15.5,' FEQP=',D15.5,'ALAM=',D15.5,'ALAMP=',D15
1.5)

```

```

301 FORMAT(10X,' AK=',D15.5,' PEFF=',D15.5,' PO2=',D15.5,/)
304 FORMAT(' PAO PAL PAVE FLUX
1L RATIO N')
305 FORMAT(D15.5,D15.5, D15.5,D15.5,D15.5,I5)
501 FORMAT(D15.5,D15.5,D15.5,D15.5,D15.5)
601 FORMAT(/,15X,'CK1P=',D15.5,'CK2P=',D15.5,'CK1=',D15.5,'CK2=',D15.5
1)
603 FORMAT( 15X,'CTP=',D15.5,'CT=',D15.5,'ALPHP=',D15.5,'ALPH=',D15.5
1)
605 FORMAT(15X,'PERMP=',D15.5,'PERM=',D15.5,'DBP=',D15.5,'PB=',D15.5,/
1)
607 FORMAT(///,
1 15X,'A=',D15.5,'RM=',D15.5,'THICK',D15.5,'PHI =',D15.5,/)
609 FORMAT( /, 25X,' HEMOL= ',D15.5)
613 FORMAT( 10X,'DB=',D15.5,'CT=',D15.5,'PERM=',D15.5,'PHI=',D15.5,'D
1BP=',D15.5)
621 FORMAT( 30X,'*****')
1000 CALL EXIT
END

```

```

C
C DATA READ IN
C

```

```

//G.SYSIN DD *
.40000E+7 .80000E02 .40000E+8 .40000E+3
.10000E00 .20000E-01 .10000E-5 .10000E-5
.10000E-10 .20000E-10 .40000E-07 .80000E-07
.20000E-3 .10000E+5 .07500E00
.40000E-3 .10000E+5 .07500E00
.50000E-3 .10000E+5 .07500E00
.10000E-0 .10000E+5 .07500E00

```



```

1*PO2+CK2))
  GAM=1./DSQRT(TAMD)
  ALAM=A/GAM
  GAMA=GAM/A
  TAMDP=( CK1P*ALPHP*PO2+CK2P)/DBP+(CK1P*CK2P*ALPHP*CTP)/(PERMP*
1 (CK1P*ALPHP*PO2+CK2P))
  FEQP=(DBP*CK1P*ALPHP*CK2P*CTP)/(PERMP*(CK1P*ALPHP*PO2+CK2P)**2)
  GAMP=1./DSQRT(TAMDP)
  ALAMP=A/GAMP
  GAMAP= GAMP/A
  IF(ALAMP.GT.100) GO TO 101
  GO TO 102
101 TP=1.
  GO TO 103
102 TP=DTANH(ALAMP)
103 R=PERMP/PERM*RM
  TANG=TP*GAMAP
  SGAMA=2.+2.*GAMA+ALAM
  SGAM=SGAMA
  GAM1=1.+GAMA
  RP=PERM/PERMP
  RF=(1.+FEQ)/(1.+FEQP)
  RF1=1.-FEQ/FEQP
  TOP1=SGAM*RP*RF1*(RP*RF*FEQ-FEQ)
  TOP2=GAM1*RP*RF1*(1.-RF)
  TOP3=(RP*FEQ/FEQP*SGAMA-2.*GAM1)*(1+FEQ)*(RP*RF-1)
  TOP4=      GAM1*(1.+FEQ)*(RP*RF-1.)*TP*ALAMP
  TOP=(1.-TANG)*(TOP1+TOP2+TOP3)+TOP4
  BOT1=SGAMA*RP*RF1*(1.-1./(1.+FEQ)+2.*RP*FEQ/(1.+FEQP))
  BOT2=2.*GAM1*RP*RF1*(FEQP-FEQ)/(1.+FEQ)/(1.+FEQP)
  BOT3=(RP*(FEQ/FEQP)*SGAMA-2.*GAM1)*(2.*RP*RF+1.)
  BOT4=GAM1*(2.*RP*RF+1.)*TP*ALAMP
  BOT=(1.-TANG)*(BOT1+BOT2+BOT3) +BOT4
  AK=TOP/BOT
  PEFF=PERM*(1.+FEQ)*((1.+FEQ)-2.*PHI*AK)/((1.+FEQ)+PHI*AK)
  WRITE(6,300) FEQ,FEQP,ALAM,ALAMP
  WRITE(6,301) AK,PEFF,PO2
  PO2=PO2+10
  IF(PO2.GT.51) GO TO 104
  GO TO 20
104 PO2=PO2+5
  20 CONTINUE
C
C      DRIVING FORCE CONDITIONS SPECIFIED.
C
777 PAO=0
  N=120
  PAL=5
  DO 400 NNN=1,20
  J=1
  WRITE(6,304)
11 J=J+1
  TOTAL=0.
  N=N*(J-1)

```

```

IF(PAL.GT.41.) GO TO 21
GO TO 22
21 N=300
22 DELPO=(PAL-PAO)/N
SUM=0
DO 75 I=1,N
PO22=PAO+I*DELPO
PO21=PO22-DELPO
KKK=0
PO2=PO22
C
C      PARAMETERS FOR IMPERMEABLE MODEL DETERMINED FOR FIXED PO2.
C      REPEATED N TIMES IN ORDER TO OBTAIN PAVE(1)
C
12 FEQ=(DB *CK1 *ALPH *CK2 *CT )/(PERM *(CK1 *ALPH *PO2 +CK2)**2)
TAMD=(CK1*      ALPH*PO2+CK2)/DB+(CK1*CK2*ALPH*CT)/(PERM*(CK1*ALPH
1*PO2+CK2))
GAM=1./DSQRT(TAMD)
ALAM=A/GAM
GAMA=GAM/A
TAMDP=( CK1P*ALPHP*PO2+CK2P)/DBP+(CK1P*CK2P*ALPHP*CTP)/(PERMP*
1 (CK1P*ALPHP*PO2+CK2P))
FEQP=(DBP*CK1P*ALPHP*CK2P*CTP)/(PERMP*(CK1P*ALPHP*PO2+CK2P)**2)
GAMP=1./DSQRT(TAMDP)
ALAMP=A/GAMP
GAMAP= GAMP/A
IF(ALAMP.GT.100) GO TO 201
GO TO 202
201 TP=1.
GO TO 203
202 TP=DTANH(ALAMP)
203 R=PERMP/PERM*RM
TANG=TP*GAMAP
SGAMA=2.+2.*GAMA+ALAM
SGAM=SGAMA
GAM1=1.+GAMA
RP=PERM/PERMP
RF=(1.+FEQ)/(1.+FEQP)
RF1=1.-FEQ/FEQP
TOP1=SGAM*RP*RF1*(RP*RF*FEQ-FEQ)
TOP2=GAM1*RP*RF1*(1.-RF)
TOP3=(RP*FEQ/FEQP*SGAMA-2.*GAM1)*(1+FEQ)*(RP*RF-1)
TOP4=      GAM1*(1.+FEQ)*(RP*RF-1.)*TP*ALAMP
TOP=(1.-TANG)*(TOP1+TOP2+TOP3)+TOP4
BOT1=SGAMA*RP*RF1*(1.-1./(1.+FEQ)+2.*RP*FEQ/(1.+FEQP))
BOT2=2.*GAM1*RP*RF1*(FEQP-FEQ)/(1.+FEQ)/(1.+FEQP)
BOT3=(RP*(FEQ/FEQP)*SGAMA-2.*GAM1)*(2.*RP*RF+1.)
BOT4=GAM1*(2.*RP*RF+1.)*TP*ALAMP
BOT=(1.-TANG)*(BOT1+BOT2+BOT3) +BOT4
AK=TOP/BOT
PEFF=PERM*(1.+FEQ)*((1.+FEQ)-2.*PHI*AK)/((1.+FEQ)+PHI*AK)
IF(KKK)24,24,30
24 PEFF2=PEFF
KKK=KKK+1

```

```

PO2=PO21
GO TO 12
30 PEFF1=PEFF
AREA=(PO22-PO21)*(PEFF1+PEFF2)/2
SUM=SUM+AREA
75 CONTINUE
FAVE=TOTAL/(PAL-PAO)
FLUXL=SUM/THICK
PAVE(J)=SUM/(PAL-PAO)
RATIO =PAVE(J)/PERM
WRITE(6,305) PAO,PAL, PAVE(J), FLUXL , RATIO,N
400 PAL=PAL+5
800 CONTINUE
IF(NITER.LT.4 ) GO TO 5
300 FORMAT(10X,' FEQ=',D15.5,' FEQP=',D15.5,'ALAM=',D15.5,'ALAMP=',D15
1.5)
301 FORMAT(10X,' AK=',D15.5,' PEFF=',D15.5,' PO2=',D15.5,/)
304 FORMAT(' PAO PAL PAVE FLUX
1L RATIO N')
305 FORMAT(D15.5,D15.5, D15.5,D15.5,D15.5,I5)
501 FORMAT(D15.5,D15.5,D15.5,D15.5,D15.5)
601 FORMAT(/,15X,'CK1P=',D15.5,'CK2P=',D15.5,'CK1=',D15.5,'CK2=',D15.5
1)
603 FORMAT( 15X,'CTP=',D15.5,'CT=',D15.5,'ALPHP=',D15.5,'ALPH=',D15.5
1)
605 FORMAT(15X,'PERMP=',D15.5,'PERM=',D15.5,'DBP=',D15.5,'DB=',D15.5,/
1)
607 FORMAT(///,
1 15X,'A=',D15.5,'RM=',D15.5,'THICK',D15.5,'PHI =',D15.5,/)
609 FORMAT( /, 25X,' HEMOL= ',D15.5)
613 FORMAT( 10X,'DB=',D15.5,'CT=',D15.5,'PERM=',D15.5,'PHI=',D15.5,'D
1BP=',D15.5)
621 FORMAT( 30X,'*****')
1000 CALL EXIT
END

```

FOUR STEP PROGRAM (NONEQUILIBRIUM)

THIS IS THE ADAIR FOUR STEP REACTION SCHEME PERMEABILITY PROGRAM.

THE AVERAGE EFFECTIVE PERMEABILITY IS OBTAINED BY NUMERICAL INTEGRATION.

THE PROGRAM FIRST SOLVES A FOUR BY FOUR MATRIX TO DETERMINE THE FOUR EIGENVALUES. THEN THE CONSTANTS E(J,M)

ARE EVALUATED. ONCE THESE

PARAMETERS ARE KNOWN THE TEN BY TEN MATRIX IS SOLVED IN ORDER TO DETERMINE THE CONSTANT A. WITH THIS IN HAND THE AVERAGE EFFECTIVE PERMEABILITY CAN BE CALCULATED.

PEFF IS OBTAINED BY NUMERICAL INTEGRATION.

PERM- CONTINUOUS PHASE PERMEABILITY. PRIME- DISPERSED PHASE

PERMEABILITY. B(J)- BACKWARD RATE CONSTANTS. K(J)- FORWARD

RATE CONSTANTS. CT-DISPERSED PHASE CARRIER CONCENTRATION.

ALF- SOLUBILITY IN DISPERSED PHASE. DB- DIFFUSIVITY OF

CARRIER. PHI- VOLUME FRACTION. EO- GRADIENT(IMPOSED).

LR(J) EIGENVALUES. A(I,J) COEFFICIENTS OF 4X4 MATRIX.

G(I,J)- COEFFICIENTS OF 10X10 MATRIX. AK -THE CONSTANT A.

PEFF-(AVERAGE) EFFECTIVE PERMEABILITY.

```

REAL K(4),KEQ(4), LR(4),LI(4)
DIMENSION C(6),B(4),D(4),A(4,4),IANA(4),AA(4,4),COE(3,3)
DIMENSION X(10),CONE(3)
DIMENSION E(5,4),G(10,10),AL(10)

```

PARAMETERS ARE READ IN.

```

READ(5,600) DA,DB,CT
READ(5,600) ALF,PERM,EO
DO 4 J=1,4
READ(5,600) K(J),B(J)
B(J)=1.20*B(J)
4 KEQ(J)=K(J)/B(J)
PRIME=DA*ALF
WRITE(6,605)
WRITE(6,610)PERM,PRIME,CT,DB,ALF,EO
WRITE(6,625)
WRITE(6,628) K(1),K(2),K(3),K(4)
WRITE(6,635)
WRITE(6,638) B(1),B(2),B(3),B(4)
44 READ(5,600)AR
WRITE(6,620)AR
NQ=0

```

DRIVING FORCE SPECIFIED

```

46 READ(5,600) PAO,PAL
   NQ=NQ+1
   PHI=0.2
   DO 800 II=1,5
   WRITE(6,676) PHI
   N=120
   IF(PAO.GT.99)      N=240
   DELPO=(PAO-PAL)/N
   SUM=0.
   JCON=0
   DO 275 IR=1,N
   PO22=PAL+IR*DELPO
   PO21= PO22-DELPO
   PO2=PO22
   KKK=0
212 C(1)=ALF*PO2

```

```

C
C      EQUILIBRIUM PARAMETERS AND CONCENTRATIONS CALCULATED. THE
C      COEFFICIENTS A(I,J) SPECIFIED.
C

```

```

CALL EQUIL(C,KEQ,K,B,A,CT,ALF,DA,DB)

```

```

C
C      EIGENVALUES,LR(J) ,ARE CALCULATED USING THE SCIENTIFIC
C      SUBROUTINE PACKAGE SUBROUTINES HSBG AND ATEIG.
C      SINCE THE MATRIX A(I,J) IS NON-SYMMETRICAL, IT WAS FIRST
C      CONVERTED BY A SIMILARITY TRANSFORM TO THE UPPER ALMOST-
C      TRIANGULAR HESSENBURG FORM USING SUBROUTINE HSBG. SUBROUTINE
C      ATEIG THEN COMPUTES THE EIGENVALUES.
C

```

```

   DO 23 I=1,4
   DO 23 J=1,4
23  AA(I,J)=A(I,J)
   CALL HSBG(4,AA,4)
   CALL ATEIG(4,AA,LR,LI,IANA,4)
   DO 24 J=1,4
24  LR(J)=1./SQRT(LR(J))
640 FORMAT(15X,'LR(1)= ',E15.5,' LR(2)= ',E15.5,' LR(3)= ',E15.5,'
      1LR(4)= ',E15.5)
650 FORMAT(15X,'LI(1)= ',E15.5,' LI(2)= ',E15.5,' LI(3)= ',E15.5,'
      1LI(4)= ',E15.5)

```

```

C
C      E(J,M) ARE CALCULATED USING THE SUBROUTINE SIMQ FROM THE
C      SCIENTIFIC SUBROUTINE PACKAGE.
C

```

```

   DO 33 M=1,4
   E(1,M)=1
   DO 28 I=1,3
   CONE(I)=-A(I+1,1)
   DO 28 J=1,3
   IF(I-J) 27,25,27
25  COE(I,J)=A(I+1,J+1)-1./LR(M)**2
   GO TO 28
27  COE(I,J)=A(I+1,J+1)
28  CONTINUE

```

```

CALL SIMQ(COE,CONE,3,KS)
DO 29 J=2,4
29 E(J,M)=CONE(J-1)
33 CONTINUE
DO 9 I=1,4
9 E(5,I)=PRIME/DB -(4.* E(2,I)+3.* E(3,I)+2* E(4,I))

```

```

C
C THE COEFFICIENTS G(I,J) ARE SPECIFIED AND THE TEN UNKNOWNNS
C ARE CALCULATED UTILIZING THE SUBROUTINE SIMQ.
C THE TEN UNKNOWNNS ARE AL(J) WHERE AK IS AL(10)
C

```

```

GRAD=EO
G(1,1)=(K(1)*C(2)+K(2)*C(3)+K(3)*C(4)+K(4)*C(5))/DA
G(1,2)=(K(1)*C(1)+B(4))/PRIME
G(1,3)=(K(2)*C(1)-B(1)+B(4))/PRIME
G(1,4)=(K(3)*C(1)-B(2)+B(4))/PRIME
G(1,5)=(K(4)*C(1)-B(3)+B(4))/PRIME
G(2,1)=K(1)*ALF*C(2)/DB
G(2,2)= K(1)*C(1)/DB
G(2,3)= -B(1)/DB
G(2,4)=0
G(2,5)=0
G(3,1)=(K(2)*C(3)-K(1)*C(2))*ALF/DB
G(3,2)=-K(1)*C(1)/DB
G(3,3)=(K(2)*C(1)+B(1))/DB
G(3,4)=-B(2)/DB
G(3,5)=0
G(4,1)=(K(3)*C(4)-K(2)*C(3))*ALF/DB
G(4,2)=0
G(4,3)=-K(2)*C(1)/DB
G(4,4)=(K(3)*C(1)+B(2))/DB
G(4,5)=-B(3)/DB
DO 6 I=1,4
DO 6 J=6,10
6 G(I,J)=0
DO 7 I=1,4
7 D(I)=SINH(AR/LR(I))*(1+(AR/LR(I))**2/2) -COSH(AR/LR(I))*AR/LR(I)
DO 8 I=5,10
DO 8 J=1,5
8 G(I,J)=0
G(5,2)=-1
G(6,3)=-1
G(7,4)=-1
G(8,5)=-1
DO 10 I=5,8
DO 10 J=6,9
10 G(I,J)=2.* E(I-3,J-5)*D(J-5)
DO 12 I=5,8
12 G(I,10)=0
G(9,1)=1
DO 14 J=6,9
14 G(9,J)=SINH(AR/LR(J-5))-(AR/LR(J-5))*COSH(AR/LR(J-5))
G(9,10)=-AR*GRAD
G(10,1)=1

```

```

DO 16 J=6,9
16 G(10,J)=-2.*D(J-5)
G(10,10)=2.*PERM*GRAD*AR/PRIME
DO 18 J=1,8
18 AL(J)=0
AL(9)=AR*GRAD
AL(10)=PERM*GRAD*AR/PRIME
CALL SIMQ(G,AL,10,KS)
AK=AL(10)

```

```

C
C     EFFECTIVE PERMEABILITY CALCULATED, AND THE WHOLE PROCESS
C     REPEATED (INTEGRATION) IN ORDER TO OBTAIN THE AVERAGE EFFECTIVE
C     PERMEABILITY
C

```

```

PEFF=PERM*(1-2.*PHI*AK)/(1.+PHI*AK)
IF(KKK) 224,224,230
224 IF(JCON) 225,225,229
225 PEFF2=PEFF
KKK=KKK+1
PO2=PO21
GO TO 212
229 PEFF1=PEFF2
PEFF2=PEFF
GO TO 231
230 PEFF1=PEFF
231 AREA=DELPO*(PEFF1+PEFF2)/2
SUM=SUM+AREA
JCON=JCON+1
275 CONTINUE
PEFF=SUM/(PAO-PAL)
RATIO=PEFF/PERM
FLUX=PEFF*(PAO-PAL)/.0803
WRITE(6,674) PAO,PAL,PEFF,FLUX,RATIO
800 PHI=PHI+0.2
1000 WRITE(6,681)
IF(NQ-3) 46,599,599
599 IF(KKK) 598,44,44
598 PHI=PHI+.1
600 FORMAT(5E15.5)
605 FORMAT(10X,'PERM',11X,'PRIME',13X,'CT',13X,'DB',12X,'ALF',9X,'EO')
610 FORMAT(5X,6E15.5)
620 FORMAT(//////////,25X,' AR= ',E15.5,///)
628 FORMAT (5X,5E15.5)
635 FORMAT(/,10X,'B(1)',11X,'B(2)',11X,'B(3)',11X,'B(4)')
638 FORMAT (5X,5E15.5)
625 FORMAT(/,10X,'K(1)',11X,'K(2)',11X,'K(3)',11X,'K(4)')
676 FORMAT(/,30X,'PHI=',E15.5)
674 FORMAT(5X,'PAO=',E12.5,' PAL= ',E12.5,' PEFF= ',E12.5,' FLUX= ',
1E12.5,' RATIO= ',E12.5)
681 FORMAT(//////////)
CALL EXIT
END

```

```

C
C

```



```

C
SUBROUTINE EQUIL(C,KEQ,K,B,A,CT,ALF,DA,DB)
C
C      SUBROUTINE CALCULATES EQUILIBRIUM PARAMETERS AND A(I,J)
C
REAL KEQ(4),K(4)
DIMENSION C(6),A(4,4),B(4)
F1=1+KEQ(1)*C(1)*(1.+KEQ(2)*C(1)*(1.+KEQ(3)*C(1)*(1.+KEQ(4)*C(1)
1)))
C(2)=CT/F1
DO 5 J=3,6
5 C(J)=KEQ(J-2)*C(1)*C(J-1)
PRIME=DA*ALF
A(1,1)=(K(1)*C(2)+K(2)*C(3)+K(3)*C(4)+K(4)*(C(5)+C(1)*DA/DB)+
1 DA/DB*(B(4)-B(3)))/DA
A(1,2)=(K(1)*C(1)+4.*B(3)-3.*B(4)-4.*K(4)*C(1))/PRIME
A(1,3)=(C(1)*(K(2)-3.*K(4))-B(1)+3*B(3)-2*B(4))/PRIME
A(1,4)=(C(1)*(K(3)-2.*K(4))-B(2)+2*B(3)-B(4))/PRIME
A(2,1)=K(1)*ALF*C(2)/DB
A(2,2)=K(1)*C(1)/DB
A(2,3)=-B(1)/DB
A(2,4)=0
A(3,1)=(K(2)*ALF*C(3)-K(1)*ALF*C(2))/DB
A(3,2)=-K(1)*C(1)/DB
A(3,3)=(K(2)*C(1)+B(1))/DB
A(3,4)=-B(2)/DB
A(4,1)=(K(3)*C(4)-K(2)*C(3)-B(3)*DA/DB)*ALF/DB
A(4,2)=4.*B(3)/DB
A(4,3)=(3.*B(3)-K(2)*C(1))/DB
A(4,4)=(K(3)*C(1)+B(2)+2.*B(3))/DB
RETURN
END

```

```

C
C      DATA READ IN
C

```

```

//G.SYSIN DD *
.73750E-05      .60000E-07      .50900E-05
.16000E-08      .34600E-13      -.10000E+05
.17700E+11      .19000E+04
.33200E+11      .15800E+03
.48900E+10      .53900E+03
.33000E+11      .50000E+02
.10000E-03
.24300E+02      .20000E+01
.50000E+02      .33000E+01
.89700E+02      .48000E+01
.40000E-03
.24300E+02      .20000E+01
.50000E+02      .33000E+01
.89700E+02      .48000E+01

```

FOUR STEP EQUILIBRIUM PROGRAM

THIS PROGRAM GIVES THE EQUILIBRIUM SOLUTION OF THE ADAIR
FOUR STEP REACTION SCHEME . PERMP- DISPERSED PHASE PERMEABILITY.
KEQ(J) EQUILIBRIUM CONSTANTS. PAO- UPSTREAM PRESSURE AT X=0.
PAL- DOWNSTREAM PRESSURE AT X=L. FLUX- FLUX THROUGH SLAB.
OTHER PARAMETERS SIMILAR TO THE NONEQUILIBRIUM PROGRAM.
AVERAGE EFFECTIVE PERMEABILITY OBTAINED BY NUMERICAL INTEGRATION.

```

REAL K(4),KEQ(4)
DIMENSION C(6), B(4)
READ(2,600) DA,ALF,PERM
READ(2,600) DB,CT
DO 44 J=1,4
READ(2,600) K(J),B(J)
R(J)=1.2*B(J)
44 KEQ(J)=K(J)/B(J)
PERMP=DA*ALF
WRITE(3,605) DA,ALF,PERMP,PERM
WRITE(3,606) DB,CT
WRITE(3,628) K(1),K(2),K(3),K(4)
WRITE(3,638) B(1),B(2),B(3),B(4)
WRITE(3,648) KEQ(1),KEQ(2),KEQ(3),KEQ(4)
46 READ(2,600) PAO,PAL,PHI
DO 500 II=1,5
WRITE(3,676) PHI
N=250
N=120
DELPO=(PAO-PAL)/N
SUM=0.
DO 275 I=1,N
PO22=PAL+I*DELPO
PO21= PO22-DELPO
PO2=PO22
KKK=0
212 C(1)=ALF*PO2
DIV=1+KEQ(1)*C(1)*(1.+KEQ(2)*C(1))*(1.+KEQ(3)*C(1))*(1+KEQ(4)*C(1)
1)))
DBDP=KEQ(1)*ALF*(1.+KEQ(2)*C(1))*(4.+KEQ(3)*C(1))*(9+16*KEQ(4)*C(1)
1)))
BTOP=KEQ(1)*C(1)*(1.+KEQ(2)*C(1))*(2.+KEQ(3)*C(1))*(3.+4.*KEQ(4)*
1C(1) )))
DSDP=DBDP/4/DIV-BTOP**2/PO2/4/(DIV**2)
SAT=BTOP/4/DIV
FEQ=DB*CT*DSDP/PERMP*4
AK=- (PERMP*(1+FEQ)-PERM)/ (PERMP*(1+FEQ)+2*PERM)
PEFF=PERM*(1-2*PHI*AK)/(1.+PHI*AK)
IF(KKK) 224,224,230

```

```

224 PEFF2=PEFF
    KKK=KKK+1
    P02=P021
    GO TO 212
230 PEFF1=PEFF
    AREA=DELPO*(PEFF1+PEFF2)/2
    SUM=SUM+AREA
275 CONTINUE
    PEFF=SUM/(PAO-PAL)
    RATIO=PEFF/PERM
    FLUX=PEFF*(PAO-PAL)/.0803
    WRITE(3,304) PAO,PAL,PEFF,FLUX,RATIO
500 PHI=PHI+0.20
    IF(KKK) 599,599,46
599 PHI=PHI+.1
600 FORMAT(4E15.5)
605 FORMAT(5X,' DA= ',E15.5,' ALF= ',E15.5,' PERMP= ',E15.5,' PERM= ',
1E15.5)
606 FORMAT(5X,' DB= ',E15.5,' CT= ',E15.5)
628 FORMAT(5X,' K(1)= ',E15.5,' K(2)= ',E15.5,' K(3)= ',E15.5,' K(4)=
1',E15.5)
638 FORMAT(5X,' B(1)= ',E15.5,' B(2)= ',E15.5,' B(3)= ',E15.5,' B(4)=
1',E15.5)
648 FORMAT(5X,' KEQ(1)= ',E15.5,' KEQ(2)= ',E15.5,' KEQ(3)= ',E15.5,
1' KEQ(4)= ',E15.5)
304 FORMAT(5X,'PAO=',E12.5,' PAL= ',E12.5,' PEFF= ',E12.5,' FLUX= ',
1E12.5,' RATIO= ',E12.5)
676 FORMAT(/,30X,'PHI=',E15.5)
    CALL EXIT
    END
// XEQ
    .73750E-05      .16000E-08      .34600E-13
    .60000E-07      .50000E-05
    .17700E+11      .19000E+04
    .33200E+11      .15800E+03
    .48900E+10      .53900E+03
    .33000E+11      .50000E+02
    .24300E+02      .20000E+01      .20000E+00
    .89700E+02      .48000E+01      .20000E+00

```

POTENTIAL, CONCENTRATION, AND FLUX
PROGRAM FOR CASE 4 ONE STEP MODEL.

FOR PARTIAL PRESSURE, CONCENTRATION, OR FLUX DIFFERENCE THE
PROGRAM FIXES THE LOCI AT CERTAIN VALUES AND THEN CALCULATES
THESE LOCI AT VARIOUS POINTS IN SPACE AS A FUNCTION OF THE
NORMALIZED RADIUS AND THE ANGLE.

PRIME= OUTSIDE PERMEABILITY, PERM= INSIDE PERMEABILITY
DA=DIFFUSIVITY OF A IN THE DISPERSED PHASE, DB= DIFFUSIVITY
OF B, CKON= EQUILIBRIUM CONSTANT, CK1= FORWARD REACTION RATE
RA=IS THE NORMALIZED RADIUS WHICH IS R/A
EO= THE IMPOSED GRADIENT, CT= TOTAL CARRIER CONCENTRATION
IN THE DISPERSED PHASE, ALPHA= SOLUBILITY OF A IN THE
DISPERSED PHASE, A= SPHERE RADIUS, PAO= PARTIAL PRESSURE
OF A AT THE CENTER OF THE SPHERE, CBO= CONCENTRATION OF
SPECIES B AT THE CENTER OF THE SPHERE (EQUILIBRIUM)
PHI= ANGLE IN RADIANS, DEGR= ANGLE IN DEGREES
FEQ= EQUILIBRIUM FACILITATION FACTOR, F= FACILITATION FACTOR
SZI= VALUE OF CONSTANT FLUX DIFFERENCE

DIMENSION ZSIN(20)

SET UP OF PHYSICAL PARAMETERS

```

99 READ(2,543) CK1
543 FORMAT(E15.5)
PAO=10.
A=1.E-4
PAQ=3.25*(A/.0001)
PADIF=0.25*(A/.0001)
PRIME=2.804E-11
CT=0.02
ALPHA=1.745E-6
DB=.76E-7
DA=.65E-5
PERM=DA*ALPHA
CKON=7.E+4
CK2=CK1/CKON
EO=-1./A
CBO=(CK2*CT)/(CK1*ALPHA*PAO+CK2)
WRITE(3,342) PAO,CBO,A,EO
WRITE(3,352) DA,DB,CT,ALPHA
WRITE(3,354) PERM,CK1,CK2 ,PRIME
CKON=CK1/CK2

```

```

C      CALC OF GAM, ALAMB, GAMAA
C
C      Y=(CKON*ALPHA*PAO)/(1.+CKON*ALPHA*PAO)
      TAMDA= CK1*ALPHA*PAO*((CT*(1.-Y))/(DA*ALPHA*PAO) + (1./DB) +
1(1.-Y)/(Y*DB))
      GAM=1./ SQRT(TAMDA)
      ALAMB=A/GAM
      GAMAA=GAM/A
      WRITE(3,361) GAM,ALAMB,GAMAA
C
C      CALC OF TERMS AND CONSTANTS
C
      U=DSINH(ALAMB)
      V=DCOSH(ALAMB)
      FEQ=(DB*CKON*CT)/(DA*((CKON*ALPHA*PAO+1.0)**2))
      R=FEQ
      FETA=((3.*(GAMAA**2)+1.)*(U/V)-3.*GAMAA)/((2.*(GAMAA**2)+1.)*(U/V)
1-2.*GAMAA)
      Q=FETA
      F=(R*Q)/(1.+R*(1.-Q))
      B1=((PERM*(1.+F)-PRIME)/(PERM*(1.+F)+2.*PRIME))*(-1.)
      TERM=(CK1*ALPHA*PAO+CK2)/DB
      QQQ=SQRT(GAMAA)
      QQQQ=QQQ*GAMAA
      C1= (TERM*(PRIME/PERM)*(GAMAA**2)*(1.-2.*B1)*(A**2)-(1.+B1))/
1(-(QQQQ      )*U +(QQQ      )*V )
      WRITE(3,371) F,FEQ,B1,C1
C
C      OUTSIDE PA
C
C
C
C
C      LOCI OF PARTIAL PRESSURE LINES OUTSIDE THE SPHERE ARE
C      CALCULATED
C
      WRITE(3,801)
      PA=PAO+PAQ
      DO 50 I=1,13
C      VALUE OF THE PARTIAL PRESSURE IS SET.
      PA=PA-PADIF
      RA=4.25
      WRITE(3,310) PA,RA
      RDEL=.25
      KKK=0
      DO 60 JJ=1,24
      KKK=KKK+1
      IF( 9-KKK) 4,5,5
4 IF(14-KKK) 7,6,6
7 RDEL=0.05
      GO TO 5
6 RDEL=0.1
C      RA FIXED AND ANGLE CALCULATED

```

```

5 RA=RA-RDEL
  AR=1./RA
  ANGLE=(PA-PAO)/ (-EO*RA*A*(1.+B1*(AR**3)))
  IF(1.0-ANGLE) 83,11,11
11 PHI=DARCS(ANGLE)
  DEGR=(180./3.1415927)*PHI
  WRITE(3,704) RA,DEGR,PHI
60 CONTINUE
83 RA=1.
C   AT ZERO DEGREE ANGLE THE NORMALIZED RADIUS IS SEARCHED FOR
  PHI=0.
  DEGR=0.
  DIFF=-0.1
  J=1
66 AR=1./RA
  J=J+1
  TA=PAO-EO*A*RA*(1.+B1*AR**3)
  DELL=ABS(TA-PA)
  IF(DELL-1.E-3) 68,68,71
71 IF(PA-TA) 80,68,72
72 RA=RA-DIFF
  GO TO 77
80 RA=RA+DIFF
  DIFF=DIFF*0.1
  RA=RA-DIFF
77 IF(J-50) 66,66,68
68 WRITE(3,355) TA,RA,DEGR,PHI,J
50 CONTINUE

C
C   INSIDE PA
C
C   LOCI OF PARTIAL PRESSURES INSIDE THE SPHERE FIXED AND
C   SEARCHED FOR.
C
  WRITE(3,804)
  CRIT=.001
  PASET=PAO
  DO 100 I=1,8
C   PARTIAL PRESSURE SET
  PASET=PASET+PADIF
  PHI=-3.1415927/36
  WRITE(3,307) PASET
  DO 109 II=1,18
  J=1
C   ANGLE IN RADIANS (PHI ) SET AND RA SEARCHED FOR
  PHI=PHI+3.1415927/36.
  DIFF=-0.1
  RA=1.0
107 AR=1./RA
  J=J+1
  PROD=RA*ALAMB
  REV=1./PROD
  UR=DSINH(PROD)

```

```

VR=DCOSH(PROD)
FSTAR=C1*(AR**0.5)*(-(REV**1.5)*UR+(REV**0.5)*VR)-TERM*(PRIME /
1PERM)*(GAMAA**2)*      (1.-2.*B1)*RA*(A**2)
PA=PAO+EO*A*FSTAR*      COS(PHI)

```

C
C

```

DEL=(PA-PASET)
DELL= ABS(DEL)
IF(DELL-CRIT) 108,108,111
111 IF(PA-PASET)130,108,112
112 RA=RA+DIFF
GO TO 177
130 RA=RA-DIFF
DIFF=DIFF*0.1
RA=RA+DIFF
IF(1.000-RA) 109,177,177
177 IF(J-50) 107,107,108
108 DEGR=(180./3.1415927)*PHI
WRITE(3,355) PA,RA,DEGR,PHI,J
109 CONTINUE
100 CONTINUE

```

C
C
C
C
C
C
C
C

INSIDE CB CALC

CONCENTRATION LOCI OF B INSIDE SPHERE FIXED AND LOCI
DETERMINED AS A FUNCTION OF RA AND DEGR

```

WRITE(3,806)
RA=1.

```

C

CONC OF B AT RA=1 DETERMINED

```

AR=1./RA
PROD=RA*ALAMB
REV=1./PROD
UR=DSINH(PROD)
VR=DCOSH(PROD)
FSTAR=C1*(AR**0.5)*(-(REV**1.5)*UR+(REV**0.5)*VR)-TERM*(PRIME /
1PERM)*(GAMAA**2)*      (1.-2.*B1)*RA*(A**2)
CBSET=CBO+(PERM/DB)*EO*A*(FSTAR+(1.-2.*B1)*(PRIME/PERM)*RA)
BBB=CBSET-CBO
CRIT=.1E-6

```

```

WRITE(3,666) CBSET ,CBO
DO 200 II=1,9

```

C

A CONCENTRATION FOR B IS SET

```

CBSET=CBSET-0.10*BBB

```

C

ANGLE IN RADIANS IS FIXED AND RA IS SEARCHED

```

999 PHI=-3.1415927/36
WRITE(3,666) CBSET ,CBO
DO 209 IJ=1,18
J=1
PHI=PHI+3.1415927/36.
DIFF=-0.1
RA=1.0

```


C NOW THAT VALUES OF CONSTANT FLUX DIFFERENCE HAVE BEEN
 C SET THE LOCI FOR THE REACTIVE SPHERE IN THE NONREACTIVE MEDIUN
 C CAN BE GENERATED. A SIMILAR PROCEDURE IS USED AS BEFORE.
 C
 C
 C
 C
 C

SZI OUTSIDE SPHERE

C WRITE(3,807)
 DO 460 II=1,10
 C VALUE OF SZI IS SET
 SZI=ZSIN(II)
 RA=4.25
 WRITE(3,631) SZI
 RDEL=0.25
 KKK=0
 DO 450 IJ=1,24
 KKK=KKK+1
 IF(9-KKK)1,2,2
 1 IF(14-KKK) 21,22,22
 22 RDEL=0.1
 GO TO 2
 21 RDEL=0.05
 C RA FIXED AND ANGLE CALCULATED
 2 RA=RA-RDEL
 ANGLE=(SZI)/(PRIME*EO*(A**2)*(B1/RA-(RA**2)/2))
 ANGLE=SQRT(ANGLE)
 IF(1.0-ANGLE) 463,461,461
 461 PHI=DARSN(ANGLE)
 DEGR=(180./3.1415927)*PHI
 WRITE(3,704) RA,DEGR,PHI
 450 CONTINUE
 463 DIFF=-0.1
 J=1
 C RA IS CALCULATED AT 90 DEGREES
 RA=1.
 306 AR=1./RA
 J=J+1
 SZI=PRIME * A**2 * EO*(B1/RA - RA**2/2.)
 DEL= (ZSIN(II)-SZI)
 DELL=ABS(DEL)
 IF(DELL-1.E-19)308,308,311
 311 IF(ZSIN(II)-SZI)330,308,312
 312 RA=RA-DIFF
 GO TO 377
 330 RA=RA+DIFF
 DIFF=DIFF*0.1
 RA=RA-DIFF
 377 IF(J-50) 306,306,308
 308 WRITE(3,655)SZI,RA,J
 655 FORMAT(20X,'SZI=',E15.5,'RA=',E15.5,'J=',I5)
 460 CONTINUE
 C
 C

SZI INSIDE SPHERE

```

C
C
C
DO 470 I=6,12
C   VALUE OF SZI IS SET
SZI=ZSIN(I)
RA=1.0
WRITE(3,631) SZI
DO 465 JJ=1,19
C   RA FIXED AND ANGLE CALCULATED
RA=RA-0.05
AR=1./RA
PROD=RA*ALAMB
UR=DSINH(PROD)
VR=DCOSH(PROD)
DFDR=-TERM*(PRIME/PERM)*(GAM**2)*(1.-2.*B1)*(1./A)+C1*(-(AR**2))*
1(GAMAA**1.5)*(1./GAM)*VR + 2.*(AR**3)*(1./A)*(GAMAA**1.5)*UR+AR*
2(GAMAA**0.5)*(1./GAM)*UR -(1./A)*(AR**2) *(GAMAA**0.5)*VR)
ANGLE=(SZI)/(PERM*EO*(RA**2)*(A**3)*DFDR/2.)
ANGLE=(SZI)/(PRIME*EO*(RA**2)*(A**2)*(-(1.-2.*B1))/2.)
ANGLE=SQRT(ANGLE)
IF(1.0-ANGLE)773,471,471
471 PHI=DARSN(ANGLE)
DEGR=(180./3.1415927)*PHI
WRITE(3,704) RA,DEGR,PHI
465 CONTINUE
773 DIFF=-0.1
J=1
C   RA IS CALCULATED AT 90 DEGREES
RA=1.E-7
706 AR=1./RA
J=J+1
SZI=-PRIME*EO*RA**2*A**2*(1.-2.*B1)/2.
DEL=ZSIN(I)-SZI
DELL=ABS(DEL)
IF(DELL-1.E-21) 708,708,711
711 IF(ZSIN(I)-SZI) 730,708,712
712 RA=RA-DIFF
GO TO 777
730 RA=RA+DIFF
DIFF=DIFF*0.1
RA=RA-DIFF
777 IF(J-50) 706,706,708
708 WRITE(3,655) SZI,RA,J
470 CONTINUE
C
C
631 FORMAT(/,20X,'SZISET=',E15.5)
704 FORMAT(15X,'RA=',E15.5,'DEGR=',E12.5,'PHI=',E12.5)
310 FORMAT(/,20X,' PAINITIAL=',E15.5,' RA INITIAL=',E15.5,/)
342 FORMAT(//,10X,' PAO=',E15.5,' CBO=',E15.5,' A=',E15.5,' EO=',E15.5
1)
352 FORMAT(10X,' DA=',E15.5,' DB=',E15.5,' CT=',E15.5,' ALPHA=',E15.5)
354 FORMAT(20X,' PERM=',E15.5,' CK1=',E15.5,' CK2=',E15.5,' PRIME=',

```

```
1E15.5,////)
361 FORMAT(20X,' LAMDA=',E15.5,' A/LAMDA=',E15.5,' LAMDA/A=',E15.5)
371 FORMAT(/,10X,' F=',E12.5,' FEQ=',E12.5,' BI=',E12.5,' C1=',E12.5)
356 FORMAT(1X,' CB=',E12.5,' PHI=',E12.5,' RA=',E12.5,' DEGR=',E12.5,
1' J=',I2)
307 FORMAT(/,' PASET=',E12.5,/)
355 FORMAT(5X,' PA=',E12.5,' RA=',E12.5,' DEGR=',E12.5,' PHI=',E12.5,
1' J=',I2)
801 FORMAT(/,30X,' OUTSIDE PA CALC',/)
804 FORMAT(/,30X,' INSIDE PA CALC',/)
806 FORMAT(/,30X,' INSIDE CB CALC',/)
807 FORMAT(/,30X,' SZI CALC',/)
532 FORMAT( 30X,' RA=',E15.5,' ZSIN=',E15.5)
531 FORMAT(/,20X,' ZSIN CALCULATION ',/)
666 FORMAT(/,30X,' CBSET=',E15.5,' CBO=',E15.5,/)
1000 CALL EXIT
END
```

GENERAL PROGRAM FOR PRESSURE AND CONSTANT
FLUX DIFFERENCE LOCI AROUND AND INSIDE A
REACTING SPHERE IN A REACTING MEDIUM.

THE PROGRAM FIXES CERTAIN VALUES OF THE PRESSURE AND THE
TOTAL FLUX (IN A REGION OF SPACE) FOR SPECIES A AND THEN
DETERMINES THE LOCUS OF THESE VALUES IN SPACE AS A
FUNCTION OF THE NORMALIZED RADIUS AND THE ANGLE.
FOR A FIXED SET OF PHYSICO-CHEMICAL PARAMETERS THE
EQUILIBRIUM FACILITATION FACTORS CAN BE DETERMINED.
THESE PARAMETERS ARE FED IN WITH THE VALUES OF
THE CHARACTERISTIC LENGTHS FOR A GIVEN SPHERE RADIUS A.
THE PROGRAM CAN CALCULATE PROFILES AND FLUX LINES FOR ANY
OF THE HETEROGENEOUS MEDIA SHOWN IN FIGURE 2.2 .
PHYSICO CHEMICAL PARAMETERS INSIDE THE SPHERE ARE
USUALLY DENOTED BY A P AT THE END (P=PRIME)
PERM= PERMEABILITY, EO= IMPOSED GRADIENT
FA= IMPOSED FLUX, PAO= PARTIAL PRESSURE AT CENTER OF SPHERE.
A= SPHERE RADIUS, ALAM= CHARAC. LENGTH,
FEQ= EQUILIBRIUM FACILITATION FACTOR.
AK, PK1,PK2,PK4, ARE THE FOUR CONSTANTS DETERMINED FROM
THE BOUNDARY CONDITIONS.

DIMENSION ZSIN(15)

PARAMETERS ARE READ IN.

```

READ(2,501) PERM,PERMP,EO,PAO
READ(2,501) FEQ,FEQP
17 READ(2,501) ALAM,ALAMP,A
   JJJ=0
   GAM=A/ALAM
   GAMP=A/ALAMP
   GAMA=1./ALAM
   GAMAP=1./ALAMP
   PAQ=3.25*A/.0001
   PADIF=.25*A/.0001
   WRITE(3,605) PERMP,PERM
   WRITE(3,607) EO,PAO,A
   WRITE(3,609) GAM,ALAM,GAMA
   WRITE(3,611) GAMP,ALAMP,GAMAP
   WRITE(3,612) FEQ,FEQP
605 FORMAT(15X,'PERMP=',E15.5,'PERM=',E15.5)
607 FORMAT(15X,'EO=',E15.5,'PAO=',E15.5,'A=',E15.5)
609 FORMAT(/,15X,'GAM=',E15.5,'ALAM=',E15.5,'GAMA =',E15.5)
611 FORMAT(/,15X,'GAMP=',E15.5,'ALAMP=',E15.5,'GAMAP=',E15.5)

```

```
612 FORMAT(15X,'FEQ=',E15.5,' FEQP=',E15.5)
      JK=1
```

```
      CALC OF TERMS AND CONSTANTS
```

```
      U=DSINH(ALAM)
      V=DCOSH(ALAM)
      UP=DSINH(ALAMP)
      VP=DCOSH(ALAMP)
      IF(ALAMP-75.) 102,101,101
```

```
101 TP=1.
```

```
      GO TO 103
```

```
102 TP=DSINH(ALAMP)/DCOSH(ALAMP)
```

```
103 READ(2,502) NPATH,RM
```

```
      R=PERMP/PERM*RM
```

```
      VALUE OF NPATH DETERMINES WHAT MODEL WILL BE USED.
      NPATH=1.....IMPERMEABLE, NPATH=2 .....PERMEABLE
```

```
      IF(NPATH-1 ) 1,1,2
```

```
1 WRITE(3,705)
```

```
      TERMS AND CONSTANTS FOR THE IMPERMEABLE MODEL ARE CALC.
```

```
      SGAMA =-2. -2.*GAMA-ALAM
```

```
      UVP=1.-GAMAP*TP
```

```
      QUVP=-2.*UVP+ALAMP*TP
```

```
      RFAC=PERM/PERMP*(1.+FEQ)/(1.+FEQP)
```

```
      R=1.
```

```
      TERM2=FEQ*R*(1.+GAMA)*QUVP
```

```
      TERM3=RFAC*FEQP*R*UVP*SGAMA
```

```
      TOP=QUVP*SGAMA*( -R+RFAC*R)-TERM2+TERM3
```

```
      BOT=QUVP*SGAMA*( + R/2+RFAC*R) -TERM2+TERM3
```

```
      AK=(1.+FEQ)/2*TOP/BOT
```

```
      WRITE(3,501) SGAMA,UVP,QUVP,RFAC,TERM2,TERM3
```

```
      TERMT=QUVP*SGAMA*(-R+RFAC*R)
```

```
      TERMB=QUVP*SGAMA*(R/2+RFAC*R)
```

```
      WRITE(3,501) TERMT,TERMB
```

```
      PK2=1.-2.*AK/(1.+FEQ)
```

```
      QRT= SQRT(GAMA)
```

```
      VU= EXP(-ALAM)
```

```
      PK1=FEQ*(-1+TOP/BOT)/QRT/SGAMA/VU
```

```
      DQRT= SQRT(GAMAP)
```

```
      QUVP=QUVP*DCOSH(ALAMP)
```

```
      PK4=(-FEQP/(1.+FEQP)*(1.-TOP/BOT))/(DQRT )/QUVP
```

```
      GO TO 3
```

```
2 WRITE(3,707)
```

TERMS AND CONSTANTS FOR THE PERMEABLE MODEL ARE CALCULATED

```

C
C
TANG=TP*GAMAP
SGAMA=2.+2.*GAMA+ALAM
SGAM=SGAMA
GAM1=1.+GAMA
RP=PERM/PERMP
RF=(1.+FEQ)/(1.+FEQP)
RF1=1.-FEQ/FEQP
TOP1=SGAM*RP*RF1*(RP*RF*FEQ-FEQ)
TOP2=GAM1*RP*RF1*(1.-RF)
TOP3=(RP*FEQ/FEQP*SGAMA-2.*GAM1)*(1+FEQ)*(RP*RF-1)
TOP4=      GAM1*(1.+FEQ)*(RP*RF-1.)*TP*ALAMP
TOP=(1.-TANG)*(TOP1+TOP2+TOP3)+TOP4
ROT1=SGAMA*RP*RF1*(1.-1./(1.+FEQ))+2.*RP*FEQ/(1.+FEQP)
ROT2=2.*GAM1*RP*RF1*(FEQP-FEQ)/(1.+FEQ)/(1.+FEQP)
ROT3=(RP*(FEQ/FEQP)*SGAMA-2.*GAM1)*(2.*RP*RF+1.)
ROT4=GAM1*(2.*RP*RF+1.)*TP*ALAMP
BOT=(1.-TANG)*(BOT1+BOT2+BOT3) +BOT4
AK=TOP/BOT
VUP=(1.-TANG)*DCOSH(ALAMP)
PK2=1.-(2./(1.+FEQ))*AK
QRT= SQRT(GAMA)
DQRT= SQRT(GAMAP)
PK4=((1.+FEQ-2.*AK)*RP *RF - (1+FEQ+AK))/((1. + FEQ)*RP *RF1*
1DQRT*VUP)
VU= EXP(-ALAM)
PK1=((1.+AK/(1.+FEQ))- (1.-2.*AK/(1.+FEQ))*RP *RF + ((1.+FEQ-2.*AK)
1 *RP*RF - (1.+FEQ +AK))/RF1)/( QRT      *GAM1*(VU))
3 FA=-PERM*(1.+FEQ)*EO
WRITE(3,614) TOP,BOT,FA,RM
WRITE(3,613) AK,PK1,PK2,PK4

```

OUTSIDE PA

A VALUE FOR PA IS SET AND THE ANGLE IS CALCULATED AS
THE NORMALIZED RADIUS RA IS VARIED.

```

C
C
WRITE(3,701)
PA=PAO+PAQ
DO 50 I=1,12
C PARTIAL PRESSURE PA IS SET
PA=PA-PADIF
RA=4.25
WRITE(3,615) PA
RDEL=.25
KKK=0
DO 60 JJ=1,16
KKK=KKK+1
IF(11-KKK) 4,5,5
4 RDEL=.1
C RA IS SET
5 RA=RA-RDEL

```

```

AR=1./RA
RATIO=RA/GAMA
VRUR=EXP(-RATIO)
F1=-1./(1.+FEQ)          *AK/RA**2
F2=                        PK1*SQRT(AR)*SQRT(GA)
1MA/RA) *(1.+GAMA/RA)*(VRUR)
FR=F1+F2
C   THE ANGLE FOR FIXED PA AND RA IS CALCULATED.
ANGLE=(PA-PAO)/(-FA/PERM/(1.+FEQ)*A*(RA-FR))
IF(1.-ANGLE) 83,11,11
11 PHI=DARCS(ANGLE)
C   THE ANGLE IN DEGRS IS CALCULATED
DEGR=(180/3.1415927)*PHI
POT=-FA*A*COS(PHI)*(RA+AK/(1+FEQ)/(RA**2))
WRITE(3,617) RA,DEGR,PHI,POT
60 CONTINUE
83 IF(RA-1.001) 50,50,84
84 RA=1.
C   AT ZERO DEGREES THE NORMALIZED RADIUS IS SEARCHED FOR.
PHI=0.
DEGR=0.
DIFF=-1.
J=1
66 AR=1./RA
RATIO=RA/GAMA
VRUR=EXP(-RATIO)
F1=-1./(1.+FEQ)          *AK/RA**2
F2=                        PK1*SQRT(AR)*SQRT(GA)
1MA/RA) *(1.+GAMA/RA)*(VRUR)
FR=F1+F2
J=J+1
TA=PAO-FA*A/PERM/(1.+FEQ)*(RA-FR)
DELL=ABS(TA-PA)
IF(DELL-1.E-4) 68,68,71
71 IF(PA-TA) 80,68,72
72 RA=RA-DIFF
GO TO 77
80 RA=RA+DIFF
DIFF=DIFF*0.1
RA=RA-DIFF
77 IF(J-50) 66,66,68
68 WRITE(3,619) TA,RA,DEGR,PHI,J
POT=-FA*A*COS(PHI)*(RA+AK/(1+FEQ)/(RA**2))
WRITE(3,617) RA,DEGR,PHI,POT
50 CONTINUE
C
C
C   INSIDE PA
C
C   PROCEDURE SAME AS BEFORE. FIRST PA IS SET, THEN RA IS
C   SET AND THE ANGLE IS CALCULATED. FINALLY AT ZERO DEGREES
C   RA IS SEARCHED FOR.
C
C

```

```

WRITE(3,621)
PA=PAO
DO 150 I=1,10
C   PA IS SET
PA=PA+PADIF
RA=1.05
WRITE(3,615) PA
RDEL=.05
DO 160 JJ=1,20
C   RA IS SET
RA=RA- RDEL
AR=1./RA
C   FOR A FIXED PA , THE ANGLE IS CALCULATED FOR EACH RA
VRP=DCOSH(RA/GAMAP)
URP=DSINH(RA/GAMAP)
VRURP=VRP-URP/(RA/GAMAP)
H1=-PK2*FA/PERMP*(1./(1.+FEQP)) *A*RA
H2= FA*A/
1 PERMP*PK4*AR**0.5*(GAMAP/RA)**0.5*(VRURP)
HR=H1+H2
ANGLE=(PA-PAO)/HR
IF(1.-ANGLE) 183,111,111
111 PHI=DARCS(ANGLE)
DEGR=(180/3.1415927)*PHI
POT=-FA*A* COS(PHI)*(RA*PK2+ 3*AK/(1+FEQ))
WRITE(3,617) RA,DEGR,PHI,POT
160 CONTINUE
183 RA=1.
C   AT ZERO DEGREES RA IS SEARCHED FOR.
DEGR=0.
PHI=0.
DIFF=0.1
J=1
166 AR=1./RA
J=J+1
VRP=DCOSH(RA/GAMAP)
URP=DSINH(RA/GAMAP)
VRURP=VRP-URP/(RA/GAMAP)
H1=-PK2*FA/PERMP*(1./(1.+FEQP)) *A*RA
H2= FA*A/
1 PERMP*PK4*AR**0.5*(GAMAP/RA)**0.5*(VRURP)
HR=H1+H2
TA=PAO+HR
DELL=ABS(TA-PA)
IF(DELL-1.E-4) 168,168,171
171 IF(TA-PA) 180,168,172
172 RA=RA-DIFF
GO TO 177
180 RA=RA+DIFF
DIFF=DIFF*0.1
RA=RA-DIFF
177 IF(J-50) 166,166,168
168 WRITE(3,619) TA,RA,DEGR,PHI,J
POT=-FA*A* COS(PHI)*(RA*PK2+ 3*AK/(1+FEQ))

```



```

WRITE(3,617) RA,DEGR,PHI,POT
IF(RA-1.)150,150,151
150 CONTINUE
151 WRITE(3,629)

```

```

C
C
C          POTENTIAL      FLOW
C
C
C

```

```

C          FOR THE LOCI OF CONSTANT FLUX DIFFERENCE THE VALUES
C          ARE SET UP FOR THE CASE OF A REACTING SPHERE AT EQUILIBRIUM
C          IN A CONTINUOUS MEDIUM AT EQUILIBRIUM. ALSO THE INSIDE
C          PARAMETERS ARE ANALOGOUS TO THE OUTSIDE PARAMETERS. FOR
C          THIS CASE LINES OF CONSTANT FLUX DIFFERENCE ARE PARALLELL.
C          THIS BASE CASE SETS THE VALUES FOR FLUX DIFFERENCES.
C          BY CALCULATING THEM AT 90 DEGREES AND EACH RA=.25
C          THE LINES WILL BE EQUIDISTANT. FOR THE SITUATION OF INTEREST
C          THE LINES OF CONSTANT FLUX DIFFERENCE WILL APPROACH
C          THE LINES OF THE BASE CASE AT LARGE DISTANCES AWAY FROM
C          THE SPHERE. (EFFECTS OF THE REACTING SPHERE DECAY RAPIDLY)
C

```

```

WRITE(3,531)

```

```

RA=3.25

```

```

C          EQUILIBRIUM VALUE OF AK WOULD BE

```

```

AE=(1.+FEQ)*(PERM*(1+FEQ)-PERMP*(1+FEQP))/(2.*PERM*(1+FEQ)+PERMP*
1 (1+FEQP))

```

```

C          HOWEVER FOR EQUAL PARAMETERS IT IS ZERO

```

```

AE=0.

```

```

C          ZSIN(IJ)= SZI SET VALUES. CALCULATED OUTSIDE SPHERE

```

```

DO 440 IJ=1,9

```

```

RA=RA-.25

```

```

SZI=-FA*A**2*(RA**2-2*AE/(1+FEQ))/RA)

```

```

ZSIN(IJ)=SZI

```

```

WRITE(3,532) RA,ZSIN(IJ)

```

```

440 CONTINUE

```

```

RA=RA+.25

```

```

C          ZSIN(IJ)= SZI SET VALUES. CALCULATED INSIDE SPHERE

```

```

DO 441 IJ=9,12

```

```

RA=RA-.25

```

```

SZI=-RA**2*A**2*FA*(1.-2*AE/(1+FEQ))

```

```

ZSIN(IJ)=SZI

```

```

WRITE(3,532) RA,ZSIN(IJ)

```

```

441 CONTINUE

```

```

C
C
C          SZI OUTSIDE SPHERE
C
C
C

```

```

C          SAME PROCEDURE AS BEFORE IS USED. FOR EACH SET VALUE
C          OF SZI RA IS VARIED AND EACH ANGLE CALCULATED . THE POINTS
C          IN SPACE WILL THEN GIVE A LINE. AT 90 DEGREES RA IS SEARCHED.
C

```

```

WRITE(3,807)
DO 460 II=1,12
SZI=ZSIN(II)
RA=4.25
WRITE(3,731) SZI
RDEL=0.25
KKK=0
DO 450 IJ=1,24
KKK=KKK+1
IF(9-KKK)21,22,22
21 IF(14-KKK) 23,24,24
24 RDEL=0.1
GO TO 22
23 RDEL=0.05
22 RA=RA-RDEL
ANGLE=(SZI)/(-FA*A**2*(RA**2-2*AK/(1.+FEQ)/RA))
ANGLE=SQRT(ANGLE)
IF(1.0-ANGLE) 463,461,461
461 PHI=DARSN(ANGLE)
DEGR=(180./3.1415927)*PHI
WRITE(3,704) RA,DEGR,PHI
450 CONTINUE
IF(RA-1.01) 460,463,463
463 DIFF=-0.1
J=1
RA=1.
406 AR=1./RA
J=J+1
SZI=-FA*A**2*(RA**2-2*AK/(1+FEQ)/RA)
DEL=(ZSIN(II)-SZI)
DELL=ABS(DEL)
IF(DELL-1.E-19)408,408,411
411 IF(ZSIN(II)-SZI)430,408,412
412 RA=RA-DIFF
GO TO 477
430 RA=RA+DIFF
DIFF=DIFF*0.1
RA=RA-DIFF
477 IF(J-50) 406,406,408
408 WRITE(3,655)SZI,RA,J
655 FORMAT(20X,'SZI=',E15.5,'RA=',E15.5,'J=',I5)
460 CONTINUE

```

```

C
C           SZI INSIDE SPHERE
C

```

```

WRITE(3,803)
803 FORMAT(///,20X,'INSIDE SZI',/)
DO 470 I=6,12
SZI=ZSIN(I)
RA=1.05
WRITE(3,731) SZI
DO 465 JJ=1,19
RA=RA-0.05
AR=1./RA

```

```

ANGLE=SZI/(-FA*A**2*RA**2*(1.-2.*AK/(1.+FEQ)) )
ANGLE=SQRT(ANGLE)
IF(1.0-ANGLE)773,471,471
471 PHI=DARSN(ANGLE)
DEGR=(180./3.1415927)*PHI
WRITE(3,704) RA,DEGR,PHI
465 CONTINUE
773 DIFF=-0.1
J=1
RA=1.E-7
706 AR=1./RA
J=J+1
SZI=-RA**2*A**2*FA*(1.-2*AK/(1+FEQ))
DEL=ZSIN(I)-SZI
DELL=ABS(DEL)
IF(DELL-1.E-21) 708,708,711
711 IF(ZSIN(I)-SZI) 730,708,712
712 RA=RA-DIFF
GO TO 777
730 RA=RA+DIFF
DIFF=DIFF*0.1
RA=RA-DIFF
777 IF(J-50) 706,706,708
708 WRITE(3,655) SZI,RA,J
470 CONTINUE
731 FORMAT(/,20X,'SZISET=',E15.5)
704 FORMAT(15X,'RA=',E15.5,'DEGR=',E12.5,'PHI=',E12.5)
807 FORMAT(/,30X,' SZI CALC',/)
532 FORMAT( 30X,'RA=',E15.5,' ZSIN=',E15.5)
531 FORMAT(/,20X,' ZSIN CALCULATION ',/)
JK=JK+1
IF(3-JK) 1000,1000,1
501 FORMAT(E15.5,E15.5,E15.5,E15.5,E15.5,E15.5)
629 FORMAT(////,15X,' CONSTANT FLUX DIFFERENCE LINES',/)
502 FORMAT(I5,E15.5)
613 FORMAT(15X,
1 ' AK=',E15.5,'PK1=',E15.5,'PK2=',E15.5,'PK4=',E15.5)
614 FORMAT(15X,'TOP=',E15.5,' BOT=',E15.5,' FA=',E15.5,' RM=',E15.5)
615 FORMAT(///,25X,'PA=',E15.5,/)
617 FORMAT(9X,'RA=',E15.5,'DEGR=',E15.5,'PHI=',E15.5,' POT=',E15.5)
619 FORMAT(5X,'TA=',E15.5,'RA=',E15.5,'DEGR=',E15.5,'PHI=',E15.5,'J=',
1I4)
621 FORMAT(/,30X,'INSIDE PA CALCULATION',/)
701 FORMAT(///,30X,' OUTSIDE PA',/)
705 FORMAT(////////,25X,'NPATH=1 *****IMPERMEABLE*****',/)
707 FORMAT(////////,25X,'NPATH=2 *****PERMEABLE*****',/)
1000 CALL EXIT
END
// XEQ
.20000E-10 .10000E-10 +.10000E+05 .10000E+02
.25000E+01 .10000E+02
.16700E+02 .20900E+02 .10000E-03
2 .10000E+19

```

APPENDIX F

SAMPLE CALCULATION FOR DATA REDUCTION

A calculation is given here as an example in order to demonstrate how the permeability (average effective permeability) is obtained. Some common parameters for most of the runs are

$$\begin{aligned} A &= 25.5 \text{ cm}^2 \\ V_d &= 30.48 \text{ cm}^3 \\ P_m &= 1.214 \times 10^{-6} \frac{\text{cm}^2\text{-cc (STP)}}{\text{sec-cc-atm}} \\ T &= 25^\circ\text{C} \\ L &= 803 \text{ } \mu\text{m} \\ 2L_m &= 94.5 \text{ } \mu\text{m} \end{aligned}$$

First the partial pressure drop through each membrane can be obtained from equation (6.10). Substitution of the above parameters yields

$$\Delta p_m = 0.74 \times 10^{-1} \frac{dp}{dt}$$

Consider the ninth run. The experimental conditions of interest are:

$$\begin{aligned} \phi &= 0.909 \\ p_{\text{O}_2}^{\text{up}} &= 91.1 \text{ mm Hg}, \quad p_{\text{O}_2}^{\text{down}} = 3.0 \text{ mm Hg} \\ \frac{dp}{dt} &= 22.9 \frac{\mu\text{m Hg}}{\text{min}} \end{aligned}$$

so that the pressure drop through each membrane is

$$\begin{aligned} \Delta p_m &= (0.74 \times 10^{-1}) (2.29 \times 10^1) \\ &= 1.7 \text{ mm Hg} \end{aligned}$$

The partial pressures at $x = 0$ and $x = L$ can now be calculated from (6.11) and (6.12)

$$p_{O_2}^{x=0} = 91.1 - 1.7 = 89.5 \text{ mm Hg}$$

$$p_{O_2}^{x=L} = 3.0 + 1.7 = 4.7 \text{ mm Hg}$$

Finally equation (6.9) gives the permeability which is with the earlier set of parameters

$$\bar{P}_{AVE} = 1.465 \times 10^{-6} \frac{dp/dt}{(p_{O_2}^{x=0} - p_{O_2}^{x=L})}$$

so that

$$\begin{aligned} \bar{P}_{AVE} &= \frac{(1.465 \times 10^{-6})(2.29 \times 10^1)}{(84.8)} \\ &= 3.96 \times 10^{-7} \frac{\text{cm}^2\text{-cc (STP)}}{\text{sec-cc-atm}} \end{aligned}$$

APPENDIX G
NOMENCLATURE

a	sphere radius
A	constant in the outside potential function
A, A_E	cross-sectional area
A_n	constant used in Appendix A
b_i	backward rate constant in Adair scheme $i = 1, 2, 3, 4$
B	constant used in Appendix C, defined by equation (C.29)
B_n	constant used in Appendix A
C	concentration
\bar{C}, C^0	equilibrium concentrations
C_A	concentration of species A
C_B	concentration of species B
$C_{A_i B}$	concentration of species $A_i B$, $i = 1, 2, 3, 4$
\bar{C}_A	equilibrium concentration of A
C_A^0	concentration of A at $x = 0$ (or $r = 0$ in which case it is an equilibrium concentration)
C_A^L	concentration of A at $x = L$
$C_{ij}^{(k)}$	constant used in Appendix C ($i = 1, 2, 3, 4$; $k = 1, 2, 3, 4$; $j = 1, 2$)
C_T	total carrier concentration
C_1	a constant used in Chapter 4
C_2	a constant used in Chapter 4
d_c	size contact points of support material
d_i	average particle diameter for class i
\bar{d}_n	number average diameter
\bar{d}_v	volume mean diameter

D	diffusivity
\bar{D}	effective diffusivity
D_A	diffusivity of species A
D_B	diffusivity of carrier species B
D_{A_iB}	diffusivity of carrier species A_iB
D_1	constant defined by equation (5.8)
D_2	constant defined by equation (5.9)
$e_i^{(k)}$	constant used in Appendix C ($i = 2,3,4,5$; $k = 1,2,3,4$)
E	constant used in Appendix C
E_m	constant used in Appendix A
$f(r)$	function defined by equation (4.43)
$f(r)$	function defined by equation (C.44a)
$f_1(r)$	function defined by equation (5.42)
$f_2(r)$	function defined by equation (5.43)
f_c	function defined by equation (4.70)
F	facilitation factor
F^{Adair}	Adair facilitation factor
F_{eq}	equilibrium facilitation factor
F_d	dispersed phase facilitation factor $F_d \rightarrow F'_{\text{eq}}$ as $a/\lambda' \rightarrow \infty$
$F_{\text{eq}}^{\text{Adair}}$	Adair equilibrium facilitation factor
F_i	constant used in Appendix C ($i = 1,2$)
$g(r)$	function defined by equation (4.33)
$g(r)$	function defined by equation (C.44a)
G_i	constant used in Appendix C ($i = 1,2$)
$h(r)$	function defined by equation (C.44c)
H_i	constant used in Appendix C ($i = 1,2$)

$H(r)$	function defined by equation (4.55)
$I_p(z)$	modified Bessel function of the first kind
$i(r)$	function defined by equation (C.44d)
I_i	constant used in Appendix C ($i = 1,2$)
$j(r)$	function defined by equation (C.44e)
J_i	constant used in Appendix C ($i = 1,2$)
k_1	forward rate in one-step model
k_2	backward rate in one-step model
k_i	forward reaction rate in four-step model ($i = 1,2,3,4$)
K	equilibrium constant for one-step model
K_i	equilibrium constants for the four-step model ($i = 1,2,3,4$)
K_d	ratio of the dispersed phase to the continuous phase permeability
K_m	ratio of the effective permeability to the continuous phase permeability
K_p	equilibrium constant based on activity
K_1	a constant used in Chapter 4
K_2	a constant used in Chapter 4
K'_2	a constant used in Chapter 4
K'_4	a constant used in Chapter 4
L	film thickness
L_m	support membrane thickness
L_s	skin thickness
L_i	a constant
n	integer
n_i	number of particles in class i

N_A	flux of A
N_A^T	flux of A (implies carrier in continuous phase)
N_{O_2}	flux of oxygen
N_{Gr}	Grashof number
N_{Ra}	Rayleigh number
N_{Sc}	Schmidt number
p	pressure
p_A^o	partial pressure at $x = 0$ (or $r = 0$ in which case it is an equilibrium pressure)
p_A	partial pressure of the species A
p_B	activity of carrier species B
p_{AB}	activity of carrier species AB
p_{O_2}	partial pressure of oxygen
$p_A^{x=0}$	partial pressure of species A at $x = 0$
$p_A^{x=L}$	partial pressure of species A at $x = L$
$p_{O_2}^{up}$	oxygen pressure in upstream volume
$p_{O_2}^{down}$	oxygen pressure in downstream volume
$p_{O_2}^{x=0}$	partial pressure of oxygen in liquid slab at $x = 0$
$p_{O_2}^{x=L}$	partial pressure of oxygen in liquid slab at $x = L$
P	permeability ($P = D\alpha$)
\bar{P}	effective permeability
P_c	continuous phase permeability
P_d	dispersed phase permeability
P_{saline}	oxygen permeability of saline
P_{oil}	oxygen permeability of S-100N mix
\bar{P}_{AVE}	average effective permeability
$P_n^m(\cos \theta)$	Legendre function

q	function defined by equation (5.19)
Q	function defined by equation (4.126)
Q^*	function defined by equation (4.136)
r	radial distance
r	function defined in equation (5.22)
R	radial distance at $r = R$
$R(r)$	function used in Appendix A
$R_{d/c}$	equilibrium solute distribution coefficient between dispersed phase and continuous phase
R_m	parameter defined by equation (4.72)
s	function defined by equation (5.21)
t	time
t	function defined by equation (5.22)
T	temperature
v_i	average volume of particles in class i
V_d	downstream volume
W	parameter defined by equation (3.8)
X	distance
Y	fractional saturation

Greek Alphabet

α	solubility of species A
$\bar{\alpha}$	solubility of medium
α_A	solubility of species A
α_B	activity coefficient of carrier species B
α_{AB}	activity coefficient of carrier species AB
$\alpha_{i,j}$	coefficient in 4x4 matrix

β_i	eigenvalues $i = 1,2,3,4$
$\gamma_{i,j}$	coefficient in 10×10 matrix
θ	angle
Θ	function used in Appendix A
Θ, Θ'	"time" lag
λ	characteristic length
Λ	defined by equation (C.49)
μ	viscosity
ν	kinematic viscosity
ρ	density
σ	standard deviation
ϕ	potential (in continuous phase)
Φ	volume fraction of the dispersed phase
ψ	flux

Subscripts

A	species A
$A_i B$	species $A_i B$ ($i = 1,2,3,4$)
B	species B
c	continuous phase
d	dispersed phase
eq	equilibrium
m	medium or membrane
s	shell or skin around particle
T	total
v	volume

Superscripts

'	(prime) denotes dispersed phase
0	at $x = 0$ (or $r = 0$)
L	at $x = L$
T	denotes total

APPENDIX H
BIBLIOGRAPHY

- Abramowitz, M., and I. A. Stegun (1968).
Handbook of Mathematical Functions, National Bureau of Standards,
Applied Math Series, 55, Washington, D. C.
- Adair, G. S. (1923).
"Comparison of Osmotic Pressure of Oxyhaemoglobin, Reduced
Haemoglobin and Methaemoglobin," J. Physiol. 58, xxxix.
- Adair, G. S. (1925).
"The Hemoglobin System. VII. The Oxygen Dissociation Curve of
Hemoglobin," J. Biol. Chem. 63, 529.
- Adams, L. R., and I. Fatt (1967).
"The Diffusion Coefficient of Human Hemoglobin at High
Concentrations," Resp. Physiol. 2, 293.
- Altman, P. L., and D. S. Dittmer (1971).
Respiration and Circulation, Fed. of Am. Soc. for Exp. Biol.,
Bethesda, Md.
- Antonini, E., and M. Brunori (1971).
Hemoglobin and Myoglobin in Their Reactions with Ligands,
North-Holland, Amsterdam.
- Barrer, R. M. (1939).
"Permeation, Diffusion and Solution of Gases in Organic
Polymers," Trans. Far. Soc. 35, 628.
- Barrer, R. M., G. Skirrow (1948).
"Transport and Equilibrium Phenomena in Gas-Elastomer Systems
I. Kinetic Phenomena," J. Polymer Sci. 3, 549.
- Barrer, R. M. (1965).
"Surface Flow of Adsorbed Gases and Vapours," Proc. Brit.
Ceram. Soc. 5, 21.
- Barrer, R. M. (1968).
"Diffusion and Permeation in Heterogeneous Media," in Diffusion
in Polymers, J. Crank and G. S. Park, Ed., Academic Press, London.
- Barrer, R. M. and J. H. Petropoulos (1961).
"Diffusion in Heterogeneous Media: Lattices of Parallelepipeds in
a Continuous Phase," Brit. J. Appl. Phys. 12, 691.
- Bassett, R. J. and J. S. Schultz (1970).
"Nonequilibrium Facilitated Diffusion of Oxygen Through Membranes
of Aqueous Cobaltodihistidine," Biochim. Biophys. Acta 211, 194.

Bauer, C. (1971).

"Influence of 2,3 DPG and Hydrogen Ions on the Kinetics of the Oxygen Hemoglobin Reaction," in Oxygen Affinity of Hemoglobin and Red Cell Acid Base Status, M. Rorth and P. Astrup, Ed., Munksgaard, Copenhagen.

Battino, R., F. D. Evans, and W. F. Danforth (1968).

"The Solubilities of Seven Gases in Olive Oil with Reference to Theories of Transport Through the Cell Membrane," J. Am. Oil Chem. Soc. 4, 830.

Becher, P. (1967).

"Effect of Preparation Parameters on the Initial Size Distribution Function in Oil-in-Water Emulsions," J. Colloid Interf. Sci. 24, 91.

Benesch, R., and R. E. Benesch (1967).

"The Effect of Organic Phosphates from the Human Erythrocyte on the Allosteric Properties of Hemoglobin," Biochem. Biophys. Res. Comm. 26, 162.

Benesch, R., R. E. Benesch, and C. I. Yu (1968).

"Reciprocal Binding of Oxygen and Diphosphoglycerate by Human Hemoglobin," Proc. Nat. Acad. Sci. USA 59, 526.

Benesch, R. and R. E. Benesch (1969).

"Intracellular Organic Phosphates as Regulators of Oxygen Release by Hemoglobin," Nature 221, 618.

Bishop, C. and D. M. Surgenor (1964).

The Red Blood Cell, Academic Press, London.

Bottcher, C. J. (1945).

"The Dielectric Constant of Crystalline Powders," Rec. Trav. Chim. Pays-Bas 64, 47.

Braunitzer, G., R. Gehring-Muller, N. Hilschmann, K. Hilsen, G. Hobom, V. Rudloff and B. Witthmann-Liebold (1961).

"Die Konstitution des Normalen adulten Humanhamoglobins," Hoppe-Seyler's Z. Physiol. Chem. 325, 283.

Braunitzer, G., K. Hilse, V. Rudloff and N. Hilschmann (1964).

"The Hemoglobins," Advan. Protein Chem. 19, 1.

Brian, P. L. T. and R. C. Reid (1962).

"Heat Transfer with Simultaneous Chemical Reaction: Film Theory for a Finite Reaction Rate," A.I.Ch.E.J. 8, 322.

Brokaw, R. S. (1961).

"Thermal Conductivity and Thermal Kinetics," J. Chem. Phys. 35, 1969.

Bruggeman, D. (1935).

"Berechnung Verschiedener Physikalischer Konstanten von Heterogenen Substanzen, I. Dielektrizitätskonstanten und Leitfähigkeiten der Mischkörper aus isotropen Substanzen," Ann. Physic. LPZ 5 (24), 636.

Buckles, R. G., E. W. Merrill, and E. R. Gilliland (1968).
"An Analysis of Oxygen Absorption in a Tubular Membrane Oxygenator," A.I.Ch.E.J. 14, 703.

Buse, G. (1971).

"The Present Position of Hemoglobin REsearch," Angewandte Chemie, Intl. Ed. 10, 663.

Carr, C. W. and K. Sollner (1944).

"The Structure of the Colloidoin Membrane and It's Electrical Behaviour. XI. The Preparation and Properties of Megapermselective Colloidion Membranes Combining Extreme Ionic Selectivity with High Permeability," J. Gen. Physiol. 28, 119.

Chang, T. M. S. (1964).

"Semipermeable Aqueous Microcapsules," Science 146, 524.

Chang, T. M. S., F. C. MacIntosh, and S. G. Mason (1965).

"Semipermeable Aqueous Microcapsules. I. Preparations and Properties," Can. J. Physiol. Pharmacol. 44, 115.

Chang, T. M. S. and M. J. Poznansky (1968).

"Semipermeable Microcapsules Containing Catalase for Enzyme Replacement in Acatalasemic Mice," Nature 218, 243.

Change, T. M. S. and M. J. Poznansky (1968a).

"Semipermeable Aqueous Microcapsules (Artificial Cells) V. Permeability Characteristics," J. Biomed. Mat. Res. 2, 187.

Chang, T. M. S. (1972).

Artificial Cells, Thomas Books, Springfield, Ill.

Chanutin, A. (1971).

Red Cell 2,3-Diphosphoglycerate (DPG). Metabolism and Function in Health and Disease, U.S. Army Medical Research and Development Command, Washington, D. C. (AD 733466).

Chanutin, A. and R. R. Curnish (1967).

"Effect of Organic and Inorganic Phosphates on the Oxygen Equilibrium of Human Erythrocytes," Arch. Biochem. Biophys. 121, 96.

Chowhan, Z. T., T. Yotsuyanagi and W. I. Higuchi (1972).

"Model Transport Studies Utilizing Lecithin Spherules. I. Critical Evaluation of Several Physical Models in the Determination of the Permeability Coefficients for Glucose," Biochim. Biophys. Acta 266, 320.

- Cole, P. V. and L. H. Hawkins (1967).
 "The Measurement of the Oxygen Content of Whole Blood," Bio-Medical Engr., February, p. 56.
- Collins, R. E. (1961).
 "Transport of Gases Through Hemoglobin Solution," Science 133, 1593.
- Colton, C. K., K. A. Smith, E. W. Merrill, and P. C. Farrell (1971a).
 "Permeability Studies with Cellulosic Membranes," J. Biomed. Mater. Res. 5, 459.
- Colton, C. K., K. A. Smith, P. Stroeve, and E. W. Merrill (1971b).
 "Laminar Flow Mass Transfer in a Flat Duct with Permeable Walls," A.I.Ch.E.J. 17, 773.
- Crank, J. (1964).
The Mathematics of Diffusion, Oxford Univ. Press, London.
- Cullis, A. F., H. Muirhead, M. F. Perutz, M. G. Grossmann, and A. C. T. North (1962).
 "The Structure of Haemoglobin. IX. A Three-dimensional Fourier Synthesis of 5.5 Å Resolution: Description of the Phase Angles," Proc. Roy. Soc. (London) A265, 161.
- Danckwerts, P. V. (1970).
Gas-Liquid Reactions, McGraw-Hill, New York.
- Danielli, J. F. (1954).
 "The Present Position in the Field of Facilitated Diffusion and Selective Active Transport," Proc. Symp. Colston Res. Soc. 7, 1.
- Davidson, J. F. and E. J. Cullen (1957).
 "The Determination of Diffusion Coefficients for Sparingly Soluble Gases in Liquids," Trans. Instn. Chem. Engrs. 35, 51.
- Davies, J. T. and E. K. Rideal (1963).
Interfacial Phenomena, Academic Press, New York.
- De La Rue, R. M. and C. W. Tobias (1959).
 "On the Conductivity of Dispersions," J. Electro-Chem. Soc. 106, 827.
- Duc, G. and K. Engel (1970).
 "A Method for Determination of Oxyhemoglobin Dissociation Curves at Constant Temperature, pH and p_{CO_2} ," Resp. Physiol. 8, 118.
- Duvelleroy, M. A., R. G. Buckles, S. Rosenkaimer, C. Tung, and M. B. Laver (1970).
 "An Oxyhemoglobin Dissociation Analyzer," J. Appl. Physiol. 28, 227.

- Edwards, M. J. and T. J. Martin (1966).
"Mixing Technique for the Oxygen-Hemoglobin Equilibrium and Bohr Effect," J. Appl. Physiol. 21, 1898.
- Eichbaum, B. R. (1959).
"The Dielectric Behaviour of Solids Embedded in a Homogeneous Medium," J. Electro-Chem. Soc. 106, 804.
- El-Twaty, A. I. (1972).
"Preparation and Characterization of Emulsions Prepared with the Brown Emulsor," B.S. Thesis, Chem. Engr. Dept., Mass. Inst. of Technology, Cambridge, Mass. 02139.
- Emmer, S. (1972).
Undergraduate Research Project, Chem. Engr. Dept., Mass. Inst. of Technology, Cambridge, Mass. 02139.
- Enns, T. (1964).
"Molecular Collision-Exchange Transport of Oxygen by Hemoglobin," Proc. Natl. Acad. Sci. 51, 247.
- Evans, E. and Y. Fung (1972).
"Improved Measurements of the Erythrocyte Geometry," Microvascular Res. 4, 335.
- Fatt, I. and R. C. La Force (1961).
"Theory of Oxygen Transport Through Hemoglobin Solutions," Science 133, 1919.
- Fatt, I. and R. C. La Force (1963).
"Dispersion Conductivity Theory Applied to Oxygen Diffusion in Blood," J. Phys. Chem. 67, 2260.
- Ridelle, T. P. and R. S. Kirk (1971).
"A Study of Unidirectional Versus Tridirectional Heat Flux Models and the Effect of Particle Size on Heat Conduction in Composite Solids," A.I.Ch.E.J. 17, 1427.
- Finkelstein, A. (1972).
"Thin Liquid Membranes," Arch. Intern. Med. 129, 229.
- Fricke, H. (1924).
"A Mathematical Treatment of the Electric Conductivity and Capacity of Disperse Systems. I. The Electric Conductivity of a Suspension of Homogeneous Spheroids," Physiol. Rev. 24, 575.
- Friedlander, S. K. and K. H. Keller (1965).
"Mass Transfer in Reacting Systems near Equilibrium," Chem. Eng. Sci. 20, 121.
- Gibson, Q. H. (1959).
"The Kinetics of Reactions Between Haemoglobin and Gases," Prog. Biophys. Biophys. Chem. 9, 1.

Gibson, Q. H. (1970).

"The Reaction of Oxygen with Hemoglobin and the Kinetic Basis of the Effect of Salt on Binding of Oxygen," J. Biol. Chem. 245, 3285.

Gibson, Q. H. (1973).

"The Contribution of the α and β Chains to the Kinetics of Oxygen Binding to and Dissociation from Hemoglobin," Proc. Nat. Acad. Sci. USA 70, 1

Gibson, Q. H. and F. J. W. Roughton (1957a).

"The Kinetics and Equilibria of the Reactions of Nitric Oxide with Sheep Haemoglobin," J. Physiol. 136, 507.

Gibson, Q. H. and F. J. W. Roughton (1957b).

"The Determination of the Velocity Constants of the Four Successive Reactions of Carbon Monoxide with Sheep Haemoglobin," Proc. Roy. Soc. B 146, 206.

Gibson, Q. H. and F. J. W. Roughton (1957c).

"The Kinetics of Dissociation of the First Ligand Molecule from Fully Saturated Carboxyhaemoglobin and Nitric Oxide Haemoglobin in Sheep Solution," Proc. Roy. Soc. B 147, 44.

Goddard, J. D., J. S. Schultz, and R. J. Bassett (1970).

"On Membranes Diffusion with Near-Equilibrium Reaction," Chem. Engr. Sci. 25, 665.

Goldman, R., O. Kedem, I. H. Silman, S. R. Caplan, and E. Katchalski (1968).

"Papain-Collodion Membranes. I. Preparation and Properties," Biochem. J. 7, 486.

Goldman, R., L. Goldstein and E. Katchalski (1972).

"Water-Insoluble Enzyme Derivatives and Artificial Enzyme Membranes," in Biochemical Aspects of Reactions on Solid Supports, G. R. Stark, Ed., Academic Press, New York.

Goldstick, T. K. (1966).

"Diffusion of Oxygen in Protein Solutions," Ph.D. Thesis, University of California, Berkeley, California.

Goldstick, T. K. and I. Fatt (1970).

"Diffusion of Oxygen in Solutions of Blood Proteins," Chem. Engr. Symp. Ser. 66, 101.

Grody, E. and D. L. Drabkin (1957).

"Spectrophometric Studies. XVI. Determination of the Oxygen Saturation of Blood by a Simplified Technique, Applicable to Standard Equipment," J. Biol. Chem. 227, 285.

Gregor, H. P. and K. Sollner (1946).

"Improved Methods of Preparation of Permselective Collodion Membranes Combining Extreme Ionic Selectivity with High Permeability," J. Phys. Chem. 50, 53.

- Griffin (1949).
J. Soc. cosmet. Chem. 1, 311.
- Griffin (1954)
J. Soc. cosmet. Chem. 5, 4.
- Guyton, A. C. (1968).
Textbook of Medical Physiology, 3rd ed., W. G. Saunders,
Philadelphia.
- Hartridge, H. and F. J. W. Roughton (1923).
"A Method of Measuring the Velocity of Very Fast Chemical
Reactions," Proc. Roy. Soc. London, Ser. A. 104, 376.
- Hartridge, H. and F. J. W. Roughton (1925).
"The Kinetics of Haemoglobin, III. The Velocity with Which
Oxygen Combines with Reduced Haemoglobin," Proc. Roy. Soc.
A107, 654.
- Hatta, S. (1928-9).
"On the Adsorption Velocity of Gases by Liquids," Tohoku
Imp. Univ. Tech. Rep. 8, 1.
- Hauser, H., M. C. Phillips, and M. Stubbs (1972).
"Ion Permeability of Phospholipids Bilayers," Nature, 239, 342.
- Hemmingsen, E. and P. F. Scholander (1960).
"Specific Transport of Oxygen Through Hemoglobin Solutions",
Science 132, 1379.
- Hershey, D. and T. Karhan (1968).
"Diffusion Coefficients for Oxygen Transport in Whole Blood,"
A.I.Ch.E.J. 14 (6), 969).
- Higuchi, W. I. (1958).
"A New Relationship for the Dielectric Properties of Two Phase
Mixtures," J. Phys. Chem. 62, 649.
- Hill, A. V. (1910).
"The Possible Effects of the Aggregation of the Molecules of
Haemoglobin on Its Dissociation Curve," J. Physiol. 40, iv.
- Hill, A. V. (1928).
"The Diffusion of Oxygen and Lactic Acid Through Tissues,"
Roy. Soc. of London, Ser. B 104, 39.
- Hill, T. L. and O. Kedem (1966).
"Models for Steady State and Active Transport Across Membranes,"
J. Theoret. Biol. 10, 399.
- Himmelblau, D. H. (1964).
"Diffusion of Dissolved Gases in Liquids," Chem. Rev. 64, 527.
- Hufner, G. (1903).
Arch. Ges. Physiol. (Pflugers), 217.

Ingram, V. M. (1963).

The Hemoglobins in Genetics and Evolution, Columbia Univ. Press, New York.

Jefferson, T. B., O. W. Witzell and W. L. Sibbitt (1958).

"Thermal Conductivity of Graphite-Silicone Oil and Graphite-Water Suspensions," Ind. Eng. Chem. 50, 1589.

Keller, K. H. (1969).

"Mass Transport Phenomena in Biological Systems," in Biomaterials, L. Stark and G. Agarwall, ed., Plenum Press, New York.

Keller, K. H. and S. J. Friedlander (1966a).

"The Steady-State Transport of Oxygen Through Hemoglobin Solutions," J. Gen. Physiol. 49, 663.

Keller, K. H., and S. J. Friedlander (1966b).

"Diffusivity Measurements of Human Methemoglobin," J. Gen. Physiol. 49, 681.

Keller, K. H., E. R. Canales, and S. I. Yum (1971).

"Tracer and Mutual Diffusion Coefficients of Proteins," J. Phys. Chem. 75, 379.

Klug, A., F. Kreuzer and F. J. W. Roughton (1956).

"The Diffusion of Oxygen in Concentrated Haemoglobin Solutions," Helv. Physiol. Acta 14, 121.

Klug, A., F. Kreuzer, and F. J. W. Roughton (1956).

"Simultaneous Diffusion and Chemical Reaction in Thin Layers of Haemoglobin Solutions," Proc. Roy. Soc. B 145, 452.

Klute, C. H. (1959).

"Diffusion of Small Molecules in Semicrystalline Polymers: Water in Polyethylene," J. Appl. Polym. Sci. 1, 340.

Koningsberg, W., G. Guidotti, and R. J. Hill (1961).

"The Amino Acid Sequence of the α Chain of Human Hemoglobin," J. Biol. Chem. 236, PC 55.

Koningsberg, W., and R. J. Hill (1962).

"The Structure of Human Hemoglobin. V. The Digestion of the α Chain of Human Hemoglobin with Pepsin," J. Biol. Chem. 237, 3157.

Koningsberg, W., J. Goldstein, and R. J. Hill (1963).

"The Structure of Human Hemoglobin. VII. The Digestion of the β Chain of Human Hemoglobin with Pepsin," J. Biol. Chem. 238, 2028.

Koshland, D. E., G. Nemethy, and D. Filer (1966).

"Comparison of Experimental Binding Data and Theoretical Models in Proteins Containing Subunits," Biochemistry 5, 365.

Kreuzer, F. (1950).

"Ueber die Diffusion von Sauerstoff in Serumweiweisslosungen verschiedener Konzentration," Helv. Physiol. Pharmacol. Acta 8, 505.

Kreuzer, F. (1953).

"Modellversuche zum Problem der Sauerstoffdiffusion in den Lungen," Helv. Physiol. Pharmacol. Acta, Suppl. 9, 99.

Kreuzer, F. (1970).

"Facilitated Diffusion of Oxygen and Its Possible Significance; A Review," Respir. Physiol. 9, 1.

Kreuzer, F. and L. J. C. Hoffd (1970).

"Facilitated Diffusion of Oxygen in the Presence of Hemoglobin," Respir. Physiol. 8, 280.

Kreuzer, F. and L. J. C. Hoffd (1972).

"Factors Influencing Facilitated Diffusion of Oxygen in the Presence of Hemoglobin and Myoglobin," Respir. Physiol. 15, 104.

Kreuzer, F. and Yahr (1960).

"Influence of Red Cell Membrane on Diffusion of Oxygen," J. Appl. Physiol. 15, 117.

Kutchai, H., and N. C. Staub (1969).

"Steady-State, Hemoglobin-Facilitated O₂ Transport in Human Erythrocytes," J. Gen. Physiol. 53, 576.

Kutchai, H., J. A. Jacquez, and F. J. Mather (1970).

"Nonequilibrium Facilitated Oxygen Transport in Hemoglobin Solution," Biophys. J., 10, 38.

La Force, R. C. and I. Fatt (1962).

"Steady-State Diffusion of Oxygen Through Whole Blood," Trans. Farad. Sci. 58, 1451.

Lenfant, C. and C. Aucutt (1966).

"Measurement of Blood Gases by Gas-Chromatography," Resp. Physiol. 1, 3908.

Li, N. N. and A. L. Shrier (1972).

"Liquid Membrane Water Treating," in Recent Developments in Separation Science, N. N. Li, Ed., Chemical Rubber Co., Cleveland, Ohio.

Lorenz, L. (1880).

"Ueber die Refractionconstante," Ann. Phys. Lpz. 11, 70.

Lorentz, A. H. (1880).

"Ueber die Beziehung Zwischen der Fortpflanzungsgeschwindigkeit des Lichtes und der Korperdichte," Ann. Phys. Lpz. 9, 641.

- Malchesky, P. S. and Y. Nose (1970).
"Inert Organic Liquid as a Biological Oxygen Carrier," J. Surg. Res. 10, 559.
- Maxwell, J. C. (1881).
A Treatise on Electricity and Magnetism, Clarendon Press, London, Vol. I, p. 440 (3rd ed., 1904).
- May, S. W. and N. N. Li (1972).
"The Immobilization of Urease Using Liquid-Surfactant Membranes," Biochem. Biophys. Res. Comm. 47, 1179.
- Mc Farlane, R. G. and A. H. Robb-Smith (1961).
Functions of the Blood, Academic Press, London.
- Meldon, J. H. (1973).
"Reaction-Enhanced Mass Transfer in Thin Liquid Films," Ph.D. Thesis, Mass. Inst. of Technology, Cambridge, Mass. 02139.
- Meredith, R. E. and C. W. Tobias (1960).
"Resistance to Potential Flow Through a Cubical Array of Spheres," J. Appl. Phys. 31 (7), 1270.
- Meredith, R. E. and C. W. Tobias (1961).
"Conductivity in Emulsions," J. Electrochem. Soc. 108, 286.
- Meredith, R. E. and C. W. Tobias (1962).
"Conduction in Heterogeneous Systems," in Advances in Electrochemistry and Electrochemical Engineering, Vol. 2, P. Delahay and C. W. Tobias, Ed., Interscience Publishers, New York, p. 15.
- Meyer, J. (1967).
"A Study of the Erythrocyte Sedimentation Rate and of the Possible Improvement of Its Clinical Applicability," Sc.D. Thesis, Mass. Inst. of Technology, Cambridge, Mass. 02139.
- Mickley, H. S., T. K. Sherwood and C. E. Reed (1957).
Applied Mathematics in Chemical Engineering, 2nd Ed., McGraw-Hill Book Co., New York.
- Moll, W. (1966).
"The Diffusion Coefficient of Haemoglobin," Resp. Physiol. 1, 357.
- Moll, W. (1969).
"Measurements of Facilitated Diffusion of Oxygen in Red Blood Cells at 37°C," Pflugers Arch. 305, 269.
- Monod, J., J. Wyman and J. P. Changeux (1965).
"On the Nature of Allosteric Transitions: A Plausible Model," J. Mol. Biol. 12, 88.

- Niesel, V. W. (1953).
"Energieverteilung bei Mischung zweier Dielectrika im elektrischen Feld und Berechnung des Verlustwinkels quasi-stationärer Vorgänge," Ann. Physik 6 (12), 410.
- Olander, D. R. (1960).
"Simultaneous Mass Transfer and Equilibrium Chemical Reaction," A.I.Ch.E.J. 6, 233.
- Panofsky, W. K. H., and M. Phillips (1962).
Classical Electricity and Magnetism, 2nd ed., p. 81, Addison-Wesley Publishing Co., Reading, Mass.
- Pasternak, R. A., M. V. Christensen and J. Heller (1970).
"Diffusion and Permeation of Oxygen, Nitrogen, Carbon Dioxide, and Nitrogen Dioxide through Polytetrafluoroethylene," Macromol. 3, 366.
- Pasternak, R. A., G. L. Burns and J. Heller (1971).
"Diffusion and Solubility of Simple Gases through a Copolymer of Hexafluoropropylene and Tetrafluoroethylene," Macromol., 4, 470.
- Pearce, C. A. R. (1955).
"The Electrical Conductivity and Permittivity of Mixtures with Special Reference to Emulsions of Water in Fuel Oil," Brit. J. Appl. Phys. 6, 113.
- Perelson, A. S. and A. Katchalsky (1972).
"The Relationship Between the Thermodynamic and Kinetic Diffusion Parameters," Chem. Eng. Sci. 27, 1190.
- Perutz, M. F. (1948).
"Submicroscopic Structure of the Red Cell," Nature 161, 204.
- Perutz, M. F. (1970).
"Stereochemistry of Cooperative Effects in Haemoglobin," Nature 228, 726.
- Pircher, L. (1952).
"Die Diffusionskonstante des Sauerstoffs in Methämoglobinlösungen verschiedener Konzentrationen," Herv. Physiol. Pharm. Acta 10, 110.
- Rayleigh, J. W. (1892).
"On the Influence of Obstacles Arranged in Rectangular Order upon the Properties of a Medium," Phil. Mag. 5 (34), 481.
- Reynolds, J. A. and G. M. Hough (1957).
"Formulae for Dielectric Constant of Mixtures," Proc. Phys. Soc. (London) B70, 769.
- Richterich, R. (1969).
Clinical Chemistry, Basel: S. Karger, p. 333.

- Riveros-Morenos, V. and J. B. Wittenberg (1972).
"The Self-Diffusion Coefficients of Myoglobin and Hemoglobins in Concentrated Solutions," J. Biol. Chem. 247, 895.
- Robb, W. L. (1971).
"Gas Permeability in Polymeric Materials," in Biomaterials, A. L. Bement, Ed., Univ. of Washington Press, Seattle, Wash.
- Roughton, F. J. W. (1927).
"The Rate of Distribution of Dissolved Gases Between the Red Blood Cell Corpuscle and Its Fluid Environment. Part I. Preliminary Experiments on the Rate of Uptake of Oxygen and Carbon Monoxide by Sheep's Corpuscles," J. Physiol. (London) 62, 232.
- Roughton, F. J. W. (1932).
"Diffusion and Chemical Reaction Velocity as Joint Factors in Determining the Rate of Uptake of Oxygen and Carbon Monoxide by the Red Blood Corpuscle," Proc. Roy. Soc., B., 111, 1.
- Roughton, F. J. W. (1949).
"The Intermediate Compound Hypothesis in Relation to the Equilibria and Kinetics of the Reactions of Haemoglobin with Oxygen and Carbon Monoxide," in Haemoglobin; Bacroft Memorial Conference, Butterworth Scientific Publications, London.
- Roughton, F. J. W. (1959).
"Diffusion and Simultaneous Chemical Reaction Velocity in Haemoglobin Solutions and Red Blood Cell Suspensions," Prog. Biophys. Chem. 9, 55.
- Roughton, F. J. W., E. C. DeLand, J. C. Kernohan, and J. W. Severinghaus (1971).
"Some Recent Studies of the Oxyhaemoglobin Dissociation Curve of Human Blood under Physiological Conditions and the Fitting of the Adair Equation to the Standard Curve," in Oxygen Affinity of Hemoglobin and Red Cell Acid Base Status, M. Rørth and P. Astrup, Ed., Munksgaard, Copenhagen.
- Runge, I. (1925).
Z. Tech. Phys. 6, 6.
- Schmolka, I. (1970).
"Theory of Emulsions," Fed. Proc. 29, 1717.
- Scholander, P. F. (1960).
"Oxygen Transport through Hemoglobin Solutions," Science 131, 585.
- Schroeder, W. A. (1963).
"The Hemoglobins," Ann. Rev. Biochem. 32, 301.
- Schroeder, W. A. and W. R. Holmquist (1968).
"A Function for Hemoglobin A_{1C}?" in Structural Chemistry and Molecular Biology, A. Rich and N. Davidson, ed., W. H. Freeman and Co., San Francisco, p. 238.

- Sendroy, J., R. T. Dillon, and D. D. Van Slyke (1934).
"Studies of Gas and Electrolyte Equilibria in Blood. XIX. The Solubility and Physical State of Uncombined Oxygen in Blood," J. Biol. Chem. 105, 597.
- Seufert, W. D. (1970).
"Model Membranes: Spherical Shells Bounded by One Bimolecular Layer of Phospholipids," Biophysik 7, 60.
- Silman, I. H. and E. Katchalski (1966).
"Water-Insoluble Derivatives of Enzymes, Antigens and Antibodies," Ann. Rev. Biochem. 35, 873.
- Slawinsky, A. (1926).
"Conductivity of an Electrolyte Containing Dielectric Bodies," J. Chim. Phys. 23, 710.
- Sloviter, H. A., M. Petkovic, S. Ogoshi and H. Yamada (1969).
"Dispersed Fluorochemicals as Substitutes for Erythrocytes in Intact Animals," J. Appl. Physiol. 27, 666.
- Smith, K. A., J. H. Meldon and C. K. Colton (1973).
"An Analysis of Carrier-Facilitated Transport," A.I.Ch.E.J. 19, 102.
- St. Denis, C. E. and C. J. D. Fell (1971).
"Diffusivity of Oxygen in Water," Canad. J. Chem. Engr. 49, 885.
- Stein, W. D. (1967).
The Movement of Molecules Across Cell Membranes, Academic Press, New York, p. 126.
- Stein, T. R. (1968).
"Augmented Diffusion of Oxygen," Ph.D. Thesis, Univ. of Minnesota, Minneapolis, Minn.
- Stein, T. R., J. C. Martin and K. H. Keller (1971).
"Steady-State Oxygen Transport through Red Blood Cell Suspensions," J. Appl. Physiol. 31, 397.
- Stewart, G. N. (1899).
"The Relative Volume or Weight of Corpuscles and Plasma in Blood," J. Physiol. 24, 356.
- Stricoff, S. (1971).
"Emulsion Studies," Undergraduate Research Report, Chemical Engr. Dept. Mass. Inst. of Technology, Cambridge, Mass. 02139.
- Szabo, G., G. Eisenman, and S. M. Ciani (1970).
"Ion Distribution Equilibria in Bulk Phases and the Ion Transport Properties of Bilayer Membranes Produced by Neutral Macrocyclic Antibiotics," in Physical Principles of Biological Membranes, F. Snell, J. Wolken, G. Iverson, and J. Lam, Ed., Gordon and Breach Science Publ., New York.

Tavlarides, L. L., C. A. Coulaloglou, M. A. Zeitlin, G. E. Klinzing, and B. Gal-Or (1970).

"Bubble and Drop Phenomena," Ind. Engr. Chem. 62 (11), 6.

Tien, H. T. (1972).

"Bilayer Lipid Membranes: An Experimental Model for Biological Membranes," in The Chemistry of Biosurfaces, Vol. I, M. L. Hair, Ed., Marcel Dekker, Inc., New York.

Topper, L. (1955).

"Analysis of Porous Thermal Insulating Materials," Ind. Eng. Chem., 47, 1377.

Tuntunjian, R. S. (1973).

"Model Systems for Transport in Reactive Heterogeneous Media," M.S. Thesis, Mass. Inst. of Technology, Cambridge, Mass. 02139.

Tyuma, I., and U. Yoshihiro (1972).

"A Note on the Oxygen Consumption of Human Adult Hemoglobin Solutions Prepared by Various Methods," in Oxygen Affinity of Hemoglobin and Red Cell Acid Base Status, M. Rorth and P. Astrup, Ed., Munsgaard, Copenhagen.

Van Slyke, D. D. and J. M. Neill (1924).

"The Determination of Gases in Blood and Other Solutions by Vacuum Extraction and Manometric Measurement," J. Biol. Chem. 61, 523.

Vieth, W. R., S. G. Gilbert and S. S. Wang (1972).

"Performance of Collagen-Invertase Complex Membrane in a Biocatalytic Module," Trans. N.Y. Aca. Sci. 34, 454.

Wang, J. H. (1961).

"Transport of Oxygen through Hemoglobin Solutions," Science 133, 1770.

Ward, W. J. (1970).

"Analytical and Experimental Studies of Facilitated Transport," A.I.Ch.E.J. 16, 405.

Ward, W. J., and W. I. Robb (1967).

"Carbon Dioxide-Oxygen Separation and Facilitated Transport of Carbon Dioxide Across a Liquid Film," Science 156, 1481.

Watson, H. C. and J. C. Kendrew (1961).

"Comparison Between the Amino-Acid Sequences of Sperm Whale Myoglobin and of Human Hemoglobin," Nature 190, 670.

Weetal, H. H. and R. A. Messing (1972).

"Insolubilized Enzymes on Inorganic Materials," in The Chemistry of Biosurfaces, M. L. Hair, Ed., Marcel Dekker, New York.

Weisz, P. B. (1973).

"Diffusion and Chemical Transformation," Science 179, 433.

Wittenberg, J. B. (1959).

"Oxygen Transport - A New Function Proposed for Myoglobin,"
Biol. Bull. 177, 402.

Wittenberg, J. B. (1966).

"The Molecular Mechanism of Hemoglobin - Facilitated Oxygen
Diffusion," J. Biol. Chem. 241, 104.

Woods, M. E., J. S. Dodge, and I. M. Krieger (1968).

"Monodisperse Latices: I. Emulsion Polymerization with Mixtures
of Anionic and Nonionic Surfactants," J. Paint Techn. 40, 541.

Woodside, W. and J. H. Messmer (1961).

"Thermal Conductivity of Porous Media. I. Unconsolidated Sands,"
J. Appl. Physics 32 (9), 1688.

Wyllie, M. R. J. and A. R. Gregory (1953).

"Formation Factors of Unconsolidated Porous Media: Influence of
Particle Shape and Effect of Cementation," Trans. AIME 198, 103.

Zahka, J. (1971).

"Oxygen Transport Through Partially Immobilized Hemoglobin Films,"
M.S. Thesis, M.I.T., Cambridge, Mass. 02139.

BIOGRAPHICAL NOTE

The author, Pieter Stroeve, was born in the Netherlands, the second son of four children of Antonie Stroeve and Frederika Johanna Wilhelmina Stroeve-Smolders. The author lived for a number of years in the Netherlands and Indonesia. In 1959, the author's family emigrated to the United States of America. He received his secondary education from Oakland and Berkeley High Schools.

The author entered Contra Costa College in 1962, and later transferred to the University of California where he received his B.S. degree in 1967 from the Department of Chemical Engineering. In September of that year the author commenced graduate study at MIT and was awarded a M.S. degree in June 1969. That same month he started a literature search for a suitable doctoral thesis topic in the area of biomedical science. During his time at MIT the author has had a National Science Foundation Traineeship, a National Institutes of Health Predoctoral Fellowship, and a Du Pont de Nemours Fellowship.

The author has spent two summers as a research engineer for the Naval Ordnance Laboratory, and Esso Production Research, and has served as a part-time consultant for Durham Associates Inc.

Reflecting for a moment on his life for the past quarter of a century, the author can only conclude that he has been a very lucky man. He can deduce that conclusion from the following good influences:

- a healthy life
- a "new" country that offered him many educational opportunities
- two loving parents
- two brothers, Antonie and Wilbert, and a sister, Hanneke
- uncles and aunts in the "old" country
- a devoted and loving wife, Barbara
- Barbara's family
- two beautiful daughters, Dale Corinna Johanna and Maryke Abbe.

What more could a young man ask for?

PUBLICATIONS

"Laminar Flow Mass Transfer in a Flat Duct with Permeable Walls," A.I.Ch.E.J., 17, 773 (1971). Co-authors: C. K. Colton, K. A. Smith, and E. W. Merrill.

"Diffusion with Reversible Chemical Reaction in Heterogeneous Media - A Model for Oxygen Transport through Whole Blood," paper presented at the 72nd Annual A.I.Ch.E. Meeting, St. Louis, Missouri, May 22, 1972. Co-authors: K. A. Smith and C. K. Colton.

"Mechanism of Oxygen Transport in Hemoglobin Solutions," to be published by the Journal of Applied Physiology. Co-authors: C. K. Colton and J. G. Zahka.